Electrochemical Society

Chicago Meeting Program Issue

GLC EXPANDS PRODUCTION WITH GRAPHITE PLANT SERVING WESTERN STATES

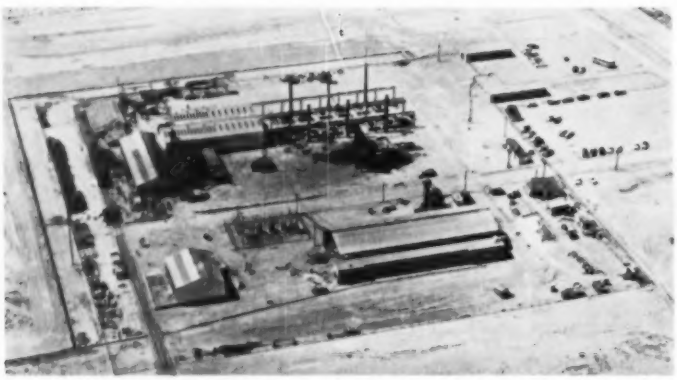

The GLC graphite plant at Antelope Valley, California.

We are glad to inform the electrometallurgical and electrochemical industries in the Western States area that we recently acquired the plant and physical assets of Crescent Carbon Corporation in California.

Carbon and graphite users in the Western States and those overseas in the Pacific area will shortly have a greatly improved source of supply at their command.

Plans now under way at the GLC graphite plant, Antelope Valley, California, call for a substantially increased inventory of electrodes, anodes and mold stock, not only in tonnage but in a variety of shapes and sizes as well. Customers can look forward to faster service on their shipments and to closer cooperation in solving their technical problems.

Technicians from our plants at Niagara Falls, N.Y. and Morganton, N.C. are establishing the most modern production techniques at the Antelope Valley plant, so that its products will meet established GLC standards of quality and uniformity.

As these forward steps are taken, we hope to have the privilege of widening the scope of our service to customers, old and new.

PRODUCTS ELECTRODE GLC DIVISION YOU CAN TRUST ®

GREAT LAKES CARBON CORPORATION

18 EAST 48TH STREET, NEW YORK 17, N. Y.

PACIFIC COAST OFFICE: 671F OAK GROVE AVENUE
MENLO PARK, CALIFORNIA • PHONE: DAVENPORT 3-4152

EDITORIAL STAFF

H. H. Uhlig, Chairman, Publication Committee

Cecil V. King, Editor

Norman Hackerman, Technical Editor

Ruth G. Sterns, Managing Editor

U. B. Thomas, News Editor

H. W. Salzberg, Book Review Editor

Natalie Michalski, Assistant Editor

DIVISIONAL EDITORS

W. C. Vosburgh, Battery

Milton Stern, Corrosion, I

R. T. Foley, Corrosion, II

T. D. Callinan, Electric Insulation

Seymour Senderoff, Electrodeposition

H. C. Froelich, Electronics

Ernest Paskell, Electronics—Semiconductors

Sherlock Swann, Jr., Electro-Organic, I

Stanley Wawzonek, Electro-Organic, II

John M. Blocher, Jr., Electrothermics and Metallurgy, I

A. U. Seybolt, Electrothermics and Metallurgy, II

N. J. Johnson, Industrial Electrolytic

C. W. Tobias, Theoretical Electrochemistry, I

A. J. deBethune, Theoretical Electrochemistry, II

ADVERTISING OFFICE

ECS
1860 Broadway, New York 23, N. Y.

ECS OFFICERS

W. C. Gardiner, President
Olin Mathieson Chemical Corp., Niagara Falls, N. Y.

R. A. Schaefer, Vice-President
The Bunting Brass and Bronze Co., Toledo, Ohio

Henry B. Linford, Vice-President
Columbia University, New York, N. Y.

F. L. LaQue, Vice-President
International Nickel Co., Inc., New York, N. Y.

Lyle I. Gilbertson, Treasurer
Air Reduction Co., Murray Hill, N. J.

I. E. Campbell, Secretary
National Steel Corp., Weirton, W. Va.

Robert K. Shannon, Executive Secretary
National Headquarters, The ECS, 1860 Broadway, New York 23, N. Y.

Manuscripts submitted to the Journal should be sent, in triplicate, to the Editorial Office at 1860 Broadway, New York 23, N. Y. They should conform to the Instructions to Authors, last published in the August 1959 issue, pp. 232C-233C. Manuscripts so submitted become the property of The Electrochemical Society and may not be published elsewhere, in whole or in part unless permission is requested of and granted by the Editor.

Inquiries re positive microfilm copies of volumes should be addressed to University Microfilms, Inc., 313 N. First St., Ann Arbor, Mich.

Journal of the Electrochemical Society

MARCH 1960 **VOL. 107 • NO. 3**

CONTENTS

Editorial

The Census 44C

Technical Papers

Observations on the Fe-Cr-O System. *A. U. Seybolt* 147

A Model of the Mechanism of Electrochemical Conversion from Active to Passive States. *W. A. Mueller* 157

Kinetics of the Dissolution of Copper in Aqueous Solutions of Aliphatic Amines. *S. C. Sircar and D. R. Wiles* 164

The Attack of Copper-Gold, Silver-Gold, Nickel-Copper, and Silver-Copper Alloys by Sulfur at Elevated Temperatures. *B. D. Lichter and C. Wagner* 168

Influence of Electrode Surface Conditions on the Electrical Strength of Liquified Gases. *D. W. Swan and T. J. Lewis* 180

Molecular Structure and the Electrical Strength of Liquid Hydrocarbons. *T. J. Lewis* 185

A New Statistical Theory for the Breakdown of Liquid Hydrocarbons. *B. W. Ward and T. J. Lewis* 191

Kinetics of the Oxidation of Antimony. *A. J. Rosenberg, A. A. Menna, and T. P. Turnbull* 196

CaS:Cu,Eu Electroluminescent Phosphors. *A. Wachtel* 199

Influence of Crystal Size on the Spectral Response Limit of Evaporated PbTe and PbSe Photoconductive Cells. *W. D. Lawson, F. A. Smith, and A. S. Young* 206

Relation of Some Surface Chemical Properties of Zinc Silicate Phosphor to Its Behavior in Fluorescent Lamps. *D. E. Harrison* 210

The System BaO-TiO_2-P_2O_5: Phase Relations, Fluorescence, and Phosphor Preparation. *D. E. Harrison* 217

An Apparatus for the Preparation of Semiconductor Grade Silicon by Film Boiling. *R. C. Ellis, Jr.* 222

Imaging-Furnace Developments for High-Temperature Research. *P. E. Glaser* 226

Metal Mists and Aluminum Losses in the Hall Process. *W. E. Haupin* 232

Anodic Precipitation of Tracer Manganese as Dioxide. *E. A. Heintz and L. B. Rogers* 236

Mass Transfer and Current Distribution under Free Convection Conditions. *K. Asada, F. Hine, S. Yoshizawa, and S. Okada* 242

Technical Notes

On the Influence of Combinations of Impurities on the Electrolysis of Zinc. *G. Steintveit and H. Holtan, Jr.* 247

Dendritic Inclusions in AlSb Grown-Junction Diodes. *H. C. Gorton* 248

Ohmic Contacts to Semiconducting Ceramics. *D. R. Turner and H. A. Sauer* 250

Preparation of InAs, InP, GaAs, and GaP by Chemical Methods. *D. Effer and G. R. Antell* 252

Chicago Meeting Program 47C-79C

Current Affairs 81C-90C

Published monthly by The Electrochemical Society, Inc., from Manchester, N. H., **Executive Offices, Editorial Office** and **Circulation Dept.,** and **Advertising Office** at 1860 Broadway, New York 23, N. Y., combining the JOURNAL and TRANSACTIONS OF THE ELECTROCHEMICAL SOCIETY. Statements and opinions given in articles and papers in the JOURNAL OF THE ELECTROCHEMICAL SOCIETY are those of the contributors, and The Electrochemical Society assumes no responsibility for them. Nondeductible subscription to members $5.00; subscription to nonmembers $18.00. Single copies $1.25 to members, $1.75 to nonmembers.

Copyright 1960 by The Electrochemical Society, Inc.

Entered as second-class matter at the Post Office at Manchester, N. H., under the act of August 24, 1912.

Editorial

The Census

The 1960 Population Census will be conducted as of April 1. Every fourth household will be asked to answer the question, for each person 14 years of age or older, "What kind of work are you doing?"

In order that the statistics on scientific and engineering manpower be developed as accurately as possible, the Census Bureau has asked that we pass along to our readers a reminder that this question on occupation should be answered completely and precisely. The entry should consist of two or more words in many cases.

Some examples of acceptable entries are: analytical chemist, chemist, chemical engineer, electrochemist, physical chemist, process chemical engineer, etc.

* * *

THE above statement was prepared for us by the Census Bureau, which has requested that we give it prominent display. Similar statements will appear in thousands of publications throughout the country. The Census Bureau will not prepare a complete list of scientific manpower; this is a function of other agencies, such as the National Research Council. The Census Bureau has the task of preparing accurate statistics concerning the population, including occupations, which it wishes to break down into categories smaller than just Chemist or Engineer or Businessman.

The sampling of every fourth household is a huge undertaking, which would be impossible for any other agency, or in any other way. A private statistical agency would consider a careful sampling of a few thousand households, properly chosen to be representative in all fields, to be sufficient to give a reasonably reliable survey of the entire nation.

The actual gathering of census data can be completed very quickly, because it will be done by many thousands of workers in their spare time. There will, unfortunately, be many errors, but they will be a surprisingly small per cent of the total. Analysis of the data, on the other hand, will take many months. The results of this vast undertaking will be of immense practical value to the nation's business, as well as to units of Government from the national to the local level. The casual citizen will perhaps be more interested in learning where the new center of population is to be located, whether California is really more popular than Florida for retired couples, and in the various statistics which eventually will filter into the World Almanac.

—CVK

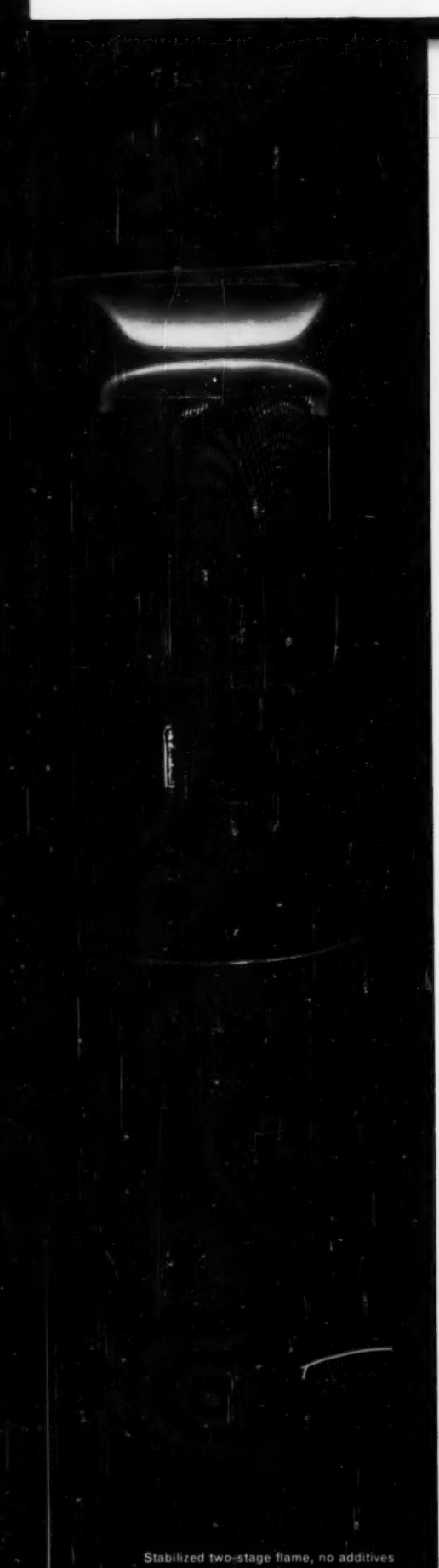

Stabilized two-stage flame, no additives

One of a series

The burning question of cool flames

Between the brief stage of not burning and burning, many hydrocarbons react with oxygen at temperatures well below that of normal flame combustion. But the reactions are usually transient and hard to analyze. At the General Motors Research Laboratories, we have been able to investigate the *effect of chemical additives on cool preflames.*

To do this, the almost invisible cool flames are stabilized for hours in a flat-flame burner, permitting careful examination of the retardation or acceleration effects of the additives. From more than twenty additives studied, experimental results indicate that some chemicals affect combustion through the mechanism of preflame reactions. We are now accumulating new information on these additives' mode of operation. For instance: emission spectra support the conclusion that tetraethyl lead reacts with the oxygenated compounds formed in cool flames to yield lead oxide vapor. These findings of when and how lead oxide is formed are important in resolving a current controversy of science — the combustion behavior of tetraethyl lead.

Studies such as this may lead to more economical and effective means of controlling unrestrained combustion — such as "knock" in reciprocating engines. The work is typical of GM Research's effort to provide useful information for a moving America. And in this way continue to keep our promise of "More and better things for more people."

General Motors Research Laboratories

Warren, Michigan

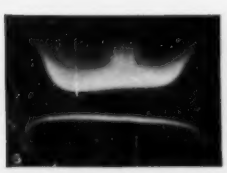

Iron carbonyl, an antiknock

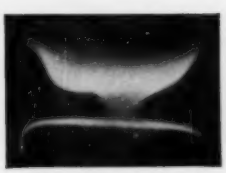

Ethyl nitrate, a proknock

Iron carbonyl retards, ethyl nitrate accelerates central portion of cool flames.

HE X-RAYS WOOD...

to help make telephone poles last longer

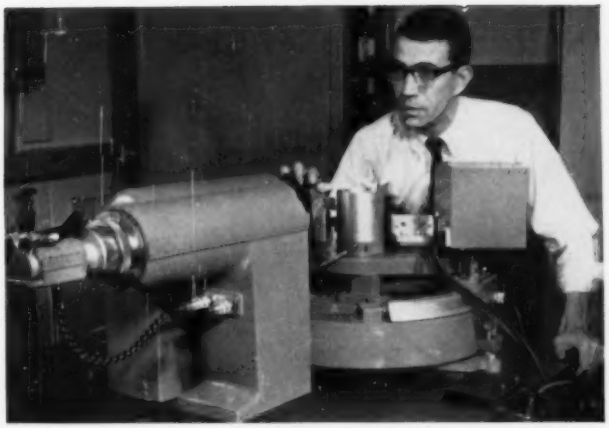

Chemist Jack Wright developed the use of this X-ray fluorescence machine for testing the concentration of preservatives in wood. Here he bombards a boring from a test telephone pole with X-rays.

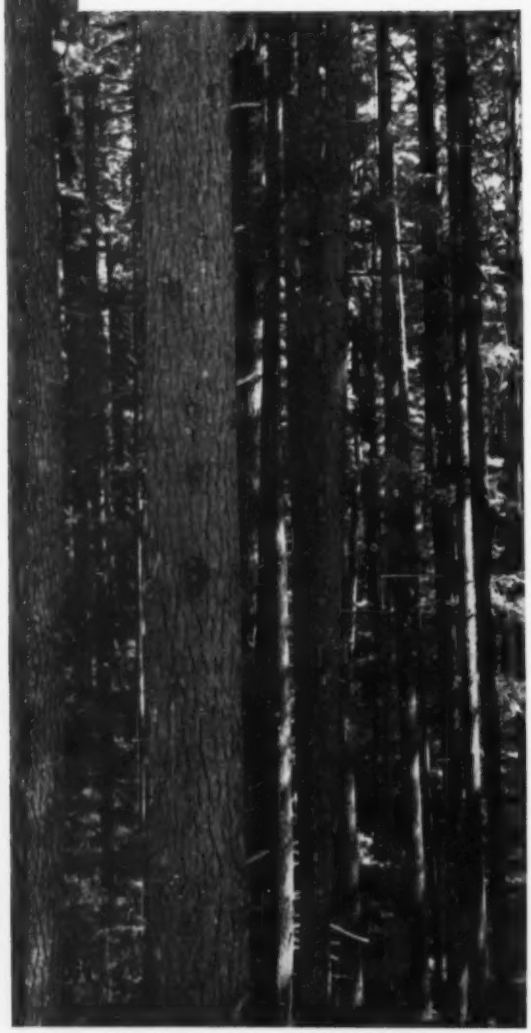

This Bell Labs chemist is using a fast, new technique for measuring the concentration of fungus-killing preservative in telephone poles.

A boring from a test pole is bombarded with X-rays. The preservative—pentachlorophenol—converts some of the incoming X-rays to new ones of different and characteristic wave length. These new rays are isolated and sent into a radiation counter which registers their intensity. The intensity in turn reveals the concentration of preservative.

Bell Laboratories chemists must test thousands of wood specimens annually in their research to make telephone poles last longer. Seeking a faster test, they explored the possibility of X-ray fluorescence—a technique developed originally for metallurgy. For the first time, this technique was applied to wood. Result: A wood specimen check in just two minutes—at least 15 times faster than before possible with the conventional microchemical analysis.

Bell Labs scientists must remain alert to *all* ways of improving telephone service. They must create radically new technology or improve what already exists. Here, they devised a way to speed research in one of telephony's oldest and most important arts—that of wood preservation.

Nature still grows the best telephone poles. There are over 21 million wooden poles in the Bell System. They require no painting, scraping or cleaning; can be nailed, drilled, cut, sawed and climbed like no other material. Scientific wood preservation cuts telephone costs, conserves valuable timber acres.

BELL TELEPHONE LABORATORIES

World Center of Communications Research and Development

Observations on the Fe-Cr-O System

A. U. Seybolt

Research Laboratory, General Electric Company, Schenectady, New York

ABSTRACT

An isothermal phase diagram for the Fe-Cr-O system is presented for 1300°C which, with a minor modification, holds for 1000°C. It is observed that Fe-Cr alloys containing over 13% Cr are in equilibrium with Cr_2O_3 containing a little dissolved Fe_2O_3. Alloys of lower chromium content are in equilibrium with iron chromite of variable composition of the type $FeCr_2O_4$. Evidence is presented indicating that when the spinel forms next to the metal a pronounced internal oxidation occurs. However, higher chromium alloys with Cr_2O_3 next to the metal show no tendency for internal oxidation. An oxygen pressure-composition diagram for the entire system is also presented. Marker experiments made during the oxidation of 20% Cr and 30% Cr alloys suggest that Cr_2O_3 is formed almost entirely by cation (Cr^{+3}) diffusion.

Many investigators have been concerned with the oxidation kinetics of the industrially important Fe-Cr alloys. However, before the kinetics can be evaluated properly, the equilibria involved should be well established. The work of Yearian, Randell, and Longo (1), conducted between 700° to 1160°C, was primarily a kinetic study, but these workers presented an approximate phase diagram which agrees in many essentials with the present investigation and with the slightly later work of Woodhouse and White (2). The investigation of Yearian, *et al.* (1) as just mentioned was not primarily an equilibrium study, and in addition the scales they observed were influenced by the presence of significant amounts of manganese, silicon, and carbon in the commercial steels they studied.

The work of Richards and White (3), and in particular the closely related investigation of Woodhouse and White (2), presented considerable information on equilibria in this system. Only very little of the findings of Richards and White (3) can be compared directly with the present study since these investigators were more concerned with the effects of rather wide variation in temperature than with establishing phase boundaries at constant temperature, as in the present case. In addition, they studied equilibria which were stable in the partial pressure of oxygen in air. On the other hand, their qualitative findings relating to the M_2O_3-M_3O_4 equilibria are in agreement with results presented here.

However, the tentative isothermal phase diagram presented by Woodhouse and White (2) (for temperatures between 560°C and the solidus) can be compared directly and qualitatively with the present investigation. It should be emphasized that Woodhouse and White considered their Fe-Cr-O isothermal phase diagram as only semiquantitative. Considering the limited amount of information available to these investigators, it is remarkable that their estimation of the nature of the system should agree so well, on a qualitative basis, with the findings to be reported in the present investigation. This agreement is particularly remarkable in view of the fact that Woodhouse and White conducted no equilibrium studies involving a metal phase, but confined themselves experimentally to the study of oxide equilibria.

It would require an inordinate amount of space to review in detail the results of the various observations made on the oxidation of Fe-Cr type materials, including stainless steels. However, the nature of the scales observed in a few of the more significant papers might be listed briefly. Rickett and Wood (4) oxidized 12-28% Cr-Fe alloys in oxygen at 980° and 1090°C and found spinel ($FeCr_2O_4$) and Cr_2O_3 on the inside and Fe_2O_3 on the outside of the scale. The nature and number of the layers depended on chromium content and temperature. McCullough and Fontana (5) found that on stainless steels heated in oxygen to 980°C spinel formed next to the metal, but as the oxidation proceeded Fe_2O_3 was predominant in the scale. Caplan and Cohen (6) used commercial Fe-Cr alloys containing 11-26% Cr with 0.3% Si, and oxidized their alloys at 1600°F to 2000°F in dry and moist air. Cr_2O_3 and spinel in various proportions were observed as the principal scale components. No essentially pure iron oxides, such as Fe_2O_3, were observed apparently under the conditions of their experiments. Moreau (7) studied a wide range of Fe-Cr alloys at 800°-1250°C and is one of the few authors who reports FeO as a stable oxide (mixed with $FeCr_2O_4$) next to the metal. Moreau apparently observed this mixed scale regardless of the chromium concentration. Yearian, Randell, and Longo (1) found practically all possible oxides depending on the parameters of composition and temperature. Their main findings can be summarized as characterizing two kinds of scale: type A (low rates of attack) consisting primarily of Cr_2O_3 with some dissolved Fe_2O_3, and type

B scales where attack is severe. In the latter scales, the spinel of the type $FeCr_2O_4$ is predominant.

In reviewing the literature of the oxidation of Fe-Cr alloys, the somewhat confused summary just presented is quite typical. This lack of agreement is due primarily to the fact that the types of scale formed are a sensitive function of temperature, chromium content, atmosphere, time of exposure, impurities present, and possibly other factors. However, it seems reasonably clear that the following oxides can be present depending on composition and oxygen partial pressure: FeO, Fe_3O_4, Fe_2O_3, Cr_2O_3, and $FeCr_2O_4$. These last two oxides require additional discussion. It has been established by Wretblad (8) and by others that Fe_2O_3 and Cr_2O_3 form a continuous series of solid solutions. In addition, Yearian, *et al.* (1) and Caplan and Cohen (6) found evidence for some Fe_2O_3 dissolved in the Cr_2O_3-type scales. The spinel $FeCr_2O_4$ is not necessarily stoichiometric, but this cubic oxide forms a solid solution series with Fe_3O_4. This has been demonstrated very well by Yearian, Kartwright, and Langenheim (9) who found that the lattice parameter of these solid solutions is not a single valued function of the composition, due to lattice sites being occupied differently as Cr^{+3} ions are replaced by Fe^{+3} ions.

In the work which follows, the primary object has been to outline the isothermal sections at 1000° and 1300°C. The oxygen equilibrium pressure is in general different in different parts of the system.

Experimental Methods

Fe-Cr alloys in the range 1-70% Cr were made using Ferrovac (vacuum-melted electrolytic iron) and hydrogen-treated electrolytic chromium. In order to maintain good control over composition, the alloys were prepared as 50-g buttons in an inert arc furnace. After homogenizing heat treatments at 1000°C or above in a hydrogen atmosphere during the processing, the alloys were mainly finished as hot-rolled (600°C) strip 0.015 in. thick. Samples used for the oxidation treatment were usually ½ x 1 in. rectangles, whose flat surfaces were abraded with various grades of wet or dry carborundum paper. The 180 grade of paper was found to be better than some of the finer grits because the oxide formed subsequently during high-temperature oxidation treatments tended to be better anchored to the sample. It was desired to keep the oxide on the metal surface to secure equilibration with the metal phase.

The general procedure for oxidation was to form a thin oxide layer on the surface and then to "equilibrate" the oxide with the metal by heating at 1000° or 1300°C in an argon atmosphere. By forming a comparatively thin oxide layer on the surface, insufficient metal was used up in forming the oxide to change the alloy composition appreciably, at least in most instances. Where considerable oxidation occurred, the experiment was repeated or the sample was not used for determining a phase boundary. True equilibration between the metal and oxide phase would require accurate control of the oxygen partial pressure and, in general, each Fe-Cr alloy would require a different oxygen pressure. However, as will be demonstrated shortly, most of the alloys are in equilibrium with Cr_2O_3 containing a small amount of Fe_2O_3. Since the dissociation pressure of Cr_2O_3 is so low, about 10^{-16} atm at 1300°C, the rate of breakdown of Cr_2O_3 in pure argon would be very small. Hence, the practical difference between controlling the oxygen pressure at 10^{-16} atm and using argon is negligible for equilibria involving Cr_2O_3. This same reasoning can be applied to cases where $FeCr_2O_4$ or more accurately, Fe $Fe_{(3-x)}Cr_xO_4$ [x-=O—2] solid solution, is stable. This is true for compositions near $FeCr_2O_4$ but not for spinels of low chromium content. In the vicinity of Fe_3O_4 or Fe_2O_3, the dissociation pressure is sufficiently high so that rapid breakdown of the oxides in argon occurs.

The primary object of the phase equilibrium study was to establish the tie lines between metal phase and oxide phase. While the identification of the oxide-oxide equilibria was of secondary importance, it was possible to establish these boundaries also.

Alloy-Oxide Equilibration Experiments

It is obvious of course that as long as one is using alloys far removed from a phase boundary, the amount of chromium removed from the alloy during oxidation is not critical. However, if one is close to a critical composition, one should not remove an appreciable fraction of chromium from the alloy if the phase boundary is to be located with a high degree of accuracy. The accuracy aimed at was about ± 1% Cr.

In general, the small ½ x 1 in. strips were oxidized briefly in 1 atm of dry oxygen for 1-5 min at temperatures ranging from 600° to 1000°C depending on chromium content. The higher chromium alloys required more severe oxidizing conditions to secure enough scale for Debye camera x-ray or electron diffraction identification. After a few milligrams of oxide were formed on the surface, the samples were transferred to a furnace operated at 1000° or 1300°C and equipped with a vacuum-tight mullite tube containing a stagnant argon atmosphere. The equilibration treatment was usually at least 24-hr long and sometimes over 65 hr in duration. The samples standing on edge on a ceramic boat could be pushed into or out of the hot zone without disturbing the argon atmosphere. The object of the equilibration was twofold: (*a*) to allow sufficient time for the composition of the oxide to adjust to the equilibrium composition of the metal phase, and (*b*) to smooth out local concentration gradients in the metal at the metal/oxide interface. Because the surface of the alloy was robbed to some extent of chromium to form a chromium-containing scale, the equilibration treatment served to reestablish a uniform chromium content across the thickness of the sheet.

For very low chromium alloys where oxidation was severe, or in cases where better control over the degree of oxidation was necessary, samples were

sealed in SiO_2 capsules. In these capsules, samples were mounted on molybdenum brackets to prevent contact with SiO_2. Also sealed into the capsule was a small amount of FeO wrapped in iron foil. The Fe/FeO equilibrium pressure at 1300°C is about 10^{-11} atm, which was more than enough to stabilize any equilibrium scale in the entire system. These capsules were partially filled with purified argon, after exhausting the air, to prevent collapse of the SiO_2 at 1300°C. Equilibrations usually were carried out on the encapsulated samples by again encapsulating them in a SiO_2 tube without the FeO.

Experimental Results

Oxidizing and equilibrating runs are summarized in Tables I and II, which give x-ray and electron diffraction results, visual and metallographic observations at 1000° and 1300°C, respectively. It will be noted that spinel solid solution ($FeFe_{(2-x)}Cr_xO_4$) was formed at low chromium concentrations, and that Cr_2O_3 constituted the scale at high chromium contents; this was true both at 1000° and 1300°C. However, at a chromium level centering about 13%, both Cr_2O_3 and the spinel were sometimes observed. It will be noted, however, that as the chromium content gradually increases, the spinel pattern becomes weaker, and the Cr_2O_3 pattern becomes correspondingly stronger. This is indicated in both Table I and II.

It was sometimes observed that the color of the scale could be a very sensitive indicator of composition, particularly since Cr_2O_3 and the spinel are so different in color. Note the visual observations in center of Table I near 14% Cr. According to this, the critical composition for spinel or Cr_2O_3 formation is between 12.8 and 13.6% Cr, whereas the x-ray data showed no Cr_2O_3 for the 13.6% Cr alloy. This last result is probably due to the fact that x-ray diffraction frequently fails to indicate a phase present in minor amount.

While in the absence of a subscale two oxide layers would signify lack of equilibrium, this is not true for the subscales formed here in the vicinity of 13% Cr. This is because, as will be demonstrated shortly, at this composition a three-phase field makes its appearance. This three-phase field widens with increasing oxygen content, and it is therefore to be expected that if much internal oxidation occurs, both spinel and Cr_2O_3 as well as the alpha solid solution can coexist.

However, for this same reason it was desired, in establishing the critical Fe-Cr alloy composition which divides Cr_2O_3 scales from the spinel scales, to avoid excessive oxidation, both external and internal. This was necessary in order to shrink the composition width over which both oxides coexist to a point on the Fe-Cr binary boundary of the isothermal phase diagram. In order to accomplish this aim the capsule experiment described above under experimental methods was used. In this manner, by the use of the decomposition pressure of iron-saturated FeO at 1000° and 1300°C, it was possible to form such a thin film of oxide (about 200 $\mu g/cm^2$) that an inconsequential amount of chromium was used up. Hence, concentration variations across the critical chromium content could be avoided, and

Table I. 1000°C scaling experiments

% Cr analysis	Oxidation treatment	Equilibration in argon	X-ray or electron diffraction results	Visual & metallographic exam.	Run No.
0.954	1 min O_2 1000°C	24 hr 1000°C	Spinel		915
1.94	1 min O_2 1000°C	24 hr 1000°C	Spinel		916
2.87	1 min O_2 1000°C	24 hr 1000°C	Spinel		917
3.91	1 min O_2 1000°C	24 hr 1000°C	Spinel	Metallography qualitatively the same	918
4.95	1 min O_2 1000°C	24 hr 1000°C	Spinel + small amt. FeO		919
5.86	1 min O_2 1000°C	24 hr 1000°C	—		920
6.83	1 min O_2 1000°C	24 hr 1000°C	Spinel		921
7.90	1 min O_2 1000°C	24 hr 1000°C	—		922
8.84	1 min O_2 1000°C	24 hr 1000°C	Spinel + some αFe_2O_3		923
9.94	5 min O_2 1000°C	64 hr 1000°C	Spinel		927
10.78	5 min O_2 1000°C	64 hr 1000°C	Spinel		928
11.02	5 min O_2 1000°C	64 hr 1000°C	Spinel		929
12.8	5 min O_2 1000°C	64 hr 1000°C	Spinel	No sign of green Cr_2O_3	930
13.6	5 min O_2 1000°C	64 hr 1000°C	Spinel	Some green color	931
14.4	5 min O_2 1000°C	64 hr 1000°C	Cr_2O_3 + spinel	More green color	932
16.4	5 min O_2 1000°C	64 hr 1000°C	Strong Cr_2O_3 weak spinel		933
18.7	5 min O_2 1000°C	64 hr 1000°C	Strong Cr_2O_3 v. weak spinel		934
20	1½ hr O_2 1000°C	64 hr 1000°C	Cr_2O_3		853
30	1½ hr O_2 1000°C	64 hr 1000°C	Cr_2O_3		854
40	1½ hr O_2 1000°C	64 hr 1000°C	Cr_2O_3		855
48.3	1½ hr O_2 1000°C	64 hr 1000°C	Cr_2O_3		856
59.5	1½ hr O_2 1000°C	64 hr 1000°C	Cr_2O_3		857
68.0	1½ hr O_2 1000°C	64 hr 1000°C	Cr_2O_3		858
			Results of SiO_2 Capsule Experiments		
10.78	FeO 30 min 1000°C	48 hr 1000°C	Spinel		1018
11.02	FeO 30 min 1000°C	48 hr 1000°C	Spinel		
12.8	FeO 30 min 1000°C	48 hr 1000°C	Spinel		
13.6	FeO 30 min 1000°C	48 hr 1000°C	Cr_2O_3		

Table II. 1300°C scaling experiments

% Cr analysis	Oxidation treatment	Equilibration in argon	X-ray or electron diffraction results	Visual & metallographic exam.	Run No.
0.954	2 min O_2 800°C	24 hr 1300°C	Spinel	Metallographic results were essentially the same for all these alloys. Some Cr_2O_3 present.	948
3.91	2 min O_2 800°C	24 hr 1300°C	Spinel		951
4.95	1 min O_2 1000°C	24 hr 1300°C	Spinel		943
5.86	1 min O_2 1000°C	24 hr 1300°C	—		944
6.83	1 min O_2 1000°C	24 hr 1300°C	—		945
7.90	1 min O_2 1000°C	24 hr 1300°C	—		946
8.84	1 min O_2 1000°C	24 hr 1300°C	Spinel		947
9.94	5 min O_2 1000°C	24 hr 1300°C	—		938
10.78	5 min O_2 1000°C	24 hr 1300°C	Mostly spinel, some Cr_2O_3 SS*		939
11.02	5 min O_2 1000°C	24 hr 1300°C	—	Visual examination showed mostly spinel	940
11.02	1 min O_2 1000°C	88 hr 1300°C	Mostly spinel, some Cr_2O_3		969
12.8	5 min O_2 1000°C	24 hr 1300°C	Spinel + Cr_2O_3		941
12.8	5 min O_2 1000°C	24 hr 1300°C	Strong spinel, weak Cr_2O_3		957
12.8	1 min O_2 1000°C	88 hr 1300°C	—	Visual observation showed mostly spinel	970
12.8	5 min O_2 800°C	67 hr 1300°C	Spinel	Very thin film	995
13.6	5 min O_2 1000°C	64 hr 1300°C	Spinel + Cr_2O_3	Metallography showed nearly 100% Cr_2O_3	955
13.6	5 min O_2 1000°C	24 hr 1300°C	Stronger Cr_2O_3, weaker spinel	Metallography showed nearly 100% Cr_2O_3	958
14.4	1 min O_2 1000°C	88 hr 1300°C	Weak spinel, strong Cr_2O_3	Metallography showed nearly 100% Cr_2O_3	972
15.7	5 min O_2 1000°C	24 hr 1300°C	Weak spinel, strong Cr_2O_3	Metallography showed nearly 100% Cr_2O_3	960
16.4	5 min O_2 1000°C	24 hr 1300°C	Weak spinel, strong Cr_2O_3	Metallography showed nearly 100% Cr_2O_3	961
20	1½ hr O_2 1000°C	23 hr 1300°C	—	Cr_2O_3 only	896
30	1½ hr O_2 1000°C	24 hr 1300°C	Cr_2O_3		877
48.3	1½ hr O_2 1000°C	24 hr 1300°C	Cr_2O_3		879
68	1½ hr O_2 1000°C	24 hr 1300°C	Cr_2O_3		881
			Results of SiO_2 Capsule Experiments		
10.78	FeO, 30 min 1000°C	20 hr 1300°C	Spinel		1016
11.02	FeO, 30 min 1000°C	20 hr 1300°C	Spinel		
12.8	FeO, 30 min 1000°C	20 hr 1300°C	Spinel		
13.6	FeO, 30 min 1000°C	20 hr 1300°C	Cr_2O_3		

* Cr_2O_3-Fe_2O_3 solid solution.

single equilibrium scales could be observed by electron diffraction as recorded in the last part of Tables I and II.

X-ray and electron diffraction observations on "equilibrated" oxide films may be summarized by stating that the transition between the spinel at low chromium content and Cr_2O_3 at high chromium contents lies at about 13% Cr ± 0.5% Cr.

Metallography

Besides the primary tool of scale identification by x-ray or electron diffraction and the occasional assistance provided by visual color observations, metallography was found to be only second in importance to x-ray diffraction. It was found possible to make a sharp division more readily between compositions which form Cr_2O_3 and those which form spinel by this technique than by use of x-rays. The pronounced separation between these two classes of alloys was made possible by the fact that alloys which form the spinel show very prominent internal oxidation, while the alloys richer in chromium, which oxidize to Cr_2O_3, do not. This is made clear in the following photomicrographs (Fig. 1-8).

The oxidized strips were given an evaporated silver coating and after a flash of copper were nickel plated to prevent washing out of the oxide layer during metallographic preparation. Four different compositions were chosen to show characteristic scales for both spinel-type and Cr_2O_3-type oxidation. Two compositions near 5 and 10% Cr in the spinel region, one near the critical 13% Cr composition and one well into the Cr_2O_3 region are shown. Figures 1 and 2 show a layer of alpha iron next to the nickel plate. The black layer between the iron layer and the beginning of the internal oxidation is spinel. The reason for the presence of an iron layer appears to be as follows: Because the chromium content is

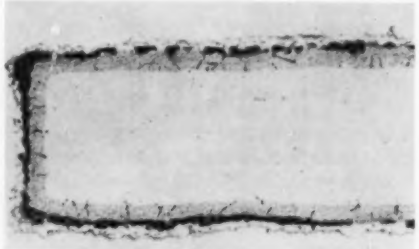

Fig. 1. 4.95% Cr oxidized 1½ hr, 1000°C; equilibrated 64 hr argon, 1000°C. Note layer of internal spinel. Magnification 100X before reduction for publication.

Fig. 2. 9.94% Cr oxidized 1½ hr, 1000°C; equilibrated 64 hr argon, 1000°C. Note layer of internal spinel. Magnification 100X before reduction for publication.

fairly low in these two alloys, some iron oxide, perhaps both Fe_2O_3 and Fe_3O_4, are formed during the oxidation treatment in pure oxygen gas. These oxides form at the surface, while the more stable spinel forms next to the metal. During the subsequent argon "equilibration" treatment the iron oxides decompose to pure iron because their dissociation pressures are quite high and, hence, the kinetics tend to be fast. However, the spinel with its very low dissociation pressure and sluggish decomposition kinetics remains after heating in argon. It is interesting to note that Fig. 3 shows both the internal oxide and areas where only the surface scale of Cr_2O_3 is present; hence this sample represents a transition structure. Since Cr_2O_3 shows a brilliant green under polarized light, while the spinel appears red to yellow depending on thickness, it was easy to ascertain that the surface scale was essentially pure Cr_2O_3 while the internal oxide was mostly all spinel. Some samples showed very small particles of Cr_2O_3 as an internal oxide which occurred with the more massive and prominent spinel. The existence of spinel above 13% Cr or of Cr_2O_3 below this concentration was always insignificant in amount compared with the major oxide present.

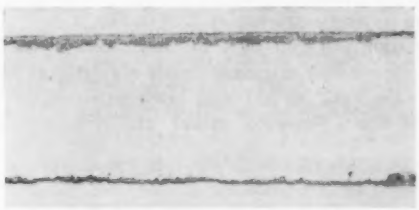

Fig. 3. 12.8% Cr oxidized 5 min, 1000°C; equilibrated 65 hr argon, 1000°C. Note transition scale: partly internal oxide, partly surface oxide. Magnification 100X before reduction for publication.

Fig. 4. 20% Cr oxidized 1½ hr, 1000°C; equilibrated 64 hr argon, 1000°C. All surface oxide. Internal oxide inclusions were present in sheet prior to oxidation. Magnification 500X before reduction for publication.

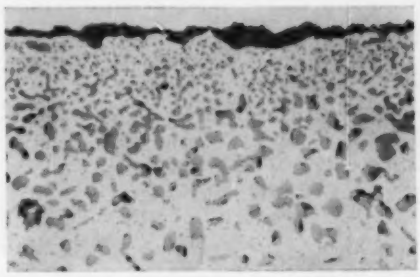

Fig. 5. 4.95% Cr oxidized 1 min, 1000°C; equilibrated 24 hr argon, 1300°C. Exaggerated internal oxidation apparently caused by some air leakage at 1300°C. Large particles are spinel. Magnification 500X before reduction for publication.

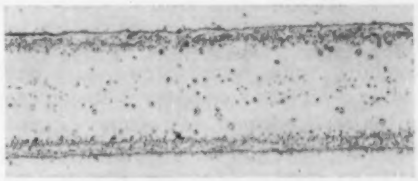

Fig. 6. 10.78% Cr oxidized 5 min, 1000°C; equilibrated 24 hr argon, 1300°C. Prominent internal oxidation. Oxide phase is spinel. Magnification 100X before reduction for publication.

Fig. 7. 13.6% Cr oxidized 5 min 1000°C; equilibrated 24 hr argon, 1300°C. Note absence of internal oxidation. Magnification 100X before reduction for publication.

Therefore, it caused no confusion in interpretation, nor in allowing the choice of about 13% Cr as the critical chromium concentration. Although not shown here, there was essentially no difference in scale appearance nor in its kinetics of formation once the chromium content exceeded about 20%.

Figure 8 is of particular interest from the standpoint of oxidation mechanism. It is shown here that a 1-mil platinum wire spot-welded to a 30% Cr-Fe strip becomes covered with Cr_2O_3 during oxi-

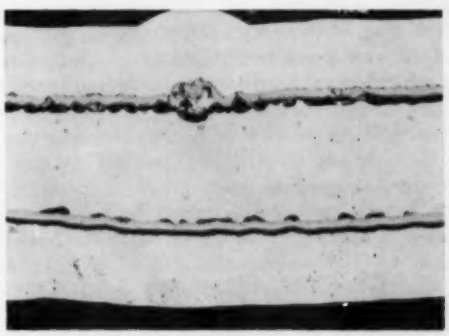

Fig. 8. 30% Cr oxidized 1½ hr, 1300°C; equilibrated 22½ hr argon, 1300°C. Note oxide covering platinum marker. Magnification 100X before reduction for publication.

Table III. Per cent Fe_2O_3 found in Cr_2O_3 scales

Alloy	Oxidation	Equilibration	% Fe_2O_3 in scale
1st sample 20% Cr-Fe	5 min 1000°C—O_2	1000°C—45 hr argon	2.7
			2.3 (check analysis)
	5 min 1000°C—O_2	1300°C—40 hr argon	0.32
		1300°C—40 hr argon	0.7 (check analysis)
2nd sample	5 min 1000°C—O_2	1000°C—64 hr argon	2.57
	5 min 1000°C—O_2	1300°C—16 hr argon	0.46

dation at 1300°C. It will be noted that many (Kirkendall) voids were formed just below the oxide layer, suggesting one-way diffusion of chromium to the scale without any countercurrent diffusion into the alloy. This observation corroborates the platinum marker behavior. Identical behavior was observed at 1000°C except that no voids just below the scale were observed. In addition, the same behavior was noted at both temperatures for a 20% Cr-Fe alloy. Since no oxide at all was formed underneath the wires, the tentative conclusion is that Cr_2O_3 on binary Fe-Cr alloys forms by cation (Cr^{+3}) diffusion, and that no appreciable diffusion of oxygen anions occurs from the gas phase. This mechanism is also suggested by the nature of the defect structure of Cr_2O_3 (10, 11).

Composition of the Two Equilibrium Scales

It has been shown above that from x-ray and metallographic evidence only two kinds of scale can be in equilibrium with binary Fe-Cr alloys: iron chromite or spinel below about 13% Cr, and Cr_2O_3 above this composition. So far, however, no evidence has been presented on the composition of these scales. To check the amount of Fe_2O_3 dissolved in Cr_2O_3, the following experiment was carried out. Two different samples of 20% Cr-Fe sheet were given a thin scale of Cr_2O_3 by a 5-min oxidation treatment in pure oxygen at 1000°C. The oxide film thus formed was equilibrated in argon at 1000° and 1300°C with the results indicated in Table III.

An alloy well over 13% Cr was chosen deliberately so that, in forming some Cr_2O_3 on the surface, the alloy would not be robbed of chromium to the point where spinel would make its appearance. However, on the basis of experience obtained in these experiments, it seems safe to assume that the nominal 20% Cr was not altered significantly by the very short oxidation treatments given this alloy. The reason for the lack of agreement between the check analyses at 1300°C must lie in the analytical technique since it was the same sample of scale. However, the main point is that if 0.5% Fe_2O_3 is taken as the average for the solubility of Fe_2O_3 in Cr_2O_3 on a 20% Cr alloy scale at 1300°C then there is an increase by a factor of five in Fe_2O_3 content by lowering the temperature to 1000°C.

The lattice parameters of the spinel phase from pure Fe_3O_4 to $FeCr_2O_4$ has been studied by Yearian, Kartwright, and Langenheim (9) as mentioned previously. While lattice parameters in this system cannot be used alone as an indication of composition, it can be used in conjunction with auxiliary information. For example, if the composition of the spinel is between approximately $Fe_{1.7}Cr_{1.3}O_4$ and $FeCr_2O_4$, one then can make use of the data of Yearian, *et al.* (9) to find the spinel composition. Fortunately, it developed that a key spinel composition fell within this range. Therefore, it was possible by suitable oxide phase equilibrations to determine all of the most important phase boundaries in the isothermal section. Before proceeding with the spinel equilibria and spinel compositions, it will be helpful to show the isothermal section of the Fe-Cr-O system at 1300° or 1000°C (Fig. 9). All of the evidence (except the maximum Fe_2O_3 solubility in Cr_2O_3) points to essentially no shift in phase boundaries between these two temperatures. At least any shift, if it occurs, seems to be less than 1% in composition. Starting at the top of the diagram, the first horizontal line joining Fe_2O_3 and Cr_2O_3 represents the continuous series of solid solutions formed by these two oxides. Just below it is the horizontal join between Fe_3O_4 and $FeCr_2O_4$; the latter composition is denoted at point S_3 in Fig. 9. The Fe_3O_4-$FeCr_2O_4$ join has a finite width according to the accepted Fe-O phase diagram and according to Yearian, *et al* (9). These authors find that $FeCr_2O_4$ contains a maximum of 0.002 cation vacancies per mole or about 2.9% vacancies, corresponding to somewhat less than 2 a/o maximum excess oxygen. Fe_3O_4 at 1300°C appears to have a homogeneity range of approximately 0.6 a/o oxygen (13). This indicates that the Fe_3O_4-$FeCr_2O_4$ join is actually a narrow band of something like 1 a/o oxygen average width. This width is indicated by the extra heavy line in Fig. 9.

The diagram can best be described by referring to the three, three-phase fields starting at the left with γ Fe, FeO, spinel and then proceeding to the right to the α Fe, γ Fe, spinel, and finally to spinel,

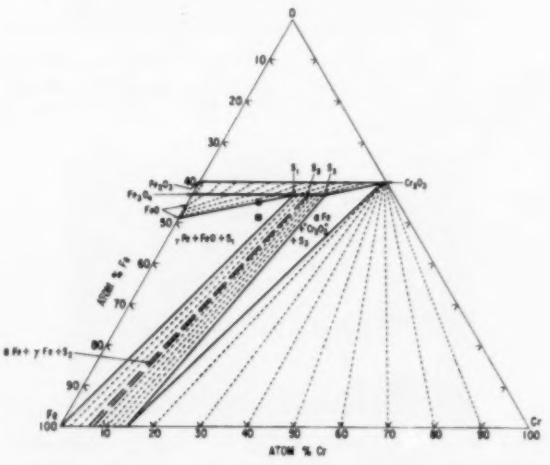

Fig. 9. Isothermal phase diagram at 1300°C for Fe-Cr-O system.

α Fe or (13 wt % Cr-Fe), "Cr_2O_3". The quotation marks around Cr_2O_3 refer to the fact that this oxide contains some Fe_2O_3 in solution. It has already been demonstrated that there are two kinds of two-phase equilibria involving the metal phase: Fe, spinel; and Fe, "Cr_2O_3." It will, of course, be understood that the spinel is of different composition in each of the three-phase fields mentioned above, and that its composition as a scale is a function of the alloy composition.

Spinel-FeO Equilibria and the Adjoining Spinel-FeO-Fe Equilibrium

The spinel composition S_1 corresponds to approximately $Fe_{1.5}Cr_{1.5}O_4$ or 21.4 a/o Cr as against 28.6 a/o Cr for $FeCr_2O_4(S_2)$. The location of point S_1 was determined by heating together FeO (high iron) and $FeCr_2O_4$ at 1300°C. Samples were prepared by mixing −200 mesh FeO powder prepared by H_2/H_2O treatment of Fe_2O_3, and $FeCr_2O_4$ prepared by synthesis from FeO and Cr_2O_3. The starting composition was 50% by weight FeO and 50% by weight $FeCr_2O_4$. In one experiment the 2-g pressed compact was heated to 1300°C in argon for 20 hr with some FeO present to supply a small oxygen pressure. Metallographic examination and x-ray diffraction results showed a mixture of FeO and spinel of lattice parameter 8.398Å. The original lattice parameter of the $FeCr_2O_4$ used had a lattice parameter of 8.377Å which agrees with the value given by Yearian, *et al.* (9) for stoichiometric spinel. Yearian's curve shows that, if the composition is near $FeCr_2O_4$, a lattice parameter of 8.398Å corresponds to $Fe_{1.5}Cr_{1.5}O_4$ or 21.4 a/o Cr as indicated above. Chemical analysis of this oxide mixture yielded 49.5% total iron, 0% free iron, and 23.2% Cr. This analysis corresponds to 29.1 a/o Fe and 14.7 a/o Cr. If this composition is plotted on the isothermal section, it falls on the phase boundary between FeO and point S_1, as it should, at the spot marked with a circled X. Hence, the lattice parameter-located point S_1 agrees with the chemical analysis of the oxide mixture.

Two additional 50-50 wt % mixtures of FeO-$FeCr_2O_4$ were made at 1300°C but sintered in argon without using FeO to supply some oxygen. In these cases some decomposition of the FeO allowed the formation of free iron, resulting in one instance in the following analysis: free iron, 14.6%; total iron 51.6%; chromium, 24.7%. Plotting this point in terms of atom per cent results in the point in the three-phase field marked with an x inside a square. The lattice parameter (8.397Å) of spinel phase in all these three-phase compacts was within the experimental error the same as in the two-phase mixture.

Figure 10 shows the microstructure of the three-phase FeO + spinel + Fe specimen. The bright spots are iron and the lighter of the two oxide phases is the FeO phase. It will be noted that the dark chromite phase is completely surrounded by the FeO, and that it has many flat sides and sharp corners evidently indicating crystallographic growth from a liquid. Therefore, it appears that this composition touches the solidus surface at 1300°C. Not enough liquid was formed to allow deformation of the pressed compacts; there was no slumping or rounding off of sharp edges.

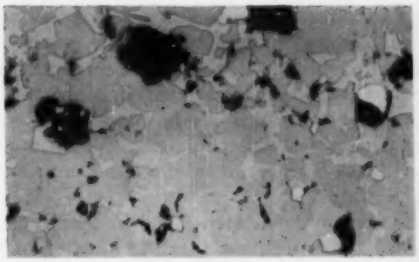

Fig. 10. αFe(γ at temperature), FeO, and spinel, demonstrating three-phase equilibrium. As polished. Black areas are voids. Magnification 250X before reduction for publication.

The FeO-$FeCr_2O_4$ experiments just cited seem to leave no doubt that the three-phase region of FeO, spinel, Fe exists as shown with the spinel composition as given above.[1] Furthermore, there appears to be no doubt that FeO of variable composition is in equilibrium with spinel of variable composition, as indicated qualitatively by the dotted tie lines. It must be emphasized, however, that these tie lines are purely qualitative, and are shown for purposes of illustration only; the precise location of these lines has *not* been determined.

Spinel-Rhombohedral Solid Solution Equilibria

The existence of this equilibria was first demonstrated by Richards and White (3), and was observed here by heating an equimolar mixture of Fe_2O_3 and Cr_2O_3 at 1800°C for 1 hr in a gas kiln. X-ray diffraction of the resulting body showed a mixture of iron chromite (spinel) and rhombohedral solution of approximately 50% Cr_2O_3 by weight. It was not possible to estimate the composition of the spinel phase from the x-ray pattern.

Figure 11 shows the microstructure of the spinel and rhombohedral solid solution compact. The black areas are voids (as in Fig. 10). The light phase which has formed on the boundary of the grains is the rhombohedral solid solution, and the darker of the two oxides is the spinel or chromite phase. Evidently at 1800°C the structure was principally spinel, but

[1] *Note added after MS preparation:* Birchenall (12) has evidence that in very dilute Fe-Cr alloys containing about 0.2% Cr, a FeO layer is formed *below* the spinel layer, e.g., next to the alloy. This evidently indicates a small amount of Cr solubility in FeO, and makes necessary a narrow two-phase region of gamma Fe solid solution—$FeO_{(Cr)}$ along the inside of the Fe-O side of the isothermal phase diagram (Fig. 9).

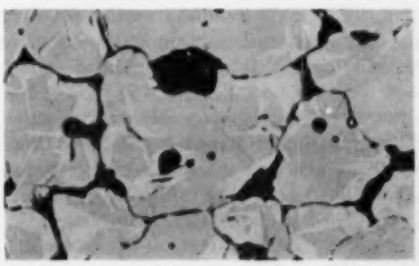

Fig. 11. Spinel (dark) plus Cr_2O_3-Fe_2O_3 solid solution (light). Black areas are voids. As polished. Magnification 500X before reduction for publication.

on cooling to lower temperatures the spinel becomes more susceptible to oxidation to the rhombohedral solid solution. Nucleation of the rhombohedral solution evidently occurred at the edges of the spinel grains where there was ready access to air, and as cooling progressed, the rhombohedral solid solution fingered into the interior of the cubic iron chromite (spinel) grains.

It has already been mentioned in connection with the spinel-FeO equilibria that the location of the tie lines were not determined but are only shown approximately for purposes of illustration. The same statement must be made about the spinel-rhombohedral solid solution equilibria. The tie lines could be established if it were possible to analyze either of these two equilibrium oxide systems for chromium, and both bivalent and trivalent iron. However, no current technique seems to be available for dissolving such oxide mixtures without oxidizing the Fe^{+2} to Fe^{+3}. In principle, probably it would be possible to obtain these tie lines merely from a knowledge of the chromium and total iron content together with lattice parameter measurements. This procedure, however, would have at least two drawbacks: (*a*) because of the lattice parameter of the spinel phase is not a single-valued function of composition, some trial and error would be involved, and (*b*) in some of the oxide mixtures the x-ray diffraction patterns may not be of sufficiently good quality to obtain the precision needed.

α Fe-*γ* Fe-*Spinel Equilibrium*

Spinel composition S_2 is the oxide in equilibrium with both ferrite and austenite as demanded by the Fe-Cr binary phase diagram.

In Fe-Cr binary alloys at 1300°C the alpha plus gamma region extends from about 6% Cr to 7% Cr as judged from the curve shown by Hansen's (13) recent review. Hence, there must be a three-phase triangle based on approximately 6% Cr and 7% Cr with the apex lying at some point S_2 on the spinel solid solution. An attempt was made to obtain a lattice parameter from the spinel "equilibrated" with an alloy lying near the critical chromium composition, but the grain size of the oxide was too fine to exhibit a satisfactory diffraction pattern. Hence, point S_2 in Fig. 9 is shown as lying approximately midway between points S_1 and S_3.

Equilibrium Oxygen Pressure as a Function of Composition

Figure 12 shows a pressure-composition diagram based mainly on data available in the literature, but to some extent on information obtained in this investigation. These data are marked with filled circles.

The pressure level of the α Fe-spinel-rhombohedral oxide equilibrium where $\log Po_2 = -13$ was calculated from the equation given by Richardson, Jeffes, and Withers (14): $2FeCr_2O_4 = 2Fe + O_2 + 2Cr_2O_3$ $\Delta F = +131{,}600 - 24.2T$ and from the relation $\Delta F = -RT \ln K$. Although Richardson, *et al.*, were apparently not aware of it, this reaction should be written in some manner to indicate that it is not pure iron here, but a solid solution of 13% Cr in Fe.

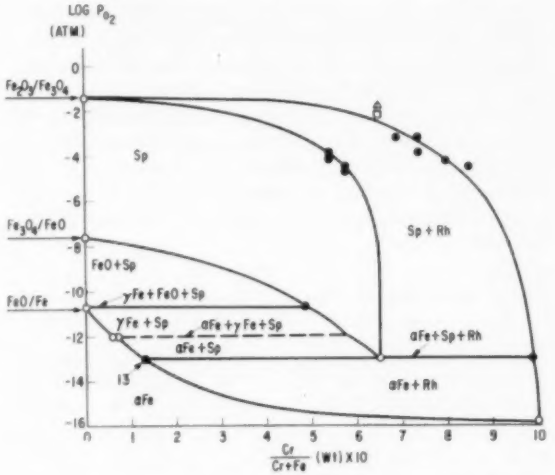

Fig. 12. Oxygen pressure-composition plot for 1300°C. Sp, spinel (based on $FeCr_2O_4$); Rh, rhombohedral (Fe_2O_3-Cr_2O_3) solid solution; αFe, pure bcc Fe or bcc Fe-Cr solid solution; ●, this investigation; O, various sources, △, Schmahl; □, calculated from Richardson, et al.

This equilibrium is graphically shown as the lowest reaction horizontal in Fig 12. The left-hand terminus is the 13% Cr-Fe composition as explained above, and at the right-hand end is shown the 0.5% Fe_2O_3 in solution in Cr_2O_3.

It should be mentioned that the composition axis of this figure is the fractional weight chromium X10, referred to the metallic constituents only.

The α Fe, γ Fe, spinel equilibrium pressure has not been determined, but its left-hand terminus is at approximately 6-7% Cr at 1300°C as given by the binary phase diagram.

The top reaction horizontal corresponding to γ Fe, FeO, spinel equilibrium has a pressure level determined by the established Fe/FeO equilibrium pressure, and its right-hand terminus is at a value of 48.5% Cr or a Cr/Cr + Fe × 10 value of 4.85.

In the spinel + rhombohedral solution two-phase region in the top of the drawing, several experimental points are shown which were obtained by controlled pressure oxidation of $FeCr_2O_4$ (see Table IV). Small pellets of $FeCr_2O_4$ powder were heated to 1300°C for various periods of time using oxygen pressures varying from 15 μ to 500 μ, obtained by a variable vacuum leak.

The datum point (open square) near the curve describing stability for the rhombohedral solution

Table IV. Controlled oxidation of $FeCr_2O_4$ at 1300°C

O_2 pressure, microns	Log Po_2, atm	Oxidation time, hr	Lattice parameter (a_o) and Cr wt ratio a_o	$\frac{Cr}{Cr+Fe}$	Rhombohedral oxide Cr/Cr + Fe wt ratio based on high angle line measurements
15	—4.70	24	8.3851 ±.0005	0.575	Too diffuse
25	—4.48	8	8.3848 ±.001	0.575	0.85-0.90
50	—4.18	8	8.3909 ±.002	0.54	0.80-0.83
100	—3.88	8	8.389 ±.002	0.54	0.74
500	—3.18	24	Too weak		0.69
500	—3.18	3	No pattern		0.74

was calculated from the Richardson, *et al.* equation plus the following two:

$$2Fe_2O_3 = 4Fe + 3\ O_2 \text{ and } 2Fe_2O_3 \cdot 4Cr_2O_3 =$$

$$2Fe_2O_3 + 4Cr_2O_3$$

The free energy for this last equation was calculated on the basis of an ideal solution. In view of the fact that there is a complete series of solid solutions between Cr_2O_3 and Fe_2O_3, the assumption of ideality might be approximately correct. In any case, the free energy change involved in the formation of the $Fe_2O_3 \cdot 2Cr_2O_3$ solid solution must be small compared to the other processes involved.

By summing up the above equations of known ΔF, one arrives at the change in free energy for the following equation

$$2Fe_2O_3 \cdot 4Cr_2O_3 = 4FeO \cdot Cr_2O_3 + O_2$$

$$\Delta F = +\ 124{,}250 - 68.7T$$

Solving for ΔF for 1300°C (1573°K) and substituting in $\Delta F = -RT \ln K = -RT \ln Po_2$, one finds $Po_2 = 4.48$ mm and log Po_2 in atmospheres is −2.23. This oxygen pressure is that required to oxidize completely the spinel of composition $FeO \cdot Cr_2O_3$ to the rhombohedral oxide of identical Cr/Fe ratio at 1300°C. In addition, Schmahl (15) has given an oxygen pressure for the dissociation of $Fe_2O_3 \cdot 2Cr_2O_3$ at 1323°C as 1.05×10^{-2} atm or log $Po_2 = -1.79$. This is plotted as an open triangle just above the open square point. Because his data refers to 1323°C, this point should be somewhat too high, as it is. Hence, it appears to be essentially in agreement with the Richardson, *et al.* point as calculated above.

It should be emphasized that the data plotted in this region are not of high accuracy, and in particular, the composition estimates of the rhombohedral solution from x-ray data are of poor accuracy, mainly because of poor x-ray photograms. However, the fact that these points cluster reasonably well to a smooth curve passing close to the other data (open points) offers some assurance that the experimental points may not be too far off.

The course of the curves bounding the two phase spinel + rhombohedral region provides the information necessary for establishing the tie lines between these two phases on the isothermal phase diagram, Fig. 9. However, in view of the questionable accuracy of these curves, it seems hardly worthwhile to attempt to draw in "accurate" tie lines. Anyone interested can do this readily from the information given.

Rate of Internal Oxidation in 5% Cr-Fe and in 10% Cr-Fe Alloys

Some measurements were made in the above two alloys on thick samples (about 0.2 in. thick) at 1000° and 1300°C. Fairly thick samples were chosen so that the diffusion distance would be small compared to the sample thickness. The samples were rectangular in shape and were encapsulated in SiO_2 with iron-saturated FeO as an oxygen source. The depth of penetration of the spinel subscale is shown in Table V.

Table V. Rate of penetration of spinel subscale

1000°C	Hours	Penetration, cm
5% Cr	20	0.0034
	40	0.0045
10% Cr	20	0.0031
	40	0.0048
1300°C		
5% Cr	1	0.0058
	64	0.0250
10% Cr	1	0.0071
	2	0.0071
	4	0.0150
	8	0.0155
	64	0.0451

Results at 1000°C are not very meaningful since the accuracy of measurement was poor. However, in the case of the 10% Cr alloy at 1300°C, it is possible to demonstrate that the data plotted as cm vs. $t^{1/2}$ yield a straight line which passes through the origin. If time is plotted in seconds, the slope is found to be about 7×10^{-8} cm²/sec. Evidently the rate of progress of the subscale layer is diffusion controlled, as would be anticipated. However, there is insufficient knowledge about concentration gradients in the layer to be able to calculate an oxygen diffusion rate.

Discussion

It seems clear that the disparity between various investigators' work in the results of Fe-Cr alloy scaling experiments lies in the nonequilibrium nature of such experiments. Evidently there was not always a full realization that very significant changes in alloy composition occurred during the progress of an oxidation run. These alloy composition changes are reflected in changes in the nature of the scale formed.

Another complication is caused by a tendency for the scale to separate from the alloy. When this can occur, the tendency for nonequilibrium scales is enhanced since there is poor contact between metal and scale. This means that a scale can exist in a higher state of oxidation than would be possible in contact with the alloy.

Thermodynamically, the scales of lowest oxygen pressure lie closest to the metal, and the scale nearest the gas phase must be of highest dissociation pressure. In a nonequilibrium experiment, if Cr_2O_3, "Fe Cr_2O_4," and Fe_2O_3 are all found in the scale, they must be present in the order listed from metal to gas phase. This order can be seen in Fig. 12. It can be seen also from Fig. 12 that during air oxidation one should not observe spinel as the outermost layer of scale for any Fe-Cr alloy because the spinel is only stable at very low oxygen partial pressures.

The actual scales observed will depend in large measure on the severity of the oxidation, which for any chromium level might be measured by the per cent chromium converted to various oxides. Yearian, *et al.* (1) recognized the so-called A and B types of scale representing a difference in the amount of oxidation. Under light oxidation, a 20% Cr alloy will only show the equilibrium Cr_2O_3 scale. With

more drastic conditions; higher temperature, longer time or possibly higher oxygen pressure, the chromium present is not adequate to prevent iron oxides from forming. In this case, one expects an outer layer of nearly pure Fe_2O_3, next a spinel layer, and finally a Cr_2O_3-Fe_2O_3 rhombohedral solid solution of variable composition.

The occurrence of different layers of variable composition will be expected, depending on the parameters just mentioned, plus specimen geometry. Therefore, there is no fundamental significance in reporting a specific series of layers in a scale unless all the variables are very closely specified, and unless the precise thickness and composition of each layer are well documented. This has not often been done in the past. What is needed at present in this and in other systems is a better characterization of the individual layers, including their defect structure and, of particular importance, their mode and rate of growth. This would probably entail controlling oxygen pressure so that the growth characteristics of a single layer could be studied.

From a practical point of view, the appearance of Fe_2O_3, or of iron chromite, during the oxidation of Fe-Cr base alloys is evidence of failure. Either the chromium content was too low, the temperature too high, or the time of exposure too long. There is good evidence that various small additions to the Fe-Cr type alloy can improve their oxidation resistance appreciably, but this will be reported elsewhere.

Finally, one must be cautious about translating results of oxidation behavior in pure oxygen to the behavior in air. The nitrogen content of air appears to play a significant role in the structures observed during the oxidation of Fe-Cr alloys. Chromium nitrides have been observed in Fe-Cr samples heated in air. This effect apparently has been little studied.

Summary and Conclusions

An isothermal section for equilibrium conditions at 1300°C in the Fe-Cr-O system has been presented. With the exception of a minor modification, this section also represents conditions at 1000°C. With the aid of this diagram, one sees that there are two types of equilibrium scale formed on Fe-Cr alloys: spinel or iron chromite below 13% Cr, and Cr_2O_3 containing a little dissolved Fe_2O_3 at higher chromium contents. With the additional information on the gamma iron-FeO equilibrium noted by Birchenall (12), this diagram agrees qualitatively with the one suggested by Woodhouse and White (2).

The oxidation mode for alloys in equilibrium with the spinel is mainly internal oxidation, at least at temperatures over 1000°C, while the oxidation mode for alloys over 13% Cr is formation of a surface oxide. This difference is of prime importance in regard to oxidation resistance. The rate of formation of the internal oxide at 1300°C is very rapid compared to the oxidation rate for surface Cr_2O_3. Since this is the case, alloys low in chromium content fail very rapidly, while the chromium-rich alloys are comparatively resistant to oxidation.

Platinum wire marker experiments seem to show that at 1000° or 1300°C the Cr_2O_3 on 20 or 30% Cr-Fe alloys forms almost entirely by cation diffusion. Oxygen diffusion from the gas phase apparently plays an insignificant role. This indicates that, to improve the oxidation rate of Fe-Cr base alloys, one should alter in some manner the rate of diffusion of Cr^{+3} in Cr_2O_3, such as by altering the nature of the defect structure of Cr_2O_3. The subject of the Cr_2O_3 defect structure cannot be expanded here, but for those interested in this subject the work of Hauffe and Block (10) and Fischer and Lorenz (11) should be mentioned.

Acknowledgments

It is a pleasure to acknowledge the general assistance of Mr. Leo Butler. The rather extensive x-ray data were obtained by Mrs. Rose DiCerbo and Mrs. Dorothy DeCarlo. Miss Eileen Alessandrini prepared many electron diffraction studies of the scales

Manuscript received July 31, 1959.

Any discussion of this paper will appear in a Discussion Section to be published in the December 1960 JOURNAL.

REFERENCES

1. H. J. Yearin, E. C. Randell, and T. A. Longo, *Corrosion*, **12**, 515t (1956).
2. D. Woodhouse and J. White, *Trans. Brit. Ceramic Soc.*, **54**, 365 (1955).
3. R. G. Richards and J. White, *ibid.*, **53**, 422 (1954).
4. R. L. Rickett and W. P. Wood, *Trans. A.S.M.*, **22** 347 (1934).
5. H. M. McCullough, M. A. Fontana, and F. H. Beck, *ibid.*, **43**, 404 (1950).
6. D. Caplan and M. Cohen, *Trans. AIME*, **194**, 1057 (1952).
7. J. Moreau, *Compt. rend.*, **236**, 85 (1953).
8. P. E. Wretblad, *Z. anorg. Chem.*, **189**, 329 (1930).
9. H. J. Yearian, J. M. Kortwright, and R. H. Langenheim, *J. Chem. Phys.*, **22**, 1196 (1954).
10. Karl Hauffe and Jochen Block, *Z. Phys. Chem.*, **198**, 232 (1951).
11. W. A. Fischer and Gert Lorenz, *Arch. Eisenhuttenw.*, **28**, 497 (1957).
12. C. E. Birchenall, Private communication.
13. M. Hansen, "Constitution of Binary Alloys," McGraw-Hill Book Co., New York (1958).
14. F. D. Richardson, J. H. E. Jeffes, and G. Withers, *J. Iron Steel Inst., London*, **166**, 213 (1950).
15. N. G. Schmahl, *Z. Elektrochem.*, **47**, 835 (1951).

A Model of the Mechanism of Electrochemical Conversion from Active to Passive States

W. A. Mueller

Physical Chemistry Division, Pulp and Paper Research Institute of Canada, Montreal, Quebec, Canada

ABSTRACT

A model is developed of the mechanism of passivation of metals by oxide films. It is based on the assumption of the formation of a passivating film caused by the reaction of OH^- ions with the metal surface. With increased potential the film-free area decreases exponentially and with a higher exponent than does the density of the anodic dissolution current. Thus in the conversion from the active to the passive state, the current density is reduced exponentially to the constant and very low value characteristic of the passive state. This mechanism of passivation is explained by equations which describe the density of the anodic dissolution current as a function of the pH and the potential difference between the metal and the electrolyte. Good agreement with the theory is shown by published data for iron, nickel, chromium, gold, and silver. A simple method is given to derive all the constants required for the mathematical formulation of the anodic dissolution current from experimental data. Flade's equation relating to the boundary potential between the active and the passive state of iron is discussed. The principles and formulas, although derived specifically for formation of oxide films, are considered also to be applicable to the electrochemical passivation by other films.

The mechanism of the reactions which cause the formation of a passivating film on metals is of basic interest in studying the nature of passivity. These reactions can be analyzed by means of partial polarization curves, if exact polarization curves in the potential range of the conversion from active to passive states are available. A detailed description of the analysis of polarization curves is being prepared for publication in another paper (1). This paper describes a model which allows an analysis of the density of the anodic dissolution current, particularly during the conversion from active to passive states. Equations are derived for the anodic dissolution current in the active state, for the conversion to the passive state and for the Flade potential (2) and these are used to interpret a series of pertinent empirical data.

The passivity of metals caused by the formation of an oxide film is the most important case of passivity; this is the case for which equations have been derived primarily. However, calculations for other types of passivating films of electrochemical origin may be made by using the same equations. Of primary importance is the inclusion of all known facts concerning the active and passive states.[1] These include the electrochemical properties of the anodic dissolution current from the active state through the Flade potential to the passive state.

Conditions for measuring accurate polarization curves in the potential range of the conversion from active to passive states have been derived before (3,4). Potentiostatic control prevents the state of instability expressed as a "jump of the potential." Accurate polarization curves measured potentiostatically in the potential range of the conversion from the active to the passive state were published previously for iron in a solution of 100 g/l NaOH and 35 g/l Na_2S (4). These curves, which were subsequently corroborated by Kesler (5), and Uusitalo (6), show an exponential increase of the current density with increasing potential in the active state (Fig. 1 and 3a). After reaching the maximum, the current density declines exponentially, thus demonstrating the conversion from active to passive states.

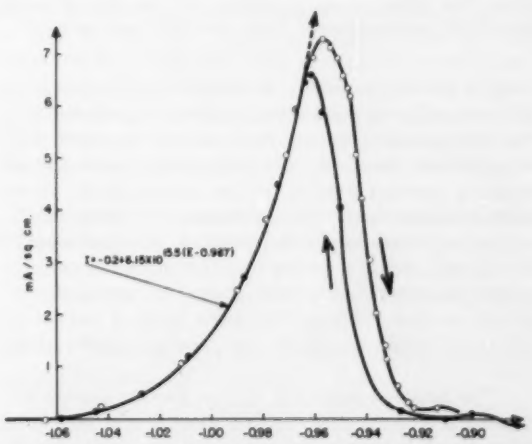

Fig. 1. Density of the anodic dissolution current of iron in a solution of 100 g/l NaOH plus 35 g/l Na_2S measured with reference to a saturated calomel cell. ○ Measured with increasing potential; ● measured with decreasing potential.

[1] For a comprehensive survey of the literature on passivity the reader is referred to the symposium in Heiligenberg, 1957 [*Z. Elektrochem.*, **61**, No. 6/7 (1958)].

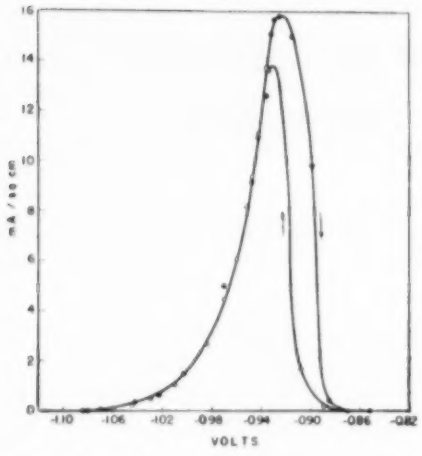

Fig. 2. Density of the anodic dissolution current of iron in a solution of 100 g/l NaOH + 35 g/l Na_2S + 30 g/l pyrogallol with reference to a saturated calomel cell. • Measured with increasing potential; ○ measured with decreasing potential.

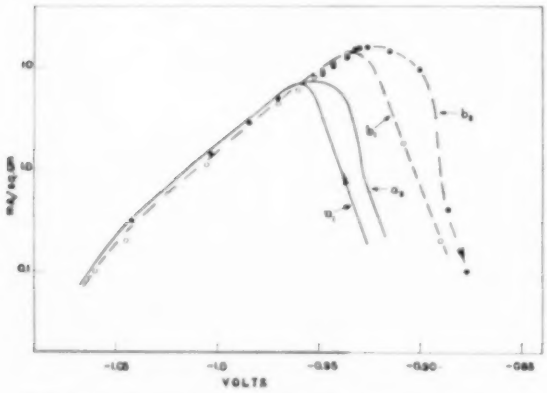

Fig. 3. Semilogarithmic plotting of the curves of Fig. 1a and b showing the exponential relations of both the increasing and decreasing current densities. The extended curves a_1 and a_2 represent the measurement without the addition of pyrogallol. The dotted curves b_1 and b_2 and the plotted points refer to the measurement in liquor containing pyrogallol.

An interesting change is noticed after adding 30 g/l pyrogallol to the above solution (Fig. 2 and 3b). The polarization curves recorded are identical with the previous curves in the range of exponentially increasing current density in the active state. However, the maximum current density is higher and is reached at a less negative potential. The decrease of the current density owing to passivation occurs also at less negative potentials. There are examples of several metals showing the same type of curves in different solutions given in recent publications (7-12).

The general equation of the anodic dissolution current I_a as a function of the measurable potential difference E between the metal and the electrolyte in the active state (1) is

$$I_a = I_o\, f(pH) \exp \frac{\alpha_a n_a F}{RT} (E - E_o) \qquad [1]$$

where α_a is symmetry factor of the reaction of anodic dissolution amounting to unity or less, n_a is the valency of the determining dissolution reaction, which in the simplest case, but not generally, is the valency of the metal dissolving in the active state, $\alpha_a n_a$ is over-all electrochemical transfer coefficient, I_o and E_o are a couple of interdependent values of current density and potential at $pH = 0$, and $f(pH)$ is the dependence of the Tafel relation on pH.

This equation is valid only if the rate of the reverse reaction, characterized by electrodeposition of the dissolved metal, is negligible in comparison to the rate of dissolution. In some cases, e.g., chromium in H_2SO_4, $f(pH) = 1$ (10). However, in the case of iron immersed in perchlorate and sulfate $f(pH) \neq 1$ according to Heusler (9).

Pourbaix (13) has shown that the relation between equilibrium pressure and potential of iron is independent of the pH value in the pH range from 0 to about 9. Similarly the valency of the iron ions formed is assumed to be 2 (14). There is some evidence, however, that the dissolution of iron in alkaline solutions leads to the formation of Fe_3O_4 as was found in a dilute solution of $NaNO_2$ (15). This reaction also would explain the average valency 2 2/3 found in the dissolution of iron in (NaOH + Na_2S) solutions (4). For this reason, and in agreement with Pourbaix's diagram (13), it is assumed that at pH values higher than 9, Eq. [1] is still valid; however, the exponent $\alpha_a n_a$ might be different.

The Flade potential E_F (2), which represents the boundary potential between the active and the passive states, depends on the pH value. For iron in the range of pH 0 to 4 Flade discovered a relationship which can be expressed by

$$E_F = E_{F_o} - \frac{RT}{F} 2.3(pH) \qquad [2]$$

where E_F is the Flade potential and E_{F_0} the Flade potential at $pH = 0$. Equation [2] has been verified by Franck (7).

The partial current density I_p of the anodic dissolution current in the passive state is independent of the potential difference between electrode and electrolyte in a considerable range of this potential (7-10). The iron ions formed in this potential range are trivalent. The anodic current density at high positive potentials (trans-passive range) is accompanied by the formation of FeO_2 and FeO_4^{--} (13).

Under the influence of a constant current density the conversion from the active to the passive state requires a time period which can be approximately expressed by the formula (7)

$$t_p = k/I - I_m \qquad [3]$$

where t_p is time during which the current passivates the metal, k constant, I current density, and I_m minimum current density sufficient for passivation. This relation was found to be valid also for metals other than iron; for gold for instance, in hydrochloric acid (16, 17), and for chromium in sulfuric acid (10). It is widely accepted (18, 8, 19-21) that the passivity of iron in many aqueous solutions is caused by an iron oxide film. The thickness of the film ap-

parently varies considerably between a film strong enough to be stripped from iron by dissolution of the backing metal (22, 23) on the one hand, and a film of molecular dimensions on the other (12, 24-27). In thick films, a layer of Fe_3O_4 adjacent to the iron surface is covered by one of Fe_2O_3 (19). At steady-state conditions the film thickness increases linearly with the potential (19-21). Visible deposits (28), usually of a bulky nature, are not considered typical features of the passive state as passivity is reached without these.

General Theory

Basic Concepts.—Since the formation of the passivating film is an electrochemical phenomenon, its rate on a film-free surface is an exponential function of the metal-electrolyte potential difference. This film originates from the reaction of anions, contained in the electrolyte, with the metal surface [Müller (29)]. For the present model the metal atoms of the film are assumed to maintain their original position in the metal lattice as surface atoms. The film is therefore very strongly bonded to the metal. In the case of iron, the electrostatic field which produces the passivating film is assumed to convert the iron atoms at the surface to the trivalent state. Thus a film is formed consisting of a monolayer of Fe_2O_3.

During the conversion from the active to the passive state, the film covering part of the surface reduces the rate of anodic dissolution because the rate of anodic dissolution is proportional to the ratio of film-free area to total area ("film-free" meaning free of the passivating film.) The corrosion rate of the film-free fraction is assumed to be undiminished.

The anodic current density in the passive state is usually very small and is caused by a very slow corrosion process. Since this current density does not depend on the potential, direct anodic dissolution is out of the question. The only alternative is to assume that a slow dissolution of the passivating film occurs continuously. The damage done to the film is immediately compensated by film reformation, which is basically an anodic process. For this reason, the anodic current-density in the passive state is proportional to the rate of film dissolution and is independent of the potential.

The variation of film thickness found empirically indicates film growth with increased potential from monomolecular dimension, reached initially by passivation at the Flade potential, to about 50 or 100A. In agreement with Vetter (20) and Weil (21), it is assumed that the increase of the thickness of passivating films is caused by the migration of iron and oxygen ions in opposite directions across the oxide film under the influence of the potential gradient. The film thickness increases with increasing potential until the rate of film growth is reduced by the decreasing gradient of the potential to the value of the rate of film dissolution. Hence, under equilibrium conditions, the film maintains a thickness which increases linearly with the potential.

With decreasing potential, the gradient of the potential in the film is decreased and so is the rate of film formation by migration. The unchanged rate of film dissolution causes a decrease of the film thickness until stable conditions are reached, i.e., when the rate of film formation has become equal to the rate of film dissolution.

The validity of these derivations is limited by the assumption that the rates of possible reverse reactions of the anodic dissolution, i.e., electrode position of the dissolved metal, and of the formation of a passive film, characterized by rebreaking the bonds, are negligible. As the reverse reactions are substantial under certain conditions, their effect has been derived in another paper (30).

Formation of an Fe_2O_3 Film on Iron as an Electrochemical Process

The electrochemical reaction involved in the formation of an Me_2O_n film on a film-free metal surface can be formulated

$$Me + n(OH)^- \rightleftharpoons Me_2O_n + n/2\ H_2O + ne^- \quad [4a]$$

or

$$Me + n(OH)^- \rightleftharpoons Me(OH)_n + ne^- \quad [4b]$$

This reaction supplies n electrons per reacting metal atom to the metal. The rate of this reaction depends on the OH^- concentration and the potential difference between metal and electrolyte. Equation [4b] formulates the reaction in agreement with the chemical analysis of passive films on iron by Neilsen and Rhodin (31). Oxygen-free solutions will now be considered. The effect of dissolved oxygen will be discussed later.

The rate of film formation r_f on a film-free surface follows Tafel's relation and is proportional to $(OH^-)^{n_{OH}}$. As $(OH^-)^{n_{OH}} = \exp 2.3 n_{OH}\ (pH - 14)$, r_f can be formulated

$$r_f = r_{14} \exp\left[2.3\ n_{OH}\ (pH - 14) + \frac{\alpha_p\ n_p\ F}{RT}\ (E - E_{14})\right] \quad [5]$$

where α_p is the symmetry factor, n_{OH} order of the process with respect to (OH^-), n_p valency controlling the rate of Me_2O_3 formation on the metal, r_{14} the rate of film formation on a film-free iron surface at pH = 14 and $E = E_{14}$, and E_{14} characteristic value of E at pH = 14. Equation [5] takes into consideration only the forward reaction which forms metal oxygen bonds at the interphase. If the backward reaction of rebreaking the bonds is so strong that equilibrium conditions are approached, Eq. [5] is no more strictly valid (30).

For reasons of simplicity the calculation is better referred to pH = 0. Thus Eq. [5] is converted to

$$r_f = r_o \exp\left[2.3\ n_{OH}\ (pH) + \frac{\alpha_p\ n_p\ F}{RT}\ (E - E_o)\right] \quad [6]$$

where r_o is the rate of film formation on a film-free metal surface at pH = 0 and $E = E_o$.

Equation [6] defines the rate of the film formation on a film-free metal surface. The rate of the film formation in an area partly covered by film is proportional to the ratio of the surface area of film-free metal to the total metal surface. This part of the derivation follows the Langmuir adsorption theory and is similar to that of Franck (7) and of Gerischer

(8). At steady state the rate of film formation is equal to the rate of film dissolution. Hence

$$a_c r_c = a_f r_f \qquad [7]$$

where a_c is film-covered area, a_f film-free area, and r_c rate of film dissolution of metal oxide or hydroxide from a film-covered area. r_c is assumed to be independent of the potential as the dissolution goes without exchange of charges. It may also be stressed that Eq. [7] does not describe an equilibrium between film formation and dissociation of the film into the original components. The ratio of the film-free area to the total area a_t is given by

$$a_f/a_t = 1/1 + \frac{r_f}{r_c} \qquad [8]$$

Combining Eqs. [6] and [8]

$$\frac{a_f}{a_t} = \frac{1}{1 + \frac{r_o}{r_c} \exp\left[2.3\, n_{OH}\,(pH) + \frac{\alpha_p n_p F}{RT}(E - E_o)\right]} \qquad (9)$$

Eq. [9] shows the very rapid decrease of the film-free area with increasing potential and pH values.

Anodic dissolution current in the potential range of the conversion from active to passive state.—The density of the anodic dissolution current I_o at totally film-free areas is given by Eq. [1]. Only the film-free area is assumed to contribute to the anodic current in this calculation. The partial coverage of the surface by an insoluble film reduces this current density to an amount which is proportional to the ratio of film-free area to total area. Thus Eqs. [1] and [9] may be combined to calculate the anodic current density I_{af} on a partly film-covered surface

$$I_{af} = \frac{f(pH) \exp\frac{\alpha_a n_a F}{RT}(E - E_o)}{1 + \frac{r_o}{r_c}\exp\left[2.3 n_{OH}\,(pH) + \frac{\alpha_p n_p F}{RT}(E - E_o)\right]} \qquad [10]$$

For the application of Eq. [10] the ratio r_o/r_c must be determined. In Eq. [3], t_p gives a reciprocal measure of r_o: however, since the potential changes continuously during the measurement, this must be regarded as approximate only. Accurate measurements of r_o should be made at constant potential in the passive state, e.g., at the Flade potential. There is, however, a clearcut relation between r_o/r_c and I_{po}/I_p ($I_{po} = I_p$ at pH = 0). When 50% of the surface is covered with the protective film, the current density $I_{o.5}$ becomes 50% of the value calculated for a film-free surface, and the potential becomes $E_{o.5}$. When $E = E_{o.5}$ in Eq. [10], I_o f (pH)-$2I_{o.5}$ and the denominator of Eq. [10] becomes 2. Thus

$$\frac{r_o}{r_c}\exp\left[2.3\, n_{OH}\,(pH) + \frac{\alpha_p n_p F}{RT}(E_{o.5} - E_o)\right] = 1 \qquad [11]$$

For the potential $E_{o.5}$ at pH = 0 the symbol $E_{o-o.5}$ may be used, and for the rate of film formation r_o at pH = 0 and $E_{o-o.5}$ the symbol $r_{o-o.5}$. According to Eq. [11] $r_{o-o.5}$ equals r_c when E_o equals $E_{o-o.5}$. Hence,

$$\frac{r_{o-o.5}}{r_c}\exp\left[2.3\, n_{OH}\,(pH) + \frac{\alpha_p n_p F}{RT}(E_{o.5} - E_{o-o.5})\right] = 1 \qquad [12]$$

The rate of film dissolution r_c at a completely film-covered area is proportional to I_p, the current density in the passive state, according to the given basic concept. At pH = 0, I_p becomes I_{po}, hence

$$r_{o-o.5}/r_c = I_{po}/I_p \qquad [13]$$

By substituting $r_{o-o.5}/r_c$ from Eq. [13] into Eq. [10] an equation results which contains only measurable quantities or constants as follows

$$I_{af} = \frac{I_o f(pH) \exp\frac{\alpha_a n_a F}{RT}(E - E_o)}{1 + \frac{I_{po}}{I_p}\exp\left[2.3\, n_{OH}\,(pH) + \frac{\alpha_p n_p F}{RT}(E - E_{o-o.5})\right]} \qquad [14]$$

The current density of the anodic dissolution current on a film-free surface as expressed in the numerator can be described by using any pair of related values of current density and potential to replace $I_o f(pH)$ and E_o, for instance, $2I_{o.5}$ and $E_{o.5}$. The second term of the denominator can be formulated

$$\frac{I_{po}}{I_p}\exp\left[2.3\, n_{OH}\,(pH) + \frac{\alpha_p n_p F}{RT}(E_{o.5} - E_{o-o.5})\right]\exp\frac{\alpha_p n_p F}{RT}(E - E_{o.5})$$

According to Eq. [12] and [13] this expression equals $\exp\frac{\alpha_p n_p F}{RT}(E - E_{o.5})$. Thus a simplified formula of the current density in the potential range of the conversion is derived

$$I_{af} = 2I_{o.5}\frac{\exp\frac{\alpha_a n_a F}{RT}(E - E_{o.5})}{1 + \exp\frac{\alpha_p n_p F}{RT}(E - E_{o.5})} \qquad [15]$$

The above derivation does not take into account the dissolution of the passivating film in the electrolyte which causes the flow of a small anodic current I_p at a completely covered surface. The partial current I_d which is caused by the film dissolution on a partly covered surface is proportional to the ratio film-covered area to total area. According to Eq. [9] and [11] the ratio film-free to total area amounts to

$$1/1 + \exp\frac{\alpha_p n_p F}{RT}(E - E_{o.5})$$

and the ratio film-covered to total area is put into Eq. [16] as factor of I_p

$$I_d = I_p \frac{\exp \frac{\alpha_p n_p F}{RT} (E - E_{0.5})}{1 + \exp \frac{\alpha_p n_p F}{RT} (E - E_{0.5})} \qquad [16]$$

In cases of typical passivity this partial current I_a is negligible in comparison with $I_{0.5}$. However, there are conditions under which I_d forms a substantial part of the combined current density I_c; then the calculation of I_c requires the addition of I_d to I_{at} as follows

$$I_c = \frac{2 I_{0.5} \exp \frac{\alpha_a n_a F}{RT} (E - E_{0.5}) + I_p \exp \frac{\alpha_p n_p F}{RT} (E - E_{0.5})}{1 + \exp \frac{\alpha_p n_p F}{RT} (E - E_{0.5})} \qquad [17]$$

Equation [17] covers the curve of the density of the anodic dissolution current as a function of the potential including the active and passive states. It is evident that Eq. [17] can be derived without special assumptions concerning type of metal and reacting ions and it is assumed to be valid if the assumptions about the mechanism of film formation are appropriate.

Comparison with experimental results.—From the above it is clear that the ratio $\beta = \alpha_p n_p : \alpha_a n_a$ determines the form of the curve of the anodic dissolution current. If β is unity the curve forms a polarographic wave, i.e., an S-shaped transition from current density 0 to a constant current density amounting to $2 I_{0.5} + I_p$ (Fig. 4). This is the shape of the curves found with silver (12) in (11M NH_3 + 1M $(NH_4)_2SO_4$), with gold (8) in 4.0*N* HCl, and with iron (8,9) in 1.0*N* H_2SO_4 at 25°C. However, this type of curve might also be caused by a film of salt, as this condition can cause the formation of a constant current density.

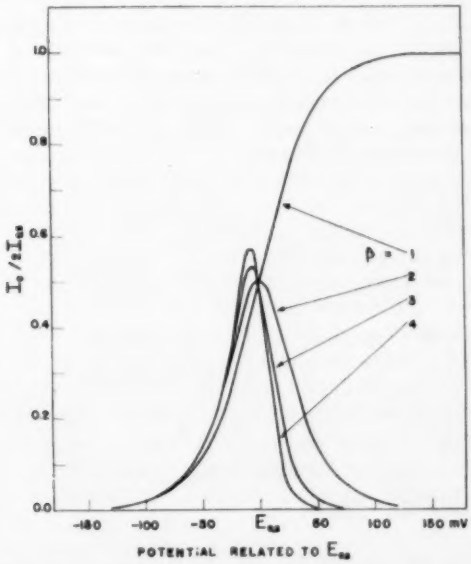

Fig. 4. Calculated curves characteristic of the density of the anodic dissolution current as a function of the potential. The ratio β of the exponent in the formula describing the anodic dissolution reaction to the exponent in the exponent in the formula of the film forming reaction control the form.

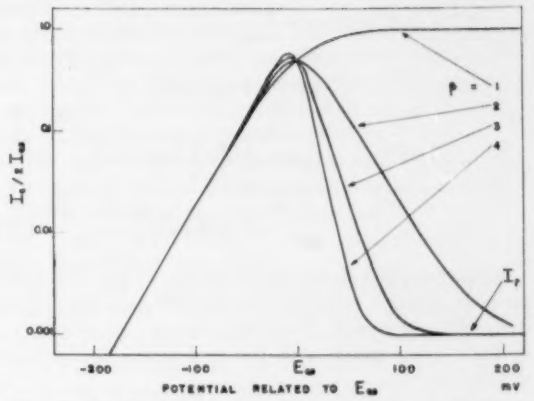

Fig. 5. Semilogarithmic plotting of the curves of Fig. 4 which shows the typical 3 ranges of nearly linear relation.

When $\beta = 2$ the curve is symmetrical, the branch covering the active state being the mirror image of the branch measured in the range of the conversion from the active to the passive state. When $\beta > 2$, the decrease of the current density in the range of the conversion from the active to the passive state becomes increasingly steeper than its increase in the active state. The curves of Fig. 1 and 2 show the typical form derived for $\beta = 3$ to 4.

In semilogarithmic plotting the calculated curve assumes a very simple form. When the second term in each numerator and denominator of Eq. [17] becomes negligible in comparison with the first term, the resulting equation in semilogarithmic plotting gives the straight line (Fig. 5)

$$\left(\frac{d \ln I_c}{dE}\right)_a = \frac{\alpha_a n_a F}{RT} \qquad [18]$$

Equation [18] is valid in the active range (subscript a). When the second term in the numerator and the first term in the denominator become negligible, another straight line is formed in semilogarithmic plotting as follows

$$\left(\frac{d \ln I_c}{dE}\right)_{a \to p} = \frac{(\alpha_a n_a - \alpha_p n_p) F}{RT} \qquad [19]$$

Equation [19] formulates the curve in the potential range of the conversion from active to passive state (subscript $a \to p$). When the first term of each nominator and denominator becomes small in comparison with the second term, I_c equals I_p.

The straight lines given by Eq. [18] and [19] cross at the coordinates $2I_{0.5}$ and $E_{0.5}$ and the second and third straight lines cross at the coordinates I_p and E_F. Thus a simple method of calculating all the characteristic constants of Eq. [17] from measured curves becomes evident. Kolotyrkin's (10) anodic current density potential curves in semilogarithmic plotting demonstrate these features. His curves obtained from chromium and nickel in H_2SO_4 consist of three straight lines representing the active state, the conversion to the passive state, and the passive state.

$E_{0.5}$ and the Flade Potential

For the current density as a function of pH a relation based on Eq. [14] and [16] can be formulated as follows

$$I_a = \frac{I_a f(pH) \exp \frac{\alpha_a n_a F}{RT} (E - E_a) + I_{p_a} \exp \left[2.3\, n_{OH} (pH) + \frac{\alpha_p n_p F}{RT} (E - E_{a-0.5}) \right]}{1 + \frac{I_{p_a}}{I_p} \exp \left[2.3\, n_{OH} (pH) + \frac{\alpha_p n_p F}{RT} (E - E_{a-0.5}) \right]} \quad [20]$$

Equation [20] shows the influence of pH and of the current density I_p in the passive state on the anodic dissolution current. The characteristic potential $E_{a.5}$ of their cross-point with the line of the active state is given by

$$E_{a.5} = E_{a-0.5} - \frac{RT}{\alpha_p n_p F} \left[2.3\, n_{OH} (pH) + \ln \frac{I_{p_a}}{I_p} \right] \quad [21]$$

because at $E_{a.5}$ the second term of the denominator equals unity (Eq. [12] and [13]). $E_{a.5}$ is independent of the function f(pH). This might be expected because the potential at which the film covers 50% of the surface does not depend primarily on the rate of anodic dissolution. Typical features of the calculated curves are the following: in the active state there is one straight line in semilogarithmic plotting if the current density which is independent of pH (f(pH) = 1). The conversion to the passive state is shown by parallel straight lines for a variation of pH as demonstrated in Fig. 6. Kolotyrkin (10) gives a demonstration of these conditions from a study of the current density of the anodic dissolution of chromium in 1.0*N*, in 0.1*N* and 0.01*N* H_2SO_4. His curves in semilogarithmic plotting consist of one straight line of the current in the active state with straight lines of the conversion to the passive state branching off at potentials of 0.05 v difference.

It is also interesting to note that the alteration of the polarization curve found after the addition of pyrogallol (Fig. 1 and 2) might be caused by an increased solubility of the passive film which effects a change of I_p. This assumption agrees with the experimental result of MacLean and Gardner (32) who studied the corrosivity of wood extractives. These

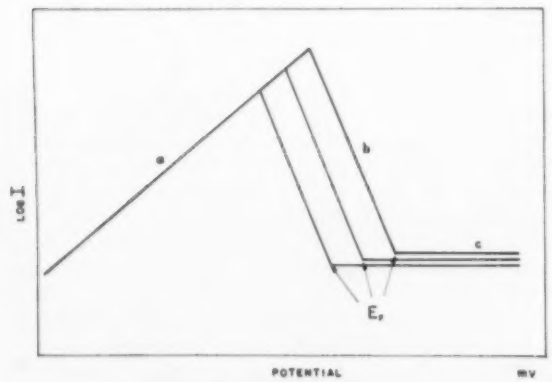

Fig. 6. Schematic semilogarithmic plotting of the density of the anodic dissolution current: (a) film-free active range, (b) conversion to the passive state, and (c) Flade potential E_F and the passive state.

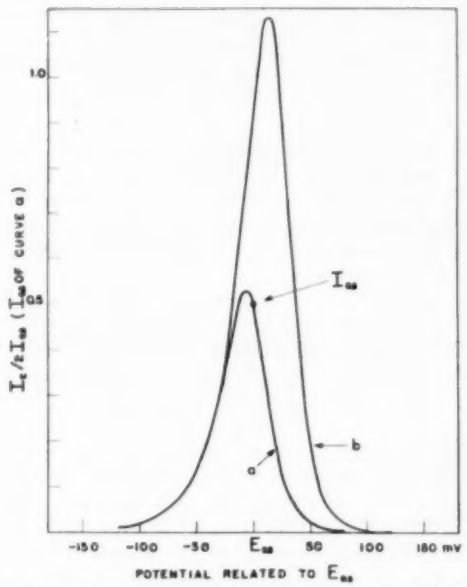

Fig. 7. Density of the anodic dissolution current calculated for a variation of the rates of film dissolution and film formation:

(a) $\frac{I_{p_a}}{I_p} \exp [2.3\, n_{OH} (pH)] = 1$;

(b) $\frac{I_{p_a}}{I_p} \exp [2.3\, n_{OH} (pH)] = 0.1$

authors suggested that the increased corrosivity of alkaline cooking liquor found by addition of 1,2 dihydroxybenzene and derivatives, such as pyrogallol, was due to increased solubility of ferric iron salts. Figure 7 demonstrates the calculated effect in two curves the shape of which agrees very well with that of Fig. 1 and 2.

Franck (7) on repeating Flade's (2) experiments, uses the expression "critical current density which causes the local activation" to describe the current density at the Flade potential. Franck does not indicate whether this critical value of the current differed at different pH values. Hence the definition of Franck's experimental values of the Flade potential is not exactly known.

In the present work, the Flade potential is defined as the potential at which the density of the anodic dissolution current I_{a_f} equals I_p, the density of the current in the passive state. It may be stated that this definition does not consider the Flade potential as an equilibrium potential for the formation and disintegration of the protective oxide film (19). According to the definition the two terms in the numerator of Eq. [20] are equal at E_F. Differentiation of the equation calculated for E_F with respect to pH results in the relation

$$E_F = E_{F_a} - (pH) \frac{RT}{F} \frac{2.3 n_{OH} - \frac{d \ln f(pH)}{d\,(pH)}}{\alpha_p\, n_p - \alpha_a\, n_a} \quad [22]$$

The meaning of Eq. [22] may be demonstrated in Fig. 8 which plots the current-potential relation on a semilogarithmic scale. The curve referring to pH = 0 is characterized by the crosspoints E_{F_a}/I_{p_a} and $E_{a-0.5}/2I_{a-0.5}$ ($I_{a-0.5} = I_{a.5}$ at pH = 0). According to Eq.

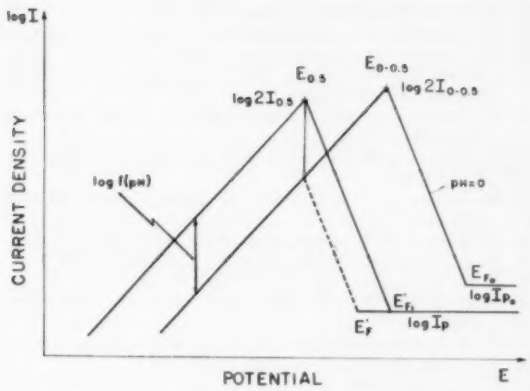

Fig. 8. Schematic semilogarithmic plotting of the anodic dissolution current showing the effect of f(pH) on the Flade potential (Eq. [22]).

[21], $E_{0.5}$ is independent of f(pH). If f(pH) equals unity the Flade potential is E'_F. If f(pH) increases with pH the resulting Flade potential E'_F reaches a value between E_{F_0} and E'_F. Equation [22] gives values of the same order of magnitude as Eq. [2]. However, exact values of the current-density-potential relation at varied pH are required for a definite decision on the validity of Eq. [22].

Comparison with Previously Developed Theories About Passivity

The theory presented is based on the accepted idea of a protective film, consisting of Fe_2O_3 in the case of iron. This theory leads to the conclusion that the electronic state of the metal surface influences the conversion process. A high value of β means a rapid decline from the maximum current density to the passive state, i.e., a typical passivity. An increase of the valency during the conversion from the active to the passive state increases β, because it means $n_p/n_a > 1$. Hence transition elements which increase the valency during the conversion are singled out as elements of typical passive behavior. Thus the original electron configuration theory (33,17,34) is corroborated, and the present theory forms a bridge between Faraday's protective film theory, and Schoenbein's theory (35) that passivation involves an essential alteration of actual metal properties.

The complementary relation between the presented theory and the theory of Vetter (20) and Weil (21) about the passive film is evident. The presented theory leads from an unprotected surface to one which is protected by a monolayer film. The growth of the film thickness is explained by their theory. Thus these two theories cover two neighboring potential ranges.

However, there is disagreement with certain previously published theories. Development of oxygen (7) or of an iron oxide higher in oxygen content than Fe_2O_3 (36) was assumed by some authors to be a necessary or characteristic condition for reaching passivity. This assumption probably has been stimulated by measurements with current controlled experimental arrangements which cause a jump of the potential from the active state over a large range of the passive state (3,4). Depending on the experimental conditions, the potential may reach stable values only in the transpassive state. With an adequate potentiostatic arrangement it is easily shown that the development of oxygen or of high iron oxides is not characteristic of the passive state of iron, but of the transpassive state.

The theory of Müller (28) assumes the deposition of porous metal salts on the rapidly corroding metal surface, particularly in strong acids. On the iron surface below the pores of the deposit, chemical passivity is assumed to be caused by the extremely high current density. Instead of this the present theory assumes that anions can form a salt film on metals. Corrosion rate and current density then are reduced to a value proportional to the solubility of the salt film. Once the potential for the formation of the oxide film is reached, the conversion from the salt-film-covered to the oxide-film-protected metal takes place.

Oxygen and oxidizing agents are well known promoters of passivity. Two different mechanisms were proposed to explain passivation by oxidation. By the first, formation of oxide films occurred by direct reaction between metal and oxygen or oxides. This is the mechanism of the formation of protective films of oxides during the exposure of metals to dry atmospheric oxygen. Dissolved oxidizing reagents, such as chromates, may also promote the formation of a protective film by direct reaction with the metal in the active state (18). By the second proposed mechanism, oxygen or oxides dissolved in water produce an electrochemical reaction between metals and oxidizing agents, consisting of removal of negative charges from the metal surface according to the equation (37)

$$\tfrac{1}{2}\,O_2 + 2e^- \rightleftharpoons O^{2-} \qquad [23]$$

An oxidizing process of this type involves a cathodic current-density according to Faraday's law. If this current density is higher than the maximum anodic current density in the active state, it causes a shift to the passive state. Thus, even though oxygen might contribute to the formation of a passive film, the decisive factors are pH and potential.

An explanation of passivity, and particularly of the Flade potential, has recently been given by Göhr and Lange (19). After a survey of the iron oxides and their properties, the basic chemical reaction involved in the formation of the Flade potential was formulated as follows:

$$Fe_3O_4 + \tfrac{1}{2}H_2O \rightarrow 3/2Fe_2O_3 + \tfrac{1}{2}H_2;\ U_H = +0.58\ v \qquad [24]$$

Even though the present theory assumes an Fe_2O_3 film in agreement with Göhr and Lange, the concept of the mechanism of film formation is different. According to the present derivation the Flade potential is not an equilibrium potential, it is a potential defined by a steady state condition as explained already.

The given derivation reaches from the active state over the range of the conversion from the active to the passive state and over the Flade potential to the passive state. The basic assumptions made and the results derived do not interfere with the theory and the facts known from Vetter (20) and Weil (21) about the neighboring passive state. At the Flade potential the proportion of film free to total area is extremely small and the film coverage almost literally complete. The present derivation studies the formation of a monolayer film. The growth of this film by inner migration which might begin before it covers the complete surface has been described by Vetter (20) and Weil (21).

Manuscript received May 21, 1959.

Any discussion of this paper will appear in a Discussion Section to be published in the December 1960 JOURNAL.

REFERENCES

1. W. A. Mueller, To be published.
2. F. Flade, *Z. physik. Chem.*, **76**, 513 (1911).
3. N. D. Green, Paper presented at N.A.C.E. Conference, March 1959.
4. W. A. Mueller, *Can. J. Tech.*, **34**, 162 (1956); *Tappi*, **40**, 129 (1957).
5. R. B. Kesler and J. F. Bakken, *Tappi*, **41**, 97 (1958).
6. E. Uusitalo, *Papper och Trä*, **8**, 393 (1958).
7. U. F. Franck, *Z. Naturforsch.*, **4a**, 378 (1949); Habilitations Schrift Goettingen (1954).
8. H. Gerischer, *Angew Chem.*, **70**, 285 (1958).
9. K. E. Heusler, *Z. Elektrochem.*, **62**, 582 (1958); K. E. Heusler, K. F. Bonhoeffer, and K. G. Weil, *Z. physik. Chem.*, in preparation.
10. Y. M. Kolotyrkin, *Z. Elektrochem.*, **62**, 664 (1958).
11. R. Olivier, Dissertation, Leiden (1955).
12. R. P. Tischer and H. Gerischer, *Z. Elektrochem.*, **62**, 50 (1958).
13. M. Pourbaix, *Chem. & Ind.*, **1953**, 780.
14. K. F. Bonhoeffer, *Z. Elektrochem.*, **55**, 151 (1951).
15. M. Cohen, Symposium on Charge Transfer Processes, Toronto, Sept. 1958, Paper No. 20; *J. Phys. Chem.*, **56**, 451 (1952).
16. G. Armstrong and J. A. V. Butler, *Trans. Faraday Soc.*, **30**, 1173 (1934).
17. U. Sborgi, *Atti Lincei*, **1**, 315, 388 (1925); *Gazz.*, **56**, 532 (1926).
18. M. Cohen and A. F. Beck, *Z. Elektrochem.*, **62**, 696 (1958).
19. H. Göhr and E. Lange, *ibid.*, **61**, 1291 (1957).
20. K. J. Vetter, *ibid.*, **58**, 230 (1954); **62**, 642 (1958).
21. K. G. Weil, *ibid.*, **59**, 711 (1955); **62**, 638 (1958).
22. U. R. Evans, *Nature*, **126**, 130 (1930); *J. Chem. Soc.*, **1930**, 478.
23. U. R. Evans, *Z. Elektrochem.*, **62**, 619 (1958).
24. P. Berge, *Compt. rend*, **245**, 1239 (1957).
25. K. F. Bonhoeffer, *Z. Elektrochem.*, **47**, 147 (1941).
26. E. S. Snavely and N. Hackerman, Symposium on Charge Transfer Processes, Toronto, Sept. 1958.
27. W. H. Wade and N. Hackerman, *Trans. Faraday Soc.*, **53**, 1636 (1957).
28. W. J. Müller, *Z. Elektrochem.*, **30**, 401 (1924); **36**, 365 (1930); **36**, 379 (1930).
29. E. Müller and K. Schwabe, *ibid.*, **38**, 407 (1932).
30. W. A. Mueller, To be published.
31. N. A. Nielsen and T. N. Rhodin, Jr., *Z. Elektrochem.*, **62**, 707 (1958).
32. H. MacLean and J. A. F. Gardner, *Pulp & Paper Mag. Can.*, **54**, 125 (Nov. 1953).
33. A. S. Russell, *Nature*, **115**, 455 (1925); **117**, 47 (1926); A. S. Russell, D. C. Evans, and S. W. Rowell, *J. Chem. Soc.*, **1926**, 1877.
34. R. Swinne, *Z. Elektrochem.*, **31**, 417 (1925).
35. C. T. Schoenbein and M. Faraday, *Phil. Mag.*, **9**, 53, 65 (1836); C. T. Schoenbein, *Pogg. Ann.*, **37**, 590 (1836).
36. H. H. Uhlig and T. L. O'Connor, *This Journal*, **102**, 562 (1955); H. H. Uhlig, *Z. Elektrochem.*, **62**, 626 (1958).
37. W. Schwartz, *Metallwissenschaft und Technik*, **10**, 513 (1956); **10**, 921 (1956).

Kinetics of the Dissolution of Copper in Aqueous Solutions of Aliphatic Amines

S. C. Sircar[1] and D. R. Wiles[2]

Department of Mining and Metallurgy, University of British Columbia, Vancouver, Canada

ABSTRACT

Studies of the rate of dissolution of copper in aqueous solutions of ammonia, and methyl-, ethyl-, and n-butylamines under a high pressure of oxygen have shown the reaction to occur in two stages: a rapid pre-equilibrium involving the free amine molecule, and a slower reaction step involving either the free amine molecule or its conjugate acid. This mechanism leads to a partial understanding of the passivity of copper surfaces in nearly neutral amine solutions.

Recent studies of the kinetics of the attack of various complexing agents on metallic copper have been extended to include the aliphatic amines. Earlier work on ammonia (1,2) and on some amine-type chelating agents (3) has suggested that the free base and its protonated form act to cause dissolution by independent paths, and that the reaction is first order in each species. Thus

$$\frac{d[Cu^{++}]}{dt} = k_1[A] + k_2[AH^+] \qquad [1]$$

where A represents the free amine, and AH^+ its singly protonated form.

The present study, involving methyl, ethyl, and n-butyl amines, was made with the thought of ob-

[1] Present address: Bakhrabad, Cuttack 2, Orissa, India.

[2] Present address: Department of Chemistry, Carleton University, Ottawa, Canada.

serving possible variation in kinetic behavior among the members of this homologous series, and also of finding out how well ammonia would fit in as a first member of such a series.

Experimental

The apparatus and procedure used were the same as those described earlier (3,1). Briefly, these were as follows.

The reaction took place in a one-gallon autoclave, under a pressure of oxygen kept constant at about 8.0 atm. The solution, about 2 l in volume, was made up by diluting stock solutions of accurately known concentrations and was maintained at an ionic strength of at least 0.1M by addition of reagent-grade sodium perchlorate. The dissolution specimen was made from conductivity grade (99.97%) copper, heat treated to give small grains of nearly random orientation. This specimen, mounted in Bakelite, was supported in the solution with its exposed face tangential to the 8-cm-diameter cylinder swept out by the impeller blades.

The amines, of Kodak White Label grade, were used without further purification. Reaction solutions were made from calculated amounts of stock solutions of the amines and of reagent-grade perchloric acid. Concentrations of the amine stock solutions were determined by titration to a methyl red end point with sulfuric acid. The composition of each solution was checked by titration. During experiments, the reacting solutions were maintained at a temperature of 25.0° ± 0.1°C. Samples, withdrawn at intervals, were analyzed colorimetrically for copper by carbamate method (4).

Results

The amines used in this work are listed in Table I along with the constants for their acid dissociation in aqueous solution:

$$K_a = \frac{[A]\,[H^+]}{[AH^+]}$$

Unfortunately, the complexes formed by these amines with cupric ion (other than the complexes with ammonia) have not been investigated. It is reasonable to assume, however, that the copper is coordinated to four amine groups, which are most likely arranged in a plane square[a] around the central atom.

The rate plots ([Cu^{++}] vs. time) were found, as in the earlier work, to be linear. This once again demonstrates the absence of such effects as autocatalysis and progressive roughening of the copper surface. The observed dependence of the rate on the amine concentration did not support the anticipated first-order behavior, but was rather of the form shown for methylamine in the lower curve of Fig. 1. The same type of behavior was found for all the amines studied.

These data can be described quite well by an expression of the form:

$$R = \frac{d[Cu^{++}]}{dt} = \frac{k_1[A]\,S}{1 + k_1[A]} \cdot k_2[A] \quad [2]$$

where S represents the exposed surface area of the copper sample. This is shown further in that a plot of $[A]^2/R$ vs. [A] gives a straight line, as would be expected from Eq. [2]. This is shown for methylamine in Fig. 2.

The observed effects of added acid, that is, the "aminium" form of the complexing agent, are such as not to support without qualification the view previously suggested (1) that the reaction of the protonated form follows an independent path. Figure 1 shows a family of curves for different values of the acidity. Some deviation from complete independence of reaction path is shown by the fact that the curves of rate vs. aminium concentration, although linear, have slopes which vary with amine concentration. These data are presented in Fig. 3.

The nature of this dependence suggests that the over-all rate equation may be of the form

$$\frac{d[Cu^{++}]}{dt} = \frac{k_1[A]\,S}{1 + k_1[A]}\{k_2[A] + k_3[AH^+]\} \quad [3]$$

A careful re-investigation of the rate dependence in the ammonia system revealed that here, too, the reaction is not simply first order as had previously been reported (1) but follows the same pattern as was found for the amines. Since the deviation from

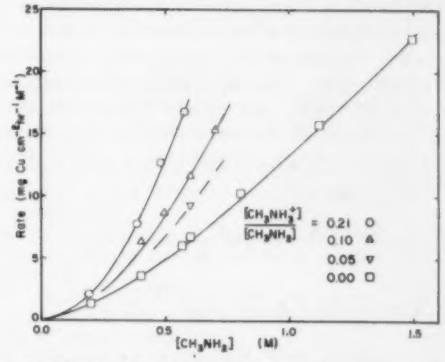

Fig. 1. Rate of dissolution of copper in aqueous methylamine solutions of various acidities.

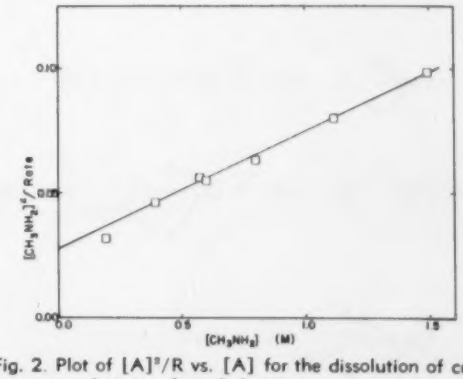

Fig. 2. Plot of $[A]^2/R$ vs. [A] for the dissolution of copper in aqueous solutions of methylamine.

[a] This assumption is based on the fact that most complexes of Cu^{++} which have been studied are square planar. See Ref. (6).

Table I. Amines used in this work

Amine	K_a*
Ammonia	5.68×10^{-9}
Methylamine	2.30×10^{-9}
Ethylamine	1.80×10^{-9}
n-Butylamine	2.46×10^{-9}

* Data adapted from Ref. (5).

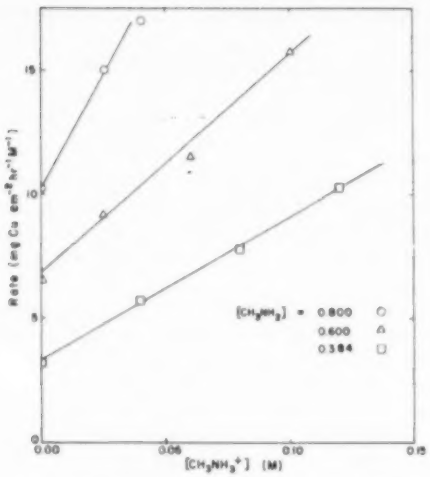

Fig. 3. Rate of copper dissolution in aqueous methylamine solutions as a function of the acidity, at constant concentration of free amine.

linearity is not great, this observation is not in disagreement with Halpern's original work, but is the result rather of a refinement in experimental sensitivity. Experimental data are summarized in Table II.

Values for the constants in Eq. [3] determined for ammonia and the various amines are presented in Table III

The form of Eq. [3] suggests that there is a pre-equilibrium involving adsorption of amine molecules on a saturable surface, producing "active sites." This equilibrium appears to be followed by reaction at the active sites via one of the two previously mentioned independent paths. The adsorption of oxygen on the surface is evidently very fast. The whole process, then, is envisioned as occurring in the following way: (The subscript $_s$ designates a species residing in the surface).

1. $Cu_s + \frac{1}{2} O_2 \xrightarrow{fast} Cu_s - O$

2. $Cu_s - O + A \overset{fast}{\rightleftarrows} Cu_s(A) - O$ $\quad k_1$

3a. $Cu_s(A) - O + A \xrightarrow{slow} Cu_s(A_2) - O$ $\quad k_2$

4a. $Cu_s(A_2) - O + H_2O \xrightarrow{fast} Cu(A)_2^{++} + 2\,OH^-$

3b. $Cu_s(A) - O + AH^+ \xrightarrow{slow}$ 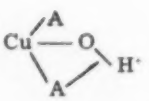 $\quad k_3$

4b. 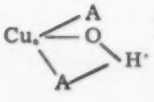 $\xrightarrow{fast} Cu(A)_2^{++} + OH^-$

Table II. Summary of kinetic data†

Complexing agent	Ionic strength	Concentration		Rate of solution, mg Cu cm⁻² hr⁻¹
		Amine	Aminium	
Methylamine	0.1	0.195	—	1.20
		0.40	—	3.40
		0.57	—	5.80
		0.60	—	6.60
		0.80	—	10.20
		1.12	—	15.60
		1.49	—	22.6
		1.49	—	22.7
Methylamine	0.2	0.80	0.025	15.0
		0.80	0.040	17.0
		0.80	0.050	18.0
		0.80	0.050	18.0
		0.80	0.075	48.8*
		0.80	0.100	55.6*
		0.80	0.125	52.0*
		0.80	0.195	50.0*
Methylamine	0.2	0.192	0.040	2.10
		0.384	0.080	7.80
		0.480	0.100	12.60
		0.576	0.120	16.7
Methylamine	0.2	0.384	0.040	5.70
		0.384	0.080	7.80
		0.384	0.120	10.30
Methylamine	0.1	0.40	0.040	6.2
		0.50	0.050	8.6
		0.60	0.060	11.6
		0.70	0.070	15.2
		0.60	0.03	9.2
		0.60	0.10	15.8
Ethylamine	0.1	0.203	—	1.30
		0.400	—	3.60
		0.535	—	6.40
		0.76	—	9.00
		0.92	—	12.60
		1.04	—	16.6
Ethylamine	0.2	0.210	0.050	2.80
	0.35	0.210	0.100	4.50
	0.2	0.210	0.150	5.80
n-Butylamine	0.1	0.187	—	1.10
		0.326	—	2.80
		0.63	—	7.60
		0.96	—	14.3
		1.29	—	20.7
		1.64	—	32.3
n-Butylamine	0.2	0.202	0.025	1.80
		0.202	0.050	2.60
		0.40	0.025	5.00
Ammonia	0.1	0.086	—	2.10
		0.165	—	5.45
		0.310	—	14.1
		0.66	—	38.0
Ammonia	0.1	0.20	0.0020	10.00
		0.20	0.0040	12.6
		0.30	0.0030	17.8
		0.30	0.0060	22.2
		0.40	0.0040	26.4
		0.40	0.0080	32.8

† Temperature: 25° ± 0.1°C; oxygen partial pressure: 8.2 atm; ionic strength adjusted with $NaClO_4$.

* No explanation has been found for these anomalously high rates.

Table III. Rate constants determined in this work

Amine	k_1*	k_2*	k_3*
Ammonia	4.7	80	2450
Methylamine	1.9	21	140
Ethylamine	2.3	20	90
n-Butylamine	1.9	23	90

* The units are: for k_1 liters per mole, and for k_2 and k_3 mg Cu^{++} cm^{-2} hr^{-1} $mole^{-1}$ liter. While the limits of error could not be determined accurately, it is felt that these values are correct to within about 5% for k_1 and k_2 and about 10% for k_3.

In the above, k_1 is an equilibrium constant, while k_2 and k_3 are the rate constants.

Since, under the conditions of the experiments, variation of the oxygen pressure makes no difference to the reaction rate, it can be assumed that the equilibrium in Step 1 is shifted very far to the right, so that the surface is completely covered with a layer of adsorbed oxygen atoms. It should be pointed out that there is no direct evidence to suggest that the oxygen adsorption precedes the amine adsorption. However, since the order of the first two steps is not at present important, the above arrangement is taken as satisfactory.

The values given in Table III for the rate constants show a marked reduction in reaction rate on going from ammonia to the amines. However, only k_3 shows any significant change as the length of the carbon chain is increased, and even here the change is not evident beyond ethylamine.

The results of the experiments done at constant total amine concentration, seen in Fig.4, in addition to confirming the nature of Eq. [3], may give some insight into the mechanism of passivation of copper in neutral or acid amine solutions. It appears that, as the concentration of free amine decreases, the position of the pre-equilibrium (Step 2) is moved far to the left, and the number of active sites is greatly reduced. Thus the reaction step (3a or 3b), involving either the free amine or its conjugate acid, is able to proceed only at a very slow rate.

The fact that the rates in nearly neutral solutions are much less than are expected from Eq. [3] (solid line in Fig. 4) cannot be accounted for on the basis of erroneous values for the rate constants. It seems possible that the surface may be closed by the adsorption of some inert species, or perhaps by the formation of an electrical double layer involving the aminium ion. Such a mechanism has been proposed (7) to explain the effect of chloride ion on the rate of dissolution of copper in acid chloride solutions.

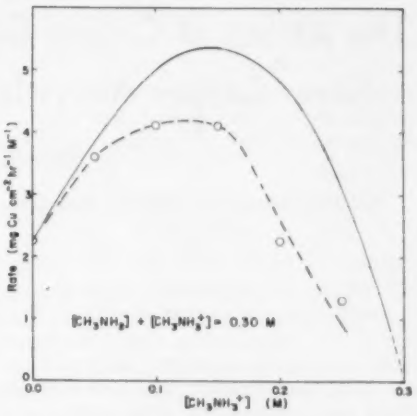

Fig. 4. Rate of copper dissolution in aqueous methylamine solutions as a function of the acidity, at constant concentration of total amine. Solid line calculated from Eq. [3], using the values given in Table III for the constants.

Acknowledgments

The authors express thanks to Dr. J. Halpern for helpful discussions. Financial support by the National Research Council (Canada) is gratefully acknowledged.

Manuscript received June 29, 1959.

Any discussion of this paper will appear in a Discussion Section to be published in the December 1960 JOURNAL.

REFERENCES

1. J. Halpern, *This Journal*, **100**, 421 (1953).
2. J. I. Fisher and J. Halpern, *ibid*, **103**, 282 (1956).
3. J. Halpern, H. Milants, and D. R. Wiles, *ibid.*, **106**, 647 (1959).
4. E. B. Sandell, "Colorimetric Analysis for Traces of Metals," p. 204, Interscience Publishers, Inc., New York (1950).
5. I. M. Kolthoff and V. A. Stenger, "Volumetric Analysis," Interscience Publishers, Inc., New York (1942).
6. J. C. Bailar, "The Chemistry of the Coordination Compounds," p. 371, Reinhold Publishing Corp., New York, (1956).
7. J. R. Weeks and G. R. Hill, *This Journal*, **103**, 203 (1956).

The Attack of Copper-Gold, Silver-Gold, Nickel-Copper, and Silver-Copper Alloys by Sulfur at Elevated Temperatures

Barry D. Lichter[1] and Carl Wagner[2]

Department of Metallurgy, Massachusetts Institute of Technology, Cambridge, Massachusetts

ABSTRACT

Copper-gold alloys involving 10 and 33 mole % Au and Ag-Au alloys involving 12 mole % Au are attacked by liquid or gaseous sulfur above 400°C very rapidly with formation of a composite scale consisting of an outer homogeneous sulfide layer and an inner two-phase layer involving Au-rich alloy and sulfide in accord with theoretical considerations regarding the instability of a plane alloy-sulfide interface. The tendency to form a rugged alloy-sulfide interface decreases with higher Au contents especially at lower temperatures and the rate of attack by sulfur decreases accordingly. Silver-copper alloys involving 40 mole % Cu are also rapidly sulfidized at 400°C and yield a single sulfide layer of uniform thickness. Nickel-copper alloys sulfidized at 400°C yield a scale consisting of an outer layer which is supposedly digenite $Cu_{1.8}S$, and an inner layer which is supposedly a solid solution of Cu_2S in nickel sulfide.

In two previous papers (1,2), diffusion processes during the oxidation of alloys involving noble metals have been considered. In particular, a theoretical analysis of the interplay of diffusion processes in the alloy and the scale shows that a plane alloy-oxide interface is not stable if only one component of a binary alloy is oxidized and diffusion in the alloy is slow in comparison to diffusion in the oxide of the less noble metal (2). Thus a highly rugged alloy-oxide interface may be formed as has been found by various authors cited previously (2). To supplement available observations, the attack of Cu-Au and Ag-Au alloys by sulfur has been investigated. The experimental methods were weight gain measurements and microscopical examination of sectioned samples, supplemented by chemical analysis of detached scales and x-ray investigations. In addition, observations are presented on the attack of Ni-Cu and Ag-Cu alloys by sulfur involving sulfidization of both alloy constituents.

Copper-gold and Ag-Au alloys were chosen because the self-diffusion coefficients of silver and copper in their sulfides stable above 300°C are as high as 10^{-6} to 10^{-5} cm²/sec (3-6), whereas the interdiffusion coefficients in solid solutions Cu-Au and Ag-Au are much lower, e.g., 10^{-12} to 10^{-11} cm²/sec at 500°C (7-12). Moreover, the solubility of sulfur in silver and copper is very low (13). In particular, the solubility of S in Cu (coexisting with Cu_2S) at 600°C has been found to be as low as 10^{-3} a/o (atomic percent) (14). Thus internal sulfidization is not likely to interfere. While this investigation was conducted, however, it was found in accord with previous observations by Maclaurin (15) that solid Ag_2S-Au_2S solutions are formed and thereby certain complications not anticipated in the theoretical analysis (2) do occur. According to Maclaurin (15), Cu_2S also dissolves Au_2S but to a minor extent.

Figure 1 shows schematically a cross section through the scale which one may expect when Cu-Au alloys react with sulfur vapor of atmospheric pressure at 500°C. Under these conditions, only cubic Cu_xS ($1.7 \leq x \leq 2$) is formed supposedly, whereas at lower temperatures several sulfide phases may be formed as discussed below. In addition to an outer layer consisting of cuprous sulfide, Fig. 1 shows an inner two-phase layer consisting of penetrating sulfide zones interspersed with metallic trunks rich in gold.

As a limiting case, one may assume that copper diffuses in the metallic trunks only in a direction parallel to the original surface of the alloy, no plastic flow of the metallic trunks takes place, and thus the local gold concentration in the two-phase scale is equal to the initial gold concentration of the alloy.

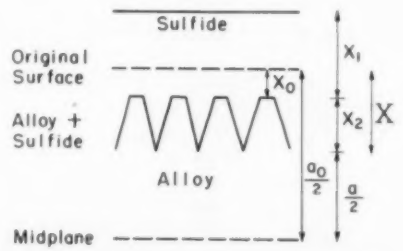

Fig. 1. Schematic section across a Cu-Au sample sulfidized at 500°C with a homogeneous layer of Cu_2S and a two-phase layer consisting of Cu_2S I and gold-rich alloy. (x_0 distance between outer boundary of the two-phase layer and initial surface, x_1 thickness of outer sulfide layer, x_2 thickness of two-phase layer, X distance between alloy-scale boundary and initial surface, a_0 initial thickness of the sample, a thickness of the unattacked core of the sample).

[1] Present address: Air Force Cambridge Research Center, Bedford, Massachusetts.

[2] Present address: Max-Planck-Institut für physikalische Chemie, Göttingen, Germany.

In this case, the outer boundary of the two-phase scale coincides with the original surface, i.e., $x_o = 0$.

In the sulfide phase, copper ions and electrons are supposed to diffuse outward, and plastic flow of the sulfide is supposed to take place so that the transition of copper from the metallic to the sulfide phase does not result in the formation of excessive voids.

Under these conditions, Cu-Au and Ag-Au alloys involving up to about 50 mole % Au are expected to be sulfidized at nearly the same rate as pure Cu and Ag with diffusion in the sulfide phase as rate-determining step.

The actual situation may deviate from the above limiting case in several respects.

1. Since metal ions and electrons move outward and plastic flow of the sulfide is limited, voids at the alloy-sulfide boundary may be formed in accord with observation by Czerski and Patzau (16), Billy and Valensi (17), Moore (18), and Rickert (19) on the sulfidization of pure Cu and Ag. In such voids, sulfur vapor originating from the dissociation of sulfide may diffuse and form sulfide farther inward whereby voids are filled at least in part.

2. Plastic flow of metallic trunks rich in gold may occur. Accordingly, the outer boundary of the two-phase scale is displaced by a distance x_o from the original surface as is shown in Fig. 1.

3. Side-branching of the penetrating sulfide zones may occur and produce a sponge-like network of gold-rich alloy.

4. In the case of excessive side-branching, individual gold-rich alloy particles in a sulfide matrix may be formed and move inward in the same fashion as inert markers move inward when a metal is oxidized and cations rather than anions migrate in the oxide. This also results in a displacement of the outer boundary between one-phase and two-phase scale toward the bulk alloy, i.e., $x_o > 0$.

5. Even under conditions where a plane alloy-sulfide interface is not stable, a nearly plane alloy-sulfide interface may occur on most of the alloy, but there may be pronounced local attack, especially along grain boundaries. Accordingly, the sulfur take-up of the sample is small, but the maximum depth of sulfide penetration may be high.

6. In the case of gold-rich alloys a plane alloy-sulfide interface, although theoretically not stable, may prevail without significant irregularities as, e.g., presumably in the case of the oxidation of Pt-rich Ni-Pt alloys (1,2). Under these conditions, diffusion of the less noble component of the alloy toward the alloy-sulfide interface becomes the rate-determining step.

7. In addition to diffusion, transfer of cations from the alloy to the sulfide may be an important rate-determining step according to recent observations by Rickert (19) on the sulfidization of pure Ag and Cu.

The experimental results reported below show that the systems investigated in this research exhibit considerable deviations from the limiting case conceived for theoretical calculations (2). In view of the complexities which have been found, results have qualitative rather than quantitative significance. No particular efforts have been made to obtain precise weight gain data because at the present stage the structure of the scale and the order of magnitude of reaction rates seem of primary interest. The discussion of the most characteristic features is stressed. Observations of seemingly minor importance are mentioned briefly but are not discussed at length.

Experimental

Materials

Copper.—Commercial Cu (99.94%) was available as 0.2 cm sheet. In addition, high-purity Cu (99.-999%) in rod form was rolled to 0.2 and 0.3 cm sheet.

Silver.—Ag shot (99.95%) was melted under nitrogen and sucked into 7 mm Vycor tubes whereby rods were obtained which were rolled to 0.2 and 0.3 cm sheet.

Nickel.—Commercial Ni (99.5% Ni, 0.32% Co, 0.15% Fe, less than 0.02% Pb) was obtained in the form of 0.1 cm sheet.

Copper-gold and silver-gold alloys.—Cu-Au alloys with mole fractions of gold $N_{Au} = 0.10$, 0.33, 0.61, and 0.74 and Ag-Au alloys ($N_{Au} = 0.12$, 0.35, and 0.56) were obtained from Baker & Co., Newark, New Jersey, where cast alloys were rolled to a thickness of 0.24 cm, annealed in nitrogen at 700°C for 15 min, quenched in water, and cross-rolled to a final thickness of 0.2 cm. These alloys are designated "as received" below. Microscopic examination of etched surfaces revealed the presence of effects of cold work and coring. To eliminate inhomogeneities and promote grain growth, samples of all alloys were annealed in a nitrogen atmosphere saturated with methanol for 100 hr approximately 100°C below the respective liquidus temperatures. The annealing time was sufficient to remove indications of a cored structure. These alloys are designated "annealed" below.

Nickel-copper alloys.—Ni-Cu alloys were prepared by J. D. Harrison. Reagent grade Cu and Ni were melted separately under hydrogen in order to remove oxygen. Alloys were prepared by vacuum melting in an induction furnace, admitting helium, and sucking samples into 9 mm Vycor tubes. The alloys contained 10, 29, and 58 atomic % Cu. Cast rods were rolled to 0.1 cm sheet.

Silver-copper alloys.—An alloy of eutectic composition ($N_{Ag} = 0.60$, $N_{Cu} = 0.40$) was prepared by melting high-purity Ag and Cu under nitrogen, sucking samples into 7 mm Vycor tubes whereby rods were obtained which were rolled to 0.3 cm sheet.

Sulfur.—U. S. P. sulfur powder was used without further purification.

Preparation of Samples

Samples were cut from the prepared sheet with a jeweller's saw, and a small hole was drilled at one end of each sample. The dimensions of samples were as follows: copper and silver, 0.5 x 1.0 x 0.2 or 0.3 cm; copper-gold and silver-gold, 0.5 x 1.0 x 0.2 cm; nickel and nickel-copper, 0.7 x 1.0 x 0.1 cm; silver-copper, 0.9 x 1.5 x 0.3 cm. The cut edges were abraided on emery paper to remove saw marks, and the large surfaces were further polished on emery

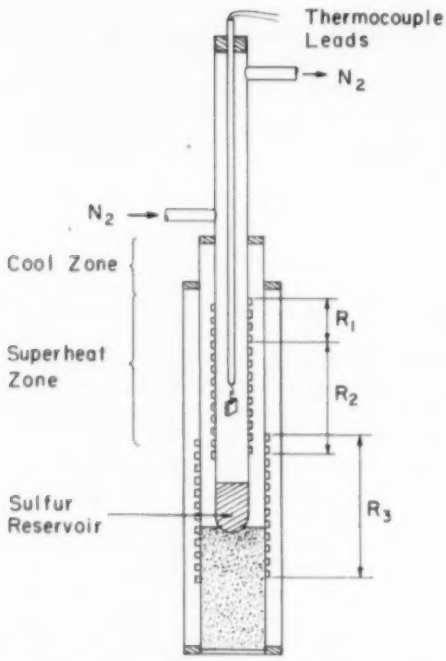

Fig. 2. Set-up for sulfidization in superheated sulfur vapor (500°-700°C) and in liquid sulfur (300°-400°C).

paper to 3/0 grade. Samples were washed with soap and water and rinsed in acetone or methanol. After surface preparation, samples were weighed immediately and inserted in the furnace.

Sulfidization Procedure

Reactions were studied (*a*) in sulfur vapor of atmospheric pressure (700°, 600°, and 500°C) and (*b*) in liquid sulfur (400° and 300°C). Figure 2 shows the set-up designed especially for tests in sulfur vapor. Power is supplied in three stages. The upper two stages ($R_1 = 8$ ohms, $R_2 = 15$ ohms) consisting of a single ribbon winding (1/16 in., "Chromel A", B and S number 28) cemented directly to the inner 25 mm Vycor tube with a common central lead were used to superheat sulfur vapor. The third stage ($R_3 = 5$ ohms) consisting of a ribbon winding ⅛ in., "Chromel A", B and S number 24) cemented to a 38 mm Vycor tube concentric with the inner tube was used to boil sulfur in the lower reservoir. A third concentric Pyrex tube was used as "storm window." Power was supplied from a constant voltage transformer and controlled by means of three variacs connected with the heating resistances R_1, R_2, and R_3. The maximum temperature which could be reached in the superheat zone was 725°C with a total electrical power imput of 1 kw. Temperature fluctuations were about ±5°C.

With the help of this design, it was possible to overcome initial difficulties which were encountered with a conventional two-stage furnace consisting of a ceramic tube surrounded by a thick packing of magnesia. When the conventional furnace was used, sulfur condensed at the upper end of the furnace and ran downward in a rather irregular manner because of the high peak of the viscosity of sulfur at 187°C (20). Applying sufficient power to the upper stage R_1 of the set-up shown in Fig. 2, liquid sulfur flowing downward was vaporized before it reached the superheat zone R_2 used for the sulfidization experiments. Boiling and recycling of sulfur and the location of the sample could be observed readily with this design.

To react samples with liquid sulfur, power was supplied only to the reservoir heated by R_3.

Samples were supported in the furnace by quartz hooks suspended on the sealed end of a Vycor tube which accommodated a thermocouple.

The samples and supporting hooks were weighed separately with a precision of 0.1 mg. At the completion of a run the Vycor tube was removed quickly from the furnace, and the sample was allowed to cool in air before weighing. For runs at 400° and 300°C, molten sulfur occasionally remained on the surface of the samples after withdrawal. The sulfur immediately ignited on contact with air and required from 5 to 10 sec for complete combustion. For most runs the weight gain was recorded as the difference in weight between the sample plus hook before and after reaction. Whenever it was possible to separate sample and hook, the weight gain was recorded as the difference in weight between the sample alone before and after reaction.

Evaluation of Weight Gain Measurements

To obtain results which are independent of the geometry of the samples and determined only by thermodynamic variables, it is necessary to conduct scaling experiments with sufficiently large samples so that the lateral dimensions are much greater than the thickness of the scale. If this condition is not satisfied, edge effects do occur, since the outer area of the sample increases and the area of the boundary between scale and metal decreases during the scaling process. Moreover, in view of local stresses, cracks within the scale and local detachment of the scale from the metallic core may occur as has been found especially in investigations on the oxidation and the sulfidization of iron (21-26).

Because of the high price of gold and the high reaction rates, it was not possible to use samples of sufficient size in order to prevent edge effects. Therefore, a definite rate law cannot be expected and, accordingly, no rate constants are reported. To represent results graphically, however, it was found expedient to plot weight gains per unit nominal area vs. the square root of time. In the calculation of the nominal area, only the large faces of the samples, approximately 0.5 x 1.0 cm, were taken into account; the smaller faces with a width of 0.1 or 0.2 cm were disregarded. Plots of this kind may in general be approximated by straight lines except when the reaction goes to completion.

Metallography

After reaction with sulfur, samples were cast in methylmetacrylate plastic. Powdered polymer was mixed with an equal volume of liquid monomer.[3] Hardening of the plastic occurs at room temperature without application of heat or pressure.

[3] Both supplied under the name "Casto-Mold" by Cosmos Products Inc., New York, N. Y.

Mounted samples were ground on a wet abrasive belt to approximately the center section. Next, samples were abraded lightly on wet silicon-carbide paper. Final polishing was performed on a "gamal" cloth wheel, using levigated gamma-alumina fine abrasive. A few samples were machine polished on lead laps, a standard procedure for preparing mineral specimens. These samples produced scale structures identical with those of manually prepared samples which indicated that the latter were representative. Samples were generally observed unetched except when it was desirable to observe the relation between the structure of the unattacked core and the structure of the scale. Unreacted samples were prepared similarly but were polished on broadcloth wheels with a coarse alumina abrasive before final polishing with "gamal" cloth. For grain size determinations a number of etchants were used. For "annealed" alloys, standard solutions of 10% KCN-2% KI and 5% $(NH_4)_2S_2O_8$ were applied separately with an eyedropper. The strength of the mixture was altered by dilution according to the gold content of the alloy. A 3% iodine solution in methanol, used (27) in studies with Cu_3Au (N_{Au} = 0.25), was found profitable only with a Cu-Au alloy with $N_{Au} = 0.33$. For as-received samples, the 10% KCN-2% KI and the 5% $(NH_4)_2S_2O_8$ etchant were used. Slightly better structures could be obtained with the help of staining etchants containing $FeCl_3$ or $K_2Cr_2O_7$. The latter revealed concentration gradients in as-received alloys.

Sulfidization of Cu-Au Alloys

Pure copper.—Weight gain curves of Cu samples reacted with sulfur at 300°, 400°, and 500°C are shown in Fig. 3. In view of the high rate of the reaction at 500°C, superheating of the samples may have occurred. Thus values for 500°C are only indicative for a very rapid reaction.

At 300° and 400°C, there may be formed three reaction products, (*a*) hexagonal chalcocite, Cu_2S II, with a variable deficit of copper, (*b*) face-centered cubic digenite with the approximate formula $Cu_{1.8}S$, and (*c*) hexagonal covellite, CuS (28-33).

At 500°C, CuS is unstable as its dissociation pressure exceeds 1 atm (34-36). Moreover, according to Hirohara (5), hexagonal Cu_2S II is unstable above 470°C. Instead, a face-centered cubic modification, Cu_2S I, is found. Its lattice is identical with that of digenite (5, 28, 29, 33). Tentatively, it may be assumed that the homogeneity of the phase Cu_2S I at 500°C extends from a Cu/S ratio of 2.0 to about 1.8. Thus face-centered cubic Cu_2S I is supposedly the only reaction product at 500°C.

Sectioned and polished samples which were sulfidized in part contained only gray sulfide. A thin outer blue layer of CuS becomes visible on samples sulfidized at 400°C only after much longer sulfidization, e.g., 24 hr. The gray sulfide may actually consist of two separate layers corresponding to hexagonal Cu_2S and digenite $Cu_{1.8}S$, or the respective transformation products formed on cooling. So far, however, no experimental evidence of Cu_2S II and digenite as separate reaction products has been obtained.

In accord with observations by Czerski and Patzau (16) and Rickert (19) sections of Cu samples sulfidized at 400°C showed numerous voids in the scale next to the metal whereas no voids were found in the outer scale. The porosity of the inner scale may be due to local detachment of the scale similar to that reported for the oxidation and sulfidization of iron (21-26).

Cu-Au *alloys.*—Weight gain plots for Cu-Au alloys involving 10 and 33 mole % Au are shown in Fig. 4 and 5.

Copper-gold alloys involving 10 mole % Au were sulfidized at about the same rate as pure copper as follows by comparing weight gain curves in Fig. 3 and 4. Microscopical examination of sectioned samples revealed an outer homogeneous sulfide layer and an inner two-phase layer consisting of sulfide

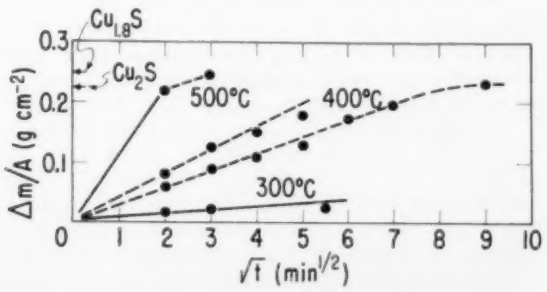

Fig. 3. Weight gain plot for pure Cu

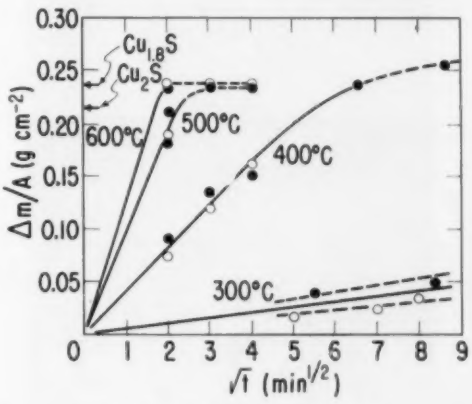

Fig. 4. Weight gain plot for Cu-Au alloy, $N_{Au} = 0.10$. ○ Annealed; ● as-received.

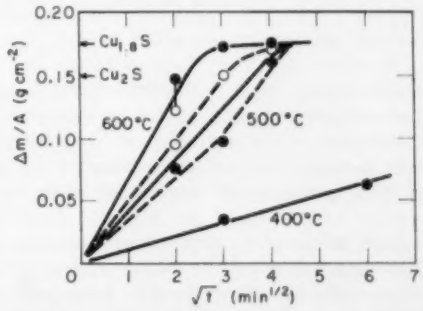

Fig. 5. Weight gain plot for Cu-Au alloy, $N_{Au} = 0.33$. ○ Annealed; ● as-received.

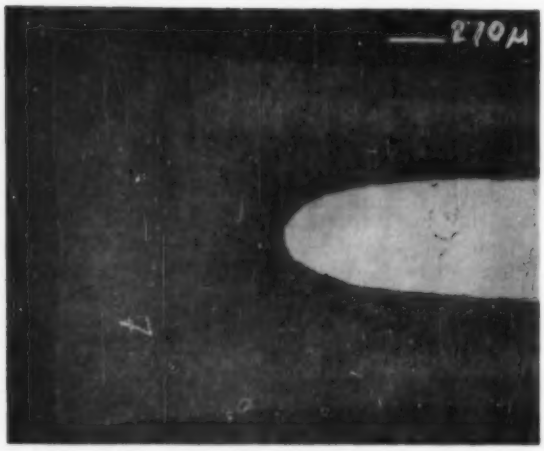

Fig. 6. Section of Cu-Au alloy ($N_{Au} = 0.10$, annealed) sulfidized at 500°C for 4 min. White region on the right-hand side is unattacked alloy, which is surrounded by a two-phase layer and an outer homogeneous sulfide layer shown only in part. Black spots in the two-phase layer are due to porosity. The width of the two-phase layer at the left-hand side is nearly equal to the original thickness. In the middle of the sample shown at the right-hand side, the two-phase layer has contracted.

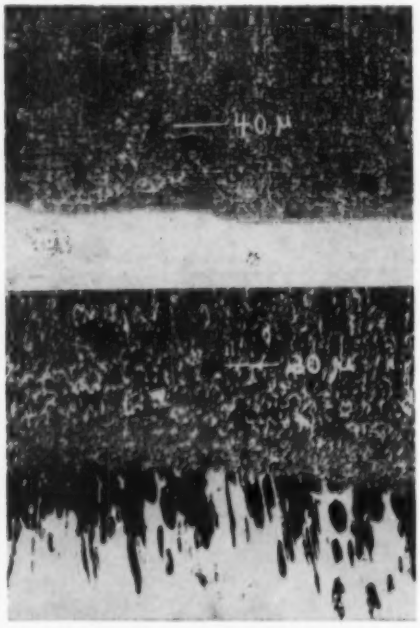

Fig. 7. Details of alloy-scale boundary of Cu-Au alloys ($N_{Au} = 0.10$) sulfidized at 500°C for 4 min. (a) (top) Annealed sample; (b) (bottom) as-received sample.

and metal. Figures 6 and 7a show that the boundaries between the various layers on annealed samples were remarkably well defined. In contrast, "as received" samples showed pronounced local sulfide penetrations presumably associated with copper-rich regions of the alloy, see Fig. 7b. Even in the outer scale, especially at the outer surface, gold particles were observed. Probably, these gold particles were formed when samples were cooled and solid Cu_2S-Au_2S solid solutions present at elevated temperatures decomposed. This interpretation is

Table I. Scale measurements for annealed Cu-Au alloys

N_{Au}	Temp, °C	t, min	x_1, mm	x_2, mm	X, mm	x_0, mm
0.10	500	4	1.1	0.6	0.7	0.1
	400	4	0.38	0.18	0.23	0.05
		9	0.60	0.32	0.39	0.07
		16	0.75	0.48	0.54	0.06
	300	25	0.08	0.07	0.07	—
		49	0.10	0.06	0.06	—
		64	0.10	0.06	0.06	—
0.33	500	4	0.3	0.35	0.35	—
		9	0.6	0.5	0.6	0.1
		16	0.65	0.9	1.0	0.1

supported especially by the observation that the amount of gold in the outer scale increased when samples were stored at room temperature for a longer time.

Scale measurements for annealed alloys are presented in Table I. The thicknesses of the outer one-phase layer and the inner two-phase layer, x_1 and x_2, respectively, were measured approximately at the middle of the large faces of the sample with the help of a movable stage micrometer. In addition, the width a of the unattacked alloy was determined. By subtracting half the thickness of the unattacked alloy from half the initial thickness of the sample $a_0/2$, the distance X between the original surface and the boundary between the scale and the unattacked alloy was obtained, $X = a_0/2 - a/2$, see Fig. 1. Finally, the distance x_0 between the original surface and the boundary between the outer one-phase and the inner two-phase scale was calculated as $x_0 = X - x_2$. Finite values of x_0 indicate either dissolution of gold in the sulfide, or a displacement of gold-rich alloy toward the middle of the sample either by plastic flow of the metallic trunks, or by inward movement of isolated gold-rich particles as has been mentioned above. From the values listed in Table I, one recognizes that the displacement x_0 does not exceed 20% of the distance X to which the attack has penetrated.

Copper-gold alloys involving 33 mole % Au were sulfidized more slowly according to weight gain curves shown in Fig. 5. Microscopical examination of sectioned samples sulfidized at 400°, 500°, and 600°C revealed the same general type of scaling as that shown in Fig. 6, but with a rather abrupt change in the width of the single-phase regions in the two-phase scale. The width in the inner part of the two-phase region was much smaller than in the outer part. Scale measurements are listed in Table I.

Copper-gold alloys involving higher gold contents ($N_{Au} = 0.61$ and 0.74) were sulfidized at much lower rates. Even at 700°C, only minor weight gains were obtained, e.g., $\Delta m/A = 0.002$ g/cm² for $N_{Au} = 0.61$ after 16 min and for $N_{Au} = 0.74$ after 64 min.

Microscopical examination of sectioned samples which had been reacted at 700°C revealed the absence of a typical two-phase scale described above for alloys involving lower gold contents. Instead, there was found a thin uniform sulfide layer containing small amounts of Au which presumably was formed by decomposition of Cu_2S—Au_2S solid solutions present at elevated temperatures. For samples

involving 61 a/o Au, isolated patches of a two-phase scale were observed between the outer sulfide and the inner unattacked core. Comparison of the alloy grain size with the width of the single-phase constituent in the two-phase patches, together with observations at the scale-alloy boundary, suggest that a considerable amount of grain boundary attack is responsible for the appearance of the patches. No patches were observed for alloys involving 74 a/o gold. However, occasional penetration along grain boundaries was observed. At lower temperatures (600° and 500°C) only a uniform sulfide layer was observed.

Additional Observations on the Structure of the Scale.

The occurrence of a sponge-like network of gold-rich alloy within the two-phase scale has been confirmed directly for Cu-Au alloys involving 33 a/o Au. Upon dissolving the sulfide phase in a mixture of equal volumes of HNO_3 and H_2O with a small addition of KNO_3, a sponge-like network of gold-rich alloy could be isolated.

When the two-phase scale from an alloy involving 10 a/o Au was treated in the same way, the details of the structure were lost. This indicates that the two-phase scale of the latter alloy involved islands of gold-rich particles or sponge in a sulfide matrix rather than a coherent network of gold-rich alloy.

The width of the single-phase regions in the two-phase scale of gold-rich alloys ($N_{Au} = 0.10$ and 0.33) was found to depend markedly on temperature. The higher the temperature, the greater was the width. This is due at least in part to coarsening of the disperse structure while the sample was at temperature as follows from microphotographs shown in Fig. 8. Two Cu-Au samples ($N_{Au} = 0.33$) were reacted to completion in sulfur vapor at 500°C. A section of one of these samples is shown in Fig. 8a. A section of the other sample which was heated to 700°C for further 16 min, is shown in Fig. 8b. The width of the single-phase regions in Fig. 8b is considerably greater than that in Fig. 8a and similar to the width in a sample reacted to completion directly at 700°C, see Fig. 8c. This shows that the residual gold-rich alloy in the two-phase layer undergoes considerable structural changes. Au_2S is dissolved in Cu_2S to some extent (15) especially at higher sulfur activities. Thus gold can be transferred between different points of the sulfide-alloy interface involving different curvatures by virtue of local dissolution and redeposition corresponding to a decrease of the area of the gold-sulfide interface and the free energy of the system. In addition, gold atoms may migrate along the gold-sulfide interface.

At all temperatures, the width of the single-phase regions in the two-phase scale was found to be considerably smaller than the grain size of the original alloy. This indicates that transgranular penetrations of sulfide do occur in accord with observations on the attack of solid alloys by liquid metals which dissolve one component of the solid alloy preferentially (37).

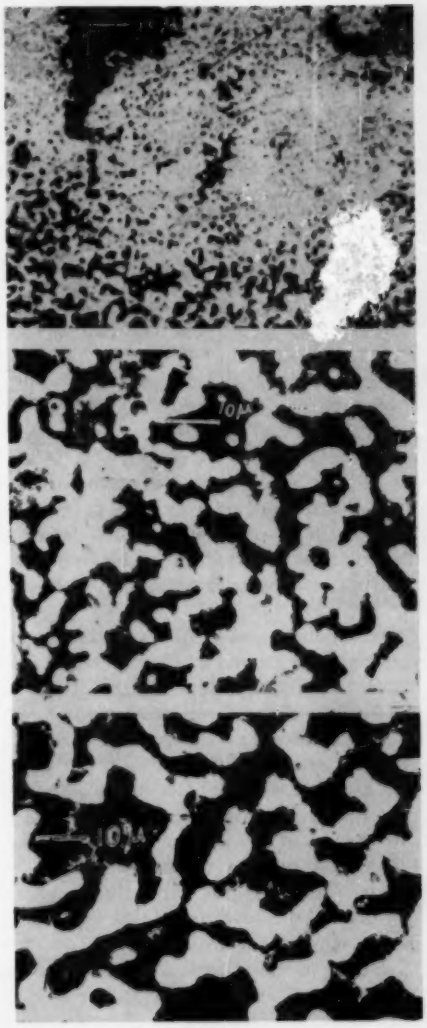

Fig. 8. Structures of two-phase layers obtained on Cu-Au alloys ($N_{Au} = 0.33$, as-received). (a) (top) Sample sulfidized at 500°C for 16 min; (b) (center) sample sulfidized at 500°C for 20 min and annealed in sulfur vapor at 700°C for 16 min; (c) (bottom) sample sulfidized at 700°C for 4 min.

Auxiliary Investigations

Chemical analysis of Cu samples completely sulfidized at temperatures ranging from 400° to 725°C yielded Cu/S atom ratios of 1.77 to 1.84 in accord with weight gain measurements. Somewhat higher Cu/S atom ratios, 1.86 to 1.89, were found in the scale detached from Cu samples which were incompletely sulfidized at 300° to 500°C. Ratios of 1.77 to 1.84 are characteristic of digenite (presumably identical with Cu_2S I) coexisting with sulfur vapor of atmospheric pressure above 500°C, or CuS below 500°C. The same Cu/S ratios were found in the scale detached from sulfidized Cu-Au alloys ($N_{Au} = 0.10$ and 0.33).

The composition of metallic particles in the two-phase scale formed on partially sulfidized Cu-rich alloys ($N_{Au} = 0.10$ and 0.33) was determined by x-ray diffraction investigations. Samples were sectioned parallel to the alloy-scale interface at several

positions in the two-phase scale. The diffraction patterns from the exposed surfaces, obtained with filtered copper radiation on a Norelco diffractometer, showed the spectra of pure gold to within $2\theta = \pm 0.2°$ where θ is the Bragg angle for Cu Kα reflections in the angular region $90° > 2\theta > 35°$. Even at that position in the two-phase scale practically adjacent to the interface between scale and remaining core of the copper-rich alloys, the spectra for virtually pure Au were observed.

Discussion

According to weight gain plots shown in Fig. 4 and 5 the rate of sulfidization of Cu-rich alloys is about the same for as-received samples and annealed samples, but there is a slight tendency for as-received samples to be sulfidized somewhat more rapidly than annealed samples as is indicated especially by results obtained for $N_{Au} = 0.10$ at 300°C shown in Fig. 4. Scale measurements are in accord herewith. In essence, however, the presence of inhomogeneities in as-received samples does not lead to a different type of attack but only modifies some characteristics of the attack found with annealed samples.

Upon extrapolating weight gain data and scale measurements for Cu-rich alloys ($N_{Au} = 0.10$ and 0.33), it follows that the final weight of a sample is reached after about the same time at which the core of unattacked alloy has disappeared. Hence most of the copper originally present in the two-phase layer is converted readily into sulfide, and accordingly the trunks of the remaining alloy consist mostly of gold. This has been confirmed by x-ray diffraction investigations reported above.

In accord with previous theoretical calculations (2), Cu and Cu-Au alloys containing 10 and 33 mole % Cu react very fast. With increasing concentration of Au, the rate of sulfidization of alloys containing up to 33 a/o Au decreases, although not considerably. To make a comparison without using a rate law explicitly, one may compare the times required for penetration of sulfide to a given depth X. For 500°C and $X = 0.05$ cm, one has $t \sim 3$ min if $N_{Au} = 0.10$ and $t \sim 5$ min if $N_{Au} = 0.33$. For 400°C and $X = 0.02$ cm, one has $t \sim 4$ min if $N_{Au} = 0.10$ and $t \sim 12$ min if $N_{Au} = 0.33$.

Gold-rich alloys ($N_{Au} = 0.61$ and 0.74) are sulfidized much more slowly than Cu-rich alloys. This is consistent with the absence of a typical two-phase scale. Thus one has a transition to the other limiting case involving a plane alloy-sulfide interface. Since diffusion in the sulfide phase is much faster than in the alloy, the activity of the sulfur at the alloy-sulfide interface is equal to that at the sulfide surface, the Cu concentration at the sulfide-alloy interface is virtually equal to zero, and diffusion of Cu toward the alloy-sulfide interface is the rate-determining step. According to Eqs. [16] to [20] of a previous, more general calculation (1) the distance x_i between the alloy-sulfide interface and the initial surface of the alloy is

$$x_i = 2u(D't)^{1/2} \qquad [1]$$

where D' is the interdiffusion coefficient of the alloy and the parameter u is determined by

$$\pi^{1/2} e^{u^2} \operatorname{erfc} u = 1 - N_{Au}^{(\infty)} \qquad [2]$$

The number of moles of metal contained in an alloy layer of thickness x_i is x_i/V' where V' is the molar volume of the alloy. Assuming the formula $Cu_{1.8}S$ as representative for the composition of the scale, sulfidization of 1 mole Cu corresponds to a weight increase of $M_s/1.8$ where $M_s = 32$ is the atomic weight of sulfur. Hence the weight increase $\Delta m/A$ per unit area is

$$\Delta m/A = x_i M_s/1.8\, V' = 2uM_s(D't)^{1/2}/1.8\, V' \qquad [3]$$

Equation [3] is evaluated for 500°C and $t = 1$ hr $= 3600$ sec with $D' = 2 \times 10^{-11}$ cm²/sec according to Jost (10), and values are compared with interpolated or extrapolated experimental values,

N_{Au}	0.33	0.61	0.74	
$\Delta m/A$ (calc.)	0.70	0.28	0.16	mg/cm²
$\Delta m/A$ (obs.)	300	2.4	1.2	mg/cm²

The experimental values $\Delta m/A$ are higher than the calculated values inasmuch as the alloy-sulfide interface was not plane under the conditions used in the present investigation. For Cu-rich alloys, the observed attack is especially high as compared to the calculated value. This illustrates the general conclusion that the instability of a plane interface may have a very large effect on the corrosion characteristics of an alloy. On the other hand, for Au-rich Cu-Au alloys for which a well-defined two-phase layer is not found and irregularities of the alloy-sulfide interface are not spectacular, the observed magnitude of attack is comparable to that calculated for a plane alloy-sulfide interface rather than to that of pure Cu or Cu-rich Cu-Au alloys.

Sulfidization of Ag-Au Alloys

Pure silver.—The reaction between pure Ag and sulfur is known to proceed very rapidly above 180°C because of easy migration of both cations and electrons in Ag_2S formed as reaction product above 180°C (38-40). In accord herewith, the time required for complete conversion of 2 mm Ag platelets into Ag_2S was found to be less than 4 min at 400° and 500°C. According to Czerski, Mrovec, Wallisch, and Werber (40) the rate is determined by a phase boundary reaction when the thickness of the Ag_2S layer is less than 0.1 cm, whereas diffusion control prevails with Ag_2S layers which are several centimeters thick according to Rickert (19).

Ag-Au *alloys.*—Weight gain curves for Ag-Au alloys involving 12 mole % Au are shown in Fig. 9. The sulfidization rate is remarkably high, although somewhat lower than for pure Ag. The total weight gain exceeds that for formation of Ag_2S alone and corresponds to the formation of a solid Ag_2S-Au_2S solution in accord with previous observations by Maclaurin (15). Microscopical examination of sectioned samples sulfidized at 400° and 500°C revealed an outer homogeneous sulfide layer and inner two-phase layer consisting of sulfide and Au-rich alloy, see Fig. 10. Scale measurements are shown in Table II. Samples sulfidized at 300°C showed only a homogeneous sulfide layer.

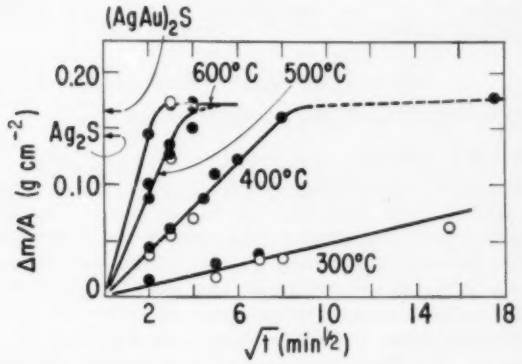

Fig. 9. Weight gain plot for Ag-Au alloy, $N_{Au} = 0.12$. ○ Annealed; • as-received.

Upon comparing microphotographs of sections of the scale in Fig. 10 and the original alloy in Fig. 11, it is clearly seen that the width of the single-phase regions in the two-phase scale is much smaller than the grain size in the original alloy. This illustrates the occurrence of transgranular attack.

According to Fig. 9, weight gain data for annealed alloys agree fairly well with data for as-received alloys. Sections of as-received samples showed a less well-defined boundary between two-phase scale and unattacked alloy, but the observed irregularities were much smaller than in the case of Cu-Au alloys shown in Fig. 7b.

Ag-Au alloys involving 35 mole % Au were found to react much more slowly. Weight gain curves are shown in Fig. 12.

Sectioned samples sulfidized at 700°, 600° and 500°C revealed considerable attack at grain boundaries together with transgranular attack. The resultant scale structure differs from that shown schematically in Fig. 1. Values of x_2 reported in Table II represent the average depth of penetration along grain boundaries. A thin two-phase region resulting from transgranular attack could be observed at the boundary between the outer sulfide scale (containing patches of alloy, presumably due to decomposition of Au_2S-Ag_2S solid solutions) and the core of the alloy. The thin two-phase layer follows the contour of the boundary between the alloy and the outer sulfide. The width of the thin two-phase layer is of the order of $x_2/10$. However, in the vicinity of a grain boundary, considerably more two-phase scale is formed, i.e., attack initiating at grain boundaries spreads into adjacent grains and results in formation of a two-phase scale.

Table II. Scale measurements for annealed Ag-Au alloys

N_{Au}	Temp, °C	t, min	x_1, mm	x_2, mm	X, mm	x_2, mm
0.12	500	9	0.92	0.31	0.65	0.34
	400	4	0.24	0.05	0.14	0.09
		9	0.37	0.06	0.20	0.14
		16	0.51	0.06	0.32	0.26
0.35	600	4	0.22	0.3	0.4	0.12
		16	0.43	0.4	0.6	0.22
	500	4	0.15	0.3	0.4	0.10
		16	0.25	0.4	0.4	0.12

Samples sulfidized at 400°C showed only a homogeneous sulfide layer. In view of the relatively low rate found at 400°C, the activity gradient of sulfur

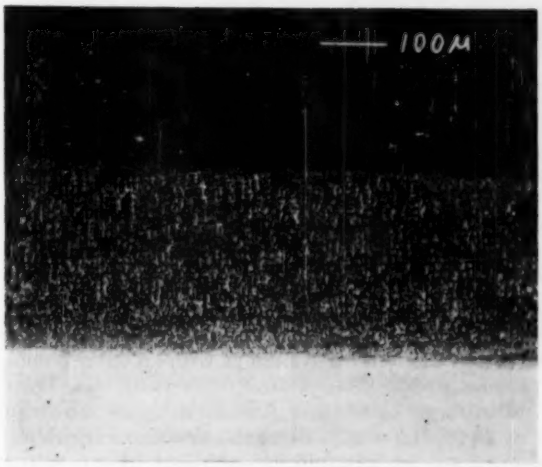

Fig. 10. Section of Ag-Au alloy ($N_{Au} = 0.12$, as-received), sulfidized at 500°C for 9 min with a homogeneous sulfide layer at the top, a two-phase layer in the middle, and unattacked alloy at the bottom.

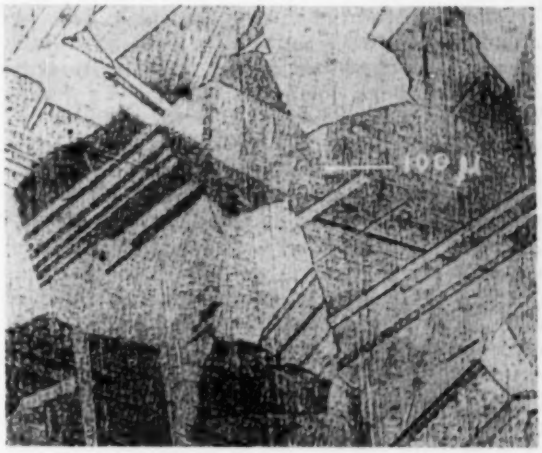

Fig. 11. Section of annealed Ag-Au alloy ($N_{Au} = 0.12$) etched with a mixture of a 10% KCN + 2% KI solution and a 5% $(NH_4)_2S_2O_8$ solution.

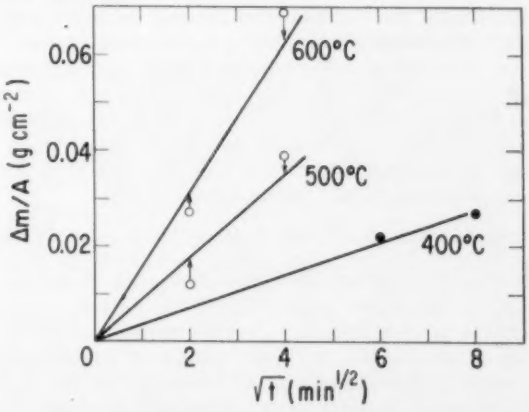

Fig. 12. Weight gain plot for Ag-Au alloy, $N_{Au} = 0.35$. ○ Annealed; • as-received.

in the sulfide must be small. Thus the activity of sulfur at the alloy-sulfide interface is nearly that of pure liquid sulfur, and accordingly a solid Ag_2S-Au_2S solution is formed.

Ag-Au alloys involving 56 a/o Au showed only slight attack. Even at 700°C, $\Delta m/A$ was as low as 0.0015 mg/cm² after 25 min. Microscopical examination of samples sulfidized at 500°, 600°, and 700°C revealed the presence of smooth sulfide layers with plane sulfide-alloy interfaces.

Discussion

In view of the formation of solid Ag_2S-Au_2S solutions (15), the behavior of Ag-Au alloys deviates from the behavior of Cu-Au alloys in several respects.

The structure of the scale may be similar to that found on Cu-rich Cu-Au alloys with an outer homogeneous sulfide layer and an inner two-phase layer consisting of sulfide and Au-rich alloy as shown in Fig. 10 for $N_{Au} = 0.12$. Since the attack is very rapid, there must be a significant gradient of the sulfur activity within the scale. The tendency for dissolution of Au diminishes with decreasing activity of sulfur, i.e., with increasing distance from the outer surface. Therefore, only little Au is dissolved at the boundary between the two-phase scale and unattacked alloy, whereas the outer parts of Au-rich alloy in the two-phase scale are gradually eaten away. Accordingly the outer boundary of the two-phase scale is displaced inward from the initial surface of the sample, i.e., $x_o > 0$, see Table II.

As an alternative, it is conceivable that Ag-rich Ag-Au alloys are sulfidized with formation of a sulfide layer of uniform thickness in which the Ag/Au ratio is virtually equal to that in the alloy. Since, the standard free energy of formation of Ag_2S is considerably more negative than that of Au_2S, the alloy coexisting with a solid solution Ag_2S-Au_2S of given composition has necessarily a much higher Au/Ag ratio than the sulfide phase. Thus there must be a thin zone of Au-rich alloy next to the sulfide phase.

To simplify calculations, it is assumed that the self-diffusion coefficients of Ag^+ and Au^+ ions in the sulfide phase are equal, and accordingly the Au/Ag ratio in the sulfide layer is independent of the distance from the surface. The driving force for outward migration of the cations is essentially a diffusion potential gradient resulting from the electrons which have a high mobility and, therefore, have the tendency to move ahead (41-43). Thus the rational rate constant k_r, defined as the rate of metal transport in equivalents per unit area per unit time for unit thickness of the sulfide layer is (42)

$$k_r = (D''/2V_{eq}'') \ln a_s^o/a_s^{(i)} \quad [4]$$

where D'' is the self-diffusion coefficient of the cations in the sulfide phase, V_{eq}'' is the volume of one equivalent of sulfide, $1/V_{eq}''$ is the cation concentration in equivalents per unit volume of the sulfide, a_s^o is the sulfur activity at the outer surface, and $a_s^{(i)}$ is the sulfur activity at the alloy-sulfide interface.

The rate constant k_{PB} introduced by Pilling and Bedworth (44) is related to k_r as has been shown previously (38),

$$k_{PB} = (\Delta m/A)^2/t = k_r M_s^2/2V_{eq}'' \quad [5]$$

From Eqs. [4] and [5] it follows that

$$\Delta m/A = (k_{PB}t)^{1/2} = (M_s/2V_{eq}'') [D''t \ln (a_s^o/a_s^{(i)})]^{1/2} \quad [6]$$

Tentatively, chemical equilibrium at the alloy-sulfide interface is assumed. In view of the high degree of disorder of the cations in Ag_2S above 180°C (28), the sulfide phase may be supposed to be an ideal solution of $Ag^+ + 0.5\ S^{2-} = AgS_{0.5}$ and $Au^+ + 0.5\ S^{2-} = AuS_{0.5}$ (45). Thus, if the law of mass action is applied to the reactions

$$Ag\ (alloy) + 1/2\ S = AgS_{0.5}\ (sulfide) \quad [7]$$

$$Au\ (alloy) + 1/2\ S = AuS_{0.5}\ (sulfide) \quad [8]$$

the activities may be replaced by the respective mole fractions. Hence

$$\frac{1-y}{2_{Ag}^{(i)} [a_s^{(i)}]^{1/2}} = K_1 \quad [9]$$

$$\frac{y}{a_{Au}^{(i)} [a_s^{(i)}]^{1/2}} = K_2 \quad [10]$$

where y is the mole fraction of $Au_{0.5}S$, equal to the ratio of the number of Au^+ ions to the sum of the numbers of the cations, $1 - y$ is the mole fraction of $AgS_{0.5}$, $a_{Ag}^{(i)}$ and $a_{Au}^{(i)}$ are the activities of Ag and Au, respectively, which are determined by the composition of the alloy at the interface, and K_1 and K_2 are constants.

Upon subtracting corresponding sides of Eqs. [7] and [8] one has

$$Ag\ (alloy) + AuS_{0.5}\ (sulfide) = Au\ (alloy) + AgS_{0.5}\ (sulfide) \quad [11]$$

with the equilibrium condition

$$\frac{a_{Au}^{(i)} (1-y)}{a_{Ag}^{(i)} y} = K_1/K_2 = K_{ex} \quad [12]$$

where K_{ex} is the equilibrium constant of the exchange reaction in Eq. [11].

The value of K_1 may be calculated from the standard free energy of formation ΔF° for $1/2\ Ag_2S = AgS_{0.5}$ deduced from emf measurements (46). Hence

$$K_1 = \exp(-\Delta F^\circ/RT) = 75 \text{ at } 445°C \quad [13]$$

Formulating Eq. [9] for the three-phase equilibrium alloy + sulfide + sulfur with starred variables and the special values $a_s^* = 1$ and $y^* \cong 0.5$ according to Maclaurin (14), one has

$$a_{Ag}^* = (1-y^*)/K_1(a_s^*)^{1/2} = 0.0067 \text{ at } 445°C \quad [14]$$

corresponding to $N_{Au}^* = 0.95$ as mole fraction of Au in the alloy, according to equations interrelating mole fractions and activities in Ag-Au alloys recommended by White, Orr, and Hultgren (47).

The value of K_{ex} may then be obtained by formulating Eq. [12] for the three-phase equilibrium alloy + sulfide + sulfur,

$$K_{ex} = \frac{a_{Au}^*(1-y^*)}{a_{Ag}^* y^*} = 141 \text{ at } 445°C \quad [15]$$

whereupon in view of Eqs. [12] and [13]

$$K_2 = K_1/K_{ex} = 0.53 \text{ at } 445°C \quad [16]$$

With the help of Eqs. [12] and [15], one may readily calculate y for arbitrarily chosen compositions of the alloy at the interface, using activities according to White, Orr, and Hultgren (47). From a plot y vs. $N_{Au}^{(i)}$ one may read $N_{Au}^{(i)}$ for a given value of y which supposedly equals the bulk mole fraction of Au in the alloy. Finally, one may calculate the value of $a_s^{(i)}$ with the help of Eq. [10]

$$a_s^{(i)} = (y/K_2 a_{Au}^{(i)})^2 \quad [17]$$

For $N_{Au} = 0.35$ in the bulk alloy one has $y = 0.35$ and obtains $N_{Au}^{(i)} = 0.93$ and $a_s^{(i)} = 0.51$ at the alloy-sulfide interface, whereas in a system free of gold according to Eqs. [9] and [13] $a_s^{(i)} = 1.78 \times 10^{-4}$ at 445°C. Hence, in view of Eq. [4], the ratio of the rate constants for a Ag-Au alloy ($N_{Au} = 0.35$) and pure Ag is

$$k_r(N_{Au} = 0.35)/k_r(N_{Au} = 0)$$

$$= \ln 0.51/\ln (1.78 \times 10^{-4}) = 0.077 \quad [18]$$

Extrapolation of data reported by Rickert (19) yields

$$k_r(N_{Au} = 0) = 17 \times 10^{-6} \text{ equiv./cm sec at } 445°C \quad [19]$$

From Eqs. [5], [18], and [19] it follows that

$$\Delta m/A = 0.38 \text{ g/cm}^2$$

$$\text{for } N_{Au} = 0.35,\ t = 3840 \text{ sec at } 445°C \quad [20]$$

which is about 14 times greater than the experimental value obtained at 400°C, $\Delta m/A = 0.027$ g/cm^2. Since the various values involved in the calculation supposedly depend on temperature only to a minor extent, the divergence between the experimental and the calculated value is an indication that equilibria at the interfaces are not readily established. This is in accord with observations on the sulfidization of pure silver especially at 200° and 300°C (19). Since Ag is sulfidized very rapidly, one may conclude tentatively that the rate of transfer of Au from the alloy to the sulfide phase is the limiting factor.

If the gold content of the alloy exceeds the maximum content of Au_2S in the sulfide phase for a given activity of sulfur, ($N_{Au} > y^*$), it is also possible that a sulfide layer of uniform thickness is formed, but with accumulation of Au in the alloy near the alloy-sulfide interface. Then diffusion in the alloy determines the rate as is shown in what follows.

Fick's second law for diffusion in the alloy reads

$$\partial N_{Au}'/\partial t = D'\partial^2 N_{Au}'/\partial x^2 \text{ at } x > x_i \quad [21]$$

where N_{Au}' is the local mole fraction of gold in the alloy, D' the interdiffusion coefficient of the alloy supposedly independent of composition, x distance from the original surface, x_i distance of the alloy-sulfide interface from the original surface, and t time.

The initial condition is

$$N_{Au}' = N_{Au} \text{ at } x = 0, t = 0 \quad [22]$$

Since $D'' >> D'$, the gradient of the sulfur activity in the sulfide layer is very small, i.e., $a_s^{(i)} \cong a_s^*$ and, therefore,

$$y \cong y^* \quad [23]$$

$$N_{Au}'(x = x_i) \cong N_{Au}^* \quad [24]$$

As long as the alloy in the middle of the sample has virtually the original composition, equations for diffusion in a semi-infinite space apply. Thus the displacement of the locus of the alloy-sulfide interface is supposed to be in accord with the parabolic law

$$x_i = 2\,u\,(D'\,t)^{1/2} \quad [25]$$

where u is a parameter calculated below.

Equations [21], [22], [24], and [25] are satisfied by

$$N_{Au}' = N_{Au} + [N_{Au}^* - N_{Au}]\ \frac{\text{erfc}\,[x/2(D't)^{1/2}]}{\text{erfc } u} \quad [26]$$

The molar volume of the alloy is denoted by V' and the surface area of the sample by A. The total number of moles of Ag and Au sulfidized per unit time is $(A/V')\ (dx_i/dt)$. Thus the number of moles of Au entering the sulfide layer per unit time is

$$dn_{Au}'/dt = y^*\,(A/V')\ (dx_i/dt) \quad [27]$$

According to Eq. [25] the alloy-sulfide interface moves by

$$dx_i = u\,(D'/t)^{1/2}dt \quad [28]$$

within the time dt. The amount of Au in the volume element $A dx_i$ is $N_{Au}^* A dx_i/V'$ and must be equal to the sum of the amount of gold diffusing backward

$$(D'A/V')\ [-(\partial N_{Au}'/\partial x)_{x=x_i}]dt$$

and the amount of gold transferred from the alloy to the sulfide phase within the time dt. Hence, using Eqs. [27] and [28] and regrouping,

$$(N_{Au}^* - y^*)\ u\,(D'/t)^{1/2} = -D'\,(\partial N_{Au}'/\partial x)_{x=x_i} \quad [29]$$

Upon substituting Eqs. [25] and [26] in Eq. [29], it follows that

$$\pi^{1/2} e^{u^2}\,\text{erfc}\ u = (N_{Au}^* - N_{Au})/(N_{Au}^* - y^*) \quad [30]$$

whereby the parameter u is determined.

Equation [30] comprises Eq. [2] stated above for Cu-Au alloys with neglect of Au in the sulfide phase. Equation [2] is obtained from Eq. [30] by letting $N_{Au}^* = 1$ and $y^* = 0$.

Sulfidization of 1 mole of Ag (or Au) corresponds to pick-up of 0.5 g-atom of sulfur, with a weight gain of $M_s/2$. The total number n of moles of Ag and Au lost from the alloy is $n = x_i A/V'$. In view of Eq. [25], the weight gain per unit area is found to be

$$\Delta m/A = M_s\,x_i/2V' = u\,M_s\,(D't)^{1/2}/V' \quad [31]$$

Equation [31] involves the diffusion coefficient D' in the alloy, whereas Eq. [6] involves the diffusion

coefficient D'' in the sulfide phase. Since $D' << D''$, one has, therefore, to expect a sharp decrease in the rate of sulfidization when the mole fraction of Au in the alloy exceeds the upper limit of the mole fraction y^* of $AuS_{0.5}$ in the sulfide phase provided that diffusion control prevails.

To evaluate Eq. [31] for $N_{Au} = 0.56$ at 500°, the values $N_{Au}^* = 0.95$ and $y = 0.5$ valid for 445° are used as an approximation. Then Eq. [30] yields $u = 1.6$. Substituting $u = 1.6$, $V' = 10.3$ cm³/mole and $D' = 3.2 \times 10^{-13}$ cm²/sec according to Jost (8), one obtains from Eq. [31]

$$\Delta m/A = 0.6 \times 10^{-3} g/cm^2 \qquad [32]$$

for $N_{Au} = 0.56$ and $t = 3840$ sec at 500°C which is about 3.5 times less than the experimental value, 2.1×10^{-3} g/cm². The divergence between the calculated and the observed value is supposedly due in part to the approximations used in the calculation and in part to the occurrence of minor irregularities of the alloy-sulfide interface.

Sulfidization of Ni-Cu Alloys

At 400°C, Ni-Cu alloys involving 10, 29, and 58 a/o Cu were found to react with sulfur at a rate which is of the same order of magnitude as that for pure Ni, but much more slowly than pure Cu. Weight gain data are shown in Fig. 13. Results obtained with samples involving 58 a/o Cu showed a large scatter.Since local detachment of the scale is suspected as the reason for irregular results, the highest weight gains observed for different samples in runs lasting the same time are reported as representative values. The parabolic rate law is obeyed approximately in contradistinction to the linear rate law reported by Hauffe and Rahmel (48) for the reaction between pure nickel and sulfur vapor at pressures ranging from 10^{-2} to 1 mm Hg and 630°C.

Microscopical examination of sectioned samples revealed the presence of two distinct, essentially homogeneous sulfide layers, see Fig. 14. The alloy-scale interface and the interface between the two sulfide layers were essentially plane. Both sulfide layers, however, showed considerable porosity. According to chemical analysis, the Cu-Ni ratio in the scale was nearly equal to the Cu-Ni ratio in the alloy. The two sulfide layers could not be separated from each other. Therefore, the two layers have not been analyzed separately.

Since the ratio of the thickness of the outer sulfide layer to that of the inner sulfide layer increases with increasing copper content of the alloy, the outer sulfide layer is supposed to be mostly copper sulfide and the inner sulfide layer mostly nickel sulfide.

At 400°C the system Ni-S involves 4 intermediate phases which may be characterized by the approximate formulas Ni_3S_2, Ni_7S_6, NiS, and NiS_2 (13, 49). According to an investigation of the ternary system Cu-Ni-S by Köster and Malfinger (50), the phase Ni_3S_2 dissolves some Cu_2S but probably less than 1 mole % at 400°C.

A tentative schematic representation of the various diffusion processes is shown in Fig. 15 where the occurrence of different sulfides of Ni and Cu is disregarded. Copper and nickel (presumably as ions and electrons) enter the inner sulfide layer I of average composition Ni_yCu_zS and migrate outward. At the interface between the two sulfide layers, most of the arriving nickel ions, some copper ions, and electrons combine with sulfur ions from the outer layer II, Cu_xS, to form Ni_yCu_zS. In the outer Cu_xS layer, copper ions and electrons migrate to the surface and react with sulfur in order to form Cu_xS. In accord with experimental results, it is assumed that Cu and Ni enter the scale and migrate across layer I at the same ratio at which Cu and Ni are present in the alloy. Since the concentration of Cu in layer I is presumably much lower than the concentration of Ni, the mobility of Cu must be sufficiently greater than the mobility of Ni. This is

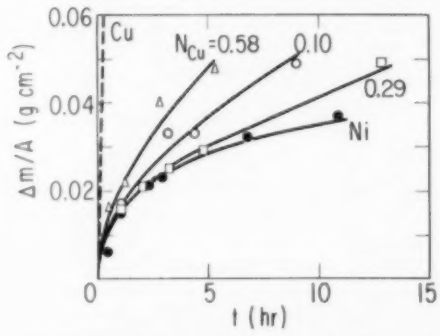

Fig. 13. Weight gain plot for Ni-Cu alloys sulfidized at 400°C.

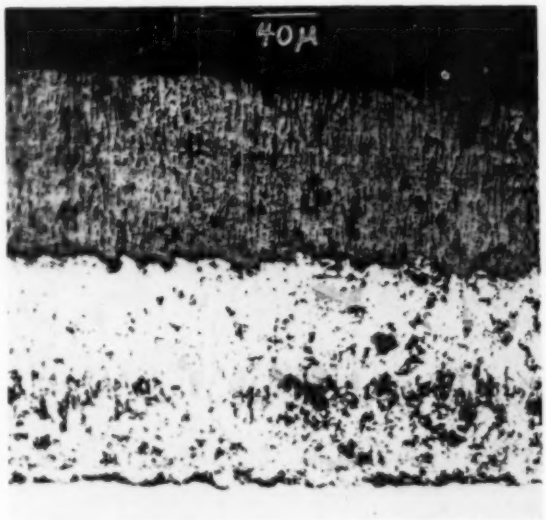

Fig. 14. Section of Ni-Cu alloy ($N_{Cu} = 0.58$) sulfidized at 400°C for 100 hr.

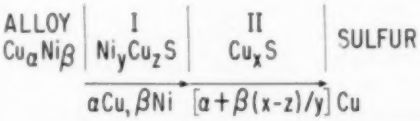

Fig. 15. Schematic representation of diffusion processes in the scale on Ni-Cu alloys exposed to sulfur at 400°C. Reaction at the Ni_yCu_zS-Cu_xS interface: αCu (in Ni_yCu_zS) + βNi in $(Ni_yCu_zS) + (\beta/y)Cu_xS = (\beta/y)\ Ni_yCu_zS + [\alpha + \beta(x-z)/y]$ Cu (in Cu_xS).

in accord with other observations according to which the mobility of monovalent ions is considerably greater than that of ions carrying a higher electrical charge.

Sulfidization of Ag-Cu Alloys

Samples of Ag-Cu alloy of eutectic composition are sulfidized in liquid sulfur at 400°C at about the same rate as the pure components. The size of the samples were 0.9 x 1.5 x 0.3 cm with a total initial surface area of 4 cm^2. The weight gains after 4, 9, 16, and 25 min were 0.369, 0.553, 0.565, and 0.660 g, respectively. The last sample was sulfidized completely. Microscopical examination of sectioned samples revealed a single sulfide layer with only minor irregularities at the alloy-sulfide interface.

Since the standard free energy of formation of Cu_2S is about twice that of Ag_2S, preferential sulfidization of copper may be expected. Actually, however, Ag and Cu enter the scale at the ratio at which they are present in the alloy as has been ascertained by chemical analysis. Presumably, the scale consists of solid solutions of the quasi-binary systems Ag_2S—Cu_2S and Ag_2S—$Cu_{1.8}S$. Various observations suggest considerable mutual solubilities (51, 52). However, complete miscibility is impossible since the terminal phases of these systems have incompatible structures at 400°C. Ag_2S has a body-centered cubic sulfur sublattice (28), Cu_2S II is hexagonal (29), and $Cu_{1.8}S$ has a face-centered cubic sulfur sublattice (28, 29).

Conclusions

High-temperature oxidation of pure metal yields, in general, oxide or sulfide layers of uniform thickness with diffusion in the scale as rate-determining step as an important limiting case. When an alloy rather than a pure metal is oxidized, one component of the alloy may be oxidized preferentially. In view of differential oxidation, diffusion processes take place in both the alloy and the scale. In special cases, the over-all ratio of the components in the scale may be the same as in the alloy, but the local ratio of the components in the scale may vary with distance from the outer surface. In addition to homogenous layers, there may occur two-phase layers either consisting of alloy enriched with respect to the more noble component and an oxide or sulfide of the less noble metal, or consisting of two oxides or sulfides of different metals. In the present research, typical examples from a large variety of possible situations have been found. The exploration of the decisive factors has been stressed. Many details have not yet been fully clarified.

Sulfidization of Cu-Au and Ag-Au alloys involving low Au contents, e.g., 10 a/o Au yields a composite scale consisting of an outer homogeneous sulfide layer and an inner two-phase layer involving Au-rich alloy and sulfide. This is in accord with theoretical considerations according to which a plane alloy-sulfide interface is not stable since the interdiffusion coefficients in the alloy are much lower than the diffusivities in the sulfide phases (2). At higher Au contents the tendency to form a rugged interface decreases especially at lower temperatures. At intermediate Au contents, local sulfide penetrations occur particularly at grain boundaries. Finally, Au-rich alloys may yield a nearly plane alloy-sulfide interface with only minor irregularities. The gradual change in the structure of the scale is reflected by a gradual decrease in the rate of attack. Alloys involving low Au contents are attacked very rapidly at about the same rate as the pure base metals since trunks of Au-rich alloy in the two-phase scale do not change the diffusion resistance of the sulfide to a large extent. In contrast, Au-rich alloys are attacked very slowly presumably with diffusion of Ag or Cu to the alloy-sulfide interface as the rate-determining step.

Silver-copper alloys also yield a sulfide layer of uniform thickness, in which the ratio of the components is the same as in the alloy in spite of the large difference in the standard free energies of formation of Ag_2S and Cu_2S. Thus only diffusion in the sulfide layer is essential and accordingly the rate of attack is about as high as that of pure Ag or Cu.

In contrast, Ni-Cu alloys immersed in liquid sulfur yield two sulfide layers. The outer layer is supposedly digenite $Cu_{1.8}S$, and the inner layer a solid solution involving nickel sulfide as solvent and Cu_2S as solute. The over-all Cu/Ni ratio in the scale is virtually the same as in the alloy. Thus only diffusion in the scale is essential. Both nickel and copper migrate presumably across the inner sulfide layer which grows by a displacement reaction between nickel ions, electrons, and copper sulfide.

Acknowledgment

This paper is based on a thesis submitted by B. D. Lichter in partial fulfillment of requirements for the degree of Sc.D. in metallurgy, Massachusetts Institute of Technology, Cambridge, Mass.

Research has been sponsored by the National Science Foundation and by Office of Ordnance Research, U. S. Army, under Contract DA-19-020-ORD-3661. The authors want to express their thanks to D. L. Guernsey for chemical analyses.

Manuscript received April 3, 1959.

Any discussion of this paper will appear in a Discussion Section to be published in the December 1960 JOURNAL.

REFERENCES

1. C. Wagner, *This Journal*, **99**, 369 (1952).
2. C. Wagner, *ibid.*, **103**, 571 (1956).
3. H. Braune and O. Kahn, *Z. physik. Chem.*, **112**, 270 (1924).
4. C. Tubandt, H. Reinhold, and W. Jost, *Z. anorg. u. allgem. Chem.*, **177**, 253 (1928).
5. E. Hirahara, *J. Phys. Soc. Japan*, **6**, 421, 428 (1951).
6. R. L. Allen and W. J. Moore, *J. Phys. Chem.*, **63**, 223 (1959).
7. H. Braune, *Z. physik Chem.*, **B110**, 147 (1924).
8. W. Jost, *ibid.*, **B9**, 73 (1930).
9. C. Matano, *J. Phys. Soc. Japan*, **9**, 41 (1934).
10. W. Jost, *Z. physik. Chem.*, **B16**, 123 (1932).
11. W. A. Johnson, *Trans. Am. Inst. Mining Met. Engrs.*, **143**, 107 (1941).
12. H. Ebert and E. Trommsdorf, *Z. Elektrochem.*, **54**, 294 (1950).
13. M. Hansen and K. Anderko, "Constitution of Binary Alloys," McGraw-Hill Book Co., Inc., New York (1958).

14. J. S. Smart and A. A. Smith, Jr., *Trans. Am. Inst. Mining Met. Engrs.*, **166**, 144 (1946).
15. J. S. Maclaurin, *J. Chem. Soc. (London)*, **69**, 1269 (1896).
16. L. Czerski and S. Patzau, *Arch Gornictwa i Hutnictwa*, **2**, 354 (1954).
17. M. Billy and G. Valensi, *J. chim. phys.*, **53**, 832, 843 (1956).
18. W. J. Moore, *ibid.*, **53**, 843 (1956).
19. H. Rickert, *Z. physik. Chem. N.F.*, in press.
20. R. F. Bacon and R. Fanelli, *J. Am. Chem. Soc.*, **65**, 639 (1943).
21. L. B. Pfeil, *J. Iron Steel Inst.*, **119**, 501 (1929).
22. B. W. Dunnington, F. H. Beck, and M. G. Fontana, *Corrosion*, **8**, 2 (1952).
23. H. Engell and F. Wever, *Acta Met.*, **5**, 695 (1957).
24. J. D. Mackenzie and C. E. Birchenall, *Corrosion*, **13**, 783t (1957).
25. D. W. Juenker, R. A. Meussner, and C. E. Birchenall, *ibid.*, **14**, 39t (1958).
26. R. A. Meussner and C. E. Birchenall, *ibid.*, **13**, 677t (1957).
27. R. Bakish and W. D. Robertson, *Trans. Am. Inst. Mining Met. Engrs.*, **203**, 424 (1955).
28. P. Rahlfs, *Z. physik. Chem.*, **B31**, 157 (1936).
29. N. W. Buerger, *Econ. Geol.*, **36**, 19 (1941).
30. M. J. Buerger and N. W. Buerger, *Am. Mineralogist*, **29**, 55 (1944).
31. W. Rühl, M. Sc. Thesis, University of Erlangen, 1952, private communication.
32. Gmelins Handbuch der anorganischen Chemie, Kupfer B, pp. 432 ff., Verlag Chemie, Weinheim (1959).
33. S. Djurle, to be published.
34. G. Preuner and I. Brockmüller, *Z. physik Chem.*, **81**, 129 (1913).
35. E. T. Allen and R. H. Lombard, *Am. J. Sci.*, (4) **43**, 175 (1917).
36. W. Biltz and R. Juza, *Z. anorg. u. allgem. Chem.*, **190**, 161 (1930).
37. J. D. Harrison and C. Wagner, to be published.
38. C. Wagner, *Z. physik. Chem.*, **B21**, 25 (1933).
39. H. Reinhold and H. Seidel, *Z. Elektrochem.*, **41**, 499 (1935).
40. L. Czerski, S. Mrowec, K. Wallisch, and T. Werber, *Arch. Hutnictwa*, **3**, 49 (1958).
41. C. Wagner, *Z. physik Chem.*, **B32**, 447 (1936).
42. C. Wagner, "Diffusion and High Temperature Oxidation of Metals" in "Atom Movements," pp. 153-173, American Society for Metals, Cleveland, Ohio (1951).
43. C. Wagner, *J. Chem. Phys.*, **21**, 1819 (1953).
44. N. B. Pilling and R. E. Bedworth, *J. Inst. Metals (London)*, **29**, 529 (1923).
45. C. Wagner, "Thermodynamics of Alloys," pp. 108 ff., Addison-Wesley Press, Cambridge, Mass. (1952).
46. K. Kiukkola and C. Wagner, *This Journal*, **104**, 379 (1957).
47. J. L. White, R. L. Orr, and R. Hultgren, *Acta Met.*, **5**, 747 (1957).
48. K. Hauffe and A. Rahmel, *Z. physik. Chem.*, **199**, 152 (1952).
49. T. Rosenquist, *J. Iron Steel Inst. (London)*, **176**, 37 (1954).
50. W. Köster and W. Malfinger, *Z. Elektrochem.*, **46**, 135 (1940).
51. C. Tubandt and H. Reinhold, *Z. physik. Chem.*, **A140**, 291 (1929).
52. N. G. Schmahl, *Angew. Chem.*, **65**, 447 (1953).

Influence of Electrode Surface Conditions on the Electrical Strength of Liquified Gases

D. W. Swan and T. J. Lewis

Electrical Engineering Department, Queen Mary College, London, England

ABSTRACT

The strengths of liquified argon, oxygen and nitrogen are of the order of 1 mv/cm but are found to depend to a marked degree on the nature of the electrode surfaces. The strength can be changed in a regular manner (sometimes by as much as 50%) by changing both the electrode metal and the degree of surface oxidation. The important discovery is that the *anode* as well as the cathode has a strong influence on the strength. This surprising result has, as yet, no obvious explanation in terms of usual breakdown mechanisms but may be very significant, not only for theories of breakdown in these liquids but for hydrocarbon liquids as well.

Studies of the electric strength of liquid dielectrics have been concerned almost exclusively with organic materials because of their practical importance as electrical insulation. Insulating oils are mixtures of complex hydrocarbons in which trace compounds can have a strong influence and, in an endeavor to simplify the studies, less complex hydrocarbons such as pure n-paraffins have been investigated extensively (1). Even for these liquids, the molecules are complex, purification is complicated, and electrode conditions difficult to assess. In addition, discharges attendant on measurements of the electric strength cause gas evolution, carbon and other deposits, and seriously disturb the electrode surfaces. Because of these difficulties, the major discharge processes cannot be studied accurately in the liquid phase. There are, however, other much simpler dielectric liquids without these disadvantages in which breakdown mechanisms can be more easily understood, and which offer the opportunity for much more precise and controlled measurements. These are liquified gases and, although they are of no importance as practical insulants, much information can be gained from them which helps in understanding the processes occurring in the organic liquids.

Of the possible liquified gases, argon, oxygen, and nitrogen are most suitable for study since they may be easily obtained by condensation. Argon is ideal

because it has a simple atomic structure and is inert; other rare gases are not so convenient since they are more expensive and not easily liquified. Oxygen and nitrogen can also be obtained with reasonable purity and are simple diatomic gases with distinctive properties. All these should produce negligible by-products when electrical breakdown occurs because the discharge merely creates gas which then recondenses. In the case of oxygen, oxidation reactions may be caused on the electrodes and surface reactions may also occur with nitrogen, but the possible processes will be few compared with those in hydrocarbons. These three liquids also possess other advantages for breakdown investigations. Thus argon does not react with the electrode surfaces and electrons will remain free in it. Oxygen readily forms negative ions, thereby trapping electrons, and also encourages surface reactions at the electrodes, especially in the craters formed by previous discharges. Nitrogen is not inert but is only slightly reactive compared with oxygen. Each liquid, therefore, produces different discharge conditions, and there is also the possibility of investigating, for example, argon with a small admixture of oxygen, so reducing the number of free electrons in the argon.

The electric strengths of these liquids have been investigated on a limited scale already by Kronig and Van de Vooren (2) who obtained values between 860 and 1040 kv/cm depending on the electrode material. No other measurements of electric strength have been made, and there is only one measurement of natural conductivity at high electric stress for liquid oxygen by Pao (3). Induced conduction has been fairly well studied, however; the liquids being irradiated with x-rays or α particles (3-9). This work has given data on ion mobilities in these liquids and has clearly demonstrated that oxygen and also nitrogen can quench electron bursts in argon by forming negative ions of low mobility. A concentration of 0.7% oxygen in liquid argon was sufficient to quench all electron pulses, but a 15% concentration of nitrogen was required for the same effect. Clearly, electrons are not likely to remain free in liquid oxygen or nitrogen except, perhaps, at the highest fields approaching the electric strength when electron detachment may occur.

The work reported here represents an initial investigation into the strength of these liquids with the intention of estimating the role of the electrode surfaces in determining the strength. It is more extensive and of greater precision than that of Kronig and Van de Vooren (2). Techniques already used for reliable measurements on hydrocarbons have been employed. It will be shown that electrode effects are dominant in argon, and this may have important implications in the studies of breakdown in hydrocarbons.

Equipment and Procedure

A diagram of the test cell arrangement is shown in Fig. 1. It consists of a long glass tube, A, sealed at the lower end and flanged at the top. The electrode mounting B is rigidly fixed at one end of a stainless steel tube C which, in turn, is sealed to a metal flange D at the top. The vacuum sealed high voltage connection E is led through tube C and terminates in a small bushing at the lower fixed electrode. The other earthed electrode with its connector F is fixed to a stainless steel shaft, G, which can be moved vertically by a micrometer H. A vacuum seal is maintained by a metal bellows J joining G and D. The flanges D and A are then sealed by an o-ring joint which also locates the electrode assembly at the lower end of the cell. Gap adjustment between the 0.5-cm diameter spherical electrodes can be made to within $\pm$ 1 μ, i.e., with $\pm$ 2% error for a 50-μ gap, and is checked several times during an experiment in order to compensate for any temperature changes. Zero gap is obtained by using a sensitive detector as already described (10). Gas is admitted via K and caused to condense by placing liquid oxygen or nitrogen in the outer Dewar vessel L. The test cell is of sufficient length above the Dewar vessel for the top flange D and micrometer to remain at room temperature during experiments. By using liquid oxygen in L when condensing oxygen and liquid nitrogen for nitrogen condensation, it is possible to effect a slow and controlled condensation with adequate temperature control. Liquid argon, which has a small temperature range (84°-87°K) is obtained by boiling liquid oxygen in L at a controlled rate at reduced pressure. Normally the cell is filled with liquid to a level just below the lower edge of B and this requires only 15 cc of liquid, i.e., about 45 liters of gas at N.T.P. In all experiments equilibrium conditions were obtained by allowing 1 hr to elapse after condensation before making measurements.

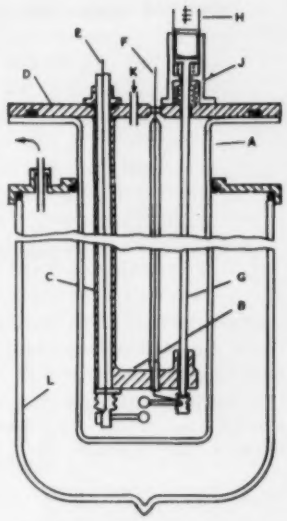

Fig. 1. Diagram of test cell

The temperature and pressure in the cell could be measured but, as Kronig and Van de Vooren have found, small pressure changes do not affect the strength. In the present series of experiments, the liquids were always in contact with their saturated vapors. For reasons given above, the temperatures were sensibly constant and are given in Table I.

The gas to be tested was passed through a P_2O_5 drying tube and a sintered glass filter of 1-μ pore

Table I. Data for gases used

	Argon	Oxygen	Nitrogen
Boiling point at atmospheric pressure, °K	87.3	90.2	77.3
Purity, %	99.95	99.5	99.9
Significant impurities, vpm	N_2 <500 O_2 <20 H_2 <10	H_2 <50 Carbon compounds <15	O_2 <10 Carbon compounds <15

size to remove dust particles. The purity of the gases is given in Table I and it is important to note that argon and nitrogen contained traces of oxygen. Since a slight internal positive pressure was maintained in the system, which was in any case vacuum tight, it is improbable that any further gas contamination occurred.

A 25 kv fully stabilized direct voltage source capable of very fine control was used for the measurements, and the voltage applied to the electrodes was measured by recording the current through a 1000 M ohm high stability resistor connected across the electrodes. The absolute error in voltage measurement was <2% and relative values could be obtained with much less error than this. When breakdown occurred the current flow was limited by using a fast electronic by-pass circuit of a type already described (10). This was capable of discharging the stored energy of the voltage supply within 1 μ sec of breakdown and so limited the energy dissipated in the liquid to the residual associated with the test cell capacitance. There was, therefore, minimum gas evolution and electrode damage. This permitted repeated measurements to be made on the same electrode surfaces without significant deterioration. Operation of the diverter also indicated breakdown without need for visual observation of the spark. Kronig and Van de Vooren report observing occasional very low electric strengths which they attribute to gas bubbles on the electrodes. Since they did not divert the discharge energy and low strengths have not been observed in the present work, their deduction seems correct.

The techniques adopted for electrode preparation were similar to those found to be reliable with hydrocarbons (1, 11). Surface scratches and previous discharge damage were removed by buffing the electrode on a rough mop with polishing compound. This was followed by further polishing on finer mops until the surface was smooth when viewed under a microscope of magnification X150. Polishing material was then removed by washing in hexane; then a soft mop, free of grease, was used to prepare the final surface. At this stage the surface was comparatively free of grease and heated by the polishing process so that initial oxidation occurred rapidly. Further oxidation could then be arrested by washing the electrodes in dust-free hexane (11). For certain measurements to be described, various oxidation thicknesses on oxidizing metals were required; these were obtained by delaying the wash in hexane and allowing the electrodes to remain for predetermined times in dry air in a dessicator. Oxidation times were then taken as measures of oxidation thickness, with zero time and minimum thickness arbitrarily chosen to correspond to that involved in directly transferring the electrodes from the final mop to hexane without delay.

The electrodes were then transferred to the test cell and washed again in dust free hexane. Finally, the whole test cell assembly was evacuated to a pressure of 10^{-5} mm Hg for a period of 18 hr to remove hexane vapors and other volatile impurities. Before condensing the gas to be tested, the cell was flushed with a sample of the same gas and re-evacuated for a short while.

Electric Strength

Electric strengths of the three liquids were measured using both stainless steel of zero oxidation

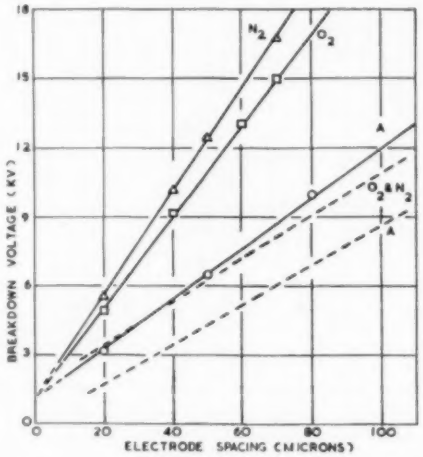

Fig. 2. Breakdown voltage vs. electrode spacing with platinum electrodes. O, Argon; □, oxygen; △, nitrogen. - - - Results from ref. (2).

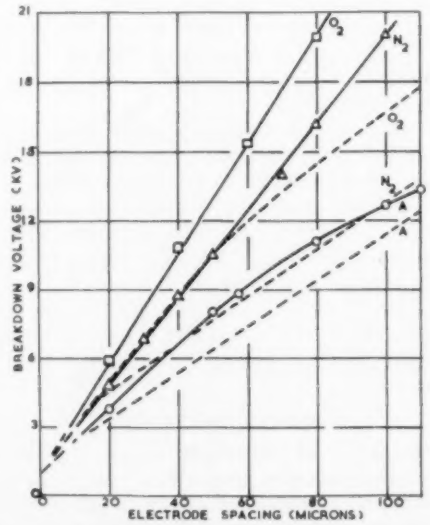

Fig. 3. Breakdown voltage vs. electrode spacing with stainless steel electrodes. O, Argon; □, oxygen; △, nitrogen. - - Results from ref. (2).

Table II. Mean strengths for liquified gases (mv/cm)

	Platinum electrodes		Stainless steel electrodes	
	from Fig. 2	from ref. (2)	from Fig. 3	from ref. (2)
Argon	1.10	0.86	1.42	1.00
Oxygen	2.00	0.93	2.38	1.04
Nitrogen	2.26	0.93	1.88	1.00

time, and platinum electrodes, in order to make direct comparison with the values obtained by Kronig and Van de Vooren. Results for a range of electrode spacings are given in Fig. 2 and 3, together with the earlier results. The coefficient of variation was found to be less than 10%. Mean strengths for the liquids, obtained from the slopes of the plots, are given in Table II. In the case of argon with stainless steel electrodes, which had been subjected to a glow discharge in hydrogen in order to reduce the oxide layer still further, a linear plot is not obtained, and the value shown in Table II is the slope for the smaller electrode spacings. The new values are higher than the previous ones in all cases. This may be due to the use of 0.5-cm diameter spherical electrodes rather than the 1-cm diameter sphere-plane arrangement used by Kronig and Van de Vooren, or to the use of the energy diverter; but, as will be shown below, the difference could be ascribed to electrode surface conditions. Argon has the lowest strength with either electrode material, but nitrogen is either stronger or weaker than oxygen according to whether platinum or stainless steel electrodes are employed (2). Good reproducibility of these results was obtained except for nitrogen with stainless steel electrodes. For this gas, results for different samples could not always be repeated even though the techniques were maintained constant. Values given in Fig. 3 are the most probable ones obtained from a large number of experiments. Similar difficulties have been found with electrical discharge measurements on nitrogen gas on a previous occasion (12), and at the moment there is no explanation of the effect. The nonlinear plot for argon and stainless steel suggests that the strength of argon for really large spacings ($> 100\ \mu$) would be much less than that quoted in Table II, and any increase for smaller spacings may be due to the influence of the electrodes, but more measurements are required to prove this.

In view of the earlier evidence from α-particle and γ-ray induced conductivity (3-9) it is expected that in argon, at least, a small percentage of oxygen (or somewhat greater amounts of nitrogen) should alter the pre-breakdown state by quenching avalanche discharges and causing electrons to attach to form negative ions. These ions would be transported to the anode and an ion concentration built up there. Although the ionization potential of oxygen (12.2 ev) is less than that of argon (15.8 ev), this does not appear to be important in deciding the strength of the liquid since addition of oxygen to argon raises the strength. For instance, addition of 20% oxygen to argon raised the strength from 1.66 to 2.42 mv/cm for a 40-μ gap with stainless steel electrodes. This is an increase of 45% but is still less than the strength of pure oxygen. In order to reveal any electrode effect in this process, stainless steel electrodes were rendered oxide-free by glow discharge and used to measure the strength of liquid argon both before and after a small quantity of oxygen had been added. Measurements of the strength at 1-min intervals showed a gradual increase amounting in all to nearly 30% over a period of 25 min. Addition of a much larger quantity of oxygen at the end of this period caused an immediate further increase of about 10%. These results suggest that the initial gradual increase could be associated with electrode oxidation and the later one with attachment processes in the bulk of the liquid.

Electrode Effects

It is obvious from the experiments described that a strong electrode influence exists. This has been further studied in two ways, both of which are described briefly. In the first, the influence of electrode metal prepared with a zero oxidation time was found for each gas. Plots similar to those of Fig. 2 and 3 were made for a range of electrode spacings and the electric strengths found as before. These strengths, given in Table III, can be changed by almost 100% by a change of electrode material. There is no correlation with work function; in fact, the order of increasing strength for the different metals is not the same for each gas even with electrodes of gold or platinum which should provide stable surfaces. Gold gives a higher strength than platinum for argon but not for oxygen or nitrogen. In any relationship between strength and cathode emission properties, platinum, having a higher work function than gold, might be expected to give a higher strength especially in argon which is inert. It is in this liquid, however, that the lower strength is found.

The next series of experiments, using argon because of its inertness, involved electrodes having various degrees of oxidation obtained by the method already outlined. Figure 4 shows the influence of this oxidation time. Each point is the mean strength found from plots similar to Fig. 2 or 3 and thus represents a large number of measurements. As expected, neither gold nor platinum produce any variation with oxidation time whereas stainless steel and brass, which oxidize readily, cause a large change. For these oxidizing metals the strength reaches a maximum after oxidation times of 15 and 70 min, respectively. Larger oxidation periods than these, i.e., greater thicknesses of oxide, cause a gradual decline in strength, and shorter times giving thinner layers also lower the strength.

The initial rise to the peak could be associated

Table III. Mean strengths as a function of electrode material

Electrodes	Work function, ev	Electric strength, mv/cm		
		Argon	Oxygen	Nitrogen
Stainless steel	—	1.40	2.38	1.88
Brass	—	1.01	1.44	1.62
Copper	4.47	1.40	1.81	—
Gold	4.58	1.16	1.24	1.50
Platinum	5.29	1.10	2.00	2.24

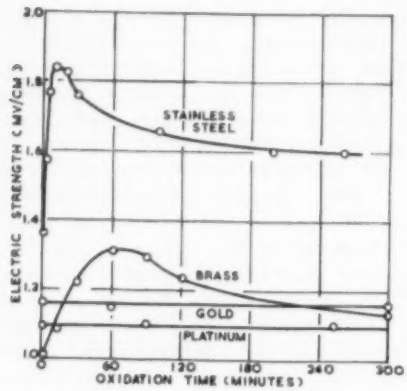

Fig. 4. Effect of electrode oxidation time on mean electric strength of argon.

with a decrease in electron emission resulting from an increase in work function caused by oxide growth. Any increase in work function in this way might be offset by a decrease caused by positive ions produced in the discharge processes coming back to this oxide layer (13). The over-all cathode emission would be determined by these opposing effects and, as the oxide layer thickened beyond a certain value, it is possible for the positive ion layer to increase in effectiveness because of the insulating properties of the oxide which would hinder ion neutralization.

For the whole range of oxidation times, therefore, the emission might initially decrease and then increase again, and if electric strength was directly related to emission, the curves in Fig. 4 are reasonable. This would be a plausible mechanism if the behavior were found to be independent of the anode, but unfortunately this is not the case. By using mixed electrodes, it has been possible to show an anode dependence also. For example, with a stainless steel anode and an aluminum cathode, the strength was practically the same as for two stainless steel electrodes, but reversal of the polarity gave a strength equal to that for aluminum electrodes. In other experiments using gold anodes and stainless steel cathodes, it was possible to change considerably the effect of oxidation time from that shown for stainless steel in Fig. 4. Thus, any mechanism of breakdown in liquid argon must include the role of the anode as being of great importance.

Conclusion

These results and others not reported indicate that the "intrinsic" strengths of the three liquified gases have not, in fact, been measured. It may well be that electrode effects will always prevent this being achieved with any certainty. The breakdown stresses are $\sim 10^6$ v/cm so that electron emission from the cathode might be expected, but it should be borne in mind that at temperatures of $\sim 90°K$ Schottky field-aided thermionic emission, which is considered to be significant for liquid breakdown at room temperature, will be negligible. At the same time the field strength does not seem to be large enough for appreciable cold field emission. Measurements of the natural conductivity of liquid argon at 10^6 v/cm confirms this since no detectable current was found. Nevertheless, individual microscopic sites might emit more freely and would then increase the probability of breakdown in these regions. The number and activity of the sites would depend on cathode material and preparation and on the incidence of positive ions generated by discharge processes as already outlined.

It is very much more difficult to suggest processes by which the anode conditions might influence the electric strength, especially when the emission from the cathode is feeble and probably confined to microscopic sites. The normal concepts of gas breakdown which we may tentatively employ here involve primary electron avalanche or α processes, followed by secondary mechanisms in the gas or at the cathode surface. In particular, positive ions produced by the avalanches may yield secondary electrons at the cathode (γ process). This mechanism does not, however, include the anode at all. If the anode is to be important, it is necessary that positive ions should be generated at the anode at a rate controlled by the conditions there and that the yield of positive ions from the rest of the liquid should be small. Two processes seem possible but there may be others. In both, the presence of oxygen in small amounts in the liquid is required in order that electrons emitted from the cathode have a good chance of forming negative ions. A negative ion approaching the anode creates a strong local field which will act across any oxide layer present, so increasing the probability either of ionization of any adsorbed molecules on the oxide layer (including neutralized oxygen ions), or of direct extraction of positive metal ions through the oxide as in an oxidation process. Ions created in this way then proceed to the cathode and by a γ process yield further electrons with the consequent possibility of a breakdown instability. An alternative process which requires positive ions to be produced by avalanches is as follows. The formation of negative oxygen ions serves to transport oxygen to the anode where the ions are neutralized. A concentration of oxygen will then build up in the immediate anode neighborhood to an equilibrium controlled by the availability of electrons and ease of neutralization of the ions. This oxygen-rich anode layer will now have a marked influence on positive-ion production which, according to avalanche growth, should be greatest in the same region. Both processes require the existence of negative ions which, for argon liquid, means the presence of an oxygen impurity. Further experiments on nitrogen and oxygen liquids need to be made to see whether anode effects are present in these liquids also.

The attachment properties of oxygen may also be responsible for the apparent intercept on the voltage axis found in Fig. 2 and 3. While this may be ascribed to the presence of a Paschen minimum as in gases, occurring for spacings of less than about 1 μ, it could also be due to an oxygen and oxygen ion layer at the anode of, perhaps, the same order of thickness. As the electrode spacing is reduced, so this layer exerts a proportionally greater influence on

the strength. It is significant that similar intercepts are found for hydrocarbon liquids containing oxygen (1).

The role of oxygen, therefore, seems the same for liquified gases and hydrocarbon liquids. The electrode effects found with the former may also exist for the latter. The present investigation is valuable in suggesting effects which may well be present in hydrocarbons, but which are masked by the more numerous side effects. Work is proceeding to discover whether this is so. Measurements in compressed gases similar to that already undertaken (14) would also be very valuable and should yield closely related information to that given here.

Acknowledgment

The authors are grateful for the generous financial assistance from the British Electrical and Allied Industries Research Association enabling equipment to be purchased. Thanks are also due to Professor M. W. Humphrey Davies for the facilities provided and for encouragement, and to the Department of Scientific and Industrial Research for a maintenance grant to one of us (D.W.S.). Dr. A. E. Guile was responsible for much of the early design of the test cell and his considerable help is acknowledged.

Manuscript received Nov. 2, 1959. This paper was prepared for delivery before the Philadelphia Meeting, May 3-7, 1959.

Any discussion of this paper will appear in a Discussion Section to be published in the December 1960 JOURNAL.

REFERENCES

1. T. J. Lewis, *This Journal*, **107**, 185 (1960).
2. R. Kronig and A. I. Van de Vooren, *Physica*, **9**, 139 (1942).
3. C. S. Pao, *Phys. Rev.*, **64**, 60 (1943).
4. G. W. Hutchinson, *Nature*, **162**, 610 (1948).
5. N. Davidson and A. E. Larsh, *Phys. Rev.*, **74**, 220, (1948); *ibid.*, **77**, 706 (1950).
6. A. N. Gerritsen and J. Koolhaas, *Physica*, **10**, 49 (1943).
7. A. N. Gerritsen, *ibid.*, **14**, 381 (1948).
8. R. L. Williams, *Can. J. Phys.*, **35**, 134 (1957).
9. R. L. Williams and F. D. Stacey, *ibid.*, **35**, 928 (1957).
10. T. J. Lewis, *Proc. Inst. Elec. Engrs. (London)*, **100**, Pt. IIa, 141 (1953).
11. R. Hancox, *Brit. J. Appl. Phys.*, **8**, 476 (1957).
12. G. A. Kachickas and L. H. Fisher, *Phys. Rev.*, **88**, 878 (1952).
13. W. B. Green, *J. Appl. Phys.*, **26**, 1259 (1955); *ibid*, **27**, 921 (1956).
14. A. H. Sharbaugh and P. K. Watson, Annual Rep. Conf. on Elec. Insul. 1957 Meeting p. 32, Nat. Acad. Sci., Nat. Res. Council (1958).

Molecular Structure and the Electrical Strength of Liquid Hydrocarbons

T. J. Lewis

Electrical Engineering Department, Queen Mary College, London, England

ABSTRACT

It is suggested that electrons moving through hydrocarbon liquids are able to excite molecular vibrations of infrared frequencies, and that this provides an effective energy loss mechanism. The relative magnitudes of this loss may be estimated for a wide range of hydrocarbons and other liquids and can be used in a criterion of breakdown. Thus the electrical strengths of these liquids measured under standard conditions may then be compared with their molecular structures. A good correlation is found.

In recent years the electric strength of a large number of hydrocarbon liquids has been measured using microsecond pulse and continuous voltages. The results published are reliable in that they are repeatable, but they do not represent the intrinsic strengths because of several influences, such as electrode effects, inherent in the measurements. In spite of this, the experiments have demonstrated that the strength is dependent on the molecular properties of these hydrocarbons and quite small changes such as that from hexane to heptane or to isopentane produce a significant effect. Because of the work of Sletten (1) of this laboratory, who has demonstrated that dissolved oxygen increases the strength of n-hexane considerably, it is now realized that the attainment of the highest strengths may not indicate the closest approach to the intrinsic value. As discussed below, many measurements already made must have been influenced strongly by oxygen in solution and, for this reason alone, it is timely to re-examine the relationship between electric strength and molecular structure. This has been discussed in various ways already (2-6) and in this paper the earlier ideas are re-stated concisely in a criterion which permits the molecular influence to be separated from the other factors. Any simple criterion of this sort is open to detailed criticism but, since the theory of breakdown is by no means clarified, the adoption of a simple criterion is advantageous. Having established the criterion, its validity will be examined using experimental results.

Basic Processes

The electric strength of a simple hydrocarbon liquid is considered to be determined by the onset of an instability initiated by the primary processes of electron emission from the cathode and electron multiplication or associated charge accumulation in the bulk of the liquid (2). These processes are

likely to be inter-related and secondary effects arising from impurities or from the measuring technique (7) may also occur. It is then difficult to separate the primary processes by measurements of the electric strength except under special conditions. Stresses greater than 10^6 v/cm are reached in these liquids before breakdown occurs, and it is commonly accepted that field extraction of electrons from the cathode must be occurring (8, 9): a major component of the infra-breakdown conduction current arising from these emitted electrons. Excluding impurities, the mode of conduction is then either by quasi-free electrons or negative ions formed by attachment and at the highest fields possibly by positive ions produced by collision ionization. The mobilities and energies of these particles depends on the collision characteristics of the liquid so that once an electron is emitted the subsequent processes are governed by the liquid and dependence on molecular properties may be expected.

Cathode Mechanisms

If the strength is to be related to liquid properties, the cathode should either play a consistent or else a negligible part in the breakdown process. Evidence from the literature suggests that the cathode effect may be both erratic and elusive, some authors reporting a dependence on electrode material and others not. The electrode surfaces in all cases is covered by complex and perhaps insulating layers of oxide, gas, and other adsorbed impurities. Charge transported to such surfaces can build up electric double layers strongly influencing the emission and preventing any direct relationship between it and the work function of the pure cathode metal. Green (8) has suggested that positive ions deposited on the cathode from the liquid are responsible for enhanced emission in n-hexane and has found a definite dependence on electrode metal and degree of oxidation.

The strengths achieved when measurements are made with pulse voltages of sufficiently short duration depends on the degree of electron availability, and cathode conditions are then important. This situation is analyzed by Ward and Lewis (7), and Hancox and Tropper (10) have also reported an effect of this kind in which cathode oxidation altered the impulse strength of transformer oil.

The relative importance of the control exercised by the separate cathode and liquid processes also determines the degree of electrode dependence. For breakdown both processes need to be above a certain threshold of activity. If the field strength required to promote the liquid mechanisms is high and at the same time the cathode is a good field-emitter, then the breakdown is liquid-controlled and cathode dependence is masked. On the other hand, a liquid of lower "intrinsic strength" with a poor cathode emitter would be expected to show cathode effects. Normal measurements might give either situation as the literature seems to indicate. In Fig. 1 these two conditions are shown by using a point-plane electrode system (11). When the liquid is relatively highly stressed, i.e., the plane negative, a cathode dependence is present, but this

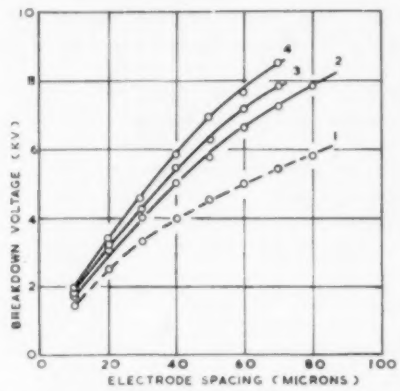

Fig. 1. Breakdown voltage of a point-plane electrode system in n-hexane, Ref. (11). 1. Point cathode, no dependence on electrode material; 2. plane cathode, aluminum electrodes; 3. plane cathode, copper electrodes; 4. plane cathode, chromium electrodes.

disappears when the polarity is reversed. A negative point insures a copious emission and the liquid, being less highly stressed, then controls the breakdown.

Since extensive experiments on various hydrocarbon series have demonstrated already that liquid effects may be observed in some detail it can be concluded that the cathodes were consistent in behavior and able to yield the required emission in these experiments. Any liquid influence on electron emission would remain reasonably constant because of the strong chemical and physical similarities in these hydrocarbon series.

Electronic Processes in the Liquid

As in gaseous or solid phases, an electron gains energy from the applied field and loses it in collisions with molecules. The efficiency of energy transfer in a collision is energy dependent and at low field strengths a stable condition is reached in which only electrons of low energy are accelerated by the field. Although the electron population will contain some electrons of much larger energies, the probability of energies sufficient for ionization will be insignificant. As the field is increased, the distribution will shift to higher energies and ionizing collisions will become more probable. Energy distributions and collision probabilities have long been known for gases (12). In liquids, the complexity of the molecules and the increased density can change the relative importance of various collisions so that these must be reconsidered. The major collision processes are:

(*a*) Elastic. At low field strengths the majority of collisions will be purely elastic involving little energy loss because of the high mass ratio of hydrocarbon molecule and electron.

(*b*) Vibrational. An energy loss, which may not be nearly so important in the gaseous phase unless the molecules are complex, arises from the excitation of molecular vibrations. The vibrations associated with the binding forces are usually in the infrared frequency band and energy quanta in the range 0.1-1 ev are involved. Vibrations excited in this way may couple to other molecules especially when

local order exists. This type of collision is considered to be a major loss process in solid breakdown.

(c) Attachment. Saturated hydrocarbons are not expected to be electronegative, but low-energy electrons could form ionic complexes or clusters by induced polarization of neighboring molecules. These clusters would behave as large ions at low fields, but the electron could be freed by thermal activation or field acceleration at higher fields, leaving the polarized molecular atmosphere behind as in the Wien effect.

(d) Excitation. Excitation transitions in the hydrocarbons requires energy quanta of several electron volts, and the excited molecule can subsequently either emit a photon or for the majority of hydrocarbons stabilize by dissociation (13). Even if photon emission occurred, it would be strongly absorbed by neighboring molecules and would not have the importance found in gas breakdown. The increased density together with the increased number of excitation and ionization levels of the complex molecules will cause the distinct energy gap between excitation and ionization of a gas to be lost in a liquid (14). Consequently, excitation will no longer form such an effective regulating mechanism to limit the ionization process as in gases.

(e) Ionization. Ionization energies are ~10 ev and decrease progressively as any particular hydrocarbon series is ascended. Positive ions of low mobility produced by the collision will disturb the field and cause enhanced emission at the cathode (8). These ions are important in causing a breakdown instability.

Apart from the major processes, electron collisions may also involve impurity molecules and give rise to a variety of effects but for conciseness, only a few of these may be mentioned. Organic impurities such as related hydrocarbons are not likely to upset the breakdown process in the pure liquid; others of a polar nature can induce a low strength. The cleaning techniques adopted reduce the effects of these latter impurities, but their presence in small controlled amounts may be useful in detecting certain breakdown processes. For instance, Darveniza (15) of this laboratory has shown that traces of anthracene cause n-hexane to emit visible light with a photon energy of about 2.5 ev when the breakdown field is approached, thus giving evidence for the presence of electrons of this energy. Water is an important impurity of which most is removed chemically, but some must remain as a trace. In dissociated form it can contribute to the conduction current and is probably regenerated at the electrodes as Plumley has suggested (16). Provided the accepted drying techniques are employed there is no evidence at the moment for it having any strong influence on breakdown.

Another important class of impurity is dissolved gas which introduces additional collision centers having energy levels which may be very different from those of the pure liquid. The excitation and ionization energies of oxygen and nitrogen, which are likely to be dissolved, are greater than the corresponding values for hydrocarbons such as n-hexane so that these transitions in the gases are not likely to occur. The most important effect to be expected is the strong electron attachment of oxygen which is discussed more fully below. The presence of an actual gas phase in the form of bubbles has been considered on many previous occasions especially for oils. Bubbles could easily initiate breakdown, but the majority of evidence suggests that the influence of dissolved gas in simple hydrocarbon liquids is through individual electron-gas molecule collisions rather than bubbles.

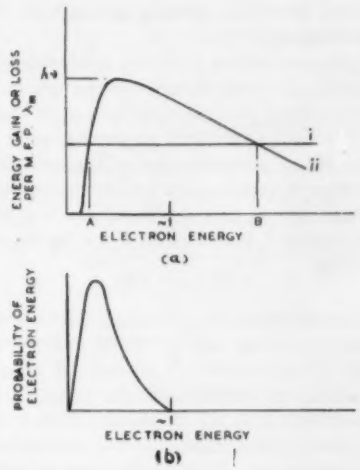

Fig. 2. Energy diagrams for vibrational collisions. (a) Energy balance below breakdown stress (i) energy gain from field E, (ii) energy loss in vibrational collisions of frequency ν; (b) electron energy distribution function corresponding to (a).

Vibrational Collisions

From the assessment above, it is concluded that vibrational collisions account for the major electron energy loss in pure hydrocarbon liquids replacing excitation collisions as the major control of collision ionization. The vibration collision loss can then be used to establish a breakdown criterion similar to that proposed for solids (14, 17). This may be done by reference to Fig. 2a which shows the hypothetical electron energy gain from the field E and loss to molecular vibrations per minimum mean free path λ_m for this collision. It is assumed that the vibration cross section reaches a peak $Q_m = (N\lambda_m)^{-1}$, where N is the number of molecules per cc, for an energy equal to a few multiples of the threshold value. Electrons in the range AB tend to shift in energy toward A, but this is opposed by thermal fluctuations repopulating the higher energy ranges. For a particular applied field below the breakdown value and constant electron emission and absorption at the electrodes, an equilibrium energy distribution is set up characterized by a severe curtailment in the excitation-ionization energy range ~ I(Fig. 2b). As the field is increased, point B moves down and more electrons will be capable of acceleration by the field toward ionization energies, but the increase will be small until the condition B = I is reached. At this field strength, many more electrons are available for acceleration. Thus the condition B = I represents the onset of a significant collision ionization or α process. At still higher fields the condition A = B will be

reached and electrons of any energy are then accelerated towards I.

The α process causes electron avalanches and, by analogy with gas breakdown, we require either that these should grow to a particular size or that an instability through secondary processes such as positive-ion emission enhancement at the cathode should occur. In any of these cases the necessary condition for an instability is that α should reach a minimum value. From Fig. 2, the condition can be expressed as

$$e\,E_m\,\lambda_m = Ch\nu \qquad [1]$$

where E_m is the breakdown field, C (≤ 1) determines the required α value, and $h\nu$ is the energy quantum transferred in a vibration collision of frequency ν. This criterion, or variations, has been utilized by several authors (2-6, 18). It should be noted that C takes account of the experimental conditions (e.g., pulse or continuous voltage measurements) and would be affected by any electrode conditions capable of altering secondary processes and thereby requiring a new α value for an instability. Because of these effects, Eq. [1] is useful for comparing liquids only when C remains reasonably constant throughout the experiments. This seems to have been achieved for the alkanes and alkyl benzenes (2-6). Through Eq. [1] it is possible to relate strength to molecular structure.

Vibration Frequency ν and Minimum Free Path λ_m

Vibration frequencies of the hydrocarbons are restricted to a few bands. Characteristic wave-numbers, determined from infrared spectra, can be associated with the carbon-hydrogen groups and with the skeletal carbon-carbon bonds (Table I). It is well known that these are characteristic of the groups and independent of the rest of the molecules. As the electron energy increases, each mode of oscillation may be excited in turn, but from our concept of the breakdown process and knowledge of the infrared absorption intensities it is expected that the major energy loss will occur in exciting 2960 cm^{-1} vibrations of the CH_1, CH_2, and CH_3 groups. This requires an energy quantum of 0.37 ev. Vibrations of the carbon skeleton in alkanes require a lower energy, and the skeleton is screened by CH bonds so that it is likely to be less effective in causing loss. The same applies to the alkyl radical of the alkyl benzenes. The benzene ring itself is best considered as a single independent group having a highest frequency as in Table I.

The independent behavior of the various groups as shown by their infrared spectra suggests that these hydrocarbon liquids may be considered to a first approximation as dense gas-like phases of the group

Table I. Infrared vibrations of hydrocarbon groups

Group	Wave number, cm^{-1}	Energy quantum, ev
CH_1, CH_2, CH_3	~2960	0.37
CH_2, CH_3	1450	0.18
CH_3	1000	0.12
C-C skeleton	890-1090	0.11-0.14
Benzene ring (CH modes)	~3000	0.37

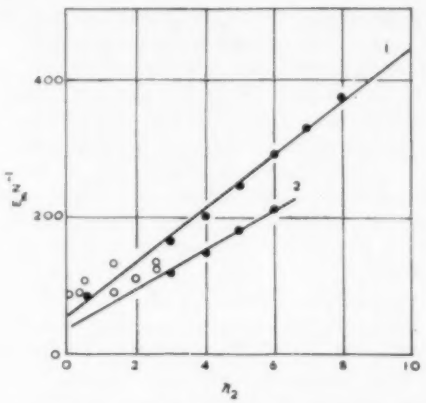

Fig. 3. E_mN^{-1} vs. n_2 for alkanes according to Eq. [4]. Curve 1, from short duration pulse measurements; curve 2, from direct voltage measurements. o Points marked thus are for branched chain alkanes containing the Q_1 cross section.

oscillators, each acting as an independent collision center and having a uniform distribution in the liquid. Thus (2, 4)

$$\lambda_m^{-1} = N\,\Sigma n_i Q_i \qquad [2]$$

where n_i is the number of i^{th} groups per molecule for which the maximum collision cross section for the 2960 cm^{-1} mode is Q_i.

Equation [1] may now be checked against the electric strength determinations reported by Sharbaugh, *et al.* and by Lewis (2-6) in which consistent techniques leading to a constant C were adopted in each series of measurements. Combining Eq. [1] and [2] and writing the constant k to include C and the common frequency of vibration ν then

$$E_mN^{-1} = k\,\Sigma n_i Q_i \qquad [3]$$

If i = 3, 2, 1 refers to CH_3 CH_2 and CH groups, then for n-alkanes C_nH_{2n+2}

$$E_mN^{-1} = k\,(n_2Q_2 + 2Q_3) \qquad [4]$$

i.e., E_mN^{-1} vs. n_2 should give a linear plot of intercept 2 k Q_3 and slope k Q_2 as is indeed confirmed for both sets of measurements in Fig. 3. Results for branched alkanes have been added to Fig. 3 and lie above the linear plot as expected because of the neglect of Q_1 in Eq. [4]. By plotting

$$(E_mN^{-1}n_1^{-1} - k\,n_3Q_3n_1^{-1}) \text{ vs. } n_2n_1^{-1}$$

for the isomers, the expected linear plot is again found which gives an estimate of k Q_1 and a check on k Q_3. It no longer appears necessary to place branched chain isomers on a separate characteristic and to ascribe a new characteristic frequency ν to them as suggested earlier (4). The relative magnitudes of Q_1, Q_2, and Q_3 agree well in the two sets of measurements in spite of the very simplified model.

For n-alkyl benzenes $C_6H_5-C_nH_{2n+1}$ Eq. [3] becomes

$$E_mN^{-1} = k\,(n_2Q_2 + Q_3 + Q_b) \qquad [5]$$

where Q_b is the cross section of the benzene ring. Results obtained by Sharbaugh, Crowe, and Cox (5) fit this law as in Fig. 4a (6, 19). Also in agreement

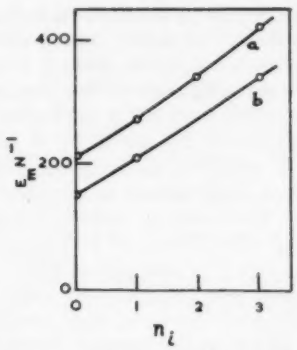

Fig. 4. $E_m N^{-1}$ as a function of molecular structure for alkyl benzenes. (a) n-Alkyl benzenes according to Eq. [5], $n_1 = n_2$; (b) branched-alkyl benzenes according to Eq. [6], $n_1 = n_3$.

with the criterion are the results for benzene, methyl benzene, and t-butyl benzene (Fig. 4b), fitting accurately the relationship

$$E_m N^{-1} = k\ (n_3 Q_3 + Q_b) \qquad [6]$$

Cross sections estimated from Fig. 4, show that Q_b is relatively large as might be expected but also that k Q_2 and k Q_3 are considerably greater (~100%) than estimates from the alkanes. This may be due in the first place to a shift in the breakdown criterion since there is no reason why C (Eq. [1]) should be the same in both series. Changes may also occur in the cross sections because the alkyl benzenes are polar with the ring negative. This would increase the interaction between the alkyl groups and electrons. It is also probable that the liquid structure differs in the two cases with a consequent effect on λ_m (see below).

Equation [1] is also supported by measurements on the dimethyl siloxane (silicone) liquids which have similar chain structures to the alkanes. The main skeleton consists of silicon-oxygen bonds, replacing the carbon-carbon bonds of the alkanes, and methyl side groups are added at the silicon sites to give a general formula $(CH_3)_3 Si - [O\ Si(CH_3)_2]_n - O\ Si(CH_3)_3$. An important difference is that the silicone skeleton is relatively exposed at the oxygen sites and the silicon oxygen bonds are polar. Equation [3] becomes

$$E_m N^{-1} = k\ (n_3 Q_3 + n_o Q_o) \qquad [7]$$

where Q_o refers to the oxygen site. The strengths found with direct voltage for the first four members of the series again give a linear characteristic when plotted according to Eq. [7] (6), bearing in mind that the dimer exhibits exceptional behavior in many of its other physical properties (20). The value of k Q_3 so obtained is identical with that from the alkanes. It has been shown already that the CH_3 group in the silicones has a vibration of ~3000 cm^{-1} very close to that found in the hydrocarbons so that the agreement in the estimates of k Q_3 appears significant.

On the whole, therefore, experiments on a large number of simple liquids can be arranged systematically according to Eq. [1] based on individual molecular groups.

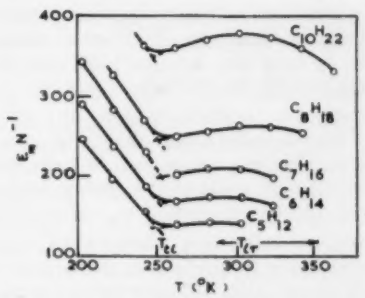

Fig. 5. Variation of E_m/N with temperature for n-alkanes showing transition temperatures.

Liquid Structure

The assumption of a uniform distribution of collision centers implies that the liquid is isotropic along individual electron paths. It is known that local order can exist in n-alkanes, however, and that this is temperature dependent. The liquid phases for pentane to decane are characterized by three states having transition temperatures T_{tt} and T_{tr} in the neighborhoods of 245° and 288°-355°K, respectively (21). Below T_{tt} the state is quasi-crystalline and the molecules pack with their long axes parallel to form crystallites. In the range T_{tt}-T_{tr} libration occurs about the long axes and above T_{tr} complete rotation is possible and local order disappears. Many physical properties change when taken through these transitions; Fig. 5 shows that the electric strength is no exception (22). By plotting $E_m N^{-1}$ against temperature in this figure normal density changes are annulled, structure effects are accentuated, and T_{tt} and T_{tr} become obvious. The change at T_{tt} is particularly abrupt. In a crystallite at low temperature the density of scattering centers due to CH_2 and CH_3 groups will be greater along the chain axis than perpendicular to it, and an electron with a trajectory along the axis will suffer the greater loss. This situation could occur as a result of field-induced orientation of the anisotropic molecule and will lead to a smaller value of λ_m in Eq. [1]. As the temperature is increased, both orientation and the crystallite size will decrease, so increasing λ_m and lowering the strength. In the range T_{tt}-T_{tr}, the onset of libration will increase the effective volume occupied by each molecular group and so increase the cross-section. The two opposing effects of decreasing orientation and increasing cross section would account for the small changes in E_m/N in this range. Normal results quoted in Fig. 3 are in this range. Above T_{tr} complete rotation is possible and the disordering processes already begun at lower temperatures cause a further fall in strength. Since the alkyl benzenes are polar, field orientation is likely to be stronger than in the alkanes and this may help to account for the increased effective cross sections found for the CH_2 and CH_3 groups in these liquids. A similar increase in orienting force would occur for the alkanes if ions attach in any way to the chain molecules.

Oxygen Effects

Account must now be taken of the study recently reported by Sletten (1) in which oxygen was shown

to have a marked influence on the strength of n-hexane (and presumably on other n-alkanes). His conclusion is that the results reported by Lewis, House, Sharbaugh, and others refer to liquids in which dissolved oxygen caused an increase in strength. He demonstrated that the strength of n-hexane may be increased from 0.9 mv/cm to the levels normally reported by dissolving oxygen in the liquid. Nitrogen did not affect the strength at all. It is necessary to determine whether the concepts in this discussion are in any way disturbed by this discovery. Because small changes in molecular structure influence the strength (2-6), even in the presence of oxygen, it is logical to seek a mechanism by which oxygen raises the strength without disturbing the controlling influence of the hydrocarbon vibrations.

Oxygen is electronegative and forms negative ions. According to the latest work (23) attachment in the gaseous phase involves a dissociative process, with the formative of an atomic ion, which has a peak at electron energies of about 6 ev lying between the vibrational and ionization energies of the hydrocarbons. If the same attachment process occurs when oxygen is dissolved, it will remove free electrons of energies above the vibration peak normally capable of contributing to the α process in the liquid. The conversion of electrons to low-mobility negative ions would also reduce the conduction current as observed (1). The attachment cross section (23) is, however, smaller than seems necessary to explain the large influence on the strength, but its effectiveness may be enhanced by transport of the oxygen ions to the anode. A layer of oxygen and oxygen ions will be built up there and brought to an equilibrium as regards oxygen concentration and electrical double-layer strength determined by the applied field. The layer would be strongly electronegative and therefore resistive to electron motion. Strong evidence for the existence of this layer on the anode has been provided recently by Ward of this laboratory who used an electrode with a layer formed in this way as the cathode in a pulse breakdown test on n-hexane. The strength was initially greater than 2.1 mv/cm and declined to the more normal value of 1.5 mv/cm as the layer diffused away and the cathode regained its emission properties. Oxygen will, therefore, tend to reduce α and restrict the volume for avalanche development. This can be accounted for in the present theory by an increase in the constant C of Eq. [1]. Further work on the role of oxygen and other gases is in progress.

The Adamczewski Theory

The theory given by Adamczewski (18) employs the same type of energy loss concept as here, but there are detailed differences which are important, especially as excellent agreement with pulse measurements (4, 5) have been obtained by him.

The major energy loss is ascribed to C—C bond vibrations of wave numbers 890 and 1090 cm^{-1}, either of which ultimately give strengths in close agreement with the pulse measurements. Reasons for not preferring this mode of vibration, which in the author's opinion cannot be overlooked, have been given already. The mean free path λ_m is also calculated differently. In the work of Sharbaugh, *et al.* (4) and Lewis (2) no attempt is made to estimate the absolute cross sections from bond dimensions and only relative magnitudes in terms of k are derived. Adamczewski, however, assumes the collision cross section to be a longitudinal geometrical section of the molecule. The n-alkane molecule is taken to be a cylinder of base radius r and length $l(n-1)$ where $2r$ ($=4.9$Å) is the mean distance between molecular axes, assuming crystal order as in the solid, l ($=1.23$Å) is the C—C bond length projected on the axis and n is the number of carbon atoms. The collision cross section is then $Q = 2r\ l(n-1)$ or $\lambda_m = [2Nr\ l(n-1)]^{-1}$. This calculation neglects thermal motion by which the molecule may be orientated randomly to the electron path. It is also doubtful whether the molecular spacing should be taken as $2r$ in determining the collision cross section. The same cylindrical model is also used for branched-chain alkanes (by adjusting r to compensate for the reduction in l due to the side groups) and for the alkyl benzenes. In the latter case the benzene ring is not considered as an entity but is used to extend the length of the alkyl radical by including two carbon atoms of the ring as part of the radical. The remaining ring bonds and any side groups then influence r. Adherence to a cylindrical model does not seem justified in these cases.

Finally, Eq. [1] is used with $C = 1$, i.e., no account is taken of other mechanisms vital to the breakdown process. Neither the oxygen effect nor the lower strengths obtained with direct rather than pulse voltages can be accommodated in the criterion. There are, therefore, great difficulties in accepting the Adamczewski theory, but the close agreement with experimental values is intriguing and demands further study.

Conclusion

The discovery of the oxygen effect and the statistical concepts given in another contribution (7) should help greatly in separating cathode from liquid effects and in determining C in Eq. [1]. By employing oxygen and perhaps other additives in controlled amounts the basic processes should be capable of investigation. Further work is also required to clarify the orientation effect over a range of temperatures including the solid state. Permanently orientated molecules in the solid might show strong directional properties and higher strengths. In the meantime the present treatment using a simple model provides a consistent relationship between measured electric strengths and molecular structure of these hydrocarbons. Up to now the reported strengths of insulating oils have been lower than what might be expected by extrapolation from simple hydrocarbons of less complexity. Careful separation of the oil will not only indicate particular molecular species which lower the strength but also provide valuable information on the relationship between electric strength and molecular structure.

Manuscript received Nov. 2, 1959. This paper was prepared for delivery before the Philadelphia Meeting, May 3-7, 1959.

Any discussion of this paper will appear in a Discussion Section to be published in the December 1960 JOURNAL.

REFERENCES

1. A. M. Sletten, *Nature*, **183**, 311 (1959).
2. T. J. Lewis, *J. Appl. Phys.*, **27**, 645 (1956).
3. R. W. Crowe, J. K. Bragg, and A. H. Sharbaugh, *ibid.*, **25**, 392 (1954).
4. R. W. Crowe, A. H. Sharbaugh, and J. K. Bragg, *ibid.*, **25**, 1480 (1954).
5. A. H. Sharbaugh, R. W. Crowe, and E. B. Cox, *ibid.*, **27**, 806 (1956).
6. T. J. Lewis, *Brit. J. Appl. Phys.*, **9**, 30 (1958).
7. B. W. Ward and T. J. Lewis, *This Journal*, **107**, 191 (1960).
8. W. B. Green, *J. Appl. Phys.*, **26**, 1257 (1956); *ibid.*, **27**, 921 (1956).
9. H. House, *Proc. Phys. Soc.*, **B70**, 913 (1957).
10. R. Hancox and H. Tropper, *Proc. Inst. Elec. Engrs. (London)*, Paper No. 2408M, Sept. 1957.
11. T. J. Lewis, *Proc. Phys. Soc.*, **B66**, 425 (1953).
12. L. B. Loeb, "Basic Processes of Gaseous Electronics," Chap. 4, University of California Press, Berkeley (1955).
13. S. A. Korff and R. D. Present, *Phys. Rev.*, **65**, 274 (1944).
14. A. von Hippel, *J. Appl. Phys.*, **8**, 815 (1937).
15. M. Darveniza, *Nature*, **183**, 743, (1959).
16. H. J. Plumley, *Phys. Rev.*, **59**, 200 (1941).
17. H. Frohlich, *Repts. Progr. Phys.*, **6**, 411 (1939).
18. I. Adamczewski, *Zesztyty Naukowe Politechniki Gdanskiej*, **3**, 3 (1957).
19. D. Berg and J. Kraitchman, Annual Report 1956, Conference on Electrical Insulation, National Academy of Sciences, National Research Council, 41 (1957).
20. N. Wright and M. J. Hunter, *J. Am. Chem. Soc.*, **69**, 803 (1947).
21. R. J. Moore, P. Gibbs, and H. Eyring, *J. Phys. Chem.*, **57**, 172 (1953).
22. T. J. Lewis, *J. Appl. Phys.*, **28**, 503 (1957).
23. J. D. Craggs, R. Thorburn, and B. A. Tozer, *Proc. Roy. Soc.*, **A240**, 473 (1957).

A New Statistical Theory for the Breakdown of Liquid Hydrocarbons

B. W. Ward and T. J. Lewis

Electrical Engineering Department, Queen Mary College, London, England

ABSTRACT

Hitherto it has been accepted that breakdown under pulse conditions occurs in liquid hydrocarbons with an insignificant statistical time lag. Theories have been developed in which the whole of any time lag measured has been assigned to a formative time, but these theories are not at all satisfactory. The paper shows that (*a*) that a significant statistical time lag does in fact exist provided the experimental procedure is correctly interpreted and (*b*) that a proper statistical analysis of the previous pulse measurements together with a statistical theory of breakdown shows that these measurements provide clear evidence *for* rather than against, a statistical time lag. Experimental results are given to show how the statistical time lag depends on electric stress and on cathode conditions.

The electric strengths of pure simple hydrocarbons indicate the possible strengths for liquid dielectrics of more commercial interest and also provide data for the determination of the breakdown mechanism in liquids. Alkanes and certain aromatic hydrocarbons have received attention in this way, but, in spite of increasingly reliable experiments, no general theory for the whole breakdown process has emerged and many conflicting ideas exist. The present contribution has the aim of presenting a new statistical model for the breakdown process, and hypotheses, supported by experimental evidence, are advanced which will help to explain many of the apparent discrepancies.

Electric strengths have been measured with both continuous and short duration voltages, but here attention will be concentrated on the latter type of test. The liquids, of which n-hexane has been most frequently tested, are given preliminary chemical purification if necessary and then further cleaned in a closed system to remove water, ionic impurity, dust particles of size $> 1\mu$, and dissolved gas. However, as Sletten has shown recently (1), most results for n-hexane, at least, and probably for other hydrocarbons refer to liquids containing significant amounts of oxygen which raise and stabilize the strength. The oxygen in these cases must have come from the air during a final stage in the cleaning process or while being stored after cleaning. The test cell is frequently integral with the cleaning system and the electrodes are usually 1 cm diameter metal spheres at a spacing of less than $\sim 10^{-2}$ cm. Electrodes are highly polished and degreased beforehand and for the experiments reported here, were stainless steel.

With this preparation, the strength of n-hexane is in excess of 1.5 mv/cm for pulse voltages of 1.5 μ sec or less (2), and at this stress field emission of electrons from the cathode must be taking place and contributing significantly to the conductivity of the liquid. A typical plot of strength vs. pulse duration (3) is shown in Fig. 1. Any point is the mean of a set of measurements having a coefficient of variation of about 5%, and a measurement is made by applying successive pulses of constant duration and increasing amplitude until a breakdown occurs. A distinct change occurs for pulse lengths $< T_s$ and the times $T \leqq T_s$ have been considered to be a measure of the formative time of the breakdown process. If the

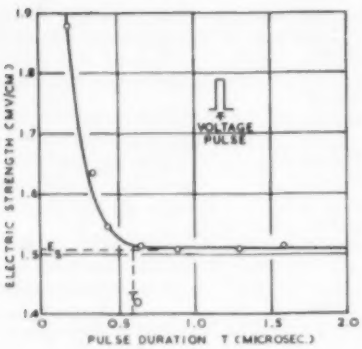

Fig. 1. Typical characteristics for a hydrocarbon liquid n-hexane (3).

pulse time T was greater than T_o, breakdown was considered to occur invariably at a time T_o provided the voltage was sufficient to cause a stress E_o (Fig. 1). This idea has been generally accepted (3, 4) and supported by statements that the statistical time lag was negligible, breakdown being easily initiated by ample electrons from the cathode (3-5). The times $T \leqq T_o$ have been related to the transit times of certain ions of mobility μ across the sphere gap d according to the law $T = d\ (\mu E)^{-1}$ (where E is the applied stress) and so compared with viscosity (4). This theory does not easily explain why the formative time should be influenced by the cathode material as observed, nor does it explain several discrepancies in published results (3-6).

There is also contrary evidence that the statistical time lag is not in fact zero from experiments using "step-function" pulse voltages in which the time lag to breakdown is measured directly for each voltage application. Strigel (7) using oil, and Saxe and Lewis (8) with n-hexane, have reported considerable random variations in the time lags even at stresses of 1.9 mv/cm. The work reported here confirms the existence of a statistical lag and also shows that it was almost certainly present in short-duration pulse experiments such as those leading to Fig. 1. By employing a statistical method, all these measurements become consistent and a physical interpretation is possible in which the roles of the liquid and cathode are clear. We begin by setting up a statistical model for the breakdown condition applicable to measurements with step-function and short duration pulse voltages.

Theory

The necessary assumptions for the model are (a) that electrons are ejected randomly from the cathode into the liquid with a mean rate I per second, and (b) that each electron has a probability W of initiating a breakdown process having a formative time t_f which is small. Cathode surface conditions will control I and liquid properties will determine W and t_f and all three quantities will be dependent on the field strength (see Fig. 2) and electrode geometry.

Step-function voltages.—If a step-function voltage is applied creating a mean stress E in the liquid, it may be shown [see (8) and references therein] that the probability of breakdown occurring within a

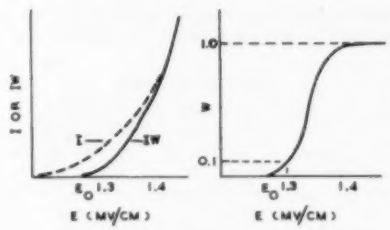

Fig. 2. I, W, and IW as functions of applied stress E. Values given are for a hypothetical liquid.

time interval t to $t + dt$ after the instant of voltage application is

$$P(E)\,dt = WI \exp\left[-WI(t - t_f)\right] dt \qquad [1]$$

From this the mean time lag before breakdown occurs, $\bar{t}$, is given by

$$\bar{t} = t_f + (WI)^{-1}$$

and the probability of a time lag $> t$ is $\exp\left[-WI(t - t_f)\right]$. These expressions are valid for $t \geqq t_f$. Equation [1] shows that the shorter time lags are most probable and according to Fig. 2 there will be a threshold condition $E = E_o$, $W = 0$ below which P is zero. As the field strength increases, the mean time lag $\bar{t}$ will decrease in accordance with the field dependence of IW. Although the theory indicates that many time lags need to be measured to obtain an accurate estimate of P, experience has shown that reliable indications may be obtained from relatively few measurements.

Short-duration pulses.—The probability of breakdown occurring with a pulse duration T, producing a stress E is

$$p(E) = 1 - \exp\left[-IW(T - t_f)\right] \qquad [2]$$

which will be zero for $E < E_o$ and $T < t_f$ and will tend to unity as E increases. The usual procedure is to apply a succession of pulses of constant T and increasing magnitude in steps ΔE until a breakdown is recorded. If at each level of stress N pulses are applied, the probability of breakdown at a stress E_m is then, assuming $t_f = 0$ for the present,

$$P_m = 1 - (1 - p_m)^N = 1 - \exp\left[-I_m W_m T N\right] \qquad [3]$$

and the probability of a breakdown first occurring at a level E_n in any succession of pulses is

$$Q_n = P_n \prod_{m=0}^{m=n-1} (1 - P_m) \qquad [4]$$

The initial level corresponds to $m = 0$ and for most applications can be taken as E_o. Using Fig. 2, it is easy to show that Q_n increases from zero at E_o, passes through a maximum and then decreases as E_n becomes large; the exact form depending on IW.

For convenience in calculation it is better to transform to a continuous variable, replacing Q_n by $Q(E)dE$ which is defined as the probability of a first breakdown in the interval E to $E + dE$ and writing λ (instead of N) as the number of pulse applications in a unit interval of stress. It is found that

$$Q = \lambda p \exp\left[-\lambda \int_{E_0}^{E} p\, dE\right] \qquad [5]$$

The distribution Q need not be symmetrical since this depends on the form of IW. It will give a most probable breakdown stress E_p and an average stress E_{av} but unless asymmetry is great $E_p \sim E_{av}$.

The same model has been used for step-function and short duration voltages, but measurements might lead to very different conclusions in the same two cases. In the first, random time lags would be obvious immediately, but with the second Q might have little spread and E_p or E_{av} could be reasonably precise. Any fluctuations in this case might then be ascribed to extraneous influences rather than to the true breakdown process. It should be noted that E_∞ will be the breakdown stress with continuous voltage and there will be a negligible chance of breakdown at this stress with pulses of microsecond duration. If the model is correct, measurements with either step-function or short duration voltages should yield information concerning the cathode and liquid function I and W. The most important result is that it gives an entirely different interpretation of the characteristic shown in Fig. 1 as will be demonstrated immediately.

Comparison with Experiment

As already mentioned, with E_p equal to 1.5 mv/cm or greater, the emission I is likely to be a field-aided thermionic process according to a Schottky law (9) which can be written as

$$I = B \exp\left(15\, E^{1/2}\right)$$

E is in mv/cm and B is a constant determined by the temperature and nature of the cathode surface. Other workers have proposed alternative field emission laws, but the exact nature is immaterial for the present argument since we require merely that I should increase rapidly with E. Making an arbitrary choice, $B = 0.01$, gives $I = 10^6$ electrons/sec for $E = 1.5$ mv/cm and using this with W for a hypothetical liquid, as in Fig. 2, in Eq. [2]-[5] it is possible to obtain Fig. 3. The formative time t_f has been neglected for ease in calculation, but it will be reintroduced below.

The agreement between the theoretical characteristic in Fig. 3 and the experimental one in Fig. 1 is striking. The parts AB and BC of the curve mainly depend on I and W, respectively, and the position of the curve on the axis of stress E_{av} may be shifted to conform with any specific liquid by adjustment of these. Adjustment on the T axis is not arbitrary however, and the discrepancy between Fig. 3 and Fig. 1 is due to the assumption $t_f = 0$ which causes the asymptotic value of T for large E_{av} to be zero in the theoretical case but not in the practical one. This can be rectified easily by including a nonzero t_f in the theoretical derivation.

The most significant result of the statistical theory is that the region of maximum curvature at B is not due to a formative time but is produced by the statistical requirements and the shape of the IW curve. Figure 3 also emphasizes that over the small range of T normally employed, the characteristic can appear to be independent of T in the range BC. Extrapolation to large T corresponding in the limit to tests with continuous voltage would yield a breakdown stress equal to E_∞. It should be noted that for ethyl alcohol and water, a strong dependence on T has been found even when T was several microseconds (5).

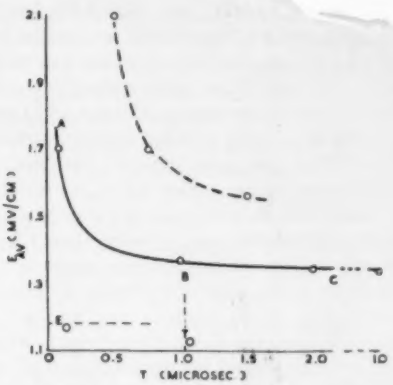

Fig. 3. Calculated breakdown stress E_{av} as a function of pulse duration for a hypothetical liquid. The region of maximum curvature at B is not due to a formative time which has been put equal to zero in the derivation.
- - - curve obtained from experiments on n-hexane similarly prepared to that employed for Fig. 4.

The procedure adopted has been to choose I and W and then derive the breakdown stress vs. pulse duration curve, but there is no reason why the procedure should not be changed and the experimental curve together with I used to determine W and t_f, for instance.

Direct support for the statistical model has recently been obtained in this laboratory. Using n-hexane and stainless steel spherical electrodes at

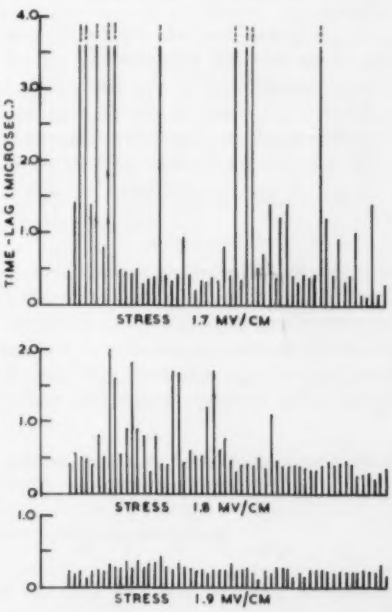

Fig. 4. Statistical time-lag sequences for n-hexane. Each vertical trace indicates the time lag for a particular step-function pulse. Electrodes were stainless steel with $d = 5 \times 10^{-5}$ cm.

a spacing of 5 x 10^{-5}cm, time lags have been measured directly using a "step-function" pulse having a front of 10^{-7} sec and lasting at maximum voltage for a time $> 10^{-4}$ sec. Time lags were recorded automatically using the technique of Saxe and Lewis (8). Figure 4 shows a series of these measurements. There is no doubt that the time lags are random and decrease in mean value as the stress is raised. At 1.7 mv/cm, lags well in excess of 3.5 μsec are recorded and even at 1.8 mv/cm lags greater than 1.5 μsec are not infrequent. These results give quite a different impression from that deduced formerly from short-duration pulses (2-6) under very similar experimental conditions. On the earlier theory, at a stress of 1.8 mv/cm, it would be considered that the time to breakdown could not exceed about 0.25 μsec, being due entirely to a formative process.

In order to confirm that Fig. 3 and 4 represent the same phenomena, measurements have been made on similar samples of n-hexane using short-duration rather than step-function voltages. All other conditions were identical. The pulses were produced by matched line techniques and increased in steps ΔE = 0.05 mv/cm with $N = 1$. Values of E_{s_v} obtained have been added to Fig. 3. The dependence on pulse duration is in general agreement with the theory and Fig. 1 and with other results (4, 5). The strength increases rapidly when the pulse duration is reduced sufficiently. Further comments concerning cathode influence on these results are given below. According to the theory, the distribution Q_{s_v}, (Eq. [4]), should shift to lower stresses when N is increased. To verify this, experiments were repeated with $N = 5$ instead of unity. The predicted shift occurred as the sample results in Table I indicate because if a procedure in which $N = 1$ had been adopted, all except measurement 4 and 5 would have resulted in higher breakdown stresses.

Thus, by comparing the theory with earlier work and by performing both types of test under otherwise identical conditions, it has been demonstrated that breakdown in n-hexane can be consistently described by the statistical model. It is inferred that the model will also be applicable to the other simple liquids tested. A few implications of this are now examined.

Discussion

Cathode effects.—According to the theory, cathode effects should predominate in the range AB (Fig. 3). Figure 5 reproduces measurements made by Crowe (3) with stainless-steel electrodes in n-hexane and other n-alkanes at two electrode spacings. Since all these liquids have common properties and the electrodes received a consistent preparation, it would be expected that the emission properties of the cathodes would be similar in all cases, i.e., that the characteristics would merge in the region AB. This is, in fact, seen to be the case in Fig. 5. Through W, liquid influences cause the curves to separate in the region BC. The differences found between the cathode regions in the experiments here (shown in Fig. 3) and those of Crowe and co-workers (2, 3, 6,) (Fig. 1) and other authors (4, 5) may be ascribed directly to differences in the emissive properties of the cathodes employed.

Table I. Influence of number of pulse applications on breakdown stress

	Breakdown measurement number							
	1	2	3	4	5	6	7	8
Breakdown stress, mv/cm	1.45	1.45	1.55	1.45	1.25	1.35	1.45	1.55
Number of pulse applications at the breakdown stress	4	5	2	1	1	2	4	2

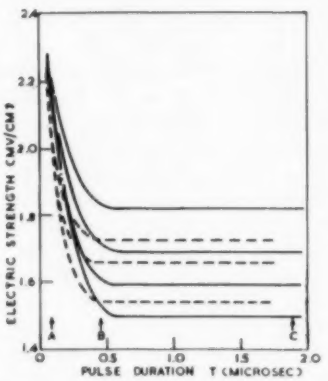

Fig. 5. Electric strength as a function of pulse duration according to Crowe (3). —— d = 6.35 x 10^{-3} cm; - - - d = 5.08 x 10^{-3} cm.

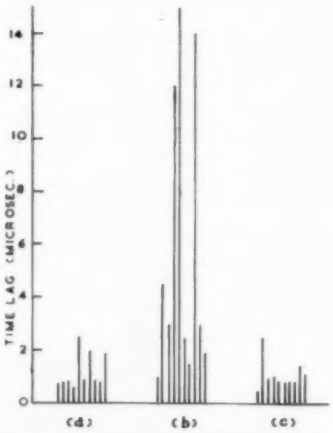

Fig. 6. Statistical time lags for n-hexane at a stress of 1.4 mv/cm, (a) and (c) roughened cathode, (b) polished cathode. Electrodes of stainless steel with d = 5 x 10^{-3} cm.

Conclusive evidence concerning the direct influence of the cathode on breakdown is shown by the time-lag measurements of Fig. 6. It is well known that an abraded metal cathode will exhibit considerably enhanced electron emission (10) and so should yield a much greater value of I than a normally polished one. Consequently, a pair of stainless steel electrodes were prepared, one being highly polished and the other roughened, and used to test n-hexane at a spacing of 5 x 10^{-3}cm. Measurements were made at a stress of 1.4 mv/cm; the polarity being reversed after every ten measurements. When the cathode was rough, time lags were short, but on reversal the

lags normally expected at that stress were obtained. A further reversal recovered the short lags once more. This experiment and others in which the degree of oxidation of the cathode was found to change the mean time lag clearly indicate the role of the cathode.

Liquid effects.—The W dependent region BC (Fig. 3) depends on the properties of the liquid and on the electrode spacing (3, 4) and thus from this region information pertaining to the breakdown mechanisms in the liquid phase may be found. Since formally T may be extended to very long times, liquid influence on pulse and continuous voltage measurements may be unified. These matters, together with the oxygen effect found by Sletten which does not alter the model proposed here, are discussed at length in a subsequent paper (11).

Formative time.—According to the statistical model, times $T < T_s$ are not measures of a true formative time t_f and even when t_f is zero (as assumed in Fig. 3) a finite T_s exists. T_s corresponds approximately to the stress at which W becomes unity and cathode conditions predominate but does not apparently have any further significance. The true formative time may be estimated at very high stresses from the experimental results because the statistical lag then tends to zero. Values estimated in this way from the work of Crowe as in Fig. 1 and 5 give t_f not greater than about 1×10^{-7} sec for a 5×10^{-3} cm gap. An estimate of similar magnitude may be made from the work of Edwards (5) and with certain reservations from that of Goodwin and Macfadyen (4). The time-lag measurements at 1.9 mv/cm, Fig. 4, also suggest a formative time not greater than 10^{-7} sec. This estimate is much less than those based on T_s and helps to explain why certain discrepancies existed in earlier interpretations. For instance, Edwards found T_s to be practically independent of the liquid but dependent on electrode separation in general agreement with Crowe and co-workers, whereas Goodwin and Macfadyen reported that T_s increased with molecular chain length and viscosity. Goodwin and Macfadyen also found that the formative time as defined by them was influenced by the cathode material and thus difficult to explain.

If t_f is about 10^{-7} sec at a stress of 1.9 mv/cm and is ascribed to the transit time of a particle, the mobility is $\sim 3 \times 10^{-5}$ cm^2/v sec which is appreciably greater than ion mobilities measured at lower fields in these liquids by Adamczewski (12) although it is possible that the mobility will decrease as the stress decreases. Further investigations are required to determine t_f and ion and electron mobilities directly in the range above 1.5 mv/cm.

A fuller study of the nature of the statistical time lag is now being made which should permit the various cathode and liquid mechanisms to be understood in more detail. If the cathode influence is understood, greater progress can then be made in establishing a theory for breakdown in liquids comparable with that in gases. The statistical hypothesis should help greatly in achieving this.

Acknowledgment

One of the authors (B.W.W.) is grateful to the Department of Scientific and Industrial Research for an award enabling this study to be made, and thanks are also due to Professor M.W. Humphrey Davies for providing facilities in the Department.

Manuscript received November 2, 1959. This paper was prepared for delivery before the Philadelphia Meeting, May 3-7, 1959.

Any discussion of this paper will appear in a Discussion Section to be published in the December 1960 JOURNAL.

REFERENCES

1. A. M. Sletten, *Nature*, **183**, 311 (1959).
2. R. W. Crowe, A. H. Sharbaugh, and J. K. Bragg, *J. Appl. Phys.*, **25**, 1480 (1954).
3. R. W. Crowe, *ibid.*, **27**, 156, (1956).
4. D. W. Goodwin and K. A. Macfadyen, *Proc. Phys. Soc.*, **66**, 85, (1953).
5. W. D. Edwards, *Can. J. Phys.*, **29**, 310 ,(1951).
6. A. H. Sharbaugh, J. K. Bragg, and R. W. Crowe, *J. Appl. Phys.*, **26**, 434 (1955).
7. R. Strigel, "Elektrische Stossfestigkeit," 2nd ed., Springer-Verlag, Berlin (1955).
8. R. F. Saxe and T. J. Lewis, *Brit. J. Appl. Phys.*, **6**, 211, (1955).
9. H. House, *Proc. Phys. Soc.*, **B70**, 913 (1957).
10. F. Llewellyn Jones and C. G. Morgan, *Proc. Roy. Soc.*, **A218**, 88 (1953).
11. T. J. Lewis, *This Journal*, **107**, 185 (1960).
12. I. Adamczewski, *Ann. Phys.*, **8**, 309, (1937).

Kinetics of the Oxidation of Antimony

A. J. Rosenberg A. A. Menna, and T. P. Turnbull

Lincoln Laboratory, Massachusetts Institute of Technology, Lexington, Massachusetts

ABSTRACT

The oxidation of antimony has been studied between 265° and 385°C. The reaction is characterized by an initially parabolic growth rate, which degenerates into a time-independent rate, controlled by the gaseous diffusion of $(Sb_2O_3)_2$ from the surface region to the cold wall outside the sample furnace. The stationary rate decreases with increasing oxygen pressure and with increasing diffusion length. A compact layer of Sb_2O_3 forms on the antimony surface and supports a further overgrowth of Sb_2O_5. Kinetic data have been analyzed to obtain thermochemical parameters for the reaction which yields $(Sb_2O_3)_2(g)$ and agreement is obtained with known data for the equilibrium $2Sb_2O_3(s) \rightleftharpoons (Sb_2O_3)_2(g)$.

Several studies now in progress in these laboratories (1) deal with the oxidation of intermetallic compounds containing antimony as a principal element. To provide a suitable frame of reference, it has been necessary to examine the oxidation of elemental antimony itself. The present article is concerned with the kinetics of this reaction in the temperature range, 265°-385°C.

Experimental

Reaction rates were determined by following the oxygen pressure at constant volume. A thermistor manometer was used, permitting instantaneous pressure measurements in the range, 1-500 μ, with a precision of better than 0.1% (2).

Single crystals of 99.999+% antimony were used. Small wafers were cleaved normal to the (0001) direction, and this plane accounted for more than 75% of the exposed surfaces, which totaled 0.5 cm^2 per sample. The samples were cleaved in air and transferred directly to an 8 mm tube which was then connected to an adsorption apparatus of the type described earlier (2). A movable tube furnace which maintained the sample temperature to ± 1°C was then raised into position. Oxygen of spectroscopic purity was used throughout.

Results

Upon exposure to oxygen at 358°C, antimony reacts readily, but the rate rapidly decreases by two orders of magnitude and becomes constant (Fig. 1). During the reaction a yellow-white crystalline material deposits on the walls of the sample enclosure at the point where it leaves the furnace. The material can be displaced by raising the position of the furnace. It was established by both x-ray and electron diffraction that the entire deposit consists of senarmontite, the cubic form of Sb_2O_3 (3). If the oxygen in the sample chamber is evacuated during the experiment, Sb_2O_3 continues to evaporate from the sample. When this evolution ceases and oxygen is readmitted to the system, the kinetics of Fig. 1 are repeated.

If the sample is quenched during the reaction by removing the furnace, an irregular crystalline overgrowth, identified as Sb_2O_3 by electron diffraction,

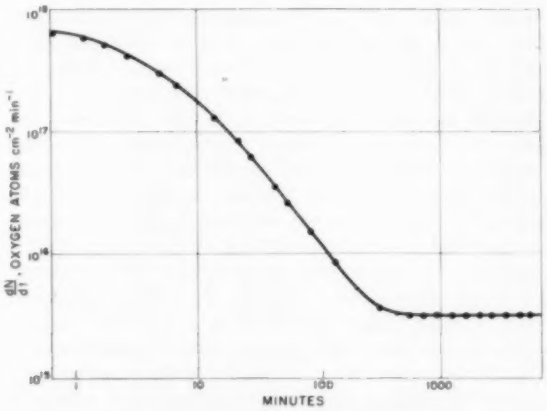

Fig. 1. Oxidation of antimony at 358°C. Oxygen pressure, 0.40-0.45 mm, surface area = 0.5 cm^2.

is observed on the surface of the sample. By sectioning the sample and scanning the exposed surface, it was further established by reflection electron diffraction that a layer of cubic Sb_2O_3 separates the Sb_2O_5 from the antimony substrate (Fig. 2).[1]

[1] Bound and Richards (4) observed the formation of senarmontite on antimony films heated in air above 250°C.

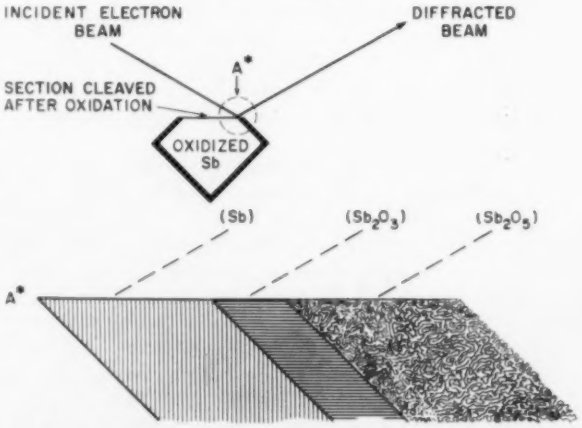

Fig. 2. Reflection electron diffraction by oxidized antimony

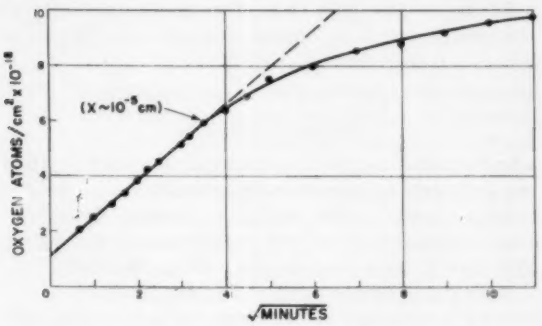

Fig. 3. Oxidation of antimony at 350°C. Oxygen pressure, 0.40-0.45 mm, surface area = 0.5 cm².

Clearly, the oxidation proceeds in at least two stages. The formation of an oxide film presumably controls the initial stage. Growth of the film requires that it be penetrated by either antimony or oxygen, so that the rate diminishes as the film thickens. Ideally, $dX/dt = kX^{-1}$ and $X = (2k)^{1/2} t^{1/2}$ where X is the film thickness, t is the reaction time, and k depends only on temperature and pressure. Figure 3 shows that the oxygen uptake does indeed increase linearly with $t^{1/2}$ during the first 15 min of reaction at 358°C. The rate then drops more rapidly than expected and approaches its stationary value.

When the steady state is attained the reaction rate is controlled by the distillation of Sb_2O_3 from the surface of the sample to the cold wall at the inlet to the sample enclosure. This is shown by two decisive results.

(i) The stationary rate varies inversely with the oxygen pressure, as shown in Table I. Accordingly, neither the primary oxidation reaction, nor the diffusion of oxygen or antimony through the oxide film, nor the diffusion of oxygen through the gas phase control the reaction since the rates of each should increase with pressure.[2] One may conclude, therefore, that oxygen acts by impeding the vapor phase diffusion of Sb_2O_3.

(ii) The stationary rate depends on the position of the sample in the furnace. Figure 4 shows that when the position of the sample relative to the top of the surrounding furnace is changed from 11 cm to 1.5 cm, the rate increases by almost an order of magnitude. Since the only effect of this manipulation is to shorten the gaseous diffusion path, the diffusion of Sb_2O_3 to the cold wall must control the rate.

[2] A chemical reaction of oxygen to inhibit vaporization of Sb_2O_3, e.g., through the equilibrium, $Sb_2O_3 + \frac{1}{2}O_2 = Sb_2O_4$ may also be disallowed since the negative pressure effect increases with increasing temperature in the range, 285°-360°C (Fig. 4). This would require that the inhibiting reaction be endothermic, and, since the entropy of any reaction which fixes gaseous oxygen is negative, the over-all free energy change would be positive.

Table I. Dependence of stationary oxidation rate on oxygen pressure, $T = 352$°C

Oxygen pressure, μ	Rate (oxygen atoms cm⁻² min⁻¹) × 10⁻¹⁵
550	1.1
270	1.2
170	1.45
90	3.2
40	7.2
15	7.9

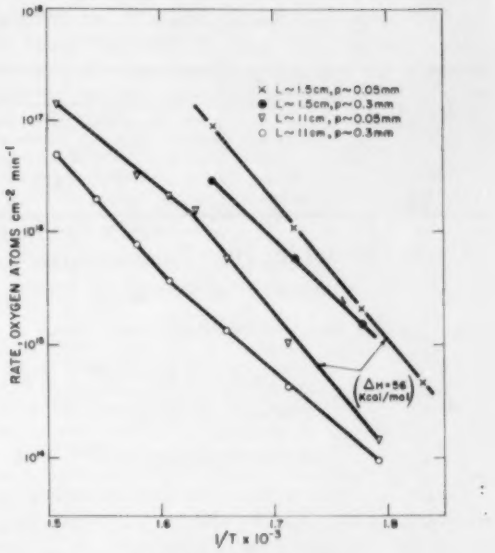

Fig. 4. Effect of temperature, pressure, and furnace level on the stationary oxidation rate. Surface area = 0.5 cm².

Discussion

The high-temperature oxidation of antimony parallels that of germanium (5) in that the diffusion of a volatile oxide through the vapor phase leads to a stationary reaction velocity. In the case of germanium the volatile species is GeO; in the case of antimony, it is $(Sb_2O_3)_2$ (6). The rate at which $(Sb_2O_3)_2$ diffuses from a gas reservoir at concentration, C_0, can be estimated from kinetic theory. We shall follow the treatment given by Law and Meigs (5) for the diffusion of GeO. The rate is given by:

$$V = \frac{\lambda \Gamma C_0 A}{\frac{\lambda \Gamma (L - \Delta)}{D} + 1} \qquad [1]$$

λ is the accommodation coefficient of $(Sb_2O_3)_2$ at the surface from which it arises; $\Gamma = (kT/2\pi m)^{1/2}$ where m is the molecular mass of $(Sb_2O_3)_2$; Δ is the mean free path in the vapor; L and A are the length and cross section of the path separating the reservoir from the cold wall where the pressure of $(Sb_2O_3)_2$ is virtually zero; D is the diffusion coefficient of $(Sb_2O_3)_2$ through oxygen. Ideally D should vary as $1/p_{O_2}$; in the present case, the dependence, while inverse, is not linear. For the present qualitative purposes we assume, as an approximation, that

$$D = D_0 (T/273)^{1.75} (760/p_{O_2}) \qquad [2]$$

where D_0 is estimated to be 0.04 cm²/sec for $(Sb_2O_3)_2$ (5, 7).

Substituting $C_0 = 1.0 \times 10^{15} PT^{-1}$ molecules/cc where P = pressure in mm of $(Sb_2O_3)_2$ in the reservoir, $\Gamma = 150T^{1/2}$ cm/sec, and $D = 1.7 \times 10^{-5} T^{1.75} p_{O_2}^{-1}$ cm²/sec, Eq. [1] becomes

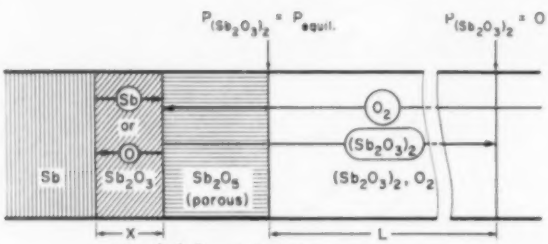

Model for High Temperature Oxidation of Antimony

Fig. 5. Model for the oxidation of antimony

$$V = \frac{1.5 \times 10^{23} \lambda A T^{-1/2} P}{9 \times 10^{4} \lambda (L - \Delta) p_{O_2} T^{-1.25} + 1} \quad [3]$$

$(Sb_2O_3)_2$ molecules/sec

Equation [3] is of the right form to account qualitatively for the negative effects of increasing p_{O_2} and L on the stationary oxidation rate. It is consistent, furthermore, with the fact that the relative effect of P_{O_2} increases with both T and L. Evaluating Eq. [3] at $L - \Delta \sim L = 11$ cm, $A = 0.5$ cm^2, $T = 600$°K, and $p_{O_2} = 0.05$ mm, we obtain

$$V\,(600°K) = \frac{3 \times 10^{15} \lambda P}{17\lambda + 1}\,(Sb_2O_3)_2 \text{ molecules/sec} \quad [4]$$

This is to equated to the rate of oxygen uptake by the sample, hence,

$$V(600°K) = \frac{1.1 \times 10^{21} \lambda P}{17\lambda + 1} \text{ oxygen atoms/min} \quad [5]$$

Since the effects of p_{O_2} and L are contained in the first term of the denominator of the rate expression, this term must be comparable with unity. Consistent with this qualitative calculation, we assume $17\lambda >> 1$ and obtain finally

$$V(600°K) \simeq 6 \times 10^{19} P \text{ oxygen atoms/min} \quad [6]$$

The observed rate of oxygen uptake under these conditions (Fig. 5) is 5×10^{16} oxygen atoms/min, whence

$$P(600°K) \simeq \frac{5 \times 10^{15}}{6 \times 10^{19}} = 8 \times 10^{-5} \text{ mm} \quad [7]$$

The purpose of this calculation is to decide whether $P = P_{equil.}$, where $P_{equil.}$ is the equilibrium vapor pressure of a plausible surface reaction yielding $(Sb_2O_3)_2(g)$. If this is the case, the standard free energy of the reaction will be given by $\Delta F° = -RT \ln(P/760)$, $= +19$ kcal/mole. The enthalpy of the reaction will be defined through Eq. [3], from which it is seen that

$$V \sim AT^{0.75} \sim BT^{0.75} \exp(-\Delta H/RT) \quad [8]$$
$$\sim C \exp(-\Delta H/RT)$$

where, C is constant for any small range of T. Thus the enthalpy corresponds approximately to the activation energy of the oxidation reaction. From Fig. 4 one obtains $\Delta H \simeq +56$ kcal/mole in the range 270°-340°C for $p_{O_2} \sim 0.05$ mm, independent of L.

With the presence of $Sb_2O_3(s)$ and $Sb_2O_5(s)$ at the surface established by electron diffraction, the four reactions given in Table II must be considered as potential sources of $(Sb_2O_3)_2(g)$. The values of ΔH, $\Delta F°$, and $P_{equil.}$ for each reaction have been calculated from the data of Hincke (8), Simon and Thaler (9), and Coughlin (10). Reactions [1],[3], and [4] are inconsistent with the kinetic analysis, giving impossibly high or low values of $P_{equil.}$. Reaction [2], on the other hand, satisfactorily accounts for the predictions of both Eq. [7] and [8].

The results give compelling evidence that the vaporization of Sb_2O_3 goes to equilibrium in the region immediately surrounding the sample, yielding a regulated pressure of $(Sb_2O_3)_2$. Although Sb_2O_5 is the most stable oxide of antimony below 360°C, it does not participate in the equilibrium. Thus, the chemical interactions of $(Sb_2O_3)_2(g)$, $Sb_2O_5(s)$, and O_2 must be very slow compared to the over-all oxidation rate. This is consistent with the observations of many workers that the interconversions of the antimony oxides through the addition or loss of O_2 are extraordinarily slow reactions (9).

A model for the oxidation is illustrated in Fig. 5. The model assumes that the primary reaction of Sb + O_2 yields $Sb_2O_3(s)$ in an isothermal system below 350°C. Continued oxidation to Sb_2O_5 is much slower. A compact film of Sb_2O_3 forms at the surface and continued reaction of Sb requires that either Sb or O_2 diffuse through the film. The rate of oxidation thus decreases with $1/X$, as observed (Fig. 3). Simultaneously $(Sb_2O_3)_2$ evaporates from the surface of the film and escapes through the oxygen atmosphere to condense on the available cold wall. The rate at which it escapes is controlled by the difference between its pressure at the surface of the sample, P, and that at the wall. The latter is virtually zero, while the maximum value that P can have is $P_{equil.}$, the equilibrium vapor pressure above $Sb_2O_3(s)$. The Sb_2O_3 film thus will thicken to a point (about 10^{-5} cm) where the further diffusion of O_2 or Sb through it exactly matches the maximum rate at

Table II. Thermochemical parameters for formation of $(Sb_2O_3)_2$ vapor at 600°K, $p_{O_2} = 0.05$ mm, standard states $p_{O_2} = P_{(Sb_2O_3)_2} = 1$ atm

Reaction	ΔH, kcal/mole	$\Delta F°$, kcal/mole	$P_{equil.}$, mm
1. $4Sb(s) + 3\,O_2(g) = (Sb_2O_3)_2(g)$	-291 ± 4	-238 ± 4	$\sim 10^{77}$
2. $2Sb_2O_3(s) = (Sb_2O_3)_2(g)$	$+47 \pm 2$	$+22 \pm 1$	4×10^{-6}-2×10^{-5}
3. $\frac{6}{5}Sb_2O_5(s) + \frac{8}{5}Sb(s) = (Sb_2O_3)_2(g)$	-18 ± 7	-44 ± 7	$\sim 10^{10}$
4. $2Sb_2O_5(s) = (Sb_2O_3)_2(g) + 2\,O_2(g)$	$+165 \pm 10$	$+86 \pm 5$	$\sim 10^{-17}$
Calculated from kinetics, Eq. [7] and [8]	$+56 \pm 3$	$+19 \pm 0.5$	8×10^{-5}

which oxygen is removed from the sample as $(Sb_2O_3)_2(g)$.

When the rate of gaseous diffusion is altered through changes in $P_{equil.}$, D, or L, the rate of transfer of Sb or oxygen across the Sb_2O_3 film is altered identically by an adjustment of the film thickness. This is best illustrated by the transient effects which are observed when the pressure, hence D, is changed. When the pressure is raised, the rate of oxidation sharply increases before falling to the lower value characteristic of the higher pressure. Conversely, when the pressure is dropped, the rate only slowly rises to the higher stationary value.

While the reaction proceeds, Sb_2O_3 is slowly oxidized to the nonvolatile Sb_2O_5 which crystallizes as a porous overgrowth atop the Sb_2O_3 film. Its rate of formation is so small as to contribute only slightly to the over-all rate of oxygen uptake. Furthermore, it does not significantly impede the escape of $(Sb_2O_3)_2$ by either physical or chemical interaction. When the supply of fresh O_2 to the sample is interrupted, however, the Sb_2O_3 film will continue to evaporate. When it is exhausted the Sb_2O_5 will collapse on the antimony substrate and be dissipated through the reaction, $8Sb + 6Sb_2O_5 \rightarrow 5(Sb_2O_3)_2$.

The model accounts for the principal experimental features of the oxidation of antimony in the temperature range 265°-350°C. The shift in mechanism above this temperature (cf. Fig. 4) is probably related to the fact that the rate of oxidation of Sb_2O_3 to Sb_2O_4 becomes appreciable above 350°C (9).

Manuscript received Oct. 5, 1959. The work reported in this paper was performed by Lincoln Laboratory, a center for research operated by Massachusetts Institute of Technology with the joint support of the U. S. Army, Navy, and Air Force.

Any discussion of this paper will appear in a Discussion Section to be published in the December 1960 JOURNAL.

REFERENCES

1. A. J. Rosenberg, M. C. Lavine, A. A. Menna, and T. P. Turnbull, to be published.
2. A. J. Rosenberg, *J. Am. Chem. Soc.*, **78**, 2929 (1956).
3. R. M. Bozorth, *ibid.*, **45**, 1621 (1923).
4. M. Bound and D. A. Richards, *Proc. Phys. Soc.*, **51**, 256 (1939).
5. J. T. Law and P. S. Meigs, *This Journal*, **104**, 154 (1957).
6. H. Biltz, *Z. Physik. Chem.*, **19**, 385 (1896).
7. A. Lonius, see L. B. Loeb, "The Kinetic Theory of Gases," p. 272, McGraw-Hill Book Co., New York (1934).
8. W. B. Hincke, *J. Am. Chem. Soc.*, **52**, 3869 (1930).
9. A. Simon and E. Thaler, *Z. Anorg. u. Allgem. Chem.*, **154**, 253 (1927).
10. J. P. Coughlin, *Bull. 542, U. S. Bur. of Mines*, 1954.

CaS:Cu,Eu Electroluminescent Phosphors

A. Wachtel

Research Department, Westinghouse Electric Corporation, Bloomfield, New Jersey

ABSTRACT

Introduction of Cu into CaS:Eu does not interfere with the red Eu^{++} emission. Excitation of the blue CaS:Cu emission is more effective by 3650Å than by 2537Å. Firing with excess Cu gives rise to deposits of free Cu_2S which may cause an efficient system of contact electroluminescence. The electroluminescent properties depend on the physical characteristics of the phosphors, including its state of agglomeration. At moderate concentrations of Eu, the blue emission of CaS:Cu is entirely suppressed in electroluminescent excitation.

This investigation was performed as part of a program to study new electroluminescent (EL) phosphors with red emission. CaS:Eu was chosen for the following reasons:

1. The red emission of this phosphor (1-3) can be excited by contact-electroluminescence (4).
2. As in ZnS, Cu is an efficient activator of alkaline earth sulfides. Excess Cu_2S has been proposed as responsible for local field intensification in ZnS EL phosphors (4). Through the use of excess Cu, a system analogous, with respect to energy transfer, to ZnS:Cu,Mn was sought.
3. Other red-emitting alkaline-earth sulfide phosphors such as CaS:Ni (5), MgS:Mn (6, 7), and MgS:Sm (8, 9) were not considered as promising because of the high sensitivity to moisture of MgS and repeated failure on the part of the writer to reproduce the CaS:Ni phosphor. Some preliminary work indicated that BaS:Sb may show a weak red emission, while the orange-red emission of BaS:Cu (10) seemed to depend on the presence of oxygen and is yellow in pure BaS:Cu phosphors.

Experimental Technique

Preparation of Raw Materials

CaS.—Most of the phosphor preparation was performed with CaS prepared by reduction of $CaSO_4$ with H_2 at 1000°C (11, 12), followed by firing in dry H_2S (12). The $CaSO_4$ for this purpose was precipitated with reagent H_2SO_4 from hot $Ca(NO_3)_2$ solution, purified according to a previously reported procedure (13). The CaS thus obtained is very voluminous. Denser materials as obtained by firing of $CaCO_3$ or CaO in H_2S (14), either directly or after reaction with sulfur (15), were investigated only at a later stage of this project.

Fluxes.—The usual fluxes were generally available in sufficiently pure form either directly or in

the form of suitable precursors from which they could be prepared easily. Halides were often added as resublimed ammonium salts which are not hygroscopic and, on thermal decomposition during firing, readily react with CaS to form the corresponding calcium halide, while the NH_3 formed furnished a reducing atmosphere.

Europium.—A convenient dry addition of the necessarily small amounts of Eu consisted of drying a solution of 99.9% Eu_2O_3[1] in dilute HNO_3 slurried with a definite weight proportion of purified sulfur. Usually, a concentration of 5% Eu on S was employed. This form of Eu addition was considered more versatile than the well-known use of a definite flux as carrier of the activator. The presence of free sulfur during the first stages of firing was also considered advantageous from the standpoint of decreasing the reactive O_2 concentration in the interstices of the powder, which is otherwise difficult to replace by N_2.

Mixing.—The usual technique of mixing consisted of directing a gentle current of dry N_2 on the mortar. This enabled the handling of hygroscopic substances such as $CaBr_2$ or CaI_2, as well as minimized decomposition of CaS without resorting to the use of a dry box and its attendant inconveniences. Whenever desirable, the preparation of oxygen-free phosphors was accomplished most reliably by conducting at least the latter part of the firings in a current of dry H_2S.

Firing.—Firing was conducted in transparent silica tubes, 15 mm ID, 17 mm OD, 75 mm long, closed at one end and charged with 2-3 g of the powder such that an empty channel was present throughout the length of the tube. While this resembles the use of boats, it also enabled the simultaneous firing of more than one sample under identical conditions in cases where appreciable interaction through atmospheric convection was not anticipated. Purified N_2 at a flow rate of about 500 ml/min was used as a protective atmosphere. H_2S, where used,[2] was passed through dioctyl phthalate followed by Ba $(OH)_2$ solution, "Drierite" (anh. $CaSO_4$) and P_2O_5. The gas inlet tube for H_2S had an ID of ½ in. and was charged with granular CaS extending into the hot zone of the furnace. Gradual discoloration of this CaS showed that it absorbed residual heavy metal impurities as well as converting to H_2S any residual gaseous impurities (H_2O, HCl) by simple metathesis.

An alternate method of firing consisted of capping the silica tube with another tube also closed at one end, and whose ID is no more than 1-2 mm larger than the OD of the tube containing the phosphor. This arrangement effectively prevents spontaneous convection of the atmosphere over the phosphor with the surrounding N_2 and thereby minimizes losses of volatile components such as ammonium halides. For this reason, however, the atmosphere over the phosphor is not replaced by N_2 during the initial flushing and about 500 mg S is added to the charge to displace this atmosphere during the initial warm-up of the system. This method is hereafter referred to as firing in a sulfur atmosphere.

[1] Obtained from Research Chemicals Inc., Burbank, Calif.

[2] Matheson "halogen-free" H_2S.

Measurements

It will be shown that the highly conducting nature of these phosphors introduced a considerable dependence of EL output on the resistance of the electrodes of the cell used for testing. Similarly, differences in conductivity between different phosphors were reflected in anomalous differences in EL output if such samples were operated simultaneously in a simple cell. It was therefore necessary to test each phosphor individually even at the expense of possibly imperfect reproduction of operating voltage and exact cell spacing. The power input with respect to the lateral dimension of the emitting area (25 mm diameter circle) was equalized by using an aluminized conducting glass of which only the necessary area of tin oxide was left uncovered. A 12 μ sheet of Mylar was laid on the conducting side of the glass by means of a thin film of castor oil. An oil-soaked paper spacer of about 110 μ thickness served to separate this from the solid Al electrode. Most measurements were performed with an applied voltage of 800 v at 10,000 cps.

All measurements were performed by means of a Spectra Brightness Spot Meter[3] which, except on rare occasions, was set on the "red" position to avoid any blue emission contributed by CaS:Cu. However, this was usually negligible.

The phosphor was screened through 200 mesh and mixed with castor oil in 1:1 weight proportion and placed between the cell electrodes. On application of the voltage, the EL output initially obtained tended to change due to simultaneous bridging (16) of the phosphor particles and decay of intrinsic EL. This resulted either in an initial increase followed by a decrease or a continuous decrease. In all cases, the maximum readings obtained were recorded.

General Conditions for Electroluminescence

Firing of CaS with Eu and more Cu than can be incorporated at a given halide concentration[4] results in discoloration due to formation of free Cu_2S and EL. Washing of the phosphor in alcoholic NaCN solution is possible without chemical decomposition other than removal of Cu_2S, but decreases EL.

In order to decrease the halide concentration present with Cu during firing and yet optimize the flux concentration with respect to enhancing the Eu emission, a two-stage procedure was found advantageous. A photoluminescent CaS:Eu phosphor is prepared, using the desired fluxes. The phosphor is slurried subsequently with anhydrous methanol containing the necessary amount of Cu as halide. Boiling causes deposition of the Cu as sulfide on the phosphor which is then washed with methanol until halide-free. After decanting, the phosphor is dried and refired either as is or with further additions. The refired phosphor is preferably again washed with methanol and then dried and screened.

The uniform deposition of Cu effected by this method is shown by almost complete disappearance of photoluminescence due to optical screening. Re-

[3] Photo Research Corp., Hollywood, Calif.

[4] Halide fluxes were usually preferred. As in ZnS, halides were noted to aid the incorporation of Cu in CaS (presumably as Cu^+) although this was not studied on a quantitative basis.

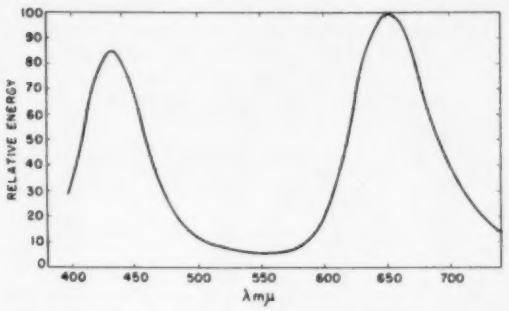

Fig. 1. Spectral distribution of 3650Å—excited emission of CaSi:Cu, Eu(0.01%) phosphor.

firing then causes a shrinkage of the precipitated layer into discrete particles of Cu_xS, and photoluminescence is restored. Electroluminescence shown at this point, when viewed through the magnification afforded by the Spectra-Meter, is seen to originate from discrete separated points which in the case of better specimens do not appear brighter but are more numerous.

Experimental Results

Photoluminescence

Introduction of Cu into CaS:Eu causes the well-known blue emission of CaS:Cu together with the red Eu^{++} emission. The Cu emission is well excited by 3650Å as shown in Fig. 1. The relative heights of the two peaks are incidental and depend on the Eu/Cu ratio and firing conditions. It is noteworthy that under 2537Å excitation, the Cu emission is largely suppressed in favor of stronger Eu emission. At low Eu concentration (0.01%),[5] the introduction of Cu, however, also enhances the otherwise weak 3650Å-excited Eu emission. This phenomenon may be analogous to the sensitized luminescence of CaS:Sm, Bi and CaS:Sm, Pb phosphors (17).

Introduction of Na^+ (and to a lesser extent Li^+) suppresses the red Eu^{++} emission. Because of the almost identical ionic sizes of Ca^{++} and Na^+, this phenomenon may well be regarded as charge compensation of substitutional Na^+ with Eu^{+++} which may thus be stabilized in the lattice. If this is so, then it tends to support Jaffe's (3) conclusion as to the divalent nature of Eu in alkaline earth sulfides. Heavier alkalies, if added as halides, do not have this effect, although the respective carbonates do.

At low Eu concentration, firing in H_2S also causes increased response to 3650Å excitation. Some of these observations are summarized in Table I which

[5] All percentages reported in this paper refer to mole or atom per cent.

Table I. Relative intensities of 6540Å peak of CaS:Eu as a function of phosphor preparation

Phosphor	3650A	2537A
1. CaS:Eu(0.01%):$CaCl_2$(5%):MgO(10%), N_2, 1050°C	1.0	29.5
2. No. 1 refired in H_2S at 1050°C	1.5	25.0
3. Like No. 2, but including 0.5% Cu	7.9	11.8
4. CaS:Eu(0.04%):NaBr(5%):Cu(1%), N_2, 1050°C	0.7	1.6

Table II. Effect of 5 mole % flux on CaS:Eu(0.02%) and CaS:Eu(0.02%):Cu(1.0%) fired in N_2 at 1050°C

	CaS:Eu:flux	CaS:Eu:Cu:flux			
		Fluor.	(3650A exc.)	EL	
	Fluor. color (3650Å exc.)	Output	Color	Output	Color
CaF_2	pink	2.0	pink	1.3	rose
$CaCl_2$	pink	3.0	pink	1.2	rose
$CaBr_2$	pink	3.0	rose	2.5	rose
CaI_2	pink	3.6	white-pink	1.9	rose
$(NH_4)_2HPO_4$	pink	2.0	white-pink	1.3	rose
$NH_4HB_4O_7$	pink	3.0	white-pink	1.6	rose
Li_2CO_3	negl.	1.2*	green	trace	yellow
Na_2CO_3	blue	20*	yel.-green	none	—
K_2CO_3	v-weak	18*	white-green	none	—
Cs_2CO_3	v-weak	10*	white-green	none	—

* Spectra Meter set on "ft-L."

shows measurements of the 6540Å peak height taken on excitation with two sources whose relative output was measured by the fluorescence of sodium salicylate. The figures refer to relative values normalized for equal number of quanta of incident 2537 and 3650Å radiation.[6] It should be mentioned that increased Eu concentration greatly increases the 3650Å-excited fluorescence, so that the low values of sample No. 4 in Table I are due to the effect of Na^+.

Effect of Phosphor Composition and Firing on EL

The effect of fluxes was investigated by firing CaS with 0.01 mole % Eu + 5 mole % flux at 1050°C in N_2 for 1 hr. The second firing was conducted with 1 mole % Cu for 20 min at 1050°C in N_2. Table II shows that $CaBr_2$ resulted in the brightest EL. CaI_2 suffers decomposition but yields similar results if used in larger quantity. The effect of alkali carbonates is the same as discussed in the previous section and, in addition, not even blue or green EL is observed. The brighter fluorescence of the green emission is probably only an effect of color. It appears to consist of a band peaked at 505 mμ as shown in Fig. 2 for a CaS:Cu,Eu,Na phosphor. Because of the halide-gettering effect of Na_2CO_3, this green center might consist of Cu^{++}. It may, however, also be identifiable with the green emission peaked at 495 mμ as obtained by Asano and Kishimoto (18) on 3CaS:$CaSO_4$:Cu,Na_2SO_4 phosphors, which these

[6] Under the simplified assumption of linear dependence of fluorescence on intensity of excitation.

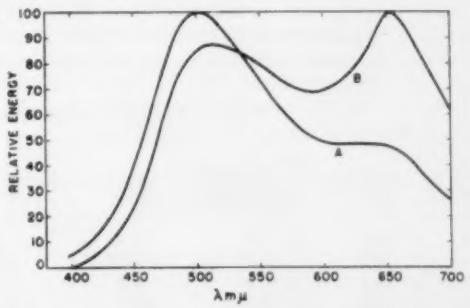

Fig. 2. Spectral distribution of emission of a CaS:Cu:Eu(0.01%):Na phosphor. A, 3650Å excitation; B, 2537Å excitation.

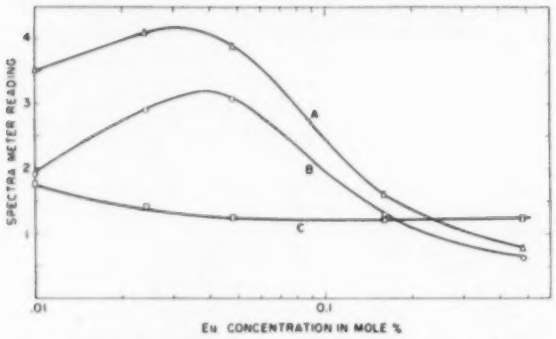

Fig. 3. Effect of Eu concentration on EL of CaS:Cu(1.-0%):Eu(x) phosphors. A, Spectra Meter set on ft-L (brightness; B, spectra Meter set on "red;" C. Ratio of A/B.

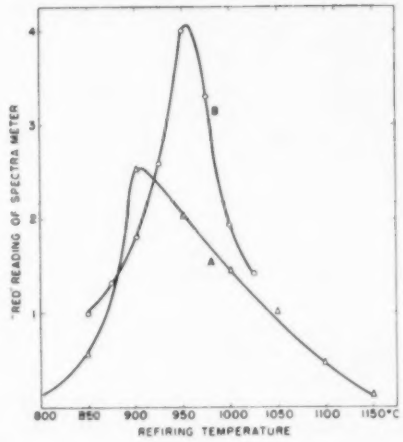

Fig. 4. Effect of refiring temperature in EL of two compositions: A, CaS+0.038% Eu+5% $NH_4HB_4O_7$+10% NH_4Br, 1050°C, N_2—15 min, H_2S—45 min, washed, +1.15CuS+2.-5% NH_4HBO_7, H_2S, 20 min; B, CaS+ 0.038% Eu+5% NH_4-HB_4O_7+10% NH_4Br, 1050°C, N_2—15 min, H_2S—45 min, +1.5% $CuCl_2$, washed, +5% $NH_4HB_4O_7$, H_2S—20 min.

authors ascribe to "CaS". The 10 mμ shift to longer wave lengths obtained here may be due to superposition of a portion of the Eu emission. Here again, 2537A excitation tends to favor the excitation of the few Eu^{++} centers still present.

Figure 3 shows the result of increasing Eu concentration in similarly prepared phosphors fluxed with $CaBr_2$. The ratios of measurements taken through the different filters of the Spectra Meter show that, at low Eu concentration, there is an appreciable blue contribution of CaS:Cu. Spectral distribution measurements showed that in the neighborhood of maximum red output (0.04 mole % Eu) the blue emission is entirely absent. In Fig. 3, this can also be estimated by the leveling-off of the ratio curve whose residual height thereafter is a function of the response of the particular photometer to the Eu emission only.

The gradual disappearance of the blue CaS:Cu emission which occurs with increasing Eu concentration is analogous to the effect observed on introducing Mn into ZnS:Cu. Inasmuch as the red Eu emission is best excited by wave lengths much shorter than the Cu emission, one is probably not dealing with an optical cascade process. The same conclusion may be drawn from the strong excitability of the blue emission by 3650A, alongside with the red Eu emission. The mechanism therefore involves sensitization as in ZnS:Cu,Mn (19) as well as many other doubly activated systems.

Inasmuch as the excess Cu_2S is thought to effect local field intensification, its particle size and distribution as well as the surface condition of the phosphor were considered to be critical. Figure 4 shows that this is probably affected by the refiring temperature in the presence of Cu which shows sharp optima with respect to EL output. Similarly, the prefiring temperature and amount of Cu added have a pronounced effect. This is shown in Table III. It will be noted that, with the exceptions of a few points showing what are believed to be accidental variations, the ratios of EL to fluorescence brightness tend to increase with increasing Cu addition and then level off in the neighborhood of maximum observed EL. This indicates that decreasing EL at higher Cu concentrations may be an optical effect due to darker body color.

It was generally noted that the parameters influencing EL output of this system appear to be more numerous than could be investigated within the scope of this study. Table IV gives a summary of some measurements taken on differently prepared phosphors. KBr as a flux was investigated because it resulted in particularly bright photoluminescent Eu emission (first firing), while $NH_4HB_4O_7$ has usually proven advantageous on EL if both firings are conducted in H_2S. It is now shown that either of these fluxes tended to reduce EL output, especially when used together.

An effort was made to shift the emission spectrum to shorter wave lengths and thus increase the visual output of these phosphors. This is known to occur upon partial substitution of Ca by Mg or Sr. In-

Table III. Effect of Cu addition on EL of phosphors prefired at three temperatures

Mole % Cu added	1020°C Prefired			1050°C Prefired			1080°C Prefired		
	EL	Fluorescence	Ratio	EL	Fluorescence	Ratio	EL	Fluorescence	Ratio
0.75	2.7	1.3	2.07	1.8	1.5	1.2	0.65	1.6	0.4
1.0	2.25	0.95	2.38	4.0	1.2	3.3	1.7	1.2	1.4
1.25	3.1	0.72	4.3	5.5	0.85	6.5	4.3	0.9	4.8
1.5	6.8	0.63	10.8	6.0	0.74	8.1	4.0	0.77	5.2
1.75	3.5	0.45	7.8	2.3	0.54	4.3	3.9	0.52	7.5
2.0	5.0	0.40	12.5	5.2	0.48	10.8	4.3	0.39	11.0
2.5	3.5	0.35	10.0	4.0	0.38	10.5	3.6	0.50	7.2
5.0	1.92	0.16	12.0	1.8	0.17	10.5	1.3	0.14	9.3

Table IV. Effect of 5 mole% KBr and 5 mole% $NH_4HB_4O_7$("AB") and firing atmosphere on CaS:Eu(0.038):Cu(1.5) prefired at 1050°C, 1 hr and refired at 950°C, 20 min

Basic composition*	First firing				Second firing				
	Additions		Atmosphere		Additions		Atmosphere, EL obtained at 10 kc, 800 v		
	AB	KBr	S	H_2S	AB	KBr	S	N_2†	H_2S
1	+	—	—	+	+	—	3.7	4.2	3.6
2	+	+	—	+	+	—	—	—	3.0
3	+	—	—	+	+	+	—	—	3.0
4	+	+	—	+	+	+	—	—	0.9
5	+	—	+	—	+	—	1.2	1.3	2.0
6	+	+	+	—	+	—	1.5	—	1.5
7	+	—	+	—	+	+	1.2	—	1.5
8	+	+	+	—	+	+	0.9	—	0.7
9	—	—	—	+	—	—	6.2	4.9	—
10	—	+	—	+	—	—	3.9	5.7	—
11	—	—	+	—	—	—	2.6	6.9	—
12	—	+	+	—	—	—	4.2	5.8	—
13	—	—	+	—	—	+	1.0	0.36	—

* 10 mole % NH_4Br for H_2S (open tube), or 1 mole % NH_4Br for S (capped tube) first firing, added in all cases.
† Open tube, but S added to mix for rapid reduction of entrained oxygen.

creased brightness was achieved, however, only on ultraviolet excitation. The substitutions generally introduced phosphorescence[7] and decreased or completely extinguished EL (20).

Additional attempts were made to optimize the nature of Cu_xS segregations. Of interest may be the effect of $CaBr_2$ or CaO in the second firing. This is shown in Fig. 5 and 6. In the case of $CaBr_2$, the effect was noted to depend on the use of H_2S and the sample size refired. Under optimum conditions, it may be postulated that partial incorporation of Cu^+ at the surface of the phosphor causes enhanced emission, while the particle size of the remaining Cu_xS is somewhat reduced. However, increased $CaBr_2$ retention (as in the case of large additions, N_2 refiring, or larger sample sizes) dissolves too much Cu. A particularly advantageous effect of the $CaBr_2$ at this stage consists of decreasing the fluxing action of the Cu_xS which is also well known in ZnS phosphors. The effect of CaO (Fig. 6) is of interest inasmuch as most if not all of this is converted to CaS during the firing in H_2S. The advantageous effect of low CaO addition, in this case, is therefore probably due to modified surface structure. Otherwise, it may be seen that oxygen in the finished phosphor is probably detrimental.

Effect of Physical Structure of CaS and Finished Phosphors on EL

A number of phosphors were prepared under conditions whereby the only variable consisted of CaS prepared by different methods and therefore differing in particle size and degree of agglomeration. Correlation of the results with microscopic examination of the phosphors showed that the highest brightness values were always obtained on phosphors consisting of thin, uniform, and fairly extended agglomerates, relatively free of fine background. No correlation of EL brightness with degree of crystallinity as obtained by x-ray powder diffraction patterns could be noted. Generally, the differences in EL output obtained here were as great as previously reported on as a result of varying phosphor composition and firing procedures. To illustrate this further, Table V shows four phosphors, each separated into two fractions 45-75 μ and <45 μ. It can be seen that the differences in EL output are considerable. Since the largest single crystals of phosphor rarely exceed 3 μ in size, it appears that the EL output of this system is a function of agglomeration.

Attempts to achieve this artifically were made by preparing phosphors from CaS derived from $CaCO_3$ or CaC_2O_4 of particle size up to 100 μ as obtained by

[7] The phosphorescence of CaS:Eu:$CaBr_2$ is quenched at Eu concentrations as low as 0.024 mole %. Most of the present phosphors were prepared with 0.04 mole % Eu.

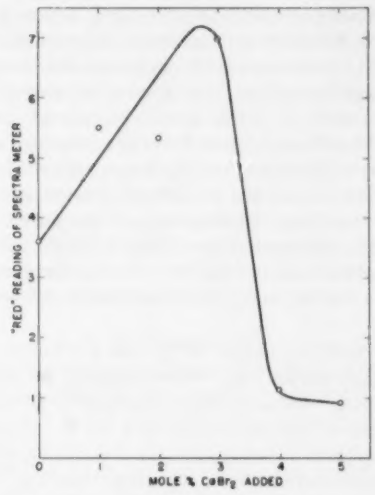

Fig. 5. Effect of $CaBr_2$ added in second firing in H_2S. One gram samples refired at 950°C for 20 min.

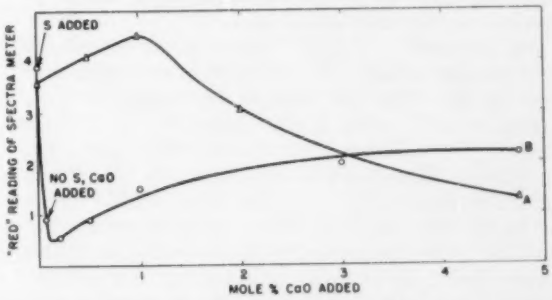

Fig. 6. Effect of CaO added in second firing in two atmospheres: A, procedure No. 1 in Table IV, H_2S refired. B, procedure No. 11 in Table IV, N_2 refired. The true abscissa of the second point is unknown. As drawn, it represents the probable oxide contamination.

Table V. EL output of different particle size fractions of CaS:Cu,Eu phosphors

Phosphor No.	45-75 μ	<45 μ	Ratio
1	3.3	2.2	1.5
2	0.95	0.26	3.6
3	1.2	0.26	4.6
4	1.0	0.33	3.0

homogenous precipitation with urea. These preparations were handled with sufficient care so as to avoid mechanical destruction of agglomerates whose outward shape remained, throughout all stages of preparation, that of the original crystals of $CaCO_3$ or CaC_2O_4. The EL output of these phosphors was, however, low and the dark body color suggested lack of penetration of the Cu beyond the outer surfaces of the agglomerates. Simultaneously prepared control phosphors obtained from finer CaS:Eu in which some agglomeration occurred during the second firing had a lighter body color and better EL performance.

Properties of CaS:Eu,Cu EL Phosphors

Chemical properties.—The chemical properties of the phosphors are essentially those of CaS, i.e., well-known. Slow decomposition as a result of exposure to atmospheric moisture has no noticeable effect on photoluminescence but does affect the EL. In connection with this, the effect of moisture absorbing additives was investigated. Table VI shows that the additives have an immediate detrimental effect. Its nature has not been determined.

EL properties.—Figure 7 and 8 show the voltage and frequency dependence of a typical phosphor. It can be seen that the voltage dependence is quite steep, possibly owing to the small intrinsic particle size of the phosphor (21). On the other hand, the frequency dependence is comparatively slight and better specimens can be excited to be readily visible at 60 cps. The luminous efficiency at 10,000 cps excitation of two phosphors is shown in Fig. 9. Under equal conditions of input (voltage and cell characteristics) the more efficient phosphor also consumed on the average 1.7 times as much power as the less efficient phosphor, i.e., was approximately 2.5 times brighter. The shape of the graphs suggests that maximum efficiency occurs at field strengths which are higher than can be achieved in practice. Somewhat similar but less reproducible results were obtained at 500 cps excitation.

Electrical properties.—As mentioned earlier, the conductivity of the CaS:Eu,Cu phosphor is very high compared to that of normal ZnS:Cu EL phosphors. Table VII shows the effect of electrode resistance on EL output of two phosphors. Under similar experimental conditions, no perceptible difference could be noted for the usual ZnS:Cu EL phosphor. Assuming a similar slope of log L vs. $V^{-1/2}$ as shown in Fig 7 and a voltage drop across the phosphor layer which is proportional to its effective resistance[5] under the particular conditions of cell operation, the respective resistances across the thickness of the 110 μ x 25 mm patch of phosphor suspension

[5] For simplicity, the calculation was made as for an ohmic resistance. Actually, the conductivity is purely an effect of ϕ, since an insulating layer of Mylar is used.

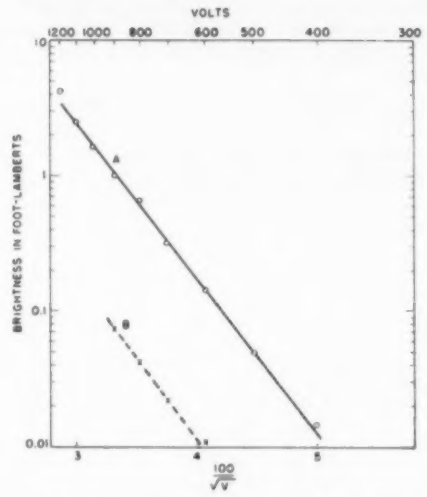

Fig. 7. Voltage dependence of EL of a CaS:Cu, Eu phosphor. Cell spacing 110 μ. A, 10,000 cps; B, 400 cps.

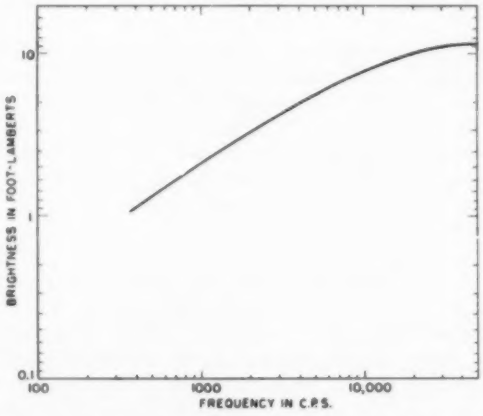

Fig. 8. Frequency dependence of EL of a CaS:Cu, Eu phosphor. Excitation at 800 v.

turn out to be about 1000 and 2000 ohms, respectively, i.e., very low values. Inasmuch as Fig. 9 suggests that a more conducting phosphor may also be more efficient (and much brighter) the difficulties in reproducible phosphor comparison with respect to different cell characteristics can readily be appreciated. It is for this reason that only values appearing within any one table or figure are comparative with each other.

Discussion

The observations made in this investigation suggest a model for the CaS:Eu,Cu EL phosphor consisting of a fine dispersion of Cu_xS particles in con-

Table VI. Effect of moisture and additives on EL output

Additive	Time of exposure to 100% relative humidity 0	1 hr	20 hr
none	2.0	1.5	0.62
1% CaO	2.0	0.8	0.49
1% MgO	1.4	0.66	0.45

Table VII. Effect of electrode resistance on EL output

Resistance from bus bar to phosphor, ohms	EL, 10 kc, 800 v	
	Phosphor a	Phosphor b
50	4.0	2.5
90	—	2.5
145	—	2.0
250	1.8	1.8

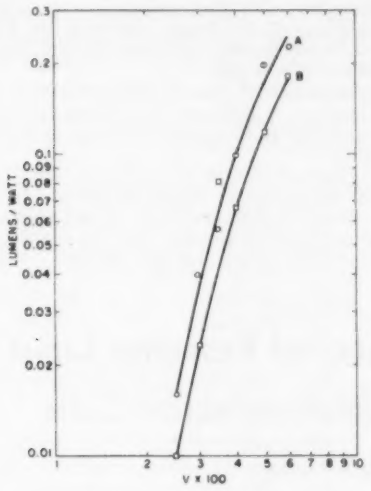

Fig. 9. Luminous efficiency of EL of two CaS:Cu, Eu phosphors excited at 10,000 cps. A, bright phosphor; B, dim phosphor.

tact with the surfaces of a red-emitting CaS:Eu,Cu phosphor. If the coated phosphor particles are agglomerated, there results increased EL output. The reason for this is not clear at present; however, one reason may be proposed on the grounds that penetration of the dielectric embedding material into the interior of the agglomerates may be poor, so that the bulk of the emitting material is subjected to greater than average field strengths. This would also explain the poorer performance of all systems in which the Cu_2S phase may be assumed to be in contact with the dielectric, i.e., either single crystal background or surface coated agglomerates.

The model is in some respects similar to the one proposed by Lehmann for ZnS:Cu EL phosphors (4) except that here one seems to be dealing with a more heterogeneous system. Phosphor formation in ZnS is associated with considerable crystal growth, and the formation of field intensifying disturbances is a process occuring during this growth and subject only to the over-all composition of the system and the firing procedure. In the present phosphor, however, there is little evidence of this, and special efforts must be made to obtain the desired physical structure by means other than relying on the usual (automatic) recrystallization process. It can, at present, only be estimated that at least one parameter responsible for high EL output should be identifiable with the concentration and state of dispersion of the Cu_2S phase on the surface of the CaS:Eu,Cu phosphor. Other parameters may be the crystallographic nature and electrical properties of the Cu_2S-CaS interface. It is probably in this respect that the comparison with ZnS:Cu EL phosphors breaks down, inasmuch as the brightness and efficiency obtainable in ZnS:Cu EL phosphors can only be explained in terms of highly specialized junctions.

The EL properties of CaS:Eu,Cu need not be regarded as an isolated case among alkaline-earth sulfides. Besides the blue-emitting CaS:Cu phosphor, yellow-emitting BaS:Cu EL phosphors were prepared successfully during preliminary phases of this study. Orange-red emitting $BaS:BaSO_4$:Cu (10) prepared with some nonincorporated Cu showed lower EL output, possibly due to presence of appreciable phosphorescence (deep traps). There is reason to believe that, under suitable conditions of preparation, any known semiconductor-type phosphor which may be coactivated by Cu may be amenable to similar treatment, provided that the phosphor tolerates the high activator concentration known to be advantageous for EL emission (22) and that deep traps can be reduced.

Summary

A method of obtaining EL in CaS:Eu has been presented, consisting of the introduction of Cu in concentrations greater than can be accommodated in the phosphor lattice. Among the various procedures tried, definite relationships have been found to exist between EL output and Cu concentration, firing temperatures and atmospheres, fluxes, and the physical nature of the raw material employed. The EL exhibited by this system appears to be a form of contact EL produced at more points than can be achieved by mechanical mixtures, and microscopic examination shows that the best specimens consist entirely of thin agglomerates of uniform size. In addition, it is visualized that the nature of the Cu_2S-CaS:Cu, Eu interface may influence the efficiency of EL produced at individual contact points. The parameters necessary to optimize this effect reproducibly are more numerous than could be investigated at present, and this difficulty is at least partially caused by the conductivity of the phosphor which influences its relative performance under slightly different conditions of excitation.

The absence of blue CaS:Cu emission shows that an energy transfer mechanism possibly analogous to that occurring in ZnS:Cu,Mn may take place. It is felt that the method can be adapted to other phosphors whose activator and trap distribution are such as not to interfere with the EL excitation process.

Acknowledgments

The writer is indebted to Miss I. Walinski for her aid in the performance of much of the experimental work, as well as to Mr. I. Meister and Drs. C. K. Lui-Wei, W. A. Thornton, and W. Lehmann for measurements. He also wishes to thank Professor E. Banks and Dr. W. Lehmann for helpful discussions and Dr. H. F. Ivey for reading and suggesting improvements in the original manuscript.

Manuscript received Aug. 27, 1959.

Any discussion of this paper will appear in a Discussion Section to be published in the December 1960 JOURNAL.

REFERENCES

1. H. M. Fernberger, U. S. Pat. 2,372,071, March 20, 1945.
2. P. Brauer, *Z. Naturforsch.*, **6a**, 561 (1951).
3. P. M. Jaffe and E. Banks, *This Journal*, **102**; 518 (1955).
4. W. Lehmann, *ibid.*, **104**, 45 (1957).
5. P. Lenard, F. Schmidt, and R. Tomaschek, "Handbuch der Experimental-physik," XXIII, 1, p. 331, Akad, Verlagsges. Leipzig (1928).

6. E. Tiede and F. Richter, *Ber. deutsch. chem. Ges.*, **55**, 69 (1922).
7. I. Schaper, *Ann. Physik*, **85**, 942 (1928).
8. R. Tomaschek, *ibid.*, **75**, 109, 561 (1924).
9. M. Travinicek, *ibid.*, **79**, 237 (1926).
10. Reference (5), p. 378.
11. K. F. Stripp and R. Ward, *J. Am. Chem. Soc.*, **70**, 401 (1948).
12. "Inorganic Syntheses," Vol. III, L. J. Audrieth, Editor, p. 20, McGraw Hill Book Co., New York (1950).
13. A. Wachtel, *This Journal*, **105**, 256 (1958).
14. "Preparation and Characteristics of Luminescent Materials," G. R. Fonda and F. Seitz, Editors, p. 30, J. Wiley & Sons, Inc., New York (1948).
15. Reference (5), p. 327.
16. W. Lehmann, *This Journal*, **103**, 24 (1956).
17. S. Rothschild, *Physik. Z.*, **37**, 757 (1936).
18. S. Asano and T. Kishimoto, *Science of Light*, **6**, 101 (1957).
19. H. C. Froelich, *J. Opt. Soc. Am.* **43**; 320 (1953) and U. S. Pat. 2,743,239 (April 24, 1956).
20. C. H. Haake, *J. Opt. Soc. Am.*, **47**, 881 (1957).
21. W. Lehmann, *This Journal*, **105**, 585 (1958).
22. W. Lehmann, *J. Opt. Soc. Am.*, **48**, 647 (1958).

Influence of Crystal Size on the Spectral Response Limit of Evaporated PbTe and PbSe Photoconductive Cells

W. D. Lawson, F. A. Smith[1], and A. S. Young

Royal Radar Establishment, Malvern, England

ABSTRACT

Photoconductive layers of PbTe have been formed by evaporation on substrates at different temperatures. The size of crystals in the layers has been estimated from electron micrographs and x-ray diffraction, and a correspondence has been obtained between crystal size and the limit of spectral response. Sensitivity up to the long wave-length limit set by the energy gap is not achieved unless the crystals are greater than a critical size; for lead telluride this is about a quarter of a micron. A similar effect has been shown to occur with PbSe.

Photoconductive layers of PbTe are commonly prepared by an evaporation technique usually in a low pressure of oxygen, followed by a sensitizing heat treatment either *in vacuo* or in a low pressure of oxygen. PbS and PbSe cells can be made similarly, or the layers can be formed by chemical precipitation from solutions and this may or may not be followed by heat treatment. It is well known that the sensitivity and the spectral response of layers depend very markedly on the preparation process and on the subsequent heat treatment, and, although some very sensitive cells have been prepared, the processes employed are mainly empirical (1) and the precise effect of each stage in the treatment is not always clear. This note shows that the long wave-length limit of the spectral response of a layer is related to the size of the crystals in the layer and that full spectral response is not developed unless the crystals are of adequate size. Thus layers prepared initially with small crystals respond only to the shorter wave lengths and one effect of heat treatment is growth of the crystals with a corresponding extension of the response to longer wave lengths.

Preparation of Layers

The layers used in this investigation were all prepared by the evaporation technique described in detail by Young (2) for PbTe, in Dewar-type cell blanks fitted with sapphire windows. Powder from crushed single crystals was used as starting material and it was first evaporated onto the sapphire window of the cell blank in a good vacuum (10^{-6} mm Hg) and then transferred to the glass substrate which carried the electrode system, through a low pressure of oxygen (10^{-2} to 10^{-3} mm Hg). The thickness of the layers was about one micron and apart from the variables noted in Table I the conditions of preparation were as nearly identical as possible for all layers.

Measurement of Spectral Response

The measurements of spectral response were made using a Leiss double monochromator (3) fitted with sodium chloride prisms. The monochromatic radiation from the output slit was divided into two beams, one of which was deflected to the layer under test, the other to Hilger thermocouple. The path lengths of the two beams were made equal in order to eliminate the effects of atmospheric absorption.

The input radiation to the monochromator, from a Nernst filament source, was chopped at two frequencies by two independent rotating sectored disks. One frequency of 5 cps was suitable for the thermocouple response time, and the other of 800 cps was used in the photoconductive response circuit. The signal from the thermocouple, after amplification at 5 cps, was used in a servosystem to control the aperture of the input slit and so maintain a constant energy output from the monochromator over the wave-length range 1 to 7 microns.

The cell under test was connected through a series load resistor to a constant voltage source and the 800 cps signal developed was amplified in a tuned high-gain amplifier (4) and fed to a pen recorder.

[1] A.E.R.E., Harwell, England.

The wave-length scale on the chart was derived from calibration pips obtained from the monochromator prism drive. The response curves are reproduced as they were drawn by the recorder; the wave-length scale is not linear because the dispersion of the prisms is not linear with either prism drive or chart drive. The response scale is linear but arbitrary as we were not concerned in this study with absolute measurements of sensitivity.

The apparatus was arranged so that spectral responses could be monitored while the cells were being processed on the pumping system and all spectral responses were measured with the cells at 90°K.

Electron Microscope Examination of the Layers

At one micron the layers are too thick to be examined directly in a transmission electron microscope and replicas have to be used. Some photographs were taken in a reflection electron microscope, but they were difficult to interpret and the replica technique was found to be the best way of examining the structure of the layers. Preshadowed aluminum replicas about 250Å thick were used, prepared by first evaporating a layer of boric oxide onto the photoconductive layer, then the shadowing material, uranium or gold-palladium alloy at an angle of ~ 30°, and finally the aluminum layer evaporated from three directions simultaneously to ensure a continuous replica. The replicas were then floated off by immersing the specimen gently in water. The magnification of all the E. M. pictures is about 10,000 times; crystal sizes were measured from these photographs.

X-Ray Photographs

Back reflection x-ray Laue photographs of the layers were taken, with the front window of the cell removed, using radiation which consisted predominantly of the $K\alpha_1$ and $K\alpha_2$ lines of copper. A half-millimeter diameter collimator directed the beam on to the specimen, and the film-specimen spacing was 3 cm. Exposure times of 3-4 hr were required.

The x-ray photographs give an indication of crystal size (5) since the scattered beams from very small crystals are broadened and the broadening from crystals up to 300Å thick is sufficient to prevent resolution of the α doublet. Between 300Å and 1000Å broadening still occurs, but the doublet can be resolved and above 1000Å the doublet is fully resolved. Crystal sizes from 1000Å up to 10,000Å give continuous sharp diffraction rings, but above that there are insufficient orientations present in the irradiated region of the layer to give continuous rings which then begin to appear spotty.

Debye-Scherrer photographs taken on powder scraped from the layers confirmed that the material was PbTe with the same lattice spacing, 6.45Å, as the original crystals.

Results

Lead Telluride.—Figures 1 to 6 show x-ray and electron microscope photographs and measurements of spectral response at 90°K, obtained from a series of lead telluride layers prepared as described in

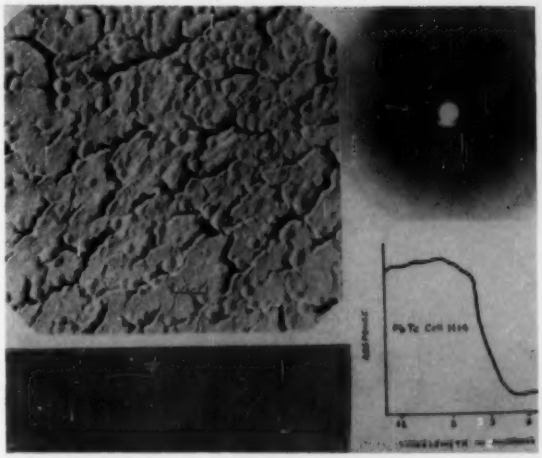

Fig. 1. PbTe cell H14 formed at 90°K. Electron micrograph, x-ray Laue photograph, and spectral response.

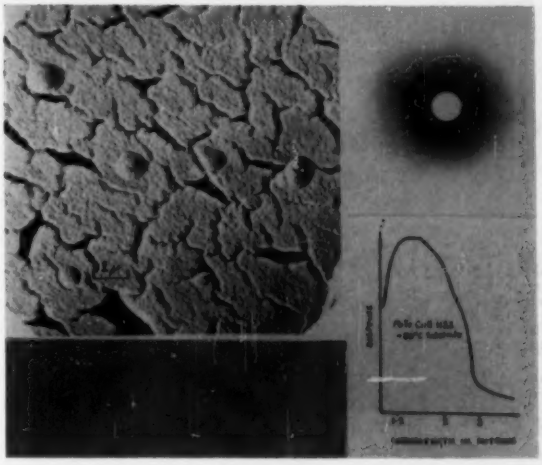

Fig. 2. PbTe cell H22 formed at 193°K. As Fig. 1

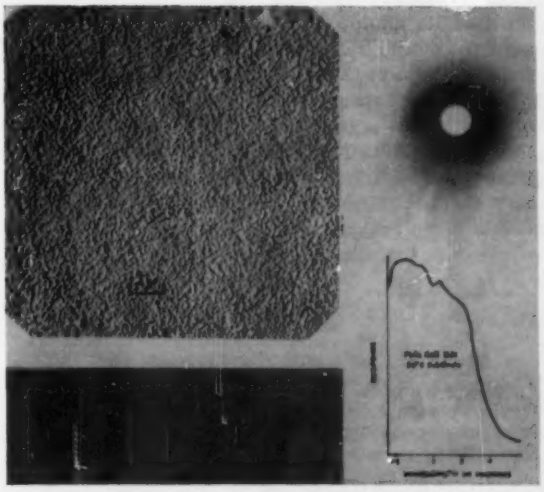

Fig. 3. PbTe cell H21 formed at 300°K. As Fig. 1

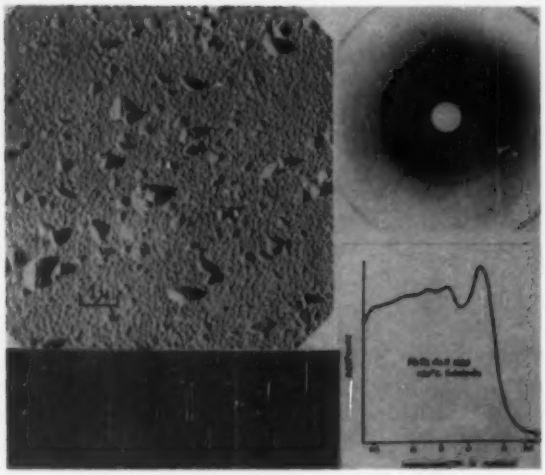

Fig. 4. PbTe cell H20 formed at 420°K. As Fig. 1

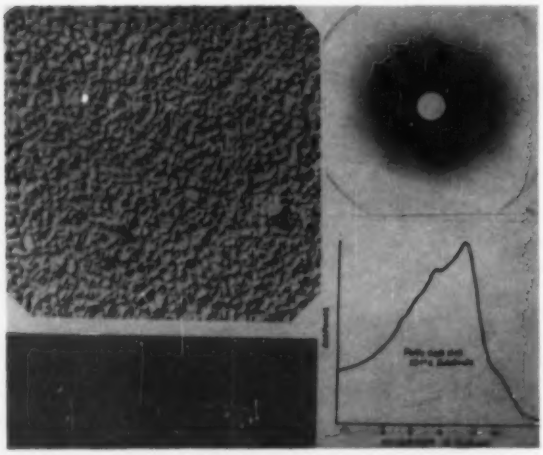

Fig. 5 PbTe cell H18 formed at 650°K. As Fig. 1

(2) but with the glass substrate held at different temperatures while the layers were being formed. Table I gives the substrate temperature at which each cell was formed and also the long wave-length limit of its photoconductive response and an estimate from the x-ray and electron micrographs of the mean size of the crystallites in the layer.

The oxygen pressure at which each layer was formed is also given in Table I, and it will be seen that the pressure has been increased with substrate temperature. This increase was found to be necessary in order to obtain a reasonable sensitivity in

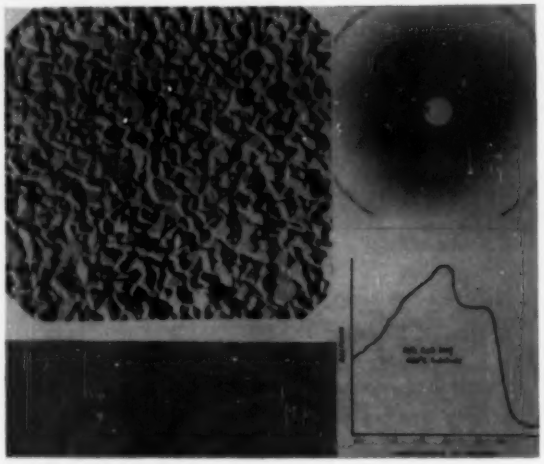

Fig. 6. PbTe cell H19 formed at 720°K. As Fig. 1

each layer, but we found that oxygen pressure by itself had no influence on the limit of response. The precise role of oxygen in the sensitizing process is not discussed in this paper. Jones (6) has shown in experiments on the oxidation of lead selenide that the amount of oxygen taken up in the sensitizing process is small (<2%).

From absorption measurements on single crystals (7) lead telluride should give a photoconductive response at 90°K extending to 5.8μ on the long wave-length side, assuming correspondence between absorption and photoconductivity. It will be seen from Fig. 1-6 that the full spectral response is obtained only from layers formed on the hotter substrates and the limit of response in layers formed on the colder substrates occurs at shorter wave lengths. The reason becomes apparent from the electron micrographs. These show a progressive increase in crystallite size with increasing substrate temperature, as might be expected, and it is only those layers which have crystallites of adequate size which exhibit the full spectral response out to 5.8μ. The critical size is between a quarter and a half a micron; crystals smaller than that are apparently unable to absorb the longer wave-length radiation and the spectral response is limited correspondingly. This explanation is confirmed by the discrepancy between the measured absorption of layers (8) and single crystals (7). The layers gave an absorption edge at about 2μ (measured at 290°K), whereas the absorption edge of single crystals at the same temperature occurs at 4.5μ. The absorption edge of single crystals varies very little

Table I

Figure No.	1	2	3	4	5	6	7
Cell No.	H14	H22	H21	H20	H18	H19	H14
Substrate temp, °K	90	193	300	420	650	720	90
Oxygen pressure, mm Hg	5×10^{-4}	10^{-6}	5×10^{-6}	7×10^{-5}	10^{-2}	10^{-3}	5×10^{-4}
Limit of response, microns	3[a]	3[a]	4	5	5.8	5.8	2.5[b]
Crystallite size, microns	<0.03[a]	<0.03[a]	0.06	0.12	0.25	0.5	

[a] After the layer had warmed up to room temperature.
[b] Before the layer had warmed up to room temperature.

with deviations from stoichiometry or with the state of strain of the crystal. The conditions of preparation of the layers in reference (8) are not given, so a comparison of their properties with ours is not possible.

The response of cell H18 formed at 650°K goes out as far as that of cell H19 formed at 720°K, but in the latter cell high sensitivity is maintained right out to 5.5μ whereas in H18 the sensitivity falls rapidly beyond 4.5μ. This again can be attributed to the difference in crystal size. An apparent anomaly occurs in the response of cell H14, prepared at 90°K, which goes to a slightly longer wave length than H22, formed at 193°K. These responses were, however, measured after each cell had been allowed to warm up to room temperature, cell H14 for a longer time than H22. Some increase in crystal size may occur at room temperature so that spectral responses measured after warming up are not truly characteristic of the temperature of formation. This is consistent with the result in Fig. 7 which shows the response curve of cell H14 taken immediately after the layer was formed at 90°K and before it had been allowed to warm up at all; the limit of response occurs at an even shorter wave length, 2.5μ. It was not possible to measure the characteristic crystal size corresponding to 90°K as an x-ray or replica could not be taken without letting the layer come to room temperature, but the result can again be explained in terms of crystal size since it is likely that the layer formed at very low temperature consists of very small crystals.

The response of H14 after a further anneal at 620°K is shown in Fig. 8 together with the x-ray and electron photographs. The doublet in the Laue diagram is now distinctly resolved, c.f. Fig. 1 showing that the crystals have grown and this is confirmed in the electron micrograph. The limit of photoconductive response has now moved out to about 5.8μ and sensitivity is well maintained to nearly 5.5μ.

The physical appearance of the layers in Fig. 1, 2, and 8 is characteristic of layers which are formed on substrates below room temperature. It is likely that the cracks develop through differential expansion during the period of warming up to room temperature.

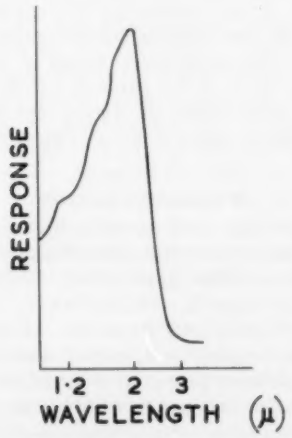

Fig. 7. Spectral response of PbTe cell H14 measured immediately after formation.

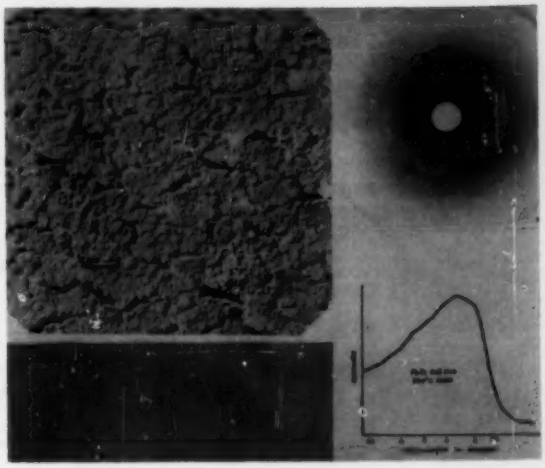

Fig. 8. Electron micrograph, x-ray Laue photograph, and spectral response of PbTe cell H14 after anneal at 620°K.

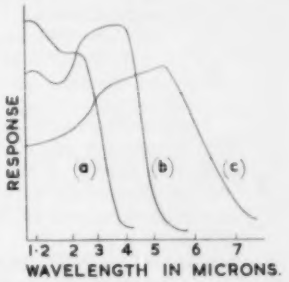

Fig. 9. Spectral responses of PbSe cells baked at different temperatures. (a) Cell H1 left at room temperature; (b) cell H3 baked at 420°K; (c) cell H8 baked at 570°K.

Lead selenide.—Lead selenide layers prepared in the same way by evaporation give similar results, and the dependence of spectral response on crystal size again occurs. The results are not given here in detail but Fig. 9 shows how the limit of response can be moved to longer wave lengths. Cell H1 was formed on a cooled substrate at 90°K through an oxygen pressure of 10^{-2} mm Hg, it was allowed to warm up to room temperature, and its response was measured (at 90°K) some time later. The response ends at about 3.5μ. Cell H3 was prepared similarly and subsequently baked *in vacuo* (10^{-4} mm Hg) at 420°K; its response extends to about 5.2μ. Cell H8 was baked instead to 570°K with a corresponding extension of response to about 7μ, the same as the limit at 90°K in single crystals (9). X-ray and electron micrographs of these layers again showed a gradual increase in crystal size with the temperature of the heat treatment.

Conclusion

The long wave-length limits of photoconductive response and absorption of evaporated layers of PbSe and PbTe are related to the size of the crystallites in the layer. By controlling crystallite size the response or the absorption of a layer can be made to terminate at any wave length up to the

limit fixed by the energy gap of the compound. Thus infrared filters and selective narrow-band filter-detector combinations can be constructed to operate anywhere within the spectral range of the material.

Acknowledgments

The authors are indebted to Miss A. E. Rennie for taking the x-ray photographs, Mr. A. A. Brooker for assistance with the preparation of cells, and Dr. C. S. Lees for helpful discussions on the electron microscope study. The paper is published by permission of the Controller, H. M. Stationery Office.

Manuscript received Sept. 9, 1959.

Any discussion of this paper will appear in a Discussion Section to be published in the December 1960 JOURNAL.

REFERENCES

1. T. S. Moss, *Proc. I.R.E.*, **43**, 1869 (1955).
2. A. S. Young, *J. Sci. Instr.*, **32**, 142 (1955).
3. V. Roberts, *ibid.*, **29**, 134 (1952).
4. D. A. H. Brown, *ibid.*, **29**, 292 (1952).
5. N. F. M. Henry, H. Lipson, and W. A. Wooster, "The Interpretation of X-ray Diffraction Photographs," Macmillan Co., New York (1951).
6. R. H. Jones, *Proc. Phys. Soc.*, **B70**, 1025 (1957).
7. A. F. Gibson, *ibid.*, **B65**, 378 (1952).
8. A. F. Gibson, *ibid.*, **B63**, 756 (1950).
9. A. F. Gibson, W. D. Lawson, and T. S. Moss, *ibid.*, **A64**, 1054 (1951).

Relation of Some Surface Chemical Properties of Zinc Silicate Phosphor to its Behavior in Fluorescent Lamps

D. E. Harrison[1]

Luminescent Materials Laboratories, Lamp Metals and Components Department, General Electric Company, Cleveland, Ohio

ABSTRACT

The importance of the surface properties of zinc silicate phosphor to fluorescent brightness and lumen maintenance has been demonstrated. A phenomenological theory is developed which accounts qualitatively for some of the changes that occur during lamp burning. Inherent in this theory is the concept of a high-temperature surface phase which is a part of the zinc silicate crystal. The surface phase may be retained at room temperature by rapid quenching, but if the phosphor is cooled slowly the surface phase dissociates, probably into its constituent oxides. As a result Mn^{2+} can be oxidized, and Zn^{2+} can be reduced either by vacuum firing or by photolysis by u.v. light. Metallic zinc is produced as a consequence of lamp burning and it amalgamates with mercury. The zinc atoms on the phosphor surface act as vapor traps for mercury and cause it to distribute itself over the surface, probably as tiny droplets. The oxidation of Mn^{2+} and the reduction of Zn^{2+} can be prevented by formation of a protective layer on the phosphor surface, e. g. $ZnSb_2O_6$. It is thought that the surface properties of zinc silicate phosphor, particularly those which affect the extent and perfection of a protective coating, greatly influence the quality of lamps produced by identical procedures.

Zinc orthosilicate activated by manganese is a phosphor which has been the subject of numerous investigations (1-5). In addition to the usual green luminescent form, red and yellow phosphors have been prepared (6-9). The green luminescent form is of value as a lamp phosphor. Unfortunately however, when it is used in fluorescent lamps it exhibits poor maintenance. Lowry (10) showed that the maintenance could be improved substantially by the addition of small amounts of Sb_2O_3 to the phosphor; the best results were observed when the addition was made to the coating suspension. Merrill and Davis (11) demonstrated similar results by incorporation of small amounts of As plus Pb in the phosphor matrix during synthesis.

The practical advantages of Sb_2O_3 additions have been used for many years, but nevertheless seemingly identical phosphor preparations and lamp-making procedures yield different lamp results.

The subject is treated as a summarization of observations which seem pertinent to an understanding of the zinc silicate phosphor. Phase studies are considered to show that under equilibrium conditions phosphor compositions consist essentially of $(Zn, Mn)_2SiO_4$ plus SiO_2. The effects of the ZnO/SiO_2 ratio and phosphor synthesis temperature on lumen output are shown. Some of the surface chemical properties of zinc silicate phosphor are given, and evidence is presented for changes in the crystallographic structure of the surface. Finally a phenomenological mechanism of fluorescent deterioration of zinc silicate phosphors in fluorescent lamps is given.

Experimental Procedure

Raw materials used where silicic acid prepared by hydrolysis of tetraethylorthosilicate, New Jersey Zinc Company USP grade ZnO, Mallinckrodt reagent grade $MnCO_3$, Sb_2O_3, As_2O_3, $(NH_4)_2HPO_4$, SnO_2, TiO_2 H_3BO_3, and Reynolds $Al_2O_3xH_2O$. Compositions were mixed in a mortar with acetone until dry. Calcines were prepared in fused silica crucibles at temperatures ranging from 1200° to 1300°C. Heat treatments were done in silicon carbide electric resistance furnaces and platinum-wound resistance furnaces.

[1] Present address: Metallurgy Department, Research Laboratories, Westinghouse Electric Corp., Pittsburgh, Pa.

The pH values of water suspensions of zinc silicate phosphor were measured in the following manner: 60 ml of distilled water were adjusted to a pH of 6.0 by absorption of a small amount of CO_2. One gram of phosphor was added to the water and the mixture was stirred sufficiently to maintain the phosphor in suspension. The polyethylene beaker which contained the suspension was covered and a stream of nitrogen was passed over the cover in order to prevent CO_2 from diffusing in around the electrodes and stirrer. Measurements were obtained by means of a Beckman glass electrode pH meter. Results were reproducible to ± 0.05 pH units.

Lumen data were obtained from 40-w fluorescent lamps using standard lamp-making and photometry procedures.

Results and Discussion

Phase Studies

The system ZnO-SiO_2 was investigated by Bunting (12) who reported that Zn_2SiO_4 is the only compound which exists in the binary system. The absence of a metasilicate is surprising, for this compound is found in other systems of the type RO-SiO_2 where RO = CaO, MgO, SrO, BaO, or MnO. Leverenz (13) postulated the existence of a deficiency structure between the ortho-and meta-silicate compositions. This opinion was based on observations from x-ray studies that no new phases appeared with ZnO/SiO_2 ratios between the ortho-and meta-silicate compositions and that the Zn_2SiO_4 pattern remained unchanged when mixtures were prepared from ZnO and silicic acid.

Re-examination of the system confirmed the earlier results of Bunting that $ZnSiO_3$ does not exist. Microscopic and x-ray examination of compositions between Zn_2SiO_4 and SiO_2 (introduced as silicic acid) revealed that the silica is very reluctant to form a crystalline modification even on prolonged heating and that it does not occur as isolated particles but rather it appears to form a "cocoon" around the Zn_2SiO_4 crystals. X-ray and microscopic data show no evidence of solid solution between Zn_2SiO_4 and SiO_2.

Studies in the system ZnO-MnO-SiO_2 (14) showed that there is a binary join between Zn_2SiO_4 and $MnSiO_3$ and that $MnSiO_3$ is soluble in Zn_2SiO_4 in excess of 10 mole % at 1300°C, which is more than twice the amount of manganese normally used as an activator. Since there appears to be no solubility of SiO_2 in either Zn_2SiO_4 or $(Zn,Mn)_2SiO_4$, phosphor compositions can be regarded as essentially a two-phase system of $(Zn,Mn)_2SiO_4$ plus SiO_2.

In order to investigate the effects of the ZnO/SiO_2 ratio and synthesis temperature of the phosphor on lamp performance, the following synthesis technique was used: over-all compositions with the desired ZnO/SiO_2 ratios were prepared at 1200°-1250°C from ZnO plus silicic acid. The required amount of manganese was introduced as the carbonate in a second firing at either 1200°, 1250°, or 1300°C. This procedure yields a wide range of phosphor compositions which have high powder brightness. If $ZnO + SiO_2 + MnO$ initially are fired together, a firing temperature of 1300°C is required to develop full brightness unless a flux is used.

Zinc silicate phosphor is excited by 2537Å or 3650Å radiation but the response to 3650 develops after firing the phosphor at higher temperatures than are required for good response to 2537. This effect was demonstrated by thermal gradient firings in air. Zinc orthosilicate was prepared at 1200°C/4 hr. To this material was added the necessary amount of $MnCO_3$ and the mixture was fired in a thermal gradient furnace in the temperature range from 600° to 1350°C. At 1200°C the phosphor had 95% of the maximum fluorescent brightness observed when excited by 2537, but it had practically no response to 3650. 1220°C increased the response both to 2537 and 3650. The maximum brightness under 2537 was obtained between 1250° and 1300°, but at 1350°C there was marked sintering and a decrease in brightness. In contrast, the brightness under 3650 increased in a uniform manner from 1250° to 1350°C.

Relation of Phosphor Preparation to Lumen Output

The effect of various ZnO/SiO_2 ratios on lamp performance is given in Fig. 1. Test phosphors were prepared by first forming zinc silicate at 1200°C and then introducing the required amount of manganese in a second firing at 1200°C. A control phosphor was prepared by firing together $ZnO + MnO + SiO_2$ at 1300°C using a ZnO/SiO_2 ratio of 1.7/1.0. In all tests an addition of 0.1 wt % Sb_2O_3 was made to the phosphor coating suspension. A line on the ordinate opposite the ZnO/SiO_2 ratio indicates the spread in lumen values obtained from a seven lamp test at zero hours. The two curves shown per test represent the extremes per variation, as measured during the time of the test. The data show that a phosphor with a mole ratio of 1.9/1.0 is comparable in lumen performance to one with a ratio of 1.5/1.0, whereas a phosphor with a ratio of 1.7/1.0 is substantially better. By some means a certain excess of silica gives an improvement in lumen output, but too large an excess cancels the initial gain. Since silicic acid in contact with $(Zn, Mn)_2SiO_4$ is reluctant to form a crystalline modification even on prolonged heating, too large an excess of silica may have a deleterious effect on lamp performance as a result of carrying water into the lamp. However, the fact that some sort of surface protection is required strongly suggests that the surface properties of zinc silicate itself may be an important factor in phosphor depreciation.

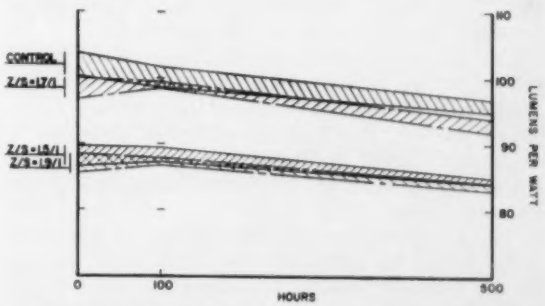

Fig. 1. Effect of ZnO/SiO_2 ratio on the efficiency and maintenance of zinc silicate phosphors.

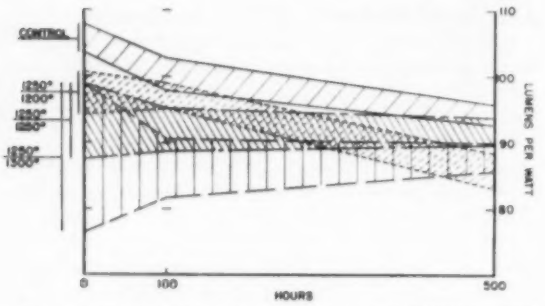

Fig. 2. Effect of firing temperature on the efficiency and maintenance of zinc silicate phosphors.

Further evidence of the possible effect of surface properties was given by the following test: zinc silicate was formed at 1250°C; the required amount of manganese was introduced in a second firing at either 1200°, 1250°, or 1300°C to yield compositions low in free silica, i.e., $(Zn_{1.99}Mn_{0.01})_2SiO_4$. Lamps were prepared from each of the three test lots; results are shown in Fig. 2. The lines on the ordinate opposite the firing temperatures and the two curves per test have the same meaning as in Fig. 1. It is seen that the spread within each group increases as the second firing temperature increases. As lamp burning progresses, changes occur which tend to minimize the differences initially present. Evidently higher firing temperatures produce changes in the phosphor which make it more susceptible to lamp making variables.

Evidence for the Formation of a Surface Phase

The suspicion that a surface alteration does occur in zinc silicate phosphor during synthesis is confirmed by comparison of x-ray and electron diffraction data. These data, which are listed in Table I, were obtained from a sample with a molar composition of $(Zn_{1.99}Mn_{0.01})_2SiO_4$ and fired three times at 1250°C/3 hr. The first column lists "d" values obtained from x-ray data which reflect the arrangement of atoms in the interior of the crystal. The fourth column lists "d" values calculated from electron diffraction data which gives the arrangement of atoms on the surface. Comparison of the two sets of "d" values shows that there is a shift in lattice spacing between the surface and interior of the crystal.

The surface phase cannot be accounted for by an accumulation of either ZnO, MnO, Mn_2O_3, Mn_3O_4, $ZnMn_2O_4$, or any of the crystalline modifications of SiO_2. Therefore, it appears that a distinct new phase develops on the surface of $(Zn,Mn)_2SiO_4$.

Zinc silicate phosphor can fluoresce either green, yellow, or red, or a combination of these colors depending on the method of preparation. As was mentioned earlier, zinc silicate phosphor develops a response to 3650Å excitation when fired at temperatures higher than about 1200°C. Since the green emission under 3650Å is the same as that under 2537Å, it appears that the development of a surface phase serves to introduce new absorption centers but not different types of luminescent centers. Comparison of the x-ray data of yellow luminescent powders studied by Rooksby and McKeag (7) and Pfeiffer and Fonda (8), respectively, and of yellow and yellow-green luminescent films examined by Feldman and O'Hara (9) showed no correlation with the surface phase postulated in the present study. The red fluorescent form is in a vitreous state as shown by Pfeiffer and Fonda.

Closely related to the phenacite structure of zinc orthosilicate is the spinel arrangement. The oxygen atoms in spinel are in a face-centered cubic order. The "d" spacings of a face-centered cubic structure were calculated on the basis of the strongest line observed in the electron diffraction data. The last column in Table I lists the calculated "d" values. There appears to be a reasonable fit between the calculated values and the "d" values obtained from electron diffraction data, particularly with the smaller "d" spacings. The data show that a surface rearrangement has occurred and that it seems to be a spinel-like structure.

The phenacite and spinel structures of A_2BO_4 compounds are similar enough that, in some cases, an increase in temperature can cause a phase transition. For example, Li_2SO_4 and Li_2MoO_4 are dimorphic with low-temperature phenacite and high-temperature spinel structures. Since bulk Zn_2SiO_4 does not have a spinel modification, and since, in general, reconstructive inversions show positive volume changes in the direction of increasing temperature, a spinel modification of zinc silicate could be expected to be stable at the surface of the crystal at temperatures nearer the melting point, e.g., 1200°-1300°C. Therefore, at some lower temperature, the postulated surface phase will become unstable and should ideally invert back to the phenacite arrangement. As will be developed later, it appears unlikely that a simple inversion occurs but rather that the surface phase dissociates into its constituent oxides.

Differential thermal analysis data seem to fit this general scheme: DTA curves of previously formed zinc silicate phosphors showed a small but reproducible exothermic effect on heating, beginning at about 1250° and exhibiting a broad maximum in the region of 1320°C. No heat effects were observed during cooling. High-temperature x-ray analysis by Hummel (15) demonstrated that the thermal effect is not the result of a "bulk" crystallographic

Table I. $(Zn_{1.99}Mn_{0.01})_2SiO_4$ thrice fired at 1250°C/3 hr

"Substrate"				"Surface"		F-cubic $a = 9.138$
d	I/I	Δd_1*	d	I	Δd_2*	d
4.055	60	+0.181	3.874	M	+0.696	4.572
3.509	90	+0.179	3.330	M	−0.101	3.229
2.850	60	+0.096	2.754	S	0	2.754
2.650	100	+0.108	2.542	M	+0.096	2.638
2.327	70	+0.085	2.242	M	+0.046	2.284
2.017	30	+0.062	1.953	W	−0.101	2.043
1.866	70	+0.060	1.806	M	+0.059	1.865
1.692	20	+0.039	1.653	W	+0.105	1.758
1.602	30	+0.015	1.587	W	+0.028	1.615
1.523	20	+0.020	1.503	W	+0.020	1.523
1.424	60	+0.023	1.401	S	−0.008	1.393
1.340	40	+0.020	1.320	M	−0.001	1.319
1.213	10	+0.022	1.191	W	−0.002	1.189
1.007	20	+0.011	0.996	WM	+0.001	0.997

* Δd_1 and Δd_2 are the differences between the "d" values of the "substrate" and the "surface" and the "surface" and the F-cubic spacings, respectively.

inversion. Since the phosphor was originally furnace-cooled from about 1250°C, a stable high-temperature surface phase has had an opportunity to invert to a low-temperature modification or to dissociate. The exothermic effect at 1250°C on reheating suggests a recombination reaction of the dissociated products of the high-temperature surface phase. If there were a simple crystallographic inversion, an endothermic rather than an exothermic effect would be expected. The sluggishness of a dissociation or inversion could prevent the appearance of any distinct thermal effects on cooling.

A rough estimate of the thickness of the surface layer can be made by comparing the patterns obtained by x-ray and electron diffraction techniques. For ionic crystals, the depth of electron penetration is of the order of 10Å (16), whereas, oxide films several hundred angstroms in thickness have insufficient volumes to produce x-ray lines. Since the x-ray pattern did not show even diffuse lines corresponding to the electron diffraction data, the surface phase may be from about ten to several hundred angstroms in thickness. A surface film with this order of volume could conceivably produce the thermal effect detected by DTA.

Some Surface Chemical Properties of Zinc Silicate Phosphor

Differences in the surface properties of the phosphor are reflected in measurements of pH and oxidizing potential. The data are shown in Fig. 3. Zinc orthosilicate, free of manganese, has a pH of about 6.80 and, of course, no oxidizing potential as evidenced by organic indicators such as benzidine (17). When the previously formed zinc silicate was activated by manganese to yield the composition $(Zn_{0.90}Mn_{0.06})_2SiO_4$, fired at 1250°C/4 hr, and cooled in the furnace, it exhibited marked oxidizing potential and a pH of 7.85. When this phosphor was quenched from temperatures above 1000°C, the oxidizing potential was lost and the pH dropped to 6.82.

Changes in pH and oxidizing potential can be explained on the basis of the properties of a surface structure. A phosphor preparation temperature of 1300°C will favor divalent manganese by the valency isobar effect. Since Mn^{2+} will substitute isomorphously for Zn^{2+}, rapid quenching of the phosphor should freeze in the surface structure in which Mn^{2+} is stable. Therefore, a quenched phosphor would have zero oxidizing potential and a pH similar to that of unactivated zinc orthosilicate. On the other hand, if the phosphor is cooled slowly, the surface phase has an opportunity to dissociate and as a result some of the divalent manganese is oxidized. Consequently the phosphor now exhibits high oxidizing potential. The higher pH over that of nonactivated zinc silicate is probably a result of the formation of $Mn_2O_3 \times H_2O$ or $MnO_2(OH)_2$ on the surface of the phosphor where it serves as another source of $(OH)^-$ ions.

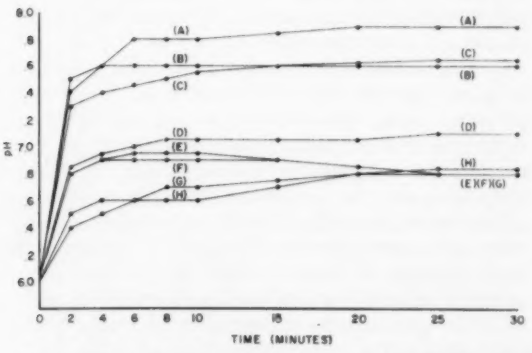

Fig. 3. Effect of surface treatment of zinc silicate phosphors on pH. (A) $(Zn_{0.90}Mn_{0.06})_2SiO_4$; (B) $(Zn_{0.90}Mn_{0.06})_2SiO_4$:$B_2O_3$; (C) ZnB_2O_4; (D) $(Zn_{0.90}Mn_{0.06})_2SiO_4$:$Sb_2O_3$; (E) $(Zn_{0.90}Mn_{0.06})_2SiO_4$:-$P_2O_5$; (F) $Zn_3(PO_4)_2$; (G) Zn_2SiO_4; (H) $(Zn_{0.90}Mn_{0.06})_2SiO_4$ air quenched from 1050°C.

A phosphor prepared at 1300°C and cooled in the furnace will acquire a tan coloration after standing a few days in air. This effect is much accelerated by reheating the material in air at 600°C. However, if the phosphor is quenched from temperatures above 1000°C, it is far more resistant to powder discoloration. Thus, higher oxides of manganese as evidenced by higher oxidizing potential and powder discoloration appear to be associated with the dissociation of a surface phase.

Froelich (18) concluded from his studies of Mn-activated silicate phosphors that oxidizing matter, presumably Mn^{3+}, is located at or near the surface of the phosphor crystals. Thus, he observed that Zn-Be silicate, which is isostructural with Zn_2SiO_4, activated by manganese acquired a tan coloration and high oxidizing potential when fired between about 350° and 1000°C. Experiments showed that the higher oxides of manganese did not develop during phosphor synthesis but only after the material was heated in the temperature range of instability previously mentioned. Summarizing, Froelich comments that, "it can be said that manganese-activated silicate phosphors, in particular Zn-Be silicates, have a rather unstable crystal surface which is subject to chemical deterioration and disintegration, depending upon the surrounding atmosphere and temperature. Small amounts of manganese oxide on or immediately below the crystal surface, held more or less loosely in the lattice, are fairly easily attacked by oxygen from the atmosphere or other oxidizing substances. They sever their bonds with the other oxides in the crystal lattice and are oxidized to free, brown manganic oxide, Mn_2O_3, giving rise to a change in the natural color and an apparent loss of fluorescent brightness. . ."

The oxidation of surface manganese can be avoided in other ways than by quenching. Refiring the phosphor with $(NH_4)_2HPO_4$ produces a film of zinc phosphate on the material at temperatures from 300° to 800°C. The oxidizing potential is lost and the pH is very nearly that of $Zn_3(PO_4)_2$ as shown in Fig. 3. Similar treatment of the phosphor with H_3BO_3 destroys the oxidizing potential and yields a material with a pH nearly that of ZnB_2O_4. However, the firing temperature is limited to 300°-500°C because of the volatility of B_2O_3. Refiring the phosphor with Sb_2O_3 produces a film of $ZnSb_2O_6$ as revealed by x-ray analysis, and again the oxidizing potential is lost.

Changes in the surface properties of zinc silicate phosphor can be produced at moderate temperatures in vacuum. The procedure was to place the phosphor sample in an alumina boat which then was sealed in a Pyrex tube and evacuated to 1μ. The tube was inserted in a furnace so that one end protruded from the furnace. Samples were heated at 600°C for 20 hr. Results obtained from untreated phosphor and phosphors with various surface modifications are shown in Table II. Zinc orthosilicate free of manganese was partially reduced, and metallic zinc collected on the cool portion of the tube. Manganese solid solutions in zinc orthosilicate substantially increased the reduction of zinc as evidenced by a darker gray powder and larger deposits of metallic zinc on the tube.

When zinc silicate phosphor is fired at 1200°-1300°C under neutral or reducing conditions, the powder turns gray in color and the fluorescent brightness is much decreased. Therefore, it appears that Zn_2SiO_4 itself may be subject to reduction quite apart from the effect of a surface phase. However, since the formation of metallic zinc can be prevented by suitable surface treatment, the surface structure of zinc silicate seems to play an important role in the process. Assuming that the surface structure does contribute directly to the formation of metallic zinc, the effect may arise from two causes. Under the same conditions of vacuum heat treatment zinc metal will distill from ZnO. Consequently the occurrence of zinc metal in the phosphor may be the result of the presence of ZnO from the dissociation of the surface at 600°C. Another possible cause may be from an oxidation-reduction reaction which occurs as a result of the instability of the surface phase. Since the coordination number of silicon in inorganic crystalline materials is invariably four, the postulation of a surface-spinel phase suggests the occurrence of a "normal" spinel structure. That is, a structure in which Si^{4+} ions are in fourfold and Zn^{2+} ions are in sixfold coordination positions. When zinc silicate which was prepared at a high temperature is reheated at a moderately low temperature, e.g., 600°C, the surface-spinel phase becomes unstable and attempts to form a phenacite structure. This requires that the Zn^{2+} ions change their coordination number from 6 back to 4 since all cation sites in the phenacite structure are fourfold coordination positions. Although the over-all cation/anion ratio has to be maintained in the structure transition, it may be that local surface conditions give rise to oxidation-reduction reactions between O^{2-} and Zn^{2+} ions. The loss of Zn and O_2 unbalances the stoichiometry so that dissociation of the surface phase results. As shown in Table II, Mn^{2+} substitutions for Zn^{2+} increases the amount of metallic zinc produced. However, consideration of the free energy changes shows that reduction of Zn^{2+} cannot result from the oxidation of Mn^{2+}. Therefore, it appears that manganese plays an indirect role in the reduction of zinc ions and it may serve to increase the instability of the surface phase. Examination of the relative field strengths of Mn^{2+} or Mn^{4+} and Zn^{2+} (where field strength is defined as ionic valence/ionic radius) shows that manganese ions have higher polarizing power than zinc ions. Consequently, oxidation of Mn^{2+} enables it to compete more successfully for oxygen ions than can Zn^{2+}. As a result, another disruptive force is introduced which would tend to cause dissociation of the high-temperature phase.

Table II. Stability of zinc silicate phosphor

Sample	Oxidizing potential	Body color after 600°C for 20 hr at 1μ Hg pressure	Deposit on tube	Fluorescent brightness (2537A rad.) $(Zn,Mn)_2SiO_4$ at 100%
Zn_2SiO_4	—	Light gray	Zinc	—
$(Zn, Mn)_2SiO_4$	Positive	Dark gray	Zinc	72%
$(Zn, Mn)_2SiO_4$: P_2O_5	Negative	Dark gray	—	72%
$(Zn, Mn)_2SiO_4$: As_2O_5	—	White	—	102%
$(Zn, Mn)_2SiO_4$: Sb_2O_5	—	White	—	97%

The reactivity of zinc silicate phosphor is demonstrated by the ease with which it will react with other oxides to form a second compound on the surface of the phosphor. For example, Al_2O_3 will react with zinc silicate at 1000°C to form a layer of $ZnAl_2O_4$, a spinel. By suitable surface treatment both the oxidation of Mn^{2+} and the reduction of Zn^{2+} ions can be prevented. Re-firing the phosphor with Sb_2O_3 or As_2O_5 forms surface films of $ZnSb_2O_6$ and probably $ZnAs_2O_6$, respectively. As a result the phosphor body color remains white and the fluorescent brightness is maintained. Since $ZnAs_2O_6$ has low u.v. absorption and causes reduction of oxidized manganese present in the untreated phosphor to the divalent state, the powder brightness is somewhat higher than that of the untreated material. A surface film of zinc phosphate prevented zinc metal from volatilizing from the phosphor, but reduction still occurred as evidenced by a gray powder color and loss of fluorescent brightness (see Table II).

A fluorescent lamp provides a low-pressure environment for the phosphor and, during exhaust, temperatures in excess of 500°C. In addition there is the possibility of reducing Zn^{2+} by photolysis from u.v. radiation produced by the mercury arc. Kressin (19a) reports that graying occurs in zinc silicate phosphors on exposure to strong u.v. light. He has attributed the observed graying to the formation of elemental manganese. Two of the experiments on which Kressin (19b) bases his conclusions are the following:

(*a*) A weighed amount of gray irradiated phosphor was placed in a silica bulb and heated in the presence of a measured small amount of oxygen until the white color of the original phosphor was restored. The oxygen then was pumped off, burned with hydrogen to form water, and the latter determined by means of Karl Fischer reagent. The amount of oxygen used up by the phosphor then was found by difference. A blank sample of unactivated zinc silicate without manganese, carried through the entire process as before, showed no oxygen consumption whatever.

(*b*) Zinc silicate with manganese was settled on a quartz plate and irradiated in vacuum with a quartz lamp. During this experiment, the vessel was connected to a mass spectrometer, and the evolution

of oxygen could be detected with this instrument. A blank run with zinc silicate free of manganese did not show the evolution of any oxygen.

Kressin's data can be equally well accounted for by the formation of elemental zinc. Thus, the consumption of oxygen in experiment (*a*) and the evolution of oxygen in experiment (*b*) could be associated with the oxidation and reduction of zinc. The fact that the blank, which contains no manganese, did not show a similar reaction is probably a result of zinc orthosilicate having low absorption for u.v. radiation.

If metallic zinc is produced by photolysis or by the mechanism described earlier, it logically can be expected to react with mercury, probably to form an amalgam. To test this hypothesis phosphor was brushed from lamps after they had burned for 3000 hr. Mercury was separated from the phosphor by shaking a suspension of 5 g of the phosphor in an NH_4OH solution, which caused dispersion of the phosphor, until a ball of mercury collected at the bottom of the tube. The 4 mg of mercury which were recovered were washed with acetic acid to dissolve traces of Zn_2SiO_4. Chemical analysis revealed that the mercury contained 5 wt % Zn but no Mn. Microscopic examination of the zinc amalgam before chemical analysis revealed that it consisted of a mixture of liquid and well defined hexagonal platelets. These platelets are described by Mellor (20) as beta-zinc amalgam. Reference to the phase diagram of the system Zn-Hg (21) shows that Zn is soluble in Hg to 2.15 wt % at 20°C. Therefore, zinc in excess of this limit separates from the liquid as crystals of beta-zinc amalgam.

Relation of Surface Properties to the Accumulation of Mercury on the Phosphor

A mechanism of lumen depreciation is indicated in which zinc metal sites on the phosphor surface act as "vapor traps" which cause the mercury to distribute itself over the phosphor surface. Of the several factors responsible for lumen depreciation, adsorption of mercury is generally regarded as the principal cause (22). The condensation of mercury in tiny droplets on the phosphor surface has been considered by Froelich (22). If it is assumed that the normal 10-20% lumen drop is the result of shadowing by mercury droplets, the size of the droplets required lies between that necessary to cover a certain fraction of the lamp surface to that required to cover the same fraction of the geometric surface of the phosphor powder. Thus, a 40-w lamp with internal surface area of 1320 cm^2 would require spheres of 0.1 to 0.05 μ in diameter to shadow 10-20% of the surface area. A 40-w fluorescent lamp contains about 3.7 g of zinc silicate phosphor which has a surface area of 1.0 to 1.3 m^2/g. Therefore, the geometric surface area is in the order of 10^4 cm^2. Again assuming that the mercury condenses in spheres, droplets with diameters in the order 0.01 to 0.001 μ would be required to cover 10-20% of the geometric phosphor surface area.

Application of the well-known Thomson equation (23) shows that a mercury sphere with a 0.1 μ diameter would have about 10% higher vapor pressure than that over a flat surface. The equation is not valid for spheres with diameters 0.01-0.001 μ since the surface tension is no longer independent of the diameter. Such classical considerations do not take into account the effect of surface forces on the behavior of small droplets of mercury nor do they consider the effect of zinc atoms in "seeding" the condensation of tiny mercury droplets.

The behavior of excess silica with Zn_2SiO_4 suggests that surface forces are appreciable. As was described earlier, excess silicic acid used in the preparation of Zn_2SiO_4 is reluctant to form a crystalline modification and tends to form a cocoon around the zinc silicate crystals. In contrast, excess silicic acid used in the preparation of $CaSiO_3$ readily forms quartz crystals which tend to remain as isolated particles. Thus, it seems possible that small droplets or patches of mercury might be particularly stable on the surface of the zinc silicate phosphor. Unfortunately, electronmicroscopy has not resolved the problem so that the distribution of mercury is still a matter of conjecture.

It is instructive to note that a lamp which has burned for some time and then is reheated to about 300°C will regain substantially all of its lumen drop, but the rate of lumen decrease on re-burning is much greater than it was initially. Evidently the sites which cause deposition of mercury on the surface of the phosphor are not destroyed by heating to 300°C with the result that the lumen drop is much more rapid because of the greater number of sites operating. Such a description is in qualitative agreement with the observation that a gray colored phosphor, which had been removed from a lamp after some hours of burning, could not be bleached by acetic acid until the sample had been reheated to about 300°C. Heating zinc amalgam to this temperature will distill off the mercury and leave a residue of zinc. Since zinc amalgam is insoluble in acetic acid whereas zinc is soluble, it is necessary to decompose the amalgam before the zinc can be dissolved.

Relation of Phosphor Surface Chemistry to Lamp Brightness

The behavior of zinc silicate phosphor during lamp making and lamp burning is complicated. However, the observations discussed serve at least qualitatively to account for the major changes in phosphor brightness. Phosphor removed from a lamp immediately after lamp making is discolored and it has suffered about a 10% loss in brightness. Two factors contribute to this effect. Since the phosphor was furnace cooled, dissociation of the surface phase has led to higher oxidation states of manganese and consequently a tan coloration. The addition of Sb_2O_3 to the coating suspension has led to the formation of $ZnSb_2O_6$ which has high u.v. absorption.

As lamp burning progresses the phosphor suffers further losses in brightness as mercury collects on the surface of the material. The body color changes from a tan coloration to a dark gray color. Metallic zinc atoms are believed to serve as "vapor traps" which cause the mercury to be distributed over the

Table III. Effect of various additives on the lumen performance of zinc silicate phosphors

Sample	0 hr, LPW	100 hr, LPW	500 hr, LPW
$(Zn, Mn)_2SiO_4$	95.7	83.3	70.9
$(Zn, Mn)_2SiO_4$: P_2O_5	110.4	81.6	65.1
$(Zn, Mn)_2SiO_4$: 0.25 wt % As_2O_5	110.3	98.0	85.8
$(Zn, Mn)_2SiO_4$: 0.10 wt % Sb_2O_3	102.6	95.2	84.2
$(Zn, Mn)_2SiO_4$: 0.10 wt % As_2O_5 + 0.10 wt % Sb_2O_3	108.4	98.3	85.1
$(Zn, Mn)_2SiO_4$: special treatment	109.0	104.1	99.0

surface of the phosphor. Two factors can lead to the production of metallic zinc: the decomposition of the surface phase; and reduction of Zn^{2+} by photolysis. Both effects may operate, but it is nevertheless clear that prevention of the oxidation of Mn^{2+} and reduction Zn^{2+} should give substantial improvements in lumen output.

The benefit of a protective coating is demonstrated by the lumen data shown in Table III. The addition of either $(NH_4)_2HPO_4$, Sb_2O_3, or As_2O_5 was made to the coating suspension. As a result the development of a surface film most probably occurs only during lehring. Lamps prepared from untreated zinc silicate gave about 71 lpw (lumens per watt) after 500 hr of burning. The addition of P_2O_5 gave only 65 lpw. This result is consistent with the data given in Table II which show that, although P_2O_5 additions prevented oxidation of Mn^{2+}, reduction of Zn^{2+} did occur. The larger lumen decrease observed than for untreated phosphor may be the deleterious effect of additional H_2O in the lamp from unreacted H_3PO_4. As is well known, the addition of 0.1 wt % Sb_2O_3 to the coating suspension gives substantial improvements both in initial lumens and lumen maintenance so that after 500 hr lamps have about 84 lpw. A mill addition of 0.1 wt % Sb_2O_3 plus 0.1 wt % As_2O_5 was better at 100 hr than either Sb_2O_3 or As_2O_5 alone. The substantial gain in zero hour lumen achieved by adding As_2O_5 alone or in combination with Sb_2O_3 is probably the result of better formed $ZnAs_2O_6$ or $ZnSb_2O_6$ on the surface of the zinc silicate crystals. Evidently the surface layer is not entirely stable since the initial gain in lumens over Sb_2O_3 alone was lost after about 500 hr of burning. By special treatment of the phosphor it is possible to achieve 99 lpw after 500 hr. Thus, appropriate surface treatment of the phosphor improves not only the lumen output but also the lumen maintenance.

Ideally, $(Zn, Mn)_2SiO_4$ stabilized by a suitable surface film should be an optimum phosphor composition. However, a certain excess of silica is required as shown by the data in Fig. 1. A phosphor with a ZnO/SiO_2 ratio of 1.9/1.0 gave lower lumens than one with a ratio of 1.7/1.0. Since Sb_2O_3 was added to the coating suspension, a film of $ZnSb_2O_6$ could form only during lehring, that is, in the minute or two that the phosphor was above about 500°C. It seems likely that any factor which affects the kinetics of formation of $ZnSb_2O_6$ also will affect lamp performance. Similar results are shown by the data in Fig. 2. A particular phosphor composition had varying susceptibility to lamp-making conditions depending on the temperature at which the phosphor was prepared. Since it is shown that surface alterations do occur in zinc silicate, it is likely that different heat treatments will produce various degrees of surface alteration. The change in response to 3650Å excitation appears to be associated with alterations in surface structure which also could conceivably have a marked effect on the kinetics of the formation of $ZnSb_2O_6$. Thus, heat treatments which produce changes in response to 3650Å excitation also yield phosphors which give lamps with different lumen outputs. Consequently, it appears that the surface properties of a phosphor, particularly those which affect the extent and perfection of a protective coating, greatly influence the quality of lamps produced by identical procedures.

The proposed mechanism of zinc silicate phosphor deterioration does not explain why some lamps actually improved in maintenance from 100 to 500 hr (see Fig. 2). Also in need of an explanation is that although zinc-beryllium silicate and zinc silicate are isostructural the former is much more stable in lamps than the latter. However, in the case of zinc-beryllium silicate there is the possibility of forming a surface film of Be_2SiO_4 which may help prevent reduction of Zn^{2+}.These results emphasize that there are many other factors needing research to explain the maintenance of lamps.

Acknowledgments

Grateful acknowledgment is given to Miss Eileen Allessandrini of General Electric Company Research Laboratory for supplying the electron diffraction data, to Miss Mary V. Hoffman for obtaining some of the lamp data, to Mr. J. G. Rabatin for supplying the DTA data, to Mr. J. W. Hunter for analysis of the zinc amalgam, and to Dr. C. A. Brown for his many stimulating discussions.

Manuscript received Sept. 16, 1959.

Any discussion of this paper will appear in a Discussion Section to be published in the December 1960 JOURNAL.

REFERENCES

1. G. R. Fonda, *J. Phys. Chem.*, **43**, 561 (1939).
2. K. H. Butler, *This Journal*, **93**, 143 (1948).
3. E. Nagy, *J. Optical Soc. Am.*, **39**, 42 (1949).
4. H. W. Leverenz, "An Introduction to the Luminescence of Solids," pp. 223-233, John Wiley and Sons, New York (1950).
5. S. Larach and J. Turkevich, *Phys. Rev.*, **89**, 1060 (1953).
6. A. Schleede and A. Gruhl, *Z. Elektrochem.*, **29**, 411 (1923).
7. H. P. Rooksby and A. H. McKeag, *Trans. Faraday Soc.*, **37**, 308 (1941).
8. H. G. Pfeiffer and G. R. Fonda, *This Journal*, **99**, 140 (1952).
9. C. Feldman and Margaret O'Hara, *J. Optical Soc. Am.*, **48**, 816 (1958).
10. E. F. Lowry, *This Journal*, **95**, 242 (1949).
11. J. B. Merrill and A. B. Davis, U.S. Pat. 2,554,999 (May 29, 1951).
12. E. N. Bunting, *J. Research Nat. Bur. Standards*, **4**, 134 (1930); R. P. 136; E. M. Levin, H. F. McMurdie, and F. P. Hall, "Phase Diagrams for Ceramists," The Am. Ceram. Soc. (1956).
13. H. W. Leverenz, *loc cit.*, p. 328.
14. D. E. Harrison, Unpublished data.
15. F. A. Hummel, Private communications.
16. C. E. Hall, "Introduction to Electron Microscopy," p. 252, McGraw-Hill Book Co., Inc., New York (1953).

17. F. Feigl, "Qualitative Analysis by Spot Tests," pp. 55, 242, Elsevier Publishing Co., Inc., Amsterdam (1947).
18. H. C. Froelich, *Trans. Electrochem. Soc.*, **87**, 429 (1945).
19a. G. Kressin, "Technisch-Wissenschaftliche Abhandlungen der Osram Gesellschaft," p. 235, Springer Verlag (1958).
19b. G. Kressin, Private communications.
20. J. W. Mellor, "Inorganic and Theoretical Chemistry," vol. IV, p. 1038, Longmans, Green & Co., London (1946).
21. E. A. Anderson, "Metals Handbook," p. 1222, The American Society for Metals, Cleveland (1948).
22. H. C. Froelich, *J. Applied Phys.*, **17**, 573 (1946).
23. Samuel Glasstone, "Textbook of Physical Chemistry," p. 495, D. van Norstrand Co., Inc., New York (1946).

The System BaO-TiO_2-P_2O_5: Phase Relations, Fluorescence, and Phosphor Preparation

D. E. Harrison[1]

Luminescent Materials Laboratory, Lamp Metals and Components Department, General Electric Company, Cleveland, Ohio

ABSTRACT

The subsolidus phase relations were determined in the system BaO-TiO_2-P_2O_5 by using x-ray and petrographic techniques. Four compounds were isolated and individually prepared: $2BaO:TiO_2:P_2O_5$ melts congruently at 1197° ± 3°C; $BaO:TiO_2:P_2O_5$ has a rapidly reversible dimorphic inversion at 967° ± 5°C and it melts congruently at 1428° ± 3°C; $4BaO:3TiO_2:P_2O_5$ melts incongruently at 1302° ± 3°C; and $BaO:4TiO_2:3P_2O_5$ melts incongruently at 1368° ± 3°C. The only compound in the system which is of the self-activated type is $2BaO:TiO_2:P_2O_5$. It has an emission similar to that of $MgWO_4$. Compositions of maximum fluorescence are restricted to the join $2BaO:P_2O_5$-$2BaO:TiO_2:P_2O_5$ since compositions off this join contain either $BaO:TiO_2:P_2O_5$, $4BaO:3TiO_2:P_2O_5$ or TiO_2 which have high u.v. absorption but are nonfluorescent phases.

Henderson and Randy (1a) developed a phosphor with a composition of $2Ba_2P_2O_7$: 0.5 to 2.5 TiO_2. (In this paper, "activator concentrations" such as 0.5 to 2.5 TiO_2 refer to moles of material per mole of $Ba_2P_2O_7$.) This phosphor, which is excited by 2537Å radiation, has an emission similar to that of $MgWO_4$ and it is of the self-activated type. It is reported that maximum fluorescence occurs with a composition of $2Ba_2P_2O_7$: 1.0 TiO_2 but that relatively large increases in the concentration of titania only slowly decrease the intensity of fluorescence.

The system BaO-TiO_2-P_2O_5 provides an unusual opportunity to relate the ternary phase relations to the fluorescent properties without the uncertainties attending the introduction of small amounts of an activator as the fourth component. The purpose of this study was to determine the subsolidus phase relations and to show how the brightness of phosphor compositions is influenced by small amounts of nonfluorescing phases which necessarily occur as a result of the ternary phase relations. Subsolidus phase relations were determined by examining compatibility triangles and isolating compounds. It is hoped that the phase data and particularly the characterization of the fluorescent compound will prove useful in a fundamental study of this self-activated phosphor.

Experimental Procedure

Reagent grade $BaCO_3$, $BaHPO_4$, TiO_2, $(NH_4)_2HPO_4$, and BaF_2 were used as starting materials. Compositions were prepared by grinding the ingredients in a mortar with acetone until dry. Calcines were prepared in either fused silica or platinum crucibles at temperatures ranging from 700° to 1100°C for periods up to 3 weeks.

X-ray data were obtained from a General Electric, XRD-5, diffractometer using $Cu_{K\alpha}$ radiation (λ = 1.540Å) filtered with nickel.

The immersion technique was used to determine the refractive index of crystals. Indices up to 1.700 were determined to an accuracy of ±0.001, from 1.71 to 1.80 to an accuracy of ±0.005, and 1.84 to 2.00 to an accuracy of ±0.02.

Differential thermal analysis (DTA) data were obtained with an automatically recording apparatus, as described by Rabatin and Card (2).

The melting points of compounds were determined by a quench technique similar to that described by Shepherd, Rankin, and Wright (3). Thermocouples were calibrated using gold (mp, 1063°C), lithium metasilicate (mp, 1201°C), and diopside (mp, 1392°C). Since it was impossible to quench 20-g samples of ternary compound compositions to glasses, calcines were used as starting materials for quench studies.

Ultraviolet absorption was measured by determining the u.v. reflected from a sample. The detector consisted of a Corning 9863 filter, a layer of zinc silicate phosphor, a green filter, and a barrier layer photocell.

Relative fluorescent brightness was measured by a barrier layer photocell corrected to eye sensitivity.

[1] Present address: Metallurgy Department, Research Laboratories, Westinghouse Electric Corp., Pittsburgh, Pa.

Results and Discussion

Phase studies, binary systems.—The system BaO-TiO_2 was examined extensively by Rase and Roy (4). Five compounds exist: $2BaO:TiO_2$, $BaO:TiO_2$, $BaO:2TiO_2$, $BaO:3TiO_2$, and $BaO:4TiO_2$. The compound $BaO:2TiO_2$ has a lower limit of stability at 1210°C; below this temperature the composition is a mixture of $BaO:TiO_2$ and $BaO:3TiO_2$. Jonker and Kwestroo (5) discovered two new compounds which belong to the binary system. These compounds, $2BaO:5TiO_2$ and $2BaO:9TiO_2$, are stabilized by small additions of SnO_2 or ZrO_2. The system TiO_2-P_2O_5 was examined recently by Harrison and Hummel (6) who showed that $5TiO_2:2P_2O_5$ and $TiO_2:P_2O_5$ are the only compounds which occur in this system.

No complete phase diagram of the system BaO-P_2O_5 is reported, but a number of compounds are claimed. Glatzel (7) reports the occurrence of $BaO:P_2O_5$, and Ouvrard (8) shows the existence of $2BaO:P_2O_5$. A cubic form of $3BaO:P_2O_5$ is listed in the ASTM X-ray Diffraction Patterns, and a rhombohedral form is reported by Zachariasen (9). Recently, Langguth, Osterheld, and Karl-Kroupa (10) presented x-ray data for a new compound $3BaO:2P_2O_5$. Re-examination of the system confirmed the existence of the four compounds claimed. Further work was done on the new compound $3BaO:2P_2O_5$. Since it was not possible to quench the entire composition to a glass, conventional quench technique could not be used to determine the melting point. After fusion the quenched product always consisted of $3BaO:2P_2O_5$ plus glass. Therefore, it is concluded tentatively that the 3:2 compound melts congruently. DTA gave an endotherm at 900°C on heating and a second endotherm at 990°C followed by melting. The thermal effect at 900°C is the result of a slowly reversible dimorphic inversion which was found by static methods to occur at 870° ± 10°C. Microscopic examination showed that the low-temperature form has maximum and minimum refractive indices of 1.628 and 1.618, respectively. The high-temperature form is nearly isotropic with a refractive index of about 1.626. Typical x-ray patterns of the high- and low-temperature forms are given in Table II and compared with the data of Langguth, Osterheld, and Karl-Kroupa. Langguth, *et al.* fired their sample of 3:2 at 550°C/12 hr, whereas in the present work the low-temperature form was prepared at 800°C/24 hr. The differences in crystal development obtained at these firing temperatures may account for the discrepancies in the x-ray data.

Phase studies, ternary system.—Compatibility triangles were determined by comparison of x-ray and microscopic data of ternary compositions with data from the binary systems. Compositions investigated are shown in Fig. 1 and listed in Table I.

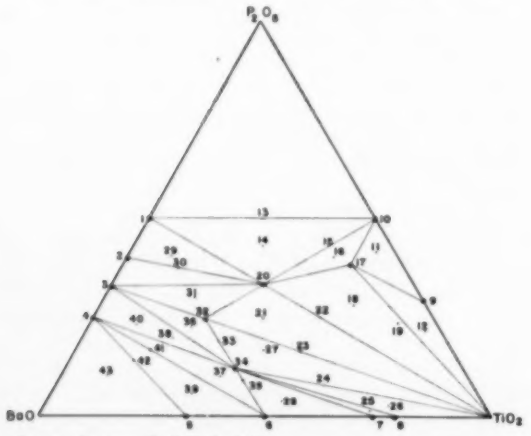

Fig. 1. System BaO-TiO_2-P_2O_5

Comp. No.
1—$BaO:P_2O_5$
2—$3BaO:2P_2O_5$
3—$2BaO:P_2O_5$
4—$3BaO:P_2O_5$
5—$2BaO:TiO_2$
6—$BaO:TiO_2$
7—$BaO:3TiO_2$

Comp. No.
8—$BaO:4TiO_2$
9—$5TiO_2:2P_2O_5$
10—$TiO_2:P_2O_5$
17—$BaO:4TiO_2:3P_2O_5$
20—$BaO:TiO_2:P_2O_5$
32—$2BaO:TiO_2:P_2O_5$
34—$4BaO:3TiO_2:P_2O_5$

Table I. Compositions in the system BaO-TiO_2-P_2O_5

Comp. No.	Mole % composition			Phases present
	BaO	TiO_2	P_2O_5	
1	50.0	—	50.0	BP
2	60.0	—	40.0	B_3P_2
3	67.0	—	33.0	B_2P
4	75.0	—	25.0	B_3P
5	67.0	33.0	—	B_2T
6	50.0	50.0	—	BT
7	25.0	75.0	—	BT_3
8	20.0	80.0	—	BT_4
9	—	71.5	28.5	T_5P_2
10	—	50.0	50.0	TP
11	5.0	55.0	40.0	BTP + BT_4P_3 + T
12	3.0	76.0	21.0	BT_4P_3 + T_5B_2 + T
13	25.0	25.0	50.0	BP + BT
14	28.5	28.0	43.5	BP + BT + BTP
15	14.3	42.8	42.8	TP + BTP
16	15.0	45.0	40.0	TP + BTP + BT_4P_3
17	12.5	50.0	37.5	BT_4P_3
18	16.0	57.0	27.0	BTP + BT_4P_3 + T
19	9.1	63.6	27.3	BTP + BT_4P_3 + T
20	33.3	33.3	33.3	BTP
21	37.5	37.5	25.0	BTP + B_2TP + T
22	25.0	50.0	25.0	BTP + T
23	33.3	50.0	16.7	B_2TP + T
24	30.8	61.5	7.7	B_4T_3P + T
25	25.5	73.5	1.0	?
26	20.0	77.5	2.5	?
27	41.6	41.6	16.8	B_2TP + B_4T_3P + T
28	43.5	53.5	3.0	B_4T_3P + BT + BT_3
29	50.0	10.0	40.0	BP + BTP + B_3P_2
30	50.0	12.5	37.5	B_3P_2 + BTP
31	50.0	20.0	30.0	B_3P + BTP + B_2TP
32	50.0	25.0	25.0	B_2TP
33	50.0	30.0	20.0	B_2TP + B_4T_3P
34	50.0	37.5	12.5	B_4T_3P
35	50.0	40.0	10.0	B_4T_3P + BT
36	55.0	22.5	22.5	B_3P + B_2TP + B_2T_3P
37	55.0	35.0	10.0	B_3P + B_4T_3P + BT
38	60.0	20.0	20.0	B_3P + B_4T_3P + B_3P
39	63.0	31.0	6.0	B_3P + BT + B_2T
40	67.0	10.0	23.0	B_3P + B_4T_3P + B_3P
41	67.0	17.0	16.0	B_3P + BT
42	71.5	14.3	14.3	B_3P + B_2T
43	80.0	10.0	10.0	?

Legend:

BP = $BaO:P_2O_5$	BT_4 = $BaO:4TiO_2$
B_3P_2 = $3BaO:2P_2O_5$	T_5P_2 = $5TiO_2:2P_2O_5$
B_2P = $2BaO:P_2O_5$	TP = $TiO_2:P_2O_5$
B_3P = $3BaO:P_2O_5$	BT_4P_3 = $BaO:4TiO_2:3P_2O_5$
B_2T = $2BaO:TiO_2$	BTP = $BaO:TiO_2:P_2O_5$
BT = $BaO:TiO_2$	B_2TP = $2BaO:TiO_2:P_2O_5$
BT_3 = $BaO:3TiO_2$	B_4T_3P = $4BaO:3TiO_2:P_2O_5$

Table II. Characteristic x-ray patterns

High-temperature $3BaO:2P_2O_5$ (25°C)		(After Langguth, *et al.*) $3BaO:2P_2O_5$		Low-temperature $3BaO:2P_2O_5$ (25°C)	
d	*I/I*	*d*	*I/I*	*d*	*I/I*
6.32	20			7.76	25
4.95	15			5.24	30
3.93	50	5.10	w	5.01	15
3.83	100			4.87	15
3.45	85	4.66	w	4.74	30
3.37	55	4.19	w	4.44	5
3.32	70	3.97	w	3.95	10
3.29	45			3.88	15
3.21	80	3.76	w	3.81	50
3.14	50	3.58	s	3.63	80
3.07	45	3.44	w	3.52	70
3.03	85	3.38	w	3.42	25
2.91	20	3.30	s	3.34	100
2.82	45	2.99	w	3.14	30
2.79	50	2.93	w	3.10	60
2.70	20	2.79	m	2.83	50
2.40	15	2.72	w	2.76	50
2.33	15	2.60	w	2.59	10
2.24	35	2.54	w	2.55	35
2.19	20			2.42	10
2.16	35			2.40	20
2.14	45			2.37	20
2.11	30			2.33	10
2.09	50	2.23	m	2.24	10
2.07	20	2.19	w	2.20	35
2.02	15			2.16	15
1.996	25	2.13	vw	2.14	25
1.951	20	2.10	m	2.09	35
1.916	15			2.07	25
1.717	15			2.05	10
1.646	20			2.04	15
				1.988	10
				1.971	10
				1.940	20
				1.909	25
				1.883	15
				1.843	20
				1.816	20
				1.799	20
				1.742	25
				1.720-1.705	15
				1.668	15
				1.589	15
				1.572	10
				1.567	10
				1.552	10
				1.520	20
				1.432-1.414	10
				1.397	15
				1.665	3
				1.338	5

$2BaO:TiO_2:P_2O_5$		Low-temperature $BaO:TiO_2:P_2O_5$ (25°C)		High-temperature $BaO:TiO_2:P_2O_5$ (1024°C)	
d	*I/I*	*d*	*I/I*	*d*	*I/I*
8.34	30	7.69	10	4.41	45
4.17	80	4.39	30	4.15	5
3.90	25	4.13	20	3.83	77
3.59	10	3.86	40	3.34	10
2.84	5	3.75	50	3.20	10
2.78	100	2.96	100	2.91	100
2.73	10	2.85	30	2.82	5
2.65	3	2.72	5	2.77	5
2.39	3	2.60	20	2.66	5
2.28	3	2.57	30	2.59	20
2.25	3	2.43	25	2.54	85
2.19	3	2.25	5	2.41	30
2.14	5	2.15	10	2.23	10
1.943	3	2.13	5	2.20	5
1.751	10	2.12	10	2.12	35
				1.940	10
				1.928	10
				1.875	10
				1.792	15
				1.738	5
				1.557	5
				1.545	5
				1.476	10
				1.462	5
				1.284	5
				1.246	5
				1.202	10
				1.030	10
				1.916	50
				1.776	25
				1.663	15
				1.627	15
				1.543	30
				1.529	30

$4BaO:3TiO_2:P_2O_5$		$BaO:4TiO_2:3P_2O_5$	
d	*I/I*	*d*	*I/I*
4.74	10	4.19	70
4.69	10	3.67	100
4.44	5	3.45	10
4.27	10	3.07	10
4.06	5	2.83	90
3.57	20	2.71	10
3.41	5	2.66	10
3.25	10	2.41	20
3.18	100	2.25	5
3.04	5	2.19	5
2.93	5	2.18	10
2.86	10	2.04	10
2.80	60	1.984	10
2.66	10	1.920	5
2.41	5	1.833	20
2.37	5	1.760	5
2.34	20	1.711	5
2.20	10	1.646	10
2.18	10	1.576	10
2.10	20	1.529	5
2.02	5	1.513	5
1.928	20	1.502	5
1.854	5	1.498	10
1.792	10	1.460	10
1.732	5	1.409	5
1.682	20		
1.617	5		
1.586	5		
1.432	5		
1.399	5		
1.383	5		
1.379	5		
1.281	5		
1.253	5		
1.201	5		
1.075	5		
1.058	5		

Since the temperature range examined was from 800° to 1100°C, $BaO:2TiO_2$ does not appear as a phase in the ternary system. Composition No. 28 consisted of a mixture of $4BaO:3TiO_2:P_2O_5$ + $BaO:TiO_2$ + $BaO:3TiO_2$ but not $2BaO:5TiO_2$. Therefore, it appears that $2BaO:5TiO_2$ does not occur as a stable phase in the ternary system in the temperature range studied. The sluggishness with which equilibrium is reached in the triangles $3BaO:P_2O_5$ — $2BaO:TiO_2$ — BaO and $4BaO:3TiO_2:P_2O_5$ — $BaO:3TiO_2$ — TiO_2 prevented determination of the phase relations within these triangles. However, the boundaries of the triangles are correct as drawn. No extensive solid solution regions exist in the ternary system. Four ternary compounds were discovered and individually prepared. A diagram of the compatibility triangles is given in Fig. 1 and the phase data are listed in Table I.

The compound $2BaO:TiO_2:P_2O_5$ has maximum and minimum refractive indices of 1.688 and 1.672, respectively. At 1197° ± 3°C, 2:1:1 melts congruently. DTA showed no thermal effects between ca. 100°C and the melting temperature. A characteristic x-ray pattern is listed in Table II.

The compound $BaO:TiO_2:P_2O_5$ has maximum and minimum refractive indices of 1.84 and 1.79, respectively, and it melts congruently at 1428° ± 3°C. DTA exhibits an endotherm at 970°C on heating and a exotherm at 905°C on cooling. The thermal effects are the result of a rapid-reversible-dimorphic inversion. High-temperature x-ray examination showed that the inversion occurs at 967° ±5°C. Characteristic x-ray diffraction data of the high- and low-temperature forms are given in Table II.

The compound $4BaO:3TiO_2:P_2O_5$ has a refractive index of about 1.71, and it melts incongruently at 1302° ± 3°C into a liquid and $3BaO:P_2O_5$. Comparison of the x-ray data of 4:3:1 and 3:1 shows that they are almost identical but differences in optical properties of these two compounds proved that 4:3:1 dissociates into 3:1 and a liquid. DTA shows no thermal effects from about 100°C to the melting temperature. A characteristic x-ray pattern is given in Table II.

The compound $BaO:4TiO_2:3P_2O_5$ has refractive indices between 1.88 and 1.92, and it melts incongruently at 1368° ± 3°C into a liquid and probably 1:1:1. X-ray examination of the dissociated product did not reveal a clearly defined phase but suggests that it might be a transition phase between the high- and low-temperature forms of 1:1:1. DTA showed no thermal effects from about 100°C to the melting temperature.

Fluorescent studies.—Reference to Fig. 1 shows that the composition region, $2Ba_2P_2O_7:0.5\text{-}2.5TiO_2$, of useful phosphors reported by Henderson and Ranby lies on the joins $2BaO:P_2O_5$-$2BaO:TiO_2:P_2O_5$ and $2BaO:TiO_2:P_2O_5$-TiO_2. Observation of the end members reveals that 2:1:1 fluoresces a blue color whereas 2:1 and TiO_2 do not fluoresce at all. The optimum phosphor composition claimed by Henderson and Ranby is $2Ba_2P_2O_7:1.0TiO_2$ or actually 50 mole % $2BaO:P_2O_5$ + 50 mole % $2BaO:TiO_2:P_2O_5$, since there is essentially no solubility between end members. Surprisingly, a composition with 50 mole % dilution by 2:1 fluoresces only slightly less brightly than the 2:1:1 compound. This may be explained by the relatively low u.v. absorption of $2BaO:P_2O_5$ and the method of measuring powder brightness. Powder brightness is measured from a sample which has effectively infinite thickness for u.v. light; therefore low absorbing, nonfluorescing particles behave as voids. In this regard it is interesting to examine the fluorescence of compositions in the compatibility triangles which terminate at the 2:1:1 compound.

Composition No. 31, for example, is a mixture of 35 mole % 2:1:1, 31 mole % 1:1:1, and 34 mole % 2:1. However, this composition has only 52% of the brightness of 2:1:1 or $2Ba_2P_2O_7:1.0TiO_2$ because of the presence of 1:1:1 which has high u.v. absorption but no fluorescence. A similar situation exists in composition No. 36 which is composed of 44 mole % 2:1:1, 28 mole % 4:3:1, and 28 mole % 2:1. Like 1:1:1, the presence of 4:3:1, which is a nonfluorescent, highly u.v. absorbing phase, causes this composition to have only 68% of the brightness of 2:1:1. Compositions Nos. 21 and 27 exhibit only 36 and 25% brightness, respectively, due to the presence of TiO_2 in addition to either 1:1:1 or 4:3:1. Absorption and brightness data are summarized in Table III.

Table III. Ultraviolet absorption and fluorescent brightness of Ba-Ti-phosphate compositions

Comp. No.	Mole % composition in terms of compatible phases					U.V. abs.	% powder brightness in terms of
	2:1:1	1:1:1	4:3:1	2:1	TiO_2	in %	2:1:1
32	100	—	—	—	—	96	100
20	—	100	—	—	—	98	0
34	—	—	100	—	—	97	0
3	—	—	—	100	—	21	0
TiO_2	—	—	—	—	100	96	0
31	35	31	—	34	—	97	52
36	44	—	28	28	—	96	68
21	47	42	—	—	11	97	36
27	57	—	26	—	17	96	25

Effect of phosphor composition on brightness.—Because of the low reactivity of TiO_2, the formation of 2:1:1 can be facilitated by using an excess of $2BaO:P_2O_5$. More satisfactory results can be achieved by employing a flux, such as BaF_2, as was used by Henderson and Ranby. Since chemical analysis shows that fluorine is lost on firing, the BaF_2 appears to be oxidized to BaO, apparently by a mass action effect. In order to remain on the 2:1 — 2:1:1 join or to arrive at the 2:1:1 compound, it is necessary to compensate for the additional BaO with P_2O_5. The use of SrF_2, as claimed in a recent patent by Uehara, Kobuke, and Tomishima (11), probably requires similar treatment, since it is likely that small amounts of Sr will substitute for Ba in the phosphor matrix.

A particularly effective method of introducing extra P_2O_5 is by use of $BaO:P_2O_5$. Conveniently, this compound melts congruently into a stable liquid at 843° ± 3°C. Since phosphor synthesis proceeds rapidly at about 1000°C, the combined effects of a fluoride flux and liquid $BaO:P_2O_5$ yield well-formed phosphor. The liquid initially produced by melting of $BaO:P_2O_5$ does not cause sintering, and a phosphor with small particle size is obtained.

The dramatic effect on phosphor brightness with compositions on either side of the 2:1:1 — 2:1 join is demonstrated by the following experiment: Three compositions were prepared (A) $4BaHPO_4 + 1.3TiO_2 + 0.07BaF_2$; (B) $4BaHPO_4 + 1.3TiO_2 + 0.07BaF_2 + 0.07BaO:P_2O_5$; and (C) $4BaHPO_4 + 1.3TiO_2 + 0.07BaF_2 + 0.14BaO:P_2O_5$. Composition (A) lies just off the join in the compatibility triangle 2:1 — 2:1:1 — 4:3:1. Composition (B) is on the join and composition (C) is again located off the join in the triangle 2:1 — 2:1:1 —1:1:1. All compositions were fired at 900°C for 2 hr, a second time at 930°C for 2 hr, and finally fired at 1000°C for 15 hr. The results of

Table IV. Relative fluorescent brightness of some Ba-Ti-phosphate compositions

Composition	Heat treatments 900°C for 2 hr	930°C for 2 hr	1000°C for 15 hr
A*	96	82	82
B*	92	92	100
C*	74	76	80
	900°C for 2 hr	930°C for 2 hr	980°C for 15 hr
D‡	98	90	69
E‡	96	96	100
F‡	57	59	69

* A: 62.4 mole % 2:1:1 + 36.7 mole % 2:1 + 0.9 mole % 4:3:1
B: 62.8 mole % 2:1:1 + 37.2 mole % 2:1
C: 57.5 mole % 2:1:1 + 39.2 mole % 2:1 + 3.3 mole % 1:1:1

‡ D: 44.5 mole % 2:1:1 + 53.5 mole % 2:1 + 2.0 mole % 4:3:1
E: 46.5 mole % 2:1:1 + 53.5 mole % 2:1
F: 37.0 mole % 2:1:1 + 56.5 mole % 2:1 + 6.5 mole % 1:1:1

powder brightness measurements are given in Table IV. Assuming loss only of water and fluorine, the fired compositions are given in Table IV in mole per cent by compatible phases.

The brightness data show that as equilibrium is attained, composition (A) which contains 0.9 mole % 4:3:1, and composition (C) which contains 3.3 mole % 1:1:1 have only 80% of the brightness of composition (B) on the join 2:1:1 — 2:1. The loss in brightness of compositions (A) and (C) shows that 4:3:1 and 1:1:1 are more effective absorbers for u.v. radiation than their mole percentages would suggest. Examination of the reaction sequence reveals that the first phase to form is $2BaO:P_2O_5$ from the decomposition of $BaHPO_4$. $2BaO:P_2O_5$ reacts with TiO_2 to form $2BaO:TiO_2:P_2O_5$ and depending on composition either 4:3:1 or 1:1:1 form as equilibrium is reached. The reaction sequence is illustrated by composition (A). An initial firing at 900°C gave a product with 96% brightness but successive firings at 930° and 1000°C lowered the brightness to 82%. Composition (C) which has the additional fluxing action of liquid $BaO:P_2O_5$ approached the equilibrium value during the initial firing at 900°C. Thus, it seems likely that the 4:3:1 and 1:1:1 phases occur on the surfaces of the 2:1:1 and 2:1 phases where they can act as more effective absorbers for u.v. light than their mole percentages would indicate.

Three other compositions were selected similar to (A), (B), and (C). The additional compositions were prepared as follows (D) $4.0BaHPO_4 + 1.0TiO_2 + 0.15BaF_2$; (E) $4.0BaHPO_4 + 1.0TiO_2 + 0.15BaF_2 + 0.15BaO:P_2O_5$; and (F) $4.0BaHPO_4 + 1.0TiO_2 + 0.15BaF_2 + 0.30BaO:P_2O_5$. Fluorescent brightness data and compositions by compatible phases are given in Table IV. The results parallel those obtained from compositions (A), (B), and (C). In addition, it is demonstrated that doubling the amount of 4:3:1 from 0.9 mole % in (A) to 2.0 mole % in (D) only further decreases the brightness by about 10%. Thus it appears that doubling the amount of 4:3:1 increases the effective u.v. absorbing area by about 10%, which again suggests that 4:3:1 occurs as patches on the surface of the phosphor.

Conclusions

1. The subsolidus phase relations were determined in the system $BaO-TiO_2-P_2O_5$. Four ternary compounds were isolated: (*a*) $2BaO:TiO_2:P_2O_5$ melts congruently at 1197° ± 3°C, and it has maximum and minimum refractive indices of 1.688 and 1.672, respectively; (*b*) $BaO:TiO_2:P_2O_5$ melts congruently at 1428° ± 3°C, and it has maximum and minimum refractive indices of 1.84 and 1.79, respectively; (*c*) $4BaO:3TiO_2:P_2O_5$ has a refractive index of about 1.71, and it melts incongruently at 1302° ±3°C, and (*d*) $BaO:4TiO_2:3P_2O_5$ melts incongruently at 1368° ± 3°C, and the refractive indices lie between 1.88 and 1.92.
2. $3BaO:2P_2O_5$ exhibits a slowly reversible dimorphic inversion at 870° ± 10°C. The low-temperature modification has maximum and minimum refractive indices of 1.628 and 1.618, respectively. The high-temperature form is nearly isotropic with a refractive index of about 1.626.
3. $2BaO:TiO_2:P_2O_5$ is the only compound in the system which is of the self-activated type. It has an emission similar to that of $MgWO_4$.
4. Compositions with maximum fluorescence are restricted to the join $2BaO:P_2O_5$-$2BaO:TiO_2:P_2O_5$, since compositions off this join contain either $BaO:TiO_2:P_2O_5$, $4BaO:3TiO_2:P_2O_5$, or TiO_2 which have high u.v. absorption but are nonfluorescent phases.

Acknowledgments

The author thanks Professor F. A. Hummel of the Pennsylvania State University for supplying the high-temperature x-ray data, and J. G. Rabatin of the General Electric Company for obtaining the differential thermal analysis data.

Manuscript received Sept. 16, 1959.

Any discussion of this paper will appear in a Discussion Section to be published in the December 1960 JOURNAL.

REFERENCES

1(a) S. T. Henderson and P. W. Ranby, *This Journal*, **98**, 479 (1951).
(b) P. W. Ranby, U.S. Pat. 2,596,509 (May 13, 1952).
2. J. G. Rabatin and C. S. Card, *This Journal*, **104**, 68C [abs. 90] (1957).
3. E. S. Shepherd, G. A. Rankin, and F. E. Wright, *Am. J. Sci.*, 4th Ser., **28**, 293 (1909).
4. D. E. Rase and Rustom Roy, *J. Am. Ceram. Soc.*, **38**, 110 (1955).
5. G. H. Jonker and W. Kwestroo, *J. Am. Ceram. Soc.*, **41**, 390 (1958).
6. D. E. Harrison and F. A. Hummel, *J. Am. Ceram. Soc.*, **42**, 487 (1959).
7. A. Glatzel, Ueber dimetaphosphorsaure and tetrametaphosphorsaure Salze, Diss., Wiirzburg, 1880, *Bull. Nat. Research Council*, **118**, 13 (1949).
8. L. Ouvrard, *Ann. chim Phys.*, **6**, (16) 289 (1889); *Bull. National Res. Council*, (118) 13 (1949).
9. W. H. Zachariasen, *Acta Cryst.*, **1**, 263 (1948); *Bull. Nat. Research Council*, **118**, 13 (1949).
10. R. P. Langguth, R. K. Osterheld, and E. Karl-Kroupa, *J. Phys. Chem.*, **60**, 1335 (1956).
11. Y. Uehara, Y. Kobuke, and H. Tomishima, U.S. Pat. 2,882,238 (April 14, 1959).

An Apparatus for the Preparation of Semiconductor Grade Silicon by Film Boiling

Ray C. Ellis, Jr.

Research Division, Raytheon Company, Waltham, Massachusetts

ABSTRACT

A film boiling technique is used to increase the rate of thermal decomposition of silicon tetraiodide. The silicon is deposited molten on a submerged induction-heated graphite shape and is collected after its departure from the hot zone by flotation. Apparatus is described for the synthesis and purification of large quantities of silicon tetraiodide.

Depending on the semiconductor application, silicon of purity of as little as one part per billion is required. Zone segregation has been of limited use for silicon. Many difficulties have been encountered when melting and solidifying silicon in known crucible materials. The most effective method of zone segregation utilizes a floating zone (1).

Semiconductor grade silicon has been prepared by the reduction of silicon tetrachloride with zinc vapor (2), the reduction of a halogenated silicon compound with hydrogen (3-8), and by the thermal decomposition of silane (9) and of silicon tetraiodide (10, 11).

Recently it was shown that the rate of deposition of titanium from the thermal decomposition of titanium tetraiodide could be increased greatly if the geometry were changed from the Van Arkel-de-Boer (12) method to a film boiling geometry (13). This is the basis of the apparatus described below.

Silicon tetraiodide is a suitable starting material. The free energy change for the decomposition $SiI_4 \rightarrow Si + 2I_2$ at 1 atm becomes zero at about 1770°K. This figure may be in considerable error because of the uncertainty of the data available (14). At this temperature, K of the reaction, $I_2 \rightarrow 2I$, is about 8 $l/mole^{-1}$ with a contribution of −7.32 kcal/mole (15).

The partial pressure of iodine which limits the reaction is supplied by the decomposition. The rate of the decomposition by film boiling is most dependent on the removal of iodine from the reaction zone (11).

Silicon tetraiodide melts at 127°C and boils at 300°C, mp 122°-122.5°C, bp 301.5°C (16). Its density is greater than that of silicon and aids in the removal of the product from the reaction zone by flotation. Silicon tetraiodide can be prepared easily in large quantities (Appendix I) and can be purified in large quantities (Appendix II).

Experimental

Apparatus.—The apparatus for the decomposition consists of a graphite heater, A in Fig. 1, heated with coils, B, driven by a 20 kw rf generator. The heater is held at its base by two molybdenum wires, C, in an inner quartz liner, D. This liner assembly can be changed without disassembling the entire

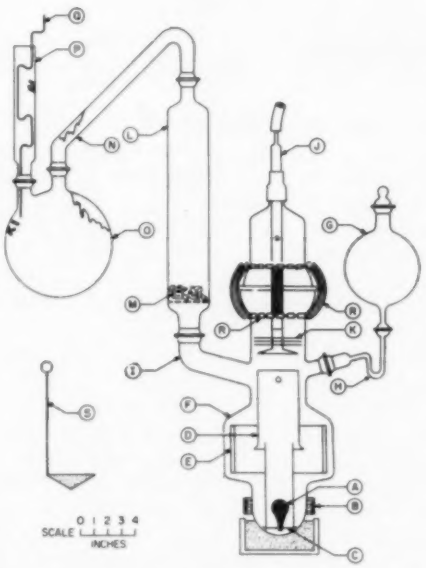

Fig. 1. Apparatus for the decomposition of silicon tetraiodide by film boiling.

apparatus. The inner liner and the outer quartz liner, E, are contained in the reactor, F, which has a total volume of about 10 l and rests in sand. The reactor is fitted with a 2-l feeding flask, G, and feeding tube, H, a sidearm, I, and a large upper joint. The upper joint contains a gas inlet tube, J, on which are hung a series of tantalum baffles, K. Attached to the side arm is the column, L, filled with quartz cullet, M. A condenser, N, leads from the top of the column to a 10-l receiving flask, O. Connected to the receiving flask is a vent or stack, P, in which is placed a cleaning crank, Q. All joints are held together with ball joint clamps except the large joint, which is held together with a chain and spring clamp, R. The chains on each side of the joint are held with springs of suitable number and strength. The chains distribute the pressure evenly.

Operation.—After the graphite heater has been put into place and about 3 l of liquid silicon tetraiodide have been added, the apparatus is flushed with an inert gas such as argon. The graphite then is heated to just below the decomposition temper-

ature (1800°C est.). The flushing gas is adjusted to the point where the heavy vapors of silicon tetraiodide just rise to the baffles. This keeps the large joint between the reactor and the top clean. As the boiling continues the condensing vapors rise in the column and heat it. This prevents clogging of the cold column later by iodine. The power put into the graphite is increased and decomposition begins. Iodine vapors obscure all the inner parts of the apparatus and the decomposition proceeds with iodine distilling out of the column and into the condenser and receiving flask. To prevent clogging, the condenser is heat-cycled periodically to melt the solidified iodine down into the receiver. The crystals in the stack are broken free with the crank.

The molten silicon builds up continuously on the graphite and breaks to the surface of the surrounding liquid in a bright display of molten droplets. The inner quartz liner directs the silicon droplets upward and dumps them out onto the surface of the liquid tetraiodide. The outer quartz liner prevents the molten droplets from floating into the side of the glass container. Very few droplets stick to any surface. Fresh silicon tetraiodide is added as it is needed during the decomposition to keep the liquid level up. This is accomplished by melting the solidified silicon tetraiodide in the feeding flask and through the feeding tube trap.

After several pounds of silicon have collected, the power is turned off, the top is opened, and the inner liner removed. The pellets then can be removed with a tantalum screen ladle (S, Fig. 1). The pellets are soaked in distilled water and then in hydrofluoric acid solution to rid them of any silica. After washing and drying, the pellets are ready for use.

In disassembling the apparatus the joints of the feeding tube and the condenser are loosened by heating and are separated. The top of the reactor is removed and the liquid contents of the reactor poured (usually with filtering) into a flask for storage. The glassware is cleaned by an overnight immersion in hot, 10% sodium hydroxide solution, followed by a scrubbing in Alconox solution and a rinse in demineralized water.

Heater.—Special attention must be paid to the surface on which the silicon deposits since naturally no contamination of the silicon by the surface material or its impurities is desired. The best material found was graphite.

The graphite selected has to be both pure and dense for this application. It was found that commercial graphite with a density of less than about 1.70 was completely disintegrated into silicon carbide by molten silicon. This destructive process was seen less frequently as more dense graphite was used. As silicon starts to form on a graphite surface a protective layer of silicon carbide forms. This prevents further reaction unless the graphite is porous. In this case the silicon runs into the pores, forming some silicon carbide. The volume of the silicon carbide is greater than that which the graphite originally occupied, resulting in a crack which relieves the strain. Silicon runs into this crack and the destructive process continues.

The shape selected for the graphite has smooth contours to encourage the least violent liquid and gas flow around it and to minimize the strains induced on its surface by the thin silicon carbide layer.

Unfortunately there is a finite solubility of carbon in molten silicon. Therefore the graphite (or silicon carbide) dissolves to an appreciable extent in the silicon that has formed. A very small amount of silicon carbide crystallizes out of the silicon pellets as they solidify. This amounts to about 0.1%. Occasionally a graphite heater had to be replaced because of extensive erosion.

Silicon carbide was used in several experiments and found to erode about as rapidly as the dense graphite samples.

Results

Product.—The product is a mass of various sized polycrystalline droplets of silicon ranging from ⅛ to ¾ in. in diameter. Many of the droplets broke after solidification. The product is pictured in Fig. 2.

Rates as high as 120 g/hr have been observed. This corresponds to 10 g of silicon/hr/cm². By suspending the graphite in the vapor, a rate of 1.0 g/hr/cm² was obtained at about 1800°C. This tenfold increase in the rate by the introduction of film boiling compares with the factor of 100 found by Petersen (13) using titanium tetraiodide.

The purity of the product was determined by drawing a test crystal from each batch and measuring its resistivity. The average resistivity of about a thousand runs was found to be about 5-10 ohm-cm, p-type. The impurity element was identified as boron by determining the segregation coefficient. The highest resistivities found were in the 300 ohm-cm range, but it is believed this was due to compensation.

Although the small carbon (or carbide) content in the silicon did not affect the resistivity, it interfered in the growth of single crystals by appearing as a dross on the molten product during crystal growing.

Several methods have been used to remove the silicon carbide from the product. The product has

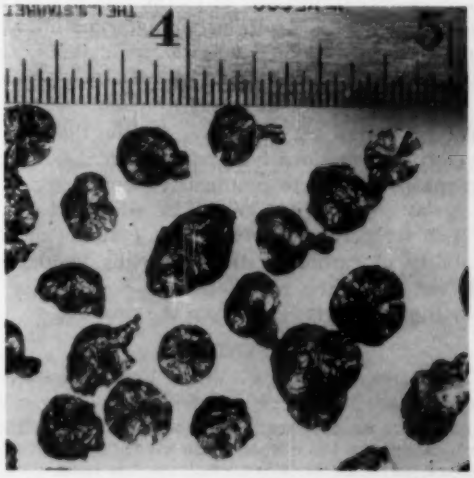

Fig. 2. The product: solidified droplets of silicon

been filtered through quartz wool and fritted quartz disks but these steps, while removing the carbide, introduce oxygen (17).

Temperature of decomposition.—The decomposition in this system starts suddenly because the sudden darkening of the contents of the reactor is seen when the temperature is increased by very small increments. Several methods have been used to estimate this temperature. Direct optical measurement was impossible because of the deep iodine color. Just prior to decomposition, the temperature is about 1700°C. When the graphite was heated in argon with the same power input as above, the temperature was about 150° higher. In one case where silicon tetraiodide was used, hydrogen was introduced just under the heater to obtain better visibility. The deep iodine color was dispelled everywhere except in the immediate neighborhood of the decomposition zone. It is interesting to note that under these conditions small quantities of triiodosilane distilled out of the column.

Placing a thermocouple inside the graphite and free from silicon tetraiodide vapors could not be accomplished without the disintegration of the thermocouple with silicon at temperatures somewhat below where the reaction appears to begin.

A further estimate of the decomposition temperature was attempted by observing the time it took the pellets to solidify. Knowing the heat of fusion and the heat capacity of molten silicon and assuming an emissivity as high as unity, one can calculate the time required for a pellet of a given size to solidify, assuming heat loss by radiation only. The calculated cooling time is still much larger than the observed, showing considerable heat loss by conduction.

Thermodynamics predicts an equilibrium decomposition temperature of 1770°K at 1 atm but this is very dependent on the iodine partial pressure. Reducing the iodine pressure reduces the temperature at which decomposition can take place. A discussion of this equilibrium has been made by Schäfer and Morcher (18, 19) and by Loonam (20). It is interesting to note that, with an adequate supply of iodine at a total pressure of 1 atm, the formation of silicon tetraiodide is self-sustaining, sometimes producing temperatures sufficient to soften quartz (Appendix I).

Summary

An apparatus has been used for the thermal decomposition of silicon tetraiodide by film boiling on a graphite surface to produce semiconductor grade silicon at a rate of 120 g/hr. The estimated decomposition temperature is 1800°C at 1 atm. The small solubility of carbon in silicon at this temperature does not affect the resistivity but does hinder the growth of single crystals from the product.

APPENDIX I

Apparatus for the Production of Large Quantities of Silicon Tetraiodide

Literature on preparation of metal halides by direct combination are too numerous to mention. Much of the preparative work on silicon halides has been done by Schumb, *et al.* (21). The following represents an improvement on Szekely's method (3) in that the apparatus can be run almost continuously and that the rate of the reaction is somewhat higher.

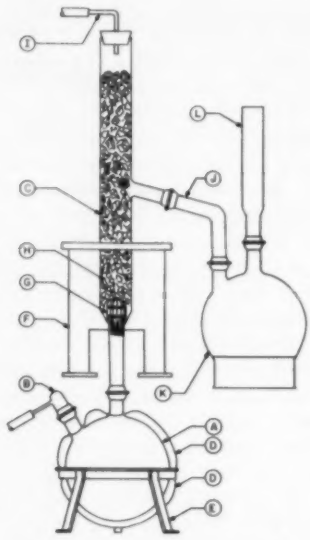

Fig. 3. Apparatus for the preparation of silicon tetraiodide

Experimental.—Resublimed iodine was purchased in 25-lb drums from J. T. Baker Chemical Company, Phillipsburg, New Jersey. The crude silicon (low aluminum grade) was purchased in 100 lb drums from the Electro-Metallurgical Division of Union Carbide and Carbon Corporation. The silicon was crushed to about 1 mesh before use.

The apparatus (Fig. 3) consists of a 5 l boiler flask, A, fitted with an inlet tube, B, and an opaque quartz burning tube, C. A heating mantle, D, surrounds the boiler and supports it. The assembly is supported by a sturdy tripod, E. The lower portion of the burning tube is surrounded by a resistance furnace, F. A tantalum or molybdenum wire plug, G, in the neck of the burning tube supports the silicon charge, H. A one-holed rubber stopper and a glass tube in the top of the burning tube act as a secondary inlet tube, I. The burning tube has a side arm which connects through an elbow, J, to a 5 l receiver, K. The receiver is fitted with an open tube, L, called a stack.

To ready the apparatus for use, the burning tube is filled with crushed silicon and the boiler is loaded with about 4 l (40 lb) of molten iodine. This material is generally iodine recovered from the decomposition of silicon tetraiodide. The system is swept with argon slowly through both inlet tubes.

The furnace is turned on and its temperature increased until the purple vapors appearing in the side arm and elbow change to a white aerosol of silicon tetraiodide. The boiler temperature is increased and the reaction proceeds vigorously as iodine distills up into the burning tube. Usually the furnace is turned off completely to avoid overheating as the reaction is self-sustaining.

As the reaction continues, the flushing gas is decreased to a very low flow rate. The necks of the receiver and the stack are heated periodically with a large soft flame to melt down any solid that has collected. Silicon in the burning tube is knocked down into the reaction zone by tapping the tube gently with a heavy wooden stick. To run the apparatus more or less continuously, the boiler and burning tube can be recharged and the receiver replaced. The washing procedure for the burning apparatus is identical to that used for the decomposition apparatus.

The impure product that distills into the receiver is usually a dark pinkish-brown liquid cooling to a brown waxy solid. The rate of production can be controlled by regulating the boiler temperature and averages 7.5

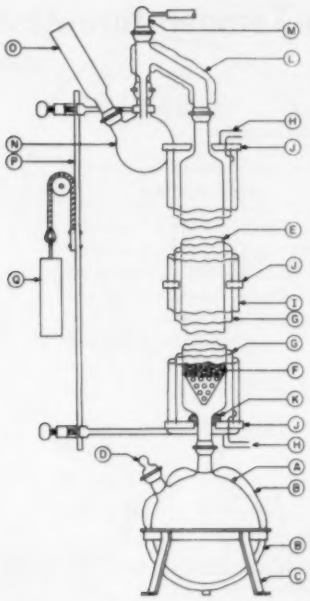

Fig. 4. Still for the distillation of silicon tetraiodide

lb/hr of crude product. The yield is essentially quantitative.

The rate of burning cannot be increased greatly because several times the opaque quartz tube had sagged dangerously because of over-heating. If pure silicon is used as the starting material, the reaction starts with great difficulty and the burning rate is quite slow.

APPENDIX II

Still for the Purification of Large Quantities of Silicon Tetraiodide

The still used for the purification is an easily built laboratory-scale still for handling of large quantities of a dense, high boiling material such as silicon tetraiodide. It is of the usual type with a few innovations for use with silicon tetraiodide. The weight of the column and receiver is counterbalanced so that a redistribution of weight during distillation will not strain the neck of the boiler flask. The thermometer was eliminated from the prototype still head because it was more convenient to take product cuts on an empirical basis.

Experimental.—The apparatus (Fig. 4) consists of a 12-l boiler pot, A, enclosed in a heating mantle, B. The mantle and flask are supported by a sturdy tripod, C. The boiler has a side arm, D, for the introduction of crude silicon tetraiodide. A column, E, 72 in. long and 3 in. in diameter is packed with ⅜ in. glass helices, F, and is connected to the boiler. The column is surrounded by two jackets. The inner jacket, G, is wound with nichrome wire, H, to balance the heat loss of the column. The outer jacket, I, is insulating. To facilitate the construction of the apparatus, the jackets were each made of two parts. The column assembly is held in position by three grooved Transite rings, J. The column rests in glass wool, K. The weight of the column assembly is supported by the bottom Transite retainer. The top of the column connects to an insulated still head, L, which is fitted with a gas inlet tube, M. The receiver, N, is attached to the still head and is fitted with a vent, O, called a stack. An internal extension on the head directs the distillate away from the joint between the head and the receiver. The column and receiver assembly is attached to a movable rack, P. The column, receiver, and rack are counterbalanced by a weight, Q, to prevent strain on the neck of the boiler flask.

Usually the charge of crude silicon tetraiodide is about 85 lb. It is contaminated largely with iodine. The first fraction is deeply colored with iodine, bp 184°C, and somewhat contaminated with boron triiodide. By the time the pure yellow distillate of silicon tetraiodide appears these impurities have been collected. The temperature of the upper part of the column is lowered slightly by decreasing the power in the winding of the upper, inner jacket. The throughput stops and the receiver is quickly changed. Product is similarly taken in batches. Crude silicon tetraiodide can be added as desired.

The distillation was carried out at 1 atm to avoid the use of vacuum equipment. This step did necessitate the introduction of suitable insulation and heating of the apparatus.

The reflux ratio during operation was about 3:1 and it is estimated that there were about seven theoretical plates.

The product is a yellow liquid or a white solid with the melting point found to be 127°C. The throughput of the column could be as large as 7 lb/hr, because there was good separation of impurities. The nearest boiling containment was boron triiodide with a boiling point of 210°C (16), a separation of 90°C from silicon tetraiodide. The product was analyzed spectroscopically and no impurities were found.

Manuscript received June 22, 1959.

Any discussion of this paper will appear in a Discussion Section to be published in the December 1960 JOURNAL.

REFERENCES

1. P. H. Keck, *Physica*, **20**, 1059 (1954).
2. D. W. Lyon, O. M. Olsen, and E. D. Lewis, *J. (and Trans.) Electrochem. Soc.*, **96**, 359 (1949).
3. G. Szekely, *This Journal*, **104**, 663 (1957).
4. H. C. Theuerer, *Bell Labs. Record*, **33**, No. 9, 337 (1955).
5. D. W. Lyon, "Rare Metals Handbook," Ch. 19, Reinhold Publishing Co., New York (1954).
6. A. E. van Arkel, *Metallwirtschaft*, **13**, 405, 511 (1934).
7. Siemens and Halske Ag. Brit. Pat. 809,250 and 795,191.
8. R. C. Sampler, E. F. Maverick, and M. L. Croutch, *This Journal*, **104**, 317 (1957).
9. Progress Reports. Contract No. DA-36-039-SC-72768 to the Lansdale Tube Co. (Philco Corporation), Lansdale, Pennsylvania.
10. F. B. Litton and H. C. Andersen, *This Journal*, **101**, 287 (1954).
11. A. F. Armington, "Some Aspects of the Decomposition of Silicon Tetraiodide," paper presented at the 113th Meeting of the Electrochemical Society, New York, May 1, 1958.
12. A. E. van Arkel and J. H. de Boer, U. S. Pat. 1,671,213 (1928).
13. A. W. Peterson, and L. A. Bromley, *J. Metals*, **8**, 284 (1956).
14. L. L. Quill, "The Chemistry and Metallurgy of Miscellaneous Materials," 1st ed., McGraw-Hill Book Co., Inc., New York (1950).
15. Stark and Bodenstein, *Z. Elektrochem.*, **16**, 961 (1910).
16. H. C. Andersen and L. H. Belz, *J. Am. Chem. Soc.*, **75**, 4828 (1953).
17. W. K. Kaiser and P. H. Keck, *J. Appl. Phys.*, **28**, 882 (1957).
18. Schafer and Morcher, *Angew. Chem.*, **68**, 583 (1956).
19. Schafer and Morcher, *Z. anorg. u. allgem. Chem.*, **29C**, 279 (1957).
20. A. C. Loonam, *This Journal*, **106**, 238 (1959).
21. W. C. Schumb and R. C. Young, *J. Am. Chem. Soc.*, **52**, 1464 (1930).

Imaging-Furnace Developments for High-Temperature Research

Peter E. Glaser

Arthur D. Little, Inc., Cambridge, Massachusetts

ABSTRACT

The principles of imaging furnaces using the sun or a high intensity electric arc are presented. The performance of imaging furnaces with the two energy sources are contrasted and the relative advantages of each source are pointed out. Details on arc performance and construction are given. Advances in instrumentation for measuring and controlling temperature and heat flux are described. The function of a flux distributor to obtain larger uniformly heated area is explained.

The goal of high-temperature research is to obtain a better understanding of the behavior of materials under conditions of extreme temperatures. Therefore, means had to be found to generate high temperatures under controlled conditions in the laboratory. Among the approaches for generating high temperatures are those relying on heat transfer by a gas, induction heating, or resistance heating, and those using only radiant heating by means of an imaging furnace.

The imaging furnace, an optical system to concentrate radiation from a suitable heat source, has been found a useful research tool in studies of high-temperature phenomena. In an imaging furnace, the heat source is far enough from the sample to transmit heat by radiation only and not by conduction or convection. The advantages of this method are freedom from contamination of the sample (both by furnace vapors and a sample container), the possibility of studying the behavior of the material in either air or a controlled atmosphere, and the ease with which instruments can be brought close to the sample without being subjected to excessive heat.

Imaging Systems

During the past few years, solar furnaces, using the sun to provide radiant energy, have created considerable interest (1), although their dependence on the weather has restricted their applications. The substitution of an artificial source to permit the use of an imaging furnace inside a laboratory has been found to offer definite advantages (2). The development of new high-intensity electric arcs (3) has provided radiant-energy-producing capabilities beyond those found in a solar furnace.

Figure 1 shows the possible arrangements by which the source can be imaged onto a sample. A single paraboloidal mirror (4) and a paraboloidal mirror in combination with a flat mirror (5) have been used to image the sun onto the sample. Ellipsoidal-(6) and paraboloidal-mirror combinations (7) have been used in conjunction with electric arcs. An optical system using an ellipsoidal mirror with the source located at the major focal distance (8) produces a reduced image and the highest flux density, while a refractive system (9) is capable of giving a uniform image irradiation. The two-paraboloidal-mirror and two-ellipsoidal-mirror systems have found wide usage; two-ellipsoidal mirrors have some advantage in convenience of controlling the radiation.

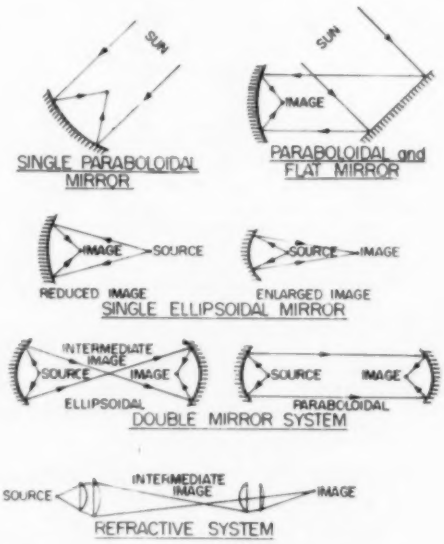

Fig. 1. Optical systems of imaging furnaces

The choice of optical system and imaging source depends on the desired characteristics of the image. A single mirror tends to have the least transmission loss, and, if the location of the source is transposed, either an enlarged or reduced image can be obtained. In addition to the type of image obtained (as determined by the optical system), the radiation flux density, distribution of the flux density at the focal zone, and fluctuation in the source output influence the usefulness of an imaging furnace.

When the sun is used as the radiation source, the flux density at the image is determined by the amount of radiation that reaches the collecting mirror system after absorption by the atmosphere (about 1.3 cal/cm^2/min). Because of the limited output of this radiation source, considerable effort had to be expended in establishing the optimum size and geometry (10) of the collecting mirrors so that a high image flux density could be attained.

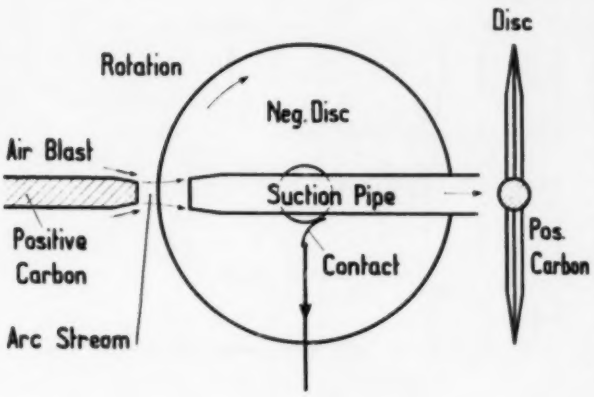

Fig. 2. Blown arc arrangement

Electric-Arc Sources

The electric arcs that have been used in imaging furnaces are of the Beck (11) type. The outstanding visible characteristic of this high-intensity electric arc is a jet of gaseous material ejected from the anode crater in the form of a vertical tail flame. The flow velocity and flow direction of this tail flame are determined by internal electromagnetic fields and thermal effects. These vaporized anode components, comprising atoms, ions, and possibly some diatomic molecules, radiate very strongly; their steady-state behavior depends on the current density. Much of the radiation that emanates from the gaseous materials of the tail flame is lost, since it cannot be concentrated into an image. A considerable improvement over the conventional high-intensity electric arc is represented by the Gretener (12) blown arc. Figure 2 shows the mechanism by which a blown arc is obtained. Tangential air jets surrounding the anode direct a conical stream of air inward toward the arc. In this manner, the gaseous materials are concentrated in the form of a cylinder of brilliantly glowing gases. In addition, the air jets surrounding the anode cool the outside surface thus allowing a higher current density without an increase in carbon consumption.

Operational Requirements

Operational requirements and experimental procedures may determine the type of source and optical system of an imaging furnace. The spatial distribution of the radiant flux density at the focal zone of the collecting mirror must be considered; it has been shown to follow approximately a Gaussian distribution (13). A useful parameter describing it is the radial distance from the optical axis at which the flux density has dropped to 90% of that measured on the axis. The nature of the optical system and the size and type of source determine what this radial distance will be.

Although a maximum image flux density is desirable, a constant flux density at the image plane is necessary. When the sun is used as the radiation source, nearly ideal constant conditions prevail at the image; no other source has been able to produce equivalent conditions.

Constancy of flux density is influenced by nonuniform composition of the arc electrodes, irregular burning of the electrodes (caused by the effects of magnetic fields), variations in the supply of voltage, unsatisfactory electrode feed devices and controls, and an unstable arc (caused by an excessive current density). The positioning of the positive carbon in the focal plane of the source mirror is critical; a movement of ⅛ in. from the electrode focal plane can cause a change of 10% in the flux density at the image.

The duration of an experiment to be performed in an imaging furnace may influence the selection of a source. Theoretically, the sun provides the longest daily operating time for an imaging furnace, but actually, this time depends on the location of the furnace and on the weather. In the northern latitudes, atmospheric conditions may limit the number of uninterrupted operating hours available; the electric arc offers a better alternative when continuous use of the imaging furnace is desired.

Considerable improvements have been made in the structure of electrodes (14) for improving the performance of electric arcs, particularly the blown arc. The improved carbon electrodes have a cored structure designed to prevent disturbing light fluctuations when the arc is being burned. A suitable electrode has a double-cored construction. The inner core contains rare earth compounds that provide a high intensity of light; the proportion of rare earth in the outer core is greater than that in the inner core. Experimentally produced electrodes using this construction allow a far greater current density to be employed and thus make possible a higher flux density.

At lower current densities, electrodes may have to be replaced in about 20 min, while at higher current densities, they may have to be changed in about 5 min. Disk cathodes can operate for several hours.

ADL-Strong Arc-Imaging Furnace

A double-ellipsoidal-mirror system has been designed on the basis of requirements posed by high-temperature research procedures. This system offers an excellent compromise between the requirements of high-radiation flux density, large image size, temperature control, duration of the radiation pulse, and flexibility for experimental measurements. Figure 3 is a diagram of the ADL-Strong arc-

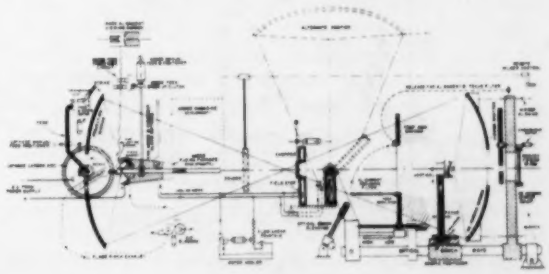

Fig. 3. Diagram of ADL-Strong arc imaging furnace

imaging furnace. The arc source is a Gretener-type arc with a 10-mm rod anode and a carbon-disk cathode. An auxiliary 6-in. diameter collecting mirror located behind the anode reflects a portion of the radiation to the main source mirror. Two ellipsoidal 21-in. diameter mirrors are used; these can be operated with the optical axis in either a horizontal or vertical position by the insertion of a flat diagonal mirror. With the optical axis in the vertical position, it is possible to melt powders and study liquid phases, with the parent materials forming the container.

Temperatures of the sample are controlled by a temperature modulator that consists of a sliding aperture with remote electric controls. An alignment and focusing disk forms part of the modulator and enables the mirrors to be aligned on the optical axis and a sample to be located in the focal plane. The sample is mounted on a positioner that permits tri-axial movement through remote electric drives. Two shutters are used, one located near the intermediate image, and the other just behind the opening in the collecting mirror. The purpose of these shutters is to permit the separation of incident and reflected radiation from the sample as well as to allow a specific radiation pulse to be obtained. The power required by the arc is 180 amp continuous to 300 amp intermittent at 75 v and is supplied by a selenium rectifier.

Measurement Techniques

Once the capability of generating high temperature with an imaging furnace had been developed, the need arose to have instruments available for the measurement of physical parameters, particularly heat flux and temperature.

Heat Flux

Calorimeter.—Figure 4 shows the cross section of the calorimeter (15), designed to meaure heat flux reaching the focal zone of the collecting mirror, where the energy arriving over a 140-degree solid angle is accumulated inside a black-body cavity and transferred to the circulating water; this energy is calculated from measurements of the temperature rise and quantity of water flowing. The device is designed with an accuracy of ± 5% and has been used as our basic calibrating calorimeter.

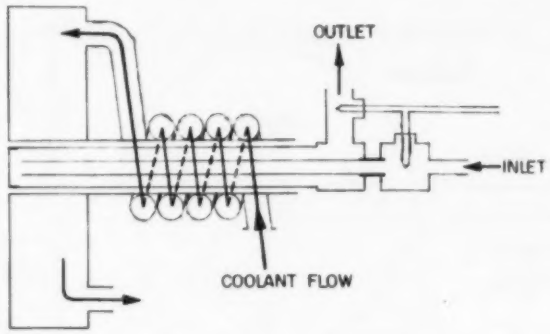

Fig. 5. Cross section of calorimeter

Figure 5 shows a cross section of the water-cooled calorimeter used to measure the radiation over 180-degree solid angle. The measuring area of the calorimeter is blackened and water-cooled, and the temperature rise and quantity of water flowing is measured. This type of calorimeter requires calibration, since some of the incident energy is radiated again at the front surface.

Radiometer.—The two calorimeters described measure the total radiation received over a specific diameter at the focal plane. In some instances, it may be of interest to measure the maximum flux density (rather than the average flux density) as well as the flux distribution across the focal plane.

Figure 6 shows a circular-foil radiometer (16). The receiving area of this water-cooled radiometer is 0.9 mm in diameter. Since it has a very short time constant, the measurement of rapidly varying fluxes or of the continuous traversal of the focal plane can be accomplished. Figure 7 shows the cross section through the radiometer. A blackened, thin circular foil of constantan fastened to a water-cooled copper block absorbs the radiation, and a thin copper wire attached to the center of the circular foil measures the temperature rise at its center.

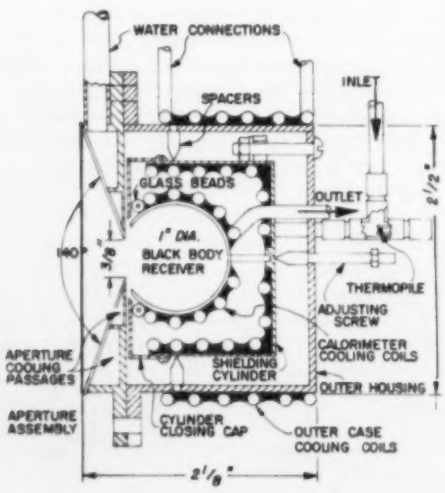

Fig. 4. Cross-section of calorimeter

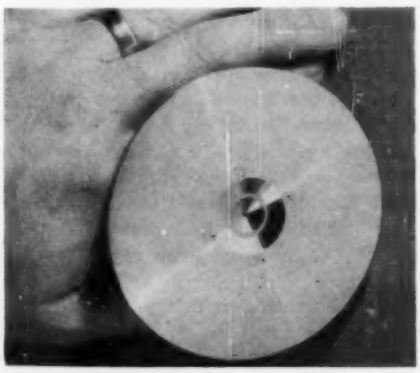

Fig. 6. Circular foil radiometer

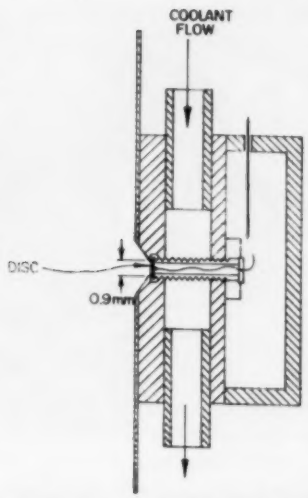

Fig. 7. Cross section of radiometer

The circular-foil radiometer calibrated with the absolute calorimeter can also measure the radiation flux density at the focal zone. Figure 8 shows the flux distribution obtained in both the solar furnace and the arc-imaging furnace with the radiometer. Also shown are the instantaneous flux variations recorded by the radiometer in the arc-imaging furnace; these variations are of the order of ± 5%. Improvements in the electric feeding device, the power supply, and the uniformity of the electrode are expected to further reduce the flux variations.

When a short-time radiation pulse is to be used, conventional calorimeters cannot be applied use-

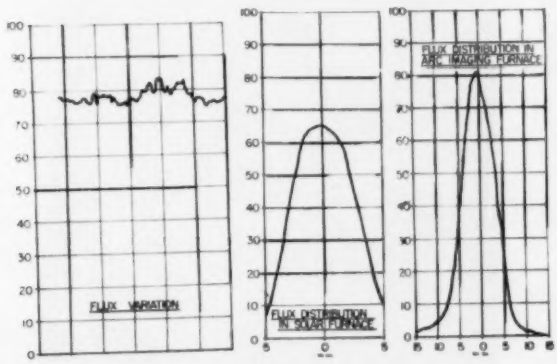

Fig. 8. Flux distribution and variation

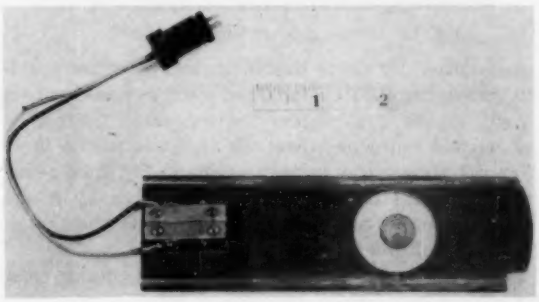

Fig. 9. Copper disk calorimeter

Table I. Performance data ADL-Strong arc imaging furnace

Device	Flux, cal/cm² sec	Equiv. black body temp, °K	Amp @ 75 v d.c.	Anode carbon type
Radiometer				
1 mm diam	265	3750	300	Experimental "Ultrex"
	225	3600	155	Modified "Ultrex"
Calorimeter				
9.5 mm diam	220	3550	300	Experimental "Ultrex"
	145	3240	155	Modified "Ultrex"

fully. Instead, a copper disk is suspended by thin wires, and its temperature is measured by a thermocouple after calibration with the calorimeter (Fig. 9).

Table I shows the performace data of the ADL-Strong arc-imaging furnace. Although in prior work 4000°K (obtained from calorimetry) was reported as the highest value attained, the lower temperatures measured in the ADL-Strong furnace are partially attributed to the use of second surface-collecting mirrors.

Temperature Measurements

Conventional optical pyrometers measure accurately only the temperatures of a black body (17), a condition that few samples are able to satisfy. Although drilling small holes into the sample surface to approximate black body conditions is valid theoretically, this expedient raises questions concerning the uniformity of cavity temperatures and may not be feasible with some of the samples to be tested.

The optical pyrometer can be used for accurate temperature measurements in an imaging furnace if suitable shutters are provided for separating emitted and reflected radiation. Radiation emitted by, or reflected from, the sample is observed with an optical pyrometer sighted through a hole at the center of the collecting mirror (Fig. 3). The shutter located near the intermediate image position rotates about an axis that is slightly displaced from the optical axis of the ellipsoidal mirrors and periodically shields the sample from the arc radiation. An off-axis shutter behind the collecting mirror is provided with a small opening that coincides with the optical axis; it is driven in synchronization with the previous shutter by means of synchronous motors. The field coils of the motors are connected in such a manner that the two shutters can be either in phase or out of phase. In the in-phase position, only radiation emitted by the sample is observed, since all other radiation is prevented from reaching the sample. In the out-of-phase position, both emitted radiation and the arc radiation reflected from the sample are observed.

The apparent surface temperature of the sample is measured with the two shutters rotating in phase. A second temperature is then measured with the shutters out of phase. Kirchhoff's equation relating reflectivity to emissivity can then be used to deter-

mine the approximate spectral emissivity; once this is known, the true temperature can be calculated

$$\frac{1}{e^{C_2/\lambda T_{p1}} - 1} = K \frac{\epsilon(\lambda,T)}{e^{C_2/\lambda T_M} - 1} \qquad [1]$$

$$\frac{1}{e^{C_2/\lambda T_{p2}} - 1} = K \frac{\epsilon(\lambda,T)}{e^{C_2/\lambda T_M} - 1} + \frac{K[1 - \epsilon(\lambda,T)]}{e^{C_2/\lambda T_s} e - 1}$$

$$\epsilon(\lambda,T) = 1 - \frac{1}{K}\left(\frac{1}{e^{C_2/\lambda T_{p2}} - 1} - \frac{1}{e^{C_2/\lambda T_{p1}} - 1}\right)(e^{C_2/\lambda T_s} e - 1)$$

$$T_M = \frac{\lambda}{C_2} \ln^{-1}\left[1 + K\epsilon(\lambda,T)(e^{C_2/\lambda T_{p1}} - 1)\right] \qquad [2]$$

The first equation relates the in-phase apparent temperature of the sample to the true sample temperature. The second equation relates the out-of-phase apparent temperature to the sample temperature and to the effective temperature of the arc source. The last term in this equation represents the reflected arc radiation received by the pyrometer.

An effective arc temperature must be used in the equation in place of the arc temperature, because the mirrors of the imaging furnace are not perfect reflectors and do not have perfect geometry. These imperfections reduce the spectral brightness of the arc image. For determination of the effective arc temperature, a plain mirror is placed about 2 in. in front of the focal zone, and the apparent temperature of the arc image is measured with an optical pyrometer provided with suitable filters. These equations can then be solved simultaneously to give a value of the spectral emissivity. The value of the emissivity is then used with the first equation so that a true temperature accurate to 5% is obtained. A comparable measuring procedure has been used to measure cathode temperatures in a cavity (18).

A modified optical pyrometer allows the measurement of temperatures automatically and provides a record of temperature variations occurring as fast as 1/100 of a second.

Flux Uniformity

The optical system used in an imaging furnace determines the spatial distribution of the radiant flux density. With the two-ellipsoidal-mirror system, a high flux density over a limited image size is obtained (Fig. 8). At times it may be desirable to enlarge the image area and, instead of a Gaussian distribution, to obtain a uniform distribution over a larger area. The usefulness of defocusing (19) depends to a large extent on the type of optical system; defocusing is usually accompanied by a decrease in uniformity even as the image size increases. Although optical systems to obtain larger images with a uniform distribution have been developed (20) low flux densities usually result. To meet the requirements for either a high temperature over a small area or a uniform flux distribution over a large area, a flux redistributor was developed. This flux redistributor (Fig. 10) can be placed in front of the focal plane of the imaging furnace; it provides a uniform distribution over a fairly large

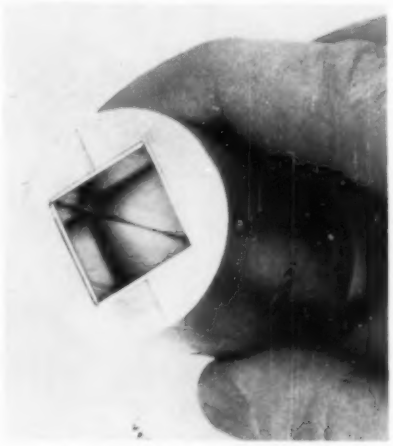

Fig. 10. Flux redistributor

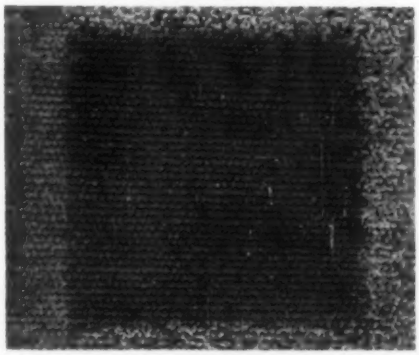

Fig. 11. Sample exposed with redistributor

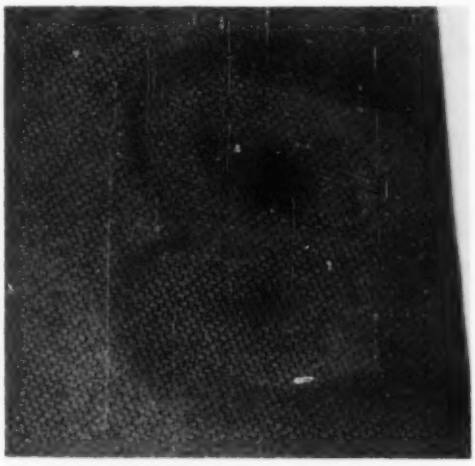

Fig. 12. Sample exposed without redistributor

image area. By using this instrument, we were able to concentrate 20 cal/cm²/sec over a ⅝-in. square area; Figure (11) shows the increased uniformity of burned patterns when the redistributor is used; Fig. 12 shows the pattern without the flux redistributor. This device intercepts the flux by means of four mirrors and redistributes it onto the sample plane in a uniformly illuminated area.

The effect of a nonuniformity in the energy beam is almost completely eliminated by the use of the flux redistributor. If U_m is the maximum nonuni-

formity expressed as a percentage of the flux distribution without a flux redistributor, then with the redistributor the nonuniformity is given by:

$$U < \frac{S_a}{100} U_m$$

where S_a is a shadow attenuation function depending on the ratio of length to inside dimension and on the reflectivity of the inside surfaces of the flux redistributor.

Conclusions

The use of imaging furnaces for the radiant heating of materials has been of considerable interest to many researchers. Because of the newness of the device, however, the lack of instrumentation, and the nonexistence of well-defined experimental procedures, its applications have not as yet been widespread. As more information accumulates, its advantages and drawbacks will become more fully appreciated and its usefulness demonstrated in a greater number of research projects. As is the case with many new research tools, it cannot be expected to solve all high-temperature-research problems; rather, it will be applicable to those research projects where the ingenuity of the experimenter and experimental requirements make it invaluable.

Acknowledgments

The author would like to thank the members of the staff of Arthur D. Little, Inc., and Strong Electric Company, Toledo, Ohio, for their interest, help, and cooperation in the design, instrumentation, and manufacture of the arc-imaging furnace. Particularly noteworthy were the designs worked out by F. Chellis, the development of the flux redistributor by M. Chen, and the temperature-measurement methods developed by H. Blau. C. Warner, A. Camus, and J. Lund made valuable contributions to the measurements of heat flux and helped make the ADL-Strong arc-imaging furnace a safe and dependable research tool.

Manuscript received July 22, 1959. This paper was prepared for delivery before the Philadelphia Meeting, May 3-7, 1959.

Any discussion of this paper will appear in a Discussion Section to be published in the December 1960 JOURNAL.

REFERENCES

1. Proceedings of the 1957 Solar Furnace Symposium, *J. Solar Energy, Science and Engineering*, **1**, April-July (1957).
2. P. E. Glaser, High Intensity Arc Symposium, p. 71, The Carborundum Co., Niagara Falls, N. Y. (1958).
3. W. Finkelnburg and J. P. Latil, *J. Opt. Soc. Am.*, **44**, 1 (1954).
4. W. M. Conn, *Am. Ceram. Soc. Bull.*, **33**, 69 (1954).
5. F. Trombe, *J. Solar Energy, Science and Engineering*, **1**, 9 (1957).
6. M. R. Null and W. W. Lozier, *Rev. Sci. Instr.*, **29**, 163 (1958).
7. J. Farber, Symposium on High Temperature, Stanford Research Institute, Menlo Park, Calif. p. 1 (1956).
8. M. R. Null and W. W. Lozier, To be published *J. of SMPTE*.
9. T. R. Broida, U. S. Naval Radiological Defense Laboratory Report, USNDRL-417 (1952).
10. N. K. Hiester, *et al.*, *Jet Propulsion*, **27**, 507 (1957).
11. F. Beck, D. R. Pat., 262913, March 1910.
12. E. Gretener, *J. of SMPTE*, **55**, 391 (1955).
13. G. A. Swope and F. C. Henriques, Report TOI 54-8, Technical Operations, Inc., Arlington, Mass. (1954).
14. C. E. Greider, U. S. Pat. 2,797,351, June 25, 1957.
15. P. E. Glaser, *Rev. Sci. Instr.*, **28**, 1084 (1957).
16. R. Gardon, *ibid.*, **24**, 366 (1953).
17. A. G. Emslie and H. H. Blau, *This Journal*, **106**, 877 (1959).
18. C. H. Prescott, "Temperature: Its Measurement and Control," p. 1199, Reinhold Publishing Co., New York (1941).
19. R. de La Rue, *J. Solar Energy, Science and Engineering*, **1**, 94 (1957).
20. R. Gardon, *Rev. Sci. Inst.*, **25**, 459 (1954).

Metal Mists and Aluminum Losses in the Hall Process

Warren E. Haupin

Alcoa Research Laboratories, New Kensington, Pennsylvania

ABSTRACT

Reaction of aluminum with Hall cell electrolyte forms aluminum monofluoride and sodium which dissolve in some form to give the bath a reducing capacity equivalent to a free aluminum content of about one tenth per cent. The so-called "metal mist" forms in the presence of moisture and consists of hydrogen bubbles containing a small partial pressure of aluminum monofluoride, sodium, and sodium tetrafluoroaluminate. Increasing the NaF/AlF_3 ratio of the electrolyte increases the sodium and decreases the aluminum monofluoride partial pressure, but sodium has a much higher partial pressure; hence, a low NaF/AlF_3 ratio is desirable to minimize metal reoxidation. Carbon dioxide is abundant in the anode gas of a smelting cell and is soluble in the bath. It oxidizes the free metal both in and over the bath. The rate of this reoxidation appears to be controlled by the rate of diffusion and convection of dissolved metal away from the metal-bath interface.

Almost any oxygen-containing gas, including water vapor, is reduced when it is bubbled through Hall bath (87% NaF-AlF_3 of various NaF/AlF_3 ratios, 8% CaF_2, 5% Al_2O_3) when the electrolyte is contacting aluminum, thereby indirectly oxidizing the aluminum. The mechanism of the aluminum reoxidation, the composition of the "mist" or "fog" that forms, and even the question of whether acid bath (excess AlF_3 over the cryolite composition) or alkaline bath (excess NaF) causes the greater metal loss have, however, been the subject of considerable controversy (1-16).

Various investigators have reported the fog to be sodium (4-9), aluminum (10-13), aluminum monofluoride (16), aluminum carbide (19), hydrogen (14,15), or some combination of these. The apparent composition of the fog was influenced by the method used to identify the fog. Investigators immersing copper strips in bath, held over aluminum, picked up aluminum in the copper, which has a high solubility for aluminum. They interpreted this as indicating the mist was aluminum. However, investigators similarly using lead, which has a high solubility for sodium, found that the lead picked up sodium.

Composition of Mist

A mist must be a separate phase, but bubbles of sodium vapor or aluminum monofluoride vapor were ruled out by thermodynamic considerations, for these vapors cannot exist at 1 atm pressure at the bath temperature in contact with molten cryolite. Thermodynamics did not rule out the presence of these gases at a much lower partial pressure, but this presupposed the presence of some other gas. There was also the possibility of a mist of finely divided aluminum suspended in the cryolite, and mechanisms for obtaining such suspensions have been postulated (12,13).

To start the present investigation, it was thought desirable to extend Grjotheim's investigation (14) of metals which form a mist in Hall baths. At 980°C in a graphite crucible, it was found that a mist formed when magnesium, aluminum, sodium, or zinc was added to the bath. Sodium and zinc caused a violent bubbling when added, but a foggy appearance remained for 15 to 30 min after the bath became still. The bath remained clear when tin, nickel, lead, copper, or silver was added. The metals that made a mist were all metals capable of displacing hydrogen from water. Since sodium and zinc were above their boiling points, it might be claimed that the mist was vapors of these metals. The other mist formers, however, were well below their boiling temperatures.

Operators of the Hoopes-type aluminum refining cells claimed that the bath in their cells did not form a mist. To investigate this and to observe the effect of lowering the sodium ion concentration of the bath, melts were prepared of the following compositions by weight:

Bath 1—30% BaF_2, 21.5% AlF_3, 37.5% Na_3AlF_6, 11% MgF_2
Bath 2—18% BaF_2, 21% AlF_3, 45% Na_3AlF_6, 16% CaF_2
Bath 3—26% AlF_3, 58% Na_3AlF_6, 16% CaF_2
Bath 4—100% Li_3AlF_6

These baths all formed a mist when aluminum was added. The most logical explanation for the bath in commercial refining cells being free from mist is that the bath had a layer of molten aluminum floating on its surface and was thereby protected from absorbing moisture.

Local cell action.—The loss of aluminum when held under fused salts in Pyrex was studied. No loss of metal was found in pure NaCl-KCl eutectic at 750°C. With the addition of 10% Na_3AlF_6 both chemical and electrochemical solution of aluminum occurred. Electrochemical solution was obtained by placing a graphite rod into the bath and contacting the aluminum. The rate of electrochemical solution was controlled by polarization of the carbon and took a carbon area approximately six times the metal area to obtain double the rate of chemical solution. A

tenfold increase in metal loss was obtained with a carbon area roughly 30 times the metal area.

Loss in inert crucibles.—To determine if mist formation in the Hall bath was the result of electrochemical action and rule out the carbide mist theory, neutral Hall bath and bath No. 3 were each melted in crucibles of sintered alumina, silicon nitride, and magnesite, respectively. These baths formed a mist upon the addition of aluminum, regardless of the crucible used.

To eliminate completely any crucible effect or local cell action, a pool of molten bath was melted in a pile of powdered Hall bath using radiant energy from an electric arc in argon between tungsten electrodes. The molten bath held in solid bath was clear. A 0.1 mg piece of aluminum was dropped in the pool. It moved about by convection currents and left a trail of mist reminding one of the tail of a comet. Eventually, the aluminum was consumed. When a 1 mg piece of aluminum was added, it rested on the bottom and a mist rose in streamers. A 1-g piece completely fogged in the bath. Since no carbon was present in the system, these tests ruled out the carbide mist theory. They also indicated that no electrolytic cell action was necessary for mist formation. Based on the foregoing evidence Grjotheim's conclusion was accepted: that a mist of hydrogen forms by the reaction between free metal and moisture that dissolves in the bath.

Howard (18) has shown that a vapor of sodium tetrafluoro aluminate ($NaAlF_4$) exists over molten cryolite. Therefore, one must conclude that the hydrogen bubbles will have a small partial pressure of $NaAlF_4$.

Formation of a Hydrogen Mist

While the tests just described gave indirect evidence of a mist of hydrogen, they did not prove that hydrogen was the only source of mist. Grjotheim (15) suggested that polynuclear metal ions may cause a foggy appearance. A more quantitative test was designed therefore to ascertain if hydrogen was the only source of fog or mist. Baths of the desired composition were mixed as dry powdered reagent grade chemicals and added to a crucible at the bottom of a sealed retort, as shown in Fig. 1. The bath was dried at 200°C for 12 hr, then melted and held at 980°C. Dry argon was flushed continuously through the retort at 100 cc/min. The retort had a replaceable copper sleeve extending from the top of the crucible to the top of the retort, a distance of 12 in. Metallic vapors condensed and partially alloyed with this sleeve. Some metal condensed also on and in the gas inlet and outlet tubes. The top of the retort was water cooled to protect the "O" ring seals and to cool the upper part of the copper sleeve. The escaping gases passed consecutively through an electrostatic precipitator to remove particulate matter, sodium fluoride pellets to remove HF, magnesium perchlorate to remove moisture, ascarite to remove CO_2, hot copper oxide to oxidize CO to CO_2 and hydrogen to water, magnesium perchlorate to absorb the oxidized hydrogen, and finally ascarite to remove CO_2 oxidized from CO. The absorption chambers

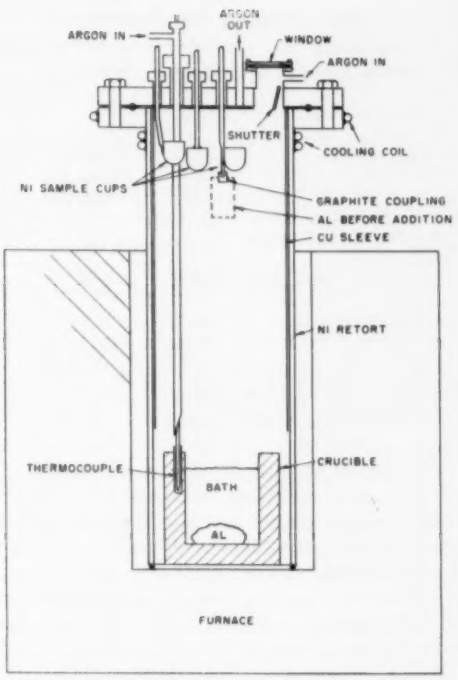

Fig. 1. Sealed system for metal mist tests

were weighed periodically during the test. Also, throughout the run, observations were made of the mist in the bath through a glass window equipped with a shutter and wiper operated through "O" ring seals. Bath samples were taken and metal addition made by control rods operated through "O" ring seals so that the system was never open to the atmosphere.

As soon as the bath became molten, bath sample No. 1 was taken. Then 100 g of aluminum were added to the remaining 750 g of molten bath. As soon as the metal melted, the bath became fogged and the surface was agitated by escaping gas bubbles. After ½ hr, the time of maximum hydrogen evolution determined by weight gain of the absorption bottle, bath sample No. 2 was taken. Since it was difficult to see clearly enough through the window to be sure of the complete absence of mist, duplicate runs were made of the first three tests. The retort was opened after 72 hr, at which time all measurable hydrogen evolution had stopped. The bath, at this time, was in each case found to be mist-free. The taking of bath sample No. 3, therefore, was set at 72 hr. Table I gives the results. The free metal in the frozen bath samples was determined by hydrogen evolution with HCl and is reported in equivalent per cent free aluminum. Both hydrogen and methane were frequently evolved. The methane, assumed to have come from Al_4C_3, represented 0-0.24% Al_4C_3 by weight in the bath. There was no correlation between the evolution of methane and the presence of mist or the NaF/AlF_3 ratio of the bath.

An attempt was made to analyze the frozen bath samples separately for metallic sodium and metallic aluminum by vacuum distillation and by mercury extraction. No free aluminum or sodium was found

Table I. Results of bath sample No. 3

Bath molten (length of time)	10 min	40 min	72 hr
Aluminum present under bath	No	Yes	Yes
Bath appearance	Clear	Fogged	Clear
H_2 evolution	None	0.2-0.25 ml/min	None
Reducing power of bath, as equivalent % free aluminum			
With 3.6%* AlF_3 in bath	0.00%	0.08%	0.09%
With neutral bath	0.00%	0.11	0.10
With 11.5%* NaF in bath	0.00%	0.12	0.11

* Initial composition, by weight.

Table II. Weight loss (in grams) of aluminum

Crucible	C	C	C	BN	SiC
NaF/AlF_3 wt ratio, start	1.34	1.50	1.86	1.50	1.50
NaF/AlF_3 wt ratio, end	1.14	1.34	1.31	1.43	ND[3]
Aluminum losses as					
Na condensate	3.1 g	5.5 g	10.0 g	0.2 g	ND[5]
Al condensate	0.8	0.6	0.4	0.5	ND[5]
Carbide	5.7	2.5	3.7	0	ND[4]
Into crucible	1.1	0.6	0.8	ND[2]	ND[2]
Oxidized by H_2O	0.5	0.4	0.4	1.3	1.6
Na+AlF dissolved in bath	0.6	0.7	0.8	ND[2]	ND[3]
Total Al loss	11.8	10.3	16.1	ND	ND
Weighed loss of Al[1]	11.1	11.3	16.9	5.1	15.9

ND—Not determined.
[1] Weight loss is not accurate because of difficulty in separating adhered bath from aluminum.
[2] Did not want to sacrifice expensive crucible.
[3] Previous data appeared sufficient.
[4] Difficult to obtain in carbide system.
[5] Cu condensing sleeve became detached during run.

by either method, but this was attributed to faulty technique. It is planned some time in the future to make a more detailed study of these techniques.

An apparent separation of the aluminum and sodium was obtained by hydrogen evolution, using first water and then a sodium hydroxide solution. The first evolution was assumed to represent metallic sodium, again correcting for any methane evolution. When all evolution stopped, sufficient NaOH was added to the water to make a 10% NaOH solution. The second evolution was assumed to represent aluminum. Hall bath with a NaF/AlF_3 weight ratio of 1.5 showed 0.16% Na and 0.05% Al by this technique, while bath with a NaF/AlF_3 ratio of 1.3 showed 0.10% Na and 0.05% Al. These results were not exactly consistent with Table I or with theory. Theory would lead one to expect a higher aluminum concentration in the second bath sample, for AlF in the molten bath should decompose to Al and AlF_3 in the frozen bath samples. It was feared that water was giving some evolution from the aluminum. Because of this, no great reliance is placed in this method of separately analyzing for Al and Na.

A mist or fog was present only when hydrogen was being evolved. No second type of mist suspected by Grjotheim was found. No hydrogen was evolved until aluminum was added. Upon addition of aluminum, free metal was found in the bath and a mist formed. After 72 hr, hydrogen evolution had stopped, but the bath still contained free metal. Later we shall see that the free metal in solution creates a vapor pressure of aluminum monofluoride and sodium over the bath. The metal loss through reaction with moisture apparently depended on how dry the bath and crucible were initially.

Metal Losses

Table II gives the weight loss in grams of the aluminum and shows the various ways in which this aluminum was lost. The aluminum loss into the crucible was determined by a chemical analysis of the crucible for calcium, sodium, aluminum, fluorine, and aluminum carbide, all corrected for a blank of the crucible before the test. The aluminum loss into the crucible was taken as the excess of metal ions over the fluoride ion on an equivalent basis. The total carbide figure included both the carbide on the crucible and adhering to the aluminum. The aluminum loss by reaction with moisture dissolved in the bath was determined by the hydrogen evolution from the system. The aluminum loss as a vapor escaping from the bath was determined by chemical analysis of the copper shield and gas inlet and exit tubes and the condensate adhering to them. Both free aluminum and sodium were found. Naturally, much of the sodium condensing did not alloy with the copper and burned when the retort was opened. Care was taken to minimize the loss of sodium oxide fumes and the sodium that burned was determined from the sodium oxide formed.

Aluminum and Sodium Vaporization

Perhaps the manner in which the sodium and aluminum condensate varied with bath ratio, shown in Table II, is even a more significant finding than the composition of the fog. Metallic sodium in the vapor over the bath probably is accounted for by the equilibrium:

$$\underset{\text{(lig)}}{Al} + \underset{\text{(bath)}}{Na_3AlF_6} \rightleftharpoons \underset{\text{(bath)}}{3Na} + \underset{\text{(bath)}}{2AlF_3}$$

$$\downarrow\uparrow$$

$$\underset{\text{(p in argon)}}{3Na}$$

The vapor pressure of aluminum is too low to account for the transfer of aluminum. The most plausible explanation for the aluminum transfer is that the aluminum was carried as aluminum monofluoride vapor through the following sequence of reactions:

$$\underset{\text{(lig)}}{2Al} + \underset{\text{(bath)}}{AlF_3} \rightleftharpoons \underset{\text{(bath)}}{3AlF} \rightleftharpoons$$

$$\underset{\text{(p in argon)}}{3AlF} \rightarrow \underset{\text{(Cu alloy)}}{2Al} + \underset{\text{(solid)}}{AlF_3}$$

To check this theory a ⅛ in. diameter copper rod was sealed in a graphite capsule 1 in. OD x 2 in. long with ⅜ in. thick walls. The air in the pores and cavity of the capsule was replaced with argon by placing the capsule in the chamber, evacuating, and then filling with argon. The capsule was then

floated on molten bath for 24 hr. After the test the capsule was broken open. No bath penetrated the capsule, but the surface of the copper rod was covered with a white powder that was found by x-ray diffraction to be AlF_3. The copper rod had assumed the color of yellow brass and qualitative spectrographic analysis showed it to have picked up between 1 and 10% aluminum. This was taken as evidence of a sizable vapor pressure of aluminum monofluoride over the bath.

In the foregoing reasoning it was assumed that aluminum monofluoride and sodium were soluble in some form in the bath, otherwise there appeared to be no mechanism for carrying free metal from the pool of aluminum under the bath to the surface of the bath to generate a vapor pressure of aluminum monofluoride, and sodium. However, the dissolved species need not be aluminum monofluoride and sodium. Either would suffice, or any other appropriate species such as Al, Al^+, Na_2^+, or any combination of these. Through their respective equilibriums with the bath, these constituents would create a vapor pressure of aluminum monofluoride and sodium over the bath and give the bath an activity of aluminum monofluoride and sodium so that it would reduce carbon dioxide or moisture.

Since the argon flow was the same in all the metal holding tests, the ratio of the weights of aluminum and sodium condensed should, on a mole basis, be proportional to the partial pressures of the aluminum monofluoride and sodium over the bath. Even though the partial pressure of AlF was increased by a low NaF/AlF_3 ratio, sodium still had a higher partial pressure over the bath than AlF and apparently a higher activity in the bath. This to a large extent explains why acid baths give higher current efficiencies than neutral or alkaline baths.

The steps in the reoxidation of aluminum appeared to be: (*a*) a reaction at the metal-bath interface to give a solution of free metal or its equivalent in the bath, (*b*) diffusion and convection of the free metal away from this interface, (*c*) reaction between the free metal from the bath and carbon dioxide from the anode. Reoxidization of free metal by moisture cannot account for more than about 0.6% loss in current efficiency for unburned gas from commercial cells averages less than 1% hydrogen by volume.

Nozaki and Miyanchi (12), investigating industrial cells that were suddenly disconnected due to war action, found that the free metal concentration in the electrolyte varied from none near the anodes to the maximum near the metal pad. Bath samples taken in the static metal holding tests showed the equivalent of about 0.1% free aluminum. A sample of similar electrolyte taken 3 in. from the side of an anode and 3 in. above the metal pad of an operating cell showed only the equivalent of 0.02% free aluminum or about one fifth of the equilibrium value. A similar sample of electrolyte was taken and CO_2 determined as present. It appears from the concentration and distribution of free metal that the slow step in the reoxidation of aluminum in commercial cells is the transport of free metal from the cathode to the vicinity of the anode. This is confirmed further by the observation that greater anode-cathode separation improves current efficiency.

Solubility of CO_2 in Bath

Förland and Associates (17) have reported solubility of CO_2 in molten cryolite. This was confirmed by taking a quickly frozen sample of electrolyte, as described previously, from an operating cell and a similar sample as a blank from the sealed system. Both were heated to approximately 500°C in a vacuum and the gas evolved analyzed by a mass spectrograph. The 10-g sample of the bath from the reduction pot evolved approximately 21 μg of carbon dioxide. The sample from the sealed system evolved two micrograms of carbon dioxide. This was taken as confirmation of Förland's findings.

The fact that both sodium and carbon dioxide were present in the sample of electrolyte from a commercial cell indicates a highly nonequilibrium condition exists within the electrolyte. Apparently there are strata of dispersed and dissolved carbon dioxide and dissolved free metal which are being mixed and reacting.

Numerous other gases also were evolved from the sample of the electrolyte from the reduction pot. They are listed in Table III.

Other Sources of Aluminum Loss

Another major source of aluminum loss in these tests was the formation of aluminum carbide. There was some indication (Table II) that the carbide formation was more severe in acid baths, but the trend was not very distinct. The loss of free metal, probably mostly sodium, penetrating into the crucible accounts for most of the remaining metal loss.

Use of Crucibles Other than Carbon

A test in a boron nitride crucible showed an abnormally small aluminum loss. When the cell was opened and the bath poured, however, the metal pad was covered with a dark film. The test made in a silicon carbide (SiN bonded) crucible showed practically the same metal loss as in a graphite crucible. If the principal cause of metal loss were an electrochemical cell reaction between the aluminum and the carbon, then it would appear that the metal loss would be lower both with the SiC and BN crucibles because of the lower electrical conductivity of the crucibles. The fact that the loss was practically the same in SiC as in the graphite crucible would lead one to believe that, at least under the conditions of these tests, the solution of aluminum was predominantly chemical rather than electrochemical. Previ-

Table III. Gases evolved from a rapidly frozen 10-g sample of electrolyte from a reduction pot when reheated to 500°C in vacuum

Carbon dioxide	21 micrograms
Nitrogen	5
Carbon monoxide	4
Hydrogen	1
Sulfur dioxide	1
Water	1
Silicon tetrafluoride	0.1
Carbon disulfide	0.1

ous tests in Pyrex, using fluorides diluted by chlorides, showed the metal loss was increased by electrolytic cell action. Perhaps in the present case, carbide formation on the graphite crucible inhibited local cell action, or it could be that straight chemical reaction was fast enough to maintain the equilibrium concentration in the bath. Carbon dioxide bubbling through the bath in a commercial cell certainly will remove the free metals from the bath at a much greater rate. Under these conditions cell action to form sodium may become a factor. In the present test, the lower metal loss in the boron nitride crucible appeared to be associated with the presence of a boride film over the surface of the aluminum.

Conclusions

Molten Hall bath in contact with molten aluminum develops a reducing capacity equivalent to about 0.1% free aluminum dissolved in the bath. The presence of sodium and aluminum monofluoride vapors over the bath indicates solution of free metal in some form in the bath. The visible mist, on the other hand, is hydrogen formed by reaction between moisture and free metal dissolved in the bath. Naturally the bubbles contain a small partial pressure of Na, AlF, and $NaAlF_4$. Aluminum monofluoride and sodium vapors are evolved even from a clear, mist-free bath. Increasing the NaF/AlF_3 ratio of the bath increases the sodium loss and decreases the aluminum monofluoride loss. The aluminum monofluoride loss, however, is small compared to the sodium loss even from an acid bath. In an operating reduction cell the free metal concentration in the bath does not reach its equilibrium value in the bulk of the bath but varies from a maximum near metal pad to a minimum near the anode. This indicates that the process of diffusion and convection of free metal in the bath is the rate-controlling step in the reoxidation of aluminum.

Manuscript received July 6, 1959.

Any discussion of this paper will appear in a Discussion Section to be published in the December 1960 JOURNAL.

REFERENCES

1. R. Lorenz, *Z. Elektrochem.*, **13**, 582 (1907).
2. P. P. Fedotieff and Iljensky, *Z. Anorg. Chem.*, **80**, 113 (1913).
3. W. Jander and H. Herrmann, *ibid.*, **239**, 65 (1938).
4. T. G. Pearson and J. Waddington, *Discussion Faraday Soc.*, **1**, 307 (1947).
5. R. Schadlinger, *Alluminio*, **22**, 691 (1953).
6. A. Vajna, *La Matallurgia*, **44**, 585 (1952).
7. A. Vajna, *Alluminio*, **19**, 541 (1950).
8. A. Vajna, *ibid.*, **20**, 29 (1951).
9. E. Grünert, *Z. Elektrochem.*, **48**, 393 (1942).
10. E. Pruvot, *Alluminio*, **22**, 699 (1953).
11. E. Pruvot, *ibid.*, **22**, 721 (1953).
12. H. Nozaki and K. Miyanchi, *J. Chem. Soc. Japan* (Ind. Chem. Sec.), **51**, 3 (1948).
13. E. Vuignier, *Bull Soc. Franc. Electriciens, II*, **13**, 56 (1952).
14. K. Grjotheim, *Alluminio*, **22**, 679 (1953).
15. K. Grjotheim, "Contribution to the Theory of Aluminum Electrolysis," Kg 1. Norske Videnskab, Slelskabs, Skrifter 1956, Nr 5.
16. T. G. Pearson, "Chemical Background of the Aluminum Industry," Roy. Inst. Chem. Lect. Mono. Repts. No. 3 (1955).
17. T. Förland, H. Stroegraues, and S. Urnes, *Alluminio*, **22**, 631 (1953).
18. E. H. Howard, *J. Am. Chem. Soc.*, **76**, 2041 (1954).
19. Unpublished Alcoa Reports.

Anodic Precipitation of Tracer Manganese as Dioxide

Edward A. Heintz[1] and L. B. Rogers

Department of Chemistry and Laboratory for Nuclear Science,
Massachusetts Institute of Technology, Cambridge, Massachusetts

ABSTRACT

Quantitative recovery of carrier-free $10^{-6}M$ manganese (II) is possible from weakly acidic solutions. The use of lead dioxide as either a nonisotopic carrier or a chemical displacing agent makes possible high recoveries from more acidic solutions.

Electrolytic procedures for the recovery of radioactive tracers offer the advantages of being easily adaptable to remote control operation as well as being quite selective. The present study aimed to define conditions under which carrier-free manganese could be deposited quantitatively as the dioxide. In addition, the use of lead dioxide as a carrier (1) was examined because it enabled better recoveries to be made from solutions too acidic to permit deposition of tracer manganese dioxide alone.

The choice of lead as a carrier was also based on the ready availability of conditions (2) and mechanism (3) for its anodic deposition. The ability of thallium (III) oxide to carry manganese was investigated only briefly and was found, as expected, to be less satisfactory.

[1] Metals Research Laboratories, Union Carbide Metals Co., Niagara Falls, N. Y.

Results

Anodic behavior of manganese alone.—The only depositable species in solution was manganese (II) either as a radioactive tracer alone, at an estimated concentration of $10^{-6}M$ in $1.0M$ potassium nitrate solutions, or with added nonradioactive manganese up to millimolar. Figure 1 shows that, as the pH was increased, complete deposition of carrier-free manganese dioxide ($10^{-6}M$) was first attained at pH 4.

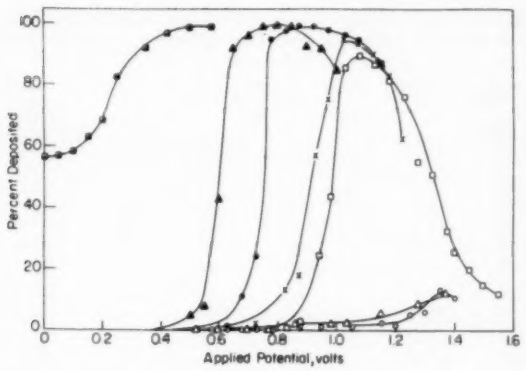

Fig. 1. Effect of initial pH on the deposition of trace manganese-52 from 1.0M potassium nitrate.

	Initial pH	Final pH
Open circle	1.00	1.00
Open triangle	2.10	1.92
Open Square	3.48	3.10
Large X	4.05	3.90
Solid circle	4.92	6.15
Solid triangle	6.02	7.05
Half & half square	9.05	9.00

The decrease found at more anodic potentials has been attributed to formation of a higher valence state having greater solubility (1).

In general, the manganese could be deposited, stripped, and redeposited at will by choosing the proper potential, thereby indicating that removal from solution was primarily an electrochemical process. However, the contribution of adsorption was evaluated by measuring at open circuit the decrease in activity of a tracer solution with time. At pH values less than 7.0, adsorption was negligible, i.e., less than 3% in 12 hr. At pH 9.0, however, virtually all of the activity was adsorbed within an hour. It was surprising to find most of the radiomanganese on the electrode.

From pH 3.5 to 6.0, the curves (at the 50% level) shifted at a rate of 155 mv/pH unit. If the reaction were

$$Mn^{++} + 2H_2O \rightarrow MnO_2 + 4H^+ + 2e \qquad [1]$$

this shift should be 120 mv at 25°C. The discrepancy may indicate that some deposited manganese was not in the tetravalent state. However, some of the discrepancy can be attributed to pH changes during a run. For example, a series of points were obtained using solutions carefully adjusted to pH 6.10 before electrolysis at each potential. These showed a spread of ±0.03 v at the level of 50% deposited whereas a comparable study at pH 4.00 showed less than ±0.01 v variation. It is interesting to note that the extent of deposition was usually in agreement with an earlier estimate (4) of 10^{-44} for the apparent solubility product of manganese dioxide.

At a given pH, one would expect the completeness of deposition to increase with the concentration of manganese. When more tracer was present, a larger percentage of manganese precipitated under a given set of conditions. Thus, 95% precipitated when three times the normal amount of tracer was used compared to 80% from the normal amount. In addition, the deposition curve proved to be the same as that for the normal amount of radiomanganese plus $10^{-6}M$ of inert manganese (II) nitrate. Decreasing the tracer to one-half the standard amount resulted in only 60% coprecipitation. Inspection of the above data showed that, regardless of the initial amount of tracer present, approximately the same amount of tracer remained in solution at the completion of the deposition. The average concentration of manganese in the tracer calculated from these data was $1 \times 10^{-6}M$, the same as estimated from activity data. Exact agreement was fortuitous but did indicate that contamination of the tracer with nonradioactive manganese was not serious.

Higher concentrations of manganese were examined by adding nonradioactive manganese. Figure 2 shows that near pH 2.0 complete deposition was attained at $10^{-4}M$ and higher. From the tracer alone a maximum of 10% was deposited. This curve served as a "blank" for later coprecipitation studies.

Coprecipitation of trace manganese with lead dioxide.—The pH region in which carrier-free manganese dioxide precipitated completely was sufficiently high to incur interferences from a number of other elements if attempts were made to apply the method to mixtures. For that reason, coprecipitation from more acidic media (1) was investigated further.

Factors which affect the coprecipitation of radiomanganese with lead are applied potential, pH, and the amount of carrier. The lower limit of potential was that at which lead deposited as its dioxide. This limit depended on the initial concentration of lead (II), shifting approximately 30 mv in a cathodic direction with each tenfold increase in concentration. The upper limit was the potential at which oxidation of manganese to a higher, more soluble valence became significant. Both the upper and lower limits were pH dependent, shifting approximately 120 mv in a cathodic direction with each tenfold increase in pH.

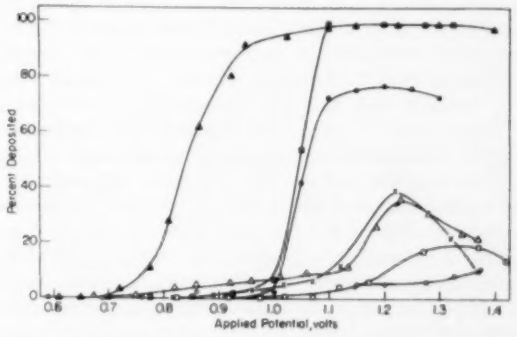

Fig. 2. Effect of total manganese concentration on the deposition of manganese from 1.0M potassium nitrate.

	Initial concentration of total manganese	Initial pH	Final pH
Open circle	Trace	2.10	1.92
Open square	1×10^{-3}M + trace	2.00	1.93
Open triangle	1×10^{-4}M + trace	2.04	1.95
Large X	1×10^{-5}M + trace	2.00	1.90
Solid circle	1×10^{-6}M + trace	2.07	1.95
Half & half square	1×10^{-4}M + trace	2.00	1.88
Solid triangle	2×10^{-3}M + trace	1.90	1.72

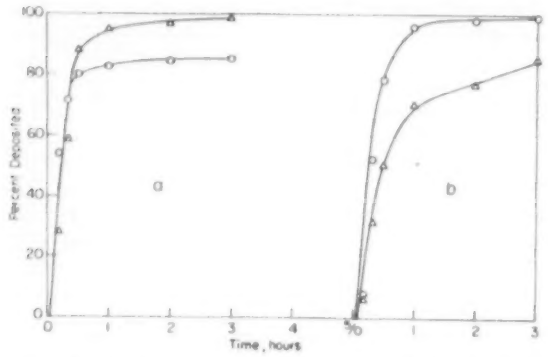

Fig. 3. Coprecipitation of manganese with 50 mg lead (II) carrier as a function of potential in 1.0M potassium nitrate at a pH of 2.0. (a) initial pH 2.00, final pH 1.85, E = +1.320 v vs. SCE; (b) initial pH 2.00, final pH 1.85, E = +1.275 v vs. SCE. Open circle, per cent manganese deposited, open triangle, per cent lead deposited.

Before starting studies of coprecipitation, depositions of lead or manganese alone were made at a number of different potentials using different initial concentrations. The relative rates later proved to be the same when both elements were deposited simultaneously.

Effect of applied potential and amount of carrier.—Figure 3 illustrates the effect of applied potential at a given pH. At the less anodic potential, lead deposited slower and gave a somewhat more adherent deposit. Use of a less anodic potential is analogous in an ordinary precipitation process to a slower rate of addition of reagent, a change which usually leads to larger and more nearly perfect crystals. However, the particles formed at both potentials were sufficiently large (greater than 1 μ) to give sharp lines on x-ray powder diffraction pictures.

At the less anodic potential, there was no reason for the potential to change the rate of deposition of the manganese because the potential was still sufficient to oxidize all of it to the tetravalent state. Hence, the net effect was greater coprecipitation for a given amount of lead. Table I shows that the effect was more striking for smaller amounts of carrier where the final fraction of manganese coprecipitated was usually smaller. The logarithmic distribution coefficient, λ, (5) was noticeably larger when the rate of deposition was slower although neither case gave a constant value during a run. For example, the values obtained for a run at +1.275 v decreased continuously from 6 to 2, whereas at +1.320 v they started at 2 and decreased to 0.3. The homogeneous distribution coefficient, D, (6) also changed during a run but it varied more than λ and in an apparently random fashion.

At potentials more anodic than +1.380 v, the efficiency of coprecipitation decreased markedly. At a potential of +1.425 v, lead was practically completely deposited at the end of 5 hr, while radiomanganese was only about one-third coprecipitated. For a similar deposition at +1.480 v only about 9% of the manganese coprecipitated. At these higher potentials, manganese was probably oxidized more or less to the more soluble heptavalent state in which form its tendency to coprecipitate should be smaller.

Table I. Effect of applied potential on the coprecipitation from 1.0M potassium nitrate of manganese-52 with lead dioxide after four hours

pH		Applied potential, v	Mg. lead present	Per cent lead deposited	Per cent manganese coprecipitated
Initial	Final				
1.00	1.00	+1.350	50	100	81
1.00	1.00	+1.320	50	70	96
2.00	1.85	+1.320	50	100	85
2.00	1.83	+1.275	50	85	98
1.00	0.98	+1.350	25	100	82
1.00	1.00	+1.320	25	44	95
2.03	1.92	+1.320	25	100	80
2.05	1.95	+1.275	25	76	96
1.05	1.05	+1.350	15	100	53
2.00	1.83	+1.350	15	100	69
0.98	0.98	+1.350	10	100	18
1.00	1.00	+1.320	10	50	74
2.08	1.90	+1.320	10	100	58
2.02	1.96	+1.275	10	78	94
1.03	1.00	+1.350	5	100	10
2.05	1.89	+1.350	5	100	24

In order to determine whether the manganese was firmly bound in the deposit or held on the surface, 50 mg of lead (II) at +1.350 v was completely deposited along with 84% of the radiomanganese. The potential was then raised to +1.480 v and the increase in the amount of manganese in the aqueous phase determined. After 4 hr, only 4% of the total manganese had returned to the solution. If the tracer had been distributed equally throughout the deposit, the 4% removed would have come from the top nine layers of lead dioxide. However, since the true area of the electrode was undoubtedly at least ten times the geometrical area, the tracer must have been stripped only from the surface.

Effect of electrode size.—A small gauze anode having a geometrical surface area of 13 cm^2 and a platinum wire anode having a geometrical surface area of 4 cm^2 were substituted, in turn, for the 79 cm^2 gauze electrode. Solutions of 1.0*M* potassium nitrate with 50 mg lead (II) plus the standard amount of radiomanganese were used after adjustment to a given pH.

At pH 1.0, a greater fraction of radiomanganese deposited than lead. This seemed reasonable because, although the rates of deposition, as measured by depletion of the solution, were considerably slower than observed for the large gauze electrode, the rate at which lead was depositing at the small electrode after the first few minutes was actually higher in terms of millimoles per square centimeter per minute than in the more depleted solution having the larger electrode. The result is comparable to that obtained by using more carrier, or to that in which lead deposition was slowed by a change in the electrolyte (*vide infra*).

At pH 2.0, the situation was reversed, and a greater fraction of lead deposited. A change in the rate of lead deposition was observed consistently between pH 1 and 2, but no satisfactory rationalization can be suggested for its existence. Irregular behavior has also been encountered under other conditions (4).

Table II. Removal at +1.350 v of manganese-52 by successive additions of lead (II)

(A) pH 2.0 Amount lead, mg	Per cent original Mn removed Observed	Calculated*	Amount lead, mg	Per cent original Mn removed Observed	Calculated
10	55	55	5	24	24
10	20	23	5	18	19
10	13	12	5	15	14
10	7	6	5	8	7
10	3	3	5	6	6
Total coprecip.	98	99		75	70
(B) pH 1.0					
10	18		5	11	
10	19		5	8	
10	20		5	10	
10	19		5	8	
Total coprecip.	76			37	

* Calculated on the basis of the first extraction factor being constant during the successive additions.

Table III. Effect of supporting electrolyte on the coprecipitation at +1.350 v of manganese-52 with 50 mg lead (II)

(A) pH 1.0 Supporting electrolyte	γ (9)	Relative % Pb deposited per minute	Relative % Mn coprecip. per minute	% Mn coprecip.
1.0 *M* $NaClO_4$	0.58	3.18	1.13	58
1.0 *M* $LiClO_4$	0.91	1.05	0.65	58
1.0 *M* KNO_3	0.45	1.05	0.89	80
1.0 *M* $NaNO_3$	0.55	0.53	0.53	95
1.0 *M* $LiNO_3$	0.76	0.43	0.38	85
5.0 *M* $NaClO_4$	—	3.80	1.00	26
4.0 *M* $NaClO_4$ plus 1.0 *M* $NaNO_3$	—	3.18	2.00	66
4.9 *M* $NaClO_4$ plus 0.1 *M* $NaNO_3$	—	3.80	1.00	23
(B) pH 2.0				
1.0 *M* $NaClO_4$	0.53	3.18	1.13	60
1.0 *M* $LiClO_4$	0.91	1.59	0.94	56
1.0 *M* KNO_3	0.45	1.59	0.92	84
1.0 *M* $NaNO_3$	0.55	1.59	1.15	94
1.0 *M* $LiNO_3$	0.76	1.05	1.00	90

Successive additions of carrier.—Large amounts of carrier required great care in handling to avoid mechanical losses from the electrode. To decrease the total, a series using small successive additions of carrier was explored as being analogous to cross-current extraction (7). Data for successive 5 and 10 mg additions given in Table II show that, at a pH of 2.0, an approximately constant extraction factor, *E*, was obtained. Remembering that the extraction factor is defined as the ratio of the amount deposited to the amount remaining in solution of a given level of carrier, the ratio for 10 mg additions was 1:1, while for 5 mg additions it was about 1:3.

In contrast, at a pH of 1.0, *E* varied with each addition of lead such that for each 10 mg addition of lead about 20% of the *initial* amount of trace was removed; for each 5 mg, about 10% of the *initial* amount of trace present. Gordon (8) has described a type of coprecipitation in which the amount of tracer carried per unit weight of carrier was independent of the amount of tracer present initially. He attributed this to phase saturation. To test this, successive 10 mg portions of lead were added to a solution containing three times the normal amount of tracer. In this case, each 10 mg portion carried 8%, 7% and 8% of the initial tracer present. On a weight basis, the amount of tracer coprecipitated with a given amount of carrier was the same as before. Although it seems unlikely, the lead dioxide formed at pH 1.0 behaved as though it were saturated with manganese dioxide.

Effect of supporting electrolyte.—Table III shows the effect of a change in electrolyte on the deposition rates of lead and manganese. In each case lead was completely deposited, although the time required depended on the supporting electrolyte. Perchlorate generally led to faster depositions of lead than did nitrate, possibly due to inhibition by lead nitrate complexes of the type $PbNO_3^+$ (10), perchlorate having less tendency to form such complexes (11). Nitrite, at a concentration of 0.01*M*, had no effect. For a given anion, it appears that the rate of lead deposition was related inversely to the hydrated cationic radii (12) which decrease on going from lithium to potassium.

In addition to increasing the relative rate of lead deposition, perchlorate media could affect adversely the amount of radiomanganese coprecipitated in another way, especially when very concentrated supporting electrolytes were used. Thermodynamically, the reaction

$$Mn^{++} + ClO_4^- + 2H^+ \rightarrow Mn^{+++} + ClO_3^- + 2H_2O \quad [2]$$

is spontaneous as written, as it has a negative change in free energy of some 20 kcal. This was tested by observing that in a millimolar solution of manganese (II), which was 1.0*M* in sodium perchlorate and at pH 2.0, a brown precipitate formed after two days without noticeable change in the pH. At the trace level, some manganese could react in this way during a run and thus form a radiocolloid that would not deposit on the anode. Such a result was actually observed: in 5.0*M* perchlorate, only 26% of the tracer coprecipitated; in a mixture of perchlorate and nitrate, only 66% of the tracer coprecipitated (compared with 85% in the absence of the perchlorate). Even the deposition of millimolar manganese at a pH of 1.0 from 1.0*M* sodium perchlorate was only 80% complete at a potential of +1.300 v, whereas from 1.0*M* potassium nitrate solution under identical conditions, deposition was more than 99% complete.

Open-circuit studies.—Byrne (4) noted that, when an electrode was disconnected from the potentiostat following an incomplete coprecipitation and was allowed to stand overnight in the solution, almost all of the radiomanganese was found on the electrode in the morning. This phenomenon was easily checked as shown by the data run in Table IV. A similar study at pH 2.0 gave results that were virtually identical. In both cases, the change in potential was similar to that observed by Wynne-Jones and coworkers (13) for pure lead dioxide.

Thermodynamically, the reaction

$$PbO_2 + Mn^{++} \rightarrow Pb^{++} + MnO_2 \quad [3]$$

Table IV. Changes in solution characteristics with time that occurred on disconnecting the external potential (+1.350 v) from an anode in 1.0M potassium nitrate solution at pH 1.0

Time, hr	Potential, v	Per cent Mn deposited	Per cent Pb deposited
0.0	1.350	80	99
0.5	1.325	—	—
1.0	1.305	84	96
2.0	1.293	86	95
5.0	1.273	87	94
10.0	1.255	98	88

has a negative change in free energy of about 2.4 kcal. Postprecipitation of radiomanganese onto the electrode is, therefore, spontaneous and is quite probably due to chemical replacement rather than to adsorption, although some contribution from the latter cannot be entirely discounted.

Farradini and Haissinsky (14) had reported that a trace of protactinium-233 was deposited spontaneously on a freshly prepared lead dioxide electrode but not on one that had been aged overnight in distilled water. The difference between a "fresh" and an "aged" lead dioxide electrode was attributed to a layer of oxygen dissolved in the crystal lattice or held on the surface of the "fresh" oxide. After such an electrode had been stored in distilled water for 12 hr, the oxygen had escaped presumably. A comparable study for manganese-52 was undertaken so as to rule out this possibility. Both platinum and lead dioxide electrodes were examined.

Several lead dioxide electrodes were prepared by anodizing platinum gauze electrodes at +1.350 v in a 1.0*M* potassium nitrate solution containing 50 mg of lead (II) at a *p*H of 1.0. Some electrodes were used immediately ("fresh"); others were stored in distilled water overnight ("aged"). Whether the oxide was "fresh" or "aged" made no difference: about 65% of the trace manganese deposited at open circuit in the first hour; another 25%, in the next hour. The deposits reached 98% after a total of 6 hr indicating that surface oxygen was unimportant.

To rule out the unlikely possibility that oxygen alone on the surface of bare platinum could cause radiomanganese to deposit, a platinum electrode was anodized in the absence of lead. It was then disconnected from the potentiostat and a standard amount of radiomanganese added. After 4 hr, only a little more than 1% of the manganese had deposited on the electrode. To complete the circle, it was shown that if lead dioxide were deposited completely from 1.0*M* potassium nitrate at pH 1.0 before adding manganese tracer, further electrolysis at +1.350 v deposited only 8% of the manganese. Clearly, when lead was not depositing, the applied potential strongly deterred the deposition of manganese.

Coprecipitation of trace manganese with thallium (III) oxide.—The carrying ability of thallium (III) oxide was investigated briefly. Thallium was chosen because it provided a different type of oxide with regard to structure and atomic ratio. Also, thallium could be determined easily with a polarograph and its anodic deposition behavior had been noted (15). Coprecipitations were expected to be much less efficient because it presented a change in valence type.

At a *p*H of 1.0, thallium (III) oxide would not deposit on an anode from a solution containing 50 mg of thallium (I) in 1.0*M* potassium nitrate although thallium was oxidized, as evidenced by the high current flow. However, using 50 mg thallium (I) at a *p*H of 2.0, about 90% of the thallium could be deposited, presumably at Tl_2O_3, before the remainder precipitated into the bulk of the solution and ruled out further study. Approximately 6% of the manganese coprecipitated with the thallium (III) oxide that adhered to the electrode. The deposition was rapid, only 20 min being required to deposit 90% of the thallium. Because the time was rather short, it was thought that the tracer might not have had sufficient time to incorporate itself in the crystal, so a smaller electrode of 13 cm^2 geometrical area was used. As in the case of lead, somewhat more tracer deposited, but not enough to make thallium a useful carrier for manganese.

Discussion and Conclusions

The isolation and simultaneous concentration of $10^{-9}M$ carrier-free manganese-52 by anodic electrodeposition as dioxide is quantitative above *p*H 4. The potential must be limited so as to avoid low recovery due to formation of a more soluble higher valence state. A lower *p*H would probably be necessary to decrease the interference from other elements if they were present. In that case, coprecipitation with lead dioxide could be used to effect complete recovery of the manganese. The later separation of manganese from lead could be done in a variety of ways including cathodic deposition of lead into mercury.

Chemical displacement of manganese (II) from aqueous solution by reaction with electrolytic lead dioxide was slower than electrolysis but always quantitative. The use of powdered lead dioxide should make the replacement faster, but it would necessitate a filtration. Other techniques leading to slower but more nearly complete recovery for a given amount of lead dioxide are the use of smaller electrodes and of successive additions of small portions of carrier.

The mechanism for anodic coprecipitation of manganese and lead dioxide appears to be either anomalous mixed-crystal formation or internal adsorption, processes which are difficult to distinguish (16). Although the dioxides of lead and manganese crystallize in the rhombic and tetragonal systems, respectively, anomalous mixed-crystals might form. However, the fact that the logarithmic distribution constant, λ, did not have a constant value indicates internal adsorption to be the more probable mechanism.

Experimental

Chemicals.—Solutions of carrier-free six-day manganese-52 were prepared by dissolving deuteron-bombarded chromium in 10*M* sulfuric acid and distilling permanganic acid (17). Calculations from radioactivity data indicated that these solutions were about $10^{-9}M$ in manganese-52. Evidence has been cited to show that the concentration of total manganese was in the same range. Before use, all manganese-52 stock solutions were precathodized for 2

hr at a potential which insured that all of the tracer was in the divalent state. Other stock solutions, all of them nitrates, were a 0.0103*M* solution of manganese (II) standardized by the bismuthate method (18); a 50 mg/ml solution of lead (II) standardized as the sulfate (19); and a 50 mg/ml solution of thallium (I), standardized against bromate (20).

Apparatus.—Depositions were carried out using a volume of 150 ml in a glass cell 5 cm in diameter and 12.5 cm tall. A platinum gauze anode with a geometrical area of 79 cm^2 was used except in one set of experiments where a 13 cm^2 gauze and a platinum spiral with a geometrical area of 4 cm^2 were substituted. Electrodes were pre-anodized in 1.0*M* sulfuric acid. Nitrate or perchlorate salt bridges were used to connect the saturated calomel reference electrode and the isolated platinum cathode to the electrolytic solution. The solution was stirred by a magnetized Teflon-covered stirring bar. The temperature, unless otherwise specified, was maintained at 25.5° ±0.5°C.

The potential of the anode was controlled to at least ±2 mv using potentiostats (21). The potentials were adjusted at the beginning of each run and checked at intervals thereafter using a Rubicon potentiometer reading to ±0.1 mv. All pH measurements were made with a Beckman Model G pH meter.

A single-channel differential discriminator, coupled through a linear amplifier to a thallium-activated sodium iodide scintillator was used to obtain the gamma-ray spectrum in the characterization of the manganese-52 in the radiochemical studies. The same scintillator-amplifier combination coupled to a binary scaler was used to count samples withdrawn from the deposition cells.

Procedures

Electrolytic.—A typical electrolytic solution was prepared by adding 145 ml of a chosen supporting electrolyte to the deposition cell along with a predetermined volume of carrier solution, usually 0.1 to 1.0 ml from a Kirk micro-pipet. A standard volume of radiomanganese, from 1.0 to 4.0 ml, was then added so as to produce about 10,000 cpm above the average background of 250 cpm. Equilibrium was reached after 1 hr at a given potential whereupon a 500 μl sample was withdrawn for analysis and the potential adjusted for the next electrolysis. To define a curve for per cent deposited vs. potential, the potential was changed anodically in successive 50 mv increments. After reaching the desired limiting potential, the direction of change was reversed until all the deposit had been stripped off the electrode. This procedure tested both reproducibility and reversibility of the system.

Analytical.—The 500 μl sample was placed in a one-dram glass vial and counted for at least 1 min or until 10,000 counts above background had registered in order to minimize the counting error (22). In calculating the amount of tracer or carrier deposited at any given time, corrections were made for the amount of solution previously withdrawn and, in the case of the radiochemical measurements, for the background and the natural decay of the radionuclide.

Manganese was analyzed by the periodate method (23) when present in macro amounts (i.e., 10^{-4} to $10^{-3}M$). Lead and thallium were determined by conventional polarographic procedures (24, 25).

Acknowledgment

The authors are indebted to Dr. Charles F. Morrison, Jr., for assembling and calibrating the counting equipment used in this study and to Dr. A. D. Pearson for x-ray diffraction pictures of deposits.

This work was supported in part by the United States Atomic Energy Commission under Contract AT(30-1)-905.

Manuscript received Aug. 28, 1958.

Any discussion of this paper will appear in a Discussion Section to be published in the December 1960 JOURNAL.

REFERENCES

1. J. T. Byrne and L. B. Rogers, *This Journal*, **103**, 442 (1956).
2. W. T. Schrenk and P. H. Delano, *Ind. Eng. Chem., Anal. Ed.*, **3**, 27 (1931).
3. M. L. Nichols, *ibid.*, **3**, 385 (1931).
4. J. T. Byrne, Ph.D. Thesis, Mass. Institute of Technology, 1951.
5. H. Doerner and W. Hoskins, *J. Am. Chem. Soc.*, **47**, 662 (1925).
6. L. Henderson and J. Kracek, *ibid.*, **49**, 738 (1927).
7. L. Alders, "Liquid-Liquid Extraction," pp. 64-86, Elsevier Publishing Co., Houston, Texas (1955).
8. L. Gordon, J. I. Peterson, and B. P. Burtt, *Anal. Chem.*, **27**, 1770 (1955).
9. W. M. Latimer, "Oxidation Potentials," 2nd Ed., p. 349, Prentice-Hall, Inc., New York (1952).
10. H. M. Hershenson, M. E. Smith, and D. N. Hume, *J. Am. Chem. Soc.*, **75**, 507 (1953).
11. H. Remy, "Treatise on Inorganic Chemistry," Vol. I., p. 809, Elsvier Publishing Co., Houston, Texas (1956).
12. E. W. Washburn, *J. Am. Chem. Soc.*, **31**, 322 (1909).
13. W. Beck, P. Jones, and W. F. K. Wynne-Jones, *Trans. Faraday Soc.*, **50**, 1249 (1954).
14. C. Ferrandini and M. Haissinsky, *J. Chim, Physique*, **1956**, 722.
15. P. Delahay and G. L. Stiehl, *J. Am. Chem. Soc.*, **73**, 1755 (1951).
16. O. Hahn, "Applied Radiochemistry," Chapters 4 and 5, Cornell University Press, Ithaca, N. Y. (1936).
17. J. D. H. Strickland and G. Spicer, *Anal. Chim. Acta*, **3**, 543 (1949).
18. I. M. Kolthoff and E. B. Sandell, "Textbook of Quantitative Inorganic Analysis," 3rd Ed., p. 677, Macmillan Co., New York (1952).
19. *Ibid.*, p. 669.
20. *Ibid.*, p. 606.
21. R. W. Lamphere and L. B. Rogers, *Anal. Chem.*, **22**, 463 (1950).
22. R. J. Rainwater and C. S. Wu, *Nucleonics*, **1**, No. 2, 60 (1947).
23. N. H. Furman, Editor, "Scott's Standard Methods of Chemical Analysis," 5th Ed., p. 573, D. van Nostrand, Inc., New York (1939).
24. I. M. Kolthoff and J. J. Lingane, "Polarography," 2nd Ed., p. 528, Interscience Publishers Inc., New York (1952).
25. *Ibid.*, p. 520.

Mass Transfer and Current Distribution under Free Convection Conditions

Kameo Asada, Fumio Hine, Shiro Yoshizawa, and Shinzo Okada

Department of Industrial Chemistry, Faculty of Engineering, Kyoto University, Kyoto, Japan

ABSTRACT

Correlation of mass transfer with current distribution, for deposition and dissolution of metals, on vertical electrodes, under free convection conditions, is discussed. The equation of mass transfer and the Laplace equation, determining the concentration and potential distributions, respectively, are solved simultaneously. The results explain most features of observed current distributions.

This paper is concerned with current distribution for deposition and dissolution of metals at vertical electrodes. The rate of metal deposition may be controlled mainly or partly by the rate of transfer of ions to the cathode. In the absence of agitation, ions are usually transferred by free convection, a process which has received much theoretical and experimental investigation (1-14). Owing to depletion of reactive ions, the density of the cathodic region becomes lower than that of the bulk of the solution; an upward flow of solution then results. (Circumstances at the anodic region are just reversed.) A diffusion layer formed around a body is generally thicker with increasing distance from the frontal edge of the body. Hence, under limiting current conditions the current density (or the reciprocal of the thickness of the diffusion layer) is inversely proportional to the *fourth* root of the distance from the bottom of the cathode, as confirmed by Wagner (3), Ibl (8), and Wilke (11).

Even at current densities below limiting ones, the same type of current distribution would be expected, if the interface concentration of the reactive species remains uniform. Such uniformity of the interface concentration is, however, not always the case, as discussed by Ibl (5, 10) and Wagner (13). In the case of rectangular cell with vertical electrodes on opposite ends, a reduction of the electrolytic current is accompanied by more uniform current distributions, because of the predominance of ohmic drop and chemical polarization over concentration polarization. Under such circumstances the thickness of the diffusion layer tends to be proportional to the *fifth* root of the distance from the bottom; this suggests that the mass transfer process is not exclusively dependent on hydrodynamic conditions.

This paper describes a theoretical approach to the intermediate domain between the extreme cases: uniform interface concentration and uniform current density. This requires simultaneous consideration of mass transfer and current distribution. These two problems have so far been studied rather separately. Effects of mass transfer on polarization characteristics were interpreted by using the thickness of the diffusion layer calculated from the limiting current, e.g. (14); this is not rigorous unless the polarization is uniform and of the nature of concentration polarization (13). On the other hand, it has been accepted that predominance of polarization over ohmic drop improves current distributions, e.g. (15). But this conclusion is based on the tacit assumption that the relationship between current density and polarization is the same for every point on the electrode. Such a condition applies to chemical polarization but is not always realized when mass transfer plays a part in polarization. It follows from these discussions, that mass transfer, electrode kinetics, and electrical resistance of baths and electrode materials are united through transfer of electric charge or current distribution.

An integration of mass transfer with the other two factors has been treated in related fields of science. Modern theories of polarography have systematically correlated electrode kinetics to diffusion (16); in addition the effect of ohmic drop on polarographic waves has been described (17). Heat transfer from a two-dimensional solid wall to a moving fluid has been analyzed (18). Levich (19) and the present authors (20) discussed current distributions over a flat plate electrode in a longitudinal flow under the condition of uniform polarization. This problem is mathematically identical to simple mass transfer processes such as the dissolution of nonelectrolytes studied by several authors (21-23). Weaver and Parry (24) estimated current distributions at a streaming mercury electrode under nonuniform polarization, by assuming that, in this case, resistance of solution is localized to the vicinity of the electrode surface.

Theoretical

The model to be treated is a cell of rectangular vertical section with vertical electrodes full-end on opposite sides. The x-axis is chosen as the cathode surface and x measures the vertical distance from the bottom of the cell. The y-axis is the bottom of the cell and y measures the horizontal distance from the cathode toward the anode.[1] The height and breadth of the cell are denoted by h, and b, respec-

[1] A glossary of symbols will be found at the end of the paper.

tively. The cathode ($y = 0$) and anode ($y = b$) are distinguished by subscripts c and a, respectively.

Distribution of concentration C is determined by a differential equation of mass transfer. The distribution of potential follows the Laplace equation

$$\partial^2\phi/\partial x^2 + \partial^2\phi/\partial y^2 = 0 \qquad [1]$$

Equation [1] is valid if there is an excess of indifferent electrolyte in the bath so that diffusion potential gradients are negligible in comparison with ohmic ones and the conductivity κ is uniform. The boundary conditions are common to both electrode surfaces and are expressed by

$$\begin{aligned} i &= i_c\left|(^\circ C/{}^*C)\exp\left[-\alpha n\mathbf{F}(E-E_c)/RT\right]\right. \\ &\quad \left. - \exp\left[(1-\alpha)\,n\mathbf{F}\,(E-E_c)/RT\right]\right| \\ &= n\mathbf{F}D\left|{}^*C - {}^\circ C\right|/\delta \\ &= \kappa\,(\partial\phi/\partial y) \qquad \text{at } y = 0 \text{ and } y = b \end{aligned} \qquad [2]$$

In Eq. [2], i is the local current density, i_c the exchange current density, α the transfer coefficient, n the number of Faradays per gram-ion reacting, $\mathbf{F}$ the Faraday, E the local electrode potential, E_c the equilibrium electrode potential, R the molal gas content, T the absolute temperature, °C and *C the concentration of the reactive species at the electrode surface and in the bulk, respectively, D the diffusion coefficient of the reactive species, and δ the differential thickness of the diffusion layer. Although not necessary for the problem, it is convenient to assume that the same kinetics operate at the cathode and anode; in other words, common values of E_c, n, i_c, and α are assigned to both electrodes. This problem was solved by means of successive approximation.

If distribution of i is given, the equation of mass transfer may be solved approximately and one obtains

$$\delta^5 = n\mathbf{F}Dki^{-2}\int_0^x i\,dx \qquad [3]$$

where k is a constant specific to the system. The derivation of Eq. [3] and an evaluation of k is described in the following section. When the anode is concerned, x should be replaced by $h - x$ in Eq. [3].

On the other hand, Eq. [1] was solved by expansion into a Fourier series. The origin of the potential ϕ was chosen to satisfy

$$\begin{aligned} \phi_{y=0} \equiv \phi_c &= -(E_c - E_c) \\ \phi_{y=b} \equiv \phi_a &= V - (E_a - E_c) \end{aligned} \qquad [4]$$

V being the terminal voltage (constant along any current flux). Equation [4] is self-consistent, if the potential drop within electrode material is negligible and if the equilibrium emf of the cell is zero. Equation [1], the last member of Eq. [2], and the additional boundary condition at the bottom and top of the electrolyte

$$\partial\phi/\partial x = 0 \quad \text{at } x = 0 \text{ and } x = h \qquad [5]$$

are satisfied by

$$\begin{aligned} \phi = \bar{\phi}_c + \bar{i}y/\kappa \\ - (2/\kappa h)\sum_{s=1}^{\infty}\{\cos(s\pi x/h)\,[\sinh(s\pi b/h)]^{-1} \\ \cdot[\cosh(s\pi[b-y]/h)\int_0^x I_c\sin(s\pi x/h)\,dx \\ - \cosh(s\pi y/h)\int_0^x I_a\sin(s\pi x/h)\,dx]\} \end{aligned} \qquad [6]$$

where I_a, I_c are defined by

$$I_j = \int_0^x (i_j - \bar{i})\,dx \text{ (for } j = a, c) \qquad [6']$$

and where $\bar{\phi}_c$ is the mean cathode potential and $\bar{i}$ the mean current density.

A cycle of successive approximation is composed of: (i) specification of $\bar{\phi}_c$ as the given condition (instead of V), (ii) assumption of i_c and i_a, followed by calculation of $\bar{i}$, (iii) evaluation of ϕ_c and ϕ_a by means of Eq. [6], (iv) determination of i_c consistent with ϕ_c through Eqs. [2]-[4], and (v) simultaneous determination of i_a and V consistent with ϕ_a through Eqs. [2]-[4] and satisfying the condition: $\bar{i}_a = \bar{i}_c$. As the integration of i and the calculation of the resulting Fourier coefficients were done repeatedly, i_c and i_a were approximated by definite numbers of exponential and polynominal terms of (x/h), respectively. This led to no serious error except in the neighborhood of the lower edge of the cathode, where $|\partial i/\partial x|$ is very large. Such an analysis could be extended to more complicated geometry, if a prior application of conformal mapping is possible.

Thickness of Diffusion Layer

One of the special features of ionic mass transfer processes by free convection as compared with the corresponding heat transfer processes and those by forced convection is the behavior of species indifferent to electrode reactions. Those species contribute to the density difference to an extent nearly as large as the reactive ones; in this respect analysis by Wagner (3) appeared to be rigorous, and his treatment was followed. Cathodic deposition of copper from $CuSO_4 - H_2SO_4$ baths was taken as an example, with the same coordinates as in the preceding section. Wagner's analysis was modified in the following three ways. (*A*) The interface concentration °*C* was regarded as a variable with x instead of a constant. (*B*) Since the velocity profile used by Wagner gives values of the limiting current which are too high, the profile of Wilke (12) was employed,[2] and the thicknesses of the hydrodynamic boundary layer and the diffusion layers of all species present were assumed equal and denoted by δ'. (*C*) In order to take migration of H^+ into account Wagner differentiated the thickness of the H^+ diffusion layer from that of Cu^{++}. In the present paper, the concentration profile of Cu^{++} will be given by

$$(C - {}^\circ C)/({}^*C - {}^\circ C) = 2y/\delta' - 2(y/\delta')^3 + (y/\delta')^4 \qquad [7]$$

and a parameter ϵ will be introduced in the profile of H^+, *i.e.*, the latter profile will be given by a power series in y/δ' with the coefficients of the first, second, third and fourth power terms taken as $(2 + \epsilon/3)$, $-\epsilon$, $-(2 - \epsilon)$ and $(1 - \epsilon/3)$, respectively.

[2] Although the observation of boundary layers (uniform current density) by Ibl (10), published during the present study, is in favor of the former profile, discussion of the profile itself is outside the limits of this paper.

This gives a differential equation:

$$(1/8k) \cdot d\,[\delta'^{3}\,(^{*}C - {}^{\circ}C)^{2}]/dx = 2(^{*}C - {}^{\circ}C)/\delta' = i/n\mathbf{F}D$$

where

$$k = 126\,(\nu D/g)/[9\beta_1 - \beta_2\,(18 - \epsilon)/(6 + \epsilon)]$$

$$\epsilon = -(90\,t - 30)/(15\,t + 2) \qquad [8]$$

In Eq. [8], ν is the kinematic viscosity, g the acceleration of gravity, t the transference number of H^+, β_1 and β_2 the density coefficients (*i.e.*, the relative increase in density caused by unit increase in the concentrations of $CuSO_4$ and H_2SO_4, respectively), and °C, *C and D refer to Cu^{++}. Equation [8] was solved for the following three cases, with the boundary condition for δ':

$$\delta' = 0, \text{ at } x = 0 \qquad [9]$$

(i) Provided the *interface concentration °C is independent of* x, the differential thickness of the diffusion layer δ and the limiting current density i_d are expressed by

$$\delta^{3} = 4kx/3(^{*}C - {}^{\circ}C)$$

and

$$i_d = n\mathbf{F}D\,{}^{*}C(3\,{}^{*}C/4kx)^{1/3} \qquad [10]$$

respectively. Equation [10] is different from those presented by other authors (1-4, 12) only in the detail of the constant k and gives estimates of limiting currents in accordance with those observed by Wilke (11).

(ii) If the *functional dependence of* i *on* x *is known*, Eq. [8] leads to Eq. [3]. In the special case of uniform current density, it follows from Eq. [3] that

$$\delta^{3} = n\mathbf{F}Dkx/\bar{i} \qquad [11]$$

which is similar to those presented by Sparrow and others (10, 13, 25).

(iii) When the *electrode potential* E *is uniform over the electrode*, one obtains from Eqs. [2], [7], and [8]

$$d\xi/d\mu = \mu^{4}\,(3\mu + 5)/(\mu + 1)^{3}$$

where

$$\mu = k_f\delta'/2D,$$

$$\xi = k \cdot k_f^{\,5}\,x/{}^{*}C\,D^{4}\,(k_f - k_b),$$

$$k_f = (i_e/n\mathbf{F}\,{}^{*}C)\,\exp[-\alpha n\mathbf{F}(E - E_e)/RT]$$

$$k_b = (i_e/n\mathbf{F}\,{}^{*}C)\,\exp[(1 - \alpha)n\mathbf{F}(E - E_e)/RT] \qquad [12]$$

which is solved as

$$\xi = \frac{3}{4}\mu^{4} - \frac{1}{3}\mu^{3} - \frac{1}{2}\mu^{2} + 3\mu - 5\ln(1 + \mu) + 2\mu/(1 + \mu). \qquad [13]$$

At $\xi = 0$ and $\xi \to \infty$ Eq. [13] reduces to Eqs. [11] and [10], respectively. Current distributions calculated from Eq. [13] were used as the first approximation for the procedure described in the preceding section.

Experimental and Results

A methacrylate cell (5 cm width, 32 cm breadth and 15 cm depth ID) was filled with solution up to a level $x = 10$ cm from the bottom, and immersed in a bath controlled at 25°C. Copper electrodes (0.1 mm in thickness) were covered with polyvinyl chloride paint except for the electrode surfaces, which were 5 cm in width and 10 cm in depth. The cathode was placed in contact with one of the end walls. The anode was supported by grooves cut into the sides and bottom of the cell, at different distances y from the cathode. Local current densities were measured by weighing what deposited or dissolved. Since introduction of a Luggin capillary might disturb hydrodynamic conditions, local electrode potentials were measured in the following way: five holes (1 mm in diameter) were drilled on one of the side walls at different depths for each electrode position, and each hole was connected with rubber tubing to a glass vessel in which a saturated calomel electrode was inserted in turn.

As noted by Ibl (8), excess of indifferent electrolytes retards the establishment of diffusion layers typical for free convection, while shortage of indifferent electrolytes may invalidate the assumptions on which the theory is based. From these considerations a system, $0.1M$ $CuSO_4 - 1.5M$ H_2SO_4, was chosen. For this system theoretical and experimental values of current densities and electrode potentials were obtained. Typical results are represented in Fig. 1-4. The following physical properties are used in the calculation: $\kappa = 0.543$ mho/cm, $D = 5.99 \times 10^{-6}$ cm²/sec, $\nu = 1.15 \times 10^{-2}$ cm²/sec, $\beta_1 = 120.6$ cm³/mole, $\beta_2 = 53.5$ cm³/mole, and $t = 0.81$ (26-28, and International Critical Tables); kinetic data were estimated at $i_e = 10^{-1}$ ma/cm² and $\alpha = 0.5$ (20).

Figures 1 and 2 refer to the case of infinite distance between electrodes ($b = \infty$ in Fig. 1, calculated, and $b = 32$ cm in Fig. 2, experimental). Cathodic current distributions shift from an inverse fourth root dependence on x (Eq. [10]) to a virtually uniform shape, with decreasing mean current density. As already mentioned, this is attributable to the competition of concentration polarization with chemical polarization and the resistance of the bath.

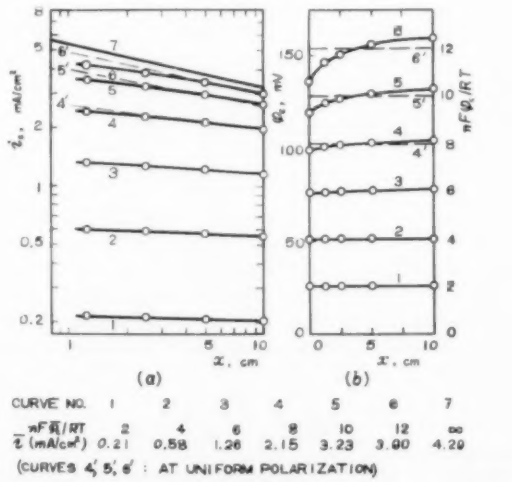
i_d, mA/cm²
φ_e, mV
$nF\varphi_e/RT$
x, cm
x, cm
(a)
(b)
CURVE NO. 1 2 3 4 5 6 7
$-nF\bar{\varphi}_e/RT$ 2 4 6 8 10 12 ∞
$\bar{i}$ (mA/cm²) 0.21 0.58 1.26 2.15 3.23 3.90 4.29
(CURVES 4', 5', 6' : AT UNIFORM POLARIZATION)

Fig. 1. Calculated distributions of (a) cathodic current density and (b) cathode potential, for b = ∞; x is the vertical distance from the bottom.

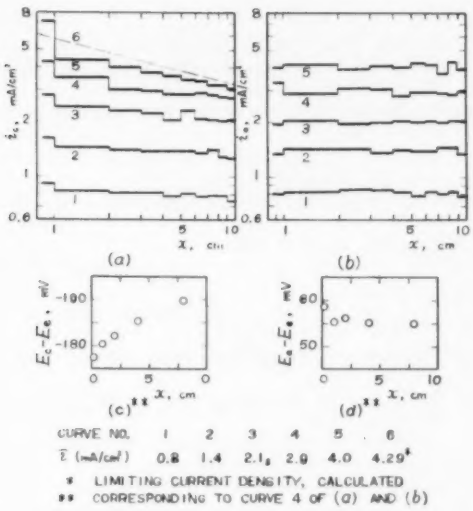
(a)
(b)
(c)
(d)
x, cm
CURVE NO. 1 2 3 4 5 6
$\bar{i}$ (mA/cm²) 0.8 1.4 2.1* 2.9 4.0 4.29*
* LIMITING CURRENT DENSITY, CALCULATED
** CORRESPONDING TO CURVE 4 OF (a) AND (b)

Fig. 2. Observed distributions of (a) cathodic current density, (b) anodic current density, (c) cathode potential, and (d) anode potential, for b = 32 cm.

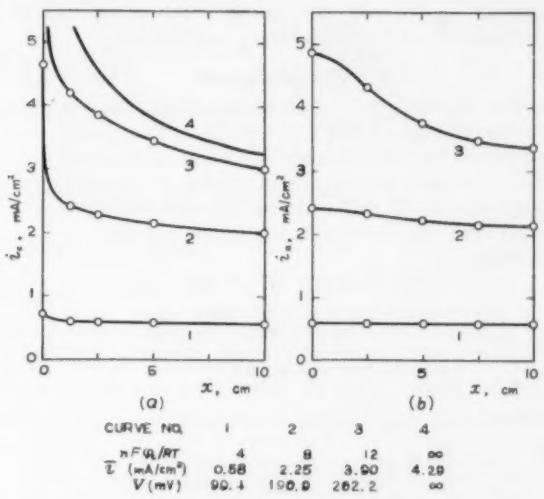

Fig. 3. Calculated distributions of (a) cathodic current density and (b) anodic current density, for b = 2 cm.

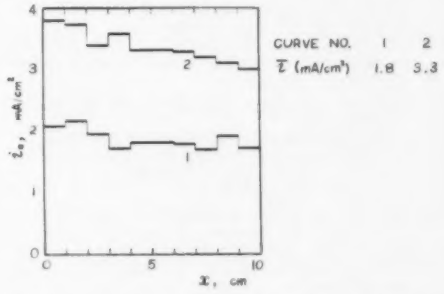

Fig. 4. Observed anodic current distributions, for b = 2 cm

The effect of the first two factors is seen separately in the dashed curves of Fig. 1, representing the case of uniform polarization [refer to (iii) of the preceding section]. The last factor results in much more uniform current distributions and nonuniform electrode potentials [see Fig. 1 (b) and Fig. 2 (c)].[3] Relatively low polarization around the lower portion of the cathode in association with relatively high current density shows plainly the peculiar effect of mass transfer on current distributions. This situation was observed also by Ibl (5). On the other hand, anodic current densities and potentials are virtually uniform (see Fig. 2), because anodic polarization is almost exclusively a chemical one as expected from Eq. [2].

Figures 3 and 4 refer to the case of finite distance between electrodes ($b = 2$ cm). The mutual influence of the cathode and the anode, whose current distributions were originally nonuniform and uniform, respectively, would cause better uniformity of current distribution at the cathode and worse uniformity at the anode. Distributions of cathodic current densities and potentials were, however, practically unaltered from the previous case ($b = \infty$) while marked change results at the anode; current densities at the anode, like those at the cathode, now become relatively high at near the bottom. This may be understood from the difference in polarization characteristics. Owing to the inclusion of concentration polarization, the slope $|\partial E/\partial i|$ of cathodic polarization curves is larger than that of anodic ones at the same current density. The larger the slope and the conductivity of the bath, the stronger is the buffering action against change in current densities (15).

Extension to Practical Conditions

The above discussions are concerned exclusively with 0.1*M* $CuSO_4$ — 1.5*M* H_2SO_4 solution at 25°C. In this system the effect of mass transfer on current distributions was remarkable, because the conductivity is high for the concentration of reacting ions. On the other hand, typical working conditions in industry are as follows: for electroplating, 0.8*M* $CuSO_4$ — 0.5*M* H_2SO_4, 20-30°C and 5-15 ma/cm²; for electrorefining, 0.6*M* $CuSO_4$ — 1.5*M* H_2SO_4, 50°C and 20 ma/cm² (29). The conductivities of these baths are not much different from those of the present study, and current densities may be less than one half of the limiting values. Such conditions would correspond to the curves on Fig. 1 numbered 4 or less. Hence failure in uniformity of current distributions due to mass transfer may be tolerable, and it would be overlooked because of probable predominance or superposition of geometrical effects.

Next, cells for testing plating conditions (such as Haring and Hull cells) are mentioned. The principle on which their use is based is such that current distributions in the vertical direction due to mass transfer are left out of consideration, and effects of polarization are interpreted in a unified way in terms of the throwing power. Such a cell is, however, operated by nature under more severe conditions than in practical plating. Indeed Ibl (5) reported that deposits appeared in a triangular form on the corner nearer to the anode and the bottom of a Hull cell. Moreover, Shreir and Smith (30) found that

[3] Except for the present case of a rectangular geometry, the resistance of the bath does not help the establishment of uniform current distributions, while chemical polarization always does.

quality of deposits was worse at the upper half of cathodes even under ordinary conditions.

Acknowledgment

The authors wish to express their appreciation to Asahi-kagaku-kogyo-shoreikai (The Asahi Association for Development of Chemical Engineering) for its support of the present study. They are grateful to Dr. R. W. Parry of the University of Michigan who read the manuscript and offered helpful suggestions.

GLOSSARY OF SYMBOLS

b — distance between electrodes (cm)
C — concentration of reactive species (mole/cm³)
^sC — concentration of reactive species at the electrode surface (mole/cm³)
$^\infty C$ — concentration of reactive species at the bulk (mole/cm³)
D — diffusion coefficient of reactive species (cm²/sec)
E — electrode potential (volt)
E_r — equilibrium electrode potential (volt)
F — the Faraday (amp sec/eq)
g — acceleration of gravity (cm/sec²)
h — height of electrodes (cm)
i — current density (amp/cm²)
i_d — limiting current density (amp/cm²)
i_o — exchange current density (amp/cm²)
k — defined by Eq. [8] (mole)
k_f, k_b — apparent rate constants of the forward and backward reactions, respectively, defined by Eq. [12] (cm/sec)
n — number of Faradays per gram-ion reacting (eq/mole)
R — molal gas constant (joules/deg K mole)
t — transference number of H^+ (dimensionless)
T — absolute temperature (deg K)
V — terminal voltage (volt)
x — vertical coordinate parallel to electrodes measured from the bottom of the cell (cm)
y — horizontal coordinate perpendicular to electrodes measured from the cathode towards the anode (cm)
α — transfer coefficient (dimensionless)
β_1, β_2 — density coefficients (see text) (cm³/mole)
δ — differential thickness of diffusion layer (cm)
δ' — integral thickness of diffusion layer (cm)
ϵ — parameter of migration for H^+ (dimensionless)
κ — conductivity (mho/cm)
μ — defined by Eq. [12] (dimensionless)
ν — kinematic viscosity (cm²/sec)
ξ — defined by Eq. [12] (dimensionless)
ϕ — potential (volt)

subscripts

$_c$ — cathode
$_a$ — anode

Manuscript received Oct. 27, 1958. This paper was abstracted from the Dissertation of K. Akada, Kyoto University and was presented before the fall meeting of the Electrochemical Society of Japan, November 28 and 29, 1957.

Any discussion of this paper will appear in a Discussion Section to be published in the December 1960 JOURNAL.

REFERENCES

1. B. Levich, *Acta Physicochim.*, **19**, 125 (1944).
2. J. N. Agar, *Discussions Faraday Soc.*, **1**, 26 (1947).
3. C. Wagner, *This Journal*, **95**, 161 (1949).
4. C. H. Keulegan, *J. Research Nat. Bur. Standards*, **47**, 156 (1951).
5. N. Ibl, W. Ruegg, and G. Trümpler, *Helv. Chim. Acta*, **36**, 1624 (1953).
6. N. Ibl, Y. Barrada, and G. Trümpler, *ibid.*, **37**, 583 (1954).
7. N. Ibl, *ibid.*, **37**, 1149 (1954).
8. N. Ibl, K. Buob, and G. Trümpler, *ibid.*, **37**, 2251 (1954).
9. N. Ibl and R. Müller, *Z. Elektrochem.*, **59**, 671 (1955).
10. N. Ibl and R. H. Müller, *This Journal*, **105**, 346 (1958).
11. C. R. Wilke, M. Eisenberg, and C. W. Tobias, *ibid.*, **100**, 513 (1953).
12. C. R. Wilke, M. Eisenberg, and C. W. Tobias, *Chem. Engr. Progr.*, **49**, 663 (1953).
13. C. Wagner, *This Journal*, **104**, 129 (1957).
14. T. Pavlopoulos and J. D. H. Strickland, *ibid.*, **104**, 116 (1957).
15. C. Wagner, *ibid.*, **98**, 116 (1951).
16. P. Delahay, "New Instrumental Methods in Electrochemistry," Interscience Publishing Co., New York (1954).
17. W. Vielstich and P. Delahay, *J. Am. Chem. Soc.*, **79**, 1874 (1957).
18. S. Sugawara and T. Sato, *Trans. Japan. Soc. Mech. Engrs.*, **19**, 13 (1953).
19. V. G. Levich and N. N. Meiman, *Chem. Abstr.*, **46**, 4892h (1952).
20. S. Okada, S. Yoshizawa, F. Hine, and K. Asada, *J. Electrochem. Soc., Japan*, **25**, 562 (1957).
21. F. Paneth and K. Ferzfeld, *Z. Elektrochem.*, **37**, 577 (1931).
22. D. A. Frank-Kamenetskii (translated by N. Thon), "Diffusion and Heat Exchange in Chemical Kinetics," Princeton University Press, Princeton (1957).
23. P. L. Chambré and A. Acrivos, *J. Appl. Phys.*, **27**, 1322 (1956); *Ind. Eng. Chem.*, **49**, 1025 (1957).
24. J. R. Weaver and R. W. Parry, *J. Am. Chem. Soc.*, **78**, 5542 (1956).
25. E. M. Sparrow and J. L. Oregg, *Trans. Am. Soc. Mech. Engrs.*, **78**, 435 (1956).
26. A. R. Gordon and A. Cole, *J. Phys. Chem.*, **40**, 73 (1936).
27. R. K. Richardson and F. D. Taylor, *This Journal*, **20**, 179 (1911).
28. M. Eisenberg, C. W. Tobias, and C. R. Wilke, *ibid.*, **103**, 413 (1956).
29. Electrochem. Soc., Japan (editor), "Denki-kagaku-binran (Handbook of Electrochemistry)", Maruzen Book Co., Tokyo, rev. ed. (1953).
30. L. L. Shreir and J. W. Smith, *This Journal*, **99**, 64, 450 (1952).

Technical Notes

On the Influence of Combinations of Impurities on the Electrolysis of Zinc

Georg Steintveit and Hans Holtan, Jr.

Det Norske Zinkkompani A/S, Eitrheim, Odda, Norway, and Metallurgy Department, Norways Institute of Technology, Trondheim, Norway, respectively

It is a well established fact that the electrolysis of zinc sulfate solutions is very sensitive to impurities present in the electrolyte, and results of experimental investigations have been reported both in textbooks (1) and in the literature (2). In recent years the subject seems to have gained increased interest (3-12). Some investigators have also applied radioactive tracers in their studies (13-15).

Metallic impurities of known poisonous action are Ge, Sb, As, Sn, Co, Ni, Se, Te, etc. Further it is also assumed that organic materials affect zinc deposition. Of particular interest in this respect is beta naphthol or alpha-nitroso-beta-naphthol (16), as this reagent is found in some technical electrolytes. Combinations of the impurities mentioned are particularly harmful. Especially is the combined effect of Co and Sb known to be very dangerous (17, 18). Nevertheless, there seems to exist some confusion regarding the subject as at least one zinc producer (19, 20) keeps a high level of Co in solution and in addition adds amounts of Sb and beta naphthol to improve zinc deposition.

Our investigations comprised the *combined action of several of said impurities* in concentrations which may occur in actual plant operation.

The influence of as much as four impurities present simultaneously was investigated. It was found that there is no law of additivity for the influence of impurities. Thus the presence of only one of two impurities may not harm the electrolysis at all, but when they are present simultaneously they may be harmful. Similar findings were reported later by Turoshima and Stender (6). Angel and co-workers (21) have performed similar experiments on chlorine-caustic electrolysis. One of our results was the observation of the very bad influence of the combination Co,Sb and beta naphthol. Below are shown the results of a series of experiments performed under identical conditions in cells fed with the following solutions:

	Pure zinc sulfate solution	% current efficiency
1.	0.003 g Co/l	90.3
2.	0.050 mg Sb/l	91.7
3.	0.030 g beta naphthol/l	91.1
4.	0.003 g Co/l + 0.050 mg Sb/l	76.8
5.	0.03 g beta naphthol/l + 0.050 mg Sb/l	91.4
6.	Co precipitated from 10 mg/l to 4 mg/l by means of beta naphthol	81.6
7.	As 6 + 0.050 mg Sb/l	25.1

Conditions during electrolysis were: current density, 4.2 amp/dm^2; cell temperature, 30°C; zinc content, 130 g/l; cell acidity, approximately 90 g H_2SO_4/l; time between stripping cathodes, 48 hr.

We see that the influence of the combinations Co,Sb, and Co,beta naphthol are harmful and that the combination Co,Sb,beta naphthol is extremely unfavorable. In the latter case the deposits were heavily corroded and showed a characteristic appearance of pinholes and of spheres under which there were voids.

There is no doubt that a real corrosion takes place even if there is present a "cathodic protection" current of 4.2 amp/dm^2. This is clearly seen also in the simple case where Co is added as the only impurity. It then formed holes in the deposits, and these holes grow as the electrolysis is continued. When a good deposit is formed from a pure solution, it is possible to start corrosion of the deposit by adding the proper combinations of impurities to the solution. When beta naphthol was present as the only impurity, we observed tiny holes in the deposits. Lashkorev and Krynkova (22) have shown that the discharge of zinc and other ions is inhibited by beta naphthol. During electrolysis, hydrogen bubbles are probably attached to the beta naphthol, thus making the holes visible.

A theoretical investigation of the phenomenon is planned.

Acknowledgment

The authors are indebted to the management of Det Norske Zinkkompani A/S for inspiring encouragement during this work and for kind permission to publish this work which was performed at the Company's Research Laboratory in 1954.

Manuscript received Sept. 25, 1959.

Any discussion of this paper will appear in a Discussion Section to be published in the December 1960 JOURNAL.

REFERENCES

1. R. Müller, "Allgemeine und Technische Electrometallurgi," Springer, Wien (1932).
2. U. C. Tainton and E. T. Clayton, *Trans. Am. Electrochem. Soc.*, **57**, 279 (1930); *Metal Ind. (London)*, **37**, 229 (1930).
3. G. Sacciati, *Ind. mineraria*, **4**, 511 (1953).
4. A. G. Pecherskaya and V. V. Stender, *Zhur. Priklad. Khim.*, **23**, (9), 920 (1950).

5. U. F. Turoshina and V. V. Stender, *J. Appl. Chem. U.S.S.R.*, **28**, 155 (1955).
6. *Ibid.*, **28**, 447 (1955).
7. *Ibid.*, **27**, 1019 (1954).
8. A. I. Levin, A. V. Pomosov, V. S. Koletova, I. E. Gurevich, E. A. Ukshe, and N. T. Rogatkina, *Korroziya i Metallopokrytiya, sbornik Stalei*, **1953**, No. 43, 5.
9. A. A. Salin, *Vestnik. Akad. Nauk. Kazakh. S. S. R.*, **12**, 73 (1956).
10. N. T. Kudryatsev and A. G. Atanasyants, *Trudy Moskow Kim. Technol. Inst. im D. I. Mendeleva*, **1956**, 143.
11. N. Matsuura, *J. Chem. Soc. Japan*, Pure Chem. Sec., **74**, 24 (1953).
12. G. T. Wever, *J. Metals*, **11**, 130 (1959).
13. N. Matsuura, *J. Chem. Soc. Japan*, Pure Chem. Sec., **74**, 239 (1953).
14. Z. A. Sheka, *Ukrain. Khim. Zhur.*, **22**, 387 (1956); **22**, 394 (1956).
15. A. I. Levin and V. S. Kolevatova, *Tswetny-Metal*, **29**, 28 (1956).
16. W. C. Snow, *Trans. Am. Inst. Mining Met. Engrs.*, **121**, 502 (1936).
17. *Can. Mining J.*, **75**, 271 (1954).
18. D. R. Zosimovich and N. F. Bogatova, *Zhur. Fiz. Khim.*, **33**, 1324 (1959).
19. W. C. Snow, *Trans. Am. Inst. Mining Met. Engrs.*, **121**, 516 (1936).
20. "Extractive Metallurgy in Australia," Frank A. Green, Editor, Australasian Institute of Mining and Metallurgy, Melbourne (1953).
21. G. Angel, T. Linden, S. Dahlerus, and R. Brännland, *This Journal*, **102**, 246 (1955).
22. M. Lashkorev and A. Krynkova, *Doklady Akad. Nauk. S.S.S.R.*, **62**, 47 (1948).

Dendritic Inclusions in AlSb Grown-Junction Diodes

H. C. Gorton

Battelle Memorial Institute, Columbus, Ohio

One of the disturbing factors in the development of solid-state devices is the anomalous behavior of individual units fabricated from material with seemingly homogeneous characteristics. One of the causes for such anomalies, found in grown-junction diodes of aluminum antimonide, has been the inclusion of impurities in the form of long filaments, which in some cases pass through the junction. The possibility of a similar mechanism for such anomalous behavior in other semiconductor devices also is suggested.

The peak inverse voltage of grown-junction AlSb diodes generally has been consistent with values expected for material of a given carrier concentration, and general uniformity has been observed in the electrical properties of different diodes cut from the same ingot.

In several AlSb crystals, p-n junctions were grown by adding tellurium or selenium to the melt after pulling had commenced. In each of the cases of interest, 0.5 a/o (atomic per cent) tantalum had been added to the melt prior to pulling the crystal (1). In one such crystal, the mobility and carrier concentration of the p-type material were 420 $cm^2\ v^{-1}\ sec^{-1}$ and $1 \times 10^{16}\ cm^{-3}$, respectively. Consequently, peak inverse voltages in excess of 150 v were expected. However, of seven diodes fabricated from single-crystal sections of the grown junction, five were linear and two broke down at about 5 v reverse potential.

Microscopic examination of the diodes, after having been etched in 1:1 HCl:HNO_3, revealed the presence of long, thin fibers about 1 to 5 μ in diameter oriented parallel with the direction of growth of the crystal and penetrating the junction. A powder Debye-Sherrer pattern of the filaments showed them to be Al_2Ta. The fortuitous fact that Al_2Ta happens to be insoluble in the etchant used to prepare the diodes made observation of the inclusions possible. Figure 1 shows a sectioned slice of an AlSb ingot containing a p-n junction. The increase in the density of the filaments toward the center of the crystals

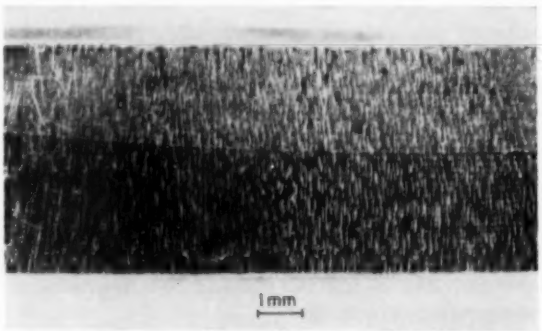

Fig. 1. Section of AlSb ingot with Al_2Ta inclusions showing p-n junction.

may be seen in the figure. Each of the two diodes mentioned above that showed some rectification was taken from near the edge of the crystal. The effect of the fibrous inclusions on the electrical properties of a p-n junction is readily apparent. The fibers appear to be shorter on the right than on the left, because they intersect the surface on the right at a slightly steeper angle.

As may be seen in Fig. 1, the growth of the filaments is inhibited at the p-n junction near the periphery of the crystal, evidently resulting from a physical disturbance due to the addition of the impurity. This discontinuity in the growth of the filaments is indicative of the fact that they are formed as the crystal is being grown and are not associated with solid-state diffusion processes subsequent to the formation of the crystal, such as the decoration of dislocations.

Figure 2 is a photomacrograph of the top side of the same specimen shown in Fig. 1. The bright spots on the dark background are the ends of the filaments protruding from the etched surface. Areas of higher and lower density of the filaments may be seen to have radial symmetry. The radial symmetry of the

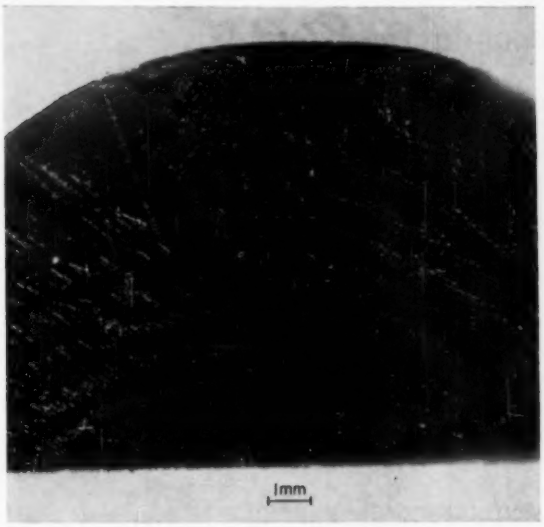

Fig. 2. Section of AlSb ingot showing filaments protruding from etched surface.

Fig. 3. Exploded view of section of Fig. 2 showing linear array of inclusions. Scale, 1⅜ in. = 1 mm.

grouping of the filaments apparently is associated with diffusion of the impurity to preferred sites at the solid-liquid interface. A detailed study of this phenomenon may lead to a greater understanding of the structure of the solid-liquid interface, under various growth conditions. It is also interesting to note that such fibrous inclusions may grow in a single-crystal matrix, without themselves acting as nucleation centers for new crystallites.

A closer examination of Fig. 2 shows several areas of parallel linear arrays of the fibrous inclusions, which are superimposed on the annular areas of high and low density of impurities. These parallel linear arrays are localized to single crystal sections of the ingot. Figure 3 is an exploded view of a small section of the crystal shown in Fig. 2. Here the linear array of the inclusions is quite apparent. Such an array immediately suggests its similarity to dislocation etch pits in other semiconducting materials.

Billig (2) showed that crystals possessing the zinc blende structure solidify dendritically when freezing takes place at a rapid rate. It is here suggested that even with the relatively slow pulling rates associated with normal crystal-growing techniques, incipient dendritic growth takes place at the solid-liquid interface. Crystal growth therefore would initiate along preferred crystal planes from which it would extend dendritically in the plane of the solid-liquid interface. An incipient dendritic lattice at the solid-liquid interface therefore would be built up whose structure would be characteristic of the crystallographic plane presenting itself to the melt. Impurities in the melt with segregation coefficients less than one therefore would tend to be trapped in the interstices of the incipient dendritic lattice. Since the different crystallographic surfaces would propagate themselves into the interstices of the dendritic lattice, any imperfections in the crystal growth would tend to form dislocations in these areas also. In either case, if the dislocations were made visible as etch pits or if the impurities were made visible either as etch pits or as insoluble inclusions, they would show ordered arrays characteristic of the dendritic growth of the matrix.

It is further suggested that certain impurities, such as Al_3Ta, segregating to the interstices of the dendritic lattice would tend to propagate themselves along the direction of growth of the crystal. Visual observation of such inclusions would be rendered impossible, except as etch pits where they would intersect a surface, if they happened to be soluble in the etchants used to process the semiconductors. Such a situation may be a factor in accounting for the disturbing fact that some crystals whose bulk properties show acceptable electrical characteristics nevertheless are unsuitable for device application.

Acknowledgment

The author wishes to thank the members of the Compound Semiconductor Research Group for their permission to publish this work.

Manuscript received June 19, 1959.

Any discussion of this paper will appear in a Discussion Section to be published in the December 1960 JOURNAL.

REFERENCES

1. M. Genser and W. P. Allred, U.S. Pat. 2,816,023.
2. E. Billig, *Proc. Roy. Soc., London*, **A235**, 37 (1956).

Ohmic Contacts to Semiconducting Ceramics

D. R. Turner and H. A. Sauer

Bell Telephone Laboratories, Incorporated, Murray Hill, New Jersey

Flaschen and Van Uitert (1) made a low-resistance ohmic contact to ferrite and semiconducting titanate ceramics with indium wetted with mercury or gallium rubbed on the surface. For investigative purposes and perhaps for some applications the low melting indium-gallium alloy is satisfactory. The difficulty of attaching terminals to indium-gallium, due to its susceptibility to physical deterioration by mechanical abuse and changes in its wetting properties, has spurred the search for a more practical contact material. This paper describes a method of preparing stable low-resistance ohmic contacts to titanate ceramics to which terminals can be soldered. The process can be used to make ohmic contacts to intermetallic compounds such as gallium-arsenide and thermoelectric semiconductors such as bismuth-telluride. The method consists of depositing metal contacts such as nickel on appropriate surfaces of the material and subsequently heat treating the contacts. Nickel is deposited most conveniently by chemical reduction, the "electroless" process (2). Electroless nickel deposition was used by Sullivan and Eigler (3) to make ohmic contacts to silicon, where a heat treatment may not be required.

Experimental

Most of the experimental work to be described here was done on lanthanum-doped barium titanate ceramics ($Ba_{0.998}La_{0.002}TiO_3$) which are n-type semiconductors. These materials exhibit large positive temperature coefficients of resistance (4). Two stable low-resistance ohmic contacts are required on devices for thermistor applications. The test specimens were wafers 1 cm in diameter and about 2 mm thick. The adhesion and surface coverage of the electroless nickel deposit on the titanate ceramic is improved if the surface is prepared by lapping, for example with No. 600 silicon carbide. The area to be coated with nickel is "activated" by dipping in stannous and palladium chloride solutions (5). This procedure deposits a thin layer of palladium on the surface which catalyzes the start of nickel deposition by chemical reduction in the "electroless" solution. Three minutes in the electroless nickel solution (solution temperature ~95°C) deposits a layer of nickel about 0.001 mm thick which is adequate for contact purposes.

Results and Discussion

The electroless nickel contact on the titanate ceramic is nonohmic as deposited. A low-resistance ohmic contact is obtained when the specimen is heat treated to at least 170°C for about 10 min. This is illustrated in Fig. 1 which gives the voltage-current curves obtained at room temperature on a typical titanate ceramic disk with electroless nickel contacts. The initial V-I curve is nonlinear, and at 0.7 v the

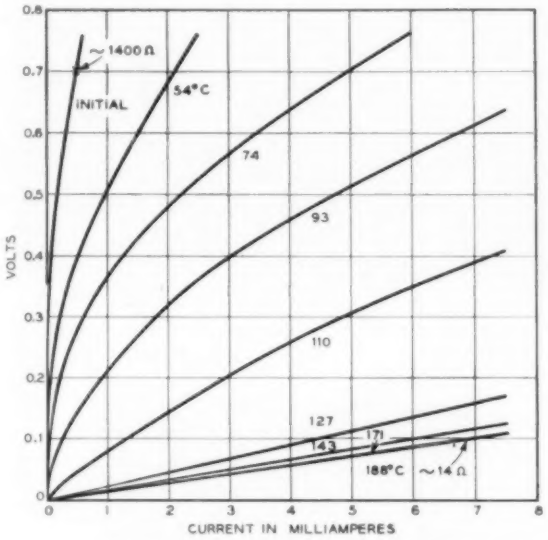

Fig. 1. Effect of heat treatment temperature on the voltage-current relation of a disk of lanthanum-doped barium titanate ceramic with electroless nickel contacts. Specimens measured at room temperature.

total resistance[1] is about 1400 ohms. After the ceramic has been heat treated for 10 min at 54°C, the contact resistance is decreased but it is still nonohmic. Higher heat treatment temperatures decrease the contact resistance still further. The contact resistance continues to decrease with increasing heat treatment temperature up to about 170°C where it approaches a minimum value. This may be considered a minimum processing temperature for obtaining low-resistance ohmic contacts. The total sample resistance of 14 ohms at this point is essentially the body resistance of the ceramic as determined by the four point probe method.

The resistance of the ohmic contact increases with time after heat treatment. This aging effect decreases if longer heat treatment times are used or the temperature of heat treatment is raised. It was found that, with heat treatment temperatures up to about 250°C, the time of heat treatment was an important factor. Longer heat treatment times decreased the rate at which the contact resistance increased with time. The time factor became less important as the heat treatment temperature approached 250°C. Above 250°C, heat treatments longer than 5 or 10 min did not change the aging characteristics of the ohmic contact. The most stable ohmic contacts were obtained when the specimen was heated to the highest temperature tried, 400°C.

[1] The total resistance includes the resistance of two contacts plus the body resistance of the sample.

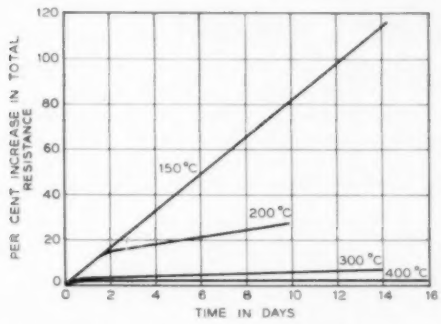

Fig. 2. Effect of heat treatment temperature on power aging of electroless nickel contacts on lanthanum-doped barium titanate disks. Samples measured at room temperature.

The effect of heat treatment temperature on contact resistance aging is shown in Fig. 2. For this experiment, electroless nickel contacts were applied to a series of 20-ohm ceramic disks and each group was heat treated at a different temperature. The heat treatment time was 30 min for 150° and 200°C and 10 min for 300° and 400°C. Those heated to 300° and 400°C were tinned with lead-tin solder to protect the electroless nickel from excessive oxidation. These aging tests were carried out at an elevated temperature of about 80°C since it was found that some heating accelerated the aging effect. The samples were heated electrically by passing either a.c. or d.c. current through the ceramics. Plotted in Fig. 2 is the per cent increase in total resistance as a function of aging time in days. The total resistance measurements were always made at room temperature. When heat treated at 150°C, the total resistance of the test pieces increased linearly with time and the resistance doubled in about 12 days. The contact resistance stability improved with higher heat treatment temperatures. At 400°C, there was a slight change during the first day after which no further resistance change was detected up to 16 days.

Long-time shelf aging tests indicate that electroless nickel contacts heat treated even at 400°C are not perfectly stabilized against increases in the contact resistance. If the contact resistance becomes too large, however, the low contact resistance obtained after the initial heat treatment can be renewed with another brief heat treatment.

The results obtained with titanate ceramics can be explained if it is assumed that the initial nonohmic behavior of electroless nickel is due to an adsorbed layer of oxygen between the ceramic and the nickel (6). The heat treatment removes the adsorbed oxygen presumably by reaction with the nickel. The deterioration of the ohmic contact is attributed to the re-formation of the insulating oxygen layer as the result of oxygen diffusion to the ceramic-nickel interface.

Electroplated nickel, copper, gold, indium, and silver have also been used to make ohmic contacts to titanate ceramics. Electroplated nickel gives the same results as electroless nickel, however, the latter is preferred over plated nickel since it is more convenient to use in this application. Indium provides an ohmic contact as plated but the adhesion is poor. Silver contacts must be heat treated in a vacuum or in an oxygen-free system to produce the ohmic contact. Oxygen diffuses through silver rapidly at elevated temperatures thus the oxygen layer at the semiconductor-silver interface is removed by chemical reaction on heating only in an oxygen-free ambient. Electroless nickel contacts on gallium-arsenide single crystals are made ohmic by tinning the nickel with a lead-tin solder. The heat treatment alone does not make the contact ohmic. Sharpless (7) has shown that tin is important in producing ohmic contacts to gallium-arsenide.

Manuscript received July 22, 1959. This paper was prepared for delivery before the Ottawa Meeting, Sept. 28-Oct. 2, 1958.

Any discussion of this paper will appear in a Discussion Section to be published in the December 1960 JOURNAL.

REFERENCES

1. S. S. Flaschen and L. G. Van Uitert, *J. Appl. Phys.*, **27**, 190 (1956).
2. A. Brenner and G. E. Riddell, U. S. Pat. 2,532,283 and 2,532,284.
3. M. V. Sullivan and J. H. Eigler, *This Journal*, **104**, 226 (1957).
4. H. A. Sauer and S. S. Flaschen, Proc. 1956 Electronic Components Symposium, pp. 41-46, May (1956).
5. F. Pearlstein, *Metal Finishing*, **53**, 59 (1955).
6. H. A. Sauer and S. S. Flaschen, *Bull. Amer. Ceram. Soc.*, to be published.
7. W. H. Sharpless, *Bell System Tech. J.*, **38**, 259 (1959).

Preparation of InAs, InP, GaAs, and GaP by Chemical Methods

D. Effer and G. R. Antell

Research Department, Metropolitan-Vickers Electrical Company Limited, Trafford Park, Manchester, England

The formation of crystals of the arsenides and phosphides of indium or gallium by a vapor phase reaction between the lower valency halides of these metals and arsenic or phosphorus has been previously reported (1). This work has now been extended to show that these basic reactions may also be used to prepare the compounds by the following methods: (*a*) continuous flow vapor phase reaction in the presence of an unreactive carrier gas; (*b*) direct reaction in the liquid phase; (*c*) by passing AsH_3 or PH_3 into the molten chlorides; and (*d*) by a replacement reaction starting with $AsCl_3$ or PCl_3 and the metal.

The following equations illustrate the over-all reactions involved.

$$2\,MCl + Y \rightarrow MCl_2 + MY \qquad [1]$$

$$3\,MCl_2 + Y \rightarrow 2\,MCl_3 + MY \qquad [2]$$

where M corresponds to In or Ga and Y to As or P.

Of the possible reactions under each heading only those involving indium monochloride and gallium dichloride were investigated. Some of the reactions resulted in the formation of colored, solid complexes which decomposed at higher temperatures to give the appropriate III-V compound. Reference is made to the possible structure of these intermediates in the discussion section.

X-ray diffraction measurements were used to establish the identity of all the III-V compounds produced.

The various methods offer alternative routes to the ultimate purification of the compounds. In this respect it has been established that chlorine has little or no effect on the electrical properties of InAs, but we have not carried out any experiments to determine the effect of this element on the other three compounds under discussion.

Experimental

Examples of the reactions given under (*a*), (*b*), (*c*) and (*d*) above are as follows:

(*a*) A continuous flow vapor phase method was carried out by passing gallium dichloride and As vapor in pure nitrogen as a carrier gas through a heated quartz tube. The reactants were introduced into the main tube from separately heated compartments such that the composition of the final mixture was in the proportions given in Eq. [2]. After mixing, the vapors passed through a furnace set at approximately 800°C followed by another at 600°C. The latter furnace served to remove any unchanged reactants and volatile products. GaAs was deposited in powdery form in this furnace, and a 75% yield was obtained by a single passage through the heaters.

(*b*) Direct reaction in the liquid phase was carried out by heating gallium dichloride with arsenic powder under a pure nitrogen gas atmosphere, at approximately 500°C for 24 hr. The gallium arsenide formed was separated mechanically from the small amount of free gallium which resulted from the heating and finally baked out under vacuum at 600°C.

To prepare the phosphides of the metals, liquid yellow phosphorus was reacted with gallium dichloride or indium monochloride at substantially 300°C in a pure nitrogen gas atmosphere for 1 hr. Normally only a temperature sufficient to keep the chloride in a molten condition was necessary to produce the reaction. Colored complexes varying from yellow to red were obtained. On heating slowly to approximately 500°C, these decomposed to give InP or GaP.

(*c*) AsH_3 and PH_3 are relatively unstable gases, AsH_3 decomposing into its elements at about 230°C and PH_3 at 440°C. Passage of AsH_3, in a carrier gas of pure hydrogen, through gallium dichloride at approximately 300°C produced an orange-colored complex which decomposed on heating slowly to 600°C to give GaAs powder. GaP was similarly prepared by passing PH_3 in a nitrogen carrier gas through gallium dichloride at approximately 300°C, the yellow complex formed being slowly heated to 500°C under vacuum to give GaP powder.

Passage of PH_3, in a pure nitrogen carrier gas, through InCl at approximately 300°C produced a red complex which yielded InP on heating slowly to 500°C under vacuum.

(*d*) A variation of the basic reactions was carried out by employing $AsCl_3$ or PCl_3 and the appropriate metal. Using the reaction between $AsCl_3$ and In as an example, when these are heated in molecular proportions an exchange reaction occurs

$$AsCl_3 + In \rightarrow InCl_3 + As$$

If the reaction takes place using an excess of In, InAs is finally produced. It is assumed that a lower halide of In is formed at one stage by the reaction between $InCl_3$ and In and that this reacts with arsenic to form indium arsenide as in the basic Eq. [1] and [2].

All of the four compounds were produced in this way by heating the chlorides to their boiling point ($AsCl_3$ 130°C; PCl_3 76°C) with the metal in sealed evacuated quartz tubes arranged vertically. As the reaction progressed, the temperature was gradually increased to approximately 350°C. Finally, the tubes were placed horizontally in a furnace and heated

slowly to 600°C with what was originally the top end of the tube protruding in order to free the III-V compound from volatile products. The tubes were sealed off in the middle and drawn off. In the case of InAs and GaAs the powders produced were melted by dropping the tubes vertically at 4 cm/hr through a furnace. In all cases except InP the compounds were produced with efficiencies greater than 95% the single experiment with *InP* yielding 65%.

Of the reactions described under the four headings, reaction (*d*) is considered to be most worthy of further investigation with regard to the preparation of the semiconducting compounds in the state of high purity. The $AsCl_3$ or PCl_3 may be purified by careful fractional distillation and finally distilled into reaction capsules containing highly purified In or Ga which are then sealed off. On completion of the reaction as detailed above InAs and GaAs may be melted directly or injected into a "floating zone" or "hanging drop" of the molten compound.

InP and GaP powders produced from the reaction are more difficult to melt due to the high pressures of phosphorus produced at the melting points of these materials. Melting of InP may be attempted in ampoules of extra thick wall or by using an autoclave pumped up to a pressure equal to the dissociation vapor pressures produced by the molten compound. Alternatively the InP powder may be used as charge material for a crystal pulling apparatus.

Discussion

The composition of the colored complexes observed during some of the reactions was not elucidated. Gallium dichloride has been denoted as $GaCl_2$ but is actually dimorphic similar to indium dichloride. Evidence for the formulation of $Ga^{I}(Ga^{III}Cl_4)$ has been given by x-ray diffraction studies with crystalline gallium dichloride (2) and by Raman spectra of the fused compound (3). Further evidence for the formulation which may have a considerable bearing on the structure of the observed complexes has been obtained by passing H_2S through gallium dichloride (4). A solid complex containing Ga, Cl, and S was obtained of variable composition, the reaction occurring with the Ga^{I} ion. It seems possible that the reactions between gallium dichloride and AsH_3, PH_3, and liquid phosphorus behave in an analogous manner.

Acknowledgment

The authors wish to thank Mr. R. W. McEvan for assistance in the experimental work and Mr. R. P. Chasmar for helpful criticisms of the manuscript. They also wish to thank Sir Willis Jackson, F.R.S., Director of Research and Education, Metropolitan-Vickers Electrical Co. Ltd., for permission to publish.

Manuscript received Sept. 8, 1959.

Any discussion of this paper will appear in a Discussion Section to be published in the December 1960 JOURNAL.

REFERENCES

1. G. R. Antell and D. Effer, *This Journal*, **106**, 509 (1959).
2. G. Garton and H. M. Powell, *J. Inorg. Nucl. Chem.*, **4**, 84 (1957).
3. L. A. Woodward, G. Garton, and H. L. Roberts, *J. Chem. Soc.*, **1956**, 3723.
4. R. C. Carlston, E. Griswold, and J. Kleinberg, *ibid.*, **80**, 1532 (1958).

FUTURE MEETINGS OF
The Electrochemical Society

Chicago, Ill., May 1, 2, 3, 4, and 5, 1960

Headquarters at the Lasalle Hotel
Sessions will be scheduled on
Electric Insulation (including a symposium on "Electrolytic Capacitors"), Electronics (including Luminescence, Semiconductors, and Thermionics), Electrothermics and Metallurgy (including symposia on Refractory Metals, "High-Purity Vanadium—Its Preparation, Properties, and Alloys," and on Rhenium, and a round table on "Methods of Reducing Iron Ores"), Industrial Electrolytics, and Theoretical Electrochemistry (general sessions, and a Symposium on "Electrochemical Engineering" co-sponsored by the Theoretical and Industrial Electrolytic Divisions)

★ ★ ★

Houston, Texas, October 9, 10, 11, 12, and 13, 1960

Headquarters at the Shamrock Hotel
Sessions probably will be scheduled on
Batteries, Corrosion, Electrodeposition, Electronics (Semiconductors), and Electrothermics and Metallurgy

★ ★ ★

Indianapolis, Ind., April 30, May 1, 2, 3, and 4, 1961

Headquarters at the Claypool Hotel

★ ★ ★

Detroit, Mich., October 1, 2, 3, 4, and 5, 1961

Headquarters at the Statler Hotel

Papers are now being solicited for the meeting to be held in Houston, Texas, October 9-13, 1960. Triplicate copies of each abstract *(not exceeding 75 words in length)* are due at Society Headquarters, 1860 Broadway, New York 23, N. Y., *not later than June 1, 1960* in order to be included in the program. *Please indicate on abstract for which Division's symposium the paper is to be scheduled and underline the name of the author who will present the paper.* Complete manuscripts should be sent in triplicate to the Managing Editor of the JOURNAL at 1860 Broadway, New York 23, N. Y.

Papers submitted for presentation at the meeting become the property of The Electrochemical Society and may not be published elsewhere, in whole or in part, unless permission is requested of and granted by the Society. Papers already published elsewhere, or submitted for publication elsewhere, are not acceptable for oral presentation except on invitation by a Divisional program Chairman.

Chicago Program

THE ELECTROCHEMICAL SOCIETY

One Hundred and Seventeenth Meeting

May 1, 2, 3, 4, and 5, 1960

Sunday through Thursday

CONDENSED TECHNICAL PROGRAM

Monday, May 2, 1960

Electric Insulation (Abstracts 1-9) 9:00 A.M.-12:00 M.; 2:00-5:00 P.M. (Parlor D, Mezzanine)

Electronics-Luminescence (Abstracts 40-54) 9:00 A.M.-12:00 M.; 2:00-4:45 P.M. (Lincoln-Douglas Rooms, 18th floor)

Electronics-Semiconductors (Abstracts 78-93) 9:15 A.M.-12:15 P.M.; 2:00-5:30 P.M. (Grand Ballroom, 19th floor)

Electrothermics and Metallurgy-Vanadium (Abstracts 121-132) 9:15-11:55 A.M.; 1:30-4:55 P.M. (Chicago Room, Mezzanine)

Industrial Electrolytic (Abstracts 178-185) 10:00 A.M.-12:00 M.; 2:45-4:45 P.M. (Illinois Room, Mezzanine)

Tuesday, May 3, 1960

Electric Insulation (Abstracts 10-20) 9:00 A.M.-12:00 M.; 2:00-4:30 P.M. (Parlor D, Mezzanine)

Electronics-Luminescence (Abstracts 55-68A) 9:00-11:55 A.M.; 2:00-4:25 P.M. (Lincoln-Douglas Rooms, 18th floor)

Electronics-Semiconductors (Abstracts 94-104) 9:00 A.M.-12:05 P.M.; 2:00-4:30 P.M. (Grand Ballroom, 19th floor)

Electrothermics and Metallurgy-Iron Ores (Abstracts 133-140) 9:15-11:55 A.M.; 2:00-4:35 P. M. (Chicago Room, Mezzanine)

Electrothermics and Metallurgy-Rhenium (Abstracts 154-164) 9:00-11:40 A.M.; 2:00-4:10 P.M. (Press Gallery, 18th floor)

Theoretical Electrochemistry—Industrial Electrolytic (Abstracts 186-190) 9:15 A.M.-12:00 M.; 2:00-4:30 P.M. (Century Room 19th floor)

Wednesday, May 4, 1960

Electric Insulation (Abstracts 21-30) 9:00-11:30 A.M.; 2:00-4:30 P.M. (Parlor D, Mezzanine)

Electronics-General (Abstracts 36-39) 2:15-3:55 P.M. (Illinois Room, Mezzanine)

Electronics—Luminescence (Abstracts 69-77B) 9:00-11:55 A.M.; 2:00-4:30 P.M. (Lincoln-Douglas Rooms, 18th floor)

Electronics-Semiconductors (Abstracts 105-120) 9:00 A.M.-12:00 M.; 2:00-4:45 P.M. (Grand Ballroom, 19th floor)

Electrothermics and Metallurgy-Iron Ores (Abstracts 141-149) 9:30 A.M.-12:00 M.; 2:00-5:05 P.M. (Chicago Room, Mezzanine)

Electrothermics and Metallurgy-Rhenium (Abstracts 165-174) 9:15-11:25 A.M.; 2:00-4:10 P.M. (Press Gallery, 18th floor)

Theoretical Electrochemistry—Industrial Electrolytic (Abstracts 191-195) 9:30 A.M.-12:00 M.; 2:00-4:30 P.M. (Century Room, 19th floor)

Thursday, May 5, 1960

Electric Insulation (Abstracts 31-35) 9:00 A.M.-12:00 M. (Parlor D, Mezzanine)

Electrothermics and Metallurgy-Iron Ores (Abstracts 150-153) 9:30 A.M.-12:00 M.; 2:00-4:00 P.M. (Chicago Room, Mezzanine)

Electrothermics and Metallurgy-Refractory Metals (Abstracts 175-177) 9:30-11:00 A.M. (Press Gallery, 18th floor)

Theoretical Electrochemistry (Abstracts 196-210) 9:00-11:20 A.M.; 2:00-4:40 P.M. (Lincoln-Douglas Rooms, 18th floor)

GENERAL INFORMATION

Convention Headquarters is the LaSalle Hotel, LaSalle at Madison St., Chicago 2, Ill.

Rates per day for rooms, with bath, are: single room, $7.50, 8.50, 9.50, 10.00, 10.50, 11.50, 13.50, 15.50; double-bed room, $11.00, 12.00, 13.00, 13.50, 14.00, 15.00, 17.00, 19.00; twin-bed room, $15.00, 17.00, 18.00, 18.50, 19.00, 20.00; 2 rooms with connecting bath, for 2—$17.00, for 3—19.00, for 4—21.00; parlor, double-bed room, for 1—$16.00, 17 50, for 2—19.50, 20.00; parlor, twin-bed room, $33.50, 45.00 50.00, 55.00; parlor, two bedrooms, $52.00, 62.50, 85.00.

Requests for room reservations should be mailed to the LaSalle Hotel, LaSalle at Madison St., Chicago 2, Ill. BE SURE to state that you will be attending The Electrochemical Society Meeting. If your wife will be attending, be sure to indicate this on your request for reservation.

The Office of the Secretary is Parlor A, Mezzanine.

The Chicago Local Section Headquarters is Parlor B, Mezzanine.

Ladies' Headquarters is Parlor F, Mezzanine.

All technical sessions will be held on the Mezzanine, 18th, and 19th floors.

REGISTRATION

The registration desk will be in the Century Room, 19th floor, on Sunday and Monday, May 1 and 2, and in the 19th floor foyer Tuesday through Thursday, May 3-5. The registration schedule is:

Sunday, May 1—3:00 to 9:00 P.M.
Monday, May 2—8:00 A.M. to 4:00 P.M.
Tuesday, May 3—8:00 A.M. to 4:00 P.M.
Wednesday, May 4—8:00 A.M. to 4:00 P.M.
Thursday, May 5—8:00 A.M. to 12:00 M.

Registration fees are:

Members, guest speakers, coauthors	$ 7.00
Nonmembers	13.00*
Ladies	5.00
Thursday only	5.00
Student Members	Complimentary
Students	2.00

* If a nonmember fills out an application form and subsequently is elected to membership in the Society, the difference between the nonmember and member registration fee will be applied to his first year's dues.

INFORMATION ABOUT CHICAGO

Information about places of interest and other attractions will be available at the Society's registration desk at the LaSalle Hotel.

SYMPOSIA AND ROUND TABLES

The Electric Insulation Division has scheduled a three-day symposium on Electrolytic Capacitors, as well as a general session.

The Electronics Division has scheduled a general session, and six sessions on Luminescence; the Semiconductor Group has symposia on: Crystal Growth; Physical Chemistry of Semiconductors; Compound Semiconductors, Surfaces; Oxide Films; Diffusion; and Device Technology.

The Electrothermics and Metallurgy Division has scheduled symposia on: Vanadium; Methods of Reducing Iron Ores; Rhenium: and Refractory and Reactive Metals.

The Industrial Electrolytic Division has scheduled two general sessions.

The Theoretical Electrochemistry Division and the Industrial Electrolytic Division have scheduled a Joint Symposium on Electrochemical Engineering including Applied Electrode Kinetics, Transport Processes in Electrolytic Cells, Distribution of Potential and Current in Electrolytic Cells, and Scale Up and Measurements on the Plant Scale.

The Theoretical Electrochemistry Division has scheduled two general sessions.

GENERAL FUNCTIONS

Symposia Chairmen Breakfasts

On Monday, Tuesday, Wednesday, and Thursday, May 2, 3, 4, and 5, special breakfasts will be held for symposia chairmen. On the day on which he presides at a symposium, each chairman should be in the Coffee Room, lower Lobby, LaSalle Hotel, where a special table will be set up, at 7:45 A.M.

Monday Evening Mixer

On Monday, May 2, all those registered at the meeting are invited to attend the mixer in the Illinois Room, Mezzanine, from 8:00 to 10:00 P.M. Beer, soft drinks, and snacks will be served on a complimentary basis. Admission is by registration badge.

Tuesday Society Luncheon and Business Meeting

The Electrochemical Society Luncheon and Business Meeting will be held on Tuesday, May 3, at 12:15 P.M. in the Illinois Room, Mezzanine. Bill Veeck, President of the American League Champion Chicago White Sox, is guest speaker.

Tuesday Palladium Medal Address

Professor A. N. Frumkin, Director of the Electrochemical Institute of the USSR, will deliver the Palladium Medal Address at 5:00 P.M. on Tuesday, May 3, in the Illinois Room, Mezzanine.

Tuesday Evening Reception and Banquet

A reception honoring President and Mrs. W. C. Gardiner will be held at 6:30 P.M. on Tuesday, May 3, in the Grand Ballroom, 19th floor. Cocktails will be served from 6:30 to 7:30 P.M., followed by dinner at 7:30 P.M. Dr. Gardiner will deliver the Presidential Address.

Wednesday Evening Party

Arrangements have been made with the famous Chez Paree for an evening including a cocktail hour, dinner, and entertainment. Red Skelton is scheduled to be featured that evening. (Price $10.00, including gratuity. Drinks ordered at the dinner table will be at the individual's expense.) Tickets for this function will be available at the Society's registration desk. Be at Chez Paree at 6:45 P.M.

LADIES' PROGRAM

All the ladies are invited to make Parlor F, Mezzanine, their headquarters during their stay in Chicago. A coffee hour will be held from 10:00 to 11:00 A.M. Monday through Thursday, May 2 to 5, in Parlor F. Members of the Ladies' Committee will be there to give information and assist in any way they can to make the stay a pleasant one.

Monday, May 2—Coffee hour at 10:00 A.M. The ladies will meet at 12:30 P.M. at the Kungsholm Restaurant, 100 East Ontario St. They will see the Puppet Opera at 2:00 P.M. Monday evening the ladies are invited to attend the Mixer from 8:00 to 10:00 in the Illinois Room, Mezzanine (see General Functions).

Tuesday, May 3—Coffee hour at 10:00 A.M. The ladies are invited to attend the Society Luncheon at 12:15 P.M. in the Illinois Room, Mezzanine, and the Reception and Banquet at 6:30 P.M. in the Grand Ballroom, 19th floor (see General Functions). The afternoon is left open.

Wednesday, May 4—Coffee hour at 10:00 A.M. The ladies will meet at Fritzel's Restaurant, State at Lake St., at 12:00 M., for lunch. Buses will leave there at 1:30 P.M. for a visit to the Oriental Institute and the Rockefeller Memorial Chapel at the University of Chicago. If time permits and the ladies so desire, the Museum of Science and Industry may be visited. The ladies are welcome to attend the party at Chez Paree at 6:45 P.M. (see General Functions).

Thursday, May 5—Coffee hour at 10:00 A.M.

LUNCHEONS AND BUSINESS MEETINGS OF DIVISIONS

Electric Insulation Division Luncheon and Business Meeting, Wednesday, May 4, at 12:30 P.M. in the LaSalle Room, 18th floor.

Electronics Division Luncheon and Business Meeting, Wednesday, May 4, at 12:15 P.M. in the Illinois Room, Mezzanine.

Electrothermics and Metallurgy Division Luncheon and Business Meeting, Wednesday, May 4, at 12:30 P.M. in Parlor E, Mezzanine.

Industrial Electrolytic Division Luncheon and Business Meeting, Monday, May 2, at 12:30 P.M. in the Illinois Room, Mezzanine.

Theoretical Electrochemistry Division Business Meeting, Thursday, May 5, at 11:30 A.M. in the Lincoln-Douglas Rooms, 18th floor.

BOARD AND COMMITTEE MEETINGS

Sunday, May 1, 2:00 P.M.—Meeting of the **Board of Directors,** Lincoln-Douglas Rooms, 18th floor.

Sunday, May 1, 7:30 P.M.—Meeting of the **Investment Advisory Panel,** LaSalle Room, 18th floor.

Monday, May 2, 2:00 P.M.—Meeting of the **Convention Advisory Committee,** LaSalle Room, 18th floor.

Monday, May 2, 4:30 P.M.—Meeting of the **Council of Local Sections,** Press Gallery, 18th floor.

Monday, May 2, 5:00 P.M.—Meeting of the **Editorial Staff** of the Journal, La Salle Room, 18th floor.

Wednesday, May 4, 5:00 P.M.—Meeting of the **Membership Committee,** LaSalle Room, 18th floor.

Thursday, May 5, 12:00 M.—Meeting of **General Chairmen of Future Meetings.** Meet in the Office of the Secretary, Parlor A, Mezzanine. Luncheon will be held in the Lotus Room, Lobby.

FALL MEETING
at the
Shamrock Hotel
HOUSTON, TEXAS
October 9, 10, 11, 12, and 13, 1960

Sessions probably will be scheduled on:

Batteries
Corrosion
Electrodeposition
Electronics-Semiconductors
Electrothermics and Metallurgy

Abstracts for the Houston Meeting (*not exceeding 75 words in length*) must reach Society Headquarters, 1860 Broadway, New York 23, N. Y., *not later than June 1, 1960* to be included in the program. *Please indicate on the abstract for which Division's symposium the paper is to be scheduled and underline the name of the author who will present the paper.*

Papers submitted for presentation at the meeting become the property of The Electrochemical Society and may not be published elsewhere, in whole or in part, unless permission is requested and granted by the Society. Papers already published elsewhere, or submitted for publication elsewhere, are not acceptable for oral presentation except on invitation by a Divisional Program Chairman.

COST OF VARIOUS FUNCTIONS

(other than registration)

Please buy tickets as early as possible.

Symposia Chairmen Breakfasts-Standard menu prices	
Monday Evening Mixer	Complimentary
Division Luncheons	$ 4.00
Tuesday Society Luncheon	4.50
Tuesday Reception and Banquet, men	9.00
ladies	7.00
Ladies' Luncheons and functions, each	1.00
Wednesday Evening, Chez Paree	10.00

JOURNALS

Copies of the January, February, March, and April issues of the "JOURNAL OF THE ELECTROCHEMICAL SOCIETY" will be available at the registration desk. The price of a single copy of the Journal is $1.25 to members and $1.75 to nonmembers.

EXTENDED ABSTRACTS

The Electronics Division is making available an extended abstract booklet containing 1000-word abstracts of most of the papers presented before the Electronics Division at the Chicago Meeting. Copies will be available at the registration desk or may be obtained about two weeks before the meeting by request to A. E. Hardy, Radio Corp. of America, New Holland Pike, Lancaster, Pa. Price $3.50 with a discount of $00.50 per copy for orders accompanied by payment and requiring no invoice.

DISCUSSION

No recordings will be made of oral discussions. Those contributing to the discussion of a paper and desiring their remarks to be published will be supplied by the symposium chairman with a printed form on which any discussion may be written. These forms should be given to the Secretary-Treasurer of the Division or to the Managing Editor of the Journal after the session; they can be mailed to the Managing Editor of the Journal, 1860 Broadway, New York 23, N. Y. The discussion will then be referred to the author for reply. Publication of the discussion and the comments of the author depends on publication of the article in the Journal.

Written discussion should be submitted within two months following publication of the article in the Journal. A Discussion Section is published semiannually in the Journal.

EMPLOYMENT POSTERS

Companies which desire to recruit employees at the Columbus Meeting will have posters to this effect on a board near the registration desk. Companies are requested to confine their announcements to this board.

NOTE

In the Index to Authors, the abstract number is used. Address of each author is included with the abstract.

Technical Program

Chicago Meeting

ELECTRIC INSULATION

Monday, May 2, 1960
Electrolytic Capacitors
with C. C. Houtz presiding

(PARLOR D, Mezzanine)

9:00 A.M.—Introductory remarks by A. J. Sherburne
9:15 A.M.—"Electrolytic Oxide Films" by J. Burnham (Abstract No. 1)
10:10 A.M.—"Conduction, Storage, and Photoelectric Phenomena in Anodic Aluminum Oxide Films" by Kurt Lehovec (Abstract No. 2)
11:05 A. M.—"Impedance Characteristics of Anodic Oxides" by L. Young (Abstract No. 3)

Electric Insulation (cont'd)
Monday, May 2, 1960
Electrolytic Capacitors (cont'd)
with R. A. Ruscetta presiding

(PARLOR D, Mezzanine)

2:00 P.M.—"Tantalum Anode Reactions" by Donald Stephenson and Robert Russ (Abstract No. 4)
2:30 P.M.—"Dielectric Characteristics of Tantalum Anodic Oxide Films As Related to Film Structure" by D. Mohler (Abstract No. 5)
3:00 P.M.—"Hydrated Oxide Films on Aluminum" by Dietrich Altenpohl (Abstract No. 6)
3:30 P.M.—"Anodic Formation of Aluminum Oxide Films, I. The Influence of Surface Preparation on Film Properties" by W. E. Tragert and J. R. Rairden (Abstract No. 7)
4:00 P.M.—"Anodic Formation of Aluminum Oxide Films, II. Effect of Various Electrical Forming Conditions on Film Properties" by W. E. Tragert and J. R. Rairden (Abstract No. 8)
4:30 P.M.—"Determination of the Thickness of Thin Porous Oxide Films on Aluminum" by M. S. Hunter and P. F. Towner (Abstract No. 9)

Electric Insulation (cont'd)
Tuesday, May 3, 1960
Electrolytic Capacitors (cont'd)
with C. C. Houtz presiding

(PARLOR D, Mezzanine)

9:00 A.M.—"Capacitor Grade Tantalum" by L. H. Belz (Abstract No. 10)
9:30 A.M.—"Measurement of the Specific Surface Area of Tantalum Powders and Sintered Anodes" by W. G. Guldner and C. C. Houtz (Abstract No. 11)
10:00 A.M.—"Some Physical Properties of Metallic Tantalum" by J. I. Budnick (Abstract No. 12)
10:30 A.M.—"Low-Temperature Sintering of Tantalum Anodes" by C. J. B. Fincham and G. J. Villani (Abstract No. 13)

MEETING ROOM SCHEDULE

Meeting	Monday		Tuesday		Wednesday		Thursday	
	A.M.	P.M.	A.M.	P.M.	A.M.	P.M.	A.M.	P.M.
Electric Insulation	G	G	G	G	G	G	G	
Electronics—General						E		
—Luminescence	C	C	C	C	C	C		
—Semiconductors	A	A	A	A	A	A		
Electrothermics and Metallurgy								
—Refractory Metals							D	
—Iron Ores			F	F	F	F	F	F
—Rhenium			D	D	D	D		
—Vanadium	F	F						
Industrial Electrolytic	E	E						
Theoretical Electrochemistry—Industrial Electrolytic			B	B	B	B		
Theoretical Electrochemistry							C	C

A = Grand Ballroom; B = Century Room; C = Lincoln-Douglas Rooms; D = Press Gallery; E = Illinois Room; F = Chicago Room; G = Parlor D.

11:00 A.M.—"Determination of the Thickness of Anodic Oxide Films by the Spectrophotometric Method in Conjunction with the Abèles Method for the Refractive Index" by L. Young and J. E. Orme (Abstract No. 14)
11:30 A.M.—"Electrolytic Etching of Dense Tantalum" by A. L. Jenny and R. A. Ruscetta (Abstract No. 15)
12:15 P.M.—Society Luncheon and Business Meeting in the Illinois Room, Mezzanine. Bill Veeck, President of the American League Champion Chicago White Sox, is guest speaker.

Electric Insulation (cont'd)
Tuesday, May 3, 1960
Electrolytic Capacitors (cont'd)
with R. A. Ruscetta presiding

(PARLOR D, Mezzanine)

2:00 P.M.—Niobium (Columbium) Solid Electrolytic Capacitors' by N. Schwartz, M. Gresh, and S. Karlik (Abstract No. 16)
2:30 P.M.—"Columbium (Niobium) Electrolytic Capacitors" by A. Shtasel and H. T. Knight (Abstract No. 17)
3:00 P.M.—"Silicon Nitride Thin Film Dielectric" by C. R. Barnes and C. R. Geesner (Abstract No. 18)
3:30 P.M.—"Properties of Anodically Formed Oxide Films on Tungsten" by H. W. Pitman and D. C. Hamby (Abstract No. 19)
4:00 P.M.—"Ion Size Effect and Mechanism of Electrolytic Rectification" by P. F. Schmidt, F. Huber, and R. F. Schwarz (Abstract No. 20)
5:00 P.M.—Palladium Medal Address by A. N. Frumkin in the Illinois Room, Mezzanine.

Electric Insulation (cont'd)
Wednesday, May 4, 1960
Electrolytic Capacitors (cont'd)
with L. Young presiding

(PARLOR D, Mezzanine)

9:00 A.M.—"The A-C Properties of Tantalum Solid Electrolytic Capacitors" by D. A. McLean (Abstract No. 21)
9:30 A.M.—"A Mathematical Model for the Porous Type Tantalum Anode Capacitor" by J. S. Fisher (Abstract No. 22)
10:00 A.M.—"Cathodic Depolarization in Tantalum Electrolytic Capacitors" by T. C. O'Nan (Abstract No. 23)
10:30 A.M.—"Cell and Thermoelectric Effects of Tantalum Electrolytic Capacitors" by J. M. Law and W. C. Richards (Abstract No. 24)
11:00 A.M.—"A Selective Electrochemical Etching Procedure to Improve D-C Characteristics of Oxide Film Capacitors" by R. W. Berry, N. Schwartz, M. J. Urban, and M. Gresh (Abstract No. 25)
12:30 P.M.—Electric Insulation Division Luncheon and Business Meeting in the LaSalle Room, 18th floor. A. J. Sherburne will speak on "Electrical Insulation in Retrospect."

Electric Insulation (cont'd)
Wednesday, May 4, 1960
Electrolytic Capacitors (cont'd)
with J. Burnham presiding

(PARLOR D, Mezzanine)

2:00 P.M.—"Equivalent Series Resistance of Anodically Formed Oxide Films on Aluminum" by W. J. Bernard (Abstract No. 26)
2:30 P.M.—"Factors Determining Allowable Ripple Current at Various Frequencies in Aluminum Electrolytic Capacitors" by R. Lane and A. Bennett (Abstract No. 27)
3:00 P.M.—"500°C Capacitors" by R. J. Stamets and R. A. West (Abstract No. 28)
3:30 P.M.—"A Novel Low Voltage Electrolytic Capacitor without Conventional Spacers" by A. J. Catotti and R. A. West (Abstract No. 29)
4:00 P.M.—"Volume Resistivity of Ammonium Ethylene Glycoborate Electrolytes" by C. C. Houtz (Abstract No. 30)

Electric Insulation (cont'd)
Thursday, May 5, 1960
General Session
with A. H. Sharbaugh presiding

(PARLOR D, Mezzanine)

9:00 A.M.—"Electrical Properties of Some Aliphatic Acids and Alcohols" by A. M. Parks (Abstract No. 31)
9:30 A.M.—"Effects of Tropical Exposure on the Electrical Properties of Insulating Materials" by L. J. Frisco (Abstract No. 32)
10:00 A.M.—"Effect of Heat on the Electrical Properties of Paper" by L. H. Wirtz and T. D. Callinan (Abstract No. 33)
10:30 A.M.—"The Electric Strength of Insulating Liquids" by A. H. Sharbaugh (Abstract No. 34)
11:15 A.M.—"Dielectric Properties of Very Thin Films of Liquid Dielectrics" by T. Salomon (Abstract No. 35)

ELECTRONICS

Wednesday, May 4, 1960
General Electronics
with A. E. Martin presiding

(ILLINOIS ROOM, Mezzanine)

2:15 P.M.—"Micromodular Solid Tantalum Capacitors" by A. W. H. Smith (Abstract No. 36)
2:40 P.M.—"Digital Programming Unit for Automatic Temperature Control" by N. L. Hozak, J. S. Cook, and D. R. Mason (Abstract No. 37)
3:05 P.M.—"An Economical, Automatic, Differential Thermal Analysis System" by C. E. Barnes and D. R. Mason (Abstract No. 38)
3:30 P.M. — "Electroluminescent-Piezoelectric Flat Panel Displays" by S. Nudelman, J. Lambe, J. Mudar, and G. Trytten (Abstract No. 39)

ELECTRONICS—LUMINESCENCE

Monday, May 2, 1960
with A. L. Smith presiding

(LINCOLN-DOUGLAS ROOMS, 18th floor)

9:00 A.M.—"Phenomenological Theory of Luminescence of Nonphotoconducting Phosphors" by Yasuo Uehara (Abstract No. 40)
9:45 A.M.—"Irreversible Thermodynamics of Solid-State Luminescence" by F. E. Williams (Abstract No. 41)
10:05 A.M.—"Shape of Absorption Bands in Solids" by J. J. Markham (Abstract No. 42)
10:35 A.M.—"Atomic Wave Functions of Activators" by K. H. Butler (Abstract No. 43)
10:55 A.M.—"The Significance of Measurements of the Temperature Dependence of Luminescence Intensity" by C. H. Haake (Abstract No. 44)
11:20 A.M.—"Absolute Spectral Reflectance of Phosphors" by J. E. Eby (Abstract No. 45)
11:40 A.M.—"Infrared Spectroscopy in Phosphor Research" by M. J. B. Thomas and C. W. Jerome (Abstract No. 46)

Electronics—Luminescence (cont'd)
Monday, May 2, 1960
with C. A. Brown presiding

(LINCOLN-DOUGLAS ROOMS, 18th floor)

2:00 P.M.—"Factors Influencing Luminescent Emission Studies of the Rare Earth Ions" by L. G. Van Uitert (Abstract No. 47)
2:20 P.M.—"Some Optical Properties of Powder and Crystal Halophosphate Phosphors" by P. D. Johnson (Abstract No. 48)
2:40 P.M.—"Energy Levels of the Antimony Center in Halophosphates" by F. E. Williams (Abstract No. 49)
3:00 P.M.—"Lead- and Manganese-Activated Calcium-Cadmium Silicate Phosphors" by Yasuo Uehara, Yoshimasa Kobuke, Isoo Masuda, and Takashi Kushida (Abstract No. 50)

3:25 P.M.—"Luminescence vs. Composition Studies of Complex Zinc and Cadmium Orthophosphates Containing Sodium and Lithium" by A. L. Smith (Abstract No. 51)
3:45 P.M.—"Cadmium Phosphate Phosphors" by R. C. Ropp (Abstract No. 52)
4:05 P.M.—"Luminescence of AlN" by I. Adams, J. W. Mellichamp, and G. A. Wolff (Abstract No. 53)
4:25 P.M.—"Crystal Structure and Spectra of Alkali Halide Phosphors" by F. D. Klement (Abstract No. 54)

Electronics—Luminescence (cont'd)
Tuesday, May 3, 1960
with Seymour Keller presiding

(LINCOLN-DOUGLAS ROOMS, 18th floor)

9:00 A.M.—"On the Hydrogen-Like Model for Traps in Zinc Sulfide" by G. Curie, N. Arpiarian, P. Guéret, and D. Curie (Abstract No. 55)
9:25 A.M.—"A Numerical Table for the Computation of Trap Depths from Thermoluminescence Experiments" by G. Curie and D. Curie (Abstract No. 56)
9:50 A.M.—"Gold-Activated (Zn,Cd)S Phosphors" by M. Avinor (Abstract No. 57)
10:10 A.M.—"Low-Temperature Luminescence of ZnSCdS Phosphors" by R. W. A. Gill and S. Rothschild (Abstract No. 58)
10:30 A.M.—"Infrared Stimulation and Quench of Zinc Sulfide Phosphors" by C. C. Klick (Abstract No. 59)
10:50 A.M.—"Synthesis and Crystallography of Structurally Pure Cubic and Hexagonal Single Crystals of ZnS" by Harold Samelson and V. A. Brophy (Abstract No. 60)
11:15 A.M.—"Infrared Absorption of n-Type (Zn,Cd)S" by R. M. Potter (Abstract No. 61)
11:35 A.M.—"Formation of Phosphor Films by Evaporation" by L. R. Koller (Abstract No. 62)
12:15 P.M.—Society Luncheon and Business Meeting in the Illinois Room, Mezzanine. Bill Veeck, President of the American League Champion Chicago White Sox, is guest speaker.

Electronics—Luminescence (cont'd)
Tuesday, May 3, 1960
with Frank Ullman presiding

(LINCOLN-DOUGLAS ROOMS, 18th floor)

2:00 P.M.—"Continuous Films of II-VI Phosphors and Photoconductors Made by Vapor Reaction" by D. A. Cusano (Abstract No. 63)
2:25 P.M.—"Transparent and Powder Phosphor Screens under High Ambient Illumination" by A. E. Hardy (Abstract No. 64)
2:50 P.M.—"Mechanism of Depreciation of Electroluminescent Phosphors" by I. L. Smith, R. M. Potter, and M. Aven (Abstract No. 65)
3:15 P.M.—"Electroluminescence Maintenance" by W. A. Thornton (Abstract No. 66)
3:40 P.M.—"Effects of Interaction among Particles in Electroluminescent Layers" by A. T. Halpin and Paul Goldberg (Abstract No. 67)
4:00 P.M.—"On the Physical Characteristics and Chemical Composition of Electroluminescent Phosphors" by Paul Goldberg and Sixdenial Faria (Abstract No. 68)
4:20 P.M.—"Detection of Ionization of Eu^{++} in the Phosphor SrS-Eu, Sm by the Paramagnetic Resonance Absorption Method" by V. V. Antonov-Romanovsky, V. G. Dubinin, A.M. Prokhorov, Z. A. Trapeznikova, and M. V. Fock (Abstract No. 68A)
5:00 P.M.—Palladium Medal Address by A. N. Frumkin in the Illinois Room, Mezzanine.

Electronics—Luminescence (cont'd)
Wednesday, May 4, 1960
with Paul Goldberg presiding

(LINCOLN-DOUGLAS ROOMS, 18th floor)

9:00 A.M.—"Copper-Chloride Relationships in Photoluminescent and Electroluminescent Zinc Sulfide Phosphors" by A. L. Solomon and P. Goldberg (Abstract No. 69)
9:25 A.M.—"Effect of CdS on the Electroluminescence of ZnS:Cu Halide Phosphors" by Arthur Dreeben (Abstract No. 70)
9:50 A.M.—"ZnS:Cu, Cl and (Zn, Cd)S:Cu, Cl Electroluminescent Phosphors" by A. Wachtel (Abstract No. 71)
10:15 A.M.—"(Zn, Hg)S and (Zn, Cd, Hg)S Electroluminescent Phosphors" by A. Wachtel (Abstract No. 72)
10.40 A.M.—"Influence of Mg and Cd on the Electroluminescence of ZnS:Cu Phosphors" by P. M. Jaffe (Abstract No. 73)
11:05 A.M.—"Influence of Halogen-Coactivator on the Electroluminescence of ZnS:Cu Phosphors, I. Green Emission" by P. M. Jaffe (Abstract No. 74)
11:30 A.M.—"Electroluminescent Time Average Light Output of a ZnS:Se Phosphor" by J. Mudar, S. Nudelman, and K. Kamyszek (Abstract No. 75)
12:15 P.M.—Electronics Division Luncheon and Business Meeting in the Illinois Room, Mezzanine.

Electronics—Luminescence (cont'd)
Wednesday, May 4, 1960
with F. E. Williams presiding

(LINCOLN-DOUGLAS ROOMS, 18th floor)

2:00 P.M.—"Temperature-Induced Color Shifts in Electroluminescence" by L. W. Strock (Abstract No. 76)
2:20 P.M.—"On the Role of a Stimulating Action of Exciting Light in the Luminescence Kinetics of the Crystalline Phosphor ZnS-Cu" by L. A. Vinokurov and M. V. Fock (Abstract No. 77)
2:45 P.M.—"On the Valency States of Manganese in Phosphor Systems" by V. V. Osiko (Abstract No. 77A)
3:10 P.M.—"Physical Processes in Alkali Halide Phosphors Activated by Mercury-Like Ions" by Ch. B. Lushchik, I. W. Jaek, G. G. Lüdja, N. E. Lushchik, and K. K. Schwarz (Abstract No. 77B)
3:30-4:30 P.M.—Round-table discussion with F. E. Williams, moderator

ELECTRONICS—SEMICONDUCTORS

Monday, May 2, 1960
Crystal Growth
with F. H. Horn presiding

(GRAND BALLROOM, 19th floor)

9:15 A.M.—"An Apparatus for the Preparation of Semiconductor Grade Silicon" by R. C. Ellis, Jr. (Abstract No. 78)
9:35 A.M.—"Twin Generation and Seeding Mechanism in Dendritic Growth" by J. W. Faust, Jr., and H. F. John (Abstract No. 79)
9:55 A.M.—"Propagation of Germanium Dendrites" by R. G. Seidensticker and D. R. Hamilton (Abstract No. 80)
10:15 A.M.—"Some Aspects of Lateral Growth in Dendrites" by H. F. John and J. W. Faust, Jr. (Abstract No. 81)
10:35 A.M.—"Dendritic Growth Studies by Pulse Plating Techniques" by R. C. Smith (Abstract No. 82)
10:55 A.M.—"Growth of Atomically Flat Surfaces on Germanium Dendrites" by A. I. Bennett, R. L. Longini, and W. J. Smith (Abstract No. 83)
11:10 A.M.—"Dendritic Growth of Indium Antimonide" by J. W. Faust, Jr., H. Nicholson, and R. Moss (Abstract No. 84)
11:25 A.M.—"Preparation of Highly Arsenic-Doped Germanium" by P. L. Moody and A. J. Strauss (Abstract No. 85)
11:45 A.M.—Recent News Papers. Titles and short abstracts will be available at the Registration Desk.

Electronics—Semiconductors (cont'd)
Monday, May 2, 1960
Physical Chemistry of Semiconductors
with C. D. Thurmond presiding

(GRAND BALLROOM, 19th floor)

2:00 P. M.—"Crystal Model Studies of Growth Phenomena in III-V Compounds" by R. C. Sangster (Abstract No. 86)
2:25 P.M.—"Orientation Dependent Distribution Coefficients of Tellurium in Indium Antimonide Crystals" by J. B. Mullin (Abstract No. 87)
2:45 P.M.—"Anisotropic Segregation in InSb" by W. P. Allred and R. K. Willardson (Abstract No. 88)
3:05 P.M.—"Study of Copper Precipitation in Silicon Single Crystals" by G. H. Schwuttke (Abstract No. 89)

3:25 P.M.—"Reactions of Oxygen in Ge" by C. S. Fuller, C. D. Thurmond, and W. Kaiser (Abstract No. 90)
3:55 P.M.—"Preparation and Properties of Pseudo-Binary System GaAs-AlAs" by E. P. Stambaugh, J. I. Genco, and R. C. Himes (Abstract No. 91)
4:15 P.M.—"Preparation and Properties of the Pseudo-Binary System GaSb-AlSb" by J. F. Miller, H. L. Goering, and R. C. Himes (Abstract No. 92)
4:45 P.M.—"Phase Diagram for the Binary System Cadmium-Tellurium" by D. R. Mason and B. M. Kulwicki (Abstract No. 93)
5:05 P.M.—Recent News Papers. Titles and short abstracts will be available at the Registration Desk.

Electronics—Semiconductors (cont'd)
Tuesday, May 3, 1960
Compound Semiconductors
with F. D. Rosi presiding

(GRAND BALLROOM, 19th floor)

9:00 A.M.—"Effect of Inhomogeneities on the Hall Coefficient in InSb" by R. T. Bate (Abstract No. 94)
9:20 A.M.—"Properties of P-Type GaAs Prepared by Copper Diffusion" by F. D. Rosi, D. Meyerhofer, and R. V. Jensen (Abstract No. 95)
9:40 A.M.—"Preparation and Properties of ZnSb" by R. C. Bourke, R. Simon, and E. H. Lougher (Abstract No. 96)
10:00 A.M.—"Preparation and Properties of Gallium Phosphide" by C. J. Frosch, M. Gershenzon, and D. F. Gibbs (Abstract No. 97)
10:35 A.M.—"Preparation and Characteristics of P-N Junctions in Gallium Phosphide" by M. Gershenzon and R. M. Mikulyak (Abstract No. 98)
11:00 A.M.—"Preparation and Properties of Grown P-N Junctions of InSb" by H. C. Gorton and F. J. Reid (Abstract No. 99)
11:25 A.M.—"Influence of Crystal Size on the Spectral Response of Evaporated PbTe and PbSe Photoconductive Cells" by W. D. Lawson, A. S. Young, and F. A. Smith (Abstract No. 100)
11:50 A.M.—Recent News Papers. Titles and short abstracts will be available at the Registration Desk.
12:15 P. M.—Society Luncheon and Business Meeting in the Illinois Room, Mezzanine. Bill Veeck, President of the American League Champion White Sox, is guest speaker.

Electronics—Semiconductors (cont'd)
Tuesday, May 3, 1960
Surfaces; Oxide Films
with H. C. Gatos presiding

(GRAND BALLROOM, 19th floor)

2:00 P.M.—"On the Mechanism of Chemically Etching Germanium and Silicon" by D. R. Turner (Abstract No. 101)
2:30 P.M.—Recent News Papers. Titles and short abstracts will be available at the Registration Desk.
3:10 P.M.—"Experimental Micro-etch Techniques on Millimeter Wave-length Diodes" by D. G. Langlais (Abstract No. 102)
3:40 P.M.—"Oxide Masking of Solid SiO_2 against Boron" by Frank Keywell and Marshall Nechtow (Abstract No. 103)
4:00 P.M.—"Oxidation-Induced Diffusion in Silicon" by H. W. Cooper, E. I. Doucette, and R. A. Mehnert (Abstract No. 104)
5:00 P.M.—Palladium Medal Address by A. N. Frumkin in the Illinois Room, Mezzanine.

Electronics—Semiconductors (cont'd)
Wednesday, May 4, 1960
Diffusion
with P. H. Keck presiding

(GRAND BALLROOM, 19th floor)

9:00 A.M.—"Gaseous Diffusion of Arsenic in Germanium" by Carl Pihl and Kurt Lehovec (Abstract No. 105)
9:20 A.M.—"Open Tube Diffusion of Antimony into Germanium" by A. E. Blakeslee (Abstract No. 106)
9:40 A.M.—"Surface Concentration of Indium in Germanium from Gaseous Diffusion, II" by Karl Busen and Earl Meeks (Abstract No. 107)
10:00 A.M.—"A Diffusion Mask for Germanium" by E. L. Jordan and D. J. Donahue (Abstract No. 108)
10:30 A.M.—"Diffusion of Phosphorus in Silicon" by I. M. Mackintosh (Abstract No. 109)
11:00 A.M.—"Experimental Evidence of Surface Damage and Precipitation in Diffused Silicon" by L. Gerlach and R. Haberecht (Abstract No. 110)
11:20 A.M.—"Precision Lapping, Damage, and Diffusion" by C. J. Spector and T. E. McGahan (Abstract No. 111)
11:40 A.M.—"A New Solution to New Diffusion Equation and a New Application of Analog Solutions" by R. Moore and J. Colburn (Abstract No. 112)
12:15 P.M.—Electronics Division Luncheon and Business Meeting in the Illinois Room, Mezzanine.

Electronics—Semiconductors (cont'd)
Wednesday, May 4, 1960
Device Technology
with W. F. Leverton presiding

(GRAND BALLROOM, 19th floor)

2:00 P.M.—"Localized Breakdown in Diffused Silicon Junctions" by B. D. James and P. S. Flint (Abstract No. 113)
2:20 P.M.—Recent News Paper. There is no Abstract No. 114.
2:40 P.M.—"Production of a Germanium PNPN Switching Transistor by Post-Alloy Diffusion" by Fred Barson and John Gow (Abstract No. 115)
3:00 P. M.—"A High-Frequency PNP Diffused Silicon Transistor Produced by the Oxide Masking Technique" by O. Stavik (Abstract No. 116)
3:25 P. M.—Recent News Paper. There is no Abstract No. 117.
3:45 P.M.—"Physical Metallurgy in Semiconductor Device Fabrication, I. Gold Electrode Attachments to Silicon and Germanium" by L. Bernstein, B. G. Bender, and W. B. Warren (Abstract No. 118)
4:05 P.M.—"Physical Metallurgy in Semiconductor Device Fabrication, II. Studies of Gold-Aluminum and Gold-Tin in Electrode Attachment" by L. Bernstein, W. B. Warren, and B. G. Bender (Abstract No. 119)
4:25 P.M.—"Effects of High Aluminum Concentration in Emitters of Germanium Alloyed Power Transistors" by H. K. Becherer and Ernest Paskell (Abstract No. 120)

ELECTROTHERMICS AND METALLURGY

Monday, May 2, 1960
High-Purity Vanadium, Its Preparation, Properties, and Alloys
with D. J. Hansen presiding

(CHICAGO ROOM, Mezzanine)

9:15 A.M.—Introductory remarks by D. J. Hansen
9:20 A.M.—"Resources of Vanadium Minerals—Domestic and Foreign" by Staff Member of the Colorado School of Mines Research Foundation (Abstract No. 121)
9:50 A.M.—"Mining and Beneficiation of Vanadium Minerals" by Staff Member of the Colorado School of Mines Research Foundation (Abstract No. 122)
10:25 A.M.—"Mineralogy and Geochemistry of Vanadium in the Colorado Plateau" by A. D. Weeks (Abstract No. 123)
10:55 A.M.—"Vanadium by Metallic Reduction of Vanadium Trichloride" by M. J. Ferrante and F. E. Block (Abstract No. 124)
11:25 A.M.—"Electrorefining of Vanadium" by D. H. Baker, Jr., and F. R. Cattoir (Abstract No. 125)

Electrothermics and Metallurgy (cont'd)
Monday, May 2, 1960
High-Purity Vanadium, Its Preparation, Properties, and Alloys (cont'd)
with M. Schussler presiding

(CHICAGO ROOM, Mezzanine)

1:30 P.M.—"Preparation of High-Purity Vanadium Metal by the Iodide Refining Process" by O. N. Carlson and C. V. Owen (Abstract No. 126)
1:55 P.M.—"Consolidation and Fabrication of Vanadium" by T. W. Merrill (Abstract No. 127)

2:20 P.M.—"Mechanical Properties of Unalloyed Vanadium" by J. W. Farrell (Abstract No. 128)
2:45 P.M.—"Lattice Parameter and Expansion Coefficient of Vanadium" by W. J. James and M. E. Straumanis (Abstract No. 129)
3:15 P.M.—"Corrosion Properties of High-Purity Vanadium" by David Schlain and C. B. Kenahan (Abstract No. 129A)
3:40 P.M.—"On the Constitution of Some Vanadium-Base Binary and Ternary Systems and the Aging Characteristics of Selected Ternary Alloys" by S. Komjathy (Abstract No. 130)
4:05 P.M.—"Development of Improved Vanadium-Base Alloys for High-Temperature Purposes" by B. R. Rajala and R. J. Van Thyne (Abstract No. 131)
4:30 P.M.—"Properties of Vanadium-Base Alloys" by S. T. Wlodek (Abstract No. 132)

Electrothermics and Metallurgy (cont'd)
Tuesday, May 3, 1960
Methods of Reducing Iron Ores
with John Convey presiding

(CHICAGO ROOM, Mezzanine)

9:15 A.M.—Introductory remarks by E. M. Sherwood
9:20 A.M.—"Canada's Interest in Methods of Reducing Iron Ores" by John Convey (Abstract No. 133)
9:50 A.M.—"Economic and Process Factors Affecting the Selection of a Direct Reduction Process" by D. C. Brown (Abstract No. 134)
10:25 A.M.—"Solid Fuels and Reductants for the Beneficiation and Reduction of Iron Ores" by H. U. Ross (Abstract No. 135)
10:55 A.M.—"Gas Reactions in Reduction Processes" by J. Huebler (Abstract No. 136)
11:25 A.M.—Discussion of papers.

Electrothermics and Metallurgy (cont'd)
Tuesday, May 3, 1960
Methods of Reducing Iron Ores (cont'd)
with B. S. Old presiding

(CHICAGO ROOM, Mezzanine)

2:00 P.M.—"Magnetizing Roasting" by D. J. Hains (Abstract No. 137)
2:30 P.M.—"How Are the Blast Furnaces Doing?" by O. R. Rice (Abstract No. 138)
3:05 P.M.—"Performance of the First Commercial H-Iron Reduction Plant" by H. H. Stotler and R. A. Lubker (Abstract No. 139)
3:35 P.M.—"The Nu-Iron Process—A Fluidized Bed Process for Reducing Iron Ore" by T. F. Reed, J. C. Agarwal, and E. H. Shipley (Abstract No. 140)
4:05 P.M.—Discussion of papers.
5:00 P.M.—Palladium Medal Address by J. N. Frumkin in the Illinois Room, Mezzanine

Electrothermics and Metallurgy (cont'd)
Wednesday, May 4, 1960
Methods of Reducing Iron Ores (cont'd)
with R. B. Mears presiding

(CHICAGO ROOM, Mezzanine)

9:30 A.M.—"Direct Reduction of Fine Iron Ore Concentrates in a Self-Agglomerating Fluidized Bed" by F. M. Stephens, Jr., and B. G. Langston (Abstract No. 141)
10:00 A.M.—"The Esso Research-Little Process" by R. W. Hyde (Abstract No. 142)
10:35 A.M.—"Present Direct Reduction Research at Stora Kopparberg, Sweden" by T. O. Dormsjo (Abstract No. 143)
11:05 A.M.—"The R-N Process" by J. S. Breitenstein (Abstract No. 144)
11:35 A.M.—Discussion of papers.
12:30 P.M.—Electrothermics and Metallurgy Division Luncheon and Business Meeting in Parlor E, Mezzanine.

Electrothermics and Metallurgy (cont'd)
Wednesday, May 4, 1960
Methods of Reducing Iron Ores (cont'd)
with A. C. Haskell presiding

(CHICAGO ROOM, Mezzanine)

2:00 P.M.—"Reasons for the Co-Current Kiln in Direct Reduction" by Horace Freeman (Abstract No. 145)
2:30 P.M.—"New Agglomeration-Reduction Process for Iron Ores" by Will Mitchell, Jr. (Abstract No. 146)
3:00 P.M.—"Direct Reduction Research at IRSID" by J. Astier (Abstract No. 147)
3:35 P.M.—"The Jet Smelting Process" by R. L. Cavanagh (Abstract No. 148)
4:05 P.M.—"New Pre-reduction Processes" by H. Walde (Abstract No. 149)
4:35 P.M.—Discussion of papers.

Electrothermics and Metallurgy (cont'd)
Thursday, May 5, 1960
Methods of Reducing Iron Ores (cont'd)
with C. L. Mantell presiding

(CHICAGO ROOM, Mezzanine)

9:30 A.M.—"Consideration of Fuel Requirements for Iron Ore Reduction" by R. Wild (Abstract No. 150)
10:00 A.M.—"Strategic-Udy Process for Smelting Iron Ores" by M. C. Udy (Abstract No. 151)
10:35 A.M.—"Technical and Economic Factors to Be Considered in the Electric Furnace Reduction of Iron Ores" by N. H. Keyser (Abstract No. 152)
11:05 A.M.—"Electric Smelting of Iron Ores" by F. C. Collin (Abstract No. 153)
11:35 A.M.—Discussion of papers.

Electrothermics and Metallurgy (cont'd)
Thursday, May 5, 1960
Methods of Reducing Iron Ores (cont'd)
with W. M. Armstrong presiding

(CHICAGO ROOM, Mezzanine)

2:00-4:00 P.M.—General discussion of methods of reducing iron ores (questions and answers, discussion and remarks from the floor). Summary of the conference by W. M. Armstrong.

Electrothermics and Metallurgy (cont'd)
Tuesday, May 3, 1960
Rhenium
with B. W. Gonser and B. J. Clemmer presiding

(PRESS GALLERY, 18th floor)

9:00 A.M.—Introductory remarks by B. W. Gonser
9:05 A.M.—"Mineralogical and Geological Occurrence of Rhenium" by S. R. Zimmerley (Abstract No. 154)
9:30 A.M.—"A Survey of the Different Methods for the Determination of Rhenium" by Suzanne Tribalat (Abstract No. 155)
9:55 A.M.—"Spectrophotometric Determination of Microgram Quantities of Rhenium by E. E. Malouf and R. J. Heaney (Abstract No. 156)
10:25 A.M.—"Some Recent Developments in the Halide and Ditertiary Arsine Chemistry of Rhenium" by J. E. Fergusson and R. S. Nyholm (Abstract No. 157)
10:50 A.M.—"Spectrochemical Analysis of Rhenium Metal Powder" by J. H. Allwein (Abstract No. 158)
11:15 A.M.—"The Crystal Chemistry of the Compounds of Rhenium with Transition Metals" by N. V. Ageev and V. Sh. Shehtman (Abstract No. 159)
12:15 P.M.—Society Luncheon and Business Meeting in the Illinois Room, Mezzanine. Bill Veeck, President of the American League Champion Chicago White Sox, is guest speaker.

Electrothermics and Metallurgy (cont'd)
Tuesday, May 3, 1960
Rhenium (cont'd)
with Chester Sims and A. D. Melaven presiding

(PRESS GALLERY, 18th floor)

2:00 P.M.—"Metallurgical Processes for Recovery of Rhenium from Flue Dusts and Gases" by E. E. Malouf, J. D. Prater, and S. R. Zimmerley (Abstract No. 160)
2:25 P.M.—"Process for Producing Pure Rhenium and Its Compounds" by Marie-Louise Jungfleisch and Henri Ruff (Abstract No. 161)
2:50 P.M.—"Rhenium Powder Metallurgy and Fabrication of Wrought Products" by J. H. Port (Abstract No. 162)
3:20 P.M.—"Behavior of Rhenium during Hot-Working" by Guy Lebert (Abstract No. 163)
3:45 P.M.—"Powder Metallurgy of Refractory Alloys Containing Rhenium" by Marie-Louise Jungfleisch and Jean Fabry (Abstract No. 164)

Electrothermics and Metallurgy (cont'd)
Wednesday, May 4, 1960
Rhenium (cont'd)
with R. I. Jaffee presiding

(PRESS GALLERY, 18th floor)

9:15 A.M.—"Certain Physical Properties of Rhenium and Its Alloys" by E. M. Savitski and M. A. Tylkina (Abstract No. 165)

9:40 A.M.—"Rhenium and Transition Metals Phase Diagrams" by E. M. Savitski and M. A. Tylkina (Abstract No. 166)

10:05 A.M.—No title received, by G. A. Geach (Abstract No. 167)

10:35 A.M.—"The Workability and Mechanical Properties of Tungsten- and Molybdenum-Base Alloys Containing Rhenium" by D. J. Maykuth, F. C. Holden, and R. I. Jaffee (Abstract No. 168)

11:00 A.M.—"Evaluation of Rhenium as an Electrical Contact Material" by V. E. Heil, T. C. Murphy, and L. F. Neely (Abstract No. 169)

12:30 P.M.—Electrothermics and Metallurgy Division Luncheon and Business Meeting in Parlor E, Mezzanine.

Electrothermics and Metallurgy (cont'd)
Wednesday, May 4, 1960
Rhenium (cont'd)
with J. H. Port presiding

(PRESS GALLERY, 18th floor)

2:00 P.M.—"Thermocouples for 3000°C Using Rhenium Alloys" by J. C. Lachman and J. A. McGurty (Abstract No. 170)

2:25 P.M.—"Rhenium in Electronics" by G. B. Gaines (Abstract No. 171)

2:50 P.M.—"Catalytic Hydrogenation of Sulfuretted Organic Compounds in the Presence of Rhenium Heptasulfide" by Constantin Aretos and Jean Vialle (Abstract No. 172)

3:20 P.M.—"On the Use of Pure or Alloyed Rhenium in Oxide Coated Cathodes" by M. P. Warin (Abstract No. 173)

3:45 P.M.—"Electroplating of Rhenium by G. S. Root and John Beach (Abstract No. 174)

Electrothermics and Metallurgy (cont'd)
Thursday, May 5, 1960
Refractory and Reactive Metals
with E. M. Sherwood presiding

(PRESS GALLERY, 18th floor)

9:30 A.M.—"Adhesion of Vapor Deposited Molybdenum Coatings'" by S. T. Wlodek and John Wulff (Abstract No. 175)

10:00 A.M.—"Kinetics of the Oxidation of Pure Tungsten from 500° to 1300°C" by E. A. Gulbransen and K. F. Andrew (Abstract No. 176)

10:30 A.M.—"Preparation and Refining of Yttrium Metal by Y-Mg Intermediate Alloy Process" by O. N. Carlson, J. A. Haefling, F. A. Schmidt, and F. H. Spedding (Abstract No. 177)

INDUSTRIAL ELECTROLYTIC

Monday, May 2, 1960
General Session
with W. D. Sherrow presiding

(ILLINOIS ROOM, Mezzanine)

10:00 A.M.—Introductory remarks by J. C. Cole

10:05 A.M.—"Graphite Anodes in Brine Electrolysis, IV. Effect of Anolyte pH on Corrosion Rate in Chlor-Alkali Cells" by L. E. Vaaler (Abstract No. 178)

10:30 A.M.—"Chemical Engineering Studies on the Decomposition Packed Tower of the Amalgam on the Chlorine-Caustic Industry" by Shinzo Okada, Shiro Yoshizawa, and Fumio Hine (Abstract No. 179)

11:00 A.M.—"A Small-Scale Electro-Organic Chemical Plant" by J. W. Drew and G. J. Moll (Abstract No. 180)

11:30 A.M.—"Intermediate Temperature Fuel Cells" by G. V. Elmore and H. A. Tanner (Abstract No. 181)

12:30 P.M.—Industrial Electrolytic Division Luncheon and Business Meeting in the Illinois Room, Mezzanine. Presentation of the Annual Chlor-Alkali Report by C. A. Hampel and N. J. Ehlers.

Industrial Electrolytic (cont'd)
Monday, May 2, 1960
General Session (cont'd)
with N. J. Ehlers presiding

(ILLINOIS ROOM, Mezzanine)

2:45 P.M.—"Electrolytic Reduction of Thorium Oxide" by L. H. Meyer (Abstract No. 182)

3:15 P.M.—"Metal Mists and Aluminum Losses in the Hall Process" by W. E. Haupin (Abstract No. 183)

3:45 P.M.—"Preparation of Boron from Boron Carbide" by D. R. Stern (Abstract No. 184)

4:15 P.M.—"Lead Dioxide Anode in the Preparation of Perchlorates" by K. C. Narasimham, S. Sundararajan, and H. V. K. Udupa (Abstract No. 185)

THEORETICAL ELECTROCHEMISTRY—INDUSTRIAL ELECTROLYTIC

Joint Symposium
Tuesday, May 3, 1960
Electrochemical Engineering
Applied Electrode Kinetics
with C. W. Tobias presiding

(CENTURY ROOM, 19th floor)

9:15 A.M.—Introductory remarks by C. W. Tobias

9:30 A.M.—"The Measurement of Polarization" by Ernest Yeager (Abstract No. 186)

10:20 A.M.—"Applied Electrochemical Kinetics" by Paul Delahay (Abstract No. 187)

11:10 A.M.—"Electrocrystallization and Surface Films" by D. A. Vermilyea (Abstract No. 188)

Theoretical Electrochemistry—Industrial Electrolytic (cont'd)
Joint Symposium
Tuesday, May 3, 1960
Electrochemical Engineering (cont'd)
Transport Processes in Electrolytic Cells
with Ralph Roberts presiding

(CENTURY ROOM, 19th floor)

2:00 P.M.—"Mass Transport in Electrolysis, Hydrodynamic Factors" by Norbert Ibl (Abstract No. 189)

2:50 P.M.—"Heat Transport and Temperature Distribution in Cells" by T. R. Beck (Abstract No. 190)

3:40 P.M.—Panel discussion, C. W. Tobias presiding. Members of the panel: Sidney Barnartt, J. V. Petrocelli, and B. E. Conway.

5:00 P.M.—Palladium Medal Address by A. N. Frumkin in the Illinois Room, Mezzanine.

Theoretical Electrochemistry—Industrial Electrolytic (cont'd)
Joint Symposium
Wednesday, May 4, 1960
Electrochemical Engineering (cont'd)
Distribution of Potential and Current in Electrolytic Cells
with R. F. Bechtold presiding

(CENTURY ROOM, 19th floor)

9:30 A.M.—"Effect of Geometry on Current Distribution in Industrial Electrolytic Cells" by Scott Lynn and C. W. Tobias (Abstract No. 191)

10:20 A.M.—"Effect of Nongeometric Factors on Current Distribution" by E. A. Grens and C. W. Tobias (Abstract No. 192)

11:10 A.M.—"Electrode Materials and Materials of Construction" by M. S. Kircher and J. E. Currey (Abstract No. 193)

Theoretical Electrochemistry—Industrial Electrolytic (Cont'd)
Joint Symposium
Wednesday, May 4, 1960
Electrochemical Engineering (cont'd)
Scale Up and Measurements on the Plant Scale
with J. C. Cole presiding
(CENTURY ROOM, 19th floor)

2:00 P.M.—"The Problem of Scale Up of Electrolytic Processes" by R. B. MacMullin (Abstract No. 194)

2:50 P.M.—"Measurements on a Plant Scale" by C. J. Dobratz (Abstract No. 195)

3:40 P.M.—Panel discussion, R. F. Bechtold presiding. Members of the panel: Norbert Ibl, N. J. Johnson, and R. B. MacMullin.

THEORETICAL ELECTROCHEMISTRY

Thursday, May 5, 1960
with L. G. Longsworth presiding

(LINCOLN-DOUGLAS ROOM, 18th floor)

9:00 A.M.—"Double Layer Structure and Relaxation Methods for Fast Electrode Processes" by Hiroaki Matsuda and Paul Delahay (Abstract No. 196)

9:20 A.M.—"The Interpretation of Measurements of Potential Decay on Open Circuit" by P. C. Milner (Abstract No. 197)
9:40 A.M.—"Cathodic Processes on Passive Zirconium" by R. E. Meyer (Abstract No. 198)
10:00 A.M.—"Kinetics of Anodic Processes in Carboxylic Acids" by B. E. Conway and M. Dzieciuch (Abstract No. 199)
10:20 A.M.—"Faradaic Rectification with Control of Alternating Potential Variations—Application to Electrode Kinetics for Fast Processes" by Hiroaki Matsuda and Paul Delahay (Abstract No. 200)
10:40 A.M.—"The Influence of Cations on the Differential Capacity of the Mercury Dropping Electrode in Methanol and Ethanol Solutions of Electrolytes" by S. Minc (Abstract No. 201)
11:00 A.M.—"Irreversible Thermodynamics in Electrochemistry" by A. J. deBethune (Abstract No. 202)
11:30 A.M.—Theoretical Electrochemistry Division Business Meeting in the Lincoln-Douglas Rooms, 18th floor.

Theoretical Electrochemistry (cont'd)
Thursday, May 5, 1960
with Paul Delahay presiding
(LINCOLN-DOUGLAS ROOMS, 18th floor)

2:00 P.M.—"Potentials in the System, Cr(II)-Cr(III), at Various Electrodes" by K. B. Morris (Abstract No. 203)
2:20 P.M.—"Electrochemical Study of Metallic Oxides in Fused Lithium Chloride-Potassium Chloride Eutectic" by H. A. Laitinen and B. B. Bhatia (Abstract No. 204)
2:40 P.M.—"Gas-Phase Charged and Electrolytically Charged β-Pd-H Alloys" by J. P. Hoare (Abstract No. 205)
3:00 P.M.—"Kinetics of Cathodic Hydrogen and Deuterium Evolution" by B. E. Conway (Abstract No. 206)
3:20 P.M.—"Behavior of Hydrogen at Oxidized Platinized Platinum Electrodes" by N. J. Ward and T. C. Franklin (Abstract No. 207)
3:40 P.M.—"Transient Strain Induced Electrode Potentials" by Eric Baum, W. F. Seyer, and Ken Nobe (Abstract No. 208)
4:00 P.M.—"Electrocapillary Studies on Solid Metals" by D. N. Staicopoulos (Abstract No. 209)
4:20 P.M.—"A New Model for Evaluating the Conductivities of Dispersions" by R. E. Meredith and C. W. Tobias (Abstract No. 210)

Abstracts

ELECTRIC INSULATION

Abstract No. 1

Electrolytic Oxide Films

J. Burnham, 10960 Verano Drive, Los Angeles 24, Calif.

The nature of the dielectric film in electrolytic capacitors has been a subject of continuing interest over the past fifty years and it is a surprising thing that not more is known about the nature of these films, their chemical and physical properties, or their mechanism of formation.

The increasing economic importance of other metals in the electrolytic capacitor field has renewed interest in the fundamental properties of anodic oxides and a considerable amount of recent work covers the determination of thickness, dielectric constant and electrical resistivity.

The advent of the diode-capacitor with voltage sensitive properties and the solid electrolytic capacitor developed by the Bell Laboratories has increased interest in the interface which is the seat of the dielectric and it appears that we are dealing in both cases with a p-n junction whose properties are not yet well understood. Recent work in the above areas is discussed.

Abstract No. 2

Conduction, Storage, and Photoelectric Phenomena in Anodic Aluminum Oxide Films

Kurt Lehovec, Sprague Electric Co., North Adams, Mass.

The paper covers unpublished work by Dr. Hans Reinheimmer, Alma Marcus, and the author. We have studied the d-c current voltage characteristic of anodically polarized aluminum oxide films sandwiched between aluminum and an electrolyte. The well-known pronounced polarization effects have been observed and the time dependence of polarization has been analyzed, using a theoretical model based on trapping centers in the oxide film. When the applied voltage is removed after a certain time of application and the anodic film is short circuited externally, it is found that an electric current flows in the external circuit which decreases approximately inversely with time over periods of many hours, and this dependence is analyzed theoretically. Illumination during this discharge period changes the discharge current and the spectral distribution of this photo effect is discussed. Results of certain measurements are also discussed.

Abstract No. 3

Impedance Characteristics of Anodic Oxides

L. Young, British Columbia Research Council, University of British Columbia, Vancouver 8, B.C., Canada

Impedance characteristics of anodic oxide films are determined by several factors which are somewhat difficult to disentangle. These are as follows: (A) Dielectric properties of the oxide material as expressed by dielectric constant and tan δ (or in alternative notation by real and imaginary dielectric constants). The dielectric losses at low frequencies are probably due largely to ionic relaxation processes which, of course, also contribute to the dielectric constant. (B) Weak places, such as fissures, pores, or local areas of conducting oxide, provide leakage circuit-elements in parallel with the film proper. (C) Interfacial effects, including electrical double layer effects at the oxide solution interface. (D) Effects due to d-c electronic conductivity of part or all of the film. A review is given of these factors and the degree to which they allow the complicated data in the literature to be explained.

Abstract No. 4

Tantalum Anode Reactions

Donald Stephenson and **Robert Russ,** Transitor Electronics, Inc., Bennington, Vt.

When tantalum is made the anode in an electrolytic cell and voltage applied, several reactions can take place. The result of these chemical reactions may be an etch, a polish, or polarization of the tantalum resulting in anodic oxidation. The variables which control these reactions may be the choice of electrolyte, or it may be current density, temperature, electrode position, and many others. An attempt to summarize and explain these effects is made.

Abstract No. 5

Dielectric Characteristics of Tantalum Anodic Oxide Films As Related to Film Structure

D. Mohler, Capacitor Dept., General Electric Co., Hudson Falls, N. Y.

The variation of the dielectric characteristics of tantalum anodic films cannot be explained on the basis of bulk metal impurities alone. The thin air oxide film on tantalum determines the structural properties of anodic films formed thereon. The dielectric characteristics in turn, are related to the physical and chemical structure of the film. Electron diffraction and spectrographic data support this view.

Abstract No. 6

Hydrated Oxide Films on Aluminum

Dietrich Altenpohl, Aluminum-Walzwerke Singen, Singen/Hohentwiel, West Germany

Hydrated oxide films on aluminum are of importance for the corrosion protection of aluminum in contact

with water solutions or in contact with atmosphere. The growth of hydrated oxide on aluminum surfaces depends on temperature and time of interaction between aluminum and H_2O, but also on the interaction with small impurities in the water or in the metal. Hydrated oxide films are of importance for the dielectric properties of electrolytic capacitors, and corresponding investigations are described.

Abstract No. 7

Anodic Formation of Aluminum Oxide Films, I. The Influence of Surface Preparation on Film Properties

W. E. Tragert and **J. R. Rairden,** Research Lab., General Electric Co., Schenectady, N. Y.

It is shown that the effect of various surface cleaning agents on anodizing behavior is attributable to the complexing action of specific anions with the residual hydrous alumina surface film. The effectiveness of matrix films formed prior to anodizing is shown to depend on the chemical as well as electrical conditions of their formation. A generalization is drawn between the ultimate dielectric properties of anodic films and the prior chemical and electrolytic treatment of the aluminum.

Abstract No. 8

Anodic Formation of Aluminum Oxide Films, II. Effect of Various Electrical Forming Conditions on Film Properties

W. E. Tragert and **J. R. Rairden,** Research Lab., General Electric Co., Schenectady, N. Y.

The two principal anodic film forming techniques, constant current and constant voltage, are examined with respect to the resultant structure and composition of the films. It is shown that the ultimate electrical properties of the film can be related to composition and hence to forming technique. The influence of reverse polarization is discussed. The effect of electrolyte composition on film structure and composition is considered.

Abstract No. 9

Determination of the Thickness of Thin Porous Oxide Films on Aluminum

M. S. Hunter and **P. F. Towner,** Aluminum Co. of America, P.O. Box 772, New Kensington, Pa.

A method is described for measuring the thickness of thin porous oxide films on aluminum employing the grazing angle interference colors characteristic of thin transparent films. In conjunction with oxide film step gauges formed under precisely controlled conditions, measurements to about 7Å are possible. Application of the method for measuring film growth in various solutions and in the evaluation of the characteristics of barrier-type electrolytes is also demonstrated.

Abstract No. 10

Capacitor Grade Tantalum

L. H. Belz, Kawecki Chemical Co., Boyertown, Pa.

The extraction and refining of tantalum metal is reviewed. The production of high-purity powder and foil is described along with a discussion of the specifications and functional quality of capacitor grade tantalum. Powder types are tabulated and powder characteristics are related to sintered anode design. The production of sintered anodes is also reviewed.

Abstract No. 11

Measurement of the Specific Surface Area of Tantalum Powders and Sintered Anodes

W. G. Guldner and **C. C. Houtz,** Bell Telephone Labs., Murray Hill, N. J.

In the production of porous anodes for electrolytic capacitors, the anodes are prepared by compressing and sintering tantalum powder. Since the capacitance of the anodes as used in capacitors is proportional to their surface area, this study was initiated to measure the surface areas of powders obtained from various suppliers and of sintered pellets prepared from these powders. The data show the loss in surface area for different powders as a result of sintering. Also, a comparison is shown of the specific surface area of pellets obtained by gas adsorption with that area calculated from capacitance measurements. Specific surface areas were measured by the Brunauer, Emmett, and Teller method using krypton at liquid nitrogen temperature.

Abstract No. 12

Some Physical Properties of Metallic Tantalum

J. I. Budnick, IBM Research Lab., Poughkeepsie, N. Y.

Studies of the purification of tantalum metal are described with emphasis on the usefulness of measurements of the superconducting properties as a powerful tool for evaluating sample perfection. Very small amounts of gaseous impurities have pronounced effects on the superconducting properties. The nuclear magnetic resonance absorption, which for tantalum is extremely sensitive to strain and impurities, has been observed in metal foil.

Abstract No. 13

Low-Temperature Sintering of Tantalum Anodes

C. J. B. Fincham and **G. J. Villani,** Metals Div., National Research Corp., Cambridge, Mass.

The sintering of tantalum anodes at temperatures lower than those customarily used in the capacitor industry appears to be a promising approach to obtaining substantially higher capacitance per unit weight or volume. Using tantalum powders of differing chemical purities and particle size distributions, a study was made of the chemical and electrical properties of anodes sintered at low temperatures, i.e., down to about 1500°C.

Abstract No. 14

Determination of the Thickness of Anodic Oxide Films by the Spectrophotometric Method in Conjunction with the Abelès Method for the Refractive Index

L. Young and **J. E. Orme,** British Columbia Research Council, University of British Columbia, Vancouver 8, B.C., Canada

The study of anodic oxide films has reached the stage at which the precise determination of the film thickness is required in absolute (as opposed to arbitrary) units. Most of the various methods of determining thickness (Faraday's law, weighing, a-c capacity) require assumptions about the true area and the composition or other properties of the film as well as a knowledge of parameters such as the density or dielectric constant, which may vary with the formation procedure and are not easily determined with sufficient accuracy. The spectrophotometric method gives a rapid and accurate measure of increments of thickness or, if the optical constants of the metal are accurately known, of absolute thickness. A knowledge of the refractive index at one wave length is required, and, if the film is uniform through its thickness, this information may be obtained with good accuracy by the Abelès method. Some applications of these techniques are discussed.

Abstract No. 15

Electrolytic Etching of Dense Tantalum

A. L. Jenny and **R. A. Ruscetta,** Capacitor Dept., General Electric Co., Irmo, S. C.

A practical method of etching dense tantalum for the purpose of magnifying its effective surface area is described. The degree of surface area magnification is related to such parameters as electrolyte composition, anodic current density, temperature, and the characteristics of metal specimens to be treated. The decrease in surface area magnification as a function of post-etch anodizing voltage apparently signifies the filling-in of certain etch pits with tantalum oxide and gives a clue to the size of these pits.

Abstract No. 16

Niobium (Columbium) Solid Electrolytic Capacitors

N. Schwartz, M. Gresh, and **S. Karlik,** Bell Telephone Labs., Inc., Murray Hill, N. J.

Field crystallization of the amorphous niobium oxide film has been found to be a determining factor for the properties of niobium solid electrolytic capacitors. Purity of the porous anodes as dependent on the sintering conditions, formation temperature and voltage, and formation electrolytes, parameters all known to control the initiation of crystallization, have been correlated with the initial and life test properties of these capacitors. The initial properties of niobium solid electrolytic capacitors compare favorably with equivalent tantalum components. However, with the current purity of niobium powder, only units with operating voltages up to 20 v survive a life test at 85°C, with the failures of capacitors rated at higher voltages attributed to the partial crystallization of the amorphous film during formation.

Abstract No. 17

Columbium (Niobium) Electrolytic Capacitors

A. Shtasel and **H. T. Knight,** Fansteel Metallurgical Corp., North Chicago, Ill.

Columbium metal was evaluated for wet and solid electrolytic capacitors. Anodic oxidation properties were studied in relation to the manufacture of capacitors. The thickness of the oxide films on columbium and tantalum as a function of the forming voltage was compared. The choice of forming and fill electrolytes was found to be more limited with columbium than with tantalum. Solid columbium capacitors with electrical properties comparable to similar tantalum units were operated as high as 35 v. Life tests at 85°C of 10-v wet and solid columbium capacitors were irradiated to a total integrated fast neutron flux of 3.9×10^{16} neutrons /cm^2 without significant damage.

Abstract No. 18

Silicon Nitride Thin Film Dielectric

C. R. Barnes and **C. R. Geesner,** Electronic Technology Lab., Wright Air Development Center, Wright-Patterson Air Force Base, Ohio

Thin adherent nonporous films of pure silicon nitride have been deposited from the vapor phase on hot molybdenum substrates by pyrolytic deposition. Such films, when incorporated between molybdenum plates to form capacitors, were found to maintain satisfactory dielectric properties up to and above 600°C. Silicon nitride coatings deposited by the method herein described also offer a convenient and effective method of encapsulation for protecting metal surfaces from atmospheric oxidation up to and above 1000°C.

Abstract No. 19

Properties of Anodically Formed Oxide Films on Tungsten

H. W. Pitman and **D. C. Hamby,** Linfield Research Institute, McMinnville, Oreg.

Properties of anodically formed oxide films on tungsten have been investigated by coulometric, optical interference, and capacitance methods in the current density range from 0.037 to 8.6 ma/cm^2. The ionic current density in film formation shows an exponential dependence on the field in the film. Properties discussed are the field in the film and current efficiency of film formation as functions of current density, and the refractive index, optical dispersion, density, and effective dielectric constant.

Abstract No. 20

Ion Size Effect and Mechanism of Electrolytic Rectification

P. F. Schmidt, Westinghouse Research Labs., Pittsburgh 35, Pa., and **F. Huber** and **R. F. Schwarz,** Philco Corp., Philadelphia 34, Pa.

The electron flow through anodic oxide films under cathodic bias has been investigated as a function of cation size. Both the magnitude of the cathodic current and the activation energies for cathodic current flow were found to depend on the size of the cation in solution. Specific adsorption of some cations may exclude other cations from the interface. The existence of a surface barrier of about 1 v and of about 250Å thickness has been proven. The barriers to electron flow inside the oxide and at its interfaces is discussed.

Abstract No. 21

The A-C Properties of Tantalum Solid Electrolytic Capacitors

D. A. McLean, Bell Telephone Labs., Inc., Murray Hill, N. J.

The a-c losses in tantalum solid electrolytic capacitors are of two kinds: those in the dielectric oxide film and those in the manganese oxide semiconductor. By making measurements at two or more suitable frequencies these losses can be separated. The method of separation is described in detail and illustrated with a number of examples. Use of this type of analysis in fundamental studies of materials and processes and in preparation of specifications is discussed. A theoretical treatment of the series losses in the MnO_2 of a cylindrical porous anode is given. A relation between losses in the dielectric and the frequency coefficient of capacitance is illustrated and discussed.

Abstract No. 22

A Mathematical Model for the Porous Type Tantalum Anode Capacitor

J. S. Fisher, Bell Telephone Labs., Inc., Merrimack Valley, Mass.

Reducing the physical size of capacitors while maintaining large values of capacitance can cause their high-frequency behavior to become affected strongly by distributed capacitance and electrode resistance. A good understanding of these effects can generally be acquired by analyzing the capacitor structure with transmission line techniques. The behavior of porous tantalum anode capacitors has been analyzed by such techniques, showing the effect of the various parameters on their high-frequency performance.

Abstract No. 23

Cathodic Depolarization in Tantalum Electrolytic Capacitors

T. C. O'Nan, P. R. Mallory & Co., Inc., Indianapolis, Ind.

For maximum capacitance and minimum internal resistance, the cathode should be nonpolarizable, nonfilming, and nongassing while being substantially inert to the electrolyte. It should respond electrochemically to pulsating (a-c) current—dissolving while anodic and redepositing while cathodic. Commonly employed cathode materials approach this circumstance, but electrochemical activity from a-c balance out, leaving no metal ions in solution. Therefore, d-c leakage currents discharge hydrogen, with attendant gas polarization and pressure increase. Cathodic depolarization minimizes these effects. Certain metal ions, which deposit and redissolve electrochemically at the cathode with high efficiency in preference to hydrogen, may perform successfully, if the deposit is adequately conductive and inert to the electrolyte. Extended depolarization capacity may be supplied through use of the proper form of excess solid material. Soluble "redox systems" may also offer cathodic depolarization. Representative systems are discussed from both theoretical and practical view points.

Abstract No. 24

Cell and Thermoelectric Effects of Tantalum Electrolytic Capacitors

J. M. Law and **W. C. Richards,** Fansteel Metallurgical Corp., North Chicago, Ill.

A voltage is normally present across the terminals of electrically isolated electrolytic tantalum capacitors. The magnitude, cause, and source impedance of this voltage were investigated. Voltages in excess of 1 v

were generally due to dielectric hysteresis, or to a charge remaining from previous electrification. Wet-electrolyte units appear to generate a small high-impedance cell emf between the tantalum anode and the silver case. Solid-electrolyte units appear to generate thermoelectrically a small high-impedance emf.

Abstract No. 25

A Selective Electrochemical Etching Procedure to Improve D-C Characteristics of Oxide Film Capacitors

R. W. Berry, N. Schwartz, M. J. Urban (present address: Weston Div., Daystrom Inc., Newark, N. J.), and **M. Gresh,** Bell Telephone Labs., Inc., Murray Hill, N. J.

The d-c leakage of anodic oxide film capacitors is presumed to be associated primarily with discrete defects in the dielectric. After the initial film has been grown by anodizing, an electrochemical etch using a halide in a nonaqueous solvent as the electrolyte removes the underlying anode metal, with its associated impurities, only at defects where appreciable current exists. A more coherent oxide film can then be regrown in a subsequent anodization, and lower d-c leakages result. The paper discusses the application of this technique to tantalum printed capacitors and to aluminum and niobium solid electrolytic capacitors.

Abstract No. 26

Equivalent Series Resistance of Anodically Formed Oxide Films on Aluminum

W. J. Bernard, Electrolytic Capacitor Div., Research and Engineering Dept., Sprague Electric Co., North Adams, Mass.

Measurement of the oxide film contribution to the equivalent series resistance of an electrolytic cell leads to an understanding of the temperature- and frequency-dependent behavior of aluminum electrolytic capacitors. An experimental procedure is described which allows accurate measurements of oxide film resistances. Interpretation and application of the data to the power factor of electrolytic capacitors are given.

Abstract No. 27

Factors Determining Allowable Ripple Current at Various Frequencies in Aluminum Electrolytic Capacitors

R. Lane and **A. Bennett,** Pyramid Electric Co., Darlington, S. C.

The variation in allowable ripple current with changes in frequency for aluminum electrolytic capacitors is discussed. The effects of various materials and processing methods on the ability to operate such capacitors at high values of ripple current are described.

Abstract No. 28

500°C Capacitors

R. J. Stamets and **R. A. West,** Capacitor Dept., General Electric Co., Hudson Falls, N. Y.

Aluminum and tantalum, the conventional electrolytic capacitor anode materials, have serious limitations for use at high temperatures. However, use of a new anode material permits operation of an anodically formed aluminum oxide dielectric in a stacked or wound foil construction at temperatures as high as 500°C (932°F). Capacitance values up to 0.06 μf have been made. Insulation resistance values as high as 40 megohm μf at 500°C have been obtained.

Abstract No. 29

A Novel Low Voltage Electrolytic Capacitor without Conventional Spacers

A. J. Catotti and **R. A. West,** Capacitor Dept., General Electric Co., Hudson Falls, N. Y.

Anodization of aluminum in certain acid solutions results in a porous oxide film. Novel low voltage electrolytic capacitors are described which utilize the barrier portion of this aluminum oxide film as the dielectric and the porous portion as the separator. Means of regulating the thicknesses of these two layers are discussed. Electrical characteristics and life test data are presented for a number of voltages and designs.

Abstract No. 30

Volume Resistivity of Ammonium Ethylene Glycoborate Electrolytes

C. C. Houtz, Bell Telephone Labs., Inc., Murray Hill, N. J.

While the ammonium ethylene glycoborates are used commonly as electrolytes in the manufacture of aluminum electrolytic capacitors, little information is available in the literature which relates composition to volume resistivity. Electrolytes were prepared in a range of proportions of ammonium hydroxide, ethylene glycol and boric acid. Resistivities at 1000 cps are shown on ternary diagrams for temperatures of 30° and 85°C. Effects on resistivity are shown for variation in reaction time and temperature and other preparation variables.

Abstract No. 31

Electrical Properties of Some Aliphatic Acids and Alcohols

A. M. Parks, International Business Machine Corp., Yorktown Heights, N. Y.

The dielectric constants and losses of some relatively low molecular weight aliphatic acids and alcohols have been measured in an Elliott cell over a frequency range of 100-100,000 cps and a temperature range of 0°-100°C. The dipole moments have been estimated from measurements on benzene solutions and the volume resistivities calculated from resistance measurements. The effect of monohydroxyl or carboxyl substitution, chain length, and position of substitution as well as the most probable configuration are discussed in terms of these electrical properties.

Abstract No. 32

Effects of Tropical Exposure on the Electrical Properties of Insulating Materials

L. J. Frisco, Dielectrics Lab., The Johns Hopkins University, Baltimore 2, Md.

Measurements of dielectric constant, dissipation factor, d-c surface and volume resistivity, flashover strength, and dielectric strength have been made on specimens which were stored at the Naval Research Laboratory, Tropical Exposure Site, Panama Canal Zone, for periods up to five years. Data are presented to demonstrate the serious degradation exhibited by several materials.

Abstract No. 33

Effect of Heat on the Electrical Properties of Paper

L. H. Wirtz and **T. D. Callinan,** International Business Machine Corp., Research Center, Yorktown Heights, N. Y.

The dielectric constants and dielectric loss factors of handsheets made from Bauer-McNett fractions of semi-bleached sulfate woodpulp were determined over the relative humidity range, 0-92%, and were compared with the electrical properties of similar handsheets which had been subjected to temperatures of 165°C.

Abstract No. 34

The Electric Strength of Insulating Liquids

A. H. Sharbaugh, Research Lab., General Electric Co., Schenectady, N. Y.

The mechanisms of dielectric rupture in liquids are reviewed critically.

Abstract No. 35

Dielectric Properties of Very Thin Films of Liquid Dielectrics

T. Salomon, Institut Francais du Petrole, Paris, France

The production of electrostatic charges in thin films of oils may possibly be explained by the fact that films 10μ thick behave like metallic conductors. This would be in line with the experimental behavior of liquid dielectrics which exhibit changes in dielectric strength and conductivity when tested in small gaps.

ELECTRONICS—GENERAL

Abstract No. 36

Micromodular Solid Tantalum Capacitors

A. W. H. Smith, P. R. Mallory & Co., Inc., 3029 E. Washington St., Indianapolis, Ind.

Solid tantalum capacitors have been made in the geometry required for the Signal Corps Micromodule Development Project. A brief description of the structures made for R.C.A., the prime contractor, is given and also the ratings and sizes currently available. The electrical characteristics of these units are presented and discussed within the frame work of the Signal Corps Requirement SCL-6402A. Evidence of reliability is also presented in the form of load life test data for up to 5000 hr.

Abstract No. 37

Digital Programming Unit for Automatic Temperature Control

N. L. Hozak, J. S. Cook, and **D. R. Mason,** Dept. of Chemical and Metallurgical Engineering, University of Michigan, Ann Arbor, Mich.

A low-cost, compact, flexible, simple, digital, temperature program unit for controlling an electric furnace has been designed and built. The set-point emf for a potentiometer-type temperature controller is derived from a series combination of a chromel-alumel thermocouple in the furnace and an auxiliary emf generator. Each 15 min a stepping switch selector-and-indicator circuit can change the magnitude of the auxiliary emf by a multiple of 25°C and, hence, the effective set point of the controller. Temperature programming is obtained from a patchboard between the emf generator and the selector circuit. The response is limited only by the time constant of the furnace.

Abstract No. 38

An Economical, Automatic, Differential Thermal Analysis System

C. E. Barnes and **D. R. Mason,** Dept. of Chemical and Metallurgical Engineering, University of Michigan, Ann Arbor, Mich.

An automatic differential thermal analysis system is described. A pulse generator, driving a motor-driven autotransformer and electric furnace combination, produces a linear heating rate which can be varied from about 1°C/min to 6°C/min from room temperature to 1200°C. The furnace holds two samples and a reference material inside a nickel block. A dual range recorder with an electrically actuated range switch is used to record the sample temperatures (0-50 mv range) and the differential temperatures between the samples and the reference material (−0.5 to +0.5 mv range). Every 20 sec the pulse generator also actuates a stepping switch which selects the appropriate thermocouple combinations and recorder ranges. Characteristic results and interpretations are presented.

Abstract No. 39

Electroluminescent-Piezoelectric Flat Panel Displays

S. Nudelman, J. Lambe (present address: Scientific Labs, Ford Motor Co., Dearborn, Mich.), **J. Mudar,** and **G. Trytten,** The University of Michigan, Willow Run Labs., Ann Arbor, Mich.

Flat display panels are under development using electroluminescent phosphors on piezoelectric materials. Electroluminescence is stimulated by strong electric fields created at the surfaces of mosaic elements when driven at their piezoelectric resonant frequencies. When all elements are placed in parallel with each resonant at different frequencies, a modulatable light spot can be made to move about in a controlled manner by varying the electrical field strength and frequency applied to the mosaic.

ELECTRONICS—LUMINESCENCE

Abstract No. 40

Phenomenological Theory of Luminescence of Nonphotoconducting Phosphors

Yasuo Uehara, Matsuda Research Labs., Tokyo Shibaura Electric Co., Ltd., Kawasaki, Japan

After a formulation of a fundamental equation of luminescence which can explain various luminescent properties of nonphotoconducting phosphors under excitation by ultraviolet of constant intensity at thermal equilibrium, calculated results of various characteristics of luminescence are compared with experimental results. Furthermore, the theory is extended to the interpretation of the luminescent properties of phosphors under excitation by charged particles.

Abstract No. 41

Irreversible Thermodynamics of Solid-State Luminescence

F. E. Williams, Research Lab., General Electric Co., Schenectady, N. Y.

Solid-state luminescence can be shown to be irreversible. Irreversible thermodynamics provides more severe limitations than does equilibrium thermodynamics. Because the second law must be satisfied locally for irreversible processes, the entropy increase associated with the radiation must balance any entropy decrease accompanying de-excitation. This requirement precludes quite generally injection electroluminescent emission intensities in excess of the electrical input. Irreversible thermodynamics also limits multiply excited antistokes photoluminescence. Common limitations of electro-and photoluminescence are discussed.

Abstract No. 42

Shape of Absorption Bands in Solids

J. J. Markham, Zenith Radio Corp., Chicago, Ill.

The theories of the shape of an optical absorption band in solid are reviewed. The shape is related to the emission and the absorption of phonons. It depends on the temperature of the crystal. The theories are related to the measured absorption bands associated with F centers in KCl and NaCl.

Abstract No. 43

Atomic Wave Functions of Activators

K. H. Butler, Sylvania Lighting Products, 60 Boston St., Salem, Mass.

The *sp* configuration is characteristic of the excited states of many primary activator ions, i.e., Sb^{3+}, Sn^{2+}, Tl^{+}. Quantum mechanical formulas show that the electron density distribution of this configuration depends strongly on the coupling of the electron spins and the magnetic quantum number of the combined electrons. The marked difference in the shapes of an ion in the $^1P_1^\circ$ and $^3P_1^\circ$ states, combined with variations in the coordinator number of the surrounding anions in different crystal structures, explains such phenomena as the polarization of luminescence in KCl:Tl and the appearance of two emission bands in many tin-activated phosphors as contrasted to the single emission band for most materials activated by lead or antimony.

Abstract No. 44

The Significance of Measurements of the Temperature Dependence of Luminescence Intensity

C. H. Haake, Research Dept., Westinghouse Electric Corp., Bloomfield, N. J.

The quantum efficiency of a phosphor and its absorptance for the exciting radiation often exhibit op-

posite temperature trends. The latter may increase while the former decreases, thus producing a luminescence maximum at a certain temperature. Unlike the quantum efficiency the absorptance is a function of various external parameters. Thus the thickness of the phosphor layer drastically influences the shape of a curve of luminescence intensity vs. temperature. Experimental data are presented and discussed.

Abstract No. 45

Absolute Spectral Reflectance of Phosphors

J. E. Eby, Sylvania Lighting Products, 60 Boston St., Salem, Mass.

Absolute measurements of the spectral reflectivity were made on a number of phosphor samples using a modified Beckman DK-1 Spectrophotometer. The method of making these measurements, which covered the range from 240 μ to 750 μ, is described and data given. These data were then used in conjunction with determinations of particle size distribution to compute the absorption coefficient of the luminescent materials.

Abstract No. 46

Infrared Spectroscopy in Phosphor Research

M. J. B. Thomas and **C. W. Jerome,** Sylvania Lighting Products, 60 Boston St., Salem, Mass.

Use of infrared spectrophotometry as a technique for the identification of compounds has become extremely important with respect to organic compounds and to a somewhat lesser extent with respect to inorganic compounds. There has been, however, no application of this technique to luminescent materials. Infrared studies of the various commercial phosphors and the starting materials used in their manufacture have been made in the 3-15 μ region. The absorption structures of many of the materials are characteristic and may be used in the study of mechanism of phosphor formation.

Abstract No. 47

Factors Influencing Luminescent Emission Studies of the Rare Earth Ions

L. G. Van Uitert, Bell Telephone Labs., Inc., Murray Hill, N. J.

Many of the rare earth ions exhibit fluorescent emission from more than one electronic level when excited. The number of emitting levels depends on the extent to which the f-electrons are perturbed by their surroundings. Increasing the concentration of terbium or europium in calcium tungstate, for example, quenches their high wave number emission states. This probably occurs through the development of exchange coupling between rare earth ions in neighboring calcium sites.

Abstract No. 48

Some Optical Properties of Powder and Crystal Halophosphate Phosphors

P. D. Johnson, Research Lab., General Electric Co., Schenectady, N. Y.

Diffuse reflectivity measurements in the far ultraviolet on halophosphate phosphors show that intrinsic optical absorption by the host lattice begins at about 1500Å in fluoroapatite and 1570Å in chloroapatite. Absorption in bands due to manganese in fluoroapatite at 1600, 1750, and 2150Å results in luminescence in the absence of antimony. Absorption due to antimony lies between 1600 and 2900Å. Optical transmission measurements on synthetic crystal apatite confirm the position of the intrinsic absorption.

Abstract No. 49

Energy Levels of the Antimony Center in Halophosphates

F. E. Williams, Research Lab., General Electric Co., Schenectady, N. Y.

It is recognized that Sb^{+++} substitutes for type II Ca^{++} in halophosphates and simultaneously $O^{=}$ replaces the halogen neighbor. We consider the energy levels of this activator system. The atomic states of Sb^{+++} are similar to those of Tl^{+} which, as an activator, has been studied theoretically. In addition, electron transfer processes can occur in the Sb^{+++} —$O^{=}$ system which may be described as a donor-acceptor pair. Configuration interaction between the atomic and transfer states is considered.

Abstract No. 50

Lead- and Manganese-Activated Calcium-Cadmium Silicate Phosphors

Yasuo Uehara, Yoshimasa Kobuke, Isoo Masuda, and **Takashi Kushida,** Matsuda Research Lab., Tokyo Shibaura Electric Co., Ltd., Kawasaki, Japan

Characteristics of lead- and manganese-activated calcium-cadmium silicate phosphors with various mole ratios of cadmium to calcium were investigated. Two group of phosphors prepared by using cadmium sulfate and carbonate as cadmium raw materials gave different characteristics. They showed different irregular shifts of emission peaks with increasing concentration of cadmium, while a similar linear relation between the lattice spacing and concentration of cadmium was obtained. Observed results are discussed.

Abstract No. 51

Luminescence vs. Composition Studies of Complex Zinc and Cadmium Orthophosphates Containing Sodium and Lithium

A. L. Smith, Electron Tube Div., Radio Corp. of America, Lancaster, Pa.

Zinc or cadmium orthophosphates react with lithium or sodium orthophosphate to form compounds of more or less complex stoichiometry. The manganese-activated luminescences of these compounds have been determined, and an attempt has been made to correlate them with x-ray diffraction studies.

Abstract No. 52

Cadmium Phosphate Phosphors

R. C. Ropp, Chemical & Metallurgical Div., Sylvania Electric Products Inc., Towanda, Pa.

A study of the preparation and properties of both $Cd_2P_2O_7$:Mn (λ max = 618 μ) and $Cd_3(PO_4)_2$:Mn (λ max = 604 μ) revealed that these phosphors become sensitized to 2537Å if heated in air or nitrogen to form the matrix followed by reheating in a reducing atmosphere. Excitation data show shifts as a function of both preparation atmosphere and phosphor formulation. Addition of zinc or magnesium gives redder phosphors, while those containing calcium are greener. Of the two systems, the pyrophosphates are by far the more efficient.

Abstract No. 53

Luminescence of AlN

I. Adams, J. W. Mellichamp, and **G. A. Wolff,** U. S. Army Signal Research and Development Lab., Fort Monmouth, N. J.

An investigation of the electroluminescence (EL), phosphorescence (Ph), and cathodoluminescence (CL) spectra of AlN has been made. The EL spectra show narrow bands in the 400-500 μ region and broad bands in the 500-700 μ region. Phosphorescence shows broad bands in the 300-600 μ region. A suggested excitation mechanism is an energy transfer between the surface and N_2 molecules. The EL was investigated by square-wave input of varying characteristics and parameters.

Abstract No. 54

Crystal Structure and Spectra of Alkali Halide Phosphors

F. D. Klement, Physics and Astronomy Institute, Academy of Sciences of the Estonian S.S.R., Tartu, U.S.S.R.

Luminescence studies were made in crystals undergoing polymorphic transitions induced by temperature and pressure. The effect of hydrostatic pressure on luminescent spectra was also investigated. Vacancies

formed in alkali halides activated by divalent impurities were found to associate with the activator ions and give rise to characteristic emission bands. Luminescence in mixed crystals were studied and indications of decomposition of the solid solutions under certain treatment were obtained. These studies also showed that there were preferential sites in the lattice for the activator impurity.

Abstract No. 55

On the Hydrogen-Like Model for Traps in Zinc Sulfide

G. Curie, N. Arpiarian, P. Guéret, and **D. Curie,** Laboratoire de Luminescence, Faculté des Sciences, Paris, France

One of us has proposed for deep traps in ZnS the model of two trapping charges $+e$, associated in neighbor substitutional sites of the lattice. Now the trap depths have been computed for all the possible trapping sites. By a convenient choice of the thermoluminescence rate, almost all the calculated trap depths have been separated effectively. Results are given also for CdS.

Abstract No. 56

A Numerical Table for the Computation of Trap Depths from Thermoluminescence Experiments

G. Curie and **D. Curie,** Laboratoire de Luminescence, Faculté des Sciences, Paris, France

The trap depth E may be computed from the "glow temperature" T^s by using the expression, derived from Randall and Wilkins' theory:

$$E^{eV} = \frac{T^{s\,°K} - T_s(\beta,s)}{K(\beta,s)}$$

which is accompanied by tables giving the coefficients T_s and K for different values of the attempt-to-escape frequency s and the rate of heating β. New calculations have been performed; the table now ranges on the interval $10^4 - 10^{15}\ s^{-1}$ of s-values. Examples of use are given; the table is also extended for the case of a bimolecular mechanism.

Abstract No. 57

Gold-Activated (Zn,CdS Phosphors) Phosphors

M. Avinor, Philips Research Labs., N. V. Philips' Gloeilampenfabrieken, Eindhoven, Netherlands

Gold was shown to produce three emission bands in CdS at 640, 800, and 1150 μ. The long wave band appears when a trivalent metal coactivator is used while the short wave bands are observed with activation by gold alone. The 1.15 μ band in CdS is shown to correspond to the 530 μ gold band in ZnS.

Abstract No. 58

Low-Temperature Luminescence of ZnSCdS Phosphors

R. W. A. Gill and **S. Rothschild,** Mullard Research Labs., Cross Oak Lane, Sulfords, Redhill, Surrey, England

Prener and Weil found little difference between the spectra of ZnSAl or ZnSGa phosphors and ZnSCl or ZnSBr phosphors. The present investigations of ZnSCdS phosphors confirmed this observation for excitation at room temperature. The spectra of self-activated ZnSCdS phosphors were, however, found to differ during excitation at liquid nitrogen temperature. A band between the self-activated emission and the edge emission, first observed by Kroger with ZnS (NaCl), appeared in several cases depending on the nature of the added impurity and the composition of the atmosphere during firing.

Abstract No. 59

Infrared Stimulation and Quench of Zinc Sulfide Phosphors

C. C. Klick, U. S. Naval Research Lab., Washington, D. C.

Experiments are described on ZnS:Ag, In and ZnS:Ag, Ga phosphors in which the phosphors are continuously excited by ultraviolet light in the region of 3600Å and are exposed to bursts of infrared light over the wave-length range from 7500 to 13,000Å. Room temperature and liquid nitrogen temperature effects are investigated. At low temperatures a large stimulation of the orange emission is found without any quenching. The wave-length dependence of the stimulation is different for the In and Ga samples. It is concluded that the infrared light frees charge carriers from traps which are not the excited states for the orange luminescence.

Abstract No. 60

Synthesis and Crystallography of Structurally Pure Cubic and Hexagonal Single Crystals of ZnS

Harold Samelson and **V. A. Brophy,** Research Lab., Sylvania Electric Products Inc., Bayside, N. Y.

Crystals of ZnS with pure zincblende and wurtzite structures have been reported to occur naturally. ZnS crystals grown synthetically usually show deviations from these pure structures; polytype formation and random faulting have been reported. In the present work, the synthesis and identification of ZnS single crystals of structurally pure zincblende and wurtzite type are discussed. The structure identifications have been made by means of x-ray single-crystal photographs and by optical microscopy using polarized light. The concept of faults in a close-packed diatomic system is discussed, and the effect of faulting on the single-crystal x-ray diffraction patterns is illustrated.

Abstract No. 61

Infrared Absorption of n-Type (Zn,Cd)S

R. M. Potter, Lamp Development Dept., General Electric Co., Cleveland, Ohio.

Free carrier absorption has been found in single crystals of CdS:In and in (Zn,Cd)S:Ga powders containing up to 60 mole % ZnS. A λ^n dependence of absorption coefficient was found, where $n = 2.2$ to 3.7. In compositions between 60 and 80 mole % ZnS, evidence was found for absorption due to electrons bound in donor states.

Abstract No. 62

Formation of Phosphor Films by Evaporation

L. R. Koller, Research Lab., General Electric Co., Schenectady, N. Y.

Thin luminescent films of zinc sulfide phosphors have been prepared by evaporation of powder phosphors *in vacuo*. The procedure consists in depositing the film on a heated substrate so that a crystalline rather than an amorphous film is formed. This is accomplished by carrying out the evaporation in a container with walls at the same temperature as the substrate. Cathodo-, photo-, and electroluminescent films have been made by this method. Other phosphors have been made by modifications of this procedure.

Abstract No. 63

Continuous Films of II-VI Phosphors and Photoconductors Made by Vapor Reaction

D. A. Cusano, Research Lab., General Electric Co., Schenectady, N. Y.

During the past several years a large number of continuous films of II-VI and other compounds have been made by improved vapor reaction techniques. Most of these have been zinc-cadmium sulfide phosphors and photoconductors, prepared with groups IB, IIIB, VB, VIIB, and manganese impurities. The salient luminescent, electrical, and electro-optical properties are discussed and, where possible, related to existing data on single crystals or granular material of similar chemical constitution. In addition, methods of fabrication and impurity introduction are described.

Abstract No. 64

Transparent and Powder Phosphor Screens under High Ambient Illumination

A. E. Hardy, Electron Tube Div., Radio Corp. of America, Lancaster, Pa.

The phosphor screen of a cathode-ray tube, operating outdoors in sunlight or in a brilliantly lighted room, is subjected principally to diffuse ambient illumination. Under this condition, better large area contrast can be obtained with certain powder phosphor screens equipped with a low transmission faceplate, than with any transparent phosphor screens now known to exist. The principal reason for this is that, for equal electrical power dissipation, the best powder screens are 10-20 times brighter than the best transparent screens. The use of a low-transmission faceplate (10-20% transmission), with a powder screen, greatly reduces the effect of diffuse ambient illumination. The brightness of truly transparent phosphor screens appears to be limited to 5-10% of their potential brightness due to internal trapping of the luminescent light.

Abstract No. 65

Mechanism of Depreciation of Electroluminescent Phosphors

I. L. Smith, R. M. Potter, and **M. Aven** (present address: Research Lab., General Electric Co., Schenectady, N. Y.), Lamp Development Dept., General Electric Co., Cleveland, Ohio

It is proposed that the short-term depreciation of copper-activated zinc sulfide electroluminescent phosphors is caused by water. The gross features of the depreciation mechanism are similar to the depreciation of zinc sulfide phosphors under ultraviolet excitation. However, while the depreciation of zinc sulfide under ultraviolet excitation affects all exposed parts of the crystallites equally, the depreciation under electroluminescence excitation is confined to localized regions.

Abstract No. 66

Electroluminescence Maintenance

W. A. Thornton, Research Dept., Westinghouse Electric Corp., Bloomfield, N. J.

The maintenance of light emission during the operating life of an electroluminescent phosphors is vital to its practical application as a light source. The maintenance of phosphors of the ZnS:Cu,Cl type has been studied. The dependence on phosphor properties, such as copper and chlorine additions and particle size, on conditions of operation, and on lamp construction is discussed. Changes in properties, other than light emission, and recent maintenance improvements are also described.

Abstract No. 67

Effects of Interaction among Particles in Electroluminescent Layers

A. T. Halpin and **Paul Goldberg,** Sylvania Research Labs., Bayside, N. Y.

The optical and electrical behavior of electroluminescent layers are discussed in terms of experimentally determined properties of individual phosphor grains modified by interactions with neighboring particles. Pronounced interaction effects were found and were studied by determining the dependence of cell brightness and electrical dissipation on variables which alter the degree of particle-particle interaction, i.e., phosphor volume fraction and fluidity of embedment medium. The role of particle interaction in determining the dielectric properties of the phosphor is discussed in terms of appropriate models.

Abstract No. 68

On the Physical Characteristics and Chemical Composition of Electroluminescent Phosphors

Paul Goldberg and **Sixdeniel Faria,** Chemistry Lab., Sylvania Research Labs., Bayside, N. Y.

Through controlled removal of surface layers, it was found that surface chemical barriers are not responsible for electroluminescence in zinc sulfide phosphors. Polycrystalline phosphors are shown to be almost uniform with respect to chemical, physical, and electroluminescent properties as one passes from the surface into the crystallite bulk. Electron micrographs show the character of the particles as successive layers of phosphor surfaces are removed by acid etching. The experimental results at progressive stages of etching are interpreted in terms of an inefficient surface layer and of changing particle size.

Abstract No. 68A

Detection of Ionization of Eu^{++} in the Phosphor SrS-Eu, Sm by the Paramagnetic Resonance Absorption Method

V. V. Antonov-Romanovsky, V. G. Dubinin, A. M. Prokhorov, Z. A. Trapeznikova, and **M. V. Fock,** P. N. Lebedev Physical Institute, Academy of Sciences of the U.S.S.R., Moscow, U.S.S.R.

When the phosphor SrS-Eu, Sm is under excitation, the paramagnetic absorption caused by Eu^{++} ions decreases appreciably (approximately to 15%). Decrease of the amount of Eu^{++} during excitation may depend either on electron trapping by Eu^{++} ion or on its further ionization, i.e., on its transition to a trivalent state. The second alternative seems to be the most probable.

Abstract No. 69

Copper-Chloride Relationships in Photoluminescent and Electroluminescent Zinc Sulfide Phosphors

A. L. Solomon and **P. Goldberg,** Sylvania Research Labs., Bayside, N. Y.

Photoluminescent ZnS:Cu,Cl prepared with copper concentrations to 3.5×10^{-4} g at./mole are analyzed for copper and chloride. Observed Cu/Cl ratios as a function of copper concentration can be understood in terms of copper and chloride solubility. Photoluminescent properties are functions of both Cu content and Cu/Cl ratios. By further thermal treatment with copper, low Cu/Cl ratios can be adjusted toward unity. A marked change in photoluminescence is produced and electroluminescence appears. The processes by which these changes are brought about are discussed.

Abstract No. 70

Effect of CdS on the Electroluminescence of ZnS:Cu Halide Phosphors

Arthur Dreeben, RCA Labs., Radio Corp. of America, Princeton, N. J.

Electroluminescent emission intensity, power dissipation, efficiency, and spectral distributions of halide-coactivated (Zn,Cd)S:Cu phosphors have been determined. The extreme sensitivity of brightness to the presence of CdS in these systems and an apparent relationship between brightness and crystal structure are discussed. Cadmium sulfide also causes a variation in the amount of copper retained, particularly in the chloride-coactivated phosphors. Hypotheses to explain these observations are offered.

Abstract No. 71

ZnS:Cu,Cl and (Zn,Cd)S:Cu,Cl Electroluminescent Phosphors

A. Wachtel, Research Dept., Westinghouse Electric Corp., Bloomfield, N. J.

Procedures for the preparation of ZnS:Cu,Cl and (Zn,Cd)S:Cu,Cl electroluminescent phosphors are based on firing in an atmosphere containing elementary S. Cl-incorporation is controlled by firing in capped silica tubes or in open boats in a current of $N_2+S_2Cl_2$. Dependence of brightness on activator concentration is established on the basis of presumably constant excess Cu as Cu_2S. The use of Pb was found to be disadvantageous. Introduction of Cd causes formation of the hexagonal phase and a (Cu,Cd)S compound and simultaneous decrease of electroluminescence brightness as well as dependence of electroluminescence emission color on Cd concentration. A two-step firing

procedure is given by means of which this effect may be avoided partially.

Abstract No. 72

(Zn,Hg)S and (Zn,Cd,Eg)S Electroluminescent Phosphors

A. Wachtel, Research Dept., Westinghouse Electric Corp., Bloomfield, N. J.

Solid solutions of (Zn,Hg)S prepared by firing in sealed silica tubes are cubic in structure. With suitable additions of Cu and a coactivator, photoluminescence and electroluminescence are obtained. The electroluminescence in the red consists of two emission bands which do not appear to be analogous to the blue and green emission bands of Cu,Cl in ZnS. The quantum efficiency is of the same order of magnitude as that of ZnS:Cu,Cl, but the emission bandwidth is about twice as large and the red electroluminescence consists of emission located to a large extent in the infrared. HgS tends to retain the cubic structure of ternary (Zn,Cd,Hg)S systems, provided that the Cd/Hg ratio does not exceed certain limits; until this is so, the introduction of Cd causes increased electroluminescence.

Abstract No. 73

Influence of Mg and Cd on the Electroluminescence of ZnS:Cu Phosphors

P. M. Jaffe, Research Dept., Westinghouse Electric Corp., Bloomfield, N. J.

The influence of MgS on the electroluminescence of ZnS:Cu phosphors prepared with additions of halogens (F,Cl,Br,I) was investigated. Increasing the MgS content from zero to 8.0 mole % results in a slight progressive decrease in the brightness. Above this concentration the emittance decreases abruptly. The abrupt change can be correlated with a transition from cubic to hexagonal structure in the region of 5.0 to 8.0 mole % MgS. Increasing the MgS concentration also causes an unexpected expansion of the lattice and a shift in emission to shorter wave lengths. In general the results are similar whether Cl, Br, or I is used while F does not appear to enter the lattice. Some investigation of the system (Zn,Cd,Mg)S:Cu,Cl was also made and is discussed.

Abstract No. 74

Influence of Halogen-Coactivator on the Electroluminescence of ZnS:Cu Phosphors, I. Green Emission

P. M. Jaffe, Research Dept., Westinghouse Electric Corp., Bloomfield, N. J.

The use of bromine as coactivator in place of chlorine in electroluminescent ZnS:Cu phosphors results in a change in some of the electroluminescent characteristics. ZnS:Cu,Br and ZnS:Cu,Cl phosphors having similar spectral distributions (green) over a wide frequency range have been prepared. Comparison of brightness as a function of voltage and frequency, brightness waveforms, maintenance, glow curves, efficiency, and temperature dependence of electroluminescence are reported.

Abstract No. 75

Electroluminescent Time Average Light Output of a ZnS:Se Phosphor

J. Mudar, S. Nudelman, and **K. Kamyszek,** Willow Run Labs., University of Michigan, Ann Arbor, Mich.

The time average light output of an electroluminescent phosphor powder has been measured from 10 kcps to 18 mops. Fatigue increases with frequency so that at megacycle operation the output diminishes to 10-25% of initial values with a 30-min period. Mechanically shaking a phosphor-air EL cell after fatigue causes a partial restimulation of light output, with successive fatigue-shake cycles showing a decreasing effect. Electroluminescence and fatigue are temperature dependent.

Abstract No. 76

Temperature-Induced Color Shifts in Electroluminescence

L. W. Strock, Sylvania Lighting Products, 60 Boston St., Salem, Mass.

The color of ZnS:Cu EL-phosphors is determined by the relative intensities of their separate blue and green band emission components for a given condition of excitation. The color of a finished phosphor may be varied over a wide range from blue to green by appropriate thermal treatment in air or other atmosphere. Regardless of Cu-content all phosphors reach their minimum blue/green color ratio at 260°C and, in general, are still green when heated to 400°C, but blue when heated to 150°C.

Abstract No. 77

On the Role of a Stimulating Action of Exciting Light in the Luminescence Kinetics of the Crystalline Phosphor ZnS-Cu

L. A. Vinokurov and **M. V. Fock,** P. N. Lebedev Physical Institute, Academy of Sciences of the U.S.S.R., Moscow, U.S.S.R.

It is shown that electrons' release from traps in ZnS-Cu phosphor by an exciting light leads to decrease of the electron concentration on deep traps with increase of excitation intensity. After removing the excitation, the distribution of electrons over traps gradually approaches equilibrium distribution. A flash under the action of an infrared light is determined mainly by release of electrons from deep levels. Therefore the above effects may be detected by measuring the value of the flash under different intensities of afterglow and at various stages of decay.

Abstract No. 77A

On the Valency States of Manganese in Phosphor Systems

V. V. Osiko, P. N. Lebedev Physical Institute, Academy of Sciences of the U.S.S.R., Moscow, U.S.S.R.

On the basis of oxidized manganese and its total content being measured in about 50 phosphors, the average valencies of manganese were calculated. Judging from these data there are three groups of phosphors differing from each other in the correlation between the luminescent properties and the valency of manganese. The model system ZnO-MnO-O_2 was studied. The cause of the different valencies of manganese is discussed.

Abstract No. 77B

Physical Processes in Alkali Halide Phosphors Activated by Mercury-Like Ions

Ch. B. Lushchik, I. W. Jaek, G. G. Lüdja, N. E. Lushchik, and **K. K. Schwarz,** Physics and Astronomy Institute, Academy of Sciences of the Estonian S.S.R., Tartu, U.S.S.R.

A number of alkali halide phosphors activated by monovalent and divalent ions having the electronic configuration of neutral mercury were prepared. Diffusion and precipitation of activator ions were investigated as were absorption, emission, and radiationless processes within the impurity center. Energy transfer by means of excitons and electron-hole pairs between the luminescent center, the host crystal and color centers were also studied.

ELECTRONICS—SEMICONDUCTORS

Abstract No. 78

An Apparatus for the Preparation of Semiconductor Grade Silicon

R. C. Ellis, Jr., Research Division, Raytheon Co., Waltham, Mass.

An apparatus is described for the production of large quantities of semiconductor grade silicon. Thermal decomposition of silicon tetraiodide by film boiling is used. The silicon is deposited molten on a submerged induction heated graphite shape and is collected after its departure from the hot zone by flotation. Apparatuses are described for the synthesis and purification of large quantities of silicon tetraiodide.

Abstract No. 79

Twin Generation and Seeding Mechanism in Dendritic Growth

J. W. Faust, Jr., and **H. F. John,** Westinghouse Research Labs., Pittsburgh, Pa.

The formation of twin lamellae at a growing crystal front is discussed in relation to the genesis of dendritic growth arms. The conditions necessary for successful seeding and propagation of a dendrite are discussed in relation to the twin structure and growth button formation. The morphology of the initial growth buttons, as well as subsequent extensions, are described for single crystal, one-twin, and multi-twin seeds.

Abstract No. 80

Propagation of Germanium Dendrites

R. G. Seidensticker and **D. R. Hamilton,** Westinghouse Research Labs., Pittsburgh, Pa.

A formal model is developed for rapid dendritic extension of germanium crystals. The role of corner nucleation is stressed. It is shown that two twin planes are required for the perpetuation of favored corner sites. Two types of sites can occur and cooperate in the extension process. Experimental evidence supports this hypothesis.

Abstract No. 81

Some Aspects of Lateral Growth in Dendrites

H. F. John and **J. W. Faust, Jr.,** Westinghouse Research Labs., Pittsburgh 35, Pa.

Results are presented which show that the lateral growth mechanism is different from that which propagates the dendrite. The growth of the dendrite outward from the central core, which contains the twin structure, to form the final, ribbon-like structure is described. The ways in which various dislocation arrays can arise from the growth process are pointed out.

Abstract No. 82

Dendritic Growth Studies by Pulse Plating Techniques

R. C. Smith, Westinghouse Research Labs., Pittsburgh, Pa.

Pulse electroplating is used to reveal sharp variations of resistivity on germanium dendrites. Good resolution of these variations is obtained in the plate deposited in the meniscus region of the plating solution. Since such resistivity variations must occur during the formation of the dendrite, certain of the growth processes can be deduced from their configuration. At least two processes are indicated, and the evolution of edge structure from small serrations to larger ones is shown to occur.

Abstract No. 83

Growth of Atomically Flat Surfaces on Germanium Dendrites

A. I. Bennett, R. L. Longini, and **W. J. Smith,** Westinghouse Research Labs., Pittsburgh, Pa.

The following theory of formation of extended flat surfaces on germanium dendrites assumes that part of the liquid-solid interface is a supercooled (111) surface. New atomic planes occasionally are nucleated thereon and grow to the melt surface, creating a step on the solid. It is proposed that the meniscus momentarily sticks to this step. Subsequent planes nucleated during this sticking period result in a step several atomic layers high, in accord with experiment.

Abstract No. 84

Dendritic Growth of Indium Antimonide

J. W. Faust, Jr., Westinghouse Research Labs., and **H. Nicholson** and **R. Moss,** Westinghouse Materials Engineering, Pittsburgh 35, Pa.

Dendrites of InSb have been grown and examined by various techniques. The effect of the polar axis is discussed. The internal twin structure and the perfection of the dendrites are described and compared to other dendrites of the zinc-blende structure.

Abstract No. 85

Preparation of Highly Arsenic-Doped Germanium

P. L. Moody and **A. J. Strauss,** Lincoln Lab., Massachusetts Institute of Technology, Lexington, Mass.

In the preparation of germanium single crystals highly doped with arsenic, sealed systems with heated walls must be used to prevent loss of arsenic from the melt by evaporation. Two such systems, a syringe-type Czochralski puller and a three-zone horizontal furnace, are described. The resistivity and Hall mobility at room temperature are reported for concentrations between 10^{19} cm^{-3} and 4.5×10^{19} cm^{-3}, the maximum attained.

Abstract No. 86

Crystal Model Studies of Growth Phenomena in III-V Compounds

R. C. Sangster, Central Research Labs., Texas Instruments Inc., Dallas, Texas

Crystal growth phenomena for III-V semiconducting compounds are discussed. A versatile model has been used to study the behavior of many low indices surfaces in the zinc blende lattice. Results are presented in a series of photographs and discussed in terms of the nature of the bonding, the type, and the packing density of surface atoms. A "stair-step" theory of crystal growth is described.

Abstract No. 87

Orientation Dependent Distribution Coefficients of Tellurium in Indium Antimonide Crystals

J. B. Mullen, Royal Radar Establishment, Malvern, England

The results of distribution coefficient determinations of tellurium in melt grown InSb crystals are discussed. The anisotropic property of the distribution coefficient has been shown to be connected with the formation during growth of planar crystallographic facets on the solid liquid interface. The "facet effect" is not due to a solute enriched boundary layer. The theoretical significance of the results is discussed.

Abstract No. 88

Anisotropic Segregation in InSb

W. P. Allred and **R. K. Willardson,** Battelle Memorial Institute, Columbus, Ohio

A large variation in segregation coefficients with respect to crystal orientation is observed in InSb. Crystals pulled on the (111) axis show high concentrations of Se and Te in the center of the ingot. This effect is thought to be caused by a segregation coefficient of Se and Te greater than unity on the (111) facet and less than unity on other planes. Radial variations in impurity content as large as a factor of ten have been observed.

Abstract No. 89

Study of Copper Precipitation in Silicon Single Crystals

G. H. Schwuttke, Sylvania Research Labs., Sylvania Electric Products Inc., Bayside, N. Y.

Copper precipitation was studied in silicon crystals of different dislocation density and different impurity concentration. In crystals of high dislocation density ($\sim 10^4/cm^2$ to $10^6/cm^2$) copper precipitates only along dislocation lines. In crystals of low dislocation density (less than $10^3/cm^2$) random precipitation exists in addition to precipitation along dislocation lines. It was found that the shape of the precipitate varies, depending on the experimental conditions and the nature of the imperfection.

Abstract No. 90

Reactions of Oxygen in Ge

C. S. Fuller, C. D. Thurmond, and **W. Kaiser,** Bell Telephone Labs., Inc., Murray Hill, N. J.

Oxygen in solid solution in Ge undergoes aggregative reactions leading to the formation of donors and ultimately to more complex aggregates. The donor forming reaction is reversible and equilibria are established depending on temperature and oxygen concentration. Solid solutions containing 0.9 to 6.0 x 10^{17} cm^{-3} oxygen have been investigated over the temperature range 325°-527°C. By assuming that four oxygen atoms react successively at a Ge atom to form the singly ionized donor structure, GeO_4, it is possible to fit the experimental curves with a single constant derived from mass action expressions and the charge and mass balance conditions.

Abstract No. 91

Preparation and Properties of the Pseudo-Binary System GaAs-AlAs

E. P. Stambaugh, J. I. Genco, and **R. C. Himes,** Battelle Memorial Institute, Columbus, Ohio

Means of preparation of homogeneous alloys in the pseudo-binary system GaAs-AlAs have been investigated with emphasis on the gallium-rich region. Degree of homogeneity and composition were determined by x-ray diffraction, electron probe, metallographic examination, microhardness determinations, and chemical analyses. Thermal, electrical, and optical properties as a function of alloy composition and/or temperature are presented.

Abstract No. 92

Preparation and Properties of the Pseudo-Binary System GaSb-AlSb

J. F. Miller, H. L. Goering, and **R. C. Himes,** Battelle Memorial Institute, Columbus, Ohio

Methods of preparation of alloys in the pseudo-binary system GaSb-AlSb were studied, and physical properties were investigated as function of composition and temperature. It has been demonstrated that, with the possible exception of the composition range between 10 and 30 mole % AlSb, solid solution prevails in this system. Melting points, unit cell sizes, energy gaps, resistivity, and hole mobility vary with composition and range between the values of the corresponding properties of the terminal compositions.

Abstract No. 93

Phase Diagram for the Binary System Cadmium-Tellurium

D. R. Mason and **B. M. Kulwicki,** Dept. of Chemical and Metallurgical Engineering, University of Michigan, Ann Arbor, Mich.

The phase diagram for the cadmium-tellurium system has been redetermined by measuring the thermal behavior of representative compositions in the system by the method of differential thermal analysis. Experimental details and the resulting data are described and discussed. Thermodynamic analysis shows that the system CdTe-Te appears to form an ideal solution. The latent heat of fusion of CdTe is estimated to be 10,700 cal/g mole. The system Cd-CdTe is an elementary solution and has a relatively large excess partial molar entropy of solution and a large partial molar enthalpy of solution. These partial molar qualities are independent functions of composition, but not of temperature. The eutectic compositions have been determined as 10^{-6} atom fraction tellurium and about 0.99 atom fraction tellurium. The validity of this work vis-a-vis that of other investigators is discussed.

Abstract No. 94

Effect of Inhomogeneities on the Hall Coefficient in InSb

R. T. Bate, Battelle Memorial Institute, Columbus, Ohio

Crystals of n-type InSb have been grown which were doped with selenium and pulled in such a way that the selenium segregated during growth to produce large impurity gradients. These impurity gradients were mapped and their effect on the galvanomagnetic coefficients determined. Results indicated very pronounced effects, such as an increase of the Hall coefficients at room temperature by nearly a factor of two, as the magnetic field is increased from 1000 to 20,000 gauss.

Abstract No. 95

Properties of P-Type GaAs Prepared by Copper Diffusion

F. D. Rosi, D. Meyerhofer, and **R. V. Jensen,** RCA Labs., Radio Corp. of America, Princeton, N. J.

Purification of arsenic by hydrogen sublimation and gallium by vacuum annealing resulted in the preparation of high resistivity (~10^5 ohm-cm), n-type GaAs crystals by the horizontal Bridgman technique. Conversion of this material to p-type was accomplished by the inward diffusion of copper from the crystal surface. Measurements of Hall mobility as a function of hole concentration in the range 2 x 10^{16} cm^{-3} to 3 x 10^{17} cm^{-3} at room temperature showed a dependence which is consistent with theory. The analysis suggests a lattice mobility for holes of 450 cm^2 v^{-1} at 300°K. The mobility varied approximately as $T^{-2.8}$ in the range 76°-300°K. At the low temperatures the number of ionized impurities ranged from 2 x 10^{15} cm^{-3} to 1 x 10^{16} cm^{-3}. Energy levels associated with copper in GaAs are 0.023 ev and 0.15 ev above the valence band.

Abstract No. 96

Preparation and Properties ZnSb

R. C. Bourke, R. Simon, and **E. H. Lougher,** Battelle Memorial Institute, Columbus, Ohio

Homogeneous specimens of ZnSb have been prepared by a modified hot-pressing method, using a graphite die. Specimens thus prepared are consistently single-phase material and, in this respect, are superior to specimens prepared by a quench-and-anneal method. The temperature dependences of resistivity, Hall coefficient, Hall mobility, and thermoelectric power of several specimens have been determined. In contrast to other reports, stoichiometric, hot-pressed ZnSb has been found to have a room temperature resistivity of 0.6 ohm-cm, a corresponding thermoelectric power of 700 v/°K and Hall mobility of 220 cm^2/v-sec. A value of 0.3 ev for the energy gap at 0°K has been calculated from electrical data. A study was made of the effect of Sn and Pb additions to stoichiometric ZnSb. Lead-doping, even to the point of saturation, failed to affect the Hall coefficient of the compound substantially. Tin, however, was found to be an effective p-type doping agent.

Abstract No. 97

Preparation and Properties of Gallium Phosphide

C. J. Frosch, M. Gershenzon, and **D. F. Gibbs** (present address: H. H. Wills Physics Lab., Bristol, England), Bell Telephone Labs., Inc. Murray Hill, N. J.

A pressure chamber is described for producing solid multicrystalline ingots of gallium phosphide at high phosphorus pressures. Bars cut from these ingots are being employed in an investigation of the floating zone technique for growing controlled single crystals of gallium phosphide. Methods for overcoming new problems encountered in the floating zone processing are described. The current status of the floating zone investigation is described. Electrical measurements are reported on single crystals cut from multicrystalline ingots and bars purified by floating zone recrystallization.

Abstract No. 98

Preparation and Characteristics of P-N Junctions in Gallium Phosphide

M. Gershenzon and **R. M. Mikulyak,** Bell Telephone Labs., Inc. Murray Hill, N. J.

Techniques for the preparation of both diffused and alloyed GaP diodes are described as well as the

thermal and chemical stability of these structures. The presence of recombination-generation centers and a highly compensated region leads to departures from ideal junction behavior in the forward and reverse currents, reverse capacity, and in long time constants found for establishing steady-state conditions. Room temperature breakdown potentials to 135 v and rectification ratios to 3 x 10^6 are reported.

Abstract No. 99

Preparation and Properties of Grown P-N Junctions of InSb

H. C. Gorton and **F. J. Reid,** Battelle Memorial Institute, Columbus, Ohio

Grown p-n junctions of InSb have been prepared by adding zinc to a high-purity melt. After the junctions had been grown, the material on the n-type side had electron mobilities greater than 350,000 cm^2/v-sec at 77°K and carrier concentrations in the $10^{14}/cm^3$ range. Junction characteristics were obtained as a function of temperature in the range of 55°-200°K. The data show the effects of surface conditions and of intrinsic carriers on the reverse current.

Abstract No. 100

Influence of Crystal Size on the Spectral Response of Evaporated PbTe and PbSe Photoconductive Cells

W. D. Lawson and **A. S. Young,** Royal Radar Establishment, Malvern, England, and **F. A. Smith,** Atomic Energy Research Establishment, Harwell, England

Photoconductive layers of PbTe have been formed by evaporation on substrates at different temperatures. The size of crystals in the layers has been estimated from electron micrographs and x-ray diffraction, and a correspondence has been obtained between crystal size and the limit of spectral response. Sensitivity up to the long wave-length limit set by the energy gap cannot be achieved unless the crystals are greater than a critical size; for lead telluride this is about a quarter of a micron. A similar effect has been shown to occur with PbSe.

Abstract No. 101

On the Mechanism of Chemically Etching Germanium and Silicon

D. R. Turner, Bell Telephone Labs., Inc., Murray Hill, N. J.

The electrode potential of germanium or silicon in a chemical etching solution is a function of: solution pH, rate of etching, physical condition of the surface, conductivity type, and resistivity. The results suggest that excess holes and electrons are produced at the surface of the semiconductor during chemical etching. Holes are injected at cathode sites, but only a portion of these holes are consumed at anode sites since the anode reaction involves current multiplication.

Abstract No. 102

Experimental Micro-etch Techniques on Millimeter Wave-length Diodes

D. G. Langlais, Philco Corp., Philadelphia, Pa.

Use of transistor micro-etch techniques has improved the sensitivity of 4.3 mm mixer diodes by approximately 3 db. Reduction of the germanium blank base thickness by jet-etching to about 0.06 mil and back-alloying have produced an "effective" base thickness of 0.02-0.03 mil (an order of magnitude less than whisker contact radius). The average spreading resistance was lowered from 14 ohm (Philco 1N2792 mixer diode) to 8 ohm as expected by micro-etch theory. Selection of jet-etching conditions yielded a flat window area diameter of approximately 6 mil, thereby reducing close alignment tolerances.

Abstract No. 103

Oxide Masking of Solid SiO_2 against Boron

Frank Keywell and **Marshall Nechtow,** Hughes Semiconductor Products, Newport Beach, Calif.

Silicon dioxide films 2000A thick on high resistivity n-type silicon were exposed at 1100°C to a boron source for a few minutes. A liquid borosilicate phase penetrated more than 700A but did not reach the parent silicon. The samples were next placed in a furnace at 950°C for 10 weeks. Boron atoms did not penetrate the solid quartz during the 10-week heat treatment, hence the diffusion coefficient of boron in solid quartz is less than 3.1 x 10^{-19} cm^2/sec. The low diffusion coefficient is due to chemical bonding between boron and oxygen atoms.

Abstract No. 104

Oxidation-Induced Diffusion in Silicon

H. W. Cooper, E. I. Doucette, and **R. A. Mehnert,** Bell Telephone Labs., Inc., Murray Hill, N. J

The formation of thermal oxide layers on silicon causes a redistribution of bulk impurities which may either be gettered at the oxide-bulk interface or be rejected into the crystal. For silicon, whose oxide grows at a parabolic rate, a rigorous solution has been obtained. The impurity concentration follows a complementary error function distribution with a constant surface concentration.

Silicon with aluminum and antimony as major and minor impurities was used to verify the theory quantitatively. The observed junction depths corresponded well in magnitude and rate of increase with that predicted. A radio-tracer technique was used to determine the segregation of indium at the silicon-silicon oxide interface. A value near unity was observed.

Abstract No. 105

Gaseous Diffusion of Arsenic in Germanium

Carl Pihl and **Kurt Lehovec,** Sprague Electric Co., North Adams, Mass.

Previous studies of the gaseous diffusion of phosphorus in germanium have been extended to include vapor diffusion of arsenic in germanium. Data are presented on surface concentration of arsenic in germanium as a function of arsenic pressure in the gas phase. At sufficiently high arsenic concentrations a liquid phase of germanium arsenide forms and this phase has been identified by electron diffraction. Evidence is presented that this liquid phase suppresses thermal conversion.

Abstract No. 106

Open Tube Diffusion of Antimony into Germanium

A. E. Blakeslee, Bell Telephone Labs., Inc., Allentown, Pa.

A two-step, three-furnace process for the diffusion of antimony into germanium is described. Sheet resistivity and junction depth data are presented as functions of time of diffusion and temperatures of the three furnaces, and empirical expressions are given for sheet resistivity in terms of the three temperatures. The impurity distributions resulting after each of the two diffusion steps are discussed. Diffusion constants found for the temperature range 600°-700°C are lower than values published for sealed tube systems.

Abstract No. 107

Surface Concentration of Indium in Germanium from Gaseous Diffusion, II

Karl Busen and **Earl Meeks,** Sprague Electric Co., North Adams, Mass.

Previous investigations on the indiffusion of indium from the vapor phase into germanium at 837°C are now extended to diffusion temperatures of 775° and 900°C. The experiments are carried out again in a specially designed closer system, and values for the surface concentration of indium in the germanium for different indium vapor pressures are presented. Diffusion coefficients of indium in germanium derived from our experiments are compared with published values.

Abstract No. 108

A Diffusion Mask for Germanium

E. L. Jordan and **D. J. Donahue,** Semiconductor and Materials Div., Radio Corp. of America, Somerville, N. J.

A technique has been developed for the deposition of a silicon dioxide diffusion mask on the surface of germanium. The silicon dioxide coatings are formed by the thermal decomposition of an organic-oxy-silane. Patterns are formed in the silicon dioxide coating by the photoresist-acid etch techniques that are well known in silicon technology. The mask is completely effective against donor impurities in all concentrations and against acceptor impurities in low and medium concentrations. The use of the mask has permitted the construction of a double diffused n-p-n mesa germanium transistor.

Abstract No. 109

Diffusion of Phosphorus in Silicon

I. M. Mackintosh, Bell Telephone Labs., Inc., Murray Hill, N. J.

A process is described for producing N-type, phosphorus-diffused layers in silicon. The diffusions are carried out in a closed system, using as the diffusion source a glass consisting of P_2O_5 and CaO. Surface concentrations between 10^{20} and 10^{16} cm^{-3} can be obtained with reproducibilities between 2% and 20%, junction depths from about 0.02 mil upward with reproducibilities between 2% and 5%. The process is compatible with the oxide masking of layers with surface concentrations as high as 10^{21} cm^{-3}. Data are presented for the diffusion coefficient, and the value of the activation energy for this process is discussed.

Abstract No. 110

Experimental Evidence of Surface Damage and Precipitation in Diffused Silicon

L. Gerlach and **R. Haberecht,** P. R. Mallory and Co., Indianapolis, Ind.

Visible evidence of surface damage and precipitation in diffused silicon is presented. Variations in the junction formation related to abnormal concentration gradients and the presence of a precipitated phase is discussed in relation to the basic mechanism of precipitation. Evidence indicates that the oxygen distribution and a critical concentration of diffusant are the important factors necessary for the presence of a precipitate.

Abstract No. 111

Precision Lapping, Damage, and Diffusion

C. J. Spector and **T. E. McGahan,** Bell Telephone Labs., Murray Hill, N. J.

Silicon slices have been lapped experimentally and polished to less than 0.003 in. with opposing faces optically plane and parallel to within 0.00002 in. Modified planetary lapping techniques have been used so that the strains usually induced by "one side at a time" processes are absent. Data are presented to correlate rate of lapping, depth of damage (measured by x-ray "rocking angle" techniques), and impurity diffusion parameters with abrasive particle size.

Abstract No. 112

A New Solution to New Diffusion Equation and a New Application of Analog Solutions

R. Moore and **J. Colburn,** General Electric Co., Syracuse, N. Y.

An analytical expression for the diffusion profile obtained during the two-step diffusion process for the germanium mesa transistor has been developed by two independent analyses. The form of this equation makes numerical solutions difficult; however, some curves obtained by digital means are presented. A more direct approach is the use of a passive electrical analog. The analogy is shown together with some of the curves obtained, and these are shown to be equivalent to the analytical results.

Abstract No. 113

Localized Breakdown in Diffused Silicon Junctions

B. D. James and **P. S. Flint,** Fairchild Semiconductor Corp., Palo Alto, Calif.

In diffused silicon junctions, localized regions of low breakdown have been found associated with "pipes" of the same doping as the bulk material that connects the bulk with the surface through the diffused layer. These pipes are much more highly doped than the bulk silicon. The frequency of their occurrence is enhanced by oxidation of the silicon prior to diffusion, and they are interpreted as arising from segregation of the bulk dopant around vacancy clusters.

Abstract No. 114

(There is no Abstract 114)

Abstract No. 115

Production of a Germanium PNPN Switching Transistor by Post-Alloy Diffusion

Fred Barson and **John Gow,** International Business Machines Corp., Poughkeepsie, N. Y.

A process has been developed for fabricating a three-terminal Germanium PNPN Switching Transistor similar to that described Klein and Kordalewski. By employing post-alloy diffusion techniques it is possible to produce the four-layer structure completely during the alloying process, with no prediffusion required. Furthermore, the device parameters can be varied within certain limits simply by changing the impurity concentration of the alloy pellets. Details of the process are described, and typical device characteristics listed.

Abstract No. 116

A High-Frequency PNP Diffused Silicon Transistor Produced by the Oxide Masking Technique

O. Stavik, Northern Electric Co., Montreal, Que., Canada

A high-frequency PNP diffused silicon transistor has been developed which has electrical characteristics very similar to the NPN diffused silicon "Mesa" transistor. Silicon slices of resistivity 0.5-0.7 ohm-cm are first diffused with arsenic to a depth of 5 μ. During this first diffusion an oxide layer is formed on the slice which is sufficiently thick to mask against the second diffusant, namely, boron. Oxide is removed from the silicon surface in the form of stripes and boron diffused through these areas to a depth of 4 μ to produce emitter junctions, thus giving a base layer of 1.0 μ. The alpha cut-off frequency ranges from 50 to 100 mcs. Grounded emitter current gain as high as 200 has been measured. V_{cb} is of the order of 50-60 v.

Abstract No. 117

(There is no Abstract 117)

Abstract No. 118

Physical Metallurgy in Semiconductor Device Fabrication, I. Gold Electrode Attachments to Silicon and Germanium

L. Bernstein, B. G. Bender, and **W. B. Warren,** Hughes Products, P. O. Box 278, Newport Beach, Calif.

Results of separate studies of large and small area attachments are discussed. Metallurgy and choice of backing material to avoid cracking is described. Compositions of gold-tin offer the most versatile attachment in a variety of atmospheres. Eleven photomicrographs and two plates of expansion curves are presented.

Abstract No. 119

Physical Metallurgy in Semiconductor Device Fabrication, II. Studies of Gold-Aluminum and Gold-Tin Electrode Attachment

L. Bernstein, W. B. Warren, and **B. G. Bender,** Hughes Products, P. O. Box 278, Newport Beach, Calif.

Electrode attachments to aluminum-silicon eutectic regions in semiconductor devices by means of gold or gold alloys often produce a condition referred to as the "purple plague," the $AuAl_2$ phase formation, with subsequent mechanical failure. Conditions which promote its formation in addition to the more desirable Au_4Al phase are discussed. Wetting and surface tension problems associated with attachments to the Al-Si surface via gold-tin alloys are described in connection with gold-aluminum compound formation. Thermal expansion data for the systems involved are presented, along with eighteen color photomicrographs of the various conditions.

Abstract No. 120

Effects of High Aluminum Concentration in Emitters of Germanium Alloyed Power Transistors

H. K. Becherer and **Ernest Paskell,** Delco Radio Div., General Motors Co., Kokomo, Ind.

This paper presents a survey of the effects of an emitter alloying with more than 2% aluminum on high power transistors. Slides show that besides the wettability between indium and germanium the regrown structure as well as the shape of the p-n junction edges will be changed. A single alloying process with Al-In alloy will give immediately the new junction shape while a re-alloying onto a pre-alloyed emitter junction will correct the previous junction. Electrical data are given to shown the gain at higher current.

ELECTROTHERMICS AND METALLURGY

Abstract No. 121

Resources of Vanadium Minerals—Domestic and Foreign

Staff Member, Colorado School of Mines Research Foundation, Inc., Golden, Colo.

This paper covers the geology and occurrence of vanadium deposits in the United States and various foreign countries including Finland, Transvaal, Quebec, Peru, and miscellaneous sources. Deposits of vanadium with uranium in sandstone and limestone ores are discussed as being one of the principal sources. Potential vanadium recovery from magnetite deposits, vanadiferous phosphates and shales, vanadate ores, and minor sources are discussed.

Abstract No. 122

Mining and Beneficiation of Vanadium Minerals

Staff Member, Colorado School of Mines Research Foundation, Inc., Golden, Colo.

Mining and beneficiation of the carnotites and roscoelite ores for vanadium recovery as practiced at present are discussed. Beneficiation processes for recovery of vanadium from other sources, including titaniferous magnetites, vanadiferous shales, ferrophosphorus from western phosphates, and as a by-product from wet process phosphoric acid production are also described.

Abstract No. 123

Mineralogy and Geochemistry of Vanadium in the Colorado Plateau

A. D. Weeks, U. S. Geological Survey, Washington, D. C.

The chief domestic source of vanadium in uraniferous sandstone in the Colorado Plateau. Vanadium is 3-, 4-, or 5-valent in nature and, as oxides or combined with other elements, it forms more than 40 minerals in the Plateau ores. These ores are discussed with regard to relative amounts of vanadium silicates and oxide-vanadates, uranium-vanadium ratios, progressive oxidation of black low-valent ores to high-valent carnotite-type ores, and theories of origin.

Abstract No. 124

Vanadium by Metallic Reduction of Vanadium Trichloride

M. J. Ferrante and **F. E. Block,** U.S. Dept. of the Interior, Bureau of Mines, P.O. Box 492, Albany, Ore.

Vanadium tetrachloride was made by chlorinating vanadium oxide with chlorine in the presence of carbon. By refluxing vanadium tetrachloride it decomposed to vanadium trichloride which is nonvolatile. The allowed volatile oxychloride to be separated. The trichloride was reduced with magnesium or magnesium-sodium mixtures under inert atmosphere. Excess reductant and by-product salts were removed from the vanadium sponge by vacuum distillation. Arc-melted vanadium was 99.8+% pure and could be cold-rolled into thin sheets.

Abstract No. 125

Electrorefining of Vanadium

D. H. Baker, Jr., and **F. R. Cattoir,** Bureau of Mines, Boulder City Metallurgy Research Lab., Boulder City, Nev.

The fused salt electrorefining technique has been applied successfully to vanadium. The electrolyte was sodium chloride containing 3-6% vanadium as vanadium dichloride. Current efficiency was approximately 91%. Oxygen and nitrogen impurities were reduced by two thirds of the amount contained in the feed material. The hardness of the product was reduced from 97 Rockwell B to 35 R_B. Arc melted ingots could be given a 99% cold reduction by rolling before edge cracking appeared.

Abstract No. 126

Preparation of High-Purity Vanadium Metal by the Iodide Refining Process

O. N. Carlson and **C. V. Owen,** Iowa State University, Ames, Iowa

The preparation of vanadium of 99.9+% purity by the Van Arkel-deBoer iodide process is described. Conditions for optimum growth rate and maximum purity were determined. Data on impurity transfer from the feed to the hot filament are presented together with a discussion of contamination by the retort. The quality of vanadium obtained from feed material prepared by bomb reduction and by a sponge process was compared. An apparatus designed to prepare several pounds per batch is described. A few physical properties were determined and are also reported.

Abstract No. 127

Consolidation and Fabrication of Vanadium

T. W. Merrill, Research Center, Vanadium Corp. of America, Cambridge, Ohio

Calcium reduction of the oxide is the commercial method used for preparation of vanadium in this country. The regulus obtained is normally arc melted in vacuum; electron beam melting also has been tried. The oxygen content is lowered by either melting process. Hot working is practicable, providing reasonable precautions are taken to avoid excessive oxygen contamination. The metal can be cold rolled, swaged, and drawn, provided the contaminated layer resulting from hot working is completely removed. Warm extrusion of small ingots was found to be a good processing method. Tubing, plates, strip, foil, rods, and wire have been produced in trial quantities.

Abstract No. 128

Mechanical Properties of Unalloyed Vanadium

J. W. Farrell, Technology Dept., Product Development Lab., Union Carbide Metals Co., Division of Union Carbide Corp., Niagara Falls, N. Y.

Mechanical properties are summarized for unalloyed vanadium consolidated by consumable-electrode arc melting. The following data are presented for both cold-worked and annealed samples with varying interstitial contents: short-time tensile properties from −196° to +1100°C, yield point and strain-aging phenomena, room temperature notched tensile properties and true stress-true strain data, the room temperature flow constants and elastic modulus, work-hardening characteristics, bend test data, Erichsen test data, crystal orientations, and metallographic techniques.

Abstract No. 129

Lattice Parameter and Expansion Coefficient of Vanadium

W. J. James and **M. E. Straumanis,** School of Mines and Metallurgy, University of Missouri, Rolla, Mo.

The lattice parameter of 99.972% pure vanadium prepared at Battelle by the Van Arkel method were determined by the asymmetric diffraction technique over the temperature range 10°-60°C using unfiltered copper radiation. From the $\alpha(321)$ line with $\theta = 72.5°$ a value of a = 3.0241Å at 25°C, corrected for refraction, was obtained. The computed closest atom-to-atom distance was 2.1384Å. The linear expansion coefficient was 9.96×10^{-6} $(°C)^{-1}$. Calculated x-ray density at 25°C was 6.121 ±0.002 g cm^{-3}. A plot of lattice parameters vs. summation of nitrogen and oxygen content when extrapolated to 0% showed a decided decrease in lattice parameter.

Abstract No. 129A

Corrosion Properties of High-Purity Vanadium

David Schlain and **C. B. Kenahan,** U. S. Dept. of the Interior, Bureau of Mines, Region V, College Park, Md.

The chemical and galvanic corrosion behavior of high-purity vanadium was investigated by the Bureau of Mines, U. S. Department of the Interior, at its College Park, Md., Metallurgical Research Center. Vanadium was found quite resistant in hydrochloric, sulfuric, and phosphoric acids, but corroded rapidly in nitric acid solutions. It resisted corrosion in substitute ocean water, 3% sodium chloride solution, 10% sodium hydroxide solution, and tap water, but not in 5% mercuric chloride or 20% ferric chloride solutions. Vanadium was resistant in acetic, lactic, citric, and tartaric acids and corroded slowly in oxalic and formic acids.

Abstract No. 130

On the Constitution of Some Vanadium-Base Binary and Ternary Systems and the Aging Characteristics of Selected Ternary Alloys

S. Komjathy, Armour Research Foundation, Technolgy Center, 10 W. 35 St., Chicago 16, Ill.

To promote development of vanadium-base alloys, binary (V-Hf, V-Re, V-Sn, V-Th, V-W) and ternary systems (V-Ti-Nb, V-Ti-Mo, V-Ti-Ta, V-Ti-W, V-Ti-O, V-Ti-Si, and V-Ti-Be) were investigated to determine: (*a*) extent of the vanadium-rich solid solution between 800° and 1500°C; (*b*) character of the second phase in equilibrium with the solid solution; and (*c*) melt reactions. The age-hardening of selected V-Ti-O, V-Ti-Si, and V-Ti-Be alloys was studied at 550°, 650°, and 750°C.

Abstract No. 131

Development of Improved Vanadium-Base Alloys for High-Temperature Purposes

B. R. Rajala and **R. J. Van Thyne,** Armour Research Foundation, Technology Center, 10 W. 35 St., Chicago 16, Ill.

Vanadium-base sheet alloys containing titanium and/or columbium, molybdenum, tantalum, and tungsten exhibit excellent strength at elevated temperatures and weldability. Since oxidation protection was not an aim of this program, tensile, creep, and short-time rupture properties were determined in enert atmospheres. These alloys with outstanding cold fricability are nearly equal to the best 2000°F sheet materials on a density corrected, 15-min rupture basis.

Abstract No. 132

Properties of Vanadium-Base Alloys

S. T. Wlodek, Metals Research Labs., Union Carbide Metals Co., P. O. Box 580, Niagara Falls, N. Y.

Development of a novel series of vanadium-base alloys combined with the IVB and VB group elements is described. High-strength, low-density compositions possessing good aqueous corrosion resistance in boiling oxidizing, or reducing, acids and sufficient oxidation resistance to allow their fabrication by conventional hot-working techniques in air can be designed. Properties estimated under inert atmosphere conditions include ultimate tensile strength of 120,000 to 35,000 psi over the temperature range 700°-1000°C and stress-rupture properties at 700°C corresponding to 100-hr life at stresses in excess of 100,000 psi. The alloy design principles responsible for these improvements of vanadium are discussed.

Abstract No. 133

Canada's Interest in Methods of Reducing Iron Ores

John Convey, Mines Branch, Dept. of Mines and Technical Surveys, Ottawa, Canada

Canada is well supplied with those resources which may be used in the production of iron, i.e., ore, coal, oil, natural gas and electric power. For that reason our metallurgical industries and research organizations have become much interested in the various methods of reducing iron ores. Our government Department of Mines and Technical Surveys in Ottawa has experimental facilities which may be used to assist in determining the reduction methods which would be most suitable in different parts of the country.

Abstract No. 134

Economic and Process Factors Affecting the Selection of a Direct Reduction Process

D. C. Brown, Jones and Laughlin Steel Corp., Pittsburgh, Pa.

A direct reduction process will prove best for all applications under all circumstances. Many process and economic factors will go together to dictate which process best fits a specific application. This paper describes the influence of physical and chemical characterization of the ore on (*a*) reduction kinetics, (*b*) type of equipment used, and (*c*) pre- or post-beneficiation or both. The effects of type in availability of fuel for both reduction requirements and process heat with the attendant effects on post-beneficiation and compaction are discussed. Other factors such as plant location, freight, use of direct reduction product, and degree of metallization are considered.

Abstract No. 135

Solid Fuels and Reductants for the Beneficiation and Reduction of Iron Ores

H. U. Ross, Dept. of Metallurgy, University of Toronto, Toronto, Ont., Canada

The advantages in using solid fuels in the beneficiation and reduction of ores are outlined. Those properties of certain types of solid fuels, which make them particularly suitable, are discussed. The great importance of the availability of coking coal on the choice of reduction process is stressed. Research and development work on direct reduction processes has been greatly stimulated by the rapid exhaustion of the reserves of low-volatile coking coals.

Abstract No. 136

Gas Reactions in Reduction Processes

J. Huebler, Surface Combustion Div., Midland Ross Corp., Toledo, Ohio

Reactions of the gases used in the reduction of the iron oxides are discussed from the standpoint of the generation of these gases either within the process or in external apparatus and from the standpoint of the reactions which occur in the reduction. An effort is made to present in a simple fashion the reasons for the reactions, reaction rates, and heat requirements for the process.

Abstract No. 137

Magnetizing Roasting

D. J. Hains, Engineering Co., Ltd., Toronto, Ont., Canada

The beneficiation of iron ores by magnetizing roasting in the rotary kiln is dealt with. The process is particularly useful in treating mixed ores due to the possibility of controlling and varying the gas atmosphere and temperature throughout the length of the kiln. Pilot and commercial plant equipment are illustrated and metallurgical results on various typical ores are reported.

Abstract No. 138

How Are the Blast Furnaces Doing?

O. R. Rice, Koppers Co., Inc., Pittsburgh, Pa.

The currently demonstrated advances in unit productivity, coke economy, etc., are dealt with, and the changed circumstances that have brought about these advances in the blast furnace art are cited. Speculation is made as to what the near future may hold with respect to blast furnace performance, as intimated by already-initiated procedures. The role played by blast furnace hot metal in the manufacture of steel is emphasized.

Abstract No. 139

Performance of the First Commercial H-Iron Reduction Plant

H. H. Stotler, Hydrocarbon Research Inc., New York, N. Y. and **R. A. Lubker,** Alan Wood Steel Co., Conshohocken, Pa.

Performance of a 50 ton per day plant in which hydrogen from coke oven gas reduces iron oxides in a fluidized bed below 1000°F and 500 psig is discussed. Operation of the plant has demonstrated the flexibility of a single unit and the versatility of the product. Operation of a three-stage unit is also discussed; performance in the commercial unit is compared with laboratory results; an economic evaluation is given of a projected 1000 ton per day plant.

Abstract No. 140

The Nu-Iron Process—A Fluidized Bed Process for Reducing Iron Ore

T. F. Reed, J. C. Agarwal, and **E. H. Shipley,** United States Steel Corp., Monroeville, Pa.

In the Nu-Iron fluidized bed reduction process preheated minus 10-mesh high-grade ore is reduced continuously with preheated hydrogen at 1300°F and 50 psig pressure in two separate steps, $Fe_2O_3 \rightarrow FeO \rightarrow Fe$. The flow of iron ore and the hydrogen are countercurrent. The unused hydrogen in the off gases from the reduction reactor is recovered and recycled. A description of the Nu-Iron pilot plant and the commercial embodiment of the process is included.

Abstract No. 141

Direct Reduction of Fine Iron Ore Concentrates in a Self-Agglomerating Fluidized Bed

F. M. Stephens, Jr., and **B. G. Langston,** Battelle Memorial Institute, Columbus, Ohio

This paper describes a process which utilizes the adhesive properties of the reduced iron particles for self-agglomeration of finely ground iron concentrates in a fluidized-bed reactor. Data are presented which show that the self-agglomeration mechanism can be controlled by the distribution of the surface areas of the particle-size fractions in the bed, the temperature, and the space velocity used in the fluidized-bed reactor.

Abstract No. 142

The Esso Research-Little Process

R. W. Hyde, Arthur D. Little Inc., Cambridge, Mass.

The Esso Research-Little process is a method for continuously reducing finely divided iron ore in a 3-stage fluidized-bed system using hydrocarbons, gaseous or liquid, as the source of both reducing agent and the heat required for the reduction. The paper includes a description of the experimental work, both laboratory and pilot plant, from which the Esso Research-Little Process was evolved.

Abstract No. 143

Present Direct Reduction Research at Stora Kopparberg, Sweden

T. O. Dormsjo, Stora Kopparberg Corp., New York, N. Y.

This paper discusses the Wiberg-Soderfors process: development, current results, possible modifications: the Stelling process using carbon monoxide. Rotary kiln reduction: the Kalling method. Magnetizing reduction for beneficiation purposes.

Abstract No. 144

The R-N Process

J. S. Breitenstein, R-N Corp., 111 Broadway, New York, N. Y.

A recent test on a 50 ton iron per day scale has demonstrated substantially greater kiln thruputs than previously projected. Large scale commercial electric and open hearth melting tests on R-N briquettes have been performed recently. This paper discusses the results of these melting tests as well as the latest information developed in the semi-commercial plant in Birmingham; in addition, a presentation is made on the new facilities installed in Birmingham, such as charring and balling, and the integration of these units in the R-N flowsheet.

Abstract No. 145

Reasons for the Co-Current Kiln in Direct Reduction

Horace Freeman, Freeman Corp., Cap-de-la-Madeleine, Quebec

The author has operated both counter-current and co-current rotary kilns for the direct reduction of iron ores. He gives his reasoning for finally adopting the co-current kiln for commercial use. In this kiln the ore, reducing carbon, and sulfur-absorbing limestone are fed together at the firing end and travel with the combustion gases to the discharge end. The results obtained with various types of natural and pretreated ores and types of reducing carbon are reported.

Abstract No. 146

New Agglomeration-Reduction Process for Iron Ores

Will Mitchell, Jr., Allis-Chalmers Manufacturing Co., Milwaukee, Wis.

(No abstract received)

Abstract No. 147

Direct Reduction Research at IRSID

J. Astier, Institut de Recherches de la Siderurgie, Maizieres-les-Metz, France

Two programs are discussed: (1) aiming to reduce low-grade French ores with coal in rotary kilns; low-temperature tests at the U.S. Bureau of Mines (Laramie, Wyo.) with beneficiation of reduced ore; Krupp Renn tests at Kraluv Dvur (Czechoslovakia); high-temperature tests at Azincourt (France) to make molten pig iron, and [2] to reduce high-grade ores or concentrates with natural gas; low-temperature gas reduction, and electric steelmaking compared with direct production of pig iron or steel.

Abstract No. 148

The Jet Smelting Process

R. L. Cavanagh, Ontario Research Foundation, Toronto, Ont., Canada

The process is outlined, and some reasons are given for the interest in this type of direct reduction process. The original research program is summarized and preliminary tests commented on. Some results of a feasibility study, including theoretical calculations, are presented. Detailed results of furnace experiments and a resume of the present status of the work are given. Approximate estimates of possible costs are made.

Abstract No. 149

New Pre-reduction Processes

H. Walde, Demag-Elektrometallurgie, GmbH, Duisburg Germany

(No abstract received)

Abstract No. 150

Consideration of Fuel Requirements for Iron Ore Reduction

R. Wild, The British Iron and Steel Research Association, London, England

The possible methods of making iron are reviewed and classified according to the quantity of reducing agent used and the energy requirements. The generation of the required energy is considered, and the effect of the efficiency of reduction is shown graphically. The known ironmaking processes are compared on the basis of their energy requirements. The influence of the available fuel, and other factors, on the choice of process is discussed.

Abstract No. 151

Strategic-Udy Process for Smelting Iron Ores

M. C. Udy, Strategic-Udy Processes Inc., Niagara Falls, N. Y.

The Strategic-Udy Process has opened a new vista of metallurgy by cutting the blast furnace into two parts. The "top part," now placed on its side and rotated, gives control of preheating and prereduction not attained in the blast furnace. Electrodes, placed in the "bottom part," provide heat and the air has been turned off. Now that carbon, silicon, phosphorus, etc., can be controlled in the product, low or off-grade ores and reductants may be used.

Abstract No. 152

Technical and Economic Factors to Be Considered in the Electric Furnace Reduction of Iron Ores

N. H. Keyser, Process Metallurgy Div., Battelle Memorial Institute, Columbus, Ohio

This paper traces changes in technology and economics that have prompted the present-day intense interest in the use of electric furnaces for reducing iron ores. The reasons for interest in "pretreatment" and "prereduction" ahead of the electric smelting furnace are explained. Emphasis is placed on the fundamentals behind the various processes that utilized electric furnaces rather than describing specific processes. Emphasis is placed on factors that influence costs rather than specific costs.

Abstract No. 153

Electric Smelting of Iron Ores

F. C. Collin, Elektrokemisk A/S, Oslo, Norway

The paper deals with growth and geographical distribution of electric pig iron smelting plants with special reference to the developments in Norway and Japan. Recent progress in preparation of sinter and the sizing of coke is emphasized. Thereby increased indirect reduction has been established, and carbon as well as power consumption reduced correspondingly. Utilization of the furnace gas as fuel, for chemical synthesis, and for pretreatment of the changes is discussed. Data from Elektrokemisk's recent research in the field are presented.

Abstract No. 154

Mineralogical and Geological Occurrence of Rhenium

S. R. Zimmerley, Research Labs., Kennecott Copper Co., Salt Lake City, Utah

(No abstract received)

Abstract No. 155

A Survey of the Different Methods for the Determination of Rhenium

Suzanne Tribalat, Laboratoire de Chimie Physique de la Faculté des Sciences, Paris, France

The study of the industrial recovery of rhenium became possible when one could determine exactly the element among large quantities of molybdenum. This paper surveys the recent works concerning the determination of rhenium. As for the determination of traces, the most sure and accurate method, tried out by thousands of analyses, is finally the extraction method of tetra phenylarsonium perrhenate, followed by the colorimetry of the thiocyanate complex, which we published a few years ago.

Abstract No. 156

Spectrophotometric Determination of Microgram Quantities of Rhenium

E. E. Malouf and **R. J. Heaney,** Research Labs., Kennecott Copper Co., Salt Lake City, Utah

(No abstract received)

Abstract No. 157

Some Recent Developments in the Halide and Ditertiary Arsine Chemistry of Rhenium

J. E. Fergusson and **R. S. Nyholm,** Dept. of Chemistry, University College of London, Gower St. WC 1, London England

Following a brief summary of the known halide complexes of the various oxidation states, recent work on the halide chemistry of tervalent and quadrivalent rhenium will be discussed. In particular, the stereochemistry of the halide complexes of rhenium III (d^4) will be discussed. The magnetism and stereochemistry will be correlated with the electron configuration. Then follows a survey of the ditertiary-arsine complexes formed by bivalent, tervalent, and pentavalent rhenium, which are, respectively, six covalent, six covalent, and eight covalent. The relationship of the spectra, magnetism, and coordination number with the electron configuration is examined.

Abstract No. 158

Spectrochemical Analysis of Rhenium Metal Powder

J. H. Allwein, Research & Development Dept., Chase Brass & Copper Co., Waterbury, Conn.

Qualitative and semiquantitative methods for the spectrochemical determination of trace impurities in

commercially pure rhenium metal powder are discussed. The semiquantitative method is based on synthetic solution standards prepared from the purest grade of rhenium. The following techniques are evaluated: (*a*) the solution-direct current arc method; (*b*) the copper spark method; and (*c*) Zink's "vacuum cup" electrode method.

Abstract No. 159

The Crystal Chemistry of the Compounds of Rhenium with Transition Metals

N. V. Ageev and **V. Sh. Shehtman,** Academy of Science, Moscow

The compounds in the systems Re-Mo, Re-Mn, Re-Fe, *et al.*, have been studied. The single crystals of the δ-phase Re-Mo are received, from which the crystal-class symmetry and the dimensions of unit cell have been determined by x-ray method. The experimental study of the structure of two compounds in the Re-Mn and Re-Fe systems has been carried out. It is found that both these compounds have a structure isomorphous to well-known δ-phases. The conditions of formation of δ- and χ-phases in binary systems of rhenium with transition metals are analyzed. It is shown that the formation of χ-phases is determined mostly by the relation of the atomic radii of rhenium and the second component. The experimental data concerning the ordering of the atoms in the cells δ-phases and χ-phases in many binary systems on the base of rhenium are received.

Abstract No. 160

Metallurgical Processes for Recovery of Rhenium from Flue Dusts and Gases

E. E. Malouf, J. D. Prater, and S. R. Zimmerley, Research Labs., Kennecott Copper Co., Salt Lake City, Utah

(No abstract received)

Abstract No. 161

Process for Producing Pure Rhenium and Its Compounds

Marie-Louise Jungfleisch and **Henri Ruff,** Ets Ch. Bertolus, Bellegarde, France

A complete process for recovering rhenium in molybdenites is described. The process consists of roasting the molybdenite in two stages, washing gases evolved during the second stage, a liquid-liquid extraction producing a solution containing 80% of the initial rhenium, precipitation of the ammonium and potassium perrhenates, transformation of the latter into perrhenic acid by cationic exchange, and, last, reduction of ammonium perrhenate into metal and the purification of the metal until the rate of 99.9% by sublimating the heptoxide.

Abstract No. 162

Rhenium Powder Metallurgy and Fabrication of Wrought Products

J. H. Port, Chase Brass & Copper Co., Waterbury 20, Conn.

(No abstract received)

Abstract No. 163

Behavior of Rhenium during Hot-Working

Guy Lebert, Conservatoire National des Arts et Metiers, Paris, France

It is known that rhenium offers the peculiarity of being very rapidly work-hardened according to the deformation. We have thought that a hot working, if precautions were taken for preventing the oxidation of the metal, would permit larger deformations than the cold working would. From rhenium powders selected because of their purity, the influence of their granulometry was studied. After sintering, a swaging under controlled and reducing atmosphere was made. Thence, it became possible to obtain deformations reaching 30%.

Abstract No. 164

Powder Metallurgy of Refractory Alloys Containing Rhenium

Marie-Louise Jungfleisch, Et. Ch. Bertolus, Bellegarde, France, and **Jean Fabry,** Société Bocuze, Lyon, France

The fabrication of refractory alloys containing rhenium is presented: determination of the characteristics of powders giving the best results (essentially, average particle diameter), blending, pressing, sintering, swaging, and drawing of fine wires (0.001 in.) A study has been started to develop the applications of these alloys in the fields where their unique properties are the most valuable.

Abstract No. 165

Certain Physical Properties of Rhenium and Its Alloys

E. M. Savitski and **M. A. Tylkina,** The Institute of Metallurgy of the Academy of Sciences of the U.S.S.R., Moscow, U.S.S.R.

Studies have been made of recrystallization of rhenium, and of alloying with tungsten, nickel (in Ni-Cr alloys), and with titanium and its alloys. Rhenium additions improve both rooom and elevated temperature properties and increase the initial recrystallization temperatures. Solid solution tungsten alloys have increased workability and electrical resistance. Applications for rhenium alloys are promising for thermocouples, electrical contacts, and some vacuum tube parts. Results are given of a study of rhenium as a contact material.

Abstract No. 166

Rhenium and Transition Metals Phase Diagrams

E. M. Savitski and **M. A. Tylkina,** Institute of Metallurgy, Academy of Sciences of the U.S.S.R., Moscow, U.S.S.R.

Binary phase diagrams of rhenium with titanium, zirconium, hafnium, vanadium, niobium, tantalum, chromium, molybdenum, tungsten, manganese, and cobalt have been determined. A number of these alloy systems are characterized by the formation of intermetallic phases of the sigma or alpha-manganese types. Comparisons are made of these and other common features of the respective diagrams on the basis of the periodicity of the binary alloy additions.

Abstract No. 167

(No title received)

G. A. Geach, Associated Electrical Industries, Ltd., Aldermaston, Berkshire, England

(No abstract received)

Abstract No. 168

The Workability and Mechanical Properties of Tungsten- and Molybdenum-Base Alloys Containing Rhenium

D. J. Maykuth, F. C. Holden, and **R. I. Jaffee,** Battelle Memorial Institute, Columbus 1, Ohio

Procedures for the fabrication of arc melted tungsten- and molybdenum-base alloys, containing 22-35 at. % rhenium, to strip, rod, and wire have been developed. Data are given on the recrystallization behavior and the effects of temperature on the tensile and bend properties of these alloys. The mechanism by which rhenium improves the ductility of tungsten and molybdenum is discussed.

Abstract No. 169

Evaluation of Rhenium as an Electrical Contact Material

V. E. Heil, T. C. Murphy, and **L. F. Neely,** P. R. Mallory & Co., Inc., Indianapolis, Ind.

(No abstract received)

Abstract No. 170

Thermocouples for 3000°C Using Rhenium Alloys

J. C. Lachman and **J. A. McGurty,** Aircraft Nuclear Propulsion Dept., General Electric Co., Cincinnati 15, Ohio

The disadvantages of limited temperature measurement capability and brittleness of rhenium/tungsten thermocouples have been overcome by the development of tungsten alloys containing rhenium. Various combinations of tungsten/rhenium alloys provide thermocouples useful to 3000°C with reasonable room temperature ductility for both wires. Calibration data and information on thermal emf stability are presented.

Abstract No. 171

Rhenium in Electronics

G. B. Gaines, Battelle Memorial Institute, Columbus 1, Ohio

The present status of the use of rhenium and rhenium alloys in electronic applications is described and, where possible, new applications are suggested with which the properties and the cost of rhenium are compatible. The information presented is based on the literature, personal correspondence, and new laboratory data. Of special interest are the present potential use of rhenium alloys in electron-tube and closely associated applications.

Abstract No. 172

Catalytic Hydrogenation of Sulfuretted Organic Compounds in the Presence of Rhenium Heptasulfide

Constantin Aretos and **Jean Vialle,** Lab of Chemistry, Faculté des Sciences, Caen, France

The rhenium heptasulfide used in this study was prepared according to W. Geilmann and H. Bode. At a temperature of 100°C, and in the presence of acetic anhydride, it catalyzes the hydrogenation of the nitro-2 thiophéne into acetylamino-2 thiophene. At 200°C, the thiophenic nucleus is hydrogenated; in this manner, we prepared the thiolane and the methyl-2 thiolane. We studied at the same time the hydrogenation at 180°-200°C of three dithole-1, 2 thiones-3. We noticed an opening of the dithiole cycle and a partial desulfuration.

Abstract No. 173

On the Use of Pure or Alloyed Rhenium in Oxide Coated Cathodes

M. P. Warin, Centre national d'etudes des Telecommunications, Paris, France

Preliminary experiences using alkaline earth oxides either pressed with rhenium powder or as a coating on metallic rhenium having proved promising, experiments were undertaken to compare in a statistical fashion the behavior during life of high transconductance pentodes using either nickel alloyed with 1-10 % rhenium, or nickel alloyed with 4% tungsten, as the base metal of the oxide coated cathode. The 10% rhenium nickel bases gave satisfactory results even at a reduced temperature. At normal heater ratings, tubes of the same batch have yielded an average life of more than 20,000 hr.

Abstract No. 174

Electroplating of Rhenium

G. S. Root and **John Beach,** Battelle Memorial Institute, Columbus 1. Ohio

(No abstract received)

Abstract No. 175

Adhesion of Vapor Deposited Molybdenum Coatings

S. T. Wlodek (present address; Union Carbide Metals Co., Niagara Falls, N. Y.) and **John Wulff,** Dept. of Metallurgy, Massachusetts Institute of Technology, Cambridge, Mass.

The adherence of molybdenum coatings produced by the reduction of molybdenum pentachloride with hydrogen at 900°C was found to depend on the purity of the plating system and the chemical nature of the surface being plated. Adherent coatings could be produced under conditions where no oxide contamination was encountered only if the surface being plated did not contain constituents whose chlorides are more stable than those of molybdenum.

Abstract No. 176

Kinetics of the Oxidation of Pure Tungsten from 500° to 1300°C

E. A. Gulbransen and **K. F. Andrew,** Westinghouse Research Labs., Churchill Boro., Pittsburgh, Pa.

Kinetic studies were made on sheet and wire specimens from 500° to 1300°C and for pressures of 0.1 atm to 0.0013 atm. Crystal structure and photographic studies were made on the oxide scale and metal. At 500°C the reaction is probably controlled by diffusion processes in the oxide. Above 1200°C the reaction appears similar to the combustion of carbon with the rate of oxidation being limited by the access of oxygen to the surface. Localized edge-type of reaction is found over the temperature range.

Abstract No. 177

Preparation and Refining of Yttrium Metal by Y-Mg Intermediate Alloy Process

O. N. Carlson, J. A. Haefling, F. A. Schmidt, and **F. H. Spedding,** Institute for Atomic Research and Dept. of Chemistry, Iowa State University, Ames, Iowa

Yttrium metal was prepared by the reduction of YF_3 with calcium or lithium forming a low melting Y-Mg alloy. The magnesium was subsequently sublimed off to produce yttrium in sponge form which was arc melted into a solid ingot. A method of removing oxygen and fluorine from the alloy by extraction with fused yttrium salts is described. The results of electron beam melting and zone refining are also presented. Some properties of yttrium metal of 99.9% purity obtained by the extraction refining process are discussed.

INDUSTRIAL ELECTROLYTIC

Abstract No. 178

Graphite Anodes in Brine Electrolysis, IV. Effect of Anolyte *p*H on Corrosion Rate in Chlor-Alkali Cells

L. E. Vaaler, Development Lab., National Carbon Co., Division of Union Carbide Corp., Niagara Falls, N. Y.

The effect of anolyte *p*H on cell efficiency and anode corrosion rate was studied in an experimental chlorine cell. With increasing *p*H, the expected decrease in current efficiency was observed with a resultant increase in the amounts of oxygen and carbon dioxide evolved. The relative increase in oxygen evolution is far greater than the carbon dioxide evolution. The results can be explained by a mechanism whereby the oxygen is formed from physically adsorbed oxygen, while carbon monoxide is formed from chemisorbed oxygen, and oxidized to carbon dioxide by oxygen or dissolved chlorine.

Abstract No. 179

Chemical Engineering Studies on the Decomposition Packed Tower of the Amalgam on the Chlorine-Caustic Industry

Shinzo Okada, Shiro Yoshizawa, and **Fumio Hine,** Dept. of Industrial Chemistry, Kyoto University, Kyoto, Japan

Kinetics on the amalgam decomposition in the cause of the local cell consist of Na-Hg(Y)/NaOH aq. (X)/H_2-graphite with emphasis on the hydrogen overpotential; the chemical engineering considerations of the decomposition tower and how to design the tower are described. This study involves representations concerning the H.T.U. and the N.T.U. of the amalgam decomposition tower from an electrochemical point of view, i.e., this tower differs from common packed towers which may be operated under the control of diffusion process.

Abstract No. 180

A Small-Scale Electro-Organic Chemical Plant

J. W. Drew and **G. J. Moll,** Ciba Pharmaceutical Products, Inc., Summit, N. J.

An electro-organic reaction unit for batch preparation of pharmaceutical intermediates on a pilot-plant and semi-commercial scale is described. Because the use of the electro-organic technique is uncommon outside of the laboratory, details of cell construction, arrangement, and instrumentation are given, with emphasis on design for versatility, safety, and accurate process control.

Examples are given of the complete reduction of an imide (N,N-dimethylaminoethyl tetrachlorophthalimide to N,N-dimethylaminoethyl tetrachloroisoindoline) using a lead cathode, and of the bimolecular reduction of a ketone to a pinacol (3-acetyl pyridine to 2, 3-bis(3-pyridyl)-2,3-butanediol) at a tin cathode.

Abstract No. 181

Intermediate Temperature Fuel Cells

G. V. Elmore and **H. A. Tanner,** Charles F. Kettering Foundation, Box 215, Yellow Springs, Ohio

New types of aqueous hydrogen-oxygen fuel cells operating at temperatures above 100°C, at atmospheric pressure, have been studied. An advantage of these cells is the removal of product water by vaporization. A cell operating in an alkaline electrolyte and a cell utilizing an acid electrolyte have been developed. Porous electrodes which have been treated with teflon have proved to be effective in resisting electrolyte penetration. Current densities in the range of 50 to 100 ma/cm^2 at 0.5 v have been achieved. The electrode mechanisms are discussed.

Abstract No. 182

Electrolytic Reduction of Thorium Oxide

L. H. Meyer, Savannah River Laboratory, E. I. du Pont de Nemours & Co., Aiken, S. C.

Thorium metal was prepared by electrolytic reduction of thorium oxide in two systems, a fused KF-ThF_4 mixture and a fused NaCl-KCl-$ThCl_4$ mixture. The average decomposition potential measured in both systems was 1.92 v. Electrolysis in the fluoride melt proved to be a superior process, the metal product having higher purity and larger average particle size than the product from the chloride melt. In addition, the recovery of thorium from recycle streams proved to be much simpler in the fluoride process than in the chloride process. The feasibility was demonstrated for all the essential steps of a complete process for production of the metal in the fluoride system.

Abstract No. 183

Metal Mists and Aluminum Losses in the Hall Process

W. E. Haupin, Alcoa Research Labs., P.O. Box 772, New Kensington, Pa.

Reaction of aluminum with Hall cell electrolyte forms aluminum monofluoride and sodium which dissolve in some form to give the bath a reducing capacity equivalent to a free aluminum content of about one tenth per cent. The so-called "metal mist" forms in the presence of moisture and consists of hydrogen bubbles containing a small partial pressure of aluminum monofluoride, sodium and sodium tetrafluoroaluminate. Increasing the NaF/AlF_3 ratio of the electrolyte increases the sodium and decreases the aluminum monofluoride partial pressure, but sodium has a much higher partial pressure; hence, a low NaF/AlF_3 ratio is desirable to minimize metal reoxidation. Carbon dioxide is abundant in the anode gas of a smelting cell and is soluble in the bath. It oxidizes the free metal both in and over the bath. The rate of this reoxidation appears to be controlled by the rate of diffusion and convection of dissolved metal away from the metal-bath interface.

Abstract No. 184

Preparation of Boron from Boron Carbide

D. R. Stern, American Potash & Chemical Corp., 3100 East 26th St., Los Angeles 23, Calif.

A process to prepare elemental boron from boron carbide is presented. Included is evidence that the process is one of anodic transfer. Boron of at least 99.8% purity can be made directly from technical grade materials. Purity is a function of electrolysis voltages and boron carbide purity. Current efficiencies in excess of 95% are obtained and preferred electrolysis conditions are stated.

Abstract No. 185

Lead Dioxide Anode in the Preparation of Perchlorates

K. C. Narasimham, S. Sundararajan, and **H. V. K. Udupa,** Central Electrochemical Research Institute, Karaikudi-3, S. India

The technique of deposition of lead dioxide on graphite or carbon base material, developed in this laboratory earlier, has now been used for obtaining suitable anodes in the preparation of sodium perchlorate from sodium chlorate. Extensive investigation has been carried out and results presented on the successful use of this type of anode in presence of certain addition agents as a replacement for platinum anode.

The influence of anodic current density, temperature, *p*H, current concentration, and duration of electrolysis on the current efficiency of perchlorate formation has been studied. Current efficiency was found to depend on anode surface transformation which took place on repeated use. Such changes could be observed visually and anode potential measurements confirm the same.

High current efficiency could be obtained even under slightly alkaline conditions of electrolysis but addition of fluoride improved the results. Addition of fluoride together with sulfate (as sulfuric acid) had the maximum effect on current efficiency under acidic conditions of *p*H.

THEORETICAL ELECTROCHEMISTRY—INDUSTRIAL ELECTROLYTIC

Abstract No. 186

The Measurement of Polarization

Ernest Yeager, Dept. of Chemistry, Western Reserve University, Cleveland 6, Ohio

Well established techniques for measuring the potentials of working electrodes are reviewed and evaluated in terms of application to the following: (*a*) polarization measurements under highly controlled conditions which are conducive to a detailed analysis of the electrode processes, and (*b*) polarization measurements in the actual systems of direct interest to electrochemical engineers for the purpose of a general analysis of the sources of polarization in the working system. Application of both steady-state and transient methods are discussed.

Abstract No. 187

Applied Electrochemical Kinetics

Paul Delahay, Dept. of Chemistry, Louisiana State University, Baton Rouge 3, La.

The necessity for quantitative knowledge on activation polarization (i.e., polarization after correction for mass transfer) is stressed for control of industrial processes. It is shown that the essential ideas of chemical kinetics can be transposed to the interpretation of polarization measurements. In many instances, polarization curves can be interpreted in terms of two kinetic parameters, the exchange current density (or standard rate constant) and the transfer coefficient. Methods of calculation are outlined. Reaction mechanisms and reaction orders are established from the study of these two kinetic parameters. The influence of the electrolyte composition and the nature of the electrode are analyzed on the basis of double layer and specific elec-

trode (adsorption, etc.) effects. Complications caused by a blocking layer of adsorbed substances (additives or impurities) are finally examined. Examples, taken from processes of industrial significance whenever possible, are given for each method of attack. Sources and critical evaluation of data are discussed.

Abstract No. 188

Electrocrystallization and Surface Films

D. A. Vermilyea, Research Lab., General Electric Co., Schenectady, N. Y.

Crystals almost always grow or evaporate by the addition or removal of atoms at surface steps. Also, surface reactions depend critically on the precise atomic arrangement of the surface. Solid surfaces are thus far from uniform in their reactivity. The inferences concerning electrode reactions which may be drawn from this fact are discussed, with particular emphasis on anodic oxide films and electrolytic crystal growth.

Abstract No. 189

Mass Transport in Electrolysis, Hydrodynamic Factors

Norbert Ibl, Federal Technological Institute, Zurich, Switzerland

The general mechanism of solution-side mass transport is reviewed. The theory of convective mass transport in electrolysis is outlined (dimensional analysis, boundary layer theory). The quantitative evaluation of limiting currents and interfacial concentrations, based on theoretical and experimental relationships, is discussed for a variety of common hydrodynamic situations and usual geometries: laminar and turbulent flow along a plate; rotating disk; rotating cylinder; natural convection, gas-evolving electrodes.

Abstract No. 190

Heat Transport and Temperature Distribution in Cells

T. R. Beck, American Potash and Chemical Co., Henderson, Nev.

Equations are presented that describe the location and the magnitude of the heat sources and sinks in an electrolytic cell. Quantitative relations describing the transport of heat within cells and to surroundings are also developed. Application of these equations to the geometry and physical properties of electrolyte and cell materials of particular cells permits calculation of such quantities as electrolyte temperature, electrode surface temperature, amount of additional heat required, amount of heat to be removed, and amount of insulation required. Examples of application to commercial electrochemical cells are given.

Abstract No. 191

Effect of Geometry on Current Distribution in Industrial Electrolytic Cells

Scott Lynn, Dow Chemical Co., Western Div., Pittsburg, Calif., and **C. W. Tobias**, Dept. of Chemistry, University of California, Berkeley 4, Calif.

The local rate of an electrode reaction depends on the distribution of current over the electrode surface. Quantitative consideration of this distribution and its effect on cell performance is required for rational cell design and for the optimization of operational procedures. The potential distribution in geometries typical of electrode arrangements in industrial cells is subjected to mathematical analysis. Numerical solutions for the more complex cases are obtained by the relaxation method using high-speed digital computers. The effect of polarization is included, and time changes in geometry due to electrode wear or solid deposits are also considered.

Abstract No. 192

Effect of Nongeometric Factors on Current Distribution

E. A. Grens and **C. W. Tobias**, Dept. of Chemistry, University of California, Berkeley 4, Calif.

Conductive properties of the electrodes and of the electrolyte regime between the electrodes can be the controlling factors in influencing current distribution. Electrode potentials and conductances depend on transport of reacting species and of products, and therefore the current distribution may be influenced by hydrodynamic factors. Some well-known examples taken from industrial practice are subjected to analysis. An apparent lack of correspondence between laboratory and plant scale performance may be resolved by considering criteria of dynamic similarity.

Abstract No. 193

Electrode Materials and Materials of Construction

M. S. Kircher and **J. E. Currey**, Hooker Chemical Corp., Niagara Falls, N. Y.

Process characteristics such as equilibrium potentials and overvoltages, electrolyte and product properties, temperature, etc., are considered in relation to materials of construction. Examples of electrode materials and cell construction materials used for some of the more important industrial cells are reviewed. Relationships between materials and design possibilities are discussed considering cost and availability as well as physical and chemical properties of materials. Specific examples of chlor-alkali cell design are included to show how a material may be selected for a given cell design and, conversely, how a cell design is derived to meet the requirements of an important material of construction. Expected trends in future cell designs are discussed with reference to availability of new materials.

Abstract No. 194

The Problem of Scale Up of Electrolytic Processes

R. B. MacMullin, R. B. MacMullin Associates, Niagara Falls, N. Y.

The industrial objective is first analyzed in full scope —feed preparation, electrolysis, and recovery of products—on the basis of existing information or analogies. A preliminary idea of cell type and capacity results, which is then scaled down to arrive at a suitable minimum prototype cell for test. Areas of ignorance are thus defined and programmed for exploration. After testing each model, the original objectives are reviewed, and the size and design of the next model is decided on the basis of scale down of a commercially desirable cell as well as scale up from the last model. The technique of complete cell design is discussed in detail and illustrated with practical applications. Procedures for economic evaluation are described.

Abstract No. 195

Measurements on a Plant Scale

C. J. Dobratz, Dow Chemical Co., Western Div., Pittsburg, Calif.

Measurements on a plant scale are complicated by problems not encountered normally in the laboratory. These are discussed along with the techniques of measurements on a plant scale of some of the operating variables peculiar to electrolytic cells. Recent developments in the use of statistical methods and automatic computers for the planning of experiments and the treatment of data are described. Examples are given of the application of these methods in an electrolytic caustic and chlorine plant.

THEORETICAL ELECTROCHEMISTRY

Abstract No. 196

Double Layer Structure and Relaxation Methods for Fast Electrode Processes

Hiroaki Matsuda and **Paul Delahay**, Dept. of Chemistry, Louisiana State University, Baton Rouge, La.

An equation is derived for the overvoltage-time characteristic in the double pulse galvanostatic method, the structure of the double layer being considered in the boundary value problem. It is shown that a previous treatment without consideration of the double

layer structure can be applied with simple modifications in the expression of the measured exchange current density. The measured transfer coefficient is seriously in error in case of strong repulsion and, especially, attraction of the discharged species in the diffuse double layer. Abnormally high transfer coefficients recently reported by other investigators are interpreted. A detailed mathematical analysis is given.

The elements of the equivalent circuit for the faradaic impedance are derived, due consideration being given to the structure of the double layer in the solution of the boundary value problem. It is shown that the classical theory is applicable but that measured exchange current densities and transfer coefficients must be corrected. The phase angle which is also affected can exceed $\pi/4$ when the reactants are strongly attracted in the diffuse double layer. Comparison is made with a similar treatment for the galvanostatic double pulse method.

Abstract No. 197

The Interpretation of Measurements of Potential Decay on Open Circuit

P. C. Milner, Bell Telephone Labs., Inc., Murray Hill, N. J.

Observations of the change in electrode potential as a function of time on open circuit have proved to be a useful method for the study of the kinetics of electrode reactions and the capacitance of the electrical double layer. The interpretation of such observations may, however, be complicated by the presence of capacitative effects resulting from faradaic processes. Consideration of these effects is included in the theory of open-circuit decay, and it is shown that in certain cases such effects are virtually indistinguishable from the capacitance of the electrical double layer and that they may be of surprising importance. The analysis of decay measurements is also considered, and a new method, which overcomes a number of objections to previous procedures, is described.

Abstract No. 198

Cathodic Processes on Passive Zirconium

R. E. Meyer, Chemistry Div., Oak Ridge National Lab., Oak Ridge, Tenn.

Measurements were made of the rates of reduction of Cu^{++}, H_2O_2, H^+, and O_2 on passive zirconium in acid solutions of sodium sulfate at temperatures ranging from 25° to 85°C. Rates of reduction at constant potential of these oxidizing agents tended to decrease with time, and Tafel slopes tended to increase with time. The kinetic orders of reduction were determined from potentiostatic experiments in which the current was determined as a function of concentration. Unit orders or nearly unit orders were observed with oxygen reduction, and fractional orders from about 0.5 to 0.65 were observed for Cu^{++} and H_2O_2. Possible mechanisms are suggested in which charge transfer through the film is assumed to play a predominant role.

Abstract No. 199

Kinetics of Anodic Processes in Carboxylic Acids

B. E. Conway and **M. Dzieciuch,** Dept. of Chemistry, University of Ottawa, Ottawa, Canada

Kinetics of the Kolbe type of reaction have been studied at gold, palladium, and platinum for anodic discharge of formate ions and trifluoroacetate ions. Linear Tafel lines are observed over three decades of current density, and the slopes are discussed. Galvanostatic charging and open-circuit decay curves indicate formation of adsorbed intermediates during the anodic reactions. Coulombic efficiencies for product formation have been determined and are discussed in relation to reaction mechanisms.

Abstract No. 200

Faradaic Rectification with Control of Alternating Potential Variations—Application to Electrode Kinetics for Fast Processes

Hiroaki Matsuda and **Paul Delahay,** Dept. of Chemistry, Louisiana State University, Baton Rouge, La.

In this method, the potential of an electrode at which a fast charge transfer process occurs is varied about the equilibrium potential according to a sinusoidal function of time. The resulting alternating current includes a rectification component because of the asymmetry of the current-potential curve. An equation is derived for this faradaic rectification current, and it is shown that the exchange current density and the transfer coefficient can be determined from the variations of the rectification current with time. Two methods of calculation are discussed. A correction for the double layer structure in the solution of the boundary value problem is derived. Conditions for frequency and circuit resistance are established. Finally, it is shown that, because the double layer capacity is in parallel with the faradaic impedance, the alternating variations of potential should in effect be controlled, except for very fast processes, even when the cell current is controlled. Analysis of faradaic rectification at controlled current developed by previous investigators thus may correspond to conditions which are seldom achieved.

Abstract No. 201

The Influence of Cations on the Differential Capacity of the Mercury Dropping Electrode in Methanol and Ethanol Solutions of Electrolytes

S. Minc, Dept. of Electrochemistry, University of Warszawa and Dept. of Electrochemistry, Polish Academy of Sciences, Warszawa, Poland

Differential capacities of the electrical double layer in region of cathodic polarization of LiCl, NaCl, KCl, $MgCl_2$, $CaCl_2$, $SrCl_2$ solutions in methanol have been measured. The effect of concentrations of the KF and LiCl solutions in methanol, ethanol, and water on the differential capacity have been determined. In addition the potential of desorption of Br^- ions in methanol in presence of Li^+ ions and K^+ ions have been investigated. The results give evidence that some cations, especially those of low polarizing ability, are specifically adsorbed at the mercury surface.

Abstract No. 202

Irreversible Thermodynamics in Electrochemistry

A. J. deBethune, Chemistry Dept., Boston College, Chestnut Hill 67, Mass.

The Onsager thermodynamics provides a unified approach to electrolytic systems out of equilibrium, such as concentration cells with transference, initial and final emf's of thermal cells, and thermal diffusion (Soret effect) of ions. For concentration cells, the method justifies the classical results of Nernst. For nonisothermal systems, the product S^*dT is the thermodynamic driving force where S^* is the entropy transported reversibly from the hot to the cold heat reservoir. The emf of a concentration cell, the initial emf of a thermal cell, and the Soret coefficient are determined by the ratios of the reversible fluxes of matter to electricity, of entropy to electricity, and of entropy to matter, respectively.

Abstract No. 203

Potentials in the System, Cr (II)-Cr (III), at Various Electrodes

K. B. Morris, Institute of Technology, Air University, Wright-Patterson AFB, Ohio

Potentials have been measured for the Cr (II)—Cr (III) system at gold, graphite, mercury, and platinum electrodes. Gold and mercury appear to be the best electrodes for two reasons, namely, (*a*) measured potentials are fairly close to theoretical potentials and (*b*) plots of log $[Cr^{+3}]/[Cr^{+2}]$ against emf are linear for those electrodes. The same plot for platinum is linear but the experimental potentials are roughly 300 mv lower than the theoretical potentials.

Abstract No. 204

Electrochemical Study of Metallic Oxides in Fused Lithium Chloride-Potassium Chloride Eutectic

H. A. Laitinen and **B. B. Bhatia,** Noyes Chemical Lab., University of Illinois, Urbana, Ill.

Owing to the relatively high solubilities of metal oxides the applicability of metal oxide electrodes to

the measurement of oxide ion activity is limited to solutions containing oxide ion in concentrations comparable with, or greater than, that contributed by dissolution of the oxides. This limit is $10^{-3}M$ or higher, depending on the system. The relatively high solubility of heavy metal oxides in this solvent is attributed to the great complexing tendency of chloride ion. It is probable that these oxides would be much less soluble in nitrate and sulfate metals and thus their utility as acidity electrodes can be extended to lower oxide concentrations.

Abstract No. 205

Gas-Phase Charged and Electrolytically Charged β-Pd-H Alloys

J. P. Hoare, Scientific Lab., Ford Motor Co., Dearborn, Mich.

Open-circuit potential-time curves were obtained from β-Pd-H electrodes in acid solution made from dry Pd wire in hydrogen gas and from Pd wire cathodes in sulfuric acid solution. Hydrogen content of the wires was determined using ceric sulfate solutions. Evidence is presented to suggest the existence of two kinds of β-Pd-H alloys. Charging mechanisms are suggested.

Abstract No. 206

Kinetics of Cathodic Hydrogen and Deuterium Evolution

B. E. Conway, Dept. of Chemistry, University of Ottawa, Ottawa, Canada

Isotopic ratios R of exchange currents for hydrogen and deuterium evolution have been obtained for palladium, platinized platinum, and copper and are discussed in relation to previous results for other metals. When surface coverage effects are considered, R has the minimum values of 7 or 2 for atom-ion and recombination desorption reactions, respectively, while for slow discharge of oxonium ions R has the minimum value 2.2 in agreement with experiment for mercury. R values for various metals are discussed in terms of rate-determining mechanism.

Abstract No. 207

Behavior of Hydrogen at Oxidized Platinized Platinum Electrodes

N. J. Ward (present address: General Chemical Div., Allied Chemical and Dye Corp., Baton Rouge, La.) and **T. C. Franklin,** Chemistry Dept., Baylor University, Waco, Texas

A study was made of the kinetics of the reaction of hydrogen with a hydrogen depleted platinized platinum electrode in order to get an idea of the mechanism of the reaction. The kinetics was investigated as functions of the pressure of the hydrogen and the area of the electrode. The electrode area was varied by: (a) varying the length of the electrode; (b) varying the coulombs of electricity passed in plating the electrode; and (c) poisoning the electrode with acetonitrile. From this data was deduced a possible mechanism of reaction of platinized platinum electrodes with hydrogen in solution in aqueous sulfuric acid.

Abstract No. 208

Transient Strain Induced Electrode Potentials

Eric Baum, W. F. Seyer, and **Ken Nobe,** Dept. of Engineering, University of California, Los Angeles 24, Calif.

Transient potentials produced when copper and zinc-plated copper wires are elastically strained in $CuSO_4$ and $ZnSO_4$ solutions, respectively, were investigated. The potential response on loading was almost instantaneous and decayed back close to the original value within several seconds. The unloading response was similar to loading but of opposite sign. The amplitude of the response was approximately proportional to the load. Theoretical considerations of the electrical double layer predict the experimental results obtained.

Abstract No. 209

Electrocapillary Studies on Solid Metals

D. N. Staicopoulos, Engineering Research Lab., Engineering Dept., E. I. du Pont de Nemours & Co., Inc., Wilmington, Del.

The use of a revolving-cup friction-measuring apparatus has made possible a study of the adsorption/desorption of ionic species on solid metal/solution interfaces, as a function of applied electrical potential. The results of this study reveal similarities between the friction characteristics at solid metal surfaces and the surface tension of liquid metals under the influence of an applied electrical potential. Specific adsorption and/or chemisorption of ionic species onto solid metal surfaces can thus be detected from the specific changes in the friction/potential characteristics.

Abstract No. 210

A New Model for Evaluating the Conductivities of Dispersions

R. E. Meredith (present address: Chemical Engineering Dept., Oregon State College, Corvallis, Oreg.) and **C. W. Tobias,** Lawrence Radiation Lab. and Dept. of Chemical Engineering, University of California, Berkeley, Calif.

Electrical conductivity measurements have been made on emulsions where the volume fractions and the conductivities of the two phases vary over a wide range. The data obtained indicate that neither Maxwell's nor Bruggeman's relation adequately predicts the effective conductivities of mixtures above a dispersed-phase volume fraction of about 0.2. A new model is proposed which corrects for some of the field interaction that exists between particles in concentrated dispersions of spherical or nonspherical particles.

INDEX TO AUTHORS

(The number in the right hand column is the abstract number used in the Technical Program and in the Abstracts)

	Abstract No.
Adams, I.	53
Agarwal, J. C.	140
Ageev, N. V.	159
Allred, W. P.	88
Allwein, J. H.	158
Altenpohl, Dietrich	6
Andrew, K. F.	176
Antonov-Romanovsky, V. V.	68A
Aretos, Constantin	172
Arpiarian, N.	55
Astier, J.	147
Aven, M.	65
Avinor, M.	57
Baker, D. H., Jr.	125
Barnes, C. E.	38
Barnes, C. R.	18
Barson, Fred	115
Bate, R. T.	94
Baum, Eric	208
Beach, John	174
Becherer, H. K.	120
Beck, T. R.	190
Belz, L. H.	10
Bender, B. G.	118, 119
Bennett, A.	27
Bennett, A. I.	83
Bernard, W. J.	26
Bernstein, L.	118, 119
Berry, R. W.	25
Bhatia, B. B.	204
Blakeslee, A. E.	106
Block, F. E.	124
Bourke, R. C.	96
Breitenstein, J. S.	144
Brophy, V. A.	60
Brown, D. C.	134
Budnick, J. I.	12
Burnham, J.	1
Busen, Karl	107
Butler, K. H.	43
Callinan, T. D.	33
Carlson, O. N.	126, 177
Catotti, A. J.	29
Cattoir, F. R.	125
Cavanagh, R. L.	148
Colburn, J.	112
Collin, F. C.	153
Convey, John	133
Conway, B. E.	199, 206
Cook, J. S.	37
Cooper, H. W.	104
Curie, D.	55, 56
Curie, G.	55, 56
Currey, J. E.	193
Cusano, D. A.	63
deBethune, A. J.	202
Delahay, Paul	187, 196, 200
Dobratz, C. J.	195
Donahue, D. J.	108
Dormsjo, T. O.	143
Doucette, E. I.	104
Dreeben, Arthur	70
Drew, J. W.	180
Dubinin, V. G.	68A
Dzieciuch, M.	199
Eby, J. E.	45
Ellis, R. C., Jr.	78
Elmore, G. V.	181
Fabry, Jean	164
Faria, Sixdeniel	68
Farrell, J. W.	128
Faust, J. W., Jr.	79, 81, 84
Fergusson, J. E.	157
Ferrante, M. J.	124
Fincham, C. J. B.	13
Fisher, J. S.	22
Flint, P. S.	113
Fock, M. V.	68A, 77
Franklin, T. C.	207
Freeman, Horace	145
Frisco, L. J.	32
Frosch, C. J.	97
Fuller, C. S.	90
Gaines, G. B.	171
Geach, G. A.	167
Geesner, C. R.	18
Genco, J. I.	91
Gerlach, L.	110
Gershenzon, M.	97, 98
Gibbs, D. F.	97
Gill, R. W. A.	58
Goering, H. L.	92
Goldberg, Paul	67, 68, 69
Gorton, H. C.	99
Gow, John	115
Grens, E. A.	192
Gresh, M.	16, 25
Guéret, P.	55
Gulbransen, E. A.	176
Guldner, W. G.	11
Haake, C. H.	44
Haberecht, R.	110
Haefling, J. A.	177
Hains, D. J.	137
Halpin, A. T.	67
Hamby, D. C.	19
Hamilton, D. R.	80
Hardy, A. E.	64
Haupin, W. E.	183
Heaney, R. J.	156
Heil, V. E.	169
Himes, R. C.	91, 92
Hine, Fumio	179
Hoare, J. P.	205
Holden, F. C.	168
Houtz, C. C.	11, 30
Hozak, N. L.	37
Huber, F.	20
Huebler, J.	136
Hummers, W. S.	54
Hunter, M. S.	9
Hyde, R. W.	142
Ibl, Norbert	189
Jaek, I. W.	77B
Jaffe, P. M.	73, 74
Jaffee, R. I.	168
James, B. D.	113
James, W. J.	129
Jenny, A. L.	15
Jensen, R. V.	95
Jerome, C. W.	46
John, H. F.	79, 81
Johnson, P. D.	48
Jordan, E. L.	108
Jungfleisch, Marie-Louise	161, 164
Kaiser, W.	90
Kamyszek, K.	75
Karlik, S.	16
Kenahan, C. B.	129A
Keyser, N. H.	152
Keywell, Frank	103
Kircher, M. S.	193
Klick, C. C.	59
Klement, F. D.	54
Knight, H. T.	17
Kobuke, Yoshimasa	50
Koller, L. R.	62
Komjathy, S.	130
Kulwicki, B. M.	93
Kushida, Takashi	50

	Abstract No.
Lachman, J. C.	170
Laitinen, H. A.	204
Lambe, J.	39
Lane, R.	27
Langlais, D. G.	102
Langston, B. G.	141
Law, J. M.	24
Lawson, W. D.	100
Lebert, Guy	163
Lehovec, Kurt	2, 105
Longini, R. L.	83
Lougher, E. H.	96
Lubker, R. A.	139
Lüdja, G. G.	77B
Lushchik, Ch. B.	77B
Lushchik, N. E.	77B
Lynn, Scott	191
Mackintosh, I. M.	109
MacMullin, R. B.	194
Malouf, E. E.	156, 160
Markham, J. J.	42
Mason, D. R.	37, 38, 93
Masuda, Isoo	50
Matsuda, Hiroaki	196, 200
Maykuth, D. J.	168
McGahan, T. E.	111
McGurty, J. A.	170
McLean, D. A.	21
Meeks, Earl	107
Mehnert, R. A.	104
Mellichamp, J. W.	53
Meredith, R. E.	210
Merrill, T. W.	127
Meyer, L. H.	182
Meyer, R. E.	198
Meyerhofer, D.	95
Mikulyak, R. M.	98
Miller, J. F.	92
Milner, P. C.	197
Minc, S.	201
Mitchell, Will, Jr.	146
Mohler, D.	5
Moll, G. J.	180
Moody, P. L.	85
Moore, R.	112
Morris, K. B.	203
Moss, R.	84
Mullin, J. B.	87
Mudar, J.	39, 75
Murphy, T. C.	169
Narasimham, K. C.	185
Nechtow, Marshall	103
Neely, L. F.	169
Nicholson, H.	84
Nobe, Ken	208
Nudelman, S.	39, 75
Nyholm, R. S.	157
Okada, Shinzo	179
O'Nan, T. C.	23
Orme, J. E.	14
Osiko, V. V.	77A
Owen, C. V.	126
Parks, A. M.	31
Paskell, Ernest	120
Pihl, Carl	105
Pitman, H. W.	19
Port, J. H.	162
Potter, R. M.	61, 65
Prater, J. D.	160
Prokhorov, A. M.	68A
Rairden, J. R.	7, 8
Rajala, B. R.	131
Reed, T. F.	140
Reid, F. J.	99
Rice, O. R.	138
Richards, W. C.	24
Root, G. S.	174
Ropp, R. C.	52
Rosi, F. D.	95
Ross, H. U.	135
Rothschild, S.	58
Ruff, Henri	161
Ruscetta, R. A.	15
Russ, Robert	4
Salomon, T.	35
Samelson, Harold	60
Sangster, R. C.	86
Savitski, E. M.	165, 166
Schlain, David	129A
Schmidt, F. A.	177
Schmidt, P. F.	20
Schwartz, N.	17, 25
Schwarz, K. K.	77B
Schwarz, R. F.	20
Schwuttke, G. H.	89
Seidensticker, R. G.	80
Seyer, W. F.	208
Sharbaugh, A. H.	34
Shehtman, V. Sh.	159
Shipley, E. H.	140
Shtasel, A.	17
Simon, R.	96
Smith, A. L.	51
Smith, A. W. H.	36
Smith, F. A.	100
Smith, I. L.	65
Smith, R. C.	82
Smith, W. J.	83
Solomon, A. L.	69
Spector, C. J.	111
Spedding, F. H.	177
Staicopoulos, D. N.	209
Stambaugh, E. P.	91
Stamets, R. J.	28
Stavik, O.	116
Stephens, F. M., Jr.	141
Stephenson, Donald	4
Stern, D. R.	184
Stotler, H. H.	139
Straumanis, M. E.	129
Strauss, A. J.	85
Strock, L. W.	76
Sundararajan, S.	185
Tanner, H. A.	181
Thomas, M. J. B.	46
Thornton, W. A.	66
Thurmond, C. D.	90
Tobias, C. W.	191, 192, 210
Towner, P. F.	9
Tragert, W. E.	7, 8
Trapeznikova, Z. A.	68A
Tribalat, Suzanne	155
Trytten, G.	39
Turner, D. R.	101
Tylkina, M. A.	165, 166
Udupa, H. V. K.	185
Udy, M. C.	151
Uehara, Yasuo	40, 50
Urban, M. J.	25
Vaaler, L. E.	178
Van Thyne, R. J.	131
Van Uitert, L. G.	47
Vermilyea, D. A.	188
Vialle, Jean	172
Villani, G. J.	13
Vinokurov, L. A.	77
Wachtel, A.	71, 72
Walde, H.	149
Ward, N. J.	207
Warin, M. P.	173
Warren, W. B.	118, 119
Weeks, A. D.	123
West, R. A.	28, 29
Wild, R.	150
Willardson, R. K.	88
Williams, F. E.	41, 49
Wirtz, L. H.	33
Wlodek, S. T.	132, 175
Wolff, G. A.	53
Wulff, John	175
Yeager, Ernest	186
Yoshizawa, Shiro	179
Young, A. S.	100
Young, L.	3, 14
Zimmerley, S. R.	154, 160

Expanding the Frontiers of Space Technology in

ELECTROCHEMISTRY

Lockheed Missiles and Space Division is making significant contributions in electrochemistry in the development of high energy batteries and fuel cells.

Basic research is being conducted in heterogenous catalysis; photochemistry; physical chemistry; solid state chemistry; electrode kinetics; and mass transfer.

Chemical engineering design and development work includes pilot plant operation; fluid flow; heat transfer; and automatic control.

Engineers and Scientists—The advanced nature of Lockheed's projects in electrochemistry provides an excellent opportunity for scientists and engineers to advance their professional status in an ideal working environment. If you are experienced in electrochemistry or in related work, you are invited to share in the future of a company with an outstanding record of achievement and make an important individual contribution to your country's scientific progress. Write: Research and Development Staff, Dept. C-26, 962 W. El Camino Real, Sunnyvale, California.
U.S. citizenship or existing Department of Defense clearance required.

Lockheed / **MISSILES AND SPACE DIVISION**

Systems Manager for the Navy POLARIS FBM; the Air Force AGENA Satellite in the DISCOVERER Program and the MIDAS and SAMOS Satellites; Air Force X-7; and Army KINGFISHER

SUNNYVALE, PALO ALTO, VAN NUYS, SANTA CRUZ, SANTA MARIA, CALIFORNIA
CAPE CANAVERAL, FLORIDA • ALAMOGORDO, NEW MEXICO • HAWAII

Current Affairs

Hiram S. Lukens

The death of Hiram Stanhope Lukens on November 25, 1959 was a great loss to the chemical profession.

Those who were fortunate enough to have technical association with him were aware of his keen scientific mind, his enormous fund of basic chemical knowledge, and his adaptability in solving problems in industrial chemical technology (since he never spoke of this side of his professional endeavors). His 23 patents (U.S., Canadian, British, and German) were principally in the electrochemical field.

Dr. Lukens served the interests of The Electrochemical Society long and well. He was Secretary of the Philadelphia Section, 1930-1931, and Chairman of the local group 1931-1932. He felt honored to be President of the national Society, 1934-1935, and served on its Executive Committee, 1934-1939. He was Chairman of the Electrodeposition Division of the Society, 1931-1932, and in later years served on the Committee on Research Projects, was Chairman of the Committee on Research Fellowships, 1949-1950, and was a member of the Ways and Means Committee of the Society, 1946-1950.

He was an Honorary Member of the American Electroplaters Society.

Dr. Lukens was equally active in the American Chemical Society. He was Chairman of the Philadelphia Section, 1924-1925, a Councilor of the national society, 1926-1947, and a member of the committee on Licensing Inquiry, 1939-1944. He was a trustee of the Philadelphia Section, 1933-1948.

In the American Institute of Chemical Engineers, he was active on the Executive Committee of the Philadelphia-Wilmington Section, 1933-1939, serving as both Vice-Chairman and then Chairman of that group. For the national society, he served on the Committee on Papers, 1936-1940, and in 1945 on the Committee for Professional Legislation.

At the Franklin Institute, during the period 1937-1956, Hiram Lukens served on many committees—on Science and the Arts, Bartol Research Foundation, Publications, Research—and was on the Board of Managers, 1942-1956.

He was on the Board of Governors of the Pennsylvania Chemical Society 1950- and was president of the University of Pennsylvania Chapter, The Society of the Sigma Xi, in 1936.

He was a civilian appointee, Chemical Warfare Service, in World War I. From 1934 to 1937, he was a member of the Division of Chemistry and Chemical Technology, National Research Council. During World War II, he was Chairman of the Committee on Flatware for Army Use, War Metallurgy Committee, Office of Scientific Research and Development.

Hiram Lukens was a native Philadelphian, graduating from Central High School in 1902. He received his B.S. degree in Chemistry from the University of Pennsylvania in 1907 and his Ph.D. in Chemistry in 1913, and from 1907 until 1953 was a faculty member at that institution. He served as the Director of the Department of Chemistry and Chemical Engineering from 1932 to 1952. His list of scientific publications numbers more than 30. His greatest pride was the product of the Department of Chemistry and Chemical Engineering, the students, both graduate and undergraduate, and the success they enjoyed in their chosen profession after leaving the university. As evidence of this, upon being chosen Director of the Department in 1932, he gave up all outside private consulting so that he might devote all of his energy to the furtherance of the department and his students, not only his former students but other fellow chemists. He was a counselor to thousands in the profession, confidant of hundreds, and a real friend to any who sought his advice or help in any matter. He was an extremely modest man, quiet spoken and beloved by all who knew him intimately.

A number of Dr. Lukens' friends have expressed a desire to establish a Hiram S. Lukens Memorial Fund, to be used for undergraduate scholarship aid in chemistry at the University of Pennsylvania. The details are now being worked out and further information will be published in the next issue of this JOURNAL.

Executive Committee of the
Philadelphia Section

Brief Communications

The JOURNAL accepts short technical reports having unusual importance or timely interest, where speed of publication is a consideration. The communication may summarize results of important research justifying announcement before such time as a more detailed manuscript can be published. Consideration also will be given to reports of significant unfinished research which the author cannot pursue further, but the results of which are of potential use to others. Comments on papers already published in the JOURNAL should be reserved for the Discussion Section published biannually.

Submit communications in triplicate, typewritten double-spaced, to the Editor, Journal of The Electrochemical Society, 1860 Broadway, New York 23, N. Y.

ACS Award to Paul Delahay for Contributions to Electrochemistry

Dr. Paul Delahay, Boyd Professor of Chemistry, Louisiana State University, received the 1959 annual Southwest Regional Award of the American Chemical Society on December 4, 1959 in Baton Rouge at the annual regional meeting of the six southwestern states sections.

The award was given in recognition of Dr. Delahay's work in various areas of electrochemistry: diffusion processes, electrode kinetics, adsorption phenomena, double layer phenomena, dry and wet corrosion, electroanalytical methods, etc. His work includes more than 70 research publications and two books, "New Instrumental Methods of Electrochemistry" and "Instrumental Analysis."

Dr. Delahay, who was born in the Netherlands, received his B.S. and an M.S. degree in chemistry from the University of Brussels, and an M.S. in electrical engineering from the University of Liege. In 1947 he received his Ph.D. degree at the University of Oregon, and was a research associate there before joining Louisiana State University in 1950. Over the last ten years, he has attracted an international group of collaborators and students to do research work at LSU under his direction.

Among his other awards are the 1951 Turner Memorial Award of The Electrochemical Society and the 1955 Award in Pure Chemistry of the American Chemical Society. He was a Guggenheim Fellow at Cambridge University in 1955 and a National Lecturer for Sigma Xi in 1958.

Dr. Delahay has been active in The Electrochemical Society since 1950, most recently serving as Chairman of the International Symposium on Electrode Processes held during the Philadelphia Meeting in May 1959.

New Members

In January 1960, the following were elected to membership in The Electrochemical Society by the Admissions Committee:

Active Members

J. B. Andelman, Dept. of Chemistry, New York University, New York 1, N. Y. (Theoretical Electrochemistry)

E. C. Bertucio, International Nickel Co., Inc., 67 Wall St., New York 5, N. Y. (Electrodeposition)

A. K. Bose, The Wheel & Rim Co. of India Private Ltd., Huzur Gardens, Sembian, Madras 11, South India (Electrodeposition)

Michael Boudart, Princeton University; Mail add: RFD 3, Princeton, N. J. (Theoretical Electrochemistry)

R. C. Brown, Delco-Remy Div., General Motors Corp., West Willard St., Muncie, Ind. (Battery)

W. G. Cople, Allison Div., General Motors Corp.; Mail add: 168 Cedar Bluff Dr., Indianapolis, Ind. (Theoretical Electrochemistry)

Floris De Boer, N. V. Philips' Gloeilampenfabrieken; Mail add: Leenderweg 218, Eindhoven, Netherlands (Electronics)

J. M. Demangone, Sylvania Electric Products Inc.; Mail add: 106 York Ave., Towanda, Pa. (Electronics)

E. E. Denhard, Jr., Armco Steel Corp., 3400 E. Chase St., Baltimore 13, Md. (Corrosion)

J. F. Dewald, Bell Telephone Labs., Inc., Murray Hill, N. J. (Theoretical Electrochemistry)

Alfred Ertel, I.T.T. Components Div., P. O. Box 412, Clifton, N. J. (Electronics)

G. E. Fitzgibbon, P. R. Mallory & Co., Inc., 3029 E. Washington Ave., Indianapolis 6, Ind. (Electronics, Electrothermics & Metallurgy)

L. E. Gierst, University of Brussels, 50 Ave. F. D. Roosevelt, Brussels, Belgium (Theoretical Electrochemistry)

A. G. Griffith, Scovill Manufacturing Co., 99 Mill St., Waterbury 20, Conn. (Electrodeposition, Electrothermics & Metallurgy)

A. H. Gropp, University of Florida; Mail add: 1715 N. W. 10 Terrace, Gainesville, Fla. (Electro-Organic)

M. T. Hagestad, Ray-O-Vac Co.; Mail add: Box 353, R.F.D. 1, McFarland, Wis. (Battery, Electro-Organic, Theoretical Electrochemistry)

D. L. Hill, Chemistry Dept., Rensselaer Polytechnic Institute, Troy, N. Y. (Electrodeposition, Theoretical Electrochemistry)

By action of the Board of Directors of the Society, all prospective members must include first year's dues with their application for membership.

Also, please note that, if sponsors sign the application form itself, processing can be expedited considerably.

D. P. Ignacz-Olasz, Fairchild Semiconductor Corp., 844 Charleston Rd., Palo Alto, Calif. (Electrodeposition)

E. W. Jensen, General Transistor Corp., 91-27 138th Pl., Jamaica 35, N. Y. (Electronics Electrothermics & Metallurgy)

W. D. Johnston, Westinghouse Research Labs.; Mail add: 2416 Collins Rd., Pittsburgh 35, Pa. (Electronics)

J. C. Jongkind, Metal & Thermit Corp.; Mail add: 15208 Leland Dr., Roseville, Mich. (Electrodeposition, Industrial Electrolytic)

G. P. Katona, Corning Glass Works; Mail add: 140 E. Denison Parkway, Corning, N. Y. (Electronics)

F. J. Krivanek, Union Carbide Consumer Products Co., Inc.; Mail add: 6197 Stanbury Rd., Parma 29, Ohio (Battery)

Costas Lagos, Sylvania Electric Products Inc.; Mail add: 1 Harbor St., Salem, Mass. (Electronics)

T. C. Manley, Welsbach Corp., 2409 W. Westmoreland St., Philadelphia 29, Pa. (Electric Insulation)

C. C. Merrick, Jr., Texas Instruments, Inc., Station 29, SC Bldg., Box 312, Dallas 21, Texas (Electronics)

R. L. Mitchell, Jr., Chlorine Institute, Inc., 342 Madison Ave., New York 17, N. Y. (Industrial Electrolytic)

L. W. Niedrach, Research Lab., General Electric Co., Schenectady 9, N. Y. (Battery)

R. C. Osthoff, Leads & Bases Engineering, Lamp Div., General Electric Co., 1133 E. 152 St., Cleveland 10, Ohio (Corrosion)

Sreenivasa Panchapakesan, T. I. Cycles of India, Ambattur, Madras, South India (Corrosion, Electrodeposition, Electronics, Electrothermics & Metallurgy, Industrial Electrolytic)

R. R. Paxton, Pure Carbon Co.; Mail add: 725 Evergreen Rd., St. Marys, Pa. (Battery)

P. Ranachandra Rao, M/S Philips India Ltd.; Mail add: 6 Tadiwala Rd., Poona 1, Bombay, India (Corrosion, Electrodeposition)

E. C. Rinker, Sel-Rex Corp., 75 River Rd., Nutley 10, N. J. (Electrodeposition)

E. L. Shriver, Allison Div., General Motors Corp.; Mail add: 39 E. 37 St., Apt. 1, Indianapolis 5, Ind. (Electrothermics & Metallurgy)

David Singman, Diamond Ordnance Fuze Labs.; Mail add: 703 Kennedy St., N. E., Washington 11, D. C. (Battery)

V. J. Spera, Electric Storage Battery Co.; Mail add: 3019 N. 22 St., Philadelphia 32, Pa. (Battery)

Neill Weber, Mellon Institute; Mail add: 1618 Williamsburg Pl., Pittsburgh 35, Pa. (Theoretical Electrochemistry)

D. R. Weiser, Champion Paper & Fibre Co., Hamilton, Ohio (Electrodeposition)

M. L. Whitehurst, R.C.A. Victor Div.; Mail add: 1811 N. Bancroft St., Indianapolis 18, Md. (Electrodeposition)

R. K. Willardson, Battelle Memorial Institute; Mail add: 3086 Gerbert Rd., Columbus 24, Ohio (Electronics-Semiconductors)

D. V. Williamson, Sylvania Electric Products Inc.; Mail add: 137 Newcastle Rd., Peabody, Mass. (Electronics)

Associate Members

L. F. Howard, P. R. Mallory & Co., Inc.; Mail add: 4101 English Ave., Indianapolis 1, Ind. (Battery, Corrosion, Electric Insulation, Electronics)

H. H. Jennison, Jr., P. R. Mallory & Co., Inc.; Mail add: 2220 N. Kitley Ave., Indianapolis 18, Ind. (Electronics)

A. R. Poirier, D. W. Onan Co.; Mail add: 4550 Central Ave., Minneapolis 21, Minn. (Battery)

D. R. Wolter, Ray-O-Vac Co., Div. of Electric Storage Battery Co., 525 University Ave., Madison, Wis. (Battery)

Student Associate Members

R. F. Steigerwald, Dept. of Metallurgical Engineering, Rensselaer Polytechnic Institute, Troy, N. Y. (Corrosion, Theoretical Electrochemistry)

Reinstatements to Active Membership

Emilio Gagliardi, Celulosa Argentina, S. A., Casilla de Correo No. 3499, Buenos Aires, Argentina, South America (Battery, Corrosion, Electric Insulation, Electronics, Industrial Electrolytic)

J. A. Keralla, Delco-Remy Div., General Motors Corp.; Mail add: 934 W. Hartman Rd., Anderson, Ind. (Battery)

E. C. Olson, The Upjohn Co., Kalamazoo, Mich. (Electro-Organic)

R. S. Spooner, Aluminium Labs. Ltd., Kingston, Ont., Canada (Corrosion, Electrodeposition)

E. M. Strohlein, Electric Storage Battery Co.; Mail add: 15 Chalfont St., Palmyra, N. J. (Battery)

Transfers from Associate to Active Membership

F. J. Marasa, International Rectifier Corp.; Mail add: 305 W. Palm Ave., El Segundo, Calif. (Electronics)

Aleksandrs Martinsons, American Potash & Chemical Corp.; Mail add: 511 Utah St., Boulder City, Nev. (Theoretical Electrochemistry)

Deceased Members

W. H. Aldridge, New York, N. Y.

S. J. Lloyd, University, Ala.

H. D. MacPherson, Philadelphia, Pa.

E. K. McMahon, Nashville, Tenn.

J. P. Oliver, Berea, Ohio

Electronics Division Enlarged Abstracts, Spring 1960

The Electronics Division will again print an "Enlarged Abstracts" booklet containing 1000-word abstracts of papers to be presented before the Division's symposia on Luminescence, Semiconductors, and General Electronics at the Chicago Meeting of The Electrochemical Society, May 1-5, 1960.

The booklets will contain about 300 pages and are expected to be ready for distribution two weeks before the meeting.

The price will be $3.50 with a discount of $00.50 per copy for orders accompanied by payment and requiring no invoicing. Orders requiring invoicing will be charged the full price even though payment does accompany the order.

Checks should be made payable to: Electronics Division, The Electrochemical Society, and should be sent to:

Austin E. Hardy
Secretary-Treasurer
c/o Radio Corp. of America
New Holland Pike
Lancaster, Pa.

Extra copies, if any, will be on sale at the convention in Chicago.

Personals

Bernard Agruss, formerly head of the Battery and Electrochemical Depts. at the National Lead Co. Research Labs. in Brooklyn, N. Y., has become affiliated with the Research Dept., Allison Div., General Motors Corp., Indianapolis, Ind., as section chief, Physical Chemistry Section.

Summer Sheff has joined the Raytheon Manufacturing Co., Semiconductor Div., Newton, Mass., as senior engineer. Previously he was with the M.I.T. Lincoln Lab. in Lexington, Mass.

Paul F. Schmidt, previously research section manager, Philco Corp., Philadelphia, Pa., is now supervising chemist, Solid State Physics Dept., Westinghouse Research Labs., Pittsburgh, Pa.

George D. Vincent has taken a position with Nortronics, a division of Northrop Corp., in charge of the maintenance and extension of their primary electrical standards in the Electrical Instrument Calibration Lab. at Anaheim, Calif. He had been director of standards at The Eppley Lab., Inc., Newport, R. I.

Harold K. Hughes has been appointed director of the Dept. of Physics at the Central Research and Engineering Div. of Continental Can Co. in Chicago. Dr. Hughes will head the company's research work on application of the principles of physics to high-speed automatic equipment for the production and quality control of metal, paper, plastic, glass, and composite containers and closures, and for any future radiation program. From 1945 to 1958, Dr. Hughes held positions in the field of applied physics with the Celanese Corp. of America, Socony-Mobil Oil Co., and the Markite Corp.

G. M. Butler, Jr., has been named as director of research of Gladding, McBean & Co., Los Angeles, Calif.

Earl J. Serfass has resigned as head of the Dept. of Chemistry at Lehigh University, Bethlehem, Pa., to accept a position as a member of the board of directors and vice-president in charge of research and development of the Milton Roy Co., Philadelphia. Dr. Serfass had been a member of the Lehigh faculty since 1936.

H. V. K. Udupa has been nominated as a member of the Sub-Committee of the Development

Council for Alkalies and Allied Industries to report on Norms of Efficiency in Caustic Soda Industry, Ministry of Commerce and Industry, Government of India. He also has been nominated as a member of the Secondary Cells and Batteries Sectional Committee, ISI.

J. Balachandra, India, has been awarded the Licentiateship, by examination, of the Institution of Metallurgists, London.

K. S. G. Doss has been nominated as a member of the Advisory Editorial Board of "Electrochimica Acta," Electrotechnical Division Council, ISI, and Advisory Committee of the Madras Branch, ISI.

K. Rajagopal has been designated as chief engineer, Mettur Chemical and Industrial Corp. Ltd., Mettur Dam R.S., India.

A. Jogarao, India, has been nominated as a member of the Electroplating Sectional Committee, ISI.

Section News

Ontario-Quebec Section

The first meeting of the 1959-1960 season was a dinner meeting held in Toronto on November 10, 1959 at the King Edward Sheraton Hotel, with Dr. W. C. Gardiner, President of the Society, as a special guest.

Two very interesting papers were presented: "Unusual Corrosion Problems" by Dr. Mars G. Fontana, chairman, Dept. of Metallurgical Engineering, Ohio State University, and "Development of the Athabaska Tar Sands Using Conventional and Nuclear Methods" by Dr. John Convey, director, Mines Branch, Dept. of Mines and Technical Surveys, Ottawa. Dr. W. B. F. MacKay, chief research and product development engineer, Atlas Steels Ltd., Welland, Canada, acted as technical chairman.

E. R. Landry, *Secretary-Treasurer*

Indianapolis Section

The Indianapolis Local Section held its second technical meeting of the current season on Tuesday, January 12, at Butler University in Indianapolis. Dr. Donald E. Koontz of the Bell Telephone Laboratories spoke on "Surface Cleaning and Treatment of Electronic Device Parts."

In his interesting and informative presentation, Dr. Koontz pointed out that the useful functions of electron tubes and semiconductor devices were the result of impurity dominated phenomena. Counteracting contaminants markedly affect characteristics, life, and reliability of devices. Results of Bell Labs. efforts to develop methods for evaluating their presence, as well as reducing their level, were discussed, together with specific examples illustrating improvement in performance resulting thereform; most instances were drawn from experiences in electron tube fabrication. The discussion included the detection and control of dust, lint, organic materials, water-soluble and chemically combined contaminants, and gaseous contaminants; also a new acid etching process which removes both imbedded and adsorbed materials. A discussion period concluded the evening's activities.

Thomas C. O'Nan,
Secretary-Treasurer

Book Reviews

Kinetics of High-Temperature Processes. Edited by W. D. Kingery. Published jointly by the Technology Press of Massachusetts Institute of Technology and by John Wiley & Sons, Inc., New York, and Chapman and Hall, Ltd., London, 1959. xvi + 326 pages; $13.50.

The fast-growing technologies of rocketry and nuclear energy place great emphasis on materials of construction which withstand high temperatures. This, together with a renaissance in the older disciplines of extractive metallurgy and glass making, has stimulated research on ceramics and inorganics generally, paced by sophisticated studies in physics and chemistry. The study of nonmetals at high temperatures is greatly increased in relative importance both as a science and as a technology. The Endicott House conference of June 1958 treated a major aspect of this field at the current research level, namely kinetics at elevated temperatures of processes in nonmetallic condensed phases (mostly solids).

The papers which issued from the conference and make up this volume are of almost uniformly high quality and will be of interest to specialists as records of important research and thought. However, the editor and the conference committee have aimed at giving this volume broader usefulness. They have attempted to select the authors and to comment editorially on their work in such a way that the collected papers might serve as an introduction to high-temperature kinetics for the general reader and a source of interdisciplinary contacts for specialists. This is a most ambitious objective and the editor and committee are to be complimented on having come quite close to their goal.

The 35 research papers reported have been divided into seven sections: I. Imperfections and Diffusion in Non-metals, II. Diffusion in Liquids and Liquid-Solid Reactions, III. Nucleation and Grain Growth, IV. Sintering and Vitrification, V. Phase Transformations, VI. Solid-Solid Reactions, and VII. Solid-Gas Reactions. The authors are largely concerned with scientific concepts rather than specific engineering applications, although a few papers are decidedly bent in the direction of applications.

The major weakness of the book for the general reader is that, inevitably, some important subjects are left out entirely and a few others are not treated in a representative way. It may not be fair to criticize a conference for this necessary weakness but the general reader should be made aware of specific limitations and this reviewer has noted the following. The kinetics covered are associated largely with slow atom movements such as diffusion. The kinetics of high-speed atom movements, as in thermal conductivity, are neglected. The kinetics of processes in melts and of phase transformations are in no way representative of current research in these extensive fields, despite the individual merits of several good papers. Only four papers are included in the section on liquids and, of these, one is on liquid metals, two are on silicates, and the fourth is only one-and-a-half pages long. It is unfortunate that the editorial introduction to the section on liquids leaves the impression that the underdeveloped area of mattes, slags, and glasses is all there is to the subject and ignores the extensive work on those materials generally denoted as fused salts.

On the other hand, the kinetics of slow atom movements in solids at high temperatures are covered with both breadth and completeness. Sections III and IV, which cover nucleation, grain growth, and sintering, are sufficient to serve virtually as a 100-page text on the subject. The two papers on the oxidation of metals in section VII and the three papers on diffusion in oxides in section I together make an exceptionally good review of the kinetics of high-tem-

perature oxidation reactions, which has become one of the most important branches of solid-state chemistry.

The value of this volume to the general reader is greatly enhanced by editorial work of unusual excellence. The editor has provided an introduction to the book in which he reviews basic concepts of kinetics, and a brief introduction to each section. These merit reading even by one who does not have the time to study the separate papers. The discussions at the end of each section are well edited and add much to the value of each paper. The entire volume is carefully indexed.

G. P. Smith

Ammonia Manufacture and Uses, by A. J. Harding. Published by Oxford University Press, New York, 1959. 41 pages; $1.05.

Electrolytic Manufacture of Chemicals from Salt, by D. W. F. Hardie. Published by Oxford University Press, New York, 1959. 74 pages; $1.20

These are two books in a series being prepared by Imperial Chemical Industries, Ltd., aimed at bridging the gap between industrial practice and the chemistry taught in the schools. Each of the books beautifully explains an essential industry as applied physical chemistry and economics. The book on electrolysis of salt starts with a general discussion of the fundamentals of electrolysis and the economic aspects of the raw material and energy supply. Manufacturing processes for production of chlorine, caustic soda, and sodium are then described in detail. Packing, storage, and transport of products, production trends and statistics, physical and chemical properties of the products, and their uses are discussed. Finally, the historical development of the industry is outlined and a chronology and bibliography are given. The book on ammonia follows much the same general outline.

Both books are well written although so concise in places as to be telegraphic. They have been prepared with the assistance of the Science Masters' Association and the Association of Women Science Teachers. This reviewer would suggest that the series, if these two books prove to be representative, would be valuable to American high school teachers who, because of the requirements for teacher's licenses, are apt to be long on education courses and short on scientific background.

H. W. Salzberg

Metallurgical Thermochemistry (Third Edition), by O. Kubaschewski and E. LL. Evans. Published by Pergamon Press Inc., New York, 1958. 426 pages; $10.00.

This new edition follows the general outline of the preceding volumes. The subject matter is divided into five major parts: 1. the theoretical basis; 2. experimental methods; 3. the estimation of thermochemical data; 4. tabulations of data; 5. examples of thermochemical treatment of metallurgical problems.

The last part of the book, dealing with the examples of thermochemical treatment of metallurgical problems, is the revised section. The changes are the substitution of the refining of iron for the reducibility of magnesium oxide and the addition of two more examples: 1. the solubility of alumina in nickel, and 2. assessment of standard values for silicon monoxide. Interpretation of experimental results in the assessment of standard values is very brusquely treated, probably because of lack of space.

The book is clearly written and precise, and stresses experimental methods and techniques. It contains a great fund of cross-referenced information assembled from scattered data and effectively presented together with independent cross checks. It is of great value both to the academic and the industrial metallurgical chemist.

Minocher Patel

Letter to the Editor

Dear Sir:

I feel that I cannot ignore the comments in your Editorial in the December 1959 issue.

You state that "if first-year college chemistry does not provide proper factual and background material for a prospective high school teacher, perhaps something is wrong with the course." It is just exactly this misconception which has led to much of our difficulty. In order to teach chemistry effectively one must understand the material, not merely know the facts. The knowledge of "thermodynamics, quantum theory, and reaction mechanism" is a necessary part of the understanding of chemistry, without which the teacher can do no more than to read the textbook to the students. Many of the misconceptions which the college chemistry teacher must help his students "unlearn" come from misstatements made by high school teachers who do not really understand chemistry.

E. C. Lingafelter
Professor of Chemistry
University of Washington
Seattle 5, Wash.

News Items

New ECS Sustaining Members

The following recently became Sustaining Members of The Electrochemical Society:

Thomas A. Edison Research Laboratory, Division of McGraw-Edison Co., West Orange, N. J.

Mallinckrodt Chemical Works, St. Louis, Mo.

Frontiers in Chemistry Lecture Series

The 19th annual Frontiers in Chemistry lectures, an activity of the Dept. of Chemistry of Western Reserve University, Cleveland, Ohio, began on February 12 and will continue through April 8. The 19th annual series covers two major topics: Part I. Surface Phenomena, and Part II. Free Radical Reactions.

The lectures are scheduled on consecutive Fridays from February 12 through April 8, with the exception of March 18. In addition to the Friday evening lectures, a special Saturday session will be held as part of Part II on March 19 on photochemistry and the radiation chemistry of organic compounds.

The complete program follows.

Part I

Feb. 12—"On Micro Emulsions and the Selective Diffusion of Ions through Oil/Water Interfaces" by Jack H. Schulman

Feb. 26—"Electrophoresis and Other Electrokinetic Phenomena" by J. J. Hermans

March 11—"New Approaches to the Study of Contact Catalysis" by Paul H. Emmett

March 25—"Surface Activity in Nonaqueous Liquids" by W. A. Zisman

April 8—"Adsorption and Exchange Processes at the Metal-Solution Interface" by J. O'M. Bockris

Part II

Feb. 19—"Directive and Solvent Effects in the Attack of Atoms and Radicals upon Carbon-Hydrogen Bonds" by Glen A. Russell

March 4—"New Polymers—New Problems" by H. F. Mark

March 19 (A.M.)—"Photochemical Production of Free Radicals" by Richard M. Noyes

March 19 (A.M.)—"The Radiation Chemistry of Organic Compounds Containing Electronegative Groups" by Amos S. Newton

April 1—"Free Radical Reactions and the Photochemistry of Ketones" by E. W. R. Steacie.

Korea to Get Soda Ash Plant

The Republic of Korea has taken a further step toward self-sufficiency with the recent signing of a loan agreement for a $5,600,000 soda ash plant to be built in that country. The loan will come from the U. S. Development Loan Fund for financing and construction.

The plant, slated to be completed in two years, will be capable of producing 37,030 tons of soda ash, 4,900 tons of caustic soda, and 2,450 tons of sodium bicarbonate annually. This plant alone will be able to meet the country's requirements for these chemical products.

This brings the DLF loans thus far approved for South Korea to a total of $12,740,000. A loan of $2,140,000 also has been approved for modernization of the Orient Cement Manufacturing Co. which operates a 150,000-ton-a-year cement plant on the Korean east coast.

Other loans approved by DLF are $1,500,000 for design work on the projected Choongjoo 150,000-kw hydroelectric power plant, and a loan of $3,500,000 for modernization of communication facilities which were badly damaged after the Korean War.

Not until after the Korean War was there an opportunity to give any attention to the need for basic, large-scale industries in South Korea. From 1945 until 1958, all heavy industry products were imported.

Pennsalt Chemicals to Build Technical Center

Pennsalt Chemicals Corp., Philadelphia, has concluded negotiations with Cabot, Cabot & Forbes to purchase a 50-acre site in the King of Prussia Park for construction of a Technical Center which will ultimately represent an investment of $6,000,000. This Park, located at the Valley Forge Interchange of the Pennsylvania Turnpike, is one of 14 industrial parks developed by Cabot, Cabot & Forbes along the Eastern Seaboard.

Plans call for a campus-type arrangement featuring a central mall. The first building in the complex will be a two-story laboratory occupying approximately 21,000 square feet. This will be devoted to product development and technical service on Pennsalt's proprietary chemicals for the metal-working industry, laundry and dry cleaning trade, food and dairy plants, as well as consumer products for the farm and home. The Isotron refrigerant and aerosol propellant technical group will also occupy expanded facilities in the new building.

Construction of the first building started early in 1960 and will be completed before the end of the year.

New Prefixes for Units

(Reprinted from the *NBS Technical News Bulletin*, October 1959.)

The National Bureau of Standards has decided to follow the recommendations of the International Committee on Weights and Measures to use new prefixes for denoting multiples and sub-multiples of units. The Committee adopted the prefixes at its meeting in Paris in the fall of 1958. In addition to the eight numerical prefixes in common use, which are given in the table below, the Committee expanded the list by adding the four prefixes marked with an asterisk. Thus, for example, 10^{-12} farad is called 1 picofarad, and is abbreviated 1 pf.

Multiples and Sub-multiples	Prefixes	Symbols
$1\,000\,000\,000\,000 = 10^{12}$	tera*	T
$1\,000\,000\,000 = 10^{9}$	giga*	G
$1\,000\,000 = 10^{6}$	mega	M
$1\,000 = 10^{3}$	kilo	k
$100 = 10^{2}$	hecto	h
$10 = 10$	deka	dk
$0.1 = 10^{-1}$	deci	d
$0.01 = 10^{-2}$	centi	c
$0.001 = 10^{-3}$	milli	m
$0.000\,001 = 10^{-6}$	micro	μ
$0.000\,000\,001 = 10^{-9}$	nano*	n
$0.000\,000\,000\,001 = 10^{-12}$	pico*	p

Announcements from Publishers

"Preparing Zircaloy-2 for Autoclave Testing the Pickling Rinsing Process," July 1959. AEC Report HW-60433,* 78 pages; $2.25.

"Electrolytic Dissolution of Stainless Steel," July 1959. AEC Report DP-396,* 10 pages 50 cents.

"Efficiency of a Thermomagnetic Generator," H. E. Strauss, Naval Research Lab., June 1959. Report PB 151736,* 9 pages; 50 cents.

"Apparatus for Measurement of the Magnetic Threshold Curves for Superconductors," J. G. Daunt, The Ohio State University Research Foundation, for Wright Air Development Center, U.S. Air Force, March 1959. Report PB 151877,* 19 pages; 50 cents.

Pergamon Institute

Pergamon Institute, a nonprofit foundation, was formed in Washington, D. C., in 1957 for the purpose of making available to English-speaking scientists, doctors, and engineers (from all countries that are members of the United Nations) the results of scientific, technological, and medical research and development in the Soviet Union and other countries in the Soviet orbit. The Institute maintains offices in Washington, London, and Oxford. Its services are available to learned societies, Government departments, trade associations, individual scientists, doctors, and engineers.

Listing and Abstracting Services

The Institute from time to time will make available, free of charge or at a nominal charge, lists of significant articles and books in various subjects from the U.S.S.R. and other countries in the Soviet orbit. The Institute also will publish in the pages of its translation journals abstracts or full titles of articles which

* Order from Office of Technical Services, U. S. Dept. of Commerce, Washington 25, D. C.

have not been accepted for publication in the translated edition. Persons interested in any article so listed may obtain a full English translation which will be supplied with a minimum of delay.

Critical Evaluation of Russian Publications

The Institute, with the assistance of its scientific staff, will undertake, on request, critical evaluation and selection of any work published in the field of science, technology, and medicine in the U.S.S.R. and other Soviet orbit countries. The Institute also will provide abstracts and résumés of such publications

Translations—Books and Journals

The Institute will undertake the additional translation of selected journals and books if suitably recommended by learned societies, Government departments, or trade assocjations.

Translations—Articles and Extracts

The Institute can undertake, with the aid of its expert panel of translators, resident all over the world, translation work in all branches of science, technology, and medicine from and into any language, including Chinese and Japanese. The charge for such a translation will be on a cooperative, cost-sharing basis (currently $6.00 per 1000 Russian words). Rates quoted under this scheme will be kept under review, with the aim of passing the benefit of increased sales over a period to all users of the translation service.

Reciprocal Services

The Institute will make available to learned societies and individual scientists, doctors, and engineers throughout the world reciprocal services on the same nonprofit basis in return for their cooperation.

Soviet Patents

The Institute receives all Soviet patents and can supply copies or translations. The journal *U.S.S.R. Patents and Inventions*, published in English for the Institute, will guide subscribers in selecting what is of interest to them.

Translators Needed

The Institute is always in need of qualified scientists, technologists, and doctors with a knowledge of the Russian language who would be able and willing to undertake translation work on a spare-time basis, for which they would be remunerated.

Further information can be obtained from Pergamon Institute, 1404 New York Ave., N.W., Washington 5, D. C.

Translation of "Optika i Spektroscopiya"

The Optical Society of America announces its translation, commencing with the January 1959 issue (Vol. 106, No. I), of *Optika i Spektroscopiya (Optics and Spectroscopy)*, the leading scientific journal of the U.S.S.R. Academy of Sciences in which is published the work of Russian scientists in all branches of optics and spectroscopy.

Optics and Spectroscopy is available free to all members of The Optical Society of America as part of their membership privileges, which include the *Journal of the Optical Society of America*, and to nonmember subscribers to the *Journal of the Optical Society of America*.

Membership dues in the OSA are $13.00 per year. Write to Dr. Mary E. Warga, Executive Secretary, Optical Society of America, 1155 Sixteenth St., N.W., Washington 6, D. C., for membership application form.

Nonmembership subscription is $28.00 per year. Send nonmember subscription orders directly to the American Institute of Physics, 335 E. 45 St., New York 17, N. Y.

Literature from Industry

UR Chargers. Technical data is available on the selection and use of specific models of Exide constant-voltage, silicon-rectifier (UR) chargers for stationary-type batteries which are claimed to provide the most accurate voltage control available for stand-by battery charging in electric utility service, emergency power and lighting, and other float-charge battery applications. The UR line, 32 basic sizes with 18 additional sizes for specialized charging jobs, has d-c outputs of from 1 to 400 amp. A revised bulletin describes the technical features of the single- and three-phase UR chargers, used for lead-acid batteries of from 5 to 124 cells. Write to Exide Industrial Div., Electric Storage Battery Co., Rising Sun and Adams Aves., Philadelphia 20, Pa.

Electronic Instruments Catalog describes and illustrates instruments for electronic, biological, and chemical measurement and control. Specifications and performance data, schematic diagrams and application circuits, as well as basic information on electrometers and micro-micro-ammeters, are included. Keithley 1960 Catalog is available on request on company letterhead from Keithley Instruments, Inc., 12415 Euclid Ave., Cleveland 6, Ohio.

Silicon Zener Diode Catalog, Bulletin SR-260, describes a complete line of hermetically sealed silicon zener diodes, including listings of 152 standard types, and instruction on selection from 1584 standard and special voltage-tolerance types. Also detailed are zener diode performance characteristics, current limits, and derating curves covering the units lisited. **Rectifier News, RN-1159,** Fall Edition, 1959, contains articles on referencing and instrumentation with zener diodes, and output regulation utilizing the switching action of zener diodes. Included are detailed circuits and performance curves covering the specific components used.

For copies, write to International Rectifier Corp., El Segundo, Calif.

Self-Curing Zinc Coating. Zinkote, a 100% inorganic, gives bare steel complete protection from water, severe weathering, salt spray, and abrasion. Applied with regular painting equipment in a single coat only a few mils thick, it cures itself to metallic hardness and adheres permanently. It is unaffected by solvents and is not flammable, volatile, or toxic, and may be used on steel structures or members of any size, before or after erection. Zinkote bulletin is available from Amercoat Corp., 4809 Firestone Blvd., South Gate, Calif.

Glass-Dielectric Wafer Capacitors. Data sheets, Reference File CE-1.02,

Notice to Members

According to the Constitution of the Society, Article III, Section 9, "Any member delinquent in dues after April 1 of each year shall no longer receive the Society's publications. . . ." Such delinquents will not receive the May issue of the JOURNAL. A reminder notice was mailed to delinquents the middle of February; a final notice will be mailed the middle of March.

describe the glass-dielectric wafer capacitors as ideally suited for printed circuit, modular, or encapsulated assemblies requiring high reliability. The items, which are flat, are said to be the smallest high-stability capacitors currently available. They meet performance requirements of MIL-C-11272A. Capacitances range from 1 to 10,000 $\mu\mu$f at 300 DCVW. **Fotoceram Micro-Module Wafers,** produced by chemically machining glass to "micro accuracy" from a photographic reduction, then converting it to a ceramic, are described in "Bulletin MMW." They are said to be nonporous, dimensionally stable, and shock resistant.

Requests should be made on company letterhead: for Reference File CE-1.02, from Electric Components Dept., and for "Bulletin MMW," from the Receiver Bulb Sales Dept., Corning Glass Works, Corning, N. Y.

Analysis of Fluorine Compounds within 30 sec by the Model 105 Nuclear Magnetic Resonance (NMR) Analyzer is described in a new report. Both quantitative and qualitative analytical results are discussed. High resolution charts and test charts for analysis of pure fluorocarbon liquids and dilutions of fluorocarbons in carbon tetrachloride are included. Material Study Report #34.58 is available from Ridgefield Instrumentation Div., Schlumberger Well Surveying Corp., Ridgefield, Conn.

A-C Catalog Guide for Process Industries. A new catalog guide of equipment for the process industries has been released by Allis-Chalmers. Included in the guide are descriptions of compressors, vacuum, centrifugal, axial flow and turbine pumps, and valves for fluid flow; crushers and grinding and roller mills for disintegration, mixing, and agglomeration; vibrating and gyratory screens for dry separation; blade mills, pool washing screens, and log washers for liquid separation; kilns, dryers, slakers, pelletizers, coolers, and liquid heaters for heat transfer. The guide also covers electrical equipment for the complete process plant, electronic metal detectors, water-conditioning equipment, chemicals, and service, as well as car shakers, lift trucks, tractors, etc.

Copies of "Allis-Chalmers Equipment for the Process Industries," 25C6177P, are available on request from Allis-Chalmers, Milwaukee 1, Wis.

Brochure on Molybdenum describes the applications, physical properties, and production processes of molybdenum. It lists the forms of molybdenum available commercially and explores the many new avenues of application opened by recent technological advances in the refractory metals field. Copies can be obtained from Sylvania Electric Products Inc., Chemical and Metallurgical Div., Towanda, Pa.

Carpenter Bulletin on Super Corrosion-Resistant Alloys. A new bulletin on tubing and pipe made of Hastelloy Alloys B and C has been issued by the Carpenter Steel Co.'s Alloy Tube Division, Union, N. J. The bulletin outlines applications of these super corrosion-resistant alloys and describes their resistance to corrosive fluids. Tables show the comparative resistance of Hastelloy Alloys B and C to various corrosive media such as hydrochloric, phosphoric, and sulfuric acids, nitric and oxidizing acid mixtures, organic acids, chlorine and hypochlorites, and acid salts at specified concentrations and temperatures. Other tables show the chemical analysis and physical and mechanical properties of the two alloys, as well as size ranges available and tolerances of pipe and tubing. Another section deals with the workability of these super corrosion-resistant steels.

For further information or to obtain a copy of this six-page bulletin, write to the Carpenter Steel Co., Alloy Tube Div., Union, N.J.

Employment Situations

Position Wanted

Chemical Engineers—M.S. Thirteen years' diversified experience in process and production control, assistant plant manager, process design, plant start-up, and trouble shooting in chloro-alkali industry. Desires responsible position in production or development. *Reply to Box 367, c/o The Electrochemical Society, 1860 Broadway, New York 23, N. Y.*

Positions Available

Metallurgist, Chemist, Chemical Engineer — Ferrous metallurgical background for research and development on high and low temperature corrosion problems of fuel burning equipment. Chattanooga, Tennessee, location. Salary commensurate with experience. *Reply to Box A-281, c/o The Electrochemical Society, 1860 Broadway, New York 23, N. Y.*

Research Chemists, Mathematicians, Metallurgists, and Physicists —The Civil Service Commission is searching for qualified scientists in the fields of chemistry, mathematics, metallurgy, and physics for research work in various Federal establishments in the Washington, D. C., area Persons appointed will work with some of the nation's foremost scientists in attractive and promising assignments and will have outstanding opportunities for advancement. The entrance salaries range from $4490 to $12,770 a year.

Most appointments are made to the following agencies: National Bureau of Standards, Dept. of the Air Force, Agricultural Research Serv-

December 1960 Discussion Section

A Discussion Section, covering papers published in the January-June 1960 JOURNALS, is scheduled for publication in the December 1960 issue. Any discussion which did not reach the Editor in time for the June 1960 Discussion Section will be included in the December 1960 issue.

Those who plan to contribute remarks for this Discussion Section should submit their comments or questions in triplicate to the Managing Editor of the JOURNAL, 1860 Broadway, New York 23, N. Y., *not later than September 1, 1960.* All discussion will be forwarded to the author(s) for reply before being printed in the JOURNAL.

ıce, Walter Reed Army Medical Center, Diamond Ordnance Fuze Labs., Geological Survey, Bureau of Mines, Food and Drug Administration, and the National Institutes of Health. The research laboratories in these agencies are among the finest equipped in the world. The basic and applied research being done is highly diversified and affords many challenges in the field of physical science.

Candidates must have completed appropriate college study leading to a bachelor's degree. In addition, for positions paying $5430 and above, graduate study or professional experience is required. College graduates may also qualify for positions paying a beginning salary of $5430 a year if they have a superior scholastic record, or through passing an appropriate written test.

Further information regarding these positions is contained in Civil Service Announcements 209B and 210B. The announcements and application forms can be obtained at many post offices throughout the country, or from the U.S. Civil Service Commission, Washington 25, D.C. Applications will be accepted by the Board of U.S. Civil Service Examiners, National Bureau of Standards, Washington 25, D.C., until further notice.

Chemists and Chemical Engineers —We need physical, organic and inorganic chemists, and chemical engineers to carry out engineering and development work in the rapidly growing power sources field. Research & Development center located in Minneapolis near University of Minnesota. Battery experience preferred but not required. Send résumés to: J. W. Baxter, Employee & Labor Relations, Gould-National Batteries, Inc., E. 1326 First National Bank Bldg., St. Paul 1, Minnesota.

Advertiser's Index

Aerovox Corporation 90C
Bell Telephone Laboratories, Inc. 46C
General Motors Research Laboratories 45C
Great Lakes Carbon Corp., Electrode Division ..... Cover 2 and 90C
Lockheed Missiles & Space Division 80C
National Cash Register Company 89C
Olin Mathieson Chemical Corporation 90C

SENIOR
Research Associate

The National Cash Register Company, a leading manufacturer of DATA PROCESSING EQUIPMENT & SYSTEMS, has need for a Senior Research Associate with a knowledge of electronics and a Ph.D. or its equivalent, in Chemical, Theoretical, or Experimental Physics.

The person we are looking for would have initiated advanced research programs in Solid State Physics (with emphasis on magnetics) and carried them through to completion with significant contributions to the field as a result.

He must be capable of planning, guiding, and evaluating future technical programs and assist in developing our research objectives. He will assist in the general administration of the programs of the department. The position is in our spacious and modern research center located in Dayton, Ohio.

Present Research Programs encompass:

- *Studies of electro luminescence and photoconductivity—materials development to circuit and system application*
- *Evaluation and application of Ferrite materials to logical systems and memory devices*
- *Deposition of magnetic materials — evaluation and application of structures into components, devices and systems*
- *Studies of the semi-conductor properties of the Ga and In series of intermetallic compounds*

Replies to this notice should be as complete as possible. All replies will be kept in confidence and should be directed to:

Mr. Thomas F. Wade, Technical Placement F-10
The National Cash Register Company
Main and K Streets, Dayton 9, Ohio

* TRADEMARK REG. U. S. PAT. OFF.
National*
ELECTRONIC DATA PROCESSING
ADDING MACHINES • CASH REGISTERS
ACCOUNTING MACHINES • NCR PAPER
DIVERSIFIED CHEMICAL PRODUCTS

THE NATIONAL CASH REGISTER COMPANY, DAYTON 9, OHIO
ONE OF THE WORLD'S MOST SUCCESSFUL CORPORATIONS
76 YEARS OF HELPING BUSINESS SAVE MONEY

SCIENTISTS AND ENGINEERS

Aerovox Corporation is Adding to Its Professional Staff

Positions for scientists and engineers of superior ability in its New Bedford Research and Engineering Laboratories for work in the following fields relating to capacitors and similar components:

DIELECTRICS

PLASTICS

ELECTROCHEMISTRY

METALLURGY

DESIGN

ENGINEERING

Comfortable salary, excellent employee benefits, including profit sharing, fine living on coast near Cape Cod, and easy access to the additional cultural centers of Boston and Providence.

For a personal interview, address your resume, in confidence, to

Mr. A. J. Warner, Manager,

Research and Engineering

Aerovox Corporation
New Bedford, Mass.

OLIN MATHIESON CHEMICAL CORPORATION METALLURGICAL LABORATORIES

Challenging research in new, fully equipped metallurgical laboratory in New Haven, Connecticut. Career positions available for research metallurgists, physical chemists, and physicists with creative problem solving ability.

PROCESS METALLURGIST

Graduate physical metallurgist for studies on the melting and continuous casting of aluminum alloys. Two to four years experience in melting and casting required. Several years research experience desirable.

PHYSICAL METALLURGIST

Graduate physical metallurgist for alloy development and studies of the effects of constitution, structure, working practices and thermal treatment on aluminum-base alloys. Two to four years research experience required. Experience in aluminum technology desirable.

PHYSICAL CHEMIST, PHYSICIST OR METALLURGIST

Ph.D. or equivalent for fundamental studies of oxidation of metals. Good background in semi-conductor technology and experimental techniques required. Familiarity with aluminum or brass metallurgy desirable.

Send detailed resume to:

E. R. Patterson, Employment Mgr.
Olin Mathieson Chemical Corporation
125 Munson Street
New Haven, Connecticut

ELECTROCHEMICAL RESEARCH AND DEVELOPMENT

Outstanding opportunity for physical chemist or chemical engineer to head up research and development program on graphite anodes for electrolysis of aqueous salt systems. Graduate with advanced degree and good academic background, or Bachelor of Science with at least two years' experience in closely related field preferred. Excellent growth potential in a rapidly expanding department housed in new facilities.

Send detailed resume indicating salary requirement to:

Manager of Research and Development
Great Lakes Carbon Corporation
Electrode Division
P. O. Box 637
Niagara Falls, New York

The Electrochemical Society

Patron Members

Aluminum Co. of Canada, Ltd.,
Montreal, Que., Canada
International Nickel Co., Inc.,
New York, N. Y.
Olin Mathieson Chemical Corp.,
Niagara Falls, N. Y.
Industrial Chemicals Div., Research
and Development Dept.
Union Carbide Corp.
Divisions:
Union Carbide Metals Co.,
New York, N. Y.
National Carbon Co., New York, N. Y.
Westinghouse Electric Corp., Pittsburgh, Pa.

Sustaining Members

Air Reduction Co., Inc.,
New York, N. Y.
Ajax Electro Metallurgical Corp.,
Philadelphia, Pa.
Allen-Bradley Co., Milwaukee, Wis.
Allied Chemical & Dye Corp.
General Chemical Div., Morristown, N. J.
Solvay Process Div., Syracuse, N. Y.
(3 memberships)
Allied Research Products, Inc.,
Detroit, Mich.
Alloy Steel Products Co., Inc., Linden, N. J.
Aluminum Co. of America,
New Kensington, Pa.
American Machine & Foundry Co.,
Raleigh, N. C.
American Metal Climax, Inc.,
New York, N. Y.
American Potash & Chemical Corp.,
Los Angeles, Calif. (2 memberships)
American Smelting and Refining Co.,
South Plainfield, N. J.
American Zinc Co. of Illinois,
East St. Louis, Ill.
American Zinc, Lead & Smelting Co.,
St. Louis, Mo.
American Zinc Oxide Co., Columbus, Ohio
M. Ames Chemical Works, Inc.,
Glens Falls, N. Y.
Auto City Plating Company Foundation,
Detroit, Mich.
Basic Inc., Maple Grove, Ohio
Bell Telephone Laboratories, Inc.,
New York, N. Y. (2 memberships)
Bethlehem Steel Co., Bethlehem, Pa.
(2 memberships)
Boeing Airplane Co., Seattle, Wash.
Burgess Battery Co., Freeport, Ill.
(4 memberships)
Canadian Industries Ltd., Montreal, Que.,
Canada
Carborundum Co., Niagara Falls, N. Y.
Catalyst Research Corp., Baltimore, Md.
Chrysler Corp., Detroit, Mich.
Ciba Pharmaceutical Products, Inc., Summit,
N. J.
Columbian Carbon Co., Brooklyn, N. Y.
Columbia-Southern Chemical Corp.,
Pittsburgh, Pa.
Consolidated Mining & Smelting Co. of
Canada, Ltd., Trail, B. C., Canada
(2 memberships)
Continental Can Co., Inc., Chicago, Ill.
Cooper Metallurgical Associates, Cleveland,
Ohio
Corning Glass Works, Corning, N. Y.
Crane Co., Chicago, Ill.
Diamond Alkali Co., Painesville, Ohio
(2 memberships)
Dow Chemical Co., Midland, Mich.
Wilbur B. Driver Co., Newark, N. J.
(2 memberships)
E. I. du Pont de Nemours & Co., Inc.,
Wilmington, Del.
Eagle-Picher Co., Chemical Div., Joplin, Mo.
Eastman Kodak Co., Rochester, N. Y.
Thomas A. Edison Research Laboratory, Div.
of McGraw-Edison Co., West Orange, N. J.
Electric Auto-Lite Co., Toledo, Ohio
C. & D. Division, Conshohocken, Pa.
Electric Storage Battery Co., Philadelphia, Pa.
Englehard Industries, Inc., Newark, N. J.
(2 memberships)
The Eppley Laboratory, Inc., Newport, R. I.
(2 memberships)
Erie Resistor Corp., Erie, Pa.
Exmet Corp., Tuckahoe, N.Y.
Fairchild Semiconductor Corp., Palo Alto,
Calif.
Federal Telecommunication Laboratories,
Nutley, N. J.
Food Machinery & Chemical Corp.
Becco Chemical Div., Buffalo, N. Y.
Westvaco Chlor-Alkali Div., South
Charleston, W. Va.
Foote Mineral Co., Paoli, Pa.
Ford Motor Co., Dearborn, Mich.
General Electric Co., Schenectady, N. Y.
Chemistry & Chemical Engineering
Component, General Engineering
Laboratory
Chemistry Research Dept.
General Physics Research Dept.
Metallurgy & Ceramics Research Dept.
General Instrument Corp., Newark, N. J.

(Sustaining Members cont'd)

General Motors Corp.
Brown-Lipe-Chapin Div., Syracuse, N. Y. (2 memberships)
Guide Lamp Div., Anderson, Ind.
Research Laboratories Div., Detroit, Mich.
General Transistor Corp., Jamaica, N. Y.
Gillette Safety Razor Co., Boston, Mass.
Globe-Union, Inc., Milwaukee, Wis.
Gould-National Batteries, Inc., Depew, N. Y.
Grace Electronic Chemicals, Inc., Baltimore, Md.
Great Lakes Carbon Corp., New York, N. Y.
Hanson-Van Winkle-Munning Co., Matawan, N. J. (3 memberships)
Harshaw Chemical Co., Cleveland, Ohio (2 memberships)
Hercules Powder Co., Wilmington, Del.
Hill Cross Co., Inc., New York, N. Y.
Hoffman Electronics Corp., Evanston, Ill.
Hooker Chemical Corp., Niagara Falls, N. Y. (3 memberships)
Houdaille Industries, Inc., Detroit, Mich.
Hughes Aircraft Co., Culver City, Calif.
International Business Machines Corp., Poughkeepsie, N. Y.
International Minerals & Chemical Corp., Chicago, Ill.
Jones & Laughlin Steel Corp., Pittsburgh, Pa.
K. W. Battery Co., Skokie, Ill.
Kaiser Aluminum & Chemical Corp.
Chemical Research Dept., Permanente, Calif.
Div. of Metallurgical Research, Spokane, Wash.
Kennecott Copper Corp., New York, N. Y.
Keokuk Electro-Metals Co., Keokuk, Iowa
Libbey-Owens-Ford Glass Co., Toledo, Ohio
M. & C. Nuclear, Inc., Attleboro, Mass.
Mallinckrodt Chemical Works, St. Louis, Mo.
P. R. Mallory & Co., Indianapolis, Ind.
McGean Chemical Co., Cleveland, Ohio
Merck & Co., Inc., Rahway, N. J.
Metal & Thermit Corp., Detroit, Mich.
Minnesota Mining & Manufacturing Co., St. Paul, Minn.
Monsanto Chemical Co., St. Louis, Mo.
Motorola, Inc., Chicago, Ill.
National Cash Register Co., Dayton, Ohio
National Lead Co., New York, N. Y.
National Research Corp., Cambridge, Mass.
National Steel Corp., Weirton, W. Va.
New York Air Brake Co., Vacuum Equipment Div., Camden, N. J.
Northern Electric Co., Montreal, Que., Canada
Norton Co., Worcester, Mass.
Olin Mathieson Chemical Corp., Niagara Falls, N. Y.
High Energy Fuels Organization (2 memberships)
Peerless Roll Leaf Co., Inc., Union City, N. J.
Pennsalt Chemicals Corp., Philadelphia, Pa.
Phelps Dodge Refining Corp., Maspeth, N. Y.
Philco Corp., Philadelphia, Pa.
Philips Laboratories, Inc., Irvington-on-Hudson, N. Y.
Pittsburgh Metallurgical Co., Inc., Niagara Falls, N. Y.
Poor & Co., Promat Div., Waukegan, Ill.
Potash Co. of America, Carlsbad, N. Mex.
Radio Corp. of America, Harrison, N. J.
Ray-O-Vac Co., Madison, Wis.
Raytheon Manufacturing Co., Waltham, Mass.
Reynolds Metals Co., Richmond, Va. (2 memberships)
Rheem Semiconductor Corp., Mountain View, Calif.
Schering Corporation, Bloomfield, N. J.
Shawinigan Chemicals Ltd., Montreal, Que., Canada
Speer Carbon Co.
International Graphite & Electrode Div., St. Marys, Pa. (2 memberships)
Sprague Electric Co., North Adams, Mass.
Stackpole Carbon Co., St. Marys, Pa.
Stauffer Chemical Co., New York, N. Y.
Sumner Chemical Co., Div. of Miles Laboratories, Inc., Elkhart, Ind.
Sylvania Electric Products Inc., Bayside, N. Y. (2 memberships)
Tennessee Products & Chemical Corp., Nashville, Tenn.
Three Point Four Corp., Yonkers, N. Y.
Titanium Metals Corp. of America, Henderson, Nev.
Tung-Sol Electric Inc., Newark, N. J.
Udylite Corp., Detroit, Mich. (4 memberships)
Universal-Cyclops Steel Corp., Bridgeville, Pa.
Upjohn Co., Kalamazoo, Mich.
Victor Chemical Works, Chicago, Ill.
Western Electric Co., Inc., Chicago, Ill.
Wyandotte Chemicals Corp., Wyandotte, Mich.
Yardney Electric Corp., New York, N. Y.